

# **Microtubules and End- Binding Proteins in Epithelial Remodelling and Breast Cancer Invasion**

**Temitope Azeezat Amodu**

*A thesis submitted in fulfilment of the requirements for the  
degree of Doctor of Philosophy*

School of Biological Sciences  
Norwich Research Park  
University of East Anglia  
August 2018

Word Count: 71,310



This copy of the thesis has been supplied on condition that anyone who consults it is understood to recognise that its copyright rests with the author and that use of any information derived therefrom must be in accordance with current UK Copyright Law. In addition, any quotation or extract must include full attribution.

# Abstract

The cytoskeleton plays vital roles in several cellular functions and disruption to its normal organisation and dynamics could lead to cancer. Cell migration is important during wound healing and tissue repair, and it is also known to take place during tumour metastasis. Microtubule reorganisation is driven by their inherent dynamic properties and influenced by plus-end tracking proteins such as the end-binding protein (EB) family. A better understanding of cell migration mechanisms could lead to more efficient treatments for invasive cancers such as breast cancer.

Random migration of MCF-7 and MDA-MB-231 cells were monitored using time-lapse microscopy. Analysis revealed that MDA-MB-231, that express relatively high levels of EB2, migrated faster compared with MCF-7 cells. Similar results were observed in EB2 overexpressing MDCKII compared with the Empty-vector MDCKII cells suggesting that elevated levels of EB2 expression is associated with increased rate of cell migration. Interestingly, immunolabelling revealed that many of these migratory cells showed EB2 accumulation at the leading edge. Resveratrol is a naturally occurring compound found in foods such as red wine and grapes and its potential in reducing the rate of cell migration in breast cancer was also investigated. Resveratrol was found to significantly reduce the migration speed of MDA-MB-231 and MCF-7 cells. In addition, resveratrol-treated cells had straighter and more radially organised microtubules with more rounded EB1 comets at the plus-ends. A dramatic redeployment of EB2 was also observed upon treatment with 50 and 75 $\mu$ M resveratrol.

Rearrangement of the microtubule cytoskeleton and its regulators are known to be essential for polarity establishment. Therefore, the project also investigated the effect of EB2 overexpression on epithelial remodelling in order to understand the processes leading to the loss of normal tissue architecture and ultimately, an invasive breast cancer state. Upon 3D culturing of MDCKII cells in Matrigel, EB2 overexpression in MDCKII cysts showed an increase in multiple lumen formation. Mechanistically, this was found to be due to loss of normal spindle orientation and specifically defects in astral microtubule cortical contact. Spindle misorientation could be rescued by Taxol treatment. Additionally, EB2 overexpression caused multipolar spindles, which are associated with supernumerary centrosomes and chromosome instability, and may contribute to cancer progression. In conclusion, this suggests a possible role for EB2 as a prognostic bio-marker for breast biopsies.

# Acknowledgements

First and foremost, I give thanks to Allah, the most gracious, the most merciful. Without his grace, this work would not have been possible.

I would like to thank my supervisors Dr Mette Mogensen and Dr Jelena Gavrilovic for giving me the opportunity to work on this exciting and challenging project. Thank you, Mette, for providing the support and guidance required for me to enjoy my work and to contribute positively. I would also like to express gratitude to Dr Paul Thomas for providing a great imaging facility and helping with subsequent analyses. Thank you to current and former lab members: Yaser, James, Debbie, Jonno and Ben for providing advice and support in the lab.

I am very grateful to Breast Cancer Now for providing the grant and supporting the project. I am also grateful for the great atmosphere and studying conditions that the School of Biological Sciences and the BMRC provided. Thanks to members of Jelena Gavrilovic and Mohammad Hajihosseini's lab; and extra special thanks goes to Irene for listening to my challenges, for several years, and providing a fun environment to work in.

Finally, I'd like to thank my entire family, particularly my mum and sister. Without your prayers, kind words and continued support throughout the years, I wouldn't have gotten this far; I hope I have made you proud. I am also extremely grateful to my friend, Vicki with whom I had numerous conversations and for keeping my sanity.

# *Table of Contents*

<b>Abstract .....</b>	<b>II</b>
<b>Acknowledgements .....</b>	<b>III</b>
<b>Table of Contents.....</b>	<b>I</b>
<b>List of Figures .....</b>	<b>VII</b>
<b>List of Tables .....</b>	<b>XVI</b>
<b>List of Abbreviations.....</b>	<b>XVII</b>
<b>Chapter I: Introduction.....</b>	<b>1</b>
<b>1.1 The Cytoskeleton .....</b>	<b>2</b>
1.1.1 Actin filaments .....	2
1.1.2 Intermediate filaments.....	5
<b>1.2 Microtubules .....</b>	<b>6</b>
1.2.1 Microtubule structure and dynamics.....	6
1.2.2 Microtubule nucleation .....	10
1.2.3 Microtubule anchorage and minus-end associated proteins.....	20
1.2.4 Microtubule plus-end tracking proteins (+TIPs) .....	21
1.2.5 Microtubule post-translational modifications.....	30
<b>1.3 Mechanisms of Epithelial Lumen Formation .....</b>	<b>33</b>
1.3.1 Lumen initiation .....	37
1.3.2 Lumen extension and expansion .....	42
<b>1.4 Spindle Orientation .....</b>	<b>44</b>
<b>1.5 Introduction to Breast Cancer .....</b>	<b>50</b>
1.5.1 Cell migration.....	53
1.5.2 Cytoskeletal organisation in migrating cells.....	54
1.5.2 Epithelial mesenchymal transition (EMT) .....	61
1.5.3 Role of EBs in breast cancer progression .....	65
<b>1.6 Treatment of Breast Cancer – Resveratrol.....</b>	<b>66</b>

1.6.1 Resveratrol and cancer .....	69
1.6.2 Resveratrol and MTs .....	71
<b>1.7 Summary.....</b>	<b>73</b>
<b>1.8 Aims and Objectives .....</b>	<b>74</b>
<b><i>Chapter II: Materials &amp; Methods.....</i></b>	<b>76</b>
<b>2.1 Model Systems .....</b>	<b>77</b>
2.1.1 Cell Lines – Breast cancer and MDCK cells .....	77
<b>2.2 Cell Culture.....</b>	<b>78</b>
2.2.1 Maintenance of cell lines.....	78
2.2.2 3D Cyst Culture.....	79
<b>2.3 Drug Treatments.....</b>	<b>79</b>
2.3.1 Double thymidine block.....	79
2.3.2 Resveratrol.....	80
2.3.3 Taxol .....	80
<b>2.4 Cell Viability Assay (MTT Assay) .....</b>	<b>81</b>
<b>2.5 Immunolabelling of 2D and 3D cultures .....</b>	<b>81</b>
2.5.1 Fixatives .....	81
<b>2.6 Microscopy.....</b>	<b>86</b>
2.6.1 Widefield fluorescence microscope.....	86
2.6.2 Confocal .....	86
2.6.3 Live Imaging .....	86
<b>2.7 Migration .....</b>	<b>87</b>
2.7.1 Random cell migration .....	87
2.7.1 Wound healing assay.....	88
2.7.3 Micropattern Coverslips .....	88
<b>2.8 Spheroid Production .....</b>	<b>89</b>
<b>2.9 Plasmid Transfection .....</b>	<b>89</b>
2.9.1 Midi-prep .....	90
<b>2.10 Western Blotting .....</b>	<b>90</b>
2.10.1 Cell lysis.....	90
2.10.2 SDS-PAGE electrophoresis .....	91
2.10.3 Protein detection .....	92

2.11 Spindle Orientation Assay and Analysis .....	93
2.12 Cold Treatment.....	94
2.13 EB1 Comet Analysis.....	94
2.14 Microtubule Acetylation Analysis .....	94
2.15 Centrosome Positioning – Two-cell stage .....	95
2.16 Centriole amplification.....	95
2.17 Centrosome Positioning Analysis.....	96
2.18 Analysis of CLIP-170 Comet Dynamics.....	96
2.19 Statistical Analysis .....	97
<b>Chapter III: Characterisation of MT Organisation and Dynamics in Breast Cancer Cell Models.....</b>	<b>98</b>
3.1 Overview.....	99
3.2 Introduction .....	99
3.3 Results .....	102
3.3.1 Characterisation of MCF-7 and MDA-MB-231 cells.....	102
3.3.2 MT dynamics and stability in MCF-7 and MDA-MB-231 cells .....	105
3.4 Discussion .....	107
<b>Chapter IV: Migration Studies in EB2 Overexpressing Cells... 132</b>	
4.1 Overview.....	133
4.2 Introduction .....	133
4.3 Results .....	136
4.3.1 Collagen-I provides a suitable ECM for cell migration in both MCF-7 and MDA-MB-231 cells .....	136
4.3.2 MDA-MB-231 cells migrated faster and further than MCF-7 cells	137
4.3.3 Localisation of EB2 in MDCKII <sup>mChEmpty</sup> and MDCKII <sup>mChEB2Hi</sup> cells.....	138
4.3.4 Increased speed of random migration associated with EB2- overexpression in MDCKII cells.....	139
4.3.5 Directional cell migration and centrosome positioning in MDCKII <sup>mChEB2Hi</sup> cells .....	140
4.4 Discussion .....	141
4.4.1 Collagen-I proved to be a suitable ECM for cell migration in both MCF-7 and MDA-MB-231 cells .....	141

4.4.2 EB2 overexpression causes increased cell migration.....	142
<b>4.5 Summary.....</b>	<b>144</b>
<b><i>Chapter V: Effects of Resveratrol on Cell Migration, MTs and End-binding Proteins in Breast Cancer Cells .....</i></b>	<b>162</b>
<b>5.1 Overview.....</b>	<b>163</b>
<b>5.2 Introduction .....</b>	<b>163</b>
<b>5.3 Results .....</b>	<b>166</b>
5.3.1 Viability assessment of resveratrol in MCF-7 and MDA-MB-231 cells .....	166
5.3.2 Resveratrol treatment causes morphological changes in both cell lines .....	166
5.3.3 Resveratrol treatment causes a significant increase in cell size and decrease in cell proliferation in both cell lines.....	167
5.3.4 Resveratrol treatment causes a reduction in speed and distance travelled during cell migration .....	168
5.3.5 Resveratrol caused reduced invasion of MDA-MB-231 cells .....	169
5.3.6 Resveratrol treatment leads to straighter MTs in MCF-7 and MDA- MB-231 cells but EB1 lattice association is observed in only MDA-MB-231 cells .....	171
5.3.7 Resveratrol treatment leads to EB2 displacement from the leading edge and detachment from MTs in MDA-MB-231 cells .....	172
5.3.8 Resveratrol treatment causes actin depolymerisation .....	173
5.3.9 Resveratrol treatment causes a decrease in size and number of focal adhesions .....	173
5.3.10 MT stability – tubulin acetylation .....	175
<b>5.4 Discussion .....</b>	<b>176</b>
5.4.1 Resveratrol caused an increase in cell area in both MCF-7 and MDA- MB-231 cells .....	176
5.4.2 Resveratrol caused a dramatic decrease in cell migration in both MCF-7 and MDA-MB-231 cells .....	177
5.4.3 Resveratrol altered MT and actin organisation and resulted in EB1 associating along the MT lattice while EB2 became cytoplasmic in MDA- MB-231 cells .....	178
5.4.4 Resveratrol caused a reduction in focal adhesions and altered MT acetylation in MDA-MB-231 cells .....	179
<b>5.5 Summary.....</b>	<b>181</b>

<b>Chapter VI: Effects of EB2 Overexpression on Epithelial Lumen Formation .....</b>	<b>216</b>
<b>6.1 Overview.....</b>	<b>217</b>
<b>6.2 Introduction .....</b>	<b>217</b>
<b>6.3 Results .....</b>	<b>222</b>
6.3.1 EB2 overexpression causes the formation of 3D cysts with multiple lumens.....	222
6.3.2 Localisation of polarity markers during 3D cyst formation.....	222
6.3.3 EB2 overexpression impairs centrosome positioning in MDCKII <sup>mChEB2Hi</sup> cells .....	223
6.3.4 EB2 overexpression alters spindle orientation in MDCKII cells.....	224
6.3.5 EB2-overexpressing cells exhibit defects in astral MT cortical contact.....	226
6.3.6 EB2 overexpression leads to increased GFP-CLIP-170 comet speed .....	227
6.3.7 Spindle misorientation in MDCKII <sup>mChEB2Hi</sup> cells could be rescued by Taxol .....	229
<b>6.4 Discussion .....</b>	<b>230</b>
6.4.1 EB2-overexpression leads to an increase in multiple lumen formation.....	230
6.4.2 EB2-overexpression leads to spindle misorientation.....	232
<b>6.5 Summary.....</b>	<b>234</b>
<b>Chapter VII: EB2 Overexpression and Multispindle Formation .....</b>	<b>259</b>
<b>7.1 Overview.....</b>	<b>260</b>
<b>7.2 Introduction .....</b>	<b>260</b>
<b>7.3 Results .....</b>	<b>263</b>
7.3.1 EB2-overexpression leads to a significant increase in cells with multipolar spindles .....	263
7.3.2 Supernumerary Centrioles.....	263
7.3.3 PLK4 is not overexpressed in EB2-overexpressing MDCKII cells ...	264
7.3.4 EB2 overexpression in MDCKII cells may induce cytokinesis failure while centriole engagement seems unaffected. ....	264
<b>7.4 Discussion .....</b>	<b>266</b>

7.4.1 EB2-overexpression leads to the formation of multipolar spindles but not through Plk4 overexpression .....	266
<b>7.5 Summary.....</b>	<b>268</b>
<b><i>Chapter VIII: General Discussion.....</i></b>	<b><i>280</i></b>
<b>8.1 Introduction .....</b>	<b>281</b>
<b>8.2 Increased EB2 expression promotes cell migration.....</b>	<b>282</b>
<b>8.3 Resveratrol alters MT organisation and reduces migration and invasion in breast cancer cells .....</b>	<b>284</b>
<b>8.4 EB2 overexpression induces formation of multiple lumens and multipolar spindle formation in MDCKII<sup>mChEB2Hi</sup> cells.....</b>	<b>285</b>
<b>8.5 Summary.....</b>	<b>290</b>
<b>8.6 Future work.....</b>	<b>290</b>
<b><i>Appendices.....</i></b>	<b><i>292</i></b>
<b><i>References.....</i></b>	<b><i>306</i></b>

# *List of Figures*

## **Chapter I**

<b>Figure 1.1 Actin filament structure.....</b>	<b>4</b>
<b>Figure 1.2 Microtubule structure.....</b>	<b>8</b>
<b>Figure 1.3 Microtubule assembly and disassembly.....</b>	<b>9</b>
<b>Figure 1.4 Centrosome Structure.....</b>	<b>14</b>
<b>Figure 1.5 Centrosome duplication.....</b>	<b>15</b>
<b>Figure 1.6 Domain structures of +TIP proteins.....</b>	<b>24</b>
<b>Figure 1.7 Regulation of MT dynamic instability by several proteins.....</b>	<b>29</b>
<b>Figure 1.8 Various mechanisms of lumen formation.....</b>	<b>36</b>
<b>Figure 1.9 Proteins involved in epithelial polarity.....</b>	<b>38</b>
<b>Figure 1.10 Spindle orientation in lumen formation.....</b>	<b>47</b>
<b>Figure 1.11 Anatomy of the breast.....</b>	<b>52</b>
<b>Figure 1.12 Cell migration process.....</b>	<b>56</b>
<b>Figure 1.13 Types of stress fibres in migrating cells.....</b>	<b>57</b>
<b>Figure 1.14 Cytoskeletal organisation in cell migration.....</b>	<b>60</b>
<b>Figure 1.15 Invasion-metastatic cascade.....</b>	<b>64</b>
<b>Figure 1.16 Resveratrol structure.....</b>	<b>68</b>

## **Chapter III**

<b>Figure 3.1 MCF-7 and MDA-MB-231 cellular morphologies....</b>	<b>113</b>
<b>Figure 3.2 MT organisation in MCF-7 cells.....</b>	<b>114</b>
<b>Figure 3.3 MT organisation in MDA-MB-231 cells.....</b>	<b>115</b>
<b>Figure 3.4: Actin and MT organisation in PHEMO fixed MCF-7 cell.....</b>	<b>116</b>
<b>Figure 3.5 Actin and MT organisation in PHEMO fixed MDA-MB-231 cell.....</b>	<b>117</b>
<b>Figure 3.6 Actin and MT organisation in PHEMO fixed</b>	

MDA-MB-231 cell.....	118
Figure 3.7 Expression of EB proteins in MCF-7 and MDA-MB-231 cells.....	119
Figure 3.8 Localisation of EB1 in MCF-7 and MDA-MB-231 cells.....	120
Figure 3.9 EB1 Comet Analysis in MCF-7 and MDA-MB-231 cells.....	121
Figure 3.10 Localisation of EB2 in MCF-7 and MDA-MB-231 cells.....	122
Figure 3.11 EB2 Comet Analysis in MCF-7 and MDA-MB-231 cells.....	123
Figure 3.12 Localisation of EB3 in MCF-7 and MDA-MB-231 cells.....	124
Figure 3.13 Increased growth lifetime but not comet speed in highly metastatic breast cancer cells.....	125
Figure 3.14 Increased growth length but not time growth in highly metastatic breast cancer cells.....	126
Figure 3.15 Detyrosinated tubulin localisation in MCF-7 and MDA-MB-231 cells.....	127
Figure 3.16 MT acetylation in MCF-7 and MDA-MB-231 cells...	128
Figure 3.17 MT acetylation in migrating MCF-7 and MDA-MB-231 cells.....	129
Figure 3.18 Fluorescence intensity analysis suggest increased MT acetylation in highly metastatic breast cancer cells but no change seen in the expression levels.....	130
Figure 3.19 Cold treatment resulted in total MT depolymerisation in most MCF-7 cells but revealed some stable MTs in MDA-MB-231 cells.....	131

## Chapter IV

Figure 4.1 Morphology of MDA-MB-231 and MCF-7 cells seeded on different ECM.....	146
---	-----

<b>Figure 4.2 Migration of MDA-MB-231 and MCF-7 cells when seeded on plastic, fibronectin and collagen I.....</b>	<b>147</b>
<b>Figure 4.3 MDA-MB-231 cells migrate with greater velocity than MCF-7 cells.....</b>	<b>148</b>
<b>Figure 4.4 MDA-MB-231 cells travel longer distances than MCF-7 cells.....</b>	<b>148</b>
<b>Figure 4.5 Confirmation of mCherry-EB2 protein expression in MDCKII<sup>EB2Hi</sup> cells.....</b>	<b>149</b>
<b>Figure 4.6 EB2 expression in MDCKII<sup>mChEmpty</sup> and MDCKII<sup>mChEB2Hi</sup> cells.....</b>	<b>150</b>
<b>Figure 4.7 EB2 localisation in MDCKII<sup>mChEmpty</sup> cell.....</b>	<b>151</b>
<b>Figure 4.8 EB2 localisation in MDCKII<sup>mChEB2Hi</sup> cells.....</b>	<b>152</b>
<b>Figure 4.9 EB2 localisation in MDCKII<sup>mChEB2Hi</sup> cells continued.....</b>	<b>153</b>
<b>Figure 4.10 Morphologies of MDCKII<sup>mChEmpty</sup> and MDCKII<sup>mChEB2Hi</sup> cells seeded on collagen-I.....</b>	<b>154</b>
<b>Figure 4.11 EB2-overexpressing in MDCKII cells leads to increased migration.....</b>	<b>155</b>
<b>Figure 4.12 Wound healing assay in MDCKII<sup>mChEmpty</sup> and MDCKII<sup>mChEB2Hi</sup> cells.....</b>	<b>156</b>
<b>Figure 4.13 Area of closure in scratch wound assays in MDCKII<sup>mChEmpty</sup> and MDCKII<sup>mChEB2Hi</sup> cells treated with DMSO.....</b>	<b>157</b>
<b>Figure 4.14 Area of closure in scratch wound assays in MDCKII<sup>mChEmpty</sup> and MDCKII<sup>mChEB2Hi</sup> cells.....</b>	<b>158</b>
<b>Figure 4.15 Centrosome positioning in directional migration of MDCKII cells.....</b>	<b>159-160</b>
<b>Figure 4.16 EB2-overexpression appears to affect centrosome positioning.....</b>	<b>161</b>

## Chapter V

<b>Figure 5.1 Resveratrol cell viability assay in breast cancer cells.....</b>	<b>183</b>
<b>Figure 5.2 Cell morphology of resveratrol-treated MCF-7 cells seeded on collagen I.....</b>	<b>184</b>
<b>Figure 5.3 Cell morphology of resveratrol-treated MDA-MB-231 cells</b>	

seeded on collagen I.....	184
Figure 5.4 Resveratrol affected the size of MCF-7 and MDA-MB-231 cells.....	185
Figure 5.5 Resveratrol caused an increase in the size of MCF-7 and MDA-MB-231 cells.....	186
Figure 5.6 Resveratrol caused a reduction in breast cancer cells proliferation.....	187
Figure 5.7 Resveratrol caused a reduction in speed and distance travelled of randomly migrating MCF-7 cells.....	188
Figure 5.8 Resveratrol caused a reduction in speed and distance travelled of random migrating MDA-MB-231 cells.....	189
Figure 5.9 Invasion of highly metastatic MDA-MB-231 cells.....	190
Figure 5.10 Invasion of highly metastatic MDA-MB-231 cells.....	191
Figure 5.11 Invasion of highly metastatic MDA-MB-231 cells continued.....	192
Figure 5.12 Effect of resveratrol on MDA-MB-231 cell invasion.....	193
Figure 5.13 EB1 expression in Resveratrol-treated MCF-7 and MDA-MB-231 cells.....	194
Figure 5.14 EB1 localisation and MT organisation in Resveratrol-treated MCF-7 cells.....	195
Figure 5.15 EB1 localisation and MT organisation in Resveratrol-treated MCF-7 cells.....	196
Figure 5.16 EB1 comet analysis in Resveratrol-treated MCF-7 cells.....	197
Figure 5.17 EB1 localisation and MT organisation in Resveratrol-treated MDA-MB-231 cells.....	198
Figure 5.18 EB1 localisation and MT organisation in Resveratrol-treated MDA-MB-231 cells.....	199
Figure 5.19 EB1 comet analysis in Resveratrol-treated MDA-MB-231 cells.....	200
Figure 5.20 EB2 expression in Resveratrol-treated MCF-7 and MDA-MB-231 cells.....	201
Figure 5.21 EB2 localisation and MT organisation in resveratrol-treated MCF-7 cells.....	202

<b>Figure 5.22 EB2 localisation and MT organisation in Resveratrol-treated MCF-7 cells continued:</b> .....	<b>203</b>
<b>Figure 5.23 EB2 localisation and MT organisation in resveratrol-treated MDA-MB-231 cells:</b> .....	<b>204</b>
<b>Figure 5.24 EB2 localisation and MT organisation in Resveratrol-treated MDA-MB-231 cells continued :</b> .....	<b>205</b>
<b>Figure 5.25 Resveratrol leads to a reduction in actin filaments in MCF-7 cells:</b> .....	<b>206</b>
<b>Figure 5.26 Resveratrol caused actin filament depolymerisation in MDA-MB-231 cells:</b> .....	<b>207</b>
<b>Figure 5.27 Analysis of the actin fluorescence intensity:</b> .....	<b>208</b>
<b>Figure 5.28 Resveratrol cause a decrease in focal adhesions in MCF-7 cells:</b> .....	<b>209</b>
<b>Figure 5.29 Resveratrol cause a decrease in focal adhesions in MCF-7 cells:</b> .....	<b>210</b>
<b>Figure 5.30 Resveratrol led to a reduction in the number of focal adhesions breast cancer cells:</b> .....	<b>211</b>
<b>Figure 5.31 Resveratrol led to a reduction in the size of focal adhesions breast cancer cells:</b> .....	<b>211</b>
<b>Figure 5.32 MT acetylation in Resveratrol-treated MCF-7 cells:</b> ....	<b>212</b>
<b>Figure 5.33 MT acetylation in Resveratrol-treated MDA-MB-231 cells:</b> .....	<b>213</b>
<b>Figure 5.34 Resveratrol decreases MT acetylation in MDA-MB-231 cells:</b> .....	<b>214</b>
<b>Figure 5.35 Acetylated tubulin expression measured by Western Blotting:</b> .....	<b>215</b>

## Chapter VI

<b>Figure 6.1 MT organisation in MDCKII<sup>mChEmpty</sup> and MDCKII<sup>mChEB2Hi</sup> cells:</b> .....	<b>236</b>
<b>Figure 6.2 Localisation of the tight junction marker ZO-1 in MDCKII<sup>mChEmpty</sup> and MDCKII<sup>mChEB2Hi</sup> cells reveal multiple lumens</b>	

in EB2 overexpressing cells.....	237
Figure 6.3 $\beta$ -catenin localises to adherens junctions in EB2 overexpressing cells.....	238
Figure 6.4 EB2-overexpressing MDCKII cysts revealed an increased number of cysts with multiple lumens.....	239
Figure 6.5 EB2 overexpression in 5 day MDCKII cysts does not affect localisation of the polarity marker Par-3 to apical junctions.....	240
Figure 6.6 EB2 overexpression in 6 day MDCKII cysts revealed maintenance of the polarity marker Par-3 localisation to apical junctions.....	241
Figure 6.7 EB2 overexpression in MDCKII cells does not affect localisation of the tight junction marker ZO-1 to the apical membrane at the two cell stage.....	242
Figure 6.8 EB2 overexpression in MDCKII cells does not affect the localisation of tight junctional marker ZO-1 to the apical membrane at the four-cell stage.....	243
Figure 6.9 EB2 overexpression in 3 day MDCKII cysts does not affect localisation of the tight junction protein ZO-1 to the apical membrane.....	244
Figure 6.10 EB2 overexpression in 4 day MDCKII cysts does not affect localisation of the tight junction protein ZO-1 to apical junctions.....	245
Figure 6.11 EB2 overexpression in 5 day MDCKII cysts does not affect localisation of the tight junction protein ZO-1 to apical junctions.....	246
Figure 6.12 EB2 overexpression in 6 day MDCKII cysts does not affect localisation of the tight junction protein ZO-1 to apical junctions.....	247
Figure 6.13 EB2 overexpression in MDCKII cells affects centrosome positioning at the two-cell stage.....	248
Figure 6.14 Cell synchronisation using Thymidine treatment in MDCKII cells.....	249
Figure 6.15 Cell synchronisation using Thymidine treatment in	

MDCKII cells.....	250
Figure 6.16 EB2 overexpression in MDCKII cells affects the angle of the bipolar spindle.....	251
Figure 6.17 EB2 overexpression affects the angle and height of bipolar spindles in MDCKII cells.....	252
Figure 6.18 EB2-overexpressing MDCKII cells exhibited defects in astral MTs making contact with the periphery.....	253
Figure 6.19 EB2-overexpressing cells exhibited no significant change in cortical NuMA intensity.....	254
Figure 6.20 EB2-overexpression leads to increased CLIP-170 comet speed but not growth lifetime events.....	255
Figure 6.21 EB2-overexpression does not alter the MT growth length and overall % time growth.....	256
Figure 6.22 EB2-overexpression led to increased acetylated and detyrosinated tubulin but reduced stability of MTs when MDCKII cells are cold treated.....	257
Figure 6.23 Taxol Treatment rescued spindle orientation defects in MDCKII <sup>mChEB2Hi</sup> cells.....	258

## Chapter VII

Figure 7.1 Multipolar spindle formation in MDCKII <sup>mChEB2Hi</sup> cells.....	269
Figure 7.2 Multipolar spindle formation in MDCKII <sup>mChEB2Hi</sup> cells.....	270
Figure 7.3 Multipolar spindle formation in MDCKII <sup>mChEB2Hi</sup> cells.....	271
Figure 7.4 Supernumerary centrioles in MDCKII cells.....	272
Figure 7.5 Supernumerary centrioles in MDCKII cells.....	273
Figure 7.6 Supernumerary centrioles in MDCKII <sup>mChEB2Hi</sup> cells.....	274
Figure 7.7 Plk4 localization in MDCKII, MDCKII <sup>mChEmpty</sup> and MDCKII <sup>mChEB2Hi</sup> cells.....	275
Figure 7.8 PLK4 is not overexpressed in MDCKII cells.....	276

**Figure 7.9 EB2 overexpressing MDCKII cells may possess more than one nucleus.....277**

**Figure 7.10 EB2 overexpressing MDCKII cells may possess more than one nucleus.....278**

**Figure 7.11 Cep215 polar localisation suggests that EB2 does not sequester Cep215 from the poles in MDCKII<sup>mChEB2Hi</sup> cells..279**

### **Chapter VIII**

**Figure 8.1 Model for a possible mechanism by which astral MTs defects may lead to multiple lumen formation.....288**

**Figure 8.2 Model for a possible mechanism by which cytokinesis failure may lead to multiple spindle formation.....289**

### **Appendix B**

**Movie S1 Time-lapse of MCF-7 cell transiently expressing GFP-CLIP-170.....300**

**Movie S2 Time-lapse of MDA-MB-231 cell transiently expressing GFP-CLIP-170.....300**

**Movie S3 Cell tracking in sub-confluent MDA-MB-231 cells seeded on tissue culture plastic.....300**

**Movie S4 Cell tracking in sub-confluent MDA-MB-231 cells seeded on fibronectin.....300**

**Movie S5 Cell tracking in sub-confluent MDA-MB-231 cells seeded on Collagen-I.....300**

**Movie S6 Cell tracking in sub-confluent MCF-7 cells seeded on tissue culture plastic.....301**

**Movie S7 Cell tracking in sub-confluent MCF-7 cells seeded on fibronectin.....301**

**Movie S8 Cell tracking in sub-confluent MCF-7 cells seeded on Collagen-I.....301**

**Movie S9 Cell tracking in sub-confluent MDCKII cells seeded on Collagen-I.....301**

**Movie S10 Cell tracking in sub-confluent MDCKII<sup>mChEmpty</sup> cells**

seeded on Collagen-I.....	301
Movie S11 Cell tracking in sub-confluent MDCKII <sup>mChEB2Hi</sup> cells seeded on Collagen-I.....	301
Movie S12 Cell tracking in sub-confluent DMSO treated MCF-7 cells.....	302
Movie S13 Cell tracking in sub-confluent 10 $\mu$ M resveratrol- treated MCF-7 cells.....	302
Movie S14 Cell tracking in sub-confluent 20 $\mu$ M resveratrol- treated MCF-7 cells.....	302
Movie S15 Cell tracking in sub-confluent 50 $\mu$ M resveratrol- treated MCF-7 cells.....	302
Movie S16 Cell tracking in sub-confluent DMSO treated MDA-MB-231 cells.....	303
Movie S17 Cell tracking in sub-confluent 20 $\mu$ M resveratrol- treated MDA-MB-231 cells.....	303
Movie S18 Cell tracking in sub-confluent 50 $\mu$ M resveratrol- treated MDA-MB-231 cells.....	303
Movie S19 Cell tracking in sub-confluent 75 $\mu$ M resveratrol- treated MDA-MB-231 cells.....	303
Movie S20 MDCKII cell bipolar spindle orientation.....	304
Movie S21 MDCKII <sup>mChEmpty</sup> cell bipolar spindle orientation.....	304
Movie S22 MDCKII <sup>mChEB2Hi</sup> cell bipolar spindle orientation.....	304
Movie S23 MDCKII cell astral MT dynamics.....	304
Movie S24 MDCKII <sup>mChEmpty</sup> cell astral MT dynamics.....	304
Movie S25 MDCKII <sup>mChEB2Hi</sup> cell astral MT dynamics.....	304
Movie S26 MDCKII <sup>mChEmpty</sup> cell GFP-CLIP-170 dynamics...304	
Movie S27 MDCKII <sup>mChEB2Hi</sup> cell GFP-CLIP-170 dynamics...305	
Movie S28 MDCKII <sup>mChEB2Hi</sup> cell multipolar spindle Formation.....	305

# *List of Tables*

<b>Table 1a List of primary antibodies.....</b>	<b>84</b>
<b>Table 1b List of secondary antibodies.....</b>	<b>85</b>
<b>Table 2 List of lasers and filters.....</b>	<b>86</b>

# *List of Abbreviations*

+TIP	plus-end tracking protein
2D	Two-dimensional
3D	Three-dimensional
ACF7	Actin cross-linking factor-7
ADP	Adenosine-5'-diphosphate
AMIS	Apical membrane initiation site
APC	Adenomatous polyposis coli
Arp	Actin related protein
ATP	Adenosine-5'-triphosphate
BCA	Bicinchoninic Acid
BRCA1/2	Breast cancer type 1/2 susceptibility protein
BSA	Bovine serum albumin
Ca <sup>2+</sup>	Calcium ions
CAMSAPs	calmodulin-regulated spectrin-associated protein
CAP-Gly	Cytoskeleton-associated Protein Glycine-rich
CDK1	Cyclin-dependent kinase 1
Cep68	Centrosomal protein 68
CH	Calponin homology domain
CLASP 1/2	Cytoplasmic linker associated protein 1/2
CLIP-170/115	Cytoplasmic linker protein 170/115
COOH	Carboxy terminal
CP110	Centriolar coiled-coil protein 110
DABCO	1,4-diazabicyclo[2.2.2]octane
DAPI	4',6-diamidino-2-phenylindole
ddH <sub>2</sub> O	double distilled water
DHC	Dynein heavy chain
DIC	Dynein intermediate chain
DLC	Dynein light chain
DLIC	Dynein light intermediate chain
DMEM	Dulbecco's modified eagle medium

DMSO	Dimethyl sulfoxide
EB1/2/3	End binding protein 1/2/3
ECL	Electrochemical luminescence
EDTA	Ethylenediaminetetraacetic acid
EMT	Epithelial mesenchymal transition
GAP	GTPase activating proteins
GAS2L1	Growth arrest-specific 2-like protein 1
GDI	RhoGDP dissociation inhibitor
GDP	Guanosine-5'-diphosphate
GFP	Green fluorescent protein
Glu tub	Detyrosinated tubulin
HEPES	N-2-Hydroxyethylpiperazine-N-2-Ethanesulfonic Acid
IQGAP 1/2/3	IQ motif containing GTPase activating protein 1/2/3
KIF2C	Kinesin-like protein 2C
LATS2	Large tumour suppressor kinase 2
LRRC45	Leucine-rich repeat-containing protein 45
Lys-40	N-terminus of $\alpha$ -tubulin on lysine 40
MAP	Microtubule associated protein
MCF-7	Michigan cancer foundation-7
MDCK	Madin darby canine kidney
MTOC	Microtubule organising centre
NuMA	Nuclear mitotic apparatus protein
Par-3	Partitioning defective-3
PAGE	Polyacrylamide gel electrophoresis
PBS	Phosphate buffered saline
PCM	Pericentriolar matrix
Plk1	Polo-like kinase 1
Plk4	Polo-like kinase 4
PLP	Pericentrin-like protein
RFP	Red fluorescent protein
Rsv	Resveratrol
SAS-5	Spindle assembly abnormal protein 5
SDS	Sodium dodecyl sulphate

TACC3	Transforming acidic coiled-coil containing protein 3
TTL	Tubulin tyrosine ligase
Tx100	Triton X100
Tyr tub	Tyrosinated tubulin
ZO-1	Zona occludins-1
$\gamma$ -TuRC	gamma tubulin ring complex
$\gamma$ -TuSC	gamma tubulin small ring complex
v/v	Volume/volume
w/v	Weight/volume

# **Chapter I: Introduction**

## 1.1 The Cytoskeleton

The internal architecture and shape of eukaryotic cells are regulated by the cytoskeleton. There are three components of the cytoskeleton – actin filaments, intermediate filaments and microtubules (MTs). Actin filaments are abundant proteins in eukaryotic cells where they have many roles including structural support. Actin filaments play roles in cell motility, muscle contraction and cell division. Intermediate filaments create cell cohesion and allows epithelial cells to withstand tension. They have a high tensile strength that is resistant to compression and bending forces. MTs form a network determining the dynamic nature of cells. They also play pivotal roles in other cellular functions such as cell growth, cell division, motility and the trafficking of vesicles, organelles, and proteins (Fife et al., 2014, Watanabe et al., 2005, Etienne-Manneville, 2013, Lowery et al., 2015).

### 1.1.1 Actin filaments

Actin was first noticed as a filament combined with myosin motors in mammalian muscle contraction (Straub, 1943, Szent-Györgyi, 1953). Actin is known to play roles in several biological processes including muscle contraction, cell migration, morphogenesis, and endocytosis (Pollard and Borisy, 2003). In terms of diameter it is the smallest cytoskeletal filament of around 5–9 nm. Each filament is a twisted chain of identical globular subunits (G-actin), a 43kDa protein, arranged in a head-to-tail fashion. Actin filaments have a distinct polarity, with plus- or barbed-end and a minus- or pointed-end (**Fig 1.1**). This polarity is important for their assembly and disassembly. Although both ends can grow, the plus-end grows faster than the minus end (Dominguez and Holmes, 2011). Assembly of G-actin into F-actin filaments (F-actin) occurs when actin monomers bound to ATP (Adenosine Triphosphate) are added to the plus-end referred to as polymerisation. After polymerisation, the ATP undergoes hydrolysis to ADP (Adenosine Diphosphate); the actin–ADP subunit is unstable in the filament, leading to actin filament disassembly (Dominguez and Holmes, 2011). Actin polymerisation proceeds until only a small concentration ( $\sim 0.1 \mu\text{M}$ ) of G-actin remains. This critical concentration is also the minimum concentration required to form F-actin filaments. It was found that the overall length of the filament remained

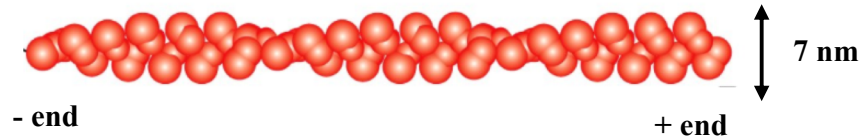
unchanged over time because there was a critical concentration of G-actin where there is a constant removal of subunits from one end of the filament while subunits are being added at the other end, in a process termed treadmilling (Wegner, 1976, Kirschner, 1980).

Actin filaments can assemble into different organisations, such as filopodia, lamellipodia, and stress fibers, which perform different functions during cell migration. Filopodia are fingerlike structures that have roles in sensing the environment during migration. They contain 15-20 parallel actin filaments cross-linked into bundles by actin-binding proteins such as fimbrin and fascin while lamellipodia are membrane protrusions that occur at the leading edge of migrating cells containing a meshwork of actin filaments that pushes on the membrane to drive the cell forward (Jacquemet et al., 2015). Moreover, actin filaments can also assemble into stress fibers. These are contractile actomyosin bundles found in several animal cells, where they play a vital role in cell adhesion and morphogenesis. Stress fibers are composed of bundles of about 10–30 actin filaments, which are crosslinked by  $\alpha$ -actinin and anchored to focal adhesions connecting the actin cytoskeleton to the ECM (Pellegrin and Mellor, 2007).

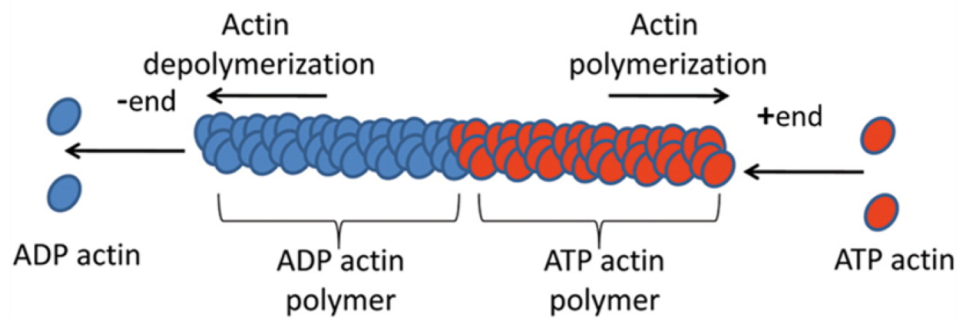
Mostly, actin filaments are assembled into two types of structures, termed ‘actin bundles’ and ‘actin networks’. In actin bundles the actin filaments are tightly packed, dense structures of cross-linked actin filaments found in, for example, microvilli. In actin networks, the actin filaments are loosely cross-linked orthogonal arrays that form a three-dimensional meshwork. These structures are regulated by a variety of actin-binding proteins such as fimbrin and fascin; where fimbrin binds actin filaments and holds two parallel filaments close together while fascin is the major actin filament bundling protein in protrusive structures such as filopodia and invadopodia (Dominguez and Holmes, 2011, Jansen et al., 2011). The activity of actin can be controlled by the Rho GTPase family - Cdc42, Rac and Rho. These proteins act as molecular switches; when bound to GTP they are considered active, and inactive when the GTP is hydrolysed to GDP. Active Cdc42, Rac and Rho have been linked to the regulation of filopodia, lamellipodia and stress fibers respectively (BurrIDGE and Wennerberg, 2004, Ridley, 2006).

## Actin filament structure

### A) Actin Filaments



### B) Actin Treadmilling



### C) Actin Branching

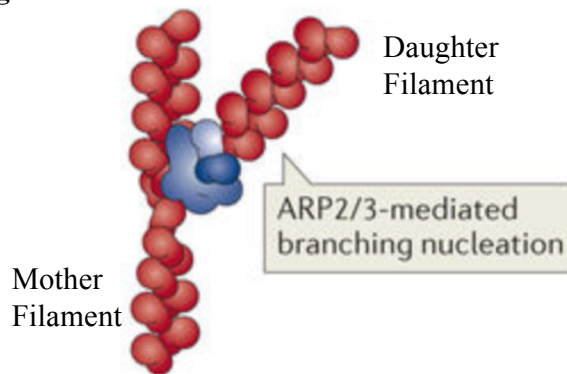


**Figure 1.1 Actin filament structure**

**A)** Actin filaments are made up of G-actin monomers and consist of two-twisted strands of a 7nm diameter with a plus and minus end. **B)** Actin treadmilling involves the simultaneous incorporation of ATP-actin at the plus-end and loss of ADP-actin at the minus-end. Actin monomers thus treadmill through the filament while the length of the filament remains the same. **C)** Actin branching - Arp2/3 binds to the sides of an existing actin filament nucleating a new actin filament. The Arp2/3 complex caps the slow-growing, minus-end (pointed-end) and promotes actin filaments elongation at the plus-end (barbed end). Adapted from Krause and Gautreau (2014).

There are two major nucleating proteins known as the Arp2/3 complex and formins that serve as nucleating sites for new actin filaments (Vinzenz et al., 2012). The Arp2/3 complex binds to the minus-end, stabilises it and promotes elongation at the plus-end. Actin nucleation plays a vital role in the regulation of the actin cytoskeleton during processes like cell motility. Arp2/3 complex can bind to the side of a preexisting filament and initiates the growth of a new-filament resulting in a branched actin network (**Fig 1.2c**) (Vinzenz et al., 2012, Pollard and Cooper, 2009). Formins are a group of multidomain proteins that are involved in the polymerisation of actin by associating with the plus-ends. Formins have essential functions in cell polarity and migration, actin assembly at the adherent junctions and formation of filopodia. They nucleate and promote actin filament elongation and bundle formation. Formins also influence MT dynamics and assist in MT actin filament alignment (Dominguez and Holmes, 2011, Breitsprecher and Goode, 2013, Palazzo et al., 2001b, Palazzo et al., 2001a).

### **1.1.2 Intermediate filaments**

Intermediate filaments provide mechanical strength and the capability to resist external stresses and possess a diameter of about 10 nm. Intermediate filaments are expandable proteins that can be stretched several times their initial length (Kreplak and Fudge, 2007). There is no documented nucleator of intermediate filaments unlike for actin and MTs, and assemble along the length of the filament. All intermediate filaments have a central alpha helical rod domain composed of four alpha helical segments. Diversity in intermediate filaments means that more than 70 genes are expressed in human tissues with more than 30 diseases being related to mutations in these genes (Hesse et al., 2001). For instance, keratins are expressed in epithelial cells and vimentins in mesenchymal cells (Hesse et al., 2001). Intermediate filaments are found in the cytoplasm and in the nucleus and are known as cytoplasmic intermediated filaments and lamins respectively.

The anti-parallel orientation of tetramers means that intermediate filaments are non-polar, unlike actin filaments and MTs. The head and tail domains play an important role in the differences between the intermediate filaments. This allows intermediate

filaments to associate with several structures, including other cytoskeletal filaments at the plasma membrane as well as connections to desmosomal junctions. Intermediate filaments undergo certain post-translational modifications – glycosylation, acetylation, ubiquitylation – with phosphorylation being the most common type and occurs mainly on the head and tail domains to regulate assembly and function. For example, phosphorylation of vimentin on Ser38 at the N-terminus regulates the cleavage furrow during cytokinesis (Goto et al., 1998). Phosphorylation of intermediate filaments regulates axonal transport, cell growth and epithelial-mesenchymal transition (Snider and Omary, 2014). Subunit exchange can occur anywhere along intermediate filaments. This was shown by fluorescence recovery after photobleaching (FRAP) that the exchange of GFP-tagged vimentin subunits within intermediate filaments occurred along the length of the bleached area (Yoon et al., 1998). These exchanges are thought to be regulated by certain phosphorylation sites (Eriksson et al., 2009). In addition, intermediate filaments determine cellular architecture by ensuring the proper targeting of adhesion proteins in polarised cells as well as regulating cell growth through protein synthesis and the cell cycle (Kim and Coulombe, 2007). However, mutations in intermediate filaments and in their associated proteins cause the loss of tissue integrity and accounts for many genetic diseases in humans such as epidermolysis bullosa simplex (Kim and Coulombe, 2007, Fuchs and Weber, 1994).

## **1.2 Microtubules**

MTs have several essential functions in biological processes, such as: cell division, cell polarity, and cell motility. MTs function in cell polarity and motility is of interest to this project (Watanabe et al., 2005, Etienne-Manneville, 2013, Ross et al., 2008). MTs provide structural support to cells and are also involved in the transportation of organelles, vesicles, and signalling molecules (Ross et al., 2008).

### **1.2.1 Microtubule structure and dynamics**

MTs are protein polymers that have polarity, which means they have two structurally distinct ends - a fast-growing plus and a slow-growing minus-end (Desai and Mitchison, 1997). The minus-end is often anchored to the centrosome at the cell

centre while the plus-end is near the cell cortex (Desai and Mitchison, 1997). MTs are comprised of  $\alpha$ - and  $\beta$ -tubulin heterodimers, that undergo catastrophe and rescue to maintain homeostasis (**Fig 1.2**) (Weisenberg, 1972, Mitchison and Kirschner, 1984, Al-Bassam and Chang, 2011). Polymerisation of MTs is an energy dependent process. GTP bound to  $\alpha$ - and  $\beta$ -tubulin dimers incorporate at the growing plus-end after which the GTP bound to the  $\beta$ -tubulin subunit is hydrolysed to GDP. It is the hydrolysis of GTP that causes the dynamic instability of MTs (Mitchison and Kirschner 1984). Generally speaking, dynamic instability is defined by four factors; 1) the speed of MT growth, 2) the speed of MT shrinkage, 3) the rate of catastrophes, and 4) the rate of rescues (van der Vaart et al., 2009). Dynamic instability at plus-ends occur due to the conformational change of the  $\alpha/\beta$ -tubulin dimer as a result of GTP hydrolysis on the  $\beta$ -subunit. To prevent the plus-ends of MTs from depolymerisation, MTs are capped by GTP-bound tubulin subunits (Akhmanova and Steinmetz, 2008). The short layer of the GTP-tubulin dimers at the plus-ends of MTs are straighter than the GDP-tubulin counterpart, which prevent MTs from depolymerisation. Therefore, the loss of the GTP-tubulin cap from the plus-end causes a kink in the MT lattice initiating depolymerisation (Kumar and Wittmann, 2012).

Development of an hMB11 antibody by Dimitrov and colleagues (2008) was used to recognise the GTP-bound conformation of tubulin. The antibody labelled for ‘specs’ of GTP-tubulin within polymerised MTs *in vivo* and *in vitro* suggesting that ‘specs’ of GTP-tubulin (termed ‘remnants’) may be buried within the MT lattice and are sites of rescue events (Dimitrov et al., 2008). Dynamic instability also takes place at the minus-end, although it occurs at a slower rate compared to the plus-ends (van der Vaart et al., 2009). The minus-end of MTs are capped by  $\gamma$ -tubulin, which itself associates with other proteins to form the  $\gamma$ -tubulin ring complex ( $\gamma$ -TuRC), the point of MT nucleation (Mogensen et al., 2000, Dammermann and Merdes, 2002). MTs undergo extensive dynamic changes (**Fig 1.3**); an example of this is treadmilling. Treadmilling occurs when there is a difference between the critical concentrations of subunits at opposite ends of MTs, whereby there is net growing at the plus ends and net shortening at the minus ends (Margolis and Wilson 1978). This process has been observed in living cells (Rodionov and Borisy 1997).

## Microtubule Structure

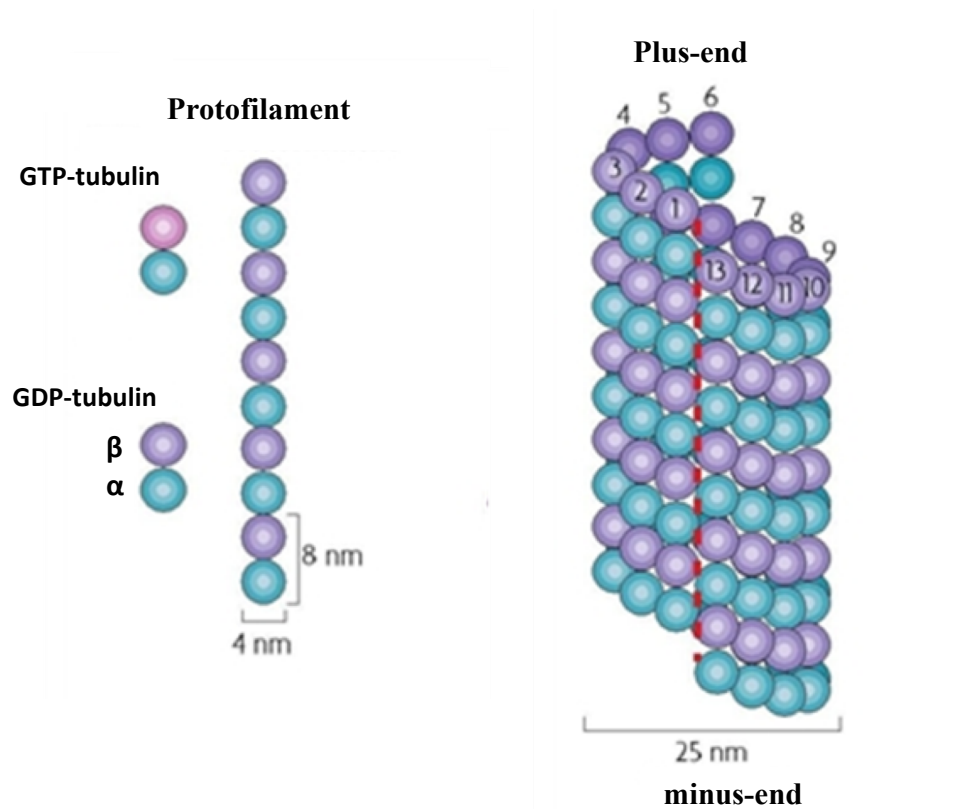


**Figure 1.2 Microtubule Structure**

MTs consist of  $\alpha$ - and  $\beta$ -tubulin heterodimers, which form protofilaments. 13-protofilaments assemble laterally in a non-symmetrical helix to form a hollow tube 25 nm in width, which rises by three monomers every turn. Note the seam in the MT wall, and the polarity of the filament. Adapted from Akhmanova and Steinmetz (2008).

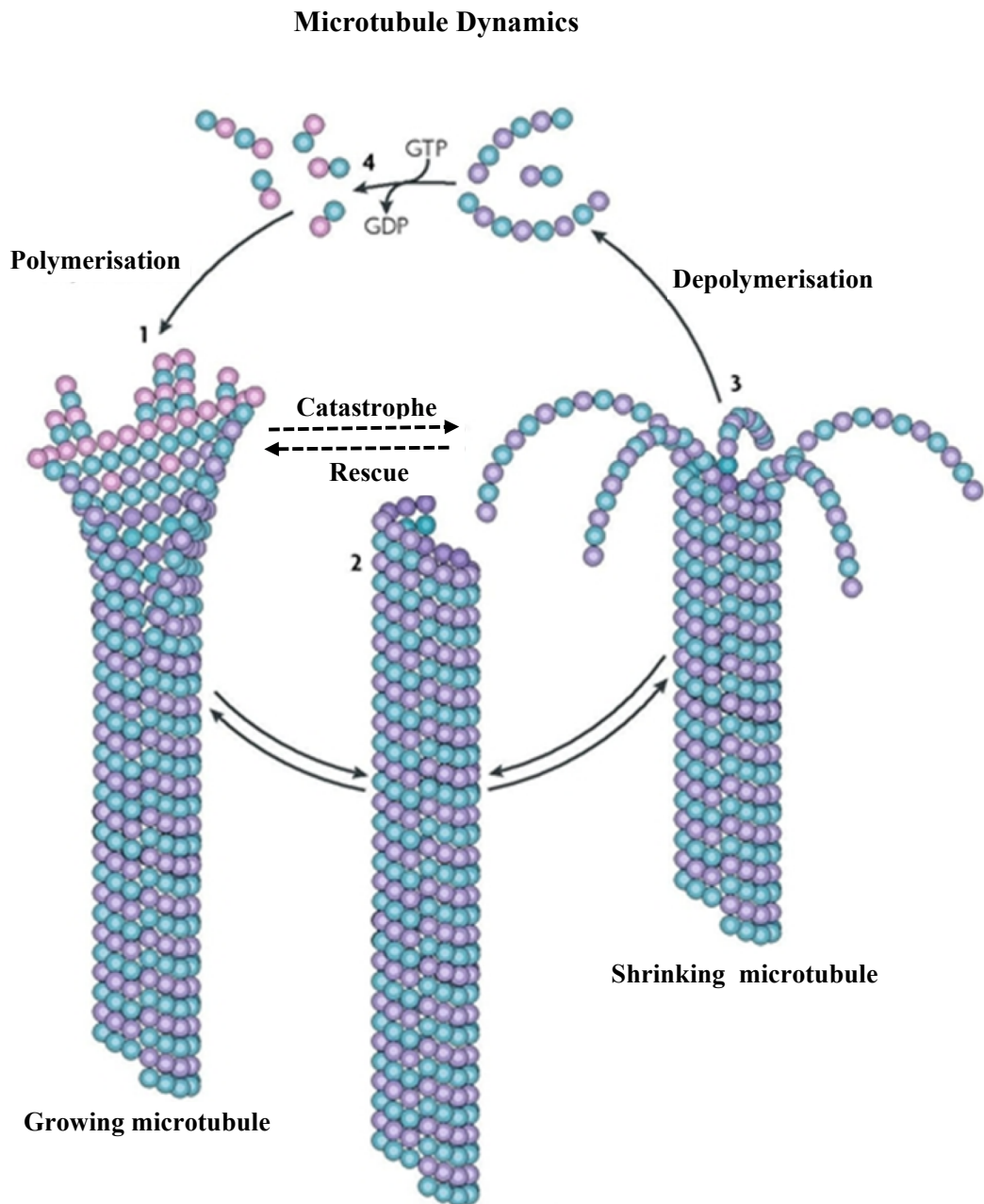


**Figure 1.3 Microtubule assembly and disassembly**

MTs can switch rapidly between phases of growth and shrinkage. Growing MTs possess a GTP-tubulin cap and the protofilaments are straight and the lattice stable, allowing incorporation of GTP-tubulin heterodimers at the plus end. Hydrolysis of GTP in  $\beta$ -tubulin causes protofilaments to curve and peel away, and the MT to shrink. Adapted from Akhmanova and Steinmetz (2008).

## 1.2.2 Microtubule nucleation

MT nucleation is the initiation of assembly of new MTs.  $\alpha/\beta$ -Tubulin heterodimers interact to form a MT seed allowing MT growth. MT organising centre (MTOC) is usually the site where MTs are nucleated from with the help of  $\gamma$ -tubulin. MTOCs can act as either nucleating and anchoring sites or anchoring sites only. The centrosome (from Latin ‘central body’) is a structure that acts as the main MTOC in most animal cells. In the centrosome, the nucleating complex consists of the small  $\gamma$ -tubulin complex ( $\gamma$ TuSC), first identified in *Aspergillus*, which combines with other  $\gamma$ -tubulin complex proteins (GCPs) to form the  $\gamma$ -tubulin ring complex ( $\gamma$ -TuRC) (Oakley and Oakley, 1989, Oakley et al., 2015). These GCPs (GCP1-6) are numbered by increasing molecular weight with  $\gamma$ -tubulin being GCP1. In budding yeast, the  $\gamma$ -tubulin complex contains only two GCP family members, the orthologues of human GCP2 and GCP3, whereas in most organisms  $\gamma$ -tubulin complexes contain additional GCP subunits. A relatively new component of the  $\gamma$ -TuRC, Dgp71WD, was discovered in *Drosophila melanogaster*. Although Dgp71WD is not related to the GCP family, its orthologue in humans, NEDD1 (GCP-WD), was shown to be a targeting factor for the  $\gamma$ -TuRC (Luders et al., 2006).

The  $\gamma$ -TuRC also acts as a cap of the minus-end of MTs while the plus-end show dynamic instability. This cap provides stability to the minus-end of MTs from enzymes that could cause its depolymerisation, in addition to inhibiting growth from the minus-end. It has now been confirmed that thirteen  $\gamma$ -tubulins are present in the  $\gamma$ -TuRC instead of the debated twelve or fourteen, since the first and seventh  $\gamma$ -TuSC overlap. This is thought to be controlled by lateral interactions between GCPs 4, 5 and 6 where they are incorporated directly into the ring rather than acting as a scaffold (Kollman et al., 2011). Post-translational modification regulates the function of GCPs. Phosphorylation of  $\gamma$ -tubulin is known to take place in *Drosophila* and budding yeast for correct MT organisation. Phosphorylation of GCP-WD controls targeting of the  $\gamma$ -TuRC to spindle MTs (Luders et al., 2006). In human cells,  $\gamma$ -TuRC integrity is regulated by mitotic spindle organising protein (MZT1), which binds to GCPs through a hydrophobic motif. MZT1 binds to fully assembled  $\gamma$ -TuRC enabling its interaction with NEDD1 as well as the CM1 domain of Cep215 thereby stimulating nucleation

activity. Depletion of MZT1 led to significant cellular defects whereby  $\gamma$ -TuRC's structure was intact suggesting that MZT1 regulates the function of  $\gamma$ -TuRC but not its assembly (Cota et al., 2017).

### 1.2.2.1 The Centrosome

Nucleation and anchorage of MTs at the minus-end are responsibilities of the centrosome (Mogensen, 2004). The centrosome comprises of a mother and daughter centriole oriented at right angles to each other and are connected by the pericentriolar matrix (PCM) (Kaverina et al., 2002) (**Fig 1.4**). Nine triplet MTs assembled in a cartwheel structure make up each centriole (Azimzadeh and Marshall, 2010). Mature centrioles (i.e. mother centrioles) can be morphologically recognised by the presence of appendages and satellites at their distal ends, which enables them to nucleate and anchor more MTs than centrioles lacking these structures (i.e. daughter centrioles) (Nigg and Stearns, 2011). Mother centrioles contain proteins such as p210 (a distal appendage protein) and cenexin (Lechtreck et al., 1999, Hung et al., 2016) while PCM-1 is usually observed in satellites (Dammermann and Merdes, 2002). During division, centrosomes move to opposite sides of the spindle pole and each become the new centrosome for each daughter cell (Nigg, 2006).

### 1.2.2.2 Centrosome duplication

Centrosomes play a key role in mitosis and are duplicated only once per cell cycle. Duplication of the centrosome occurs during the S-phase of the cell cycle. Because of this process, one centriole is more mature than the other is. Once a cell is undergoing mitosis, each centrosome moves to opposite sides of the spindle pole ready for acceptance by each daughter cell. The centrosome cycle is critical to ensure that each daughter cell receives a centrosome after cell division. The different stages of the centrosome cycle are described below (**Fig 1.5**).

Centriole disengagement defines the separation between the mother and daughter centrioles at the end of mitosis. Disengagement is a critical step that prepares the centrosome for duplication. Centrosome disengagement is complemented by the

transposition of the cohesin ring from the centrosome and is regulated by various proteins such as Polo-like kinase 1 (Plk1), CDK1, PCM and separase (Fry, 2015, Tsou et al., 2009). Astrin, a mitotic-spindle associated protein, is an inhibitor of separase (Gruber et al., 2002). A fundamental regulation of centriole disengagement is carried out by pericentrin since it prevents premature disengagement by functioning as a support of the PCM (Lee and Rhee, 2012). Furthermore, inactivity of Plk1 consequently prevents the phosphorylation of sSgo1 (a splice variant of SGO1) further augmenting the cleavage of the cohesin ring (Wang et al., 2008). It is worth mentioning a study by Oliveira and Nasmyth (Oliveira and Nasmyth, 2013), which claimed that a reduction in CDK1 activity or interaction of the PCM with cytoskeletal forces is sufficient for centriole disengagement but not the cleavage of the cohesin ring. Following disengagement, a linker is established consisting mainly of C-Nap1, Cep68, rootletin and LRRC45.

Centriole duplication begins at the G1/S transition. Here, a new daughter centriole, called a procentriole, begins to grow from the proximal end of the mother centrioles. In humans, the initial step is the recruitment of Polo-like kinase 4 (Plk4) facilitated by two proteins – Cep152 and Cep192, which are distributed in rings around the circumference of the centriole (Hatch et al., 2010, Sonnen et al., 2013). This recruitment depends on electrostatic interactions between the polo-box domain of Plk4, which is positively charged and the negatively charged regions of Cep192 and Cep152 (Sonnen et al., 2013). Plk4 in conjunction with SAS-5 and SAS-6 promotes the assembly of the symmetrical cartwheel that keeps the procentriole attached to the mother centriole (Kitagawa et al., 2011, Firat-Karalar and Stearns, 2014). How these proteins specifically interact is still under investigation. However, so far, we know from the crystal structure of Sas-6 it self-oligomerises to become the backbone of the cartwheel structure (van Breugel et al., 2011). Plk4 is also known to phosphorylate one of its substrates STIL allowing STIL to interact with SAS-6 thus enhancing SAS-6 recruitment (Kratz et al., 2015). Plk4 is a major protein that regulates centriole duplication and its overexpression leads to the generation of extra centrosomes as shown in a non-transformed mammary cell line (Godinho et al., 2014). Centrin is required for centriole duplication. The protein is a family of calcium-binding

phosphoproteins. Centrin move distally as the procentriole elongates. Depletion of centrin-2 led to centriole duplication defects in HeLa cells (Salisbury et al., 2002).

The  $\gamma$ -tubulin ring complex ( $\gamma$ -TURC) enables the nucleation of nine A-tubules at the cartwheel. A-tubules remain capped by the ring complex until the end of the process and grow from the proximal to distal end of the centriole. The length of the cartwheel structure regulates length of the centriolar MTs (Guichard et al., 2012). The other two tubules (B- and C-tubules) are nucleated until of equal length as the A-tubule. B- and C-tubules do not require  $\gamma$ -TURC for nucleation. Next, the elongation of A- and B-tubules generate the distal end of the centriole (Firat-Karalar and Stearns, 2014). Finally, when a centriole is of the desired length it is capped by CP110 and CPAP (Schmidt et al., 2009).

The G2 phase of the cell cycle is the beginning of centrosome maturation. An increase in  $\gamma$ -TURC and other PCM components eventually resulting in MT nucleation is one of the brief definitions of centrosome maturation (Palazzo et al., 2000). The two new centriole pairs obtain new PCM from the cytosol. Specifically, Aurora-A kinase is known to participate in centrosome maturation by phosphorylating the centrosomal protein TACC on three serine residues - Ser36, 620 and 626 (Brittle and Ohkura, 2005, Hannak et al., 2001). Activated Src at the golgi stimulates the activation and recruitment of Aurora-A to the centrosome (Barretta et al., 2016). In *Drosophila melanogaster*, PLK1 phosphorylates a protein called centrosomin (cnn), the human homologue of CEP215/CDK5RAP2, which then allows it to act as a framework around centrioles (Conduit et al., 2014). Further studies have revealed the role of another protein pericentrin-like protein (PLP) during centrosome maturation. Localisation of PLP to the tip of a cnn flare zone allows it to assist in efficient MT radial organisation (Lerit et al., 2015). During centrosome separation, the newly formed centrosomes separate to form two mature centrosomes. This takes place at the G2/M transition and is a prerequisite for bipolar mitotic spindle formation. A protein linker attaching both centrosomes together is severed. An example of such a protein is Nek2A, which phosphorylates CEP68 (Man et al., 2015). The activation of MT dependent motor proteins triggers the centrosomes to separate from each other and become mature centrosomes. Not only are motor proteins involved but also actin filaments and MTs.

## Centrosome Structure

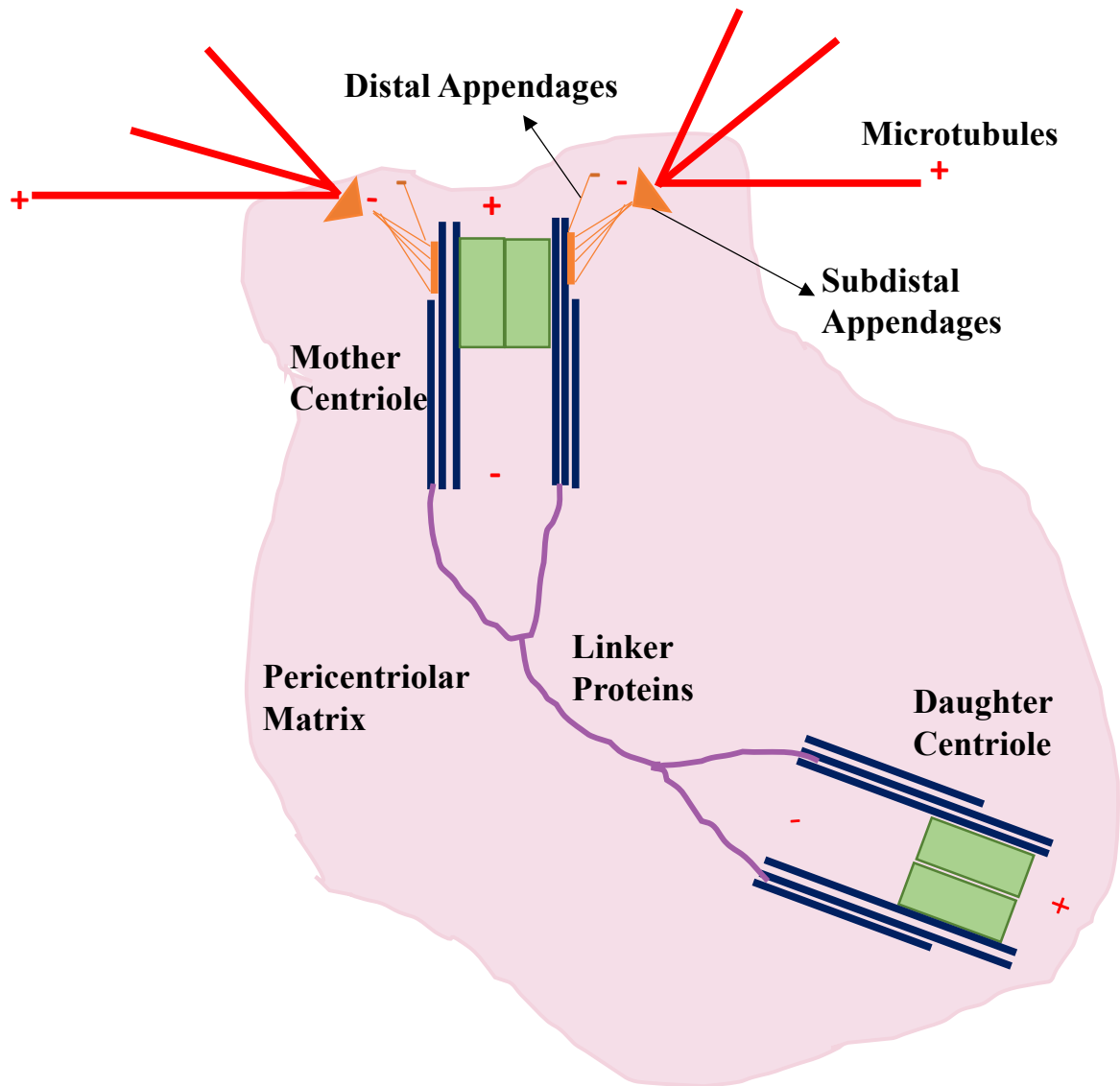


**Figure 1.4 Centrosome Structure.**

Schematic representation of the centrosome structure. The centrosome possesses two centrioles – mother and daughter – joined by linker proteins. The mother centriole possesses the appendages from which MTs are anchored while the pericentriolar matrix surrounds both centrioles.

## Centrosome Duplication Cycle

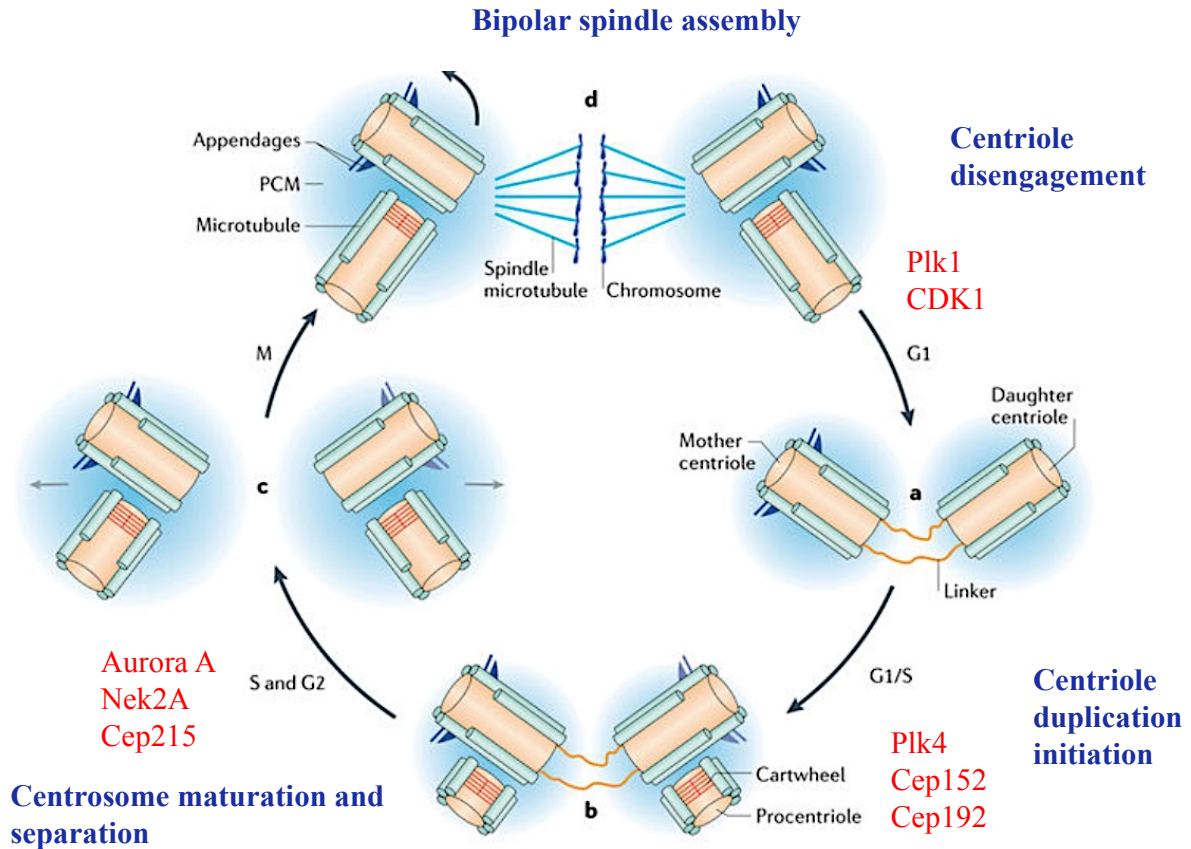


**Figure 1.5 Centrosome Duplication.**

Schematic representation of the centrosome duplication cycle. **A)** The two centrioles present in G1 phase are distinct from one another with distal and sub-distal appendages present on the mother centriole. The two centrioles are connected at their minus-ends by a proteinaceous linker. Centriole disengagement is regulated by Plk1 and CDK1. **B)** At the G1/S transition, centriole duplication is initiated. Cep152 and Cep192 recruit Plk4, which then allows the assembly of symmetrical cartwheel structures, which seeds the formation of a procentriole at the proximal ends of each mother centriole followed by procentriole elongation. **C)** Towards the end of G2 phase, both centrosomes mature and the proteinaceous linker is severed by Nek2A, thus, creating two separate centrosomes (grey arrows indicate the direction of movement). **D)** Finally, the fully separated centrosomes assemble a bipolar spindle allowing each daughter cell to inherit a pair of centrosomes. Adapted from Gonczy Pierre (2015).

There are two stages of centrosome separation – centrosome splitting and centrosome elongation (Uzbekov et al., 2002). Depolymerisation of both actin filaments and MTs separately caused inhibition of centrosome splitting therefore defects in mitotic spindle formation. However, cells can counteract this hindrance by prolonging the length of prometaphase and prophase in order for a minimum distance between the centrosomes to be achieved (Uzbekov et al., 2002). Most cells can rectify this mistake and move to the next phase of the cell cycle whilst others cannot, hence, formation or progression of tumour cells. The fact that cells can prolong the length of prometaphase and prophase during the depolymerisation of actin filaments and MTs could be classified as a checkpoint control during the cell cycle.

Growth arrest-specific 2-like protein 1 (GAS2L1), a centriole-localising protein, binds the centrosome to both actin and MTs (Stroud et al., 2011) upon linker severing therefore augmenting centrosome separation (Au et al., 2017). GAS2L1 contains a SxIP motif so can bind to EB proteins (Jiang et al., 2012). Forces applied by the GAS2L1-attached cytoskeletons also aid in centrosome separation. The main force required for centrosome separation comes from a protein Eg5 that belongs to the kinesin family (Mardin and Schiebel, 2012). Nek6 is responsible for the phosphorylation of Eg5 (Bertran et al., 2011). After separation, each centrosome moves to opposite sides of the pole.

Once each centrosome is at opposite sides of the pole, bipolar spindle formation commences. Here MTs are the main cytoskeletal structure required for this process where the regulation is catalysed by mitotic kinases. The activation of the phosphatase CDC25B is orchestrated by the kinase Aurora A (Dutertre et al., 2004). Aurora A also activates LATS2 and this protein is important for the centrosomal recruitment of  $\gamma$ -tubulin to promote MT nucleation (Abe et al., 2006). Since MTs are highly dynamic structures, they need to be stabilised briefly during spindle formation. An important protein required for this is the centrosomal adaptor TACC3/maskin, which interacts with the MT-stabilising factor ch-TOG. The complex subsequently formed enhances the affinity of ch-TOG for MTs and in turn functions to increase the stability of the kinetochore fibers hereby counteracting the activity of the MT-depolymerising kinesin KIF2C (Kinoshita et al., 2005). NuMA, is a coiled-coil nuclear protein that can interact with dynein, LGN as well as MTs and relocates to the spindle poles early in mitosis

(Kotak et al., 2012). Astral MTs interact with the cell cortex to direct spindle orientation, which is governed by dynein in complex with dynactin (Wittmann et al., 2001) and the NuMA/LGN/G $\alpha$ i complex (NuMA complex) (Kotak and Gonczy, 2013). By metaphase, the chromosomes are fully aligned at the equator with each chromosome at the spindle pole ready for the separation of sister chromatids.

### **1.2.2.3 Role of the centrosome in cancer**

A link between the centrosome and cancer has been published (Zyss and Gergely, 2009, Godinho et al., 2009). Centrosome abnormalities are thought to enhance tumour formation by stimulating chromosomal instability (Fukasawa, 2005) i.e. a process whereby cancer cells lose or gain parts or whole chromosomes during division. Khodjakov and co-workers (Khodjakov et al., 2000) were the first group to highlight a centrosome-independent pathway to regulate spindle assembly. The experiment carried out in CVG-2 cells showed that the cells were still able to form a bipolar spindle when the centrosomes had been removed by laser. These acentrosomal cells formed efficient spindles that could undergo mitosis and were also able to assemble bipolar spindles even in the presence of just one centrosome maybe suggesting their key function lies in their ability to form basal bodies which produce flagella or cilia rather than bipolar spindles.

Any of the proteins involved in the centrosome cycle could potentially be aberrant and contribute to tumour formation. Centrosome amplification is a hallmark of cancer. Monopolar spindles arise when centrosome separation fails during mitosis while multipolar spindle formation is caused by the presence of extra centrosomes. As mentioned in the previous section, Plk4 is a major regulator of centrosome number; its overexpression and the subsequent centrosome amplification causes an induction of invasive structures in 3D-cultured models. This is due to the increased centrosomal MT nucleation causing Rac1 activation and initiating epithelial remodeling and migration (Godinho et al., 2014). Though cells with extra spindle poles do not possess a checkpoint to terminate mitosis, they have different mechanisms such as centrosome clustering to suppress multipolar cell division (Godinho et al., 2009).

The best studied mechanism is the clustering of supernumerary centrosomes into two groups for mitosis to carry on with bipolar spindles (Brinkley, 2001, Nigg, 2002). The process relies greatly on motor proteins such as dynein as well as NuMA, a MT associated protein to efficiently cluster these centrosomes, which occurs during the spindle assembly checkpoint before anaphase (Quintyne et al., 2005). A genome-wide search by (Kwon et al., 2008) enabled the discovery that actin force regulators such as Formin3/INF2 in conjunction with spindle-intrinsic forces like Ncd, a kinesin-like protein, synergistically inhibit multipolar cell division by controlling the speed and extent of movement of the centrosome away from the cortex and towards the spindle. Another mechanism is by simply inactivating the extra centrosomes through silencing the MTOCs activity of the extra centrosomes. This phenomenon has been shown in polyspermic newt eggs where sperm nuclei is incorporated into the egg but ultimately only one sperm nucleus contributes to the bipolar mitosis of the zygote (Iwao et al., 2002). MTOC activity of the centrosomes is regulated by the accumulation of PCM and their phosphorylation, dependent upon cdk1/cyclin B (Ohta et al., 1993). Thus, centrosome selectivity and maintenance may be conferred due to a gradient of cyclin B1 and  $\gamma$ -tubulin in a large oocyte. Centrosome inactivation also seems to occur in flies overexpressing Plk4; brain neuroblasts overexpressing Plk4 develop into tumours and metastasise upon transplantation into their abdomen. Furthermore, centrosomes that are dispersed along spindles contain significantly less  $\gamma$ -tubulin than those at the spindle poles (Basto et al., 2008). Thus, to some degree, a decrease in PCM levels may account for the inactivation of extra centrosomes. These experiments, in flies, show that extra centrosomes can lead to tumour formation.

Conclusions drawn from other organisms where supernumerary centrosomes led to tumour formation cannot be confidently stated in mammals. In tissue culture cells, the presence of extra centrosomes acquired through overexpression of Plk4 activates p53 and causes G1 arrest probably through the activation of the Hippo pathway component large tumour suppressor homologue 2 (LATS2) preventing the initiation of tumours in these cells (Holland et al., 2012). Similarly, in p53-mutant mice overexpressing Plk4, microcephaly was observed caused by the presence of severe aneuploidy and apoptosis. This study also observed that the presence of extra centrosomes due to Plk4 overexpression led to the assembly of multipolar spindles perhaps resulting from an inefficient clustering process but most importantly, does not

promote tumourigenesis (Marthiens et al., 2013). Though centrosome amplification accelerated the initiation of tumours caused by p53 deficiency (Sercin et al., 2016).

However, a new study has established that when centrosomes are amplified through Plk4 overexpression, the consequences are chromosome missegregation and aneuploidy, and these extra centrosomes are able to direct spontaneous intestinal tumour development (Levine et al., 2017). Specifically, they found that centrosome amplification is tolerated by many tissues *in vivo* but not the skin where the mice exhibited thickened epidermis and disordered follicle morphology. Unfortunately, there were no speculations why the skin was particularly different. A doxycycline-inducible system was used to generate Plk4 overexpression and then to study its effect on centrosome number in association with a truncated APC tumour suppressor. Tumour numbers were significantly increased in the intestines of mice carrying the truncated APC allele and Plk4 overexpression without affecting the size of the tumour. The study also discovered that mice expressing Plk4 surrendered to the development of spontaneous tumours such as sarcomas, squamous cell carcinomas and lymphomas at around 9 months compared to control mice. This was partly due to the inactivation of the p53 pathway and target genes unlike the study by Holland et al., (2012); p53 was unable to fully hinder the development of tumourigenesis and proposed that centrosome amplification promoted tumour initiation by advancing the loss of chromosome 18 copy where the wild-type APC allele is located.

Mitotic spindle polarity is critical for correct chromosome segregation during mitosis. However, multiple spindles are sometimes observed in certain cancers, which are due to supernumerary centrosomes and chromosome instability that arise from centrosome overduplication or cytokinesis failure (Lingle et al., 1998, Chan, 2011). As aforementioned, one way to suppress multipolar cell division is to cluster supernumerary centrosomes into two groups for mitosis to carry on with bipolar spindles (Brinkley, 2001, Quintyne et al., 2005). There are times where multipolar spindles are not caused by centrosome amplification but rather through centriole disengagement or PCM fragmentation (Maiato and Logarinho, 2014). Cells with centrosome amplification have more than two spindle poles, each with at least two centrioles. Centriole disengagement is usually vital for the preparation of centriole duplication. It is complemented by the transposition of the cohesin ring from the

centrosome and is regulated by various proteins such as Plk1, CDK1, PCM and separase (Fry, 2015, Tsou et al., 2009). Centriole disengagement occurs when there are defects in centriole cohesion that leads to centriole separation before the end of chromatid segregation causing multipolar spindle formation (Stevens et al., 2011).

Apart from centriole disengagement, loss of spindle pole integrity might be due to PCM fragmentation. PCM fragmentation is caused by loss of centrosome integrity, which generates acentriolar fragments that can nucleate spindle MTs associating with chromosomes. Several centrosomal proteins such as ninein, centrin-2 and PCM-1 are known to accumulate at pericentriolar satellites and are then transported along MTs by dynein. Ninein, chTOG or Aurora A depletion caused PCM fragmentation and led to the formation of multipolar spindle irrespective of p53 present or not (Dammermann and Merdes, 2002, Kimura et al., 2013, De Luca et al., 2008). Therefore, these proteins are required to maintain spindle pole integrity. In conclusion, it is to be expected that a better understanding of the mechanisms governing centrosome number, structure, regulation and function will lead to a better understanding of the relationship between centrosomes and cancer and thus to therapeutic breakthroughs.

### **1.2.3 Microtubule anchorage and minus-end associated proteins**

MT anchorage is important in regulating normal cellular processes and centrosomes are partly responsible for this. Tubulin dimers are added to the plus-end while the minus end of each MT is inserted in the centrosome. A centrosome-focused radial array enables cytoplasm organisation of organelles and provides tracks for vesicular traffic (Cole and Lippincott-Schwartz, 1995a).

MTs are reorganised during epithelial cell differentiation into apico-basal arrays that are no longer anchored at the centrosome. This happens in cells such as the kidney, skin, cochlea and gastrointestinal tract (Mogensen et al., 1997, Goldspink et al., 2013, Goldspink et al., 2017b). Here, the minus-end of MTs become anchored at apical non-centrosomal MTOC (n-MTOC) associated with adherens junction (Bellett et al., 2009,

Goldspink et al., 2017b). Furthermore, ninein and calmodulin-regulated spectrin-associated protein 1-3 (CAMSAPs 1-3) are minus-end proteins that play fundamental roles in stabilising the apico-basal non-centrosomal MT array. It has been suggested that, in the inner ear CAMSAP3, may help to establish and protect the non-centrosomal site (Zheng et al., 2013). MTs released from  $\gamma$ -TuRC become free and uncapped thereby needs to be stabilised. This occurs through CAMSAPs, which regulate MT minus-end growth by decorating the polymerised MT lattice. The process leads to the formation of CAMSAP-decorated MT stretches that are now stabilised and serve as sites of non-centrosomal MT outgrowth (Jiang et al., 2014, Wu and Akhmanova, 2017).

During differentiation, ninein moves in a MT-dependent fashion to the n-MTOCs though it is not essential for apico-basal anchorage at n-MTOC. However, it is needed for the initial MT reorganisation into apico-basal arrays. Most likely the CAMSAPs compensate for lack of ninein at the n-MTOCs (Goldspink et al., 2017b, Moss et al., 2007). The formation of n-MTOCs and the recruitment of ninein to these sites is facilitated by the plus-tip protein, CLIP-170. Two models are proposed to explain the mechanism: firstly, CLIP-170 bound to MT-plus ends are targeted for cortical capture by the scaffold protein, IQGAP1, when Rac1 is activated allowing ninein to be transported along MTs to n-MTOCs. The second model proposes that CLIP-170 along with IQGAP1 and Rac1 act as a complex at adherens junctions for the recruitment of ninein to n-MTOCs (Goldspink et al., 2017b). The plus-end of a growing MT can associate with certain proteins known as the MT plus-end tracking proteins (+TIPs). These proteins regulate the behaviour of MTs and connect them to cellular structures such as the cortex. There are different types of +TIPs such as the cytoplasmic linker protein-170 (CLIP-170), end-binding proteins (EBs), cytoplasmic linker associated proteins (CLASPs), adenomatous polyposis coli (APC), ACF-7, dynactin and dynein (Akhmanova and Hoogenraad, 2005).

### **1.2.4 Microtubule plus-end tracking proteins (+TIPs)**

MT plus-end tracking proteins (+TIPs) are a group of MT-associated proteins that track the plus-end of growing MTs. They are highly conserved between several organisms and are vital because they regulate the dynamic behaviour of MTs, which

affects cellular functions such as cell division and motility. Also, +TIPs are known to form dynamic interactions that use specific sequence motifs including CH, EBH, CAP-Gly and SxIP motifs. These motifs are required for +TIPs to mediate interactions with each other and with MTs (Akhmanova and Steinmetz, 2010).

Three mechanisms by which +TIPs associate with MT plus-ends have been described. These include treadmilling, hitchhiking and motor transport. Treadmilling is the most studied mechanism and was described using live imaging of GFP-CLIP-170 and EB1. The +TIPs accumulate at the growing end of MT where the proteins remain transiently fixed with respect to the lattice (Perez et al., 1999). The addition and loss of +TIP molecules from the MT ends is not fully understood; however, some +TIPs, such as CLIP-170 and p150<sup>Glued</sup>, may co-assemble with tubulin heterodimers, and when phosphorylated increase the release from the MT. Other treadmilling +TIPs such as the EBs may use different mechanisms; by recognising the structural features or having a higher affinity for the GTP-cap of tubulin. EB1 binds to a stabilised MT in the presence of the GTP-cap. Hitchhiking involves transient binding to the MT via other +TIPs (Akhmanova and Steinmetz, 2015). For example, SxIP-motif containing proteins can bind MT plus-ends via the EB homology domain of EB proteins (Galjart, 2010). The last mechanism is by motor-mediated transport. A known example, is the kinesin family motor proteins transporting APC to the plus end of MTs (Akhmanova and Steinmetz, 2015). In summary, +TIPs can either bind to plus ends autonomously or by associating with other proteins before binding.

#### 1.2.4.1 CLIP-170

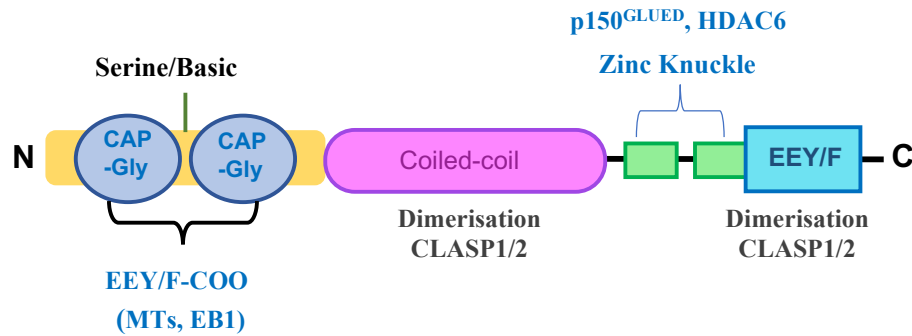
CLIP-170 has a molecular weight of 170kDa and regulates MT dynamics. Although CLIP-170 is able to bind MTs through their CAP-Gly domain (**Fig 1.6A**) they mainly bind in association with EB1 and not independently (Bieling et al., 2008). There are two CLIP proteins in mammals (CLIP-115 and 170), although lower eukaryotes only have one CLIP (Dzhindzhev et al., 2005). CLIP-115 has the CAP-Gly domain and the coiled coil domain but lacks the metal binding domain (Akhmanova et al., 2005). Further studies have shown that CLIP-170 associates with the growing ends of MTs in living cells. Thus, it has been suggested that CLIP-170 and CLIP-115 may act as rescue factors, as they were observed in the rescue but not the catastrophic phase of

MTs (Komarova et al., 2002). A recent study also reported that where MTs collide and undergo mechanical damage in the lattice, CLIP-170 recognises GTP-like remnants in these lattices, stimulating rescue. Though, how CLIP-170 specifically recognises these defects are still unclear (de Forges et al., 2016). In addition, the role of CLIP-170 in regulating angiogenesis in breast cancer cells has been established (Sun et al., 2013). CLIP-170 is highly expressed in breast cancer cells and correlates positively with breast tumour growth while the opposite is true when CLIP-170 is depleted. CLIP-170 stimulates angiogenesis by promoting the stabilisation of MTs of vascular endothelial cells, which in turn, facilitates the polarisation and migration of these cells. However, CLIP-170 had no effect on cell proliferation (Sun et al., 2013).

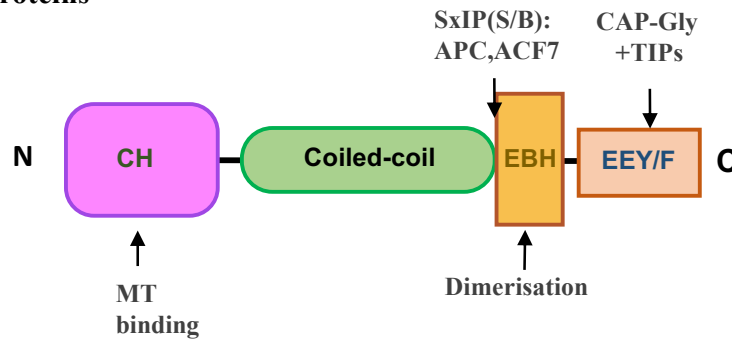
#### **1.2.4.2 End-binding proteins**

End-binding proteins (EBs) are highly conserved proteins with molecular weights around 32-39 kDa. They are the main group of +TIPs that interact with MTs but are also capable of recruiting other +TIPs to growing ends of MTs (Komarova et al., 2009). There are three types of mammalian EB proteins – EB1, EB2 (RP1) and EB3 (EBF3), which are encoded by separate MAPRE genes (Su and Qi, 2001, Lansbergen and Akhmanova, 2006). EB1 was localised to the human chromosome 20q11.2 by fluorescence in situ hybridisation, EB2 was localised to ch. 18q12 and EB3 to ch. 2p23.2 (Su et al., 1995); (Su and Qi, 2001).

**A) CLIP-170**



**B) EB Proteins**



**C) CLASP1/2**

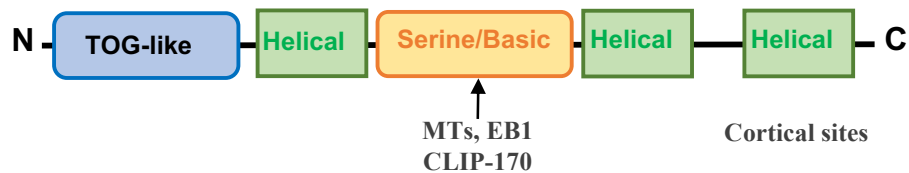


**Figure 1.6 Domain structures of +TIP proteins.**

**A)** CLIP-170 recognises the C-terminal tail of EB1 and MTs through N-terminal CAP-Gly domains. CLIP-170 can also bind further +TIPS through additional sites, and can self-inhibit via its own C-terminal tail region. **B)** In EBs, the CH domain at the N-terminus is responsible for MT binding; the coiled coil and EBH domain at the C-terminus is the region where dimerisation takes place. **C)** CLASP1/2 recognise EB1, MTs and CLIP-170 through serine/basic. Adapted from Akhmanova and Steinmetz (2008).

There is only one isoform of EB1 but two isoforms of EB2 and EB3 can exist due to alternative splicing (Bu and Su 2003). The two forms of EB2 exist because they are translated from different initiation codons while EB3 is translated from two alternatively spliced mRNAs. Though, the domain structure and functions of EB2 and EB3 isoforms are still largely unknown. EBs have a calponin homology (CH) domain at the N-terminus, which mediates interaction with MTs; and an acidic C-terminus domain that can interact with other +TIPs (**Fig 1.6B**) (Su et al., 1995; Bu and Su 2003). It has been established that EB1 and EB3 recognise the MT ends due to their high affinity for the structural conformation exhibited by GTP tubulin, or by the GTP hydrolysis at the plus end. This was shown by using MTs with incorporation of GTP $\gamma$ S (a slowly hydrolysable analogue of GTP) (Maurer et al., 2011, Maurer et al., 2012b). It was also discovered that remnants of GTP-tubulin along the MT lattice may act as rescue points for depolymerising MTs (Cassimeris, 2009). Although all EBs bind to the plus ends, they can also bind along the entire MT lattice as a result of their transient overexpression *in vivo* and *in vitro* (Goldspink et al., 2013).

Homo- and heterodimerisation of EBs occur through their C-terminal domain before they interact with MTs. All three EBs can form homodimers while EB1 and EB3 can form heterodimers (Komarova et al., 2009). More specifically, dimerisation occurs through the coiled coil domain and EBH domain at the C-terminus. This interaction produces a hydrophobic cavity at the interface of the two EB monomers and allows binding to other +TIPs (Honnappa et al., 2006). It is a prerequisite for EBs to form stable dimers in the cytoplasm before binding to the MT lattice on their own or as +TIP-EB complexes (Sen et al., 2013) Destabilisation of the EBH domain of the hydrophobic core inhibits dimer formation and therefore, EBs are not recruited to the MT plus-end (Sen et al., 2013). EBs localise to growing MTs by detecting the concentration of GTP-tubulin as well as the change in conformation of tubulin at the plus-ends (Zanic et al., 2009). They recognise a structural cap on the surface of MTs that is associated with dynamic instability and prevent MT depolymerisation (Maurer et al., 2012a, Kumar and Wittmann, 2012). The structural cap may consist of one  $\alpha/\beta$ -subunit per protofilament so, there may be 13 caps in one MT (Howard and Hyman, 2007).

CLASPs (**Fig 1.6C**) have been proposed to be vital for correct EB localisation at plus-ends of MTs. The localisation involves the interaction between CLASP1 and CLASP2, and EB protein via the hydrophobic SxIP sequence motif and electrostatic interactions (Kumar and Wittmann, 2012). The EB-SxIP motif complex can be regulated by post-translational modifications such as phosphorylation (Honnappa et al., 2009). In vitro experiments have shown that when CLASPs are present in cells, they remove EB1 from MT lattice restricting them to the plus-end. However, during depletion of CLASPs, EBs localise to the tips of MTs as well as binding to the MT lattice. It is thought that the increased lattice binding is due to the increased ratio of EB-to-MT, since the endogenous levels of EB proteins did not increase (Grimaldi et al., 2014). Another explanation for EBs binding along the lattice in addition to plus tips is due to EBs being able to recognise the GTP-tubulin remnants in MTs (Maurer et al., 2012a, Zanic et al., 2009). Generally, CLASPs prevent EB binding along the lattice by augmenting GTP hydrolysis. In CLASP-depleted cells, there is an increase in GTP-tubulin, which allows EBs to bind along the lattice. Other proteins that interact with EBs such as CLIP-170 and p150<sup>Glued</sup> also localise along the MT lattice. These CAP-Gly domain-containing proteins trail EBs to the lattice rather than being individually regulated by CLASP depletion (Grimaldi et al., 2014). CLASPs bind along MT lattice and stabilise MTs; this is important in for example, the leading edge for pioneer MTs in order for protrusion of the cell to take place during cell migration (Wittmann and Waterman-Storer, 2005). CLASPs bind to plus-end through EB1 but bind MT lattice through their TOG domain.

Although all three EBs have high sequence conservation, they have been shown to have different functions (Komarova et al., 2009). Affinity also varies in EBs, EB2 is thought to be less potent than EB1 and EB3 for binding to numerous partners such as APC hence, it is less likely that EB2 will be involved in targeting these binding partners to the growing end of MTs (Komarova et al., 2009, De Groot et al., 2010). EB1 and EB3, but not EB2, play a role in the MT plus-end regulation, by facilitating MT connections with actin, organelles, kinetochores and the cortex (Vaughan, 2005, Lansbergen and Akhmanova, 2006, Goldspink et al., 2013). Komarova and colleagues (2009) discovered that EBs compete with each other. By measuring the intensity, they found EB1 and EB3 formed comet-like structures at ends of MTs while EB2 was

consistently localised to the MT lattice. A publication by Bu and Su (2001) indicated that the overexpression of EB1 and EB3 promoted bundle formation in many cell lines while the overexpression of EB2 did not cause this effect. Furthermore, this observation was also confirmed by our lab (Goldspink et al., 2013) with the addition that the expression of EB2 is required for the initial phase of MT reorganisation during apico-basal epithelial differentiation while EB1 is essential for bundle formation. Depletion of EB2 was found to lead to EB1/EB3 lattice association in several epithelial cells including ARPE-19, TC7, U2OS and HCT116 cells while depletion of EB1 and EB2 caused EB3 lattice association as well as the plus-ends suggesting that EB3 can compensate for EB1 (Goldspink et al., 2013). The role of EB2 in centrosome duplication is currently unknown.

A major difference was found among the EB family members and their abilities to govern MT growth (Komarova et al., 2009). It was found that EB1 and EB3, but less so EB2, were needed for enhancing MT growth, and also suppressing catastrophe, instead of directly promoting growth rate or rescue. EB2 was found to have less ability to compete with other family members for contact with MT ends (Komarova et al., 2009). Phosphorylation of EB2 reduces its affinity for binding MTs and instead increases its dispersal in the cytoplasm, an effect needed for cells to undergo mitosis (Iimori et al., 2016b). A recent study showed that overexpression of EB2 is involved in the invasion of pancreatic cancer (Abiatari et al., 2009). Moreover, it has been suggested that EB2 associates with HCLS1-associated protein X-1 (HAX1) and plays a vital role in focal adhesion turnover and cell migration, where interaction between EB2 and HAX1 in skin epidermal cells promotes focal adhesion turnover while their depletion resulted in focal adhesion stability and impaired cell migration (Liu et al., 2015).

In addition to +TIPs, other MT-associated proteins (MAPs) have been identified that are also responsible for regulating MT dynamics (**Fig 1.7**). *Xenopus* MT-associated protein 215 (XMAP215) first identified in xenopus extracts as a factor that promotes MT assembly (Gard and Kirschner, 1987). It has also been found to promote the assembly of MTs in mammalian cells (van der Vaart et al., 2009). They do this by using their conserved tumour overexpressed gene (TOG) domain to bind to soluble tubulin dimers, with high affinity, and incorporating them into growing MTs (Slep and Vale,

2007, Brouhard et al., 2008). Moreover, XMAP215 binds briefly to the MT plus-end and in that time recruits 25 tubulin dimers to be incorporated for MT growth before dissociating and the cycle takes place again (Brouhard et al., 2008). Mitotic centromere-associated kinesin (MCAK) is part of the kinesin-13 motor family that augments MT depolymerisation rather than move along MTs (Howard and Hyman, 2007). MCAK is usually found at the centromere and regulates MT turnover at the kinetochore (Wordeman, 2005). Depolymerisation of MTs by MCAK is essential for the correct segregation of chromosomes during the cell cycle. Furthermore, MCAK binds to MT ends with high affinity. The protein introduces curves into protofilaments resulting in unstable MTs and ultimately, depolymerisation (van der Vaart et al., 2009). Kinesin-8 (also known as kip3 and kif18A) is another protein responsible for MT depolymerisation. It does this by increasing the rate of formation of the lattice-destabilising structures. This is useful during mitosis whereby a specific MT length has to be controlled as well as during the attachment of MTs to kinetochores (Du et al., 2010, Gardner et al., 2011).

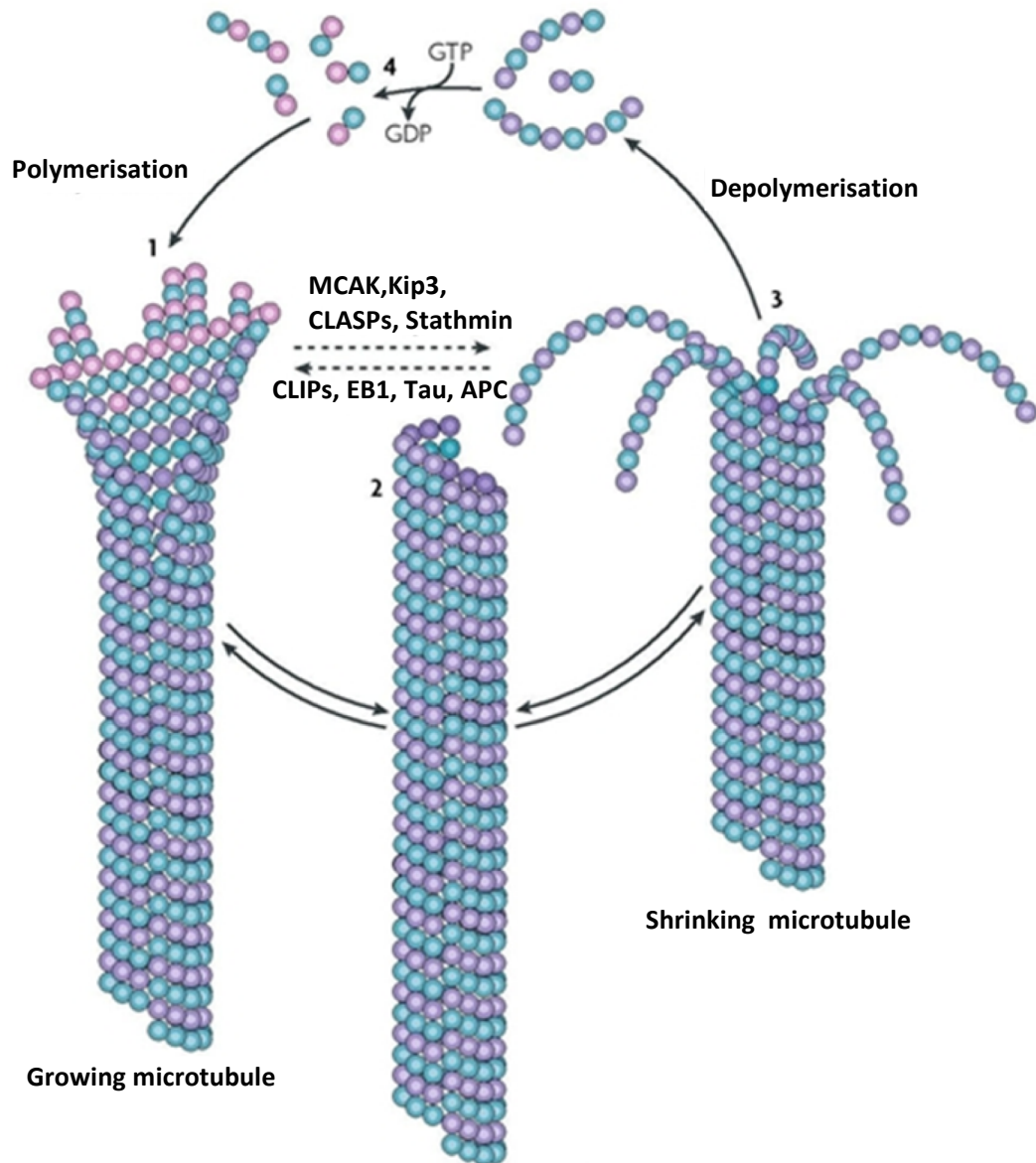


**Figure 1.7 Regulation of MT dynamic instability by several proteins.**

These proteins are required at various stages of MT growth and shrinkage. MTs can switch rapidly between phases of growth and shrinkage. Growing microtubules possess a GTP-tubulin cap. Proteins such as MCAK aid MT catastrophe while CLIPs and EB1 regulate MT rescue. Adapted from Akhmanova and Steinmetz (2008).

## 1.2.5 Microtubule post-translational modifications

MTs can undergo various post-translational modifications such as being acetylated, deacetylated, tyrosylated, detyrosylated, glycylation, glutamylation or phosphorylation, generating diversity (Westermann and Weber, 2003). Most modifications on subunits occur after MT polymerisation and are reversible processes.

### 1.2.5.1 Tyrosination/Detyrosination

This was the first post-translational modification to be identified. It is the C-terminus of the  $\alpha$ -tubulin subunit that is tyrosinated (Gundersen et al., 1984). Carboxypeptidases (CCP) are responsible for the removal of a tyrosine residue from  $\alpha$ -tubulin in a process termed detyrosination. Detyrosination leads to the exposure of glutamic acid at the C-terminus. The tyrosination-detyrosination cycle allows the recruitment of +TIP proteins and molecular motors (Hammond et al., 2008). In mammalian cells, +TIPs, especially those with a CAP-Gly domain, bind to tyrosinated tubulin while molecular motors for example, kinesin-1 binds detyrosinated tubulin. The preference of kinesin-1 for detyrosinated tubulin is said to be important in neuronal development. Deregulation of tubulin tyrosine ligase-like proteins (TTLL) proteins, which leads to detyrosinated tubulin correlates with tumour invasiveness hence, poor prognosis (Mialhe et al., 2001).

### 1.2.5.2 Acetylation and Deacetylation

This post-translational modification occurs on Lys40 of  $\alpha$ -tubulin and is a marker for MT stability. Acetylation occurs in the MT lumen and is carried out by  $\alpha$ -tubulin acetyltransferase (aTAT1). The catalytic activity of this enzyme is more than 100 times higher towards tubulin in its polymerised state compared with its unpolymerised state. It is thought that the enzyme gains access to the luminal site through cracks that appear in the polymerised tubulin or from the open MT ends. aTAT1 could use these MT faults to enter and acetylate MTs on Lys40. However, the weakness of this theory is that MTs would require a high frequency of faults in order for acetylation to spread over their entire length (Coombes et al., 2016). The other theory suggests that aTAT1 accesses the luminal sites from the open ends. This implies

that aTAT1 has a higher affinity for these ends due to the high density of exposed luminal sites, which could be used as ploys to attract the enzyme (Coombes et al., 2016, Ly et al., 2016). In cells, MTs are every now and again unprotected from mechanical forces, which can harm the MT lattice and hence result in MT depolymerisation. The perception that acetylation hotspots are frequently found at bended and curved areas of MTs, which are the same regions that amass cross-sectional breaks give an indication that these stress-induced lattice sites are the luminal passages for aTAT1. The enzyme would then acetylate the MTs, which consequently would render the region impervious to mechanical stress and permitting their repair (Schaedel et al., 2015, Janke and Montagnac, 2017).

Histone deacetylase 6 (HDAC6) (Hubbert et al., 2002) and SIRT2 (North et al., 2003) have been identified as enzymes that deacetylates  $\alpha$ -tubulin. These two proteins can act independently but they tend to form a complex to carry out their function. HDAC6 deacetylates  $\alpha$ -tubulin on polymerised MTs whereas SIRT2 can target both polymerised MTs and soluble tubulins.

### **1.2.5.3 Glutamylaton and Glycylation**

These two modifications are similar. They form as peptide side chains on the C-terminal tail domain of both  $\alpha$ - and  $\beta$ -subunit (Wloga and Gaertig, 2010). Tubulin glutamylaton is present in spindle MTs, proliferating non-neuronal cells (Bobinnec et al., 1998), axonemes (Bre et al., 1996) and basal bodies. These modifications are referred to as polymodifications because they branch off several glutamic acid side chains within the subunits. Glycylation is found in specialised ciliated cell types (Bre et al., 1996). Glutamylaton and glycylation of MT subunits are catalysed by TTLL (Janke et al., 2005). These family proteins contain several enzymes, which differ in terms of their preferred subunit, the specificity of the residue they add and whether they are chain-initiating or elongating proteins. The mechanism for polymodification takes place in two steps – initiation and elongation. Usually, different TTLL proteins catalyse these steps. Chain-initiating TTLL proteins such as TTLL1 or TTLL4 add glutamic acid or glycine residue to tubulin via an isopeptide bond. Next, chain-elongating TTLL proteins such as TTLL6 elongate the chain (Janke et al., 2005), which takes place after

MT assembly. There are shorter side chains in cellular organelles that are just forming, however this gets longer as the organelle grows (Wloga and Gaertig, 2010). As a result, side chain modifications can be used as a marker for cell growth.

## **1.3 Mechanisms of Epithelial Lumen Formation**

MT organisation is different in polarised epithelial cells. During development, epithelial cells differentiate and may polarise to form epithelial lumens. These cells organise into groups so that their apical surfaces face a central lumen whilst the basolateral surface contacts the extracellular matrix or adjacent cells (Bryant and Mostov, 2008, Nelson, 2003). The two domains are usually separated by adherens and tight junctions. Cells on the apical surface specialise to regulate the exchange of substances, for example, nutrients. Motile cells embedded in 3D matrix either migrate together and adhere or proliferate from a single precursor to form established adhesive complexes. These cells then undergo morphogenesis and polarisation to eventually form epithelial cysts with a lumen (Zegers et al., 2003). Formation and maintenance of polarity is important for the appearance of a central, fluid-filled lumen (Bryant and Mostov, 2008) whereby lumen may form from pre-existing polarised epithelia or de novo from non-polarised epithelia (Blasky et al., 2015). Three mechanisms of de novo lumen formation have been explained – cord hollowing, cell hollowing and cavitation (**Fig 1.8**), (Sigurbjornsdottir et al., 2014).

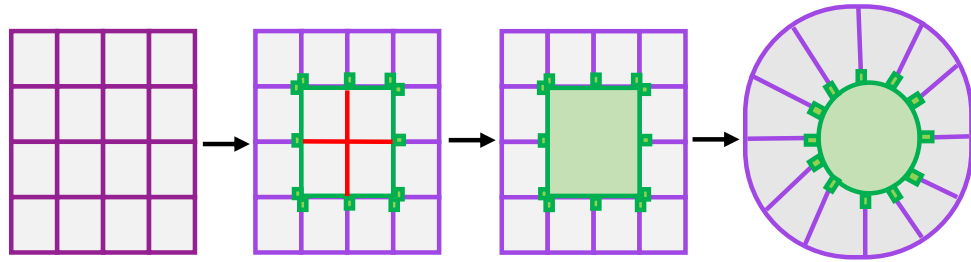
Lumen formation by cavitation involves the outer cells being in contact with the ECM, which signals differentiation and polarisation. Inability of the cells in the centre to contact the ECM causes death by apoptosis. In cell hollowing, the lumen forms and expands within a single cell. When apical vesicles are delivered to the plasma membrane, they fuse together forming a large intracellular space that expands to form the lumen. Lumens may also form by a cord hollowing process. The process takes advantage of a cell undergoing cell division. Here the formation of the midbody during the first cell division is the key event that initiates polarisation of two daughter cells. This process is dependent on targeted trafficking of apical proteins to the apical membrane initiation site (AMIS) by Rab proteins regulating AMIS formation around the midbody during late telophase (Bryant et al., 2010, Li et al., 2014b). Although only one of these mechanisms were examined in this project, others are mentioned to highlight the different mechanisms through which lumens form.

It is also worth noting that different tissues may use either of the two *de novo* mechanisms to form lumens, some tissues may require cavitation for their initial formation and hollowing for lumen expansion. In MDCK cells, lumens are formed either by cord hollowing or cavitation depending on the presence or absence of laminin. Polarity is established by forming an apical membrane domain at the interface of the two cells, a step referred to as lumen initiation (Fig 1.7c, see also subsequent section). Next, trafficking proteins such as the synaptotagmin-like protein (Slp2A) and Rab27 target vesicles containing apical proteins such as the Crumbs, Protein-associated with Lin Seven One, PALS1-associated TJ protein (Crbs/PALS1/PATJ complex) and Par complex, this constitutes the Partitioning defective protein-3 (Par-3), Par-6 and aPKC to the AMIS. These apical proteins increase their surface area, a phase required to cause apical membrane growth. The establishment of anti-adhesive factors and turgor generation represents the maturation and stabilisation of the lumen. Anti-adhesive factors such as the highly sialylated gp135 (also known as podocalyxin) forces the membrane apart while hydrostatic pressure activates apical channels and pumps (Meder et al., 2005). For instance, MDCK cysts use the ion channel cystic fibrosis transmembrane conductance regulator (CFTR) for lumen expansion, which results in the correct lumen formation. It has been established that the absence of these channels and pumps lead to the diameter of the lumen being significantly reduced (Bagnat et al., 2010). *De novo* lumen formation also occurs during development of Zebrafish vasculature. Cord hollowing is formed between two cells whereby the lumen can expand by lateral plasma membrane invagination if blood pressure is present to create a subcellular lumen (Lenard et al., 2013). In vertebrate neural tubes, the majority of tubules contain multicellular lumens. This process referred to as budding starts with a sheet of fully polarised epithelium. The sheet of cells invaginates through apical constriction so that a new tube is formed, which separates and seals from the existing sheet (Marciano, 2017).

One of the ways to characterise polarisation in epithelial cells involves the calcium switch where cells are placed in media in the presence of low calcium, this disrupts cadherin-mediated adhesion and consequently apico-basal polarity. This effect is overcome when cells are placed back in media with normal levels of calcium (Pasdar and Nelson, 1988). To establish cell polarity, epithelial cells receive cues from surrounding cells and the ECM. More specifically, these cues allow the orientation of

the axis of polarity. In 3D MDCK cultures, interaction between integrins and the ECM triggers a signalling cascade which is essential for polarity orientation (Martin-Belmonte et al., 2008). As epithelial cells polarise they form tight junctions with neighbouring cells creating a barrier that regulates permeability. Two protein complexes are first to be observed in the formation of the apical domain. One of them being the Par complex (**Fig 1.9**). The other is the Crumbs (Crb) complex made up of Crb3, which interacts with PALS) and this in turn interacts with a tight junction protein PATJ (Schluter and Margolis, 2009, Wang and Margolis, 2007).

A. Cavitation



B. Cell hollowing



C. Cord hollowing

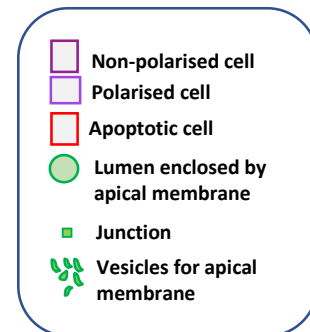


**Figure 1.8 Various mechanisms of lumen formation.**

**A)** Cavitation involves the outer cells being in contact with the ECM, which signals differentiation and polarisation. The inability of the cells in the centre to contact the ECM causes death by apoptosis. **B)** In cell hollowing, the lumen forms and expands within a single cell when apical vesicles are delivered to the plasma membrane. These vesicles fuse together forming a large intracellular space that expands to form the lumen. **C)** Cord hollowing involves a cell undergoing cell division. The lumen forms at the contact between the two cells whereby vesicles delivered fuse to the membrane. Trafficking of apical proteins triggers AMIS formation. Then lumen expansion occurs through the delivery of fluids and ion channels. Adapted from Sigurbjornsdottir et al., (2014).

### 1.3.1 Lumen initiation

In the cord hollowing model, the apical lumen forms between two cells and is dependent on the trafficking of cargo proteins to the AMIS. The AMIS is a short-lived structure containing the Par complex, Exocyst complex (consists of Sec3, Sec5, Sec6, Sec8, Sec10, Sec15, Exo70, and Exo84), tight junction protein ZO-1 and Cingulin, and Slp2a. The exocyst complex serves to direct the tethering of secretory vesicles to specific locations on the plasma membrane and to mediate their localisation to the membrane immediately before SNARE-mediated fusion (Wu and Guo, 2015). Midbody formation and midbody-dependent AMIS recruitment during telophase is the first symmetry-breaking event that determines the site of apical lumen formation.

Apical endosome targeting and fusion at the AMIS is also an important step. Before polarisation gp135 is evenly distributed on the plasma membrane. However, upon 3D cyst formation, newly synthesised gp135 is delivered to a ring at the base of the primary cilium by endosomes fusing with the plasma membrane. The site of gp135 delivery in the cilium is termed the periciliary ring. This is then followed by the cell surface pool of gp135 undergoing a MT-dependent radial motion away from the periciliary ring and towards tight junctions. Some gp135 traffics through the basolateral domain before reaching the apical membrane (Stoops et al., 2015). Rab35 is crucial for lumen formation as it couples cytokinesis with the tethering of vesicles carrying lumen-promoting gp135 at the emerging apical membrane. Gp135 acts as an effector for Rab35, interacting directly with Rab35 when activated (Klinkert et al., 2016, Ioannou and McPherson, 2016). It is common, however, for a single Rab to recruit different effectors depending on the cellular context, allowing a single Rab to initiate several cellular responses. For example, Rab35 can interact with six other effectors in addition to gp135 (Chaineau et al., 2013).

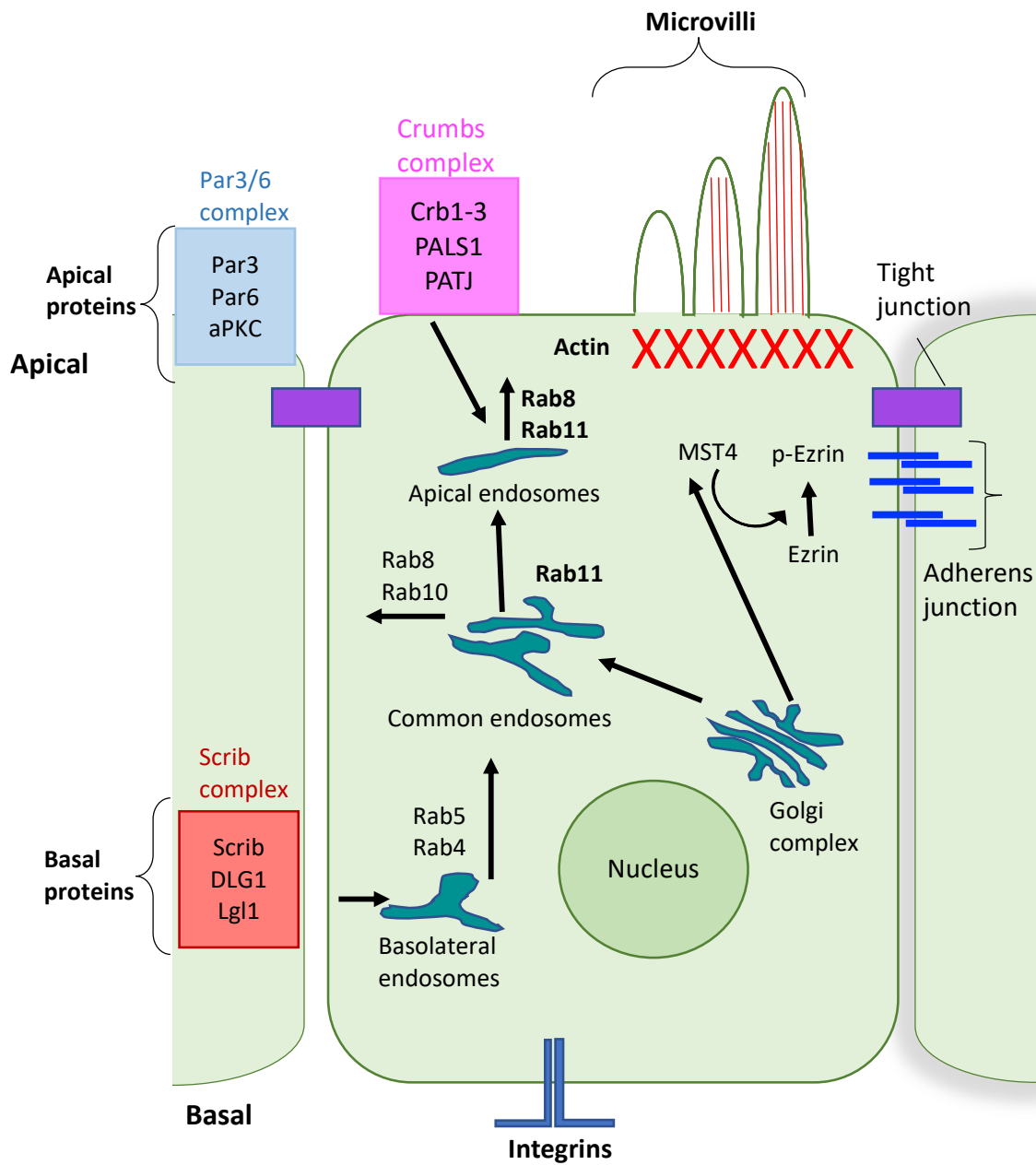


**Figure 1.9 Proteins involved in epithelial polarity**

Schematic representation of proteins involved in lumen formation. These proteins are involved in establishing and maintaining cell polarity. Par and Crumbs complexes regulate the apical and lateral domains respectively. Rab proteins are responsible for regulation and transportation of specific proteins. Tight junctions separate the apical and basolateral domains whilst providing a diffusion barrier that prevents the mixing of membrane components. Adapted from Blasky, A.J. et al., (2015).

Gp135 is internalised and rapidly transcytosed by Rabs to the AMIS. Rab11a in conjunction with rab8a activates Cdc42 (a Rho GTPase). Cdc42 becomes augmented on vesicles intended for the apical surface. In collaboration with the formins inverted formin-2 (IFN2) and MAL2, Cdc42 facilitates vesicle delivery to the AMIS (Madrid et al., 2010). Formins support the unbranched network of actin polymerisation. FMNL3 polarises actin tracks for the translocation of gp135 to the apical surface and for MAL-2 mediated transcytosis. Cdc42 activates IFN2, which then directly activates MAL-2. Depletion of IFN2 leads to defects in lumen formation. This defect is due to the loss of critical residues (Lys792, Leu976, Leu977 and Leu986) needed for actin polymerisation and depolymerisation (Madrid et al., 2010). As well as other Rab proteins being enriched on apically destined vesicles, they cooperate with Rab8a so that it binds Slp2a and 4a. This creates a link between the vesicles and syntaxin-3 for vesicle fusion with a central AMIS (Galvez-Santisteban et al., 2012). Cytokinesis provides a spatial landmark that pinpoints the formation of the AMIS and lumen (Jaffe et al., 2008, Wang et al., 2014, Li et al., 2014b, Overeem et al., 2015). During telophase, there is an accumulation of Rab11a, this protein is able to interact with a Rab11a family interacting protein (FIP5), which in turn interacts with microtubule-associated kinesin-2 (Li et al., 2014b).

During lumen initiation, gp135 and Crb3a are concentrated in Rab11a-containing trafficking vesicles. Transport of these vesicles relies on the interaction between Rab11a and its effector protein FIP5. The consecutive interactions of Rab11/FIP5 targeting complex with Sorting Nexin-18 (SNX18) and Kinesin-2 regulate apical endosome formation and transport along central spindle MTs during the first steps of lumen formation (Li et al., 2014a, Willenborg et al., 2011). Glycogen synthase kinase-3 $\beta$  (GSK3 $\beta$ ) phosphorylates FIP5, which inhibits the formation of apical carriers from recycling endosomes. Dephosphorylation of FIP5 allows the formation of apical carriers and transport along the spindle MTs to the midbody site where the lumen forms (Li et al., 2014b). However, these proteins are not solely responsible since most of the proteins required for lumen initiation reside at different subcellular locations. Cingulin was found to serve as the tethering factor that ensures the accurate targeting of apical endosomes to the AMIS. It does this by its recruitment to the AMIS through the activated Rac1-WAVE/Scar complex, which induces branched actin polymerisation.

At late telophase, Rac1 becomes concentrated at the AMIS where it colocalises with F-actin and Cingulin. Also, RhoA is inactivated, which is followed by Rac1 activation, therefore allowing Arp2/3 branched actin polymerisation. As the AMIS matures, Rac1 remains enriched at the apical membrane suggesting its involvement in maintaining the apical polarity. During late telophase, Cingulin is also able to directly bind to C-terminal tails of MTs through electrostatic interactions (Mangan et al., 2016). This shows the interactions required between endocytic membrane transport, midbody MTs and branched actin filaments during single apical lumen formation.

The main role of Par-3/6 complex is the recruitment and activation of the serine threonine kinase aPKC to tight junctions. The capacity of the Par complex to direct cell polarity depends on its ability to act on several downstream proteins. For instance, in epithelial cells, the Par complex organises junctional components while in asymmetrically dividing stem cells, it polarises fate determinants (Knoblich, 2010, Tepass, 2012). Par-3 is a multi-domain scaffold protein, with three Postsynaptic Density/Discs Large/Zonula Occludens (PDZ) domains that can interact with Par-6 and aPKC. Phosphorylation of Par-3 at S827 by aPKC is required for proper tight junction localisation of Par-3 (Nagai-Tamai et al., 2002). In addition to this phosphorylation, S144 and S885 residues of Par-3 also gets phosphorylated through Par-1 Kinase and leads to the binding of protein 14-3-3 (also known as Par-5) to Par-3 (Benton and St Johnston, 2003). The binding of 14-3-3 ensures that Par-3 stays localised to the apical membrane and not the lateral membrane. Disruption to S144 phosphorylation of Par-3 inhibits its interaction with 14-3-3, resulting in polarity defects (Hurd and Kemphues, 2003). Par-3 regulates and is regulated by GTPases. Tiam1/2 is a Rac1 guanine nucleotide exchange factor (GEF) that binds the C-terminus of Par-3A. This interaction regulates Rac1 activity at the periphery leading to a stabilisation of epithelial junctions. Furthermore, Par-3/6 complex also interacts with Cdc42 and Rac, and plays several roles during polarisation. Cdc42 main function is to regulate the recruitment of Par-3/6 to tight junctions thereby encouraging apical membrane formation (Bryant and Mostov, 2008).

Phosphorylation is necessary for the cortical displacement of proteins that are directly downstream of the Par complex and their removal from the Par domain (Tepass, 2012, Betschinger et al., 2003). These Par substrates such as Lgl, Numb and Mira bind to phospholipids at the cell cortex through electrostatic interactions and their basic and hydrophobic motifs. However, they are regulated by aPKC phosphorylation of the Par domain, which then displaces these substrates from the Par domain into the cytoplasm. This finding highlights the importance of the Par substrate basic and hydrophobic motif as key regulatory elements for polarity though, more work needs to be carried out to improve our understanding on what happens to these substrates once in the cytoplasm (Bailey and Prehoda, 2015). One of the many consequences of unregulated Par-3 protein is tumourigenesis as shown by McCaffrey and co-workers (McCaffrey et al., 2012). They found that loss of the Par-3 protein caused breast cancer and metastasis in murine mammary glands.

Firstly, Par-3 restricts aPKC at the apical membrane, resulting in the binding and phosphorylation of Par-3 by aPKC. Loss of Par-3 triggers both the mislocalisation and activation of aPKC, which then triggers JAK-dependent activation of Stat3. Stat3 in turn induces invasion from the primary tumour. Usually, Stat3 is expressed at low levels in the developing mammary gland. However, activated Stat3 is known to promote breast cancer metastasis (Barbieri et al., 2010). Though, the work was carried out in mice, it certainly suggests that Par-3 may play a significant role in human breast cancer progression.

The Exocyst complex is involved in vesicle fusion and may serve as a tether for Rab11/FIP5 at the AMIS (Datta et al., 2011). Other proteins such as the Synaptotagmin-like proteins have been implicated in the regulation of vesicular transport and targeting to the AMIS. An example is the Slp2a, which is suspected to be concentrated at the AMIS via its interactions with the phospholipid PIP<sub>2</sub>, thus mediating the transport of Rab27-containing vesicles (Galvez-Santisteban et al., 2012). So far, several Rabs – Rab8, Rab10, Rab11, Rab14, Rab17, Rab25, Rab27 and Rab35 - have been shown to be involved in epithelial transport regulation during lumen formation (Apodaca et al., 2012). Rab11a initiates a GTPase cascade, recruiting the Rab GEF Rabin8 to sub-apical vesicles, in turn activating Rab8a/b at this locale (Bryant et al., 2010). This Rab cascade directs vesicle surface delivery, possibly by activating motor proteins such as myosin-

5B (Li et al., 2007). Rab11-Rabin8-Rab8 cascade regulates not only vesicle transport steps in lumen formation but also primary cilia formation (Westlake et al., 2011). Transport and docking of these vesicles with the AMIS is promoted by the Exocyst complex (Bryant et al., 2010). As the lumen formation process progresses, the AMIS matures into a ‘pre-apical patch’ (PAP), an early apical domain between cells where the luminal space has not yet expanded (Bryant et al., 2010). At this point, the Par3/6–aPKC polarity complex, and the Exocyst subunits (Sec8–Sec10) relocate to tight junction areas. In MDCK cysts, Par-3 and aPKC kinase activity are required for apical trafficking to the AMIS to expand to a PAP (Bryant et al., 2010). Crb3a delivery to the nascent lumen may then exclude Par-3 and other junctional proteins from this region, helping to establish and expand the nascent apical domain. In *Drosophila* photoreceptor development, Par-6 along with Cdc42 recruits Crbs to the apical membrane, enabling restriction of Par-3 to the border between the apical membrane and the nascent adherens junction (Walther and Pichaud, 2010).

Furthermore, as the lumen takes shape, the AMIS develops into tight junctions that frame the border between the apical and basolateral domains (Bryant and Mostov, 2008, Li et al., 2014a). Tight junctions do this by forming a tight seal between neighbouring cells hence regulating paracellular permeability. Another example of proteins that keeps the apical membrane in place is the Zona occludens-1 (ZO-1), which is a tight junction protein encoded by the *TJPI* gene in humans and has a molecular weight of 220kDa (Shin et al., 2006). After tight junctions and polarity proteins are in place, the lumen is then ready to expand.

### 1.3.2 Lumen extension and expansion

Once lumens are formed they must expand to their mature, functional size. Turgor is generated by hydrostatic pressure. Hydrostatic pressure, regulated by apical delivery, accumulation and activation of pumps and ion channels, is thought to account for part of luminal expansion in most tissues (Bagnat et al., 2007). For instance, MDCK cysts use the ion channel cystic fibrosis transmembrane conductance regulator (CFTR) for lumen expansion, which results in the correct lumen formation. CFTR controls chloride transport in turn regulating fluid transport during lumenogenesis. In response

to increased cAMP levels, chloride currents are controlled by protein kinase A (PKA)-dependent CFTR through phosphorylation (Bagnat et al., 2010, Hallows et al., 2003). Overactivation of CFTR-dependent fluid transport results in overexpansion of lumen in MDCK cysts highlighting the relevance of CFTR in ion transport (Yang et al., 2008). In Zebrafish gut lumenogenesis, mini lumens fuse, which eventually coalesce to form a single lumen. Claudin-15 and Na<sup>+</sup>/K<sup>+</sup>-ATPase regulate the paracellular and transcellular ion transport, which drives fluid accumulation and is important in lumen expansion (Bagnat et al., 2007). Furthermore, in zebrafish ventricle lumen expansion claudin-5a regulates paracellular permeability across the neuroepithelial barrier and is crucial for ventricle lumen expansion (Zhang et al., 2010) while in *Drosophila*, the claudin equivalent Kune-Kune controls tracheal tube size (Nelson et al., 2010). These studies show that lumen expansion seems to occur in multiple organs via a conserved interplay between claudin-regulated paracellular permeability, and Na<sup>+</sup>/K<sup>+</sup>-ATPase-modulated luminal hydrostatic pressure.

Proteins required at the early stages of lumen initiation may also be required during lumen expansion. For example, the presence of negatively charged sialic acids such as gp135 is required to provide rapid expansion of the apical surface in developing blood vessels (Strilic et al., 2009). As the endothelial assembly matures, the apical pole of the cells is progressively enriched in apical actin, which links to apical proteins via ERM proteins (Strilic et al., 2010). Next, actin contraction inducing separation of adjacent apical membranes is triggered by ROCK (Ferrari et al., 2008). Subsequent actomyosin relaxation is required in some models. For instance, the expansion of the ventricular lumen of zebrafish hindbrain is regulated by Myosin phosphatase Mypt1 (Gutzman and Sive, 2010). Factors that induce proliferation may not be the primary determinant of lumen size because normal mammary ducts and acini have defined sizes despite the continuous presence of growth factors. For example, the primary ducts in a mouse mammary gland can be about 20 μm in diameter, but through expansion may get to a size of about 80 μm during lactation. It is worth noting that these size estimates may not reflect lumen size in live animals, as milk production affects lumen expansion and contraction. It is possible that lumen size is modulated by the presence of specific morphogens or by matrix composition tension in the microenvironment. An example of this has been shown in a 3D mammary organotypic culture model of lumen formation, the morphogen epimorphin/syntaxin2 cooperates with growth factor-

induced proliferation to increase lumen size (Reginato and Muthuswamy, 2006).

## 1.4 Spindle Orientation

During epithelial cyst formation, lumen initiation and expansion takes place, which mean cells undergo division. For this to occur efficiently resulting in one clear-filled lumen, the division plane needs to be parallel to the apical membrane. The orientation of the apico-basal axis determines the plane of cell division, positioning of the cells and the apical lumen therefore regulates the overall tissue architecture and diversity. One of the hallmarks of cancer is the loss of epithelial organisation and spindle misorientation, which are evident in several types of cancers. Apico-basal polarised epithelial cells, such as those lining the acini in breast, orient their spindles parallel to the apical surface causing cells to divide in the plane of the epithelial tissue. Spindle positioning defects may lead to hyperplasia – an increased amount of tissue after proliferation – and multiple lumens (Overeem et al., 2015, Hung et al., 2016).

Mechanisms regulating the apical-basal axis orientation are beginning to emerge. It has been established that the complex interactions between the ECM (O'Brien et al., 2001, Yu et al., 2005), GTPase signalling (Jaffe et al., 2008), cell division and recycling endosome dynamics are all crucial. At the ECM interface, integrins for example  $\alpha 2\beta 1$  and phosphatidylinositol (PI) 3-kinase activates Rac1 (O'Brien et al., 2001). Activation of Rac1 leads to assembly of laminin (Yu et al., 2005) although the mechanism is not clear. Integrin-mediated lumen formation requires integrin-linked kinase (ILK), a focal adhesion kinase protein.  $\beta 1$ -integrins orient apical polarity away from the cell-basement membrane interface by creating cell interactions with the basement membrane and governing signalling through ILK (Akhtar and Streuli, 2013). It was also discovered that  $\beta 1$ -integrin adhesions influence the spatial organisation of MTs (Fielding et al., 2008, Wickstrom et al., 2010). During polarisation in wild-type MDCKII cysts, MTs are aligned along the apico-basal polarity axis with EB1 pointing towards the basolateral membrane. However, in the ILK-KO MDCKII cysts, EB1 was disseminated throughout suggesting the existence of short, disorganised MTs. This led to the disruption of apico-basal polarity and lumen formation (Akhtar and Streuli, 2013). In MDCK cells, activated  $\beta 1$ -integrins reduces RhoA activity

through the recruitment of a GTP-activating protein (GAP) for RhoA. Reduced RhoA activity leads to reduced activity of one of the ERM complex protein, ezrin at the cell-ECM interface. Consequently, this allows the phosphorylation of gp135-NHERF1/EBP50-ezrin complex by PKC (Yu et al., 2008).

MTs that anchor the spindle poles to the cell membrane during mitosis are referred to as astral MTs and these MTs control spindle positioning in most epithelia. Astral MTs interact with several cortical proteins at the membrane, including NuMA, LGN and G $\alpha$ i (**Fig 1.10**) (Du and Macara, 2004, Morin et al., 2007, Peyre et al., 2011). These cortical proteins recruit and anchor dynein, which then moves towards the minus-end of the astral MTs generating pulling forces orienting and positioning the spindle poles. The N-terminus of NuMA is used for binding to dynein while the C-terminus binds both LGN and MTs, with each of these interactions being a requirement for correct spindle orientation (Seldin et al., 2016, Kotak et al., 2012). Recruitment and localisation of the LGN complex through the cell cycle require changes in cellular organisation. Levels of LGN increases as cells go through the cell cycle. In interphase, LGN is in a closed conformation and due to its weak affinity for G $\alpha$ i in this conformation, it does not get recruited to the cortex. This changes when NuMA binds LGN, opens its conformation, increasing its ability to bind G $\alpha$ i and for the complex to be at the cortex (Du and Macara, 2004).

During mitosis, LGN is augmented along the lateral and basal cortex but is excluded from the apical surface. One theory for apical exclusion is that phosphorylated LGN is bound by another protein inhibiting G $\alpha$ i binding (Hao et al., 2010). LGN tethers to the cell membrane by interacting through its C-terminal GoLoco domains with G $\alpha$ i and simultaneously links to the spindle apparatus by binding to NuMA through its N-terminal tetratricopeptide repeat (TPR) motifs (di Pietro et al., 2016). Another way LGN is recruited to the lateral cortex is by directly binding to the polarity protein Discs Large (Dlg) and E-cadherin, both of which aid its recruitment to the cortex (Gloerich et al., 2017). E-cadherin possesses an intracellular domain which LGN competes with p120-catenin for binding. Although, the full molecular mechanisms involved are still unclear, a study by (Kiyomitsu and Cheeseman, 2012) discovered that a RanGTP chromosomal gradient restricts the localisation of NuMA-LGN to the lateral cell cortex

maintaining the spindle axis. RanGTP acts in part through NuMA via its nuclear localisation sequence to proximally modify the ability of NuMA-LGN to associate with the cell cortex when chromosomes are nearby. By using a RanT24N mutant, they showed that RanGTP chromosomal gradient was accountable for excluding LGN from the cortex. Therefore, LGN is initially recruited all around the cortex during early mitosis such as prometaphase, however, by metaphase and anaphase its localisation is restricted to two cortical crescents facing the bipolar spindle and excluded from other areas. The study proposed that an innate code to control spindle orientation is caused by chromosome- and spindle pole-derived gradients and that the localisation of LGN complex is determined only when the spindle orientation is set.

NuMA is known to undergo post-translational modification. A recent study showed that cortical localisation of NuMA is regulated by its phosphorylation. During mitosis in human cells, Aurora A localises to spindle poles and phosphorylates NuMA on a serine residue. This implies that Aurora A acts at the spindle poles in order to promote the release of phosphorylated NuMA (Mud in *Drosophila*) from the poles and thereby allow its association with LGN. The finding was further confirmed by the knockdown of Aurora A, which unsurprisingly led to an increase of NuMA at the poles and a reduction at the cortex (Gallini et al., 2016). A Hippo pathway kinase, warts, can phosphorylate both NuMA and Mud. However, in *Drosophila* its phosphorylation of Mud also on a serine residue causes a conformational change that exposes its Pins (human mammalian LGN) binding domain hence allowing its interaction with Pins (Dewey et al., 2015).

Even though the LGN, NuMA and Gai complex controls spindle orientation by anchoring astral MTs to the cell cortex, the specific signals that drive mitotic spindle orientation in epithelial cells are not fully understood. IQGAP1 is known to mediate the capture and stabilisation of MTs at the cell cortex through its binding partner CLIP170, which is essential for protein polarisation and directional cell migration (Noritake et al., 2005). Its role in anchoring astral MTs to the plasma membrane during epithelial cell division has now been assessed.

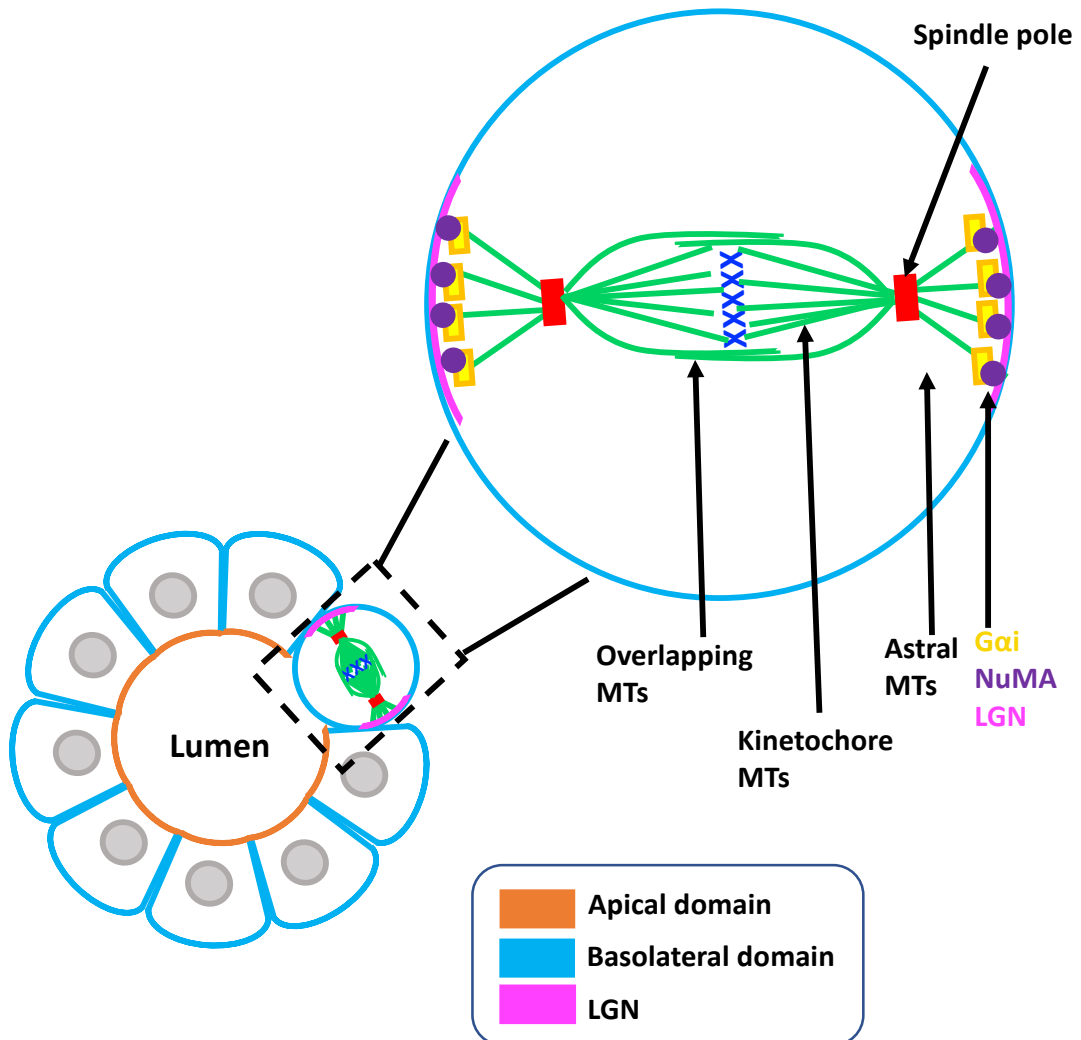


**Figure 1.10 Spindle orientation in lumen formation.**

The schematic shows cells cultured in Matrigel forming a cyst with a central lumen and distinctive polarity domains. Spindle orientation occurs in the plane of the epithelium and depends on the localisation of cortical proteins. LGN protein, which localises to the lateral cell cortex interacts with Gai membrane-anchored subunits, and with NuMA thereby regulating cortical localisation and spindle orientation. Adapted from di Pietro, F. et al., (2016).

Initially, IQGAP1 localises to the apical membrane through its N- and C-terminal domains. This effect is overcome by a stronger signal that directs IQGAP1 to the basolateral domain. Localisation of IQGAP1 to the basolateral domain relies on its IQ motif. IQGAP1 was shown to modulate EGFR activation (McNulty et al., 2011). Thus, EGFR was studied as a candidate to associate IQGAP1 to the basolateral membrane. Through co-immunoprecipitation, it was found that IQGAP1 and EGFR interacted but only when the IQ motif was present confirming the motif's role in directing IQGAP1 to the basolateral domain. In the presence of IQGAP1, NuMA and the plus-ends of astral MTs attach strongly to the membrane, resulting in correct mitotic spindle orientation. Through this, IQGAP1 is able to maintain mitotic spindle orientation (Inmaculada Banon-Rodriguez et al., 2014).

Spindle orientation also relies on MT dynamics. Cenexin functions as a scaffold protein that associates with the distal and subdistal appendages of mother centrioles and in control cells acetylated tubulin is abundant at the centrosome compared to cenexin-depleted cells suggesting that stable MTs at the centrosome are needed for positioning the centrosome (Hung et al., 2016). The maintenance of these MTs is also dependent on +TIPs such as APC, EB1 (Green et al., 2005) and CLASPs (Espiritu et al., 2012). KIF17 also plays a role in spindle orientation by interacting with MT plus-ends via APC and EB1 (Jaulin and Kreitzer, 2010). The motor head domain of KIF17 binds to EB1, APC binds to EB1 and also the tail domain of KIF17. These interactions are important for the stabilisation of MTs in epithelial cells and allows polarisation to take place. Plus-TIP proteins influence the dynamics of astral MTs and the transport of proteins that act as force generators to pull on astral MTs and orient the spindle (Tamura and Draviam, 2012). Astral MTs interact with the cell cortex to direct spindle orientation, which is governed by dynein in complex with dynactin (Wittmann et al., 2001) and the NuMA/LGN/G $\alpha$ i complex (Kotak and Gonczy, 2013). In other words, cenexin controls the positioning of the centrosome, which is essential for astral MTs. Astral MTs also modulate the localisation of NuMA and thus spindle orientation resulting in accurate positioning of the division plane and lumen formation. During epithelial morphogenesis, Cdc42 also controls spindle orientation to position the division plane and ensure correct lumen formation (Jaffe et al., 2008). Cdc42 regulates formation of the apical membrane (Martin-Belmonte et al., 2008), primary ciliogenesis (Choi et al., 2013) as well as kidney tubule development (Elias et al., 2015). Specifically, the Cdc42-

specific GEF, Intersectin-2 controls the activation of Cdc42 (Rodriguez-Fraticelli et al., 2010). Intersectin-2 localises to the centrosome and regulates the positioning of the mitotic spindle as well as the apical surface. Cdc42 can regulate the MT plus-end interaction at the actin-rich mitotic cortex (Durgan et al., 2011).

Several protein kinases and phosphatases have been described to regulate spindle orientation and positioning through different mechanisms. For example, p21 activated kinase (Bompard et al., 2013), protein phosphatase 2A (Wang et al., 2009) and ASK1 contribute to spindle orientation by controlling astral MT formation and localisation at the cortex. In particular, ASK1 controls spindle orientation by phosphorylating EB1 on Serine 40, Threonine 154 and 206 enhancing its binding affinity to the plus-ends of MTs. The resulting effect is that astral MTs become stabilised augmenting its interaction with the cell cortex, a process required for spindle orientation. Depletion of ASK1 in HeLa cells led to an increase in spindle angle and a decrease in astral MT intensity but had no effect on the length of the spindle and thus caused spindle misorientation (Luo et al., 2016). ASK1 is known to interact weakly with EB2 and does not phosphorylate it. However, CDK1 and Aurora B are kinases that phosphorylate EB2. They do this at the region connecting the CH and EBH domain, significantly reducing its binding affinity to MTs. This allows the detachment of EB2 from MTs thus ensuring mitotic progression (Iimori et al., 2016a). Par-3 and aPKC are also important as they regulate the location of the cortical complexes. Mechanisms that regulate astral MT nucleation, anchoring, dynamics and interactions with the cortex thereby control spindle orientation and the plane of division (Di Pietro et al 2016; Seldin and Macara 2017).

Two proteins have recently been identified namely Astrin and small kinetochore associated protein (SKAP). These proteins play a role at kinetochores by mediating interaction between stable kinetochore MTs and chromosomes. SKAP has an EB binding motif leading to localisation at the MT plus ends. We already know that other +TIPs can bind to MTs via EB proteins through hitchhiking. A recent study by Kern and co-workers (Kern et al., 2016) showed that mutating the EB motif in SKAP caused spindle misorientation but did not stop the recruitment of dynein to the cortex. This is probably because dynein is recruited through another +TIP or by a different protein completely. New proteins have come to light and further highlighted the roles and

regulations of cortical pulling forces. The protein Afadin in vertebrates and Canoe in *Drosophila* is responsible for localising cortical pulling forces. Canoe/Afadin links to the TPR motif of LGN in vertebrates (Niessen and Gottardi, 2008) while in *Drosophila* links the adhesion protein Echinoid to the actin cytoskeleton. Cortical localisation of LGN depends on Afadin (Carminati et al., 2016). More work carried out shows that Canoe (Afadin) enhances the interaction between Pins and Mud by acting as an accessory factor and functioning downstream of Pins (Wee et al., 2011).

Correct spindle orientation is thought to play a role in tumour suppression. Studies have shown strong correlations between spindle misorientation and carcinogenesis in *Drosophila melanogaster* and mammalian cells. For example, inhibition of spindle orientation in *Drosophila* led to invasive outgrowths caused by uncontrolled stem-cell divisions (Causinus and Gonzalez, 2005) while the loss of Par-3 promoted tumour growth in mammary glands (McCaffrey et al., 2012). Though, these studies have taken place, it is necessary to understand the role of polarity proteins, spindle orientation, and MTs in the context of the mammary gland.

## 1.5 Introduction to Breast Cancer

The mammary gland is a highly effective organ that regulates lactation in females. It performs indispensably critical immunological functions, both in giving passive immune protection to a newborn child and in immunological fight of its own tissues against diseases (Watson, 1980). Oestrogen stimulation causes the development of glandular tissue during pregnancy. During pregnancy, the oestrogen level increases causing the breast to increase in size through the enlargement of adipose tissues. The mammary gland is made up of 15-20 lobes, which drain into a major duct below the areola. Each duct is lined with layers of epithelial cells responsible for milk production. The glandular ducts are embedded in the stroma and breakdown in this structure results in breast cancer (**Fig 1.11**).

Breast cancer is a complex and heterogeneous disease. It is the third most common cause of cancer death in the UK (Cancer Research UK, 2012). In 2011, over 50,000 people were diagnosed with breast cancer in the UK and by 2012, 11,716 deaths

had occurred. These deaths occurred mainly due to metastasis (Cancer Research UK, 2013a, Cancer Research UK, 2013b). Metastasis to secondary sites is one of the hallmarks of tumour progression, which contributes to the poor prognosis of a patient (Hanahan and Weinberg, 2011). In most western countries, the incidence of breast cancer is increasing currently, 1 in 8 (women). However, mortality is decreasing, this could be due to several factors such as the initiation of mass screening and the recent introduction of new drugs (Cancer Research UK, 2014a). In addition to invasive breast cancer, there has been an increase in the type of breast cancer classified as ductal carcinoma in situ (DCIS) which characteristically show loss of normal tissue architecture. This is a direct result of an increased use of screening, which might explain why the incidence is increasing while mortality is decreasing.

#### Staging and heterogeneity of breast cancer

Breast cancer is categorised under different TNM stages and grades when diagnosed. Staging of cancer looks at how big it is and whether it has spread. This step is crucial in determining the appropriate treatment for the patient (Cancer Research UK, 2014b). T refers to the size of the tumour and there are four of these. N gives information on whether it is present in the lymph node or not especially the sentinel node, since it is the first lymph node to receive lymphatic drainage from a tumour. M refers to metastasis that is whether the tumour has spread to other parts of the body such as the bone, lungs and liver (Sobin and Fleming, 1997). There are various types of treatment available to patients with breast cancer depending on the stage. Surgery, chemotherapy, radiotherapy, hormone therapy and targeted therapy are examples of these treatments. If the mass was small when discovered, breast-conserving surgery may be used. However, if the mass was large, mastectomy will be needed in conjunction with one of the therapies (Cancer Research UK, 2014b). Breast cancer was first known to be heterogeneous through morphological classifications. The heterogeneity of breast cancer cells means that they are composed of different cell types with distinct behaviours and morphologies. This property as well as the ability of cells to migrate and invade make it challenging to treat the disease efficiently.

## Human Mammary Gland Anatomy

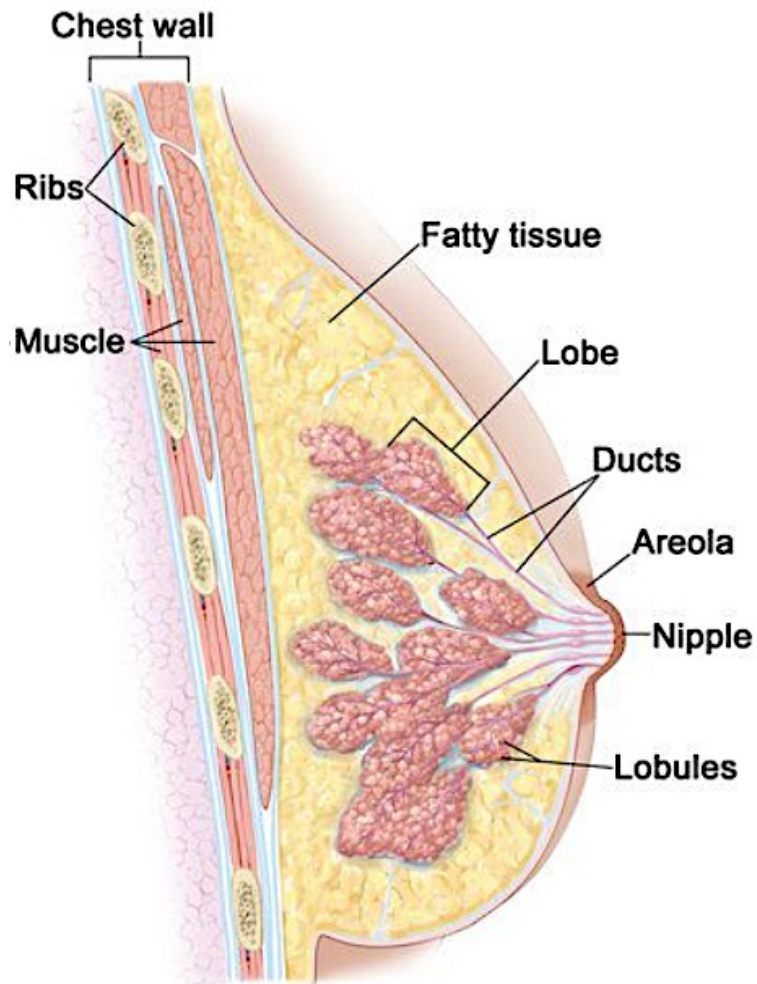


**Figure 1.11 Anatomy of the breast**

Schematic representation of the breast depicting the nipple, areola, chest wall, muscle, fatty tissue, lobe, ducts, and lobules. Each mammary gland contains about 15-20 lobes, which drains into a major duct that dilates into a lactiferous sinus below the areola opening. Each duct is lined with layers of epithelial cells responsible for milk production. The glandular ducts are embedded in the stroma and breakdown in this structure results in breast cancer. Adapted from National Breast Cancer Foundation (2013).

### 1.5.1 Cell migration

Cell migration is important for normal physiological functions such as wound healing, tissue renewal and immune responses. This process also takes place in cancer cell metastasis. The cytoskeleton is vital for the modification of cell shape during migration. Its properties provide cells with the driving force to move (Yamaguchi and Condeelis, 2007). Some cells migrate as single cells while others such as epithelial cells migrate as sheets. Migrating cells have a front to back polarity. Cell migration can be divided into four individual steps: lamellipodia protrusion, formation of new adhesions, cell body contraction, and tail retraction (Ridley, 2001) (**Fig 1.12**). Firstly, the membrane protrudes at the leading edge leading to the formation of filopodia and lamellipodia. These extensions then make contact with the substrate where they interact with the extracellular matrix through integrins. Lamellipodia extensions are made possible due to the branching filament networks of actin formed through the Arp2/3 complex (Yamaguchi and Condeelis, 2007).

Furthermore, actin filaments create contractile stress fibers (made up of  $\alpha$ -actinin, myosin II and focal adhesions), which are responsible for contraction of the cell body, retraction of the trailing edge, and connecting with focal adhesions (Skau and Waterman, 2015, Tojkander et al., 2012). There are different types of stress fibers - dorsal stress fibers lack myosin II, are connected to focal adhesions at their distal end and located at the front of the cell. Ventral stress fibres are anchored at both ends by focal adhesions. Transverse arcs are formed behind the leading edge of migrating cells and are not directly linked to focal adhesions but through dorsal stress fibres. They act as connectors for the ventral adhesion with the dorsal contractile actin network (**Fig 1.13**) (Tojkander et al., 2011).

Activation of actin polymerisation is regulated by Rho GTPases (Vega and Ridley, 2008). Rac stimulates the formation of lamellipodia while Rho is responsible for the contraction of the cell body. For example, small cell lung cancer cell migration across endothelial cells requires the disassembly of tight junctions and increased RhoA activity was observed 2h after incubating both endothelial and cancer cells. RhoA activity leads to actin reorganisation through the indirect phosphorylation of myosin

light chain. Disassembly of tight junctions on endothelial cells renders them permeable, which subsequently allows migration of small cell lung cancer (Li et al., 2006). The migration steps are controlled by different proteins but especially by Rho GTPases (Cdc42, Rac and Rho). During migration, these proteins regulate the cytoskeleton and focal adhesions. Active Cdc42 is involved in filopodia initiation while Rac is thought to influence lamellipodia projection. Actin polymerisation, actomyosin contractility, and focal adhesion turnover are regulated by activated RhoA.

In addition, filopodia and lamellipodia extensions are stabilised by the formation of new adhesions to the extracellular matrix. Contraction of the cell body occurs through actomyosin activity, which allows it to move forward and in the process disassembling the adhesion of the tail resulting in tail retraction. The cycle then takes place again.

## **1.5.2 Cytoskeletal organisation in migrating cells**

The cytoskeleton needs to undergo rearrangement in order to produce the force required for movement. Generally, the leading edge of a migrating cell extends to form a lamellipodium that is characterised by an extensive actin network. This actin network pushes forward the membrane with myosin II and actin stress fibers contracting at the back of the cell. At the same time, the centrosome and Golgi apparatus relocate to a location in front of the nucleus (**Fig 1.14**).

In epithelial cells, protrusions are mostly produced by actin however, pioneer MTs do enter the lamellipodium where they play key roles in cellular processes through their trafficking, signalling and mechanical properties (Etienne-Manneville, 2013). Lamellipodia are said to be the leading factor of directionality, which is determined by MTs. During migration, MTs are oriented towards the leading edge, where MT growth is more persistent than in the cell body. Perhaps, the reason for this is because the leading edge of the cell is the first to undergo changes and are under increased pushing forces compared to the cell body. During protrusion, MTs also act as carriers of proteins that are required at leading edge since diffusion and actin-based delivery is not sufficient (Miller et al., 2009). Therefore, the presence of MTs close to the leading edge

is vital for the delivery of proteins needed for protrusion. For example, in 3D remodelling, recycling endosomes, VAMP3, are delivered to the cell edge in an EB1 MT-dependent manner (Gierke and Wittmann, 2012). Formation of new focal adhesions occurs simultaneously as the protrusion of the lamellipodia. Indirect MT activation of Rac guanine exchange factor (GEF) TIAM2/STEF stimulates the activation of new focal adhesions (Rooney et al., 2010). Moreover, MTs can modify focal adhesions by modulating actomyosin contractility (Waterman-Storer and Salmon, 1999). It is thought that this occurs via +TIPs such as APC, CLASPs and CLIPs, which increase actin polymerisation by interacting with mDia and IQGAP (Okada et al., 2010, Brandt and Grosse, 2007).

In migrating cells, actin filaments and MTs interact with each other. Actin has been shown to be a major influence on MT organisation. For example, in lamellipodia protrusions, MTs are coupled to actin undergoing retrograde flow. This process is regulated by actomyosin activity (Waterman-Storer and Salmon, 1997). Mechanical signalling between focal adhesions and regulators of cellular contractility, such as Rho GTPases contribute to the regulation of cell migration. Furthermore, these signals are associated with cell and ECM changes during cancer formation and progression, and have an essential role in tumour growth and invasion (Provenzano and Keely, 2011). Rho GTPases regulate processes such as actin organisation, MT dynamics and adhesion sites (Wojnacki et al., 2014). The activity of Rho family proteins is regulated by stimulating the release of GDP to GTP by GEFs (Etienne-Manneville, 2013). Interaction between actin and MT could be termed as either structural or regulatory.

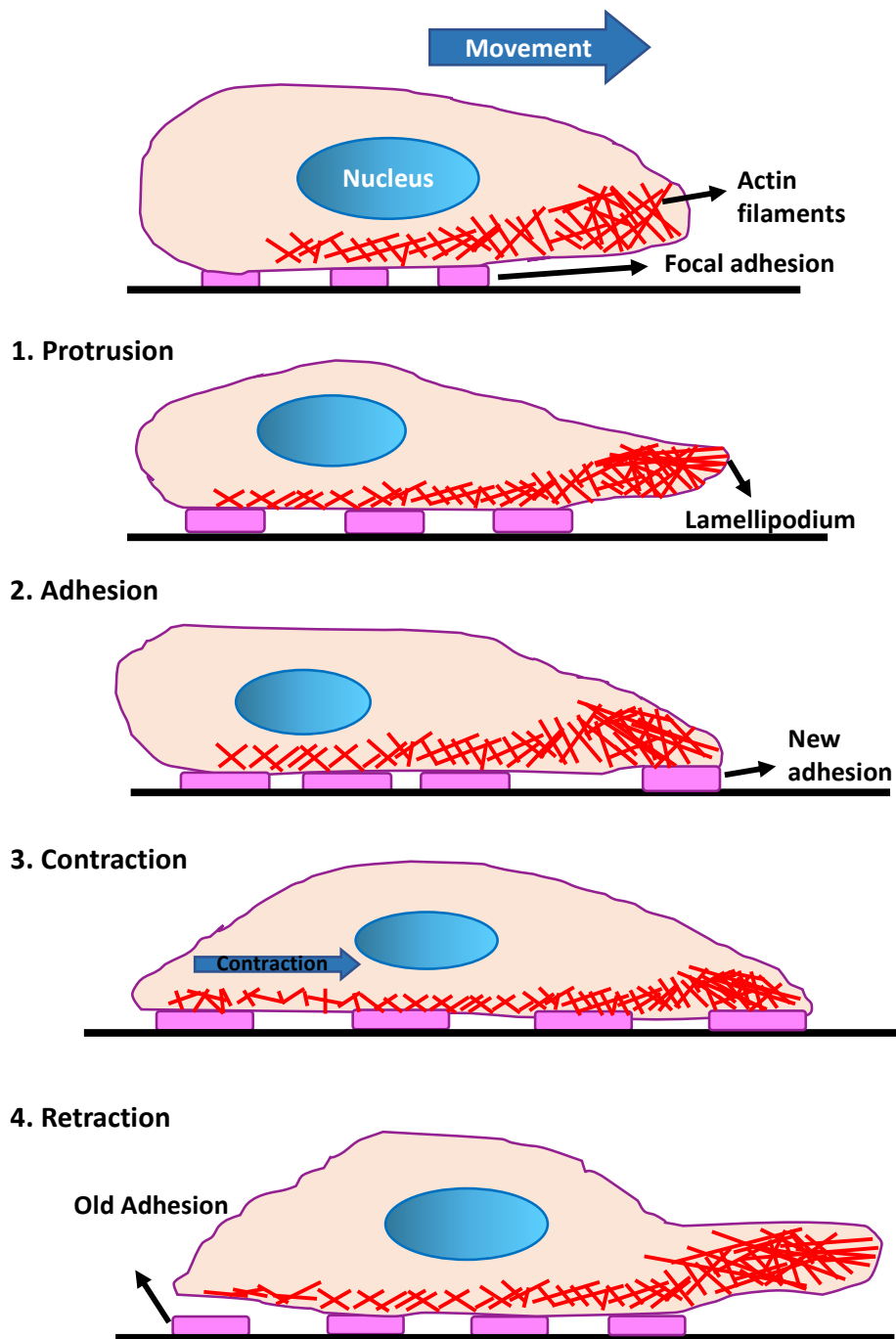


**Figure 1.12 Cell migration process**

Schematic representation of the steps in cell migration. 1. Extension of a protrusion at the leading edge forming the lamellipodium. 2. Formation of new adhesions that attach the cell to the ECM, which allows the cell to crawl over the matrix. 3. Contraction in the rear area. 4. De-adhesion at the trailing edge to start a new cycle again. Adapted from Tschumperlin (2013).

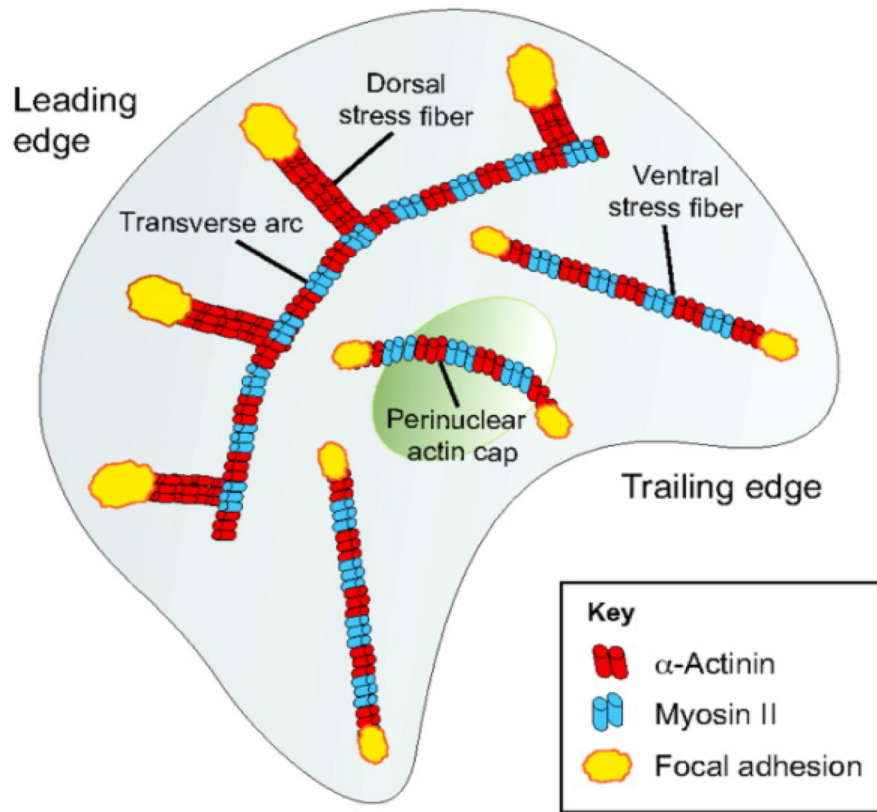


**Figure 1.13** Types of stress fibres in migrating cells.

Dorsal stress fibres are located at the front of the cell and anchored to focal adhesions close to the cell edge. Transverse arcs are formed behind the leading edge of migrating cells and are linked to focal adhesions through dorsal stress fibres. Ventral stress fibres are contractile actomyosin bundles that are anchored at both ends by focal adhesions. Perinuclear actin cap bundles are similar to ventral stress fibres but these wrap across the nucleus. Adapted from Tojkander (2011).

Regulatory interaction describes two systems that control each other indirectly through their actions on signalling pathways (Rodriguez et al., 2003b). Rho GTPase family are good examples of this, they control several processes including MT dynamics and actin organisation. For example, the formation of stress fibres (Etienne-Manneville and Hall, 2002) and MT stabilisation (Cook et al., 1998) are directed by RhoA. Rho GTPases are likely to be associated with the changes that occur in actin and MT dynamics, which determines cell migration (Etienne-Manneville and Hall, 2002). On the other hand, structural interactions can be described when actin and MTs are physically linked (Rodriguez et al., 2003b). This has not been fully verified *in vivo* because it is difficult to distinguish between filaments that simply cross over from those that are specifically bound. However, the strongest evidence of the structural interactions between actin and MTs comes from the use of multispectral time-lapse microscopy whereby different fluorophores were used to label both actin and MTs. Results revealed that MTs moved at the same trajectory and velocity as F-actin in the cell body and lamellum, but not in the lamellipodium. MTs grew along F-actin bundles showing that the movement and organisation of f-actin guides and influences the dynamic organisation of MTs during cell migration (Salmon et al., 2002). Similar findings were also observed in *xenopus* egg extracts (Waterman-Storer et al., 2000). TipAct, a cross-linker protein was engineered to show the interaction between actin and MTs. The engineered protein uses EBs to link MT plus-ends to actin. Since MT plus-ends are directed by bundles of F-actin leading to strong actin-MT communication and organisation (Kaverina et al., 1998, Stehbens and Wittmann, 2012b); the observation *in vitro* was that actin bundles are capable of capturing MT ends and redirecting MT growth. Cross-talk between actin and MTs is reliant on the concentration of the TipAct linker at both the MT tip and lattice, and also on the angle of encounter of F-actin suggesting an influence on cytoskeletal organisation (López et al., 2014).

Polarisation of the MT network during migration relies on the position of the centrosome, the nucleus and the increased MT stability at the leading edge. Centrosomal position is regulated by signalling pathways originating from Cdc42, which controls plus tip proteins and by the MT motor dynein and its accessory protein dynactin. In migrating adherent cells such as endothelial cells, the MTOC reorients toward the leading edge. MTOC reorientation repositions the Golgi toward the front of the cell and contributes to directional migration. A study by Palazzo et al., (2001)

established that MTOC reorientation is independent of Cdc42-induced changes in actin. Also, inhibition of dynein or dynactin blocked lysophosphatidic acid (LPA)- and Cdc42-activation blocking MTOC reorientation showing the importance of LPA/Cdc42. Thereby, these results establish an LPA/Cdc42 signalling pathway that regulates MTOC reorientation in a dynein-dependent manner polarising the MT network in migrating cells (Palazzo et al., 2001b). The proximity of the cis compartment of the Golgi complex to the centrosome is affected by the centrosome position. The position of the centrosome therefore causes a polarised organisation of the Golgi complex, which contributes to enhanced MT growth towards the leading edge (Efimov et al., 2007, Sütterlin and Colanzi, 2010).

Adhesion formation is an imperative step towards cell migration. It happens during the binding of adhesion receptors to ECM by means of integrins along the cell edge. The connection amongst cells and ECM produce the required power for crawling over the matrix framework, which depends on the capacity of cells to powerfully rebuild adhesion sites. Small focal complexes can be located in the lamellipodium, which later mature into large focal adhesions that connect with stress fiber ends (Wozniak et al., 2004, Parsons et al., 2010). Proteins such as focal adhesion kinase (FAK), paxillin and vinculin are focal adhesions that mediate the signalling effects of cells in response to matrix adhesion. Integrins mediate cell adhesion and ECM, and have essential roles in cell migration. They are heterodimers, which determine the receptor required for different ECM molecules. For example,  $\alpha 2\beta 1$  integrin expression in MCF-7 and MDA-MB-231 breast cancer cells is needed for its interaction with collagen-I (Taherian et al., 2011, Ramirez et al., 2011) while expression of  $\alpha 5$  and  $\alpha V\beta 3$  integrin are required for breast cancer cells interaction with fibronectin (Bauer et al., 2007, Mierke et al., 2011).

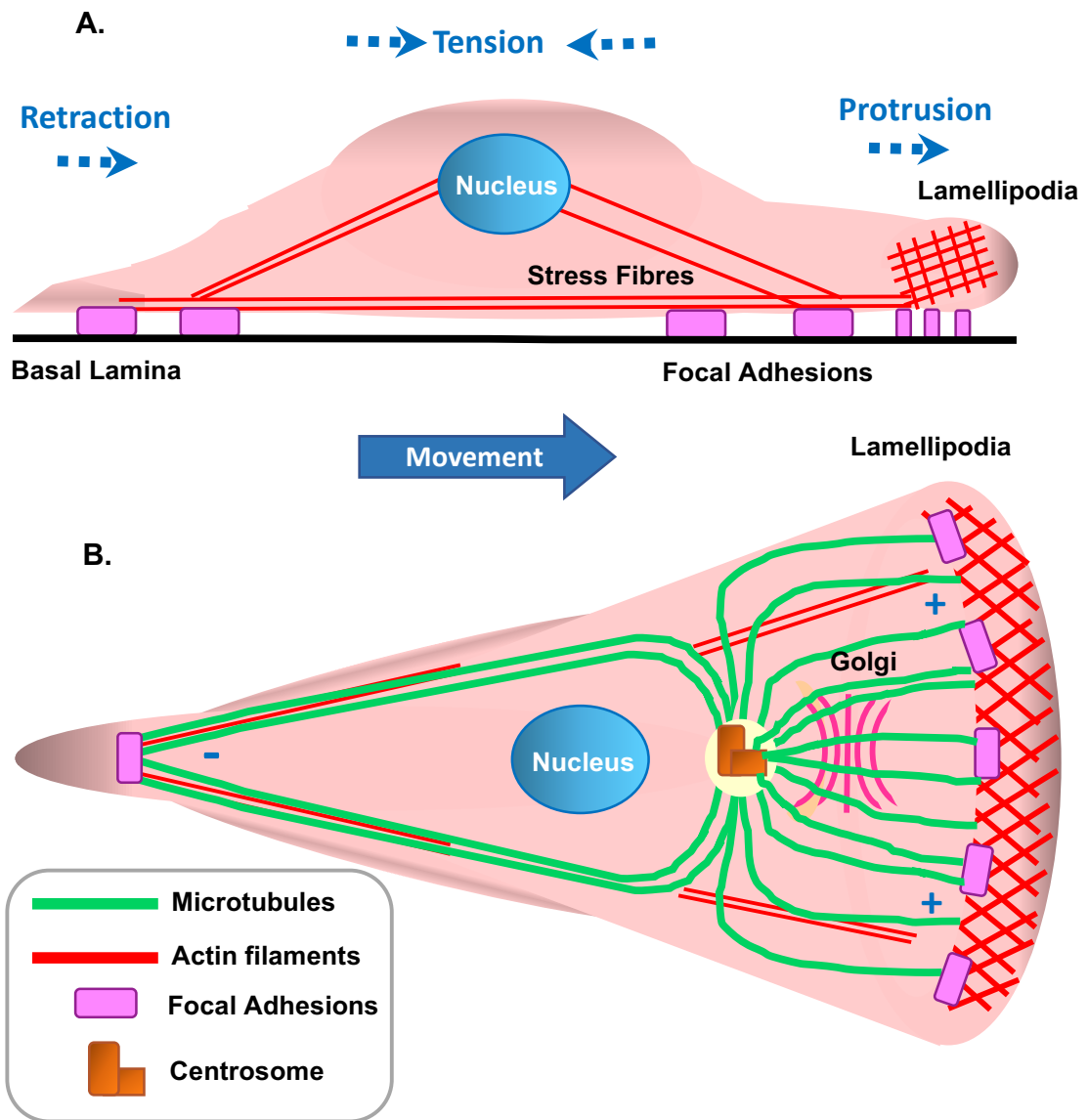


**Figure 1.14 Cytoskeletal organisation in cell migration**

A) A migrating cell undergoes different actin-related processes. During migration, polymerised actin filaments in the lamellipodium push forwards the plasma membrane at the leading edge. Focal adhesions are attached to the ECM, allowing tension exerted by actomyosin contraction in stress fibres to pull the cell forward. Finally, focal adhesions turnover and retraction of the rear. B) MTs reorganise during cell migration. The centrosome and Golgi apparatus relocate to the front of the nucleus facing the leading edge, where stable MTs extend to the leading edge and dynamic MTs found at the rear. Adapted from (Lauffenburger and Horwitz, 1996; Ridley et al. 2003).

Integrin signalling is important for the anchoring and stabilisation of MT plus ends to the cortex (Gundersen et al., 2004). The way MTs are captured may act as a platform for trafficking more molecules involved in MT stabilisation. For example, in fibroblasts, MT stabilisation is directed by FAK through RhoA and mDia (Palazzo et al., 2001b). FAK plays a role in regulating focal adhesion dynamics. Its turnover promotes breast cancer cells invasion. This is done through the formation of invadopodia, which are specialised actin-rich structures that degrades ECM. Chad and co-workers (2009) showed that endogenous FAK negatively regulates invadopodia formation and the rate at which it is formed. However, enhanced formation of invadopodia in FAK-deficient cells was not sufficient to promote invasive cell migration. Dynamic MTs are essential for focal adhesion turnover by delivering important proteins for disassembly with EBs influence. Recently, it has been shown that EB2 increases focal adhesion turnover through mitogen-activated protein kinase kinase kinase 4 (MAP4K4) association (Yue et al., 2014a). Furthermore, EB2 associates with HCLS1-associated protein X-1 (HAX1) to increase focal adhesion turnover and promote migration (Liu et al., 2015). Also, EB2 or MAP4K4 depletion resulted in focal adhesion stability (Yue et al., 2014a, Liu et al., 2015). EB2 depletion can inhibit MT dynamics and result in co-alignment between MTs and actin filaments with ACF7 associated along the lattice, which caused impaired cellular migration (unpublished data from Mogensen lab).

## **1.5.2 Epithelial mesenchymal transition (EMT)**

After the loss of apico-basal polarity and the initiation of cytoskeletal rearrangement required for cell migration, the cells may then undergo a process termed epithelial-mesenchymal transition (EMT). The primary site is where tumours begin. Some cancers grow at the primary site where they have not invaded the surrounding tissues (Cancer Research UK, 2013c). Others might remain dormant for years due to various factors, one example being the lack of blood vessel growth inside the tumour (Aguirre-Ghiso, 2007). Mutations such as the activation of oncogenes or loss of tumour suppressor genes may occur in one or more of the cells growing at the primary site giving them the ability to acquire different phenotypic properties (De Craene and Berx, 2013). An example of such phenotypic change is EMT, which promotes invasion and

metastasis (Gos et al., 2008). The shift in epithelial cell phenotype is necessary for epithelial cell layer repair during wound healing processes where the cells undergo a transient EMT in order to migrate into the wound to close the gaps in the epithelial cell sheet. This transition also occurs in embryogenesis, where individual cells peel away from the ectoderm and migrate towards the centre of the embryo to form the mesoderm (Moustakas and Heldin, 2007).

EMT involves the disruption of epithelial cell–cell junctions, loss of apico-basal polarity, breakdown of cell–basement membrane and changes in cytoskeletal organisation (Hanahan and Weinberg, 2011). During these physiological processes, the cells lose cell-cell adhesion and gain migratory properties, which allow them to move to other parts within the embryo. These changes are also important for cancer cells to acquire motility and invasive properties (Hanahan and Weinberg, 2011). In tumours derived from epithelia, the cells undergoing EMT stop producing epithelial protein markers such as E-cadherin and cytokeratin and start producing mesenchymal markers like N-cadherin and vimentin (Sarrió et al., 2008). This also requires the production of matrix metalloproteinases (MMPs) to digest the ECM as well as modify the microenvironment (Kessenbrock et al., 2010). These tumour cells sometimes appear morphologically similar to mesenchymal fibroblasts. For metastasis to occur, tumour cells disseminate from the primary tumour and invade surrounding tissues. They enter the circulation through the bloodstream or lymphatic system. After survival in the circulation, they extravasate and then migrate to secondary sites such as bones, lungs and brain (**Fig 1.15**). The highly dynamic nature of MTs is one of the many reasons cancer cells are able to metastasise to secondary sites.

During EMT, epithelial cells migrate into the underlying interstitial tissues, which is accompanied by loss of cell-cell junctions. ERM proteins influence the regulation of cell signalling and cytoskeleton during cancer progression. They are known to link actin filaments to the cell membrane (Fehon et al., 2010). It is reported that mislocalisation of ERM proteins disrupts the formation of signalling receptors, which leads to the lack of or little response to growth factors (Arpin et al., 2011). Hence, mislocalisation of ERM proteins inhibits cell-cell contact thus, aiding the invasive phenotype of cancers with epithelial origin. Cancer cells are then able to migrate into

surrounding tissues (Clucas and Valderrama, 2014). Moreover, ERM proteins regulate the activity of the Ras superfamily of small GTPases such as Rho and Rac. GEFs and guanine nucleotide dissociation inhibitors (GDI) are both essential for the activation and deactivation of Rho and Rac and these are the proteins modified by ERM proteins (Sperka et al., 2011). Furthermore, intercellular reorganisation is another important factor to be considered during EMT (Lamouille et al., 2014). A relatively new study showed that EMT is enabled by a reversal of cell polarity using MCF-10A culture as a model of mammary gland acini. This reversal results from centrosome repositioning. Specifically, centrosomes moved from their apical, actin-rich position next to intercellular junctions to the cell centre and towards extracellular matrix adhesions on the opposite side of the nucleus. This movement is supported by controlled MT network disassembly whereby TGF- $\beta$  treatment caused a reduction in the total number of MTs via a decrease in MT nucleation and polymerisation; and the release of Par-3 from intercellular junctions resulting in disengagement promotion and mesenchymal cell scattering (Burute et al., 2017).

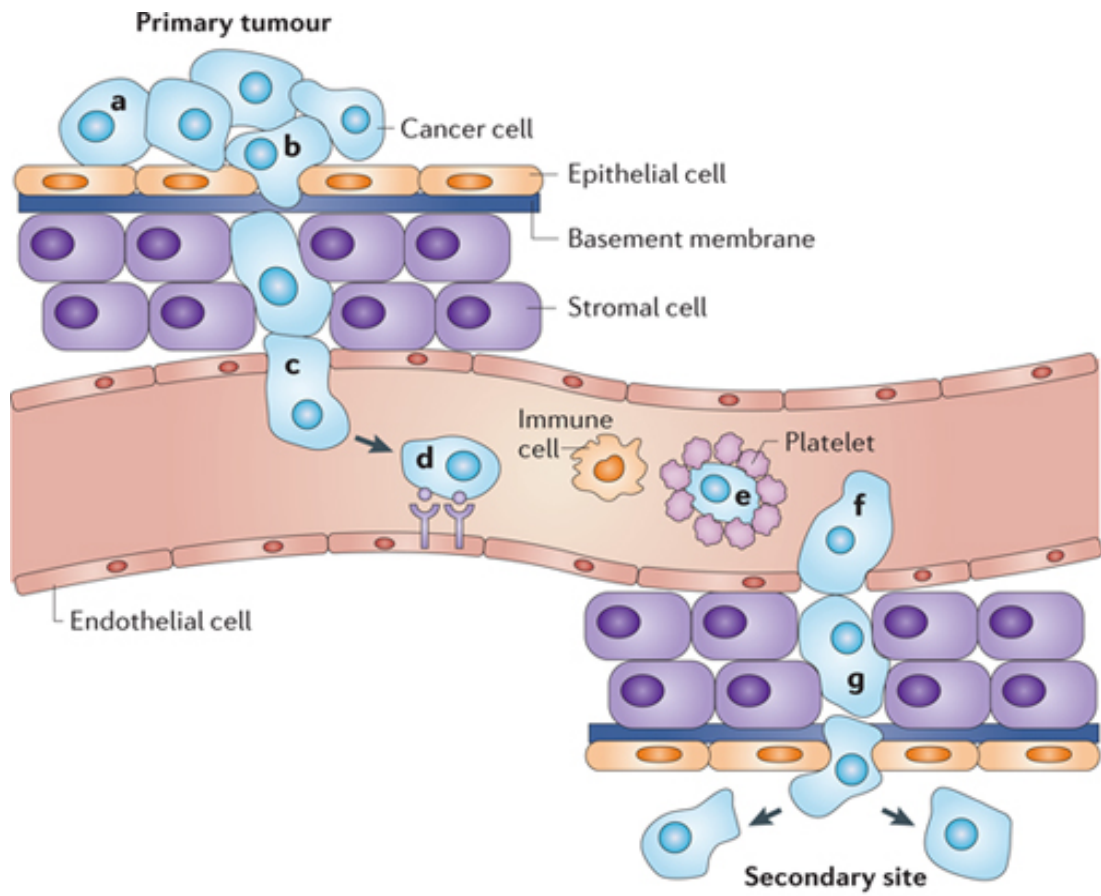


**Figure 1.15 Invasion-metastatic cascade.**

Tumour cells disseminate from the primary tumour (a) and invade local tissues (b). They enter the circulation through the bloodstream (c) or through the lymphatic system where they bind to adhesion molecules expressed on endothelial cells (d). Sometimes, platelets might coat cancer cells, which is a mechanism cancer cells use to evade detection by the immune system (e). After survival in the circulation, they extravasate (f) and migrate to secondary sites (g). (Schroeder et al., 2011).

### 1.5.3 Role of EBs in breast cancer progression

Overexpression of EB1 has been reported in certain cancers for example, gastric carcinoma, oesophageal squamous cell carcinoma, hepatocellular carcinoma and oral squamous cell carcinoma (Nishigaki et al., 2005, Wang et al., 2005, Fujii et al., 2005, Kumar et al., 2016). In addition, EB1 overexpression has been shown to increase breast cancer cell proliferation by increasing Aurora-B activity, which is a kinase required during cytokinesis thereby, enhancing tumour growth (Dong et al., 2010). Interestingly, recent studies have revealed EB1 to be involved in cancer cell apoptosis by promoting paclitaxel sensitivity in breast cancer cells. It is thought that EB1 exerts its actions through allosteric effects in a pattern similar to those seen in CLIP-170 (Sun et al., 2012). EB1 increases the ability of paclitaxel to cause cell arrest thus, resulting in multinucleated cells and eventually, increasing apoptosis (Luo et al., 2014). A contradictory recent study reported that EB1 regulates breast cancer cell sensitivity to paclitaxel, with EB1 expression decreasing the sensitivity of breast cancer cells to paclitaxel. However, EB1 depletion increased breast cancer cells sensitivity to paclitaxel by causing MT bundling in the interphase cells and inducing the formation of elongated multiple spindles in mitotic cells, demonstrating that loss of EB1 promotes paclitaxel-induced stabilisation of MTs. The study proposed that when EB1 is present and binds to the MT plus-ends, it inhibits paclitaxel from binding to the tip; though, it may not influence lattice binding, suggesting some form of competition between EB1 and paclitaxel (Thomas et al., 2015).

Upregulation of EB2 has been found to increase perineural invasion of pancreatic cancer. These changes also caused modification in actin distribution (Abiatari et al., 2009). Immunofluorescence analysis of these cells showed mainly cytoplasmic localisation of EB2. Though some were found localised in the nucleus. In pancreatic cells with highly invasive potential, EB2 was postulated to co-localise with F-actin forming stress fibres, a characteristic required for migrating cells (Abiatari et al., 2009). Furthermore, c-Myc protein has been implicated in the progression of breast cancer cells both *in vitro* and *in vivo*. Its aberrant expression promotes the growth of breast cancer cells (Wang et al., 2004). Moreover, the expression of c-Myc is dependent on the increased transcriptional activity of  $\beta$ -catenin/TCF, which is in turn reliant on

the overexpression of EB1. Here, EB1 is thought to act as an oncogene promoting growth and inhibiting apoptosis (Liu et al., 2005). A recent study also found two kinases – Aurora B and CDK1 – responsible for the phosphorylation of EB2 resulting in a reduced affinity for MTs. EB2 becomes detached from MTs and is distributed in the cytoplasm allowing the progression of mitosis (Iimori et al., 2016a). Generally, most studies found that overexpression of EB1 or EB2 appeared to enhance tumour cell growth. Understanding the role of EBs in this process would be crucial in identifying how downstream effectors affect the pathway. In addition, understanding whether EB proteins are key in providing a prognostic molecular signature is a useful addition to current signatures, which consequently will aid the development of new therapeutic strategies. For example, according to the cBio cancer genomics portal, there is a 0.18% expression signature for the MAPRE1 and 2 genes in pancreatic cancer. In breast cancer, this is 0.05, 0.09 and 0.29% for MAPRE1, 2 and 3 respectively (Cerami et al., 2012). Also, understanding the stage at which they become crucial for breast cancer progression is an area of active research.

## **1.6 Treatment of Breast Cancer – Resveratrol**

Since EB1 and EB2 overexpression have been reported to enhance tumour growth, it is necessary to understand the effects of certain treatments on these proteins. The high incidence of cancer and cost of treatment are important driving forces in the search for new and effective treatments. Several agents have been clinically tested as potential treatments for breast cancer, one of the most common types of cancer. Though, due to the poorly understood mechanisms, effective treatments for breast cancer are not yet available. Currently, there are several options for treatment, for example, radiotherapy and some combinations of paclitaxel, doxorubicin, and cyclophosphamide have shown good efficacy (Buzdar, 2007). However, since individual breast cancers are heterogeneous and portions of many individual breast tumours are resistant to existing anti-tumour agents, there is no existing "gold-standard" treatment. Hence, additional treatments need to be assessed and developed.

Phytochemicals are groups of compounds thought to have favourable health benefits including preventative properties against cancer. They are substances that

occur naturally in plants. Resveratrol is a type of phytochemical found in for example red wine, peanuts and grapes (**Fig 1.16A**). Several possible effects of resveratrol have been reported including anti-inflammatory, activation of hormones, interference with DNA replication and protecting neurons against diseases (Mattson et al., 2007, Le Corre et al., 2005).

Jang and co-workers (1997) published the first scientific paper that described resveratrol's prevention properties against cancer in mice. Most of the knowledge on resveratrol has been obtained from animal studies. Bioavailability of resveratrol has been studied. There is a rapid absorption of resveratrol in the gastrointestinal tract even when low doses of 0.03 mg/kg were given. More than half of the low dose given was recovered in the urine after 24h compared with a higher dose of 1 mg/kg, where only a quarter of the amount ingested was recovered at the same time point (Meng et al., 2004). Poor efficacy and bioavailability have prevented the use of resveratrol in clinics. To address these problems, several resveratrol analogues have been synthesised and tested for chemo-preventive effects (Ronghe et al., 2016, Mikstacka et al., 2013, Siddiqui et al., 2013). Whilst resveratrol is generally safe to use and well-tolerated, certain adverse effects have been reported in mice. For example, mice administered with varying doses of resveratrol (0-3000 mg/kg) were monitored. They found that most of the adverse events observed occurred at the highest dose administered which included nephropathy, reduced food consumption and body weight, reduced red and white blood cells (Crowell et al., 2004). The potency of resveratrol may be affected by interactions with other drugs, dietary components or vitamins (Detampel et al., 2012).

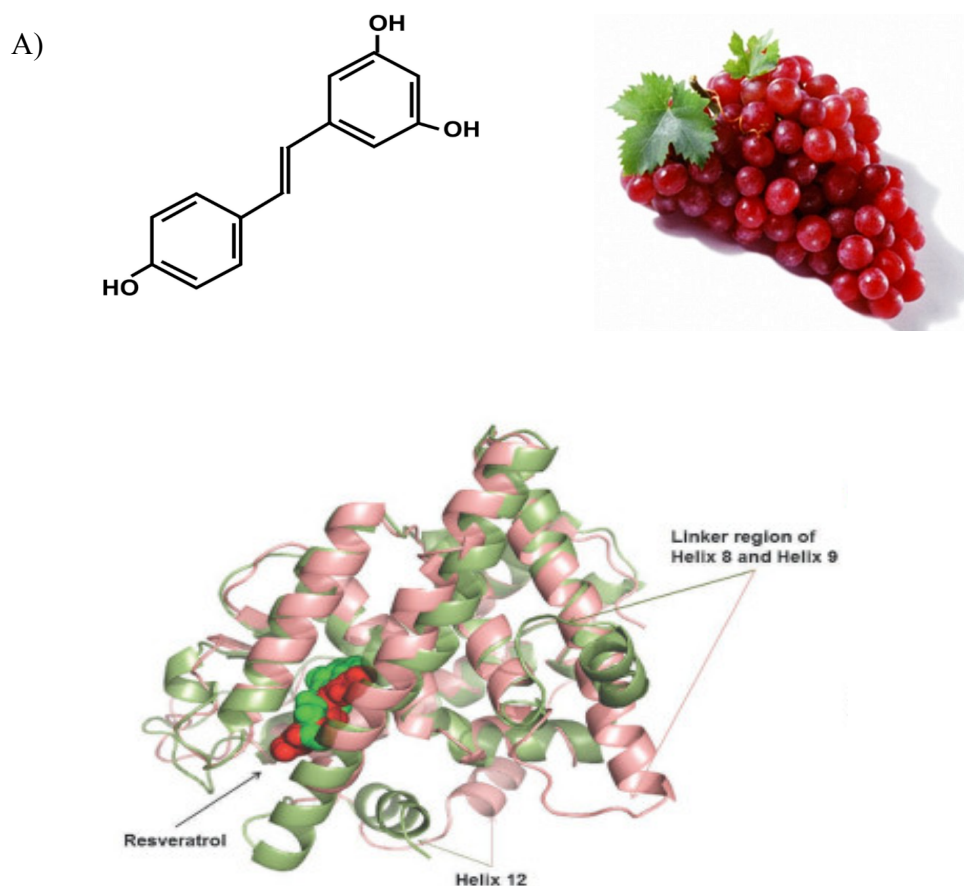


**Figure 1.16 Resveratrol Structure.**

A) Chemical structure of Resveratrol. Resveratrol (3,5,4'-trihydroxy-trans-stilbene) is found in foods such as red wine, peanuts and grapes, and is thought to have chemopreventive properties. Adapted from Camont et al., (2009). B) Schematic structure showing the interaction between resveratrol and estrogen receptor. The structures of resveratrol-ER $\alpha$  agonist (green) and resveratrol-ER $\alpha$  antagonist (red) overlap. Using visual molecular dynamics, the ER $\alpha$  is shown in cartoon representation while resveratrol is shown in space-filling mode. The side chains of some of the residues whose conformations are considerably different between the complexes are shown i.e. the linker region of helices 8 and 9, and helix12. (Chakraborty et al., 2013).

### 1.6.1 Resveratrol and cancer

Resveratrol is reported to inhibit the progression of certain types of cancer (Le Corre et al., 2005, Hong et al., 2009, Scherzberg et al., 2015). Resveratrol was found to have a preventive effect on the development of tumours in mouse mammary glands (Moon and Mehta, 1990). A study by Whitsett (2006) also found that resveratrol but not epigallocatechin-3-gallate (EGCG) – a polyphenol just like resveratrol - has chemopreventive effects against the development of mammary tumours. Female rats age 50 days were treated with 7,12-dimethylbenz(a)anthracene (DMBA) to induce mammary tumours. They found that treatment with resveratrol, but not EGCG resulted in increased lobular structure differentiation and increased apoptosis of terminal end buds making them less vulnerable to the carcinogen DMBA (Whitsett et al., 2006). However, the mechanism of action remains elusive. Resveratrol has also been found to inhibit tumour initiation by preventing the formation of free radicals when leukaemia cells were treated with 12-O-tetradecanoylphorbol-13-acetate (TPA) (Sharma et al., 1994). Another role for resveratrol has been to act as an anti-mutagen. Treatment of a bacterial strain TM677 with DMBA usually causes a mutagenic response however resveratrol was discovered to inhibit this response (Shamon et al., 1994). Moreover, resveratrol has been shown to control signalling in breast cancer cells by acting in an anti-estrogenic fashion (Le Corre et al., 2005, Azios et al., 2007). The mechanism for this involves regulating GTPases Cdc42 and Rac signalling. Consequently, these proteins modify actin cytoskeleton by allowing the induction of filopodia and lamellipodia, and reducing cell migration in a concentration-dependent fashion.

Cell migration is a critical process required during wound healing, and tumour metastasis. This process needs the activities of the cytoskeleton, cell membrane and ECM to be in agreement (Rodriguez et al., 2003a). Focal adhesions play an important role in cell migration requiring dynamic MTs (Ezratty et al., 2005). Resveratrol was found to decrease cell viability in colorectal cancer cells with as little as 5  $\mu$ M concentration. It also resulted in the suppression of focal adhesion kinase activity and invasion (Buhrmann et al., 2017). Azios et al., (2007) showed that resveratrol decreased cell migration in MDA-MB-231 breast cancer cells by altering the actin cytoskeleton

and inducing filopodia and lamellipodia extensions. Furthermore, it decreased focal adhesions and FAK activity compared to the untreated cells (Azios et al., 2007).

Resveratrol is referred to as phytoestrogens due to its ability to compete with 17 $\beta$ -estradiol (E<sub>2</sub>) for binding to and modifying the activity of estrogen receptor (ER) alpha (Gehm et al., 1997). Resveratrol has been classified as selective estrogen receptor modulators (SERM) (Levenson et al., 2002). These are classes of drugs that act on the estrogen receptor but are different from the usual full agonists or antagonists because their action is specific and different in certain tissues giving them the influence to stimulate or inhibit the estrogen-like actions (Levenson and Jordan, 1999). Binding of ligands (such as resveratrol) to the receptor results in conformational changes suitable for the receptor to dimerise, recruit co-activator proteins, bind to the estrogen response element in the promoter region of target genes, and trigger gene transcription. It was established that resveratrol bound ER $\alpha$  monomer in an antagonist conformation, in a way that Helix 12 moves away from the ligand-binding pocket and positions into the co-activator binding groove (**Fig 1.16B**) (Chakraborty et al., 2013). This conformation is more stable than resveratrol-bound ER $\alpha$  in agonist conformation, where Helix 12 positions over the ligand binding pocket. Hence, the corresponding agonist resveratrol-ER $\alpha$  dimer becomes more stable than the monomer counterpart but remains less stable compared to the corresponding dimer in the antagonist conformation (Chakraborty et al., 2013). Azios et al., (2007) has also shown the antagonistic effect of resveratrol. Since certain breast cancer cell lines, for example MCF-7 cells, are ER positive, it is possible that resveratrol will have more of an effect on MCF-7 cells compared with an ER negative cell line such as MDA-MB-231. Another mechanism was discovered on how resveratrol exerts its effects. Patients at risk of developing breast cancer were treated with 5 or 50 mg resveratrol twice a day for several weeks. From this study, they discovered that resveratrol caused a reduction in methylation of the tumour-suppressor gene *RASSF1 $\alpha$* . Usually, hypermethylation occurs at CpG islands in the promoter region and is associated with gene inactivation (Gonzalo, 2010). In this case, this would be the inactivation of the tumour-suppressor gene *RASSF1 $\alpha$* . The effect of resveratrol results in reduced hypermethylation, which is directly caused by the decreased levels of the cancer-promoting prostaglandin E<sub>2</sub> (Zhu et al., 2012).

## 1.6.2 Resveratrol and MTs

MTs play a pivotal role in cellular functions such as cell growth, cell division, motility, and trafficking of vesicles and organelles (Hawkins et al., 2010, Etienne-Manneville, 2013, Wittmann et al., 2001). Therefore, MTs have been targets for diseases such as cancer.

MT-targeting agents (MTA) are groups of compounds known to have polymerising or depolymerising effects on MTs. Examples of such agents are nocodazole and colchicine, which cause MT depolymerisation while polymerising agents are paclitaxel and docetaxel. Paclitaxel has the ability to stabilise MTs in mitotic spindle cells and arrest mitosis in proliferating cancer cells (Waters et al., 1998). In an earlier study, it was discovered that the methylated derivatives of flavonoids present a greater anti-proliferative property on cancer cells than their hydroxylated counterparts (Kandaswami et al., 1991). Thereby different studies have tested this. A resveratrol analogue called *cis*-3,4,5-trimethoxy-3'-hydroxystilbene was discovered to reduce cell proliferation in breast cancer cells by inhibiting MT polymerisation *in vitro*. Computational analysis of 3,4,5-trimethoxy-3'-hydroxystilbene and tubulin interaction indicates that the dimethoxyphenyl group of 3,4,5-trimethoxy-3'-hydroxystilbene can bind to the colchicine binding site of tubulin (Hong et al., 2009). As far as resveratrol analogues are concerned, most literature show that the trimethoxy group is the most significant part as it integrates within the colchicine-binding hydrophobic pocket in tubulin thereby blocking MT dynamics (Hong et al., 2009, Scherzberg et al., 2015, Schneider et al., 2003, Traversi et al., 2017).

Another recent study supports the notion that the methylation of the hydroxyl groups is the critical part required for tubulin polymerisation interference. They showed the anti-proliferative activity of SS28 (a methoxy derivative of resveratrol) and SS28 treatment led to G2/M arrest in multiple cell lines including the B-cell lymphoma SUDHL8 and HEK293T as well as mouse tissues. Moreover, they discovered the mechanism of action of SS28, which showed that the compound interferes with tubulin polymerisation in a concentration dependent manner, alters mitotic spindle organisation and in turn leads to cellular arrest at metaphase. Consequently, the

treatment caused mitotic cell death by triggering apoptosis. Additionally, increased lipophilic properties of SS28 support its increased uptake through the cell membrane apart from targeting tubulin resulting in better bioavailability (Thomas et al., 2016). How stilbenes affect MTs and EBs is still relatively unknown. However, some reports suggest that EBs sensitise MTs to the action of some MTAs such as paclitaxel (Mohan et al., 2013). For example, paclitaxel caused no catastrophes in the absence of EB3. Conversely, in the presence of EB3, paclitaxel reacted in the opposite way i.e. a significant increase in catastrophe frequency was detected. Whether resveratrol will have any of these effects on MTs or EBs remains to be discovered.

## 1.7 Summary

MTs are part of the cytoskeleton that is involved in maintaining cellular structures. They are highly dynamic and involved in various processes including polarisation, cell division and migration. MT plus-ends are regulated by protein such as EBs, which influence their dynamics. These proteins influence dynamics at the plus-end as well as the MT lattice depending on their expression level. Relative changes in expression could potentially affect cancer cell migration.

It is known that EB1 overexpression promotes breast cancer cell proliferation thereby, enhancing tumour growth. Similarly, EB2 overexpression has been reported to increase perineural invasion of pancreatic cancer cells. MTs contribute to cell migration and invasion by regulating cell protrusion, transport of membrane vesicles to the leading edge, and facilitating cell adhesion. Cell adhesion requires the formation, maturation and disassembly of focal adhesions whereby MTs aid in the delivery of integrins, an important process during focal adhesions turnover. Studying cells in 2D gives a brief understanding of certain processes, however, cells are more complicated and are best studied in an *in vivo* environment hence, culturing cells in 3D. Lumen formation is a complex process that involves dynamic restructuring of the cytoskeleton. It is made possible by the midbody formation, centrosome positioning, polarity proteins and mitotic spindle orientation. During mitotic spindle orientation, astral MTs are important for correct lumen formation, which is essential for maintaining the positioning of cells within a tissue and thus, controlling the overall tissue architecture.

Due to all these, MTs have been targets for cancer therapy. Most anti-cancer treatments target MT instability and dynamics to regulate their roles in various cellular functions. One such treatment is resveratrol – a product found in grapes and peanuts that is reported to have chemo-preventive properties. It is thought that the main mechanism of resveratrol occurs through the trimethoxy group, which integrates within the colchicine-binding hydrophobic pocket in tubulin thus inhibiting MT dynamics. Resveratrol suppresses/inhibits cancer cell migration, proliferation and triggers apoptosis thus reducing the invasion and metastases of these cells.

This study aims to establish whether EB2-overexpression contributes to epithelial lumen formation. In particular, epithelial remodelling and the mechanisms involved. Furthermore, the study aims to determine whether MTs, actin, EB organisation and migration of epithelial breast cancer cells are affected by resveratrol.

## **1.8 Aims and Objectives**

Loss of epithelial polarity and progression to an invasive cancer state is known to contribute to patients' poor prognosis. The overall aim of the project was therefore to investigate the role of the EBs in epithelial remodelling and migration in order to better understand these processes in breast cancer cells. In addition, the aim was also to investigate the role of EBs on epithelial cell and tissue architecture.

The four main areas of investigation were to:

1. Investigate cytoskeletal organisation in the non-invasive and highly-invasive breast cancer cell lines; MCF-7 and MDA-MB-231 and particularly with regards to:
  - MT and actin organisation.
  - Localisation and expression levels of the EBs.
  - MT dynamics and stability including posttranslational modifications.
  
2. Investigate migration in MCF-7 and MDA-MB-231 and EB2 overexpressing MDCKII cells and particularly to:
  - Determine suitable ECM substrate for the migration studies.
  - Analyse migration rates.
  - Analyse EB2 expression and localisation in MDCKII and EB2 overexpressing cells.
  - Analyse whether EB2 overexpression affects centrosome positioning in 2D cells.
  
3. Investigate the effect of resveratrol on breast cancer cell models and specifically:
  - On MT, actin and EB organisation with particular focus on EB2.

- On MT dynamics and stability.
  - On the speed of migration and focal adhesions.
  - On migration in 3D spheroids.
4. Investigate the effect of EB2 overexpression on epithelial cell and tissue architecture and specifically:
- The effect of EB2 overexpression on 3D cyst formation.
  - The effect of EB2 overexpression on centrosome positioning and polarity.
  - The effect of EB2 overexpression on MT dynamic

# **Chapter II: Materials & Methods**

## 2.1 Model Systems

### 2.1.1 Cell Lines – Breast cancer and MDCK cells

The Michigan Cancer Foundation-7 (MCF-7) cell line is an epithelial breast cancer cell line derived from the pleural effusion of a 69-year-old Caucasian woman. The cell line was obtained from American type culture collection (ATCC). The MDA-MB-231 cell line is also an epithelial breast cancer cell line that was established from a pleural effusion of a 51-year-old Caucasian woman with a metastatic mammary adenocarcinoma. The MDA-MB-231 cell line was obtained from European collection of cell cultures (ECACC).

MDCK cells were originated from the kidney tissue of an adult female cocker spaniel in 1958. The cells were initially isolated for mammalian viral infection purposes. Lelio Orci and co-workers were the first to report the response of 3D MDCK cysts to hepatocyte growth factor (HGF). MDCK cells were co-cultured with 3T3 fibroblasts in collagen gels where the cells were not in direct contact but media could exchange. They discovered that the MDCK cysts went through branching morphogenesis in which cells rearranged into a network of interconnected tubules. It was later found that fibroblasts were able to secrete HGF causing the ‘scatter factor’ effect on MDCK cells. Therefore, a connection was made between the ‘scatter factor’ and its induction of 3D cyst reorganisation (Montesano et al., 1991, Weidner et al., 1991).

Although cell lines are a powerful tool for providing reproducible results, there are certain limitations associated with their use. Limitations to cell lines used in this project is that there is a potential of cell characteristics change, over time, which may be different from those found in the initial passages. *In vivo*, human cells interact with other cell types for functional processes, however, cultured cells are being studied outside this environment, which may be critical to the hypothesis being tested.

## 2.2 Cell Culture

### 2.2.1 Maintenance of cell lines

#### 2.2.1.1 Passaging cells

Both MCF-7 and MDA-MB-231 cell lines were cultured in Dulbecco's Modified Eagle's Medium (Invitrogen) supplemented with 10% (v/v) Foetal Bovine Serum (FBS), 1% L-glutamine (Life Technologies), 100 units/mL Penicillin (Life Technologies) and 0.1 mg/mL Streptomycin (Life Technologies). The cells were cultured in a humidified incubator at 37°C/95% air/5% CO<sub>2</sub>. The medium was replaced every other day. For passaging, cells were dissociated with pre-warmed Trypsin/EDTA (Invitrogen). Once detached, the cells were re-suspended in fresh media to neutralise the effect of trypsin. Cells were usually cultured in a T-75 cm<sup>2</sup> and split 1:3 or 1:4 for culture maintenance.

MDCKII cells - The aim is to generate a 3D *in vitro* model that closely mimic the *in vivo* microenvironment. The protocol used have been adapted from (Debnath et al., 2003). The cell lines were previously generated by a lab member, Jonathan Gadsby (details in the appendix B). They were cultured in Dulbecco's Modified Eagle's Medium (Invitrogen) supplemented with 10% (v/v) Foetal Bovine Serum (FBS), 1% L-glutamine (Life Technologies), 100 units/mL Penicillin (Life Technologies) and 1 mg/mL G418 (Sigma-Aldrich). The cells were cultured in a humidified incubator at 37°C/95% air/5% CO<sub>2</sub>. The medium was replaced every other day. For passaging, cells were dissociated with pre-warmed Trypsin/EDTA (Invitrogen). Once detached, the cells were re-suspended in fresh media to neutralise the effect of trypsin. Cells were usually cultured in a T-75 cm<sup>2</sup> and split 1:20 or 1:25 for culture maintenance.

#### 2.2.1.2 Freezing cells

Cells in low passage were stocked in a liquid nitrogen dewar to avoid potential phenotypic changes associated with high passage numbers. To freeze cells, the centrifuged pellet was resuspended in appropriate medium with 10% dimethylsulphoxide (DMSO) to act as a cryopreservant. The resuspended cells were

aliquoted into several cryovials (Corning, Amsterdam, Netherlands) and immediately transferred to a Mr Frosty™ containing isopropanol before being frozen at -80°C. after 24 h, cryovials were placed in liquid nitrogen dewars. To bring up cells from frozen, the cryovials were quickly warmed in a 37°C water bath, after which the cells were immediately transferred to a sterile Falcon tube containing 9 mL of pre-warmed medium and centrifuged for 5 min at 1000 rcf to remove the DMSO. The supernatant was discarded and cell pellet resuspended in 5 ml of medium before being transferred into a T-25cm<sup>2</sup> culture flask. The medium in these flasks were changed every other day until the cells reached 80% confluency. After this level, they were passaged as mentioned in section 2.2.1.1.

## **2.2.2 3D Cyst Culture**

MDCKII cells were maintained and detached as mentioned in the previous section. Matrigel (BD Biosciences) was placed on ice overnight at 4°C. Sterile p200 pipette tips were placed in the freezer overnight to allow easy handling of the Matrigel the next day. MDCKII mCherry empty-vector and EB2-overexpressing cells were grown for the generation of 3D cysts. Matrigel at 2.5% was mixed with 1 mg/mL Collagen I diluted in DMEM and added to relevant wells before placing at 37°C for polymerisation or in some cases, only Matrigel at 2.5% was added to the wells before placing in an incubator for polymerisation. MDCKII cells were trypsinised and counted before embedding 5,000 cells in Matrigel and added to each well. After polymerisation of the Matrigel, 1 mL medium supplemented with 1 mg/mL of G418 is added to the top before placing back into the incubator. Cells are monitored daily under the microscope with medium changed every other day supplemented with 1 mg/mL of G418. Phase-contrast images were taken at various days. Cells were fixed and labelled at relevant timepoints before visualising using a confocal microscope.

## **2.3 Drug Treatments**

### **2.3.1 Double thymidine block**

Double thymidine block was used to synchronise cells, such that after thymidine

is washed out at a certain timepoint, a significant proportion of cells would simultaneously undergo mitosis. Thymidine arrest cells in the G1/S border preventing progression beyond the S phase, and to increase synchronisation, cells were blocked twice. The cells were treated with an initial thymidine block for 17 h, followed by a wash out then a 9 h passage through the cell cycle. After this, the cells were treated with thymidine for a second time for 17 h. After the second 17h time-point, thymidine was finally washed out from the cells. Cells were grown to 50% confluency on coverslips and treated with 2 mM thymidine (Sigma, Poole, Dorset) then incubated at 37°C for 17 h. After drug removal, cells were washed three times in pre-warmed medium and returned to the 37°C incubator for 9 h. This releases the cells from the block. A second 2 mM thymidine was added for a further 17 h. Cells were again released from the block by washing three times in pre-warmed medium, and allowed to go through the cell cycle in the 37°C incubator. For optimisation of time-points, cells were fixed and processed for immunolabelling at several time points after release from the second block, to determine the best time-point at which most spindles were observed.

### **2.3.2 Resveratrol**

Resveratrol (Sigma-Aldrich) was stored as a stock of 200 mM in DMSO at -20°C. Breast cancer cells were treated with varying concentrations – 2.5, 5, 10, 20, 50 and 75 µM and DMSO at a concentration of 0.038%. A MTT assay found no effect of DMSO on the cells. The cells were incubated for 24 h at 37°C and 5% CO<sub>2</sub>. This procedure was used to investigate resveratrol's effect on several experiments such as MTT assay, Western blot, cell migration and immunolabelling – all described in this chapter.

### **2.3.3 Taxol**

Taxol (Sigma-Aldrich) was stored as a stock of 10 mM in DMSO at -20°C. Stable MDCKII cells were treated with concentrations of 50 and 100 nM and DMSO at a concentration 0.001%, which is the same as the highest concentration of Taxol used (100nM). The cells were incubated for 9 h at 37°C and 5% CO<sub>2</sub>. This procedure was used to investigate Taxol's effect on spindle orientation.

## 2.4 Cell Viability Assay (MTT Assay)

The toxicity of resveratrol and cell survival was determined by MTT assay. The MTT assay is based on the cleavage of yellow dye to purple formazan crystals by intracellular NAD(P)H-oxidoreductases (based on the reduction of yellow tetrazole to purple formazan in living cells). Cells were seeded in a 96-well plate at densities of  $1 \times 10^4$  cells per well, grown overnight and treated with different concentrations of resveratrol for 24 h. 10 $\mu$ l of the MTT reagent was added in each well then incubated for 4h. 100 $\mu$ l of crystal dissolving solution was added to each well and the cellular homogenate was measured at 570nm on a spectrophotometer. Cell viability values were expressed in terms of absorbance and as means  $\pm$  SEM.

## 2.5 Immunolabelling of 2D and 3D cultures

### 2.5.1 Fixatives

#### 2.5.1.1 Methanol

Glass coverslips were coated with collagen I for 2 h at room temperature. Cells were seeded on collagen-coated glass coverslips at the relevant seeding density and incubated overnight at 37°C/95% air/5% CO<sub>2</sub> in a moist atmosphere. Cells were fixed with cold methanol at -20°C for 5 min in -20°C freezer, washed with 1% PBS goat-serum (Sigma-Aldrich) then blocked with 10% PBS goat-serum for 30 min. Cells were incubated with the appropriate primary antibodies (details in **Table 1a**). Primary antibodies were diluted in 1% PBS Goat-serum and cells were incubated for 1 h, washed followed by the secondary antibody incubation for 30 min (details in **Table 1b**). The cells were washed with 1% PBS Goat-serum, stained with DAPI then coverslips were mounted on microscope slides using hydromount mounting medium (National Diagnostics) (supplemented with 2.5% w/v DABCO). DABCO was added to prevent photobleaching of fluorophores. The slides were stored at 4°C and later visualised with the widefield microscope. All primary antibodies were raised in either rat, mouse or rabbit. Where antibodies of anti-rat and anti-mouse species were to be diluted together, a sequential staining procedure was followed. Methanol fixative has the advantage of quickly dehydrating the cells as well as removing lipids from the membrane of the cells.

For centrin antibody staining, the protocol is slightly different – once cells have been seeded and adhered for 24h, they are fixed in cold methanol for 5 min in a -20°C freezer then washed with 1% PBS goat-serum. The cells are then blocked with 15% PBS goat-serum for 30 min before incubating with centrin at 1:500 for 1h. The rest of the protocol is the same as the one described above.

For 3D cysts, the same procedure was followed though the fixation time was increased to about 30min-1h in a -20°C freezer. Cells were washed in 1% goat serum PBS every 20 min for 2h as mentioned above. After fixation, cells were blocked in 10% goat serum PBS for 1h at room temperature. Primary antibodies diluted in 1% goat serum PBS were added at 200 µL to cells as outlined in **Table 1a**. Cells were then incubated at 4°C overnight. Cells were washed in 1% goat serum PBS every 20 min for 2h then incubated in secondary antibodies. Secondary antibodies were prepared similarly to the primary antibodies, and incubated in the dark for 1h at room temperature. Cells were washed for 90 min, changing the wash every 30 min and then transferred into DAPI (1:10000, in PBS) for 10 minutes. Cells were washed in PBS a further five times over a 30 min time period, and then mounted onto slides by inverting each coverslip onto a drop of hydromount containing 2.5% (w/v) DABCO.

List of primary and secondary antibodies used are listed in **Tables 1a and 1b**.

### **2.5.1.2 Methanol-Formaldehyde**

Formaldehyde is great at cross-linking proteins and methanol is added to stabilise the aqueous formaldehyde. Stabilisation is important to prevent oxidation of the formaldehyde to formic acid and its eventual repolymerisation to paraformaldehyde. Cells were fixed in formaldehyde-methanol at -20°C for about 1h. before washing in 1% goat serum PBS containing 0.1% Triton X-100 every 20 min for 2h. After washing, cells were blocked in 10% goat serum in PBS containing 0.1% Triton X-100 for 1h at room temperature. Primary antibodies diluted in PBS with 1% goat serum were added at 200 µL to cells as outlined in Table 1a. Cells were then incubated at 4°C overnight. Cells were washed in PBS with 1% goat serum every 20 min for 2h then incubated in secondary antibodies. Secondary antibodies were prepared similarly to the primary antibodies, and incubated in the dark for 1h at room temperature. Cells were washed

for 90 min, changing the wash every 30 min and then transferred to DAPI (1:10000, in PBS) for 10 minutes. Cells were washed in PBS a further five times over a 30 min time period, and then mounted onto slides by inverting each coverslip onto a drop of hydromount containing 2.5% (w/v) DABCO.

### **2.5.1.3 PHEMO Fixation**

Some experiments were carried out using the PHEMO fixative method as it helps to reduce autofluorescence during imaging, and is great for preserving the cytoskeletal structure of cells. Cells were prepared as mentioned in the section above. PHEMO fix (3.7% Paraformaldehyde, 0.05% Glutaraldehyde and 0.5% Triton X100) was prepared in PHEMO buffer (68mM PIPES, 25mM HEPES, 15mM EGTA and 3mM Magnesium chloride). Cells were fixed in the PHEMO fix at 37°C for 10 min and for 1h in 3D cysts and washed twice with PHEMO buffer solution at 37°C for 10 min. The cells were then rinsed with PBS for 5 min at room temperature and finally, blocked in 10% goat-serum for 30 min before following the rest of the procedure outlined above.

<u>1°Antibody</u>	<u>Species</u>	<u>Dilution</u>	<u>Supplier</u>
EB1	Mouse	IF 1:500 WB: 1:500	BD Biosciences (610535)
EB2 K52	Rat	IF: 1:200 WB: 1:100	Abcam (ab45767)
EB3 KT36	Rat	IF: 1:200 WB: 1:100	Absea (010314H04)
$\alpha$ -tubulin	Rabbit	IF: 1:150 WB: 1:100	Abcam (ab15246)
Tyrosinated tubulin YL1/2	Rat	1:150	Abcam (ab11316)
Acetylated tubulin	Mouse	IF: 1:100 WB: 1:500	Sigma (T6793)
Detyrosinated tubulin	Rabbit	IF: 1:200, WB: 1:500	Abcam (ab48389)
$\gamma$ -tubulin	Rabbit	1:500	Abcam (ab16504)
$\gamma$ -tubulin	Mouse	1:500	Abcam (ab11316)
$\beta$ -actin	Rabbit	IF: 1:1000 WB: 1:10000	Abcam (ab8227)
$\beta$ -catenin	Mouse	1:500	BD Biosciences
E-cadherin	Mouse	1:200	BD Biosciences (610181)
ZO-1	Rabbit	1:200	Thermo Fisher (61-7300)
Par-3	Rabbit	1:200	Millipore (07-33D)
RFP	Rabbit	WB: 1:1000	Abcam (ab62341)
NuMA	Rabbit	1:100	Abcam (Ab86129)
Cep215	Rabbit	1:1000	Millipore (06-1398)
FAK	Rabbit	1:200	Cell signalling (8556)
Centrin	Mouse	1:500	Millipore (04-1624)

**Table 1a:** Primary antibodies used

<u>2° Antibody</u>	<u>Species</u>	<u>Dilution</u>	<u>Supplier</u>			
Alexa 488	Anti-RAT IgG	1:1000	Invitrogen Molecular (Paisley Scotland)			
	Anti-Rabbit IgG					
	Anti-Mouse IgG					
Alexa 568	Anti-RAT IgG		1:1000	Invitrogen Molecular (Paisley Scotland)		
	Anti-Rabbit IgG					
	Anti-Mouse IgG					
Alexa 647	Anti-RAT IgG			1:1000	Invitrogen Molecular (Paisley Scotland)	
	Anti-Rabbit IgG					
Cy5	Anti-Mouse IgG				1:1000	Jackson (Stratech, Newmarket, Suffolk)
DAPI		1:10000				Sigma-Aldrich
HRP-conjugated	Goat anti-MOUSE IgG	1:10000				Sigma-Aldrich
	Goat anti-RABBIT IgG					
	Goat anti-RAT IgG					
IRDye 800CW	Anti-MOUSE	1:50000	Jackson			
IRDye 680RD	Anti-RABBIT	1:50000	Jackson			
Note: All secondary antibodies were raised in goat						

**Table 1b:** Secondary antibodies used

## 2.6 Microscopy

### 2.6.1 Widefield fluorescence microscope

Cells fixed on glass coverslips were analysed using a widefield upright Zeiss Axiovert 200M microscope. Images were taken using a monochrome CCD camera. Fluorescence was detected using a 100W mercury lamp and dichroic mirror filter sets. Axiovision software (Zeiss) was used to generate multichannel images and Adobe Photoshop, CS6, was used to process the images.

### 2.6.2 Confocal

Data were acquired via Zeiss LSM Software using a Zeiss LSM510 confocal microscope. Images were collected using a 63x oil objective. Specific lasers and filters were used to visualise different fluorescent dyes as outlined in **Table 2**.

Fluorophore	Laser	Excitation (nm)
DAPI	UV	364
AlexaFluor®-488	Argon	488
AlexaFluor®-647	Helium/Neon	633

**Table 2:** Lasers and filters used to visualise fluorescently stained cellular components.

### 2.6.3 Live Imaging

Cells were seeded at 10,000 cells/well in a collagen I-coated 24-well plate and incubated at 37°C/95% air/5% CO<sub>2</sub> for 24 h in order for the cells to adhere. If the effect of a compound, for example, resveratrol was been monitored then it was added after 24h of seeding the cells and then incubated for 8h before setting up on the microscope.

Otherwise, after 24h of cell seeding, the plate was placed on a heated stage in a sealed chamber containing 37°C/95% air/5% CO<sub>2</sub> of a Zeiss Axiovert inverted microscope. The cells were left for at least 30 min in order for the cells to adapt to the environment. The experiment was set up so that the cells were tracked for 16 h with images taken every 10 min using a x10 objective. For each experimental condition, two positions were set up per well. Phase-contrast images were captured during this period from the pre-programmed positions. Data generated were analysed using Axiovision and analysed on ImageJ using the manual tracking macro.

## **2.7 Migration**

### **2.7.1 Random cell migration**

Cells were seeded at 10,000 cells/well of a 24-well plate and incubated at 37°C/95% air/5% CO<sub>2</sub> for 24 h in order for the cells to adhere. The following day, the plate was placed on a heated stage in a sealed chamber containing 37°C/95% air/5% CO<sub>2</sub> of a Zeiss Axiovert inverted microscope. The cells were left for at least 30 min in order for the cells to adapt to the environment. The experiment was set up so that the cells were tracked for 16 h with images taken every 10 min using a x10 objective. For each experimental condition, two positions were set up per well. Phase-contrast images were captured during this period from the pre-programmed positions. Data generated were imaged using Axiovision and analysed on ImageJ using the manual tracking macro. An 8 by 6 rectangular grid was drawn on an A4 paper then five random asterisks were marked, and any cell that fell into the boxes asterisked were tracked over the 16 h time-period.

Chemotaxis and migration tool from Ibidi was used to generate the spider graph. The first five columns from the tracking data (.xls) is copied into a new file and saved in a 'Tab delimited' format. The software is then calibrated by setting the number of slices (97), x/y calibration (0.167 µm) and time interval (10 min). The x/y calibration represents the edge length of a pixel in µm while the time interval represents the time between each slice. Next, click on 'Apply settings' and 'Plot data' then export the data.

### 2.7.1 Wound healing assay

Cells for each condition were seeded into 24-well plate wells and allowed to adhere overnight. Using a P200 pipette tip, a scratch was made to the cells in each well. A time-lapse microscope was used to image regions of each scratch every 2 h over a 6/8 h period and then a 24 h period. The area of scratch at the start and the relevant time periods were measured for each region using ImageJ and used in calculating the average area of closure for each condition. Analysis and graph preparation was performed in Graphpad Prism.

### 2.7.3 Micropattern Coverslips

MDCKII<sup>mChEmpty</sup> and MDCKII<sup>mChEB2Hi</sup> cells were cultured on micropatterned CYTOOchips obtained from CYTOO, Inc. The pattern of the chips was cross-bow of a 1100  $\mu\text{m}^2$  size. Chips were coated with collagen I before seeding cells on top. Collagen I solution was diluted at the recommended 2x (40ug/mL) protein in the relevant buffer. Tweezers were used to transfer the chips to a sterile 6-well plate with the writings facing upwards. Then 2ml of PBS alone was added to the chip making sure it is completely covered. This ensures the surface of the chip is completely wet. 2ml of the previously prepared collagen solution was added to the chip and incubated for 2 h at room temperature. After the time point, the chips were washed three times in PBS. This was carried out by adding fresh 2mL PBS buffer to the chip in collagen solution then removing the same volume. Importantly, the surface of the chip must not dry out during the washing steps.

Cells were collected by trypsinisation (to which an extra 2mM EDTA was added to make a final concentration of EDTA is 3 mM). EDTA is added to prevent cell clumping. Cells were resuspended to 15,000cells/mL. 60,000 cells (4mL) were added to each well ensuring that the plate was not disturbed otherwise cells will aggregate at the centre. Cells were allowed to adhere to the surface for 10 min under the hood before moving to the incubator. Once the cells had adhered (15-30min) the medium was changed to remove any floating cells. This was carried out by following the next steps:

Gently aspirating the medium from the side of the well using a pipette ensuring the plate is flat. Next, 4ml of PBS was added and aspirated again, this time starting from the centre of the chip and working towards the edge of the well. The procedure was repeated 3-4 times. Check under the microscope for floating cells. If any, repeat the washing procedure. The dish was placed in a 37°C incubator for at least 1 h to achieve full spreading. The procedure is considered successful, if approximately 10-30% of the micro-pattern is covered by single cells. Cells were fixed and immunolabelled 6-8 h after seeding because the cells would not have gone through the first round of division.

## 2.8 Spheroid Production

Cells were trypsinised and counted. 25,000 cells/150 µl of medium containing methyl cellulose was added to a round bottom 96-well plate. Cells were placed in a 37°C and 5% CO<sub>2</sub> incubator for 48 hours for spheroid formation. Using the widened pipette tips, gently remove the spheroids and place in a 1.5ml Eppendorf tube. Spheroids were washed twice in 1ml serum-free media, spinning after each wash at 13rpm (0.2 rcf in cold room) for 5 mins. Carefully resuspend spheroid in 70µl Matrigel then spread over coverslip using a widened pipette tip. Matrigel was allowed to set at 37°C for 1-2 h before adding 500 µl of the relevant media containing different concentrations of resveratrol or DMSO and incubated at 37°C. Spheroids were monitored daily for invasion for a few days (depending on migration rate).

## 2.9 Plasmid Transfection

Transformation of plasmids was carried out in the DH5α *Escherichia coli* cells. The DH5α cells were defrosted on ice for approximately 20 min, and then 1µl of plasmid (20µg/ml) was added to 50µl of DH5α cells and left on ice for another 15 min. The cells were heat-shocked for 2 min at 42°C and placed back on ice for another 1 min. Sterile growth medium for bacteria, Lysogeny Broth (500µls) was added to the cells and incubated for 1 h at 37°C under gentle agitation. Then, cells were spread onto agar and sealed with a lid, before incubating at 37°C overnight. The following day, a medium sized colony was picked from the agar plates and placed into 10 ml of LB

starter culture containing ampicillin (100 µg/ml) and incubated for 6-8 h at 37°C under gentle agitation. Two ml of the cells was placed in 250 ml of LB containing ampicillin (100 µg/ml) and placed at 37°C under gentle agitation overnight. Cells were harvested by centrifugation at 6000xg for 15 minutes at 4°C. The constructs were then isolated and purified from the *E.coli* cells using a high-speed midi kit (Macherey-Nagel), according to manufacturer's instructions and detailed below.

### **2.9.1 Midi-prep**

Midi preps were performed using the Plasmid Midi kit (Macherey-Nagel). Pellets were resuspended in 8ml of buffer RES containing RNase A then resuspended up and down before adding 8ml of buffer LYS for 5 min at room temperature. 12ml buffer EQU was used to equilibrate the column and allowed to run dry. Buffer NEU (8ml) was added to the suspension and inverted till the sample turns colourless from blue. Once a homogenous solution has been achieved, the suspension is added to the column. Buffer EQU is used to wash the column twice – one with 5ml and the other with 8ml. The plasmid DNA was eluted with buffer ELU and collected in a 50ml Falcon tube. Isopropanol is used for precipitating the eluted DNA then adding ethanol (70%) to wash the pellet. Once the pellet has air-dried, it is reconstituted in buffer TE. DNA concentration was analysed by Nanodrop (LabTech, East Sussex) and sample stored at -20°C.

## **2.10 Western Blotting**

### **2.10.1 Cell lysis**

Cell lysis buffer (see appendix for details) was prepared using Protease and Phosphatase Inhibitors, and PBS. Cells were lysed on ice to prevent protein degradation. Medium was aspirated from the plate and the wells were washed with PBS. Lysis buffer was added to each well and detached with a cell scraper (Greiner Bio-One). Supernatants were collected in fresh microfuge tubes after centrifugation at 13000 g for 10 min at 4°C. The tubes were stored at -20°C until required.

### **2.10.1.1 Protein quantification**

Protein concentrations were determined using a BCA assay (Pierce) protein kit. This is based on preparing several bovine serum albumin (BSA) standards ranging from 0-2000 $\mu$ g/ml in concentration, diluted in ddH<sub>2</sub>O. 50 $\mu$ l ddH<sub>2</sub>O, 10 $\mu$ l of each protein standard and each sample to be analysed were added to a 96-well plate in triplicates. Next, 200 $\mu$ l of the protein assay reagent (reagent A: reagent B, 50:1) was added to each well and the plate incubated for 45 min at 37°C. Absorbance readings at 550nm were measured using a spectrophotometer and the BSA values were used to generate a standard curve, from which the protein concentrations of the cell lysates were estimated.

### **2.10.2 SDS-PAGE electrophoresis**

Concentrations of the cell lysates were determined using the BCA assay and then run on SDS-PAGE. For each sample, 20 $\mu$ g of protein content (diluted in ddH<sub>2</sub>O) and 10 $\mu$ l of 5X sample buffer (Appendix A) containing 12.5%  $\beta$ -mercaptoethanol were added, and the tubes heated at 95°C in a heat block for 1 min. Gels were made between spaced glass plates by adding a 8-10% lower resolving gel (Appendix A) and left to set for approximately 20 min. Once the upper gel was added to the set lower gel, a spacing comb is added and allowed to set. These gels were transferred to a Mini Protean II tank (BioRad, Hemel Hempstead, Hertfordshire), which was filled with 1X SDS running buffer, diluted in dH<sub>2</sub>O from a 10X stock (Appendix A). The prepared samples and protein ladder (Thermo Fisher) were loaded into separate wells of the gel. The electrophoresis was performed using 30mA per gel until the sample buffer had migrated towards the bottom of the gel, taking approximately 35-45 min.

#### **2.10.2.1 Protein transfer**

After electrophoresis was completed, the proteins were transferred to a nitrocellulose transfer membrane (BioRad) by using a nitrocellulose transfer membrane and two sheets of thick blot paper. Proteins were transferred using the semi-dry transfer system (BioRad). In the transfer stage the sheets, gel and membrane were assembled as follows: thick blot paper at the bottom, the nitrocellulose membrane, the gel, and thick blot paper on the top. The sandwich created was rolled out to press out any bubbles,

which may hinder efficient protein transfer. Proteins from the gel were transferred to the nitrocellulose membrane at 15V for 35 min. The membrane was blocked with 0.5% (w/v) skimmed milk powder diluted in 1X PBS-T (i.e. PBS containing 0.5% milk powder and 0.05% Tween-20) buffer on a rocker overnight at 4°C.

## **2.10.3 Protein detection**

### **2.10.3.1 Antibody probing**

Primary antibodies directed against the appropriate proteins or  $\beta$ -actin (used as a loading control) were diluted in PBS-T + 0.5% (w/v) skimmed milk powder and used to probe the membrane, which was placed on a rocker for 1 h at room temperature or overnight at 4°C. Dilutions used are listed in **Table 1a**. All secondary antibodies are linked to the enzyme horseradish-peroxidase (HRP) (**Table 1b**). The membrane was washed and then incubated with secondary antibodies (Sigma) for 1 h at room temperature.

### **2.10.3.2 Immunodetection (Odyssey)**

Both the protein of interest and the loading control were detected at the same time without the need for stripping the membrane. This method depends on fluorescent detection using secondary antibodies labelled with infrared fluorescent dyes instead of HRP-conjugated enzymes, and on multiplex detection of multiple protein targets. The protocol for the Odyssey is the same as the one described in sections 1.10.1 and 1.10.2 until the primary antibody incubation, which is described below.

Primary antibodies were diluted in 1ml of PBS-T and 0.5% milk powder and added to the membrane and incubated for 1 h at room temperature or overnight at 4°C. After the 1<sup>st</sup> primary antibody incubation, the membrane is washed quickly three times with 0.5% PBS-T then incubated with the second primary antibody, usually the loading control. After both primary antibodies were incubated, the membrane was washed three times for 5 min with 0.5% PBS-T. Secondary antibodies (IRDye 800 or IRDye 680) were used and diluted in 10 ml of 0.5% PBS-T and 0.1% SDS, then added to the membrane for 1 h in the dark on a rocker at room temperature. Then, the membrane

washed with 0.05% PBS-T for 5 min, with a final wash of PBS alone. Finally, digital imaging was obtained by using an Odyssey scanner, with the membrane placed on the bottom left-hand side of the grid. The scanner revealed target protein signals with high sensitivity.

### 2.10.3.3 Re-probing

For detection of the loading control when the ECL developing method was used, membranes were stripped using the Re-blot solution (Merck Millipore) at a 1:10 dilution. The re-blot solution was added to the membrane and placed on a rocker for 10 min then washed with PBS-T three times every 5 min. Then the membrane was blocked with 0.5% (w/v) skimmed milk powder diluted in 1X PBS-T buffer twice for 5 min before adding the appropriate antibody. The membrane was placed on a rocker overnight at 4°C. The antibody detection step was repeated. Exposure time used was varied in order to acquire a sufficient signal.

## 2.11 Spindle Orientation Assay and Analysis

Coverslips were thinly coated with 1 mg/ml Matrigel and placed in a 37°C incubator for 30 min. Cells were trypsinised, counted, seeded onto the coated coverslips and left to adhere in a 37°C incubator overnight. To increase the number of mitotic cells, cells were synchronised twice using thymidine. Cells were fixed and immunolabelled for  $\alpha$ -tubulin and  $\gamma$ -tubulin. The confocal microscope was used to take z-stack images. Spindle orientation was analysed during metaphase.

Confocal microscopy optical sections through the entire spindle were taken at 0.2  $\mu\text{m}$  intervals. Volocity software was used for processing images ‘Tools – Contrast enhancement – Enhance’. The software was also used for obtaining the distance (D) between the centre of each spindle pole and the height of the poles. For calculating the difference in height between the poles, the measurement setting was utilised i.e. ‘Find objects – Exclude object by size – Measure – Centroid’. Spindle orientation angle in respect to the substratum in these cells were calculated. The angle  $C = \text{Sin}^{-1}$

(opposite/hypotenuse). Graphpad software was used to prepare graphs and perform statistical analysis.

## 2.12 Cold Treatment

Cells were incubated with cold medium and placed on ice for 10 min. medium was removed and cells were fixed with methanol at -20°C for 5 min, followed by three quick washes in 1% goat serum in PBS. Then, cells were immunolabelled as described previously with primary anti  $\alpha$ -tubulin and anti-EB1.

## 2.13 EB1 Comet Analysis

The EB1 comet shape was analysed by measuring the circularity of EB1 at MTs plus-end. Macron for comet analysis was applied in ImageJ. Axiovision images (14-bit; i.e., intensity values range from 0 to 16,383) were opened and analysed with ImageJ (Rasband, 1997). Background subtraction (Castle and Keller, 2007) was carried out using a rolling-ball of radius 10 pixels and the images thresholded using the algorithm of Otsu (Otsu, 1979). After background subtraction and thresholding, the circularity of objects was measured. Objects smaller than  $0.12 \mu\text{m}^2$  (i.e.,  $<12 \text{ pixels}^2$ ) and larger than  $3 \mu\text{m}^2$  (i.e.,  $>300 \text{ pixels}^2$ ) were ignored. This comet analysis code was written by Paul Thomas (Henry Wellcome Laboratory for Cell Imaging, UEA).

## 2.14 Microtubule Acetylation Analysis

To measure the extent of microtubule acetylation in fixed untreated cells, DMSO and resveratrol-treated cells. MTs were visualised with rabbit anti- $\alpha$ -tubulin primary (1:150) while acetylated MTs were visualised with mouse anti- $\alpha$ -acetylated tubulin primary antibody (1:100). The extent of MT acetylation was analysed with ImageJ. The fluorescence intensity of acetylated MTs in at least ten interphase cells per condition was analysed. The total area of acetylated tubulin divided by the area of total tubulin was used in calculating the percentage of acetylated MTs area. To do this, images were exported in two different channels and saved, one for  $\alpha$ -tubulin and the other for acetylated tubulin with grey scale (not merged image). Channel properties were

changed with length unit micron and pixel width and height to 0.102 micron when a x63 obj lens was used. To prepare for analysis the image background was subtracted and pixels in radius unit adjusted until a satisfactory image was obtained. Data were then saved to an Excel file. Finally, to determine the area of acetylated tubulin as a proportion of the total tubulin, the total area of acetylated tubulin was divided by the total area of tubulin and multiplied by 100 to give a percentage value.

## 2.15 Centrosome Positioning – Two-cell stage

Images for centrosome positioning were taken on the confocal microscope. Quantification of centrosome positioning were carried out using ImageJ. Channels for Par-3 and  $\gamma$ -tub staining were merged to generate one image. Images were processed by increasing/decreasing the brightness, removing the background and then thresholded. Next, using the ‘Analyse – Set measurements’ setting the ‘Centroid’ was calculated and redirected to the original image. The centroid values obtained were marked on the image and added to the ROI manager. Then a line was drawn from each centrosome to the centroid. The ‘ROI manager – More – Multi measure’ setting was used to calculate the distance of each centrosome from the AMIS. Finally, Graphpad software was used to prepare graphs and perform statistical analysis.

## 2.16 Centriole amplification

To count the number of centrioles per cell in all three sub-cell lines – MDCKII, MDCKII<sup>mChEmpty</sup> and MDCKII<sup>mChEB2Hi</sup> – images acquired were analysed on ImageJ. Initially, the DAPI channel was removed to allow for better analysis. Then, images containing the centriole and peripheral staining were further processed by increasing/decreasing the brightness and then removing the background. With the resulting image, the ‘Cell counter’ Plugin on ImageJ was launched. Once the ‘Cell counter’ was initialised, the centrioles within each cell was marked. This was repeated for all images and results exported. The percentage of cells with more than 4 centrioles was plotted for MDCKII<sup>mChEB2Hi</sup> cells and then compared with MDCKII<sup>mChEmpty</sup> cells.

## 2.17 Centrosome Positioning Analysis

Scaled, 3-channel, Axiovision images (14-bit; *i.e.*, intensity values range from 0 to 16,383) were opened and analysed with ImageJ (Rasband, 1997-2016). The images were split into individual channels: “Nucleus” (DAPI staining), “Cell” ( $\alpha$ -tubulin staining) and “Centrosome” ( $\gamma$ -tubulin staining).

The “Nucleus” image was thresholded using the algorithm “Triangle” (Zack et al., 1977). After thresholding, objects  $>100 \mu\text{m}^2$  were segmented and their centroids located and recorded. A similar procedure was carried out with the “Cell” image using the same threshold algorithm and the same size exclusion. For the “Centrosome” image, the procedure was the same except that the “MaxEntropy” algorithm (Kapur, 1985) was used for thresholding and the object size was limited to between  $0.2 \mu\text{m}^2$  and  $3 \mu\text{m}^2$ . Following the location of the centroids of the three objects, the *makeLine()* function of ImageJ was used to draw two lines, one between the centroid of the Nucleus and the centroid of the Centrosome the other between the centroid of the Cell and the centroid of the Centrosome. The length and angle of each line was measured and saved.

Polar plots were generated in Matlab (R2016b) using the *polarhistogram(theta, n)* command where *n* is the number of measurements and *theta* is defined by the command line: *theta = [x.x y.y z.z etc...]* placed before the *polarhistogram()* command, where *x.x*, *y.y*, *z.z...* are the line angles. Before entering into Matlab, negative angles were made positive by the addition of  $360^\circ$ , and all angles converted from degrees to radians. **Macro “Centrosome position analysis” written by Paul Thomas (Henry Wellcome Laboratory for Cell Imaging, UEA).**

## 2.18 Analysis of CLIP-170 Comet Dynamics

To assess the difference on MT dynamics, GFP-CLIP-170 comets were analysed in MCF-7 and MDA-MB-231 cells, and MDCKII<sup>mChEmpty</sup> and MDCKII<sup>mChEB2Hi</sup> cells. Cells were grown in glass-bottomed dishes and incubated overnight. Cells were transfected with  $2 \mu\text{g}$  GFP-CLIP-170 construct using jetPrime (Polypus) for 4 h, then washed with fresh medium. Cells demonstrating GFP-CLIP-170 in MTs were imaged

using live time-lapse fluorescence microscopy for a total of 2.5 min at 3 sec intervals. The live time-lapse recordings were analysed using the automated tracking software U-Track, originally packaged as 'plusTipTracker' (Applegate et al., 2011). This enabled GFP-CLIP-170 comet paths to be obtained. Next, Matlab was used to conduct all post-tracking analysis and the MT plus-tip tracking package code was written in this program. A series of TIFF files, one for each frame of the recordings were used for the plus-tip tracking to analyse dynamics of the MTs as described by Applegate and colleagues (2011). Importantly, it must be noted that stable MTs cannot be identified using this method.

## **2.19 Statistical Analysis**

GraphPad Prism software was used in the preparation of graphs and statistical analyses. Two tailed unpaired tests were used to compare the statistical significances between two groups. For experiments with multiple groups, one-way or two-way ANOVA were performed using Tukey's multiple comparisons test to assess the significance of any differences between two separate groups within the data set. Differences were regarded as significant when  $p < 0.05$ .

**Chapter III:  
Characterisation of MT  
Organisation and  
Dynamics in Breast  
Cancer Cell Models**

## **3.1 Overview**

This chapter characterises two of the model cell lines used in this project. One of the aims of this project was to investigate the role of the MT end-binding proteins (EBs) in epithelial remodelling and migration to better understand the processes leading to an invasive breast cancer state. To achieve this target, it is important first to characterise the two breast cancer cell models, the highly invasive MDA-MB-231 and the non-invasive MCF-7 cell lines. MT reorganisation is an essential process in cell remodelling and tumour metastasis and it is predicted that the expression and localisation of the EBs differ in these two breast cancer cell lines and that this is linked to their differences in invasiveness.

## **3.2 Introduction**

Breast cancer is a complex and heterogeneous disease. To understand more about the complex process, two breast cancer cell lines were used as models. The Michigan Cancer Foundation-7 (MCF-7) cell line is an epithelial breast cancer cell line derived from the pleural effusion of a 69-year-old Caucasian woman in 1970 (Levenson and Jordan, 1997). The non-invasive MCF-7 breast cancer cell line is oestrogen and progesterone receptor positive therefore, have a proliferative response to oestrogens (Horwitz et al., 1975, Lippman et al., 1976). The MDA-MB-231 cell line is also an epithelial breast cancer cell line that was established from a pleural effusion of a 51-year-old Caucasian woman with a metastatic mammary adenocarcinoma. MDA-MB-231 cells are highly aggressive, invasive and a poorly differentiated cell line. It is a triple-negative cancer cell line because it lacks the expression of oestrogen and progesterone receptor, and the human epidermal growth factor receptor 2 (Chavez et al., 2010). MDA-MB-231 cells are claudin-low and also associated with mammary cancer stem markers such as the CD44<sup>+</sup>CD24<sup>-</sup> (Holliday and Speirs, 2011). MDA-MB-231 cells have a mutant p53 (Olivier et al., 2002), which is linked to increased invasion and migratory activities (Muller et al., 2013, Muller and Vousden, 2014) whereas MCF-7 cells have a wild-type p53 (Lu et al., 2001).

Cell migration is important for normal physiological functions such as wound healing, tissue renewal and immune responses. This process is mediated by actin and

MT reorganisation, contact with the ECM and focal adhesion turnover. Therefore, MT organisation is a very important aspect to understand. Many animal cells show MTs arranged in a radial array, where the minus-ends are anchored at the centrosome, and the plus-ends grow towards the cell periphery (Desai and Mitchison, 1997, Mogensen, 2004). Disruption of the normal MT array formation is likely to contribute to a migratory phenotype. A publication by Bu and Su (2001) indicated that the overexpression of EB1 and EB3 promoted bundle formation in many cell lines while the overexpression of EB2 did not cause this effect. Furthermore, this observation was also confirmed by (Goldspink et al., 2013) with the addition that the expression of EB2 is required for the initial phase of MT reorganisation during apico-basal epithelial differentiation while that of EB1 is essential for bundle formation. EB2 was also shown to associate along the MT lattice and indirectly influence MT dynamics by preventing EB1-formin interaction, lattice binding and bundling. Therefore, correct MT bundling of polarised epithelial cells is required in order to have a functional differentiation process in tissues such as the inner ear or intestinal crypts (Goldspink et al., 2013). Essentially, EB2 overexpression has been found to increase perineural invasion of pancreatic cancer where actin distribution modifications were also observed (Abiatar et al., 2009). EB2 has also been recently suggested to contribute to focal adhesion turnover by associating with essential proteins, such as HCLS1-associated protein X-1 (HAX1) and MAP4K4, which are important in cell migration (Yue et al., 2014a, Liu et al., 2015).

Accurate regulation of MT dynamics is necessary for vital cellular functions such as cell division, cell migration and trafficking of vesicles (Mogensen, 2004). The important role of EBs lie in the regulation of MT dynamics and stability, however the exact mechanisms are still not fully understood. It has been suggested that EB1 catalyses the rescue phases of MT dynamics or suppresses the catastrophe phase (Vitre et al., 2008, Manna et al., 2008) while EB2 did not seem to have these effects (Komarova et al., 2009). The post-translation modification of tubulin subunits is an important mechanism for their stability and function. Most post-translation modifications appear on tubulin subunits after polymerisation into MTs, which allow MTs to adopt distinctive roles within the overall network (Verhey and Gaertig, 2007, Garnham and Roll-Mecak, 2012, Yu et al., 2015).

Tubulin post-translation modifications that occur on MTs that have been well characterised include acetylation and detyrosination. Acetylation of Lys 40 residue on  $\alpha$ -tubulin occurs on the luminal face of diverse MTs including cytoplasmic, spindle and centriolar MTs. Acetylation is a marker for MT stability. Acetylation is carried out by  $\alpha$ -tubulin acetyltransferase (aTAT1). It is thought that the enzyme gains access to the luminal site through cracks that appear in the polymerised tubulin or from the open MT ends. In cells, MTs are every now and again unprotected from mechanical forces, which can harm the cross-section and hence result in MT depolymerisation. The perception that acetylation hotspots are frequently found at bended and curved areas of MTs, which are the same regions that accumulate breaks give a clear indication that these stress-induced lattices are the luminal passages for aTAT1. The enzyme would then acetylate the MTs, which consequently would render the region impervious to mechanical stress and permitting their repair (Schaedel et al., 2015, Janke and Montagnac, 2017). Tubulin detyrosination occurs on  $\alpha$ -tubulin and along the MT lattice (Akhmanova and Maiato, 2017). The process involves a proteolytic removal of the C-terminal Y residue (Hallak et al., 1977). Detyrosination is likely to be generated by the enzyme cytosolic carboxypeptidase 1 (CCP1) (Kalinina et al., 2007). In addition, detyrosinated tubulin heterodimers that are released from MTs can revert to an unmodified state catalysed by tubulin tyrosine ligase (TTL) (Ersfeld et al., 1993).

To summarise, MT organisation is important for normal physiological functions, which is regulated by EB proteins. These will be looked at in both breast cancer models to understand if they affect their invasive properties as well as the role of EB proteins on MT dynamics.

## **3.3 Results**

### **3.3.1 Characterisation of MCF-7 and MDA-MB-231 cells**

#### **3.3.1.1 MCF-7 and MDA-MB-231 cell morphologies**

Cells seeded sparsely in 24-well plates were left to adhere overnight before live-imaging. Images from live time-lapse recordings of subconfluent MCF-7 and MDA-MB-231 cells showed different cellular morphologies. MCF-7 cells displayed round or elongated morphologies some with relatively large lamellipodia (Fig. 3.1Ai) while others formed protrusions (Fig. 3.1Aii). The MDA-MB-231 also included cells with relatively large lamellipodia while other cells had a spindle-like morphology with some showing two or more long relatively thin protrusions (Fig 3.1B i and ii).

#### **3.3.1.2 MT organisation in MCF-7 and MDA-MB-231 cells**

MCF-7 and MDA-MB-231 cells were seeded on coverslips and immunelabelled with an anti- $\alpha$ -tubulin antibody. Different MT organisations were observed in MCF-7 and MDA-MB-231 cells. Some MCF-7 cells, showed MTs forming bundles around the nucleus (Fig 3.2A) while others showed an intertwined MT network curved around the periphery (Fig 3.2B). Some spindle shaped cells were noticed with MTs extending to the periphery and bundles evident in thin projections (Fig 3.2C). In other cells, MTs curved around the nucleus with slight bundling at one end while other MTs appear straighter extending towards the cortex (Fig 3.2D). Microscopic images of MDA-MB-231 cells showed some cells with disorganised arrays of MTs with some bundling (Fig 3.3A). Some cells displayed distinct MTs curved around the periphery with MT bundles in thin protrusions (Fig 3.3B and C). Interestingly, in other cells, MTs appear to cluster in the centre of the cell radiating out into multiple thin elongated protrusions (Fig 3.3D).

#### **3.3.1.3 Actin organisation in MCF-7 and MDA-MB-231 cells**

Actin is an essential component of the cytoskeleton and plays various important roles including in cell movement and shape change and maintenance. MCF-7 and MDA-MB-231 cells seeded on coverslips were PHEMO fixed and immunolabelled

with an anti- $\alpha$ -tubulin antibody and stained with phalloidin conjugated to Alexafluor488 for visualisation of actin filaments. Widefield fluorescence microscope images of MCF-7 cells showed that MTs were preserved following PHEMO fixation, similar to Methanol-MES fixation. MTs and F-actin appeared at the leading edge. There is also localisation of actin at the cell periphery, mainly stress fibres, which are parallel to the edge (Fig 3.4). The results illustrate that in MDA-MB-231 cells, there is localisation of MTs and F-actin with concentration of actin at the leading edge of cells, including transverse arcs (these are stress fibres formed behind the leading edge of migrating cells and are connected to dorsal stress fibres) that are formed behind the leading edge of migrating cells (Fig 3.5). In addition, actin filaments formed a network at the periphery with stress fibres running parallel to the axis of the cell while MTs radiate out from the centrosome (Fig 3.5 and 3.6).

#### **3.3.1.4 Different expression levels of EBs are evident in MCF-7 and MDA-MB-231 cells**

In order to determine the expression levels of the three EBs in MCF-7 and MDA-MB-231 cells Western blot analysis were carried out. Western blots were carried out with  $\beta$ -actin as a loading control. It was noted that EB1 expression was higher in MDA-MB-231 cells (Fig 3.7A). Likewise, the expression of EB2 was higher in MDA-MB-231 cells than in MCF-7 cells (Fig 3.7B). There were two bands detected for EB2 expression in both cell lines, this is probably due to the two forms of EB2 which exist because they are translated from different initiation codons (Bu and Su, 2003) or post translational modification however, further validation is required to confirm this. However, there was a higher expression of EB3 in MCF-7 than in MDA-MB-231 cells (Fig 3.7C). Quantification was not carried out as only two repeats were obtained.

#### **3.3.1.5 Localisation of the EBs and comet analysis in MCF-7 and MDA-MB-231 cells**

EB1 and EB3 have been shown to play important roles in the regulation of MT dynamics (Komarova et al., 2009). It is therefore important to understand their localisation in cells with the aim of investigating their possible effects in cancer models.

Therefore, to further characterise these breast cancer cell lines, they were seeded on glass coverslips and then immunolabelled for MTs, EB1, EB2 and EB3 proteins using highly specific antibodies (see section 2.5). In MCF-7 cells, all cells expressed EB1 with the majority localising to the plus-end of MTs, however, some EB1 localisation was also evident along the MT lattice. EB1 comets appeared dot-like (Fig 3.8A). MDA-MB-231 cells also expressed EB1 with most localising as comets at the plus-end of the MTs but some EB1 was also present along the MT lattice. Some MDA-MB-231 cells formed interlaced MT networks at the front of the cell. EB1 comets appeared more elongated in MDA-MB-231 cells compared to the comets in MCF-7 cells (Fig 3.8B).

Comet analysis (details in chapter 2) was carried out on EB1 comets in order to determine differences in comets shape between the two breast cancer cell lines. Comet length is likely to reflect the extent of the GTP-cap and thus MT growth. ImageJ was used to analyse the comets in 10 cells per cell line from one experiment. The comets were measured in terms of the circularity and feret's diameter. Circularity refers to the roundness of comets while feret's diameter denotes the longest distance across the comet. EB1 comets in MCF-7 cells were more circular, around 0.7 out of 1 compared to the comets in MDA-MB-231 cells of around 0.5 (Fig 3.9A), which explains why the feret's diameter is higher in the MDA-MB-231 cells (Fig 3.9B). Thus, the results revealed that EB1 comets in MDA-MB-231 were more elongated compared to MCF-7 cells. This suggests EB1 in MDA-MB-231 cells have an increased affinity for GTP-cap, therefore, allowing more MT polymerisation.

In MCF-7 cells, EB2 localised along MTs (Fig 3.10A). Analogous to EB1, EB2 comets were also dot-like. Previously, EB2 had been localised in ARPE-19 cells and was established to be rod-like and mainly along the lattice (Goldspink et al., 2013) as well as in CHO-K1 cells (Komarova et al., 2009). In most MDA-MB-231 cells, EB2 appeared to be cytoplasmic (Fig 3.10B). An interesting observation was that EB2 was concentrated at protruding parts of the cell (Fig 3.10B). This may suggest a role in lamellipodia formation/function, a key step in cell migration.

Comet analysis was also carried out on EB2 to determine the differences between the two cell lines. Analysis by unpaired t-test revealed a significant decrease

in comet circularity in MDA-MB-231 cells compared to MCF-7 cells with a significant increase in feret's diameter in MDA-MB-231 cells compared to MCF-7 cells. The same trend was also observed for the EB2 comet analysis. EB2 comets in MCF-7 cells were more circular, around 0.7 out of 1 compared to the comets in MDA-MB-231 cells of around 0.5, this explains why the feret's diameter is higher in the MDA-MB-231 cells (Fig 3.11A and B). However, the average number of EB2 comets in MDA-MB-231 cells was higher compared to MCF-7 cells.

In MCF-7 cells, there was sporadic expression of EB3 with most cells having a low expression. EB3 did not localise to the plus-ends of MTs in most cells but was concentrated at the centrosome (Fig 3.12A). Like the observation for EB1 and EB2 in MCF-7 cells, EB3 comets were dot-like. In MDA-MB-231 cells, EB3 appeared to be strongly localised near the centrosome and the Golgi apparatus, in most cells (Fig 3.12B). Due to the substantial differences in EB3 expression in both cell lines, it was not possible to quantify the comets.

### **3.3.2 MT dynamics and stability in MCF-7 and MDA-MB-231 cells**

#### **3.3.2.1 MT dynamics in MCF-7 and MDA-MB-231 cells**

The comet analyses revealed longer EB1 comets suggesting greater MT growth in MDA-MB-231 compared to MCF-7 cells. This was studied further by analysing the MT dynamics in these two breast cancer cell lines. GFP-CLIP-170 comet dynamics was analysed in MCF-7 and MDA-MB-231 cells using live time-lapse imaging. Both cell lines were grown in 3 cm glass-bottomed dishes and allowed to adhere overnight. Cells were then transfected with 2  $\mu$ g GFP-CLIP-170 construct and left for 6 h then replaced with normal medium. Cells expressing GFP-CLIP-170 were imaged using live time-lapse widefield fluorescence microscopy for three minutes, with frame acquisition every three seconds. GFP-CLIP-170 comets were analysed using the U-Track automated tracking software, formerly packaged as plusTipTracker (Applegate et al., 2011). Post-tracking analyses were conducted using the software MATLAB. It is worth mentioning that stable MTs are usually not detected by using this method.

U-Track analysis of GFP-CLIP-170 comets were over a three-minute period. Analysis by unpaired t-test showed that GFP-CLIP-170 comet speed was not significantly different in MDA-MB-231 when compared to MCF-7 cells (Fig 3.13A). GFP-CLIP-170 tracking images established that there was a reduced growth lifetime in the highly invasive MDA-MB-231 compared to MCF-7 cells (Figure 3.13B, Movie S1 and S2). On the other hand, GFP-CLIP-170 growth length was significantly increased in MDA-MB-231 when compared to MCF-7 cells (Fig 3.14A). Further analysis however revealed no significant difference in the total percentage time MTs spend in the growth phase, termed percentage time growth in both cell lines (Fig 3.14B).

### **3.3.2.2 MT stability and tubulin modifications**

Tubulin modification is known to generate diversity of MTs, which differs with development, differentiation and the cell cycle. Tubulin modifications affect MT dynamics as well as their organisation and interaction with other cellular components. In MCF-7 cells, a high proportion of MTs were tyrosinated, with some detyrosinated tubulin observed in the central area of the cell, sometimes extending towards the periphery (Fig 3.15A). Detyrosinated tubulin localisation was sparse in MDA-MB-231 cells with many MTs containing tyrosinated tubulin (Fig 3.15B).

Acetylated tubulin is often associated with stable MTs and leads to reduced MT dynamics (Al-Bassam and Corbett, 2012, Howes et al., 2014) thus the extent of acetylation was analysed in both cell lines. MCF-7 and MDA-MB-231 cells were labelled for acetylated tubulin, tyrosinated tubulin and detyrosinated tubulin. This was done to evaluate the extent of these tubulin modifications in the two cell lines. In MCF-7 cells, some acetylated tubulin was evident in the central cell area. This formed a bundle and sometimes revealing a curly nature (Fig 3.16A and 3.17A). In MDA-MB-231 cells, there was an extensive area of acetylated tubulin compared to MCF-7 cells (Fig 3.16B and 3.17B). Western blot analysis proved difficult but suggested no difference in acetylated tubulin level between MCF-7 and MDA-MB-231 cells based on one Western (Fig 3.18A). Fluorescent intensity analysis of cells immuno-labelled for  $\alpha$ -tubulin and acetylated tubulin was therefore carried out. The proportional area of

acetylated tubulin was compared to the total  $\alpha$ -tubulin using ImageJ. Analysis by unpaired t-test suggested a significant greater area of acetylated tubulin in MDA-MB-231 cells compared to MCF-7 cells (Fig 3.18B). This suggests that MDA-MB-231 cells contain relative more acetylated tubulin than MCF-7 cells. To further characterise MT stability in both cell lines, cells were cold treated by incubating them on ice for 10 min before fixing and immuno-labelling for  $\alpha$ -tubulin and EB1. Widefield fluorescent images showed that cold treatment resulted in total MT depolymerisation in most MCF-7 cells (Fig 3.19A). However, some stable MTs were observed in the MDA-MB-231 cells and these showed EB1 lattice association (Fig 3.19B), though, images were not quantified. The acetylated data and cold treatments thus both points to MDA-MB-231 cells having more stable MTs than MCF-7 cells.

### **3.4 Discussion**

MTs are part of the cytoskeleton, which forms a network determining the dynamic nature of cells. They also play a pivotal role in other cellular functions such as cell growth, cell division, motility and the trafficking of vesicles, organelles, and proteins (Mogensen, 2004). The centrosome is a structure that nucleates and anchors the minus-end of MTs allowing the plus-end to grow towards the periphery and explore the environment (Cole and Lippincott-Schwartz, 1995b, Mogensen et al., 1997, Cole and Lippincott-Schwartz, 1995a). Importantly, +TIPs associating with plus-ends of MTs regulate their dynamics and function. Binding of EB1 and EB3 proteins to MTs allows the binding of other +TIPs such as CLASPs making them hubs for protein interaction networks at the growing MT ends (Komarova et al., 2005, Lansbergen and Akhmanova, 2006). This property is important and allows them to carry out their functions. Therefore, disruptions in MT organisation or association with +TIPs may affect their dynamics, stability and cause loss of normal function.

In this study, it was observed that MT organisation in both MCF-7 and MDA-MB-231 cells contained disorganised arrays. +TIP proteins including EB1, EB2 and EB3 regulate MT dynamics. EB1 has a higher affinity for the GTP-cap, which is at the plus-end of MTs therefore, it binds to all growing plus-ends. A typical EB1 comet-like structure was found at the plus-ends of MTs in MCF-7 cells while longer comets were

evident in MDA-MB-231 cells. An explanation for the longer comets seen in MDA-MB-231 cells could be that EB1 recognises a longer GTP cap as proposed by (Zanic et al., 2009), which may confer growing MTs and increased MT elongation. Longer EB2 comets were also confirmed in MDA-MB-231 compared to MCF-7 cells (Fig 3.11). Elongated comets in MDA-MB-231 cells indicates an increased MT plus-end and this fits with the increased MT growth length and lifetime observed during MT dynamics experiments in this study.

The localisation of EB2 in MDA-MB-231 cells was different to the one seen in MCF-7 cells as it associated with protruding parts of the cell and was apparent in the cytoplasm. This may suggest a role in lamellipodia formation, a key step in cell migration and but may also suggest co-localisation with actin filaments. It has been shown that depletion of EB2 inhibits MT dynamics leading to bundles of MTs co-aligned with actin filaments and EB1 and ACF7 lattice association (Goldspink et al., 2013). Not only was EB2 found at protruding parts, it was also found concentrated in the cytoplasm of most MDA-MB-231 cells. Attempts were made to quantify the amount of cytoplasmic to MT bound EB2 in MDA-MB-231 cells but it proved unsuccessful. EB2 distribution in the cytoplasm may be due to the phosphorylation of EB2 as phosphorylation by Aurora B and CDK1 on entry to mitosis leads to MT detachment (Iimori et al., 2016a). The proportion of phosphorylated EB2 could be analysed using phospho-tag gels. The phospho-tag will only bind to the phosphorylated EB2, which can then be visualised on a Western blot.

EB1 comet analyses revealed longer comets in the MDA-MB-231 cells suggesting longer GTP-caps and thus MTs elongating. This may also mean longer GTP-remnants found within the cell that may allow rescue to occur much quicker as GTP-remnants and rescue have been linked (Dimitrov et al., 2008). Using an hMB11 antibody, Dimitrov and colleagues (2008) discovered that the antibody bound to GTP-tubulin present at growing MT tips as well as along short lengths of polymerised MTs suggesting that GTP-tubulin “remnants” remain within the MT lattice. These remnant spots were found to be an increased area for rescue events *in vivo* hence the link between GTP-tubulin caps and rescue. Another explanation for longer comets could be that because these cells have higher levels of EB1 than in MCF-7 cells, the effect of EB1 is to protect the ends of the MTs allowing growth thus, longer comet tails. Further work

needs to be done to explore the GTP-cap size in a typical protofilament length in both cell lines. This could possibly be done by using the antibody that is thought to detect GTP-tubulin that could be used to see if anti-GTP-tubulin labelling co-localises with fluorescently-tagged EB1. An average GTP cap size found in epithelial LLCPK1 kidney cell line was about 750 tubulin subunits whereby the tail of the cap promotes MT rescue (Seetapun et al., 2012).

It could be speculated that high levels of EB2 expression in MDA-MB-231 cells could likely increase cell migration since EB2 has been shown to co-localise with actin and IQGAP1 at the leading edge (published in Jonathan Gadsby's thesis, 2014; MMM lab). Potentially, this interaction and reorganisation could allow the cell to protrude, receive signals from its surroundings and eventually migrate. Focal adhesions are constantly being assembled and disassembled as a cell migrates (Etienne-Manneville, 2013). New focal adhesions are known to form at the leading edge, which EB2 has been reported to contribute to focal adhesion turnover by associating with proteins, such as MAP4K4 and HAX1 (Yue et al., 2014a, Liu et al., 2015). So, it could be speculated that EB2-overexpression may contribute to an increase in migration by increasing focal adhesion turnover through MAP4K4 and HAX-1. Effect of EB2 on cell migration will be discussed in Chapter 4. Focal adhesion turnover would be monitored by carrying out FRAP. Cells will be transfected with GFP-paxillin and then a particular area of focal adhesion is bleached. The mean fluorescence time needed for that focal adhesion to recover and occupy the space will be measured. The results will be compared between the MCF-7 and MDA-MB-231 cells.

EB3 expression and localisation was sporadic in MCF-7 cells with most cells having a low expression. In MDA-MB-231 cells, EB3 was highly concentrated at centrosomes and the Golgi apparatus as well as near the periphery (Fig 3.12B). However, to fully confirm EB3 localisation at the centrosome and the Golgi, further immunolabelling needs to be carried out in the MDA-MB-231 cells, and labelled with antibodies against Golgi and centrosomal proteins such as  $\gamma$ -tubulin or pericentrin simultaneously with EB3 and a Golgi antibody e.g. GM130. Furthermore, the increased level of EB3 expression observed in MCF-7 cells (Fig 3.7C) could be due to the reduced expression of EB1 in MCF-7. EB3 has been observed to have an increased expression

in cells when EB1 has been depleted suggesting that EB3 might be able to compensate for EB1 (Goldspink et al., 2013).

Actin polymerisation drives forward the leading edge of migrating cells. This process depends on elongation of filaments at the growing barbed ends, organisation of filaments into mechanically stable networks, and regulated filament disassembly (Pollard and Borisy, 2003). Actin network at the lamellipodia membrane is driven by Arp2/3 nucleation while stress fibres assembly are driven by formins. A signalling cascade between the Rho family GTPases – Rho and Rac control these processes. The Rho family controls stress fibre induction through myosin light chain phosphorylation (Ridley, 2006, Burridge and Wennerberg, 2004). In both cell lines, actin filaments were observed mainly at the front of the cell with some stress fibres observed in the cell body. Stress fibres are contractile actomyosin bundles found in many cells where they have a central role in cell migration and adhesion. In particular, curved transverse arcs, which are curved actomyosin bundles that flow towards the cell centre and are connected to focal adhesions through interactions with dorsal stress fibres, and ventral stress fibres are observed in MDA-MB-231 cells, which may help drive cell movement.

An important characteristic of transverse arcs in migrating cells is their ability to flow from the cell's leading edge towards the cell centre (Hotulainen and Lappalainen, 2006) and are not directly linked by focal adhesion but pass on contractile force to the surrounding environment through their associations with dorsal stress fibres (Tojkander et al., 2012, Parsons et al., 2010). Dorsal stress fibres are located at the front of the cell and are usually anchored to focal adhesions at their distal end. Due to the lack of myosin II, they do not possess the ability to contract (Tojkander et al., 2011). On the other hand, ventral stress fibres are contractile actomyosin bundles that are associated with focal adhesions at both ends. They are located at the trailing edge of the cell where they promote cell contraction (Small et al., 1998). All three types of stress fibres - dorsal stress fibres, transverse arcs and ventral stress fibres - can be seen in MDA-MB-231 cells (Fig 3.5 and 3.6). Finally, during cell migration, actin filaments within stress fibres will be recycled by a process of retrograde actin flow (Tojkander et al., 2012). The leading edge of cells can be demonstrated by using a scratch assay whereby the cells are fluorescently labelled with actin and monitored as the wound is closed. This should give an indication of the leading edge as it is characterised by an

intense actin polymerisation. An alternative would be to fluorescently label the cells and then use a chemoattractant to direct migration. The chemoattractant creates a chemical concentration gradient, which the cells move towards.

MT dynamics is central to their biological functions, which allow them to adopt spatial arrangements that can change rapidly in response to cellular needs or to perform mechanical work. Dynamic instability is an inherent property of MTs to undergo phases of growth and shrinkage. This process occurs due to the energy acquired through GTP hydrolysis. Immunolabelling for detyrosinated and tyrosinated tubulin in MCF-7 and MDA-MB-231 cells showed that most of the MTs were tyrosinated in both cell lines, which implies there are more dynamic MTs. Tyrosinated tubulin has been showed to recruit some plus tip proteins such as CLIP-170 that is known to influence MT dynamics (Garnham and Roll-Mecak, 2012, Yu et al., 2015). A small amount of detyrosinated MTs were evident at the cell centre in MCF-7 cells compared to speckles observed in MDA-MB-231 cells.

The effect of tubulin acetylation on MT dynamics is not fully clear. However, acetylated tubulin has been used as marker for stable MTs (Palazzo et al., 2003, Dompierre et al., 2007). Moreover acetylated MTs provide tracks for some motor proteins, including dynein (Garnham and Roll-Mecak, 2012). Immunolabelling and analysis for acetylated tubulin in MCF-7 and MDA-MB-231 cells showed that there was an increased area of acetylated MTs in MDA-MB-231 compared to MCF-7 cells suggesting more stable MTs though both dynamic and stable MTs work in synergy and not exclusively. U-Track live data (Movies S1 and S2) and analysis of GFP-CLIP-170 suggests that the more invasive MDA-MB-231 cells, which show increased EB2 expression is associated with increased MT plus-end growth length that may be attributed to the elongated comets observed. The EB family has been shown to be key regulators of MT dynamics (Komarova et al., 2009). Although, not significant in our study, the average comet speed (12.0  $\mu\text{m}/\text{min}$ , Fig 3.13A, Movie S1) found in MCF-7 were similar to those already reported by (Azarenko et al., 2008) at 14.5  $\mu\text{m}/\text{min}$  also in MCF-7 cells. It should be mentioned that the study by Azarenko and colleagues (2008) based their MT dynamics on a few MTs while ours are based on total MTs found in cells. Most MTs have a half-life of 5-10 min whereas this study found the growth

lifetime of MTs to be around 9.5-10.3 sec. The result in Fig 3.13B is referring to only growing ends of MTs rather than the entire MTs within a cell. Increase in MT growth length in MDA-MB-231 cells (Fig 3.14A, Movie S2) may be attributed to the significant elongated comets thus, allowing more growing MTs. This finding is also supported by the observation of an increased growth lifetime in our study, which implies that more MTs are in the growth phase as opposed to shrinking.

In summary, the results showed distinct cellular morphologies between MCF-7 and MDA-MB-231 cells with MDA-MB-231 cells having more elongated protrusions. There was a disorganised array of MTs in both cell lines though most MCF-7 cells had MTs forming bundles around the nucleus. Actin filaments were also evident in both MCF-7 and MDA-MB-231 cells but more importantly were the formation of stress fibres – dorsal, transverse arcs and ventral, which may aid cell movement in MDA-MB-231 cells. The level of EB1 and EB2 expression was found to be higher in MDA-MB-231 cells compared to MCF-7 cells. Most MDA-MB-231 cells revealed distinct EB2 localisation, which were more concentrated at protruding parts and the centre of cells rather than as classic comets. Furthermore, analysis of MT dynamics suggested an increased growth length and lifetime in MDA-MB-231 cells, which may be attributed to elongated comets observed, hence allowing growing MTs. Finally, a significant increase in acetylated tubulin area but no difference in expression level was found in MDA-MB-231 cells suggesting more stable MTs are present compared with MCF-7 cells. More stable MTs in the MDA-MB-231 cells compared with MCF-7 cells suggest that the intricate balance between stable and dynamic MTs required for cell migration is greater in the MDA-MB-231 cells and may contribute to its increased random cell migration. Further investigation is required to determine the implications of this.

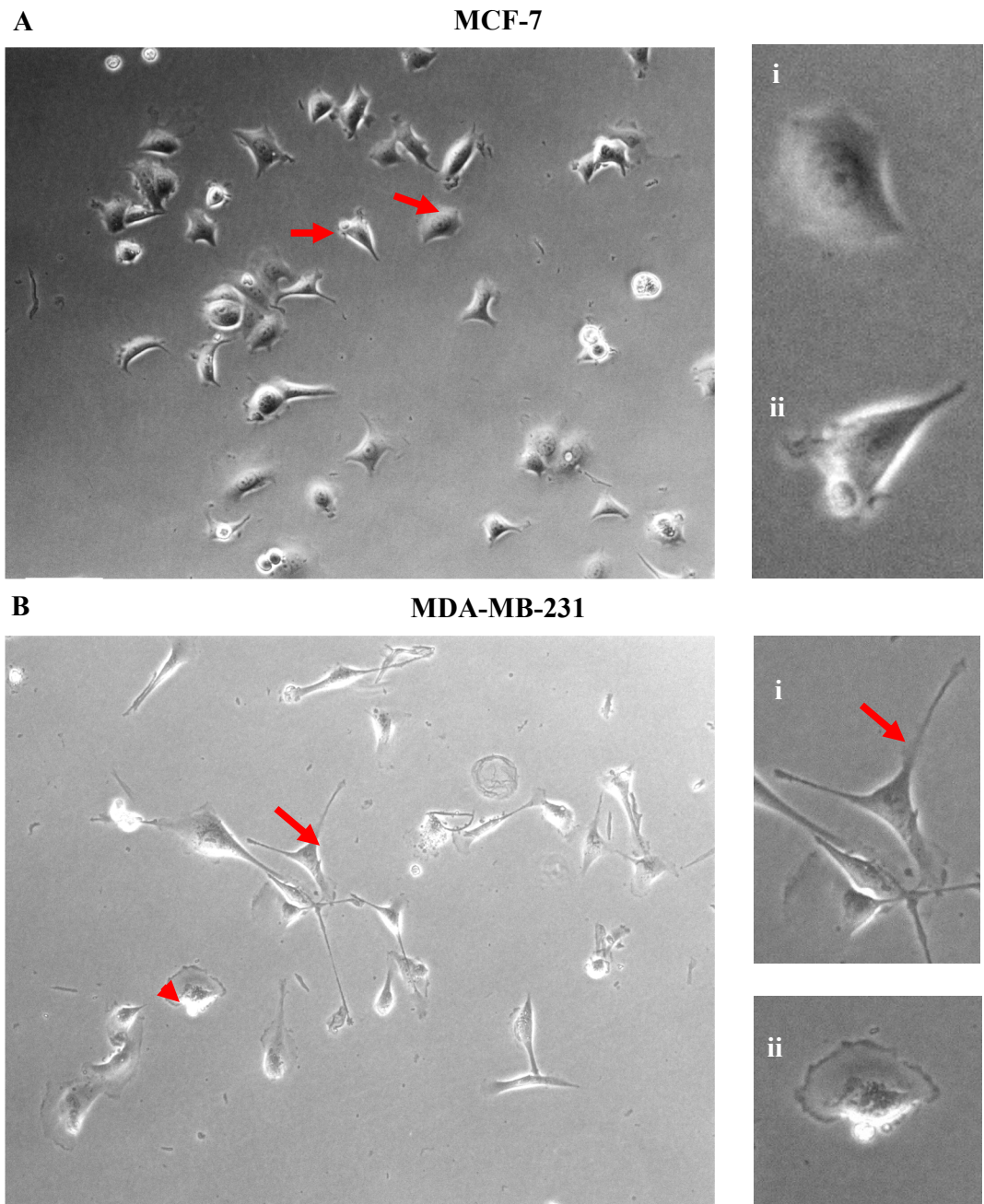


**Figure 3.1: MCF-7 and MDA-MB-231 cellular morphologies.** Image frames from live time-lapse recordings of subconfluent random migrating MCF-7 and MDA-MB-231 cells showing different cell morphologies. A) Some MCF-7 cells displayed a ‘fried-egg’ like morphology with relatively broad lamellipodia evident in some cells (enlarged region in ai) while other cells have short protrusions (aaii). B) Some MDA-MB-231 cells appear to have a spindle-like morphology with multiple elongated thin processes (highlighted by the arrow in bi) while other cells appear flat with curved lamellipodia and no processes present (arrowhead in bii). Scale bar = 100 $\mu$ m.

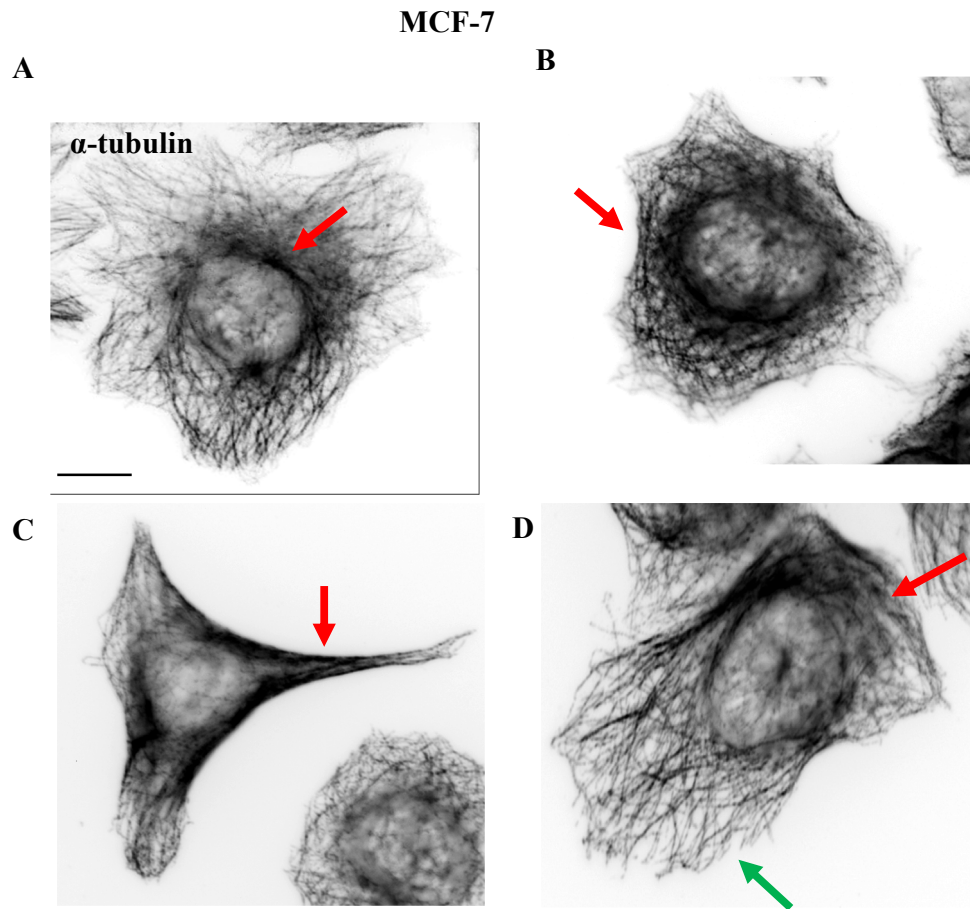


**Figure 3.2: MT organisation in MCF-7 cells.** MCF-7 cells immunolabelled with an anti- $\alpha$ -tubulin antibody (pAb, ab15246). Images were taken using a widefield fluorescence microscope. A) Cell shows MTs forming bundles around the nucleus (red arrow) with others radiating out towards the periphery (inverted image), with a trend towards this phenotype being the majority. B) Cell with circular morphology showing an intertwined MT network with distinct bundles around the nucleus (red arrow). C) A spindle shaped cell with MTs extending to the periphery and bundles evident in a thin process (red arrow). D) Cell shows curved MTs around the nucleus (red arrow) with slight bundling at one end while at the other end, MTs appear straighter extending towards the cortex (green arrow). Scale bar = 10 $\mu$ m.

MDA-MB-231

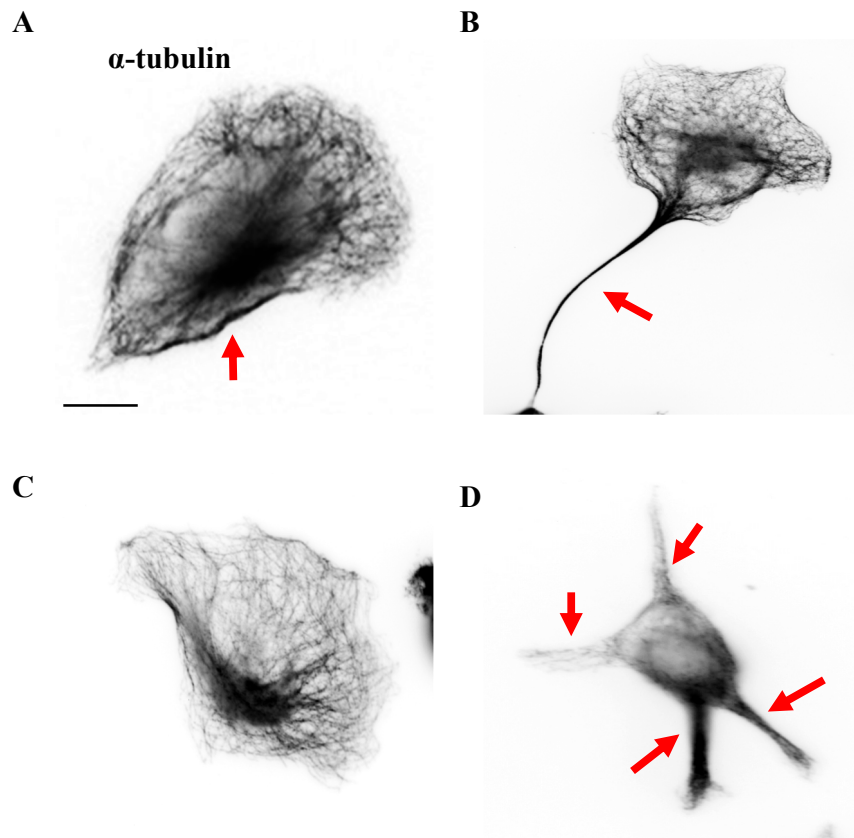


**Figure 3.3: MT organisation in MDA-MB-231 cells.** MDA-MB-231 cells immunolabelled with an anti- $\alpha$ -tubulin antibody (pAb, ab15246). Images were taken using a widefield fluorescence microscope. A) Cell shows a disorganised array of MTs with some bundling observed towards the side (red arrow). B) Cell displaying a migratory phenotype with MT bundles in a thin processes, which may be the trailing end (red arrow). C) Distinct MTs are radiated out from the centrosome, concentrated and curved towards one side of the cell. D) MTs appear to cluster in the centre of the cell radiating out into thin elongated protrusions (red arrows). Scale bar = 10 $\mu$ m.

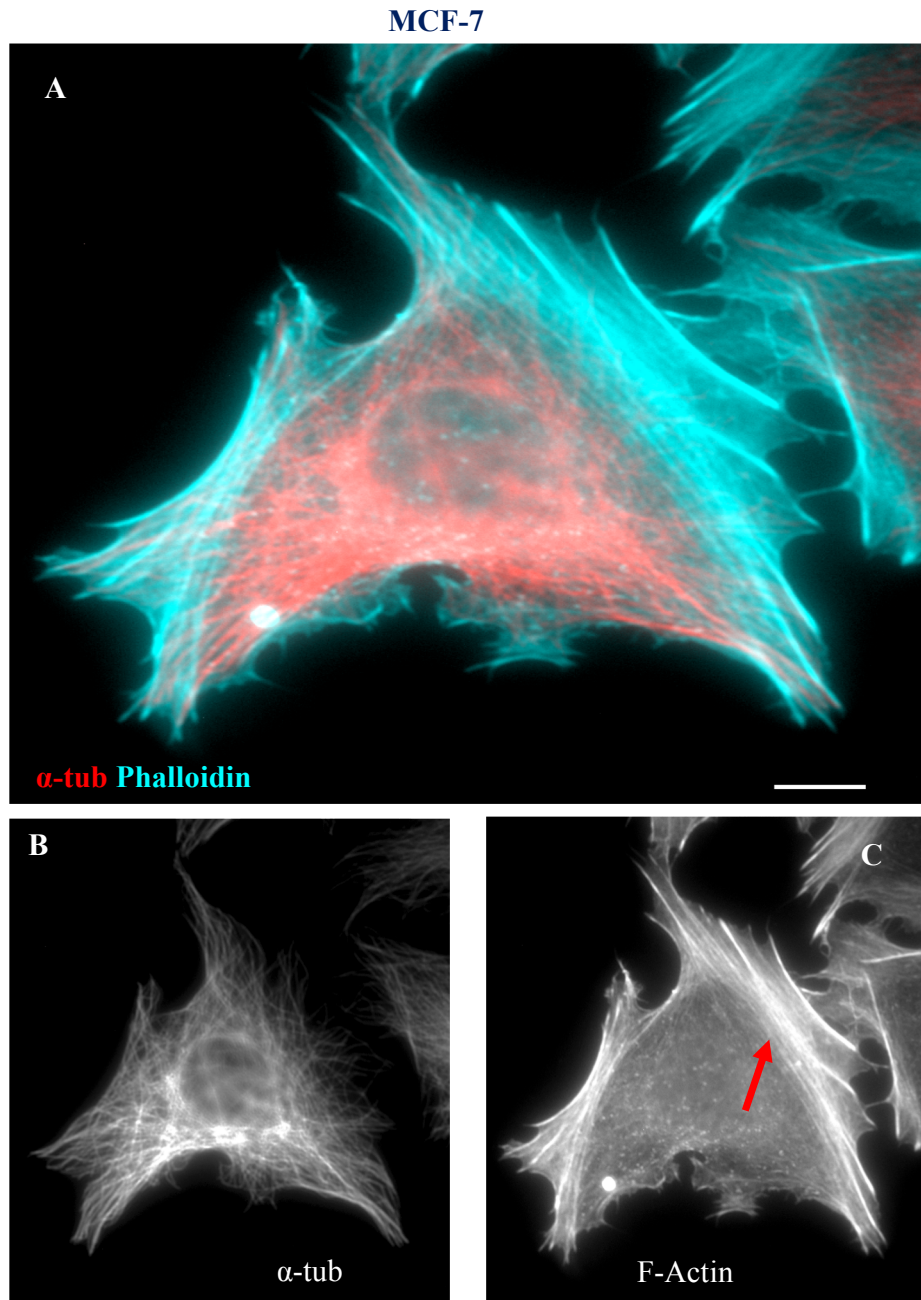


**Figure 3.4: Actin and MT organisation in PHEMO fixed MCF-7 cell.** MCF-7 cells immunolabelled with an anti- $\alpha$ -tubulin antibody (red, pAb, ab15246) and phalloidin (actin) staining (cyan). Widefield fluorescent images show good MT preservation following PHEMO fixation. A) Actin filaments concentrated around the periphery of the cell. B) Single channel image shows a disorganised array of MTs, with some parallel to the cortex. C) Single channel image shows that there is a strong localisation of actin filaments around the cell where it appears as stress fibers (red arrow). Scale bar = 10 $\mu$ m.

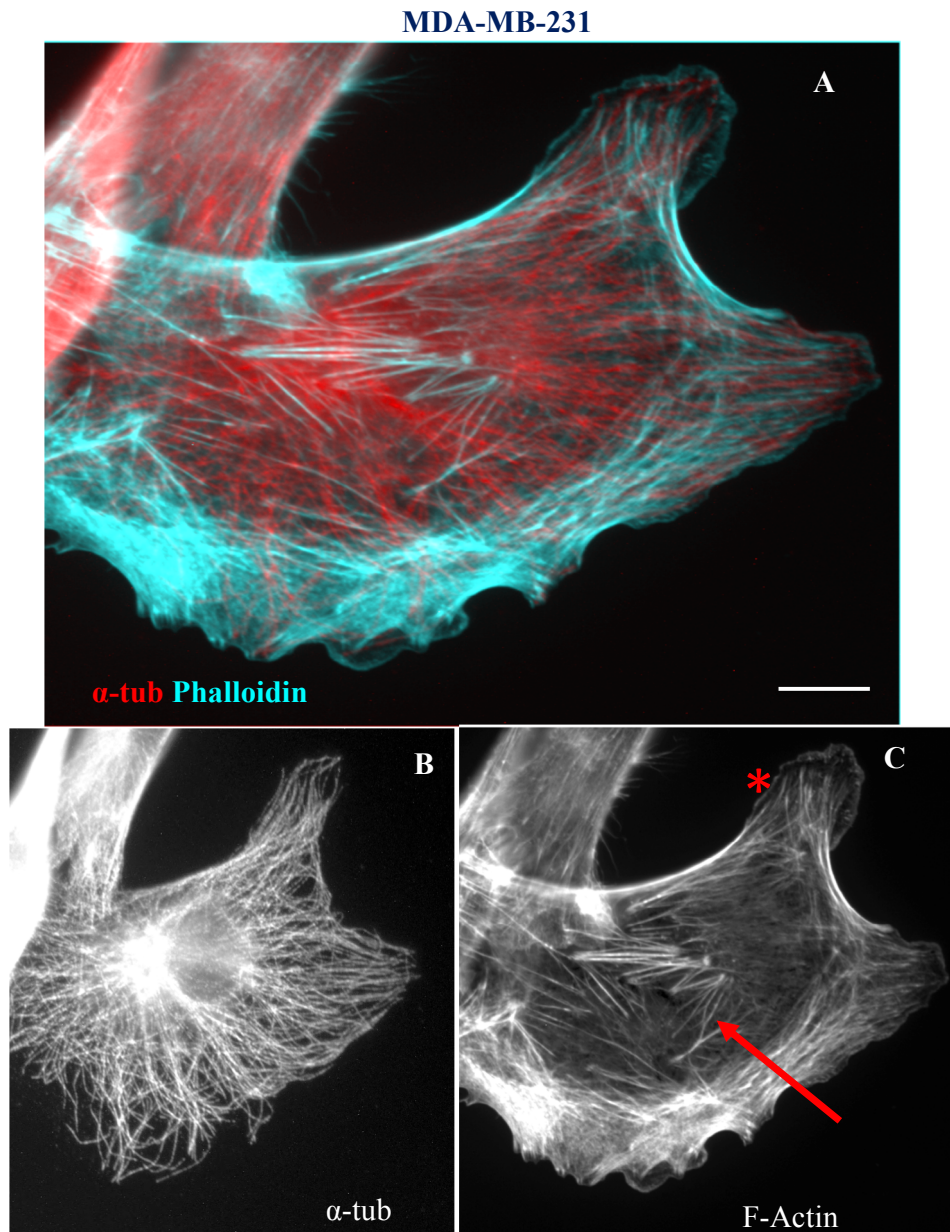


**Figure 3.5: Actin and MT organisation in PHEMO fixed MDA-MB-231 cell.** MDA-MB-231 cell immunolabelled with an anti- $\alpha$ -tubulin antibody (red, pAb, ab15246) and phalloidin (actin) staining (cyan). Widefield fluorescent images show good MT preservation following PHEMO fixation. A) Actin is observed to be concentrated mainly at the periphery of the cell, with some MTs penetrating the peripheral actin network. B) Single channel highlights a radial organisation of MTs. C) Single channel showing actin localisation at the leading edge of the cell with some ruffling at the other end (denoted with an asterisk). Actin appears to form ventral stress fibers in the centre of the cell (red arrow). Scale bar = 10 $\mu$ m.

MDA-MB-231

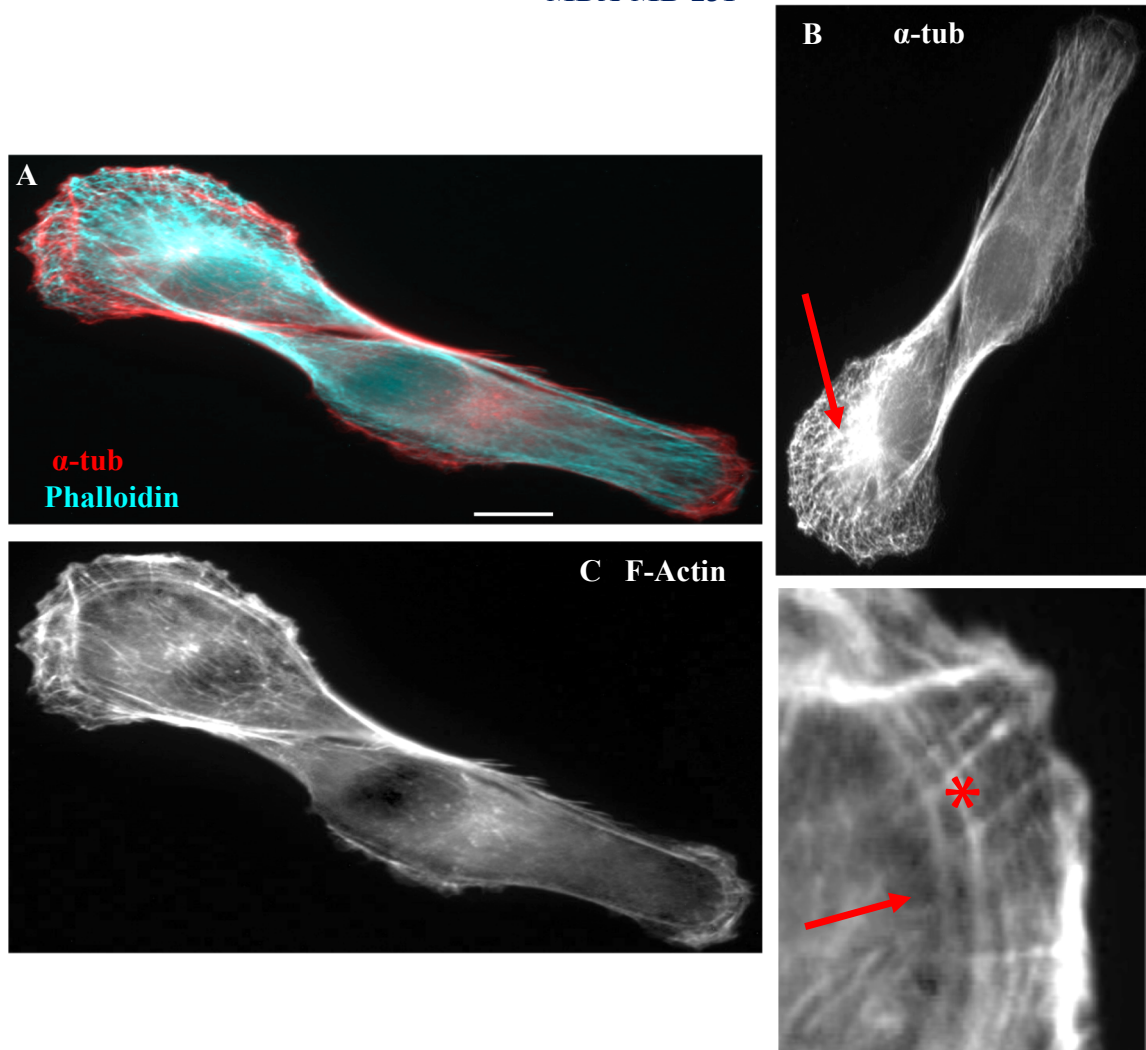


**Figure 3.6: Actin and MT organisation in PHEMO fixed MDA-MB-231 cell.** MDA-MB-231 cell immunolabelled with an anti- $\alpha$ -tubulin antibody (red, pAb, ab15246) and phalloidin (actin) staining (cyan). Widefield fluorescent images show good MT preservation following PHEMO fixation. A) Merged image showing both actin and MT organisation. B) Single channel showing MTs radiate out from the centrosome of the cell (red arrow) towards the periphery. C) Single channel showing actin filaments concentrated at the leading edge, where curved transverse arcs (red arrow in enlarged region) are formed behind the leading edge of migrating cells. There are also dorsal stress fibres running parallel to the axis of the cell (asterisks) where they connect transverse arcs. Scale bar = 10 $\mu$ m.

### Expression of EB1, EB2 and EB3

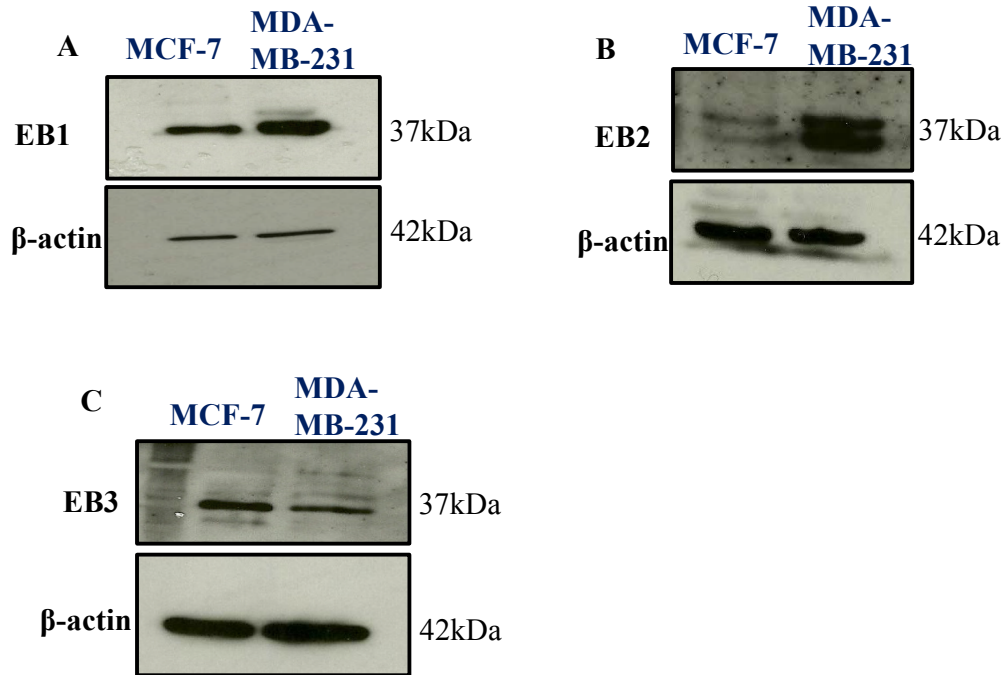


**Figure 3.7: Expression of EB proteins in MCF-7 and MDA-MB-231 cells.** Western blots of cell lysates of MCF-7 and MDA-MB-231 cells showing EB1, EB2, EB3 and  $\beta$ -actin expression levels. A and B) The expression of both EB1 and EB2 appears higher in MDA-MB-231 cells compared to MCF-7 cells. C) EB3 expression appears higher in MCF-7 compared to MDA-MB-231 cells. The molecular weight of all three proteins is approximately 37kDa.  $\beta$ -actin was used as the loading control. Blots shown is from 1 of 2 experiments.

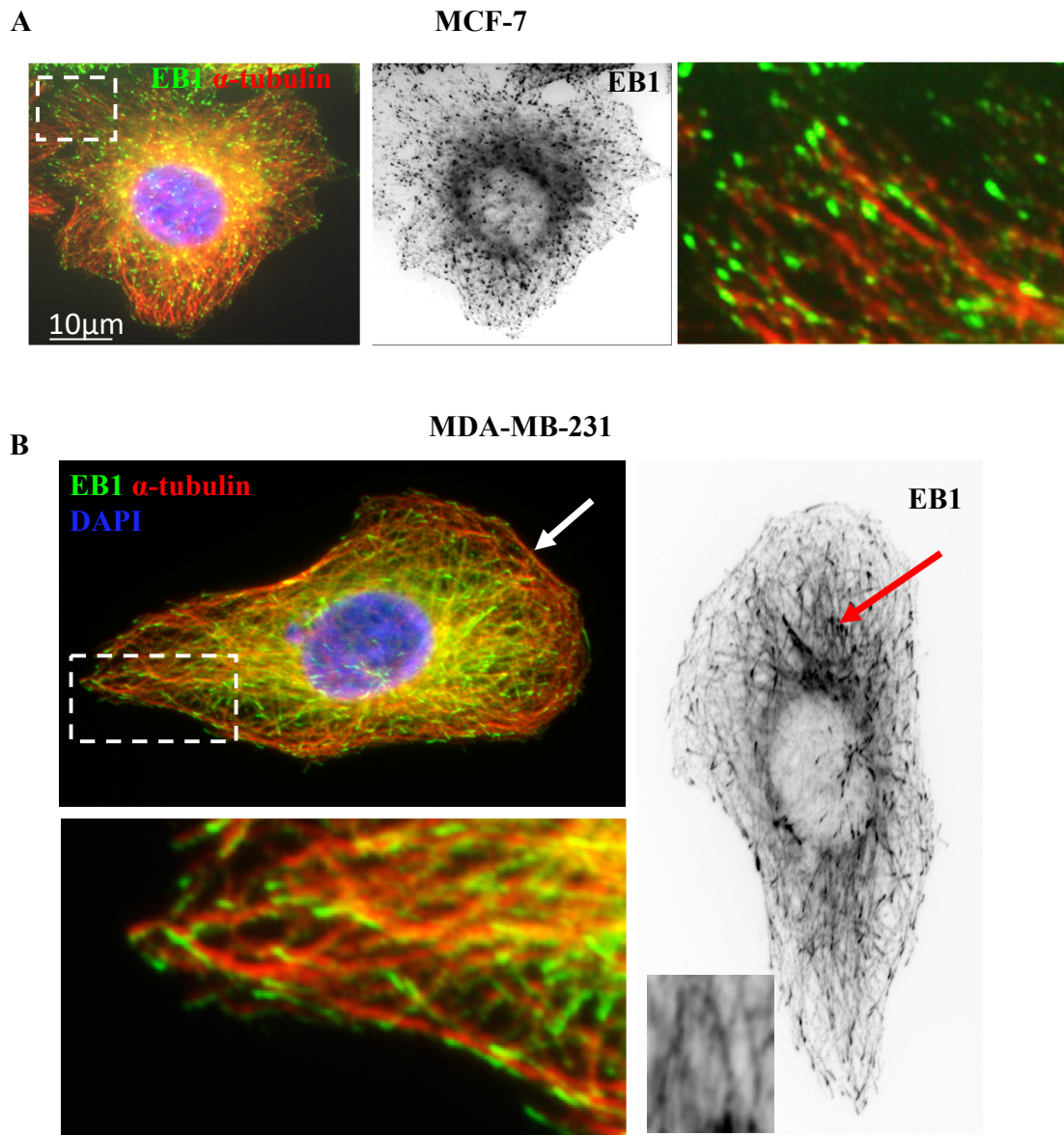
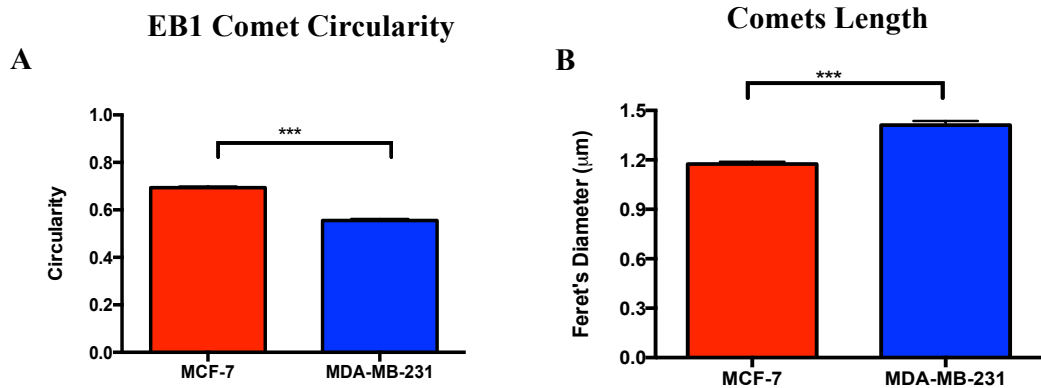


**Figure 3.8: Localisation of EB1 in MCF-7 and MDA-MB-231 cells.** Cells were immunolabelled with an anti- $\alpha$ -tubulin antibody (red, pAb, ab15246) and anti-EB1 antibody (green, mAb, BD 610535). Widefield fluorescent images of MCF-7 and MDA-MB-231 cells. A) EB1 appear as dot-like shaped comets at MT plus-ends in the MCF-7 cell. MTs are disorganised and radiates out from the centre. Enlarged image shows EB1 forming comet-like structures mainly at the plus-ends. B) MTs are highly disorganised, forming interwoven networks (white arrow). The majority of EB1 localise to the +TIP, which are elongated in shape compared to MCF-7 cells (enlarged region) but some show lattice association (red arrow in inverted image and enlarged in inset). Scale bar = 10  $\mu$ m.



MCF-7: Average number of comets in one cell = **194**

MDA-MB-231: Average number of comets in one cell = **111**

**Figure 3.9: EB1 Comet Analysis in MCF-7 and MDA-MB-231 cells.** ImageJ was used to analyse the comets. Statistical analysis using two-tailed unpaired t-test. A) EB1 circularity is higher in MCF-7 cells at 0.7 compared to 0.5 in MDA-MB-231 cells. B) Feret's diameter of comets is higher in MDA-MB-231 cells compared to MCF-7 cells. Analysis by unpaired t-test revealed a significant increase in feret's diameter in MDA-MB-231 cells at 1.4  $\mu\text{m}$  compared to MCF-7 cells 1.2  $\mu\text{m}$ . \*\*\* $p < 0.0001$ . Error bars = SEM. No of cells measured = 10. Based on one experiment.

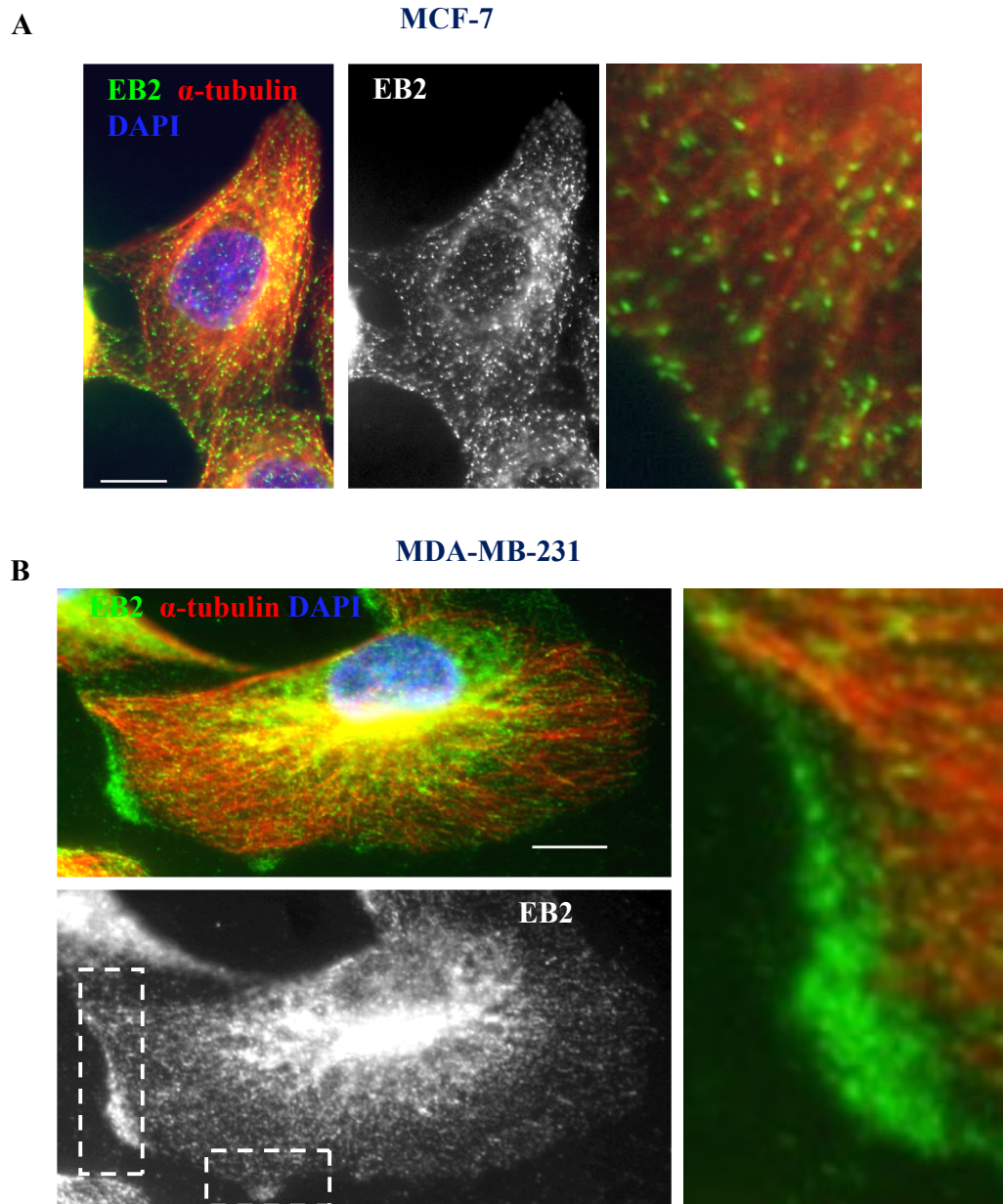
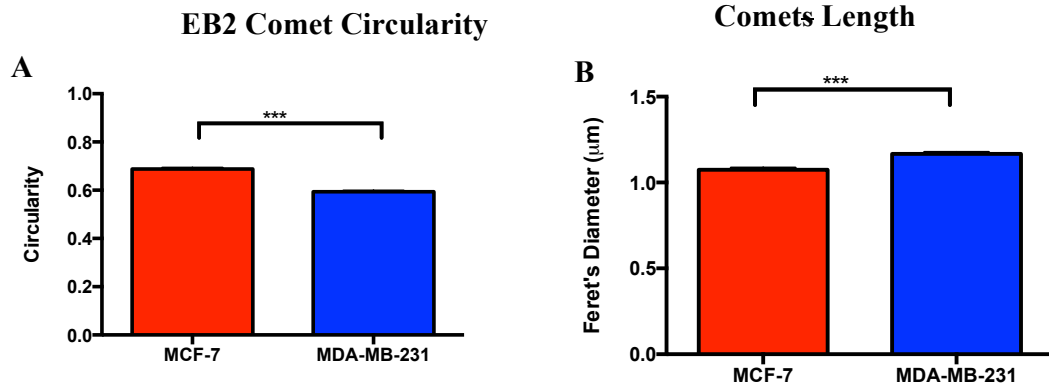


**Figure 3.10: Localisation of EB2 in MCF-7 and MDA-MB-231 cells.** Cells immunolabelled with an anti- $\alpha$ -tubulin antibody (red, pAb, ab15246) and anti-EB2 (K52, ab45767) monoclonal antibody (green). Widefield fluorescent images of MCF-7 and MDA-MB-231 cells. A) EB2 is expressed throughout the MCF7 cell with dot-like shaped comets at the plus-end of MTs (enlarged region). B) EB2 is not specific to the plus-end and can be seen concentrated in the cytoplasm and protruding parts of the MDA-MB-231 cell (enlarged region). Scale bar = 10 $\mu$ m.



MCF-7: Average number of comets in one cell = **258**

MDA-MB-231: Average number of comets in one cell = **418**

**Figure 3.11: EB2 Comet Analysis in MCF-7 and MDA-MB-231 cells.** ImageJ was used to analyse the comets. Statistical analysis using two-tailed unpaired t-test. A) There is a significantly higher EB2 circularity in MCF-7 cells compared to MDA-MB-231 cells. B) Feret's diameter is higher in MDA-MB-231 compared to MCF-7 cells. Analysis by unpaired t-test revealed a significant increase in feret's diameter in MDA-MB-231 cells compared to MCF-7 cells. \*\*\* $p < 0.0001$ . Error bars = SEM. No of cells measured = 10.

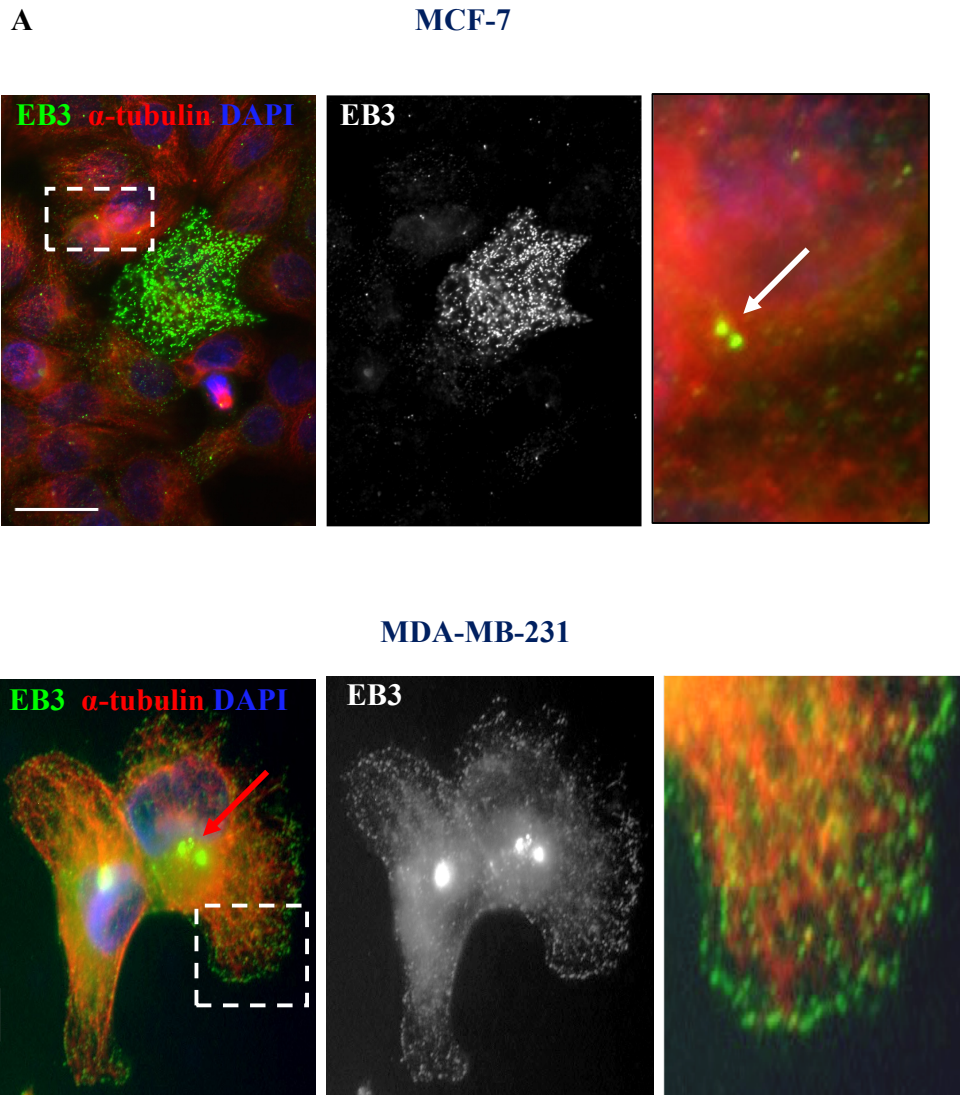


**Figure 3.12: Localisation of EB3 in MCF-7 and MDA-MB-231 cells.** Cells immunolabelled with an anti- $\alpha$ -tubulin antibody (red, pAb, ab15246) and anti-EB3 (K36) monoclonal antibody (green). Widefield fluorescent images of MCF-7 and MDA-MB-231 cells. A) There is sporadic expression of EB3 in MCF7 cells. In the cell with the upregulation of EB3, EB3 comets associate with plus ends of MTs. In other cells, EB3 is evident at the centrosome specifically concentrated at the centrioles (enlarged region & white arrow). B) EB3 is highly concentrated at centrosomes (bright region; red arrow), some observed as punctate in the cytoplasm and near the periphery (enlarged region) Scale bar = 10 $\mu$ m.

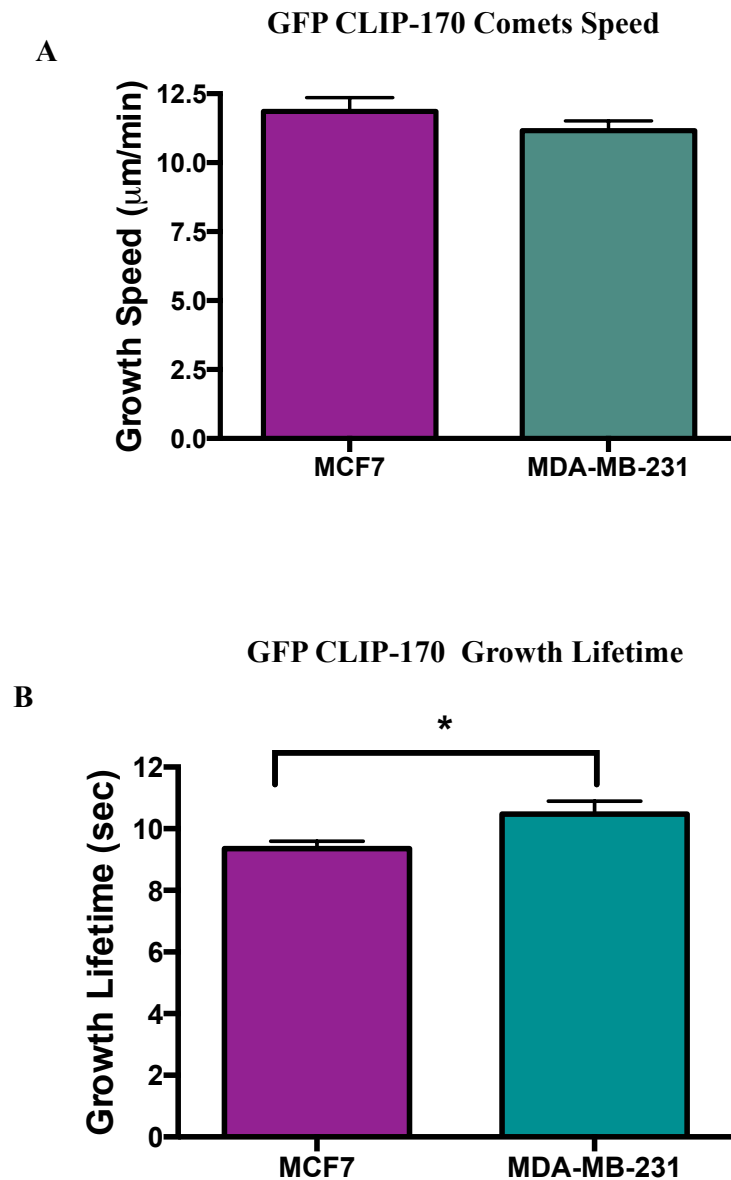


**Figure 3.13: Increased growth lifetime but not comet speed in highly metastatic breast cancer cells.** A) Analysis by unpaired t-test showed that GFP-CLIP-170 comet speed was not significantly different in MDA-MB-231 compared to MCF-7 cells. B) GFP-CLIP-170 growth lifetime was significantly increased in MDA-MB-231 compared to MCF-7 cells. \* $p < 0.05$ . Error bars = SEM. No of cells measured = 10. Based on one experiment.

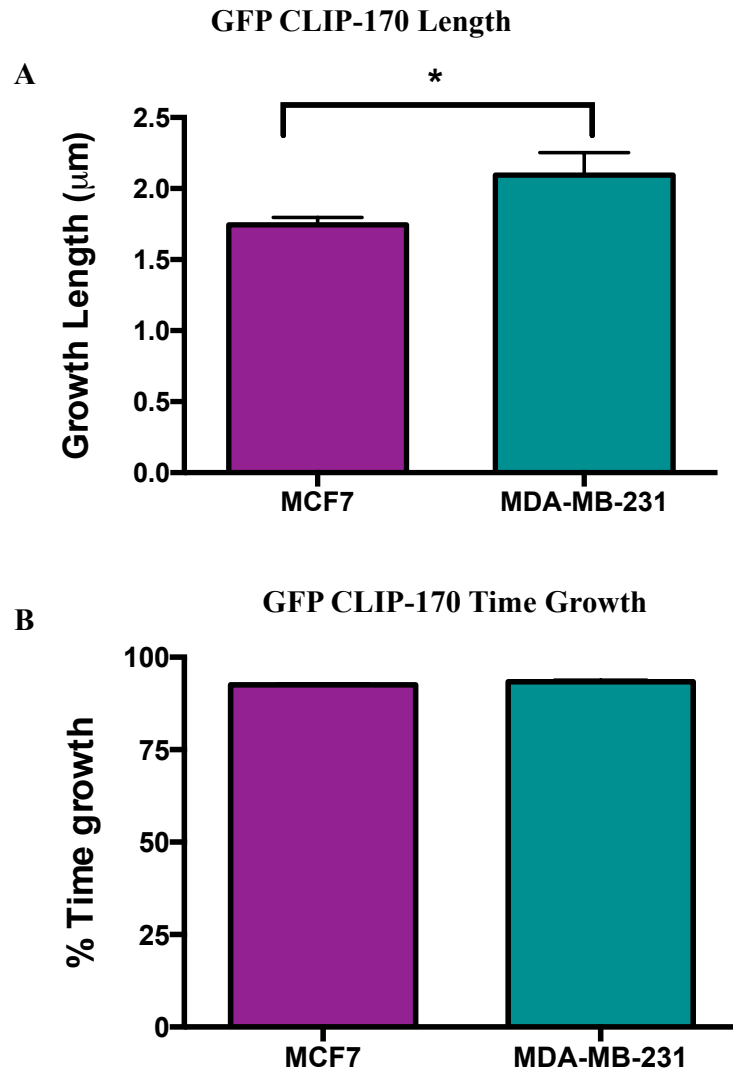


**Figure 3.14: Increased growth length but not time growth in highly metastatic breast cancer cells.** A) Analysis by unpaired t-test showed that GFP-CLIP-170 growth length was significantly increased in MDA-MB-231 when compared to MCF-7 cells. B) GFP-CLIP-170 % time spent in growth was not significantly different in MDA-MB-231 when compared to MCF-7 cells. This is the total percentage time MTs spend in the growth phase. \* $p < 0.05$ . Error bars = SEM. No of cells measured = 10. Based on one experiment.

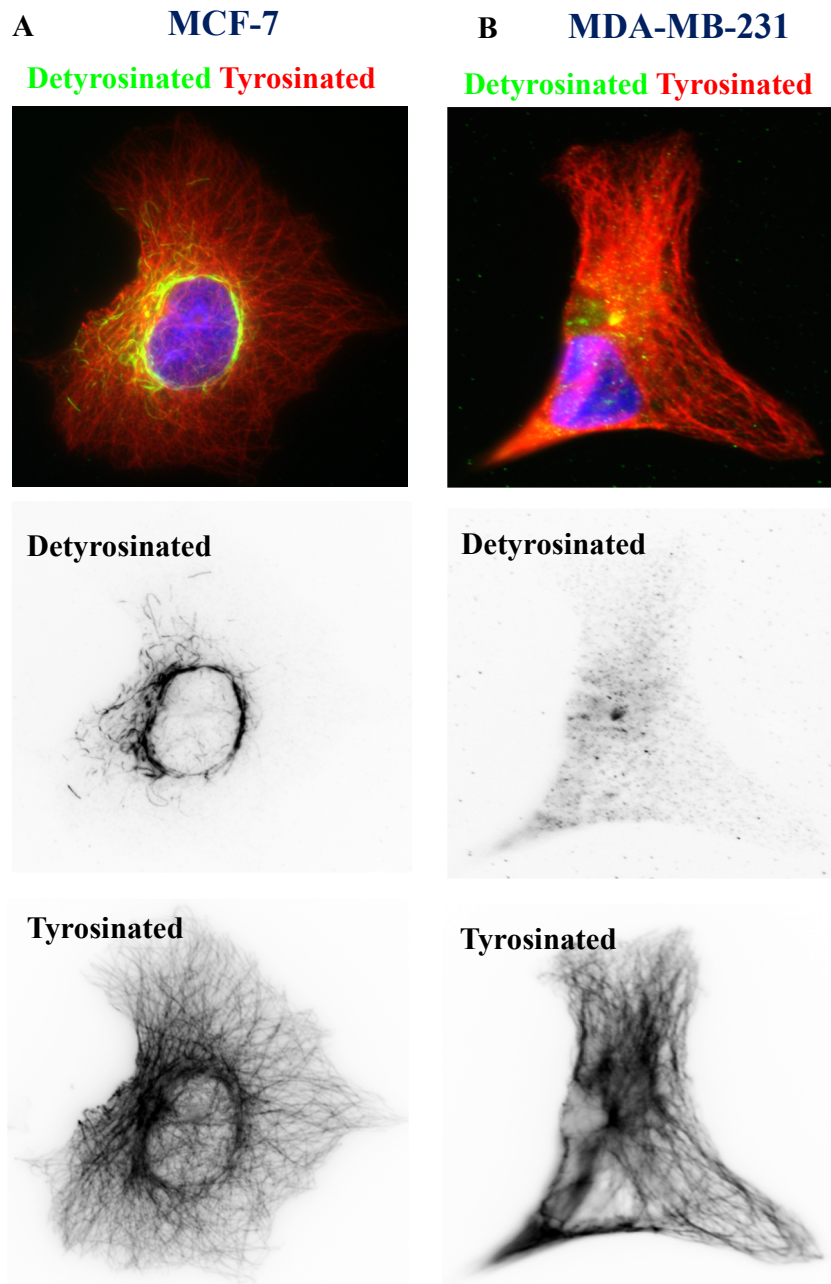


**Figure 3.15: Detyrosinated tubulin localisation in MCF-7 and MDA-MB-231 cells.** Cells immunolabelled for detyrosinated tubulin (green, mAb, ab48389) and tyrosinated tubulin (red, YL1/2, ab6160). A) Merged image shows that there were some detyrosinated MTs localised at the centre of the cell with most of the MTs being tyrosinated. Single channel shows detyrosinated tubulin clustered around the nucleus. B) Image of an MDA-MB-231 cell shows that most of the MTs are tyrosinated with a few speckles of detyrosinated MTs seen in the single channel image. Scale bar = 10 $\mu$ m.

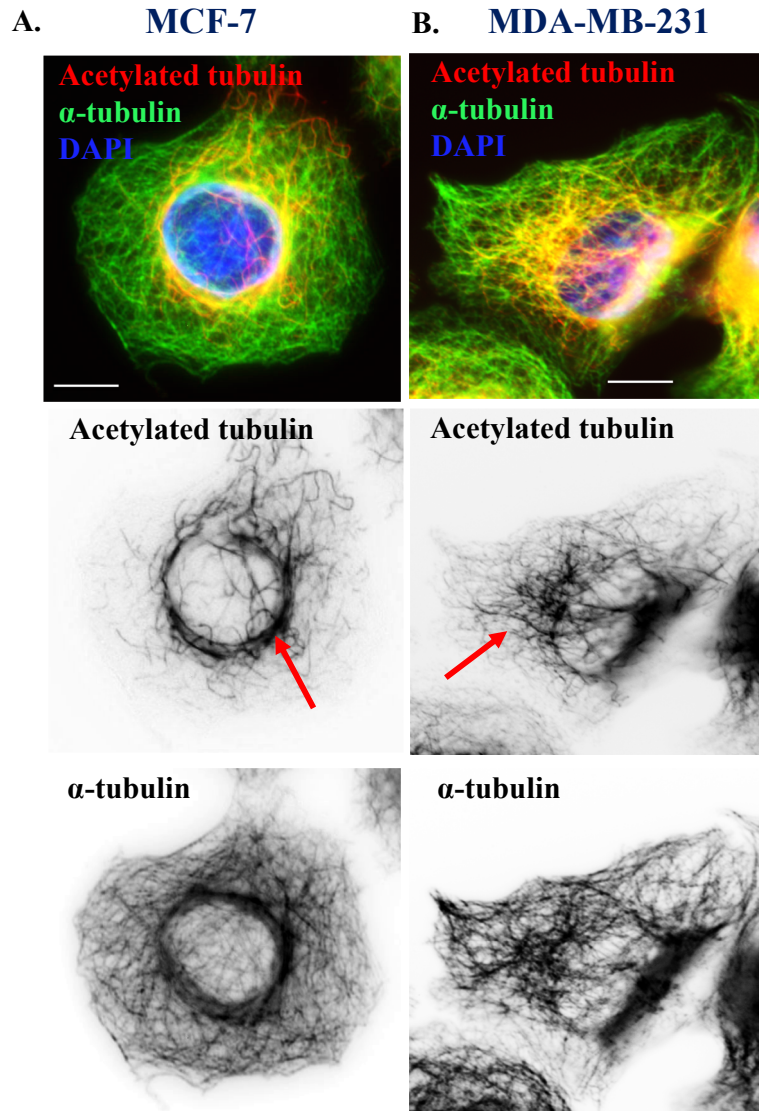


**Figure 3.16: MT acetylation in MCF-7 and MDA-MB-231 cells.** Cells immunolabelled for acetylated tubulin (red, mAb) and  $\alpha$ -tubulin (green, pAb, ab15246). A) In a MCF-7 cell, MTs appear disorganised and bundled around the nucleus with acetylated tubulin curled around the nucleus towards the periphery (red arrow). B) MDA-MB-231 cell also exhibit a disorganised MT network but with straighter acetylated tubulin (red arrow) compared to the MCF-7 cell. Scale bar = 10 $\mu$ m.

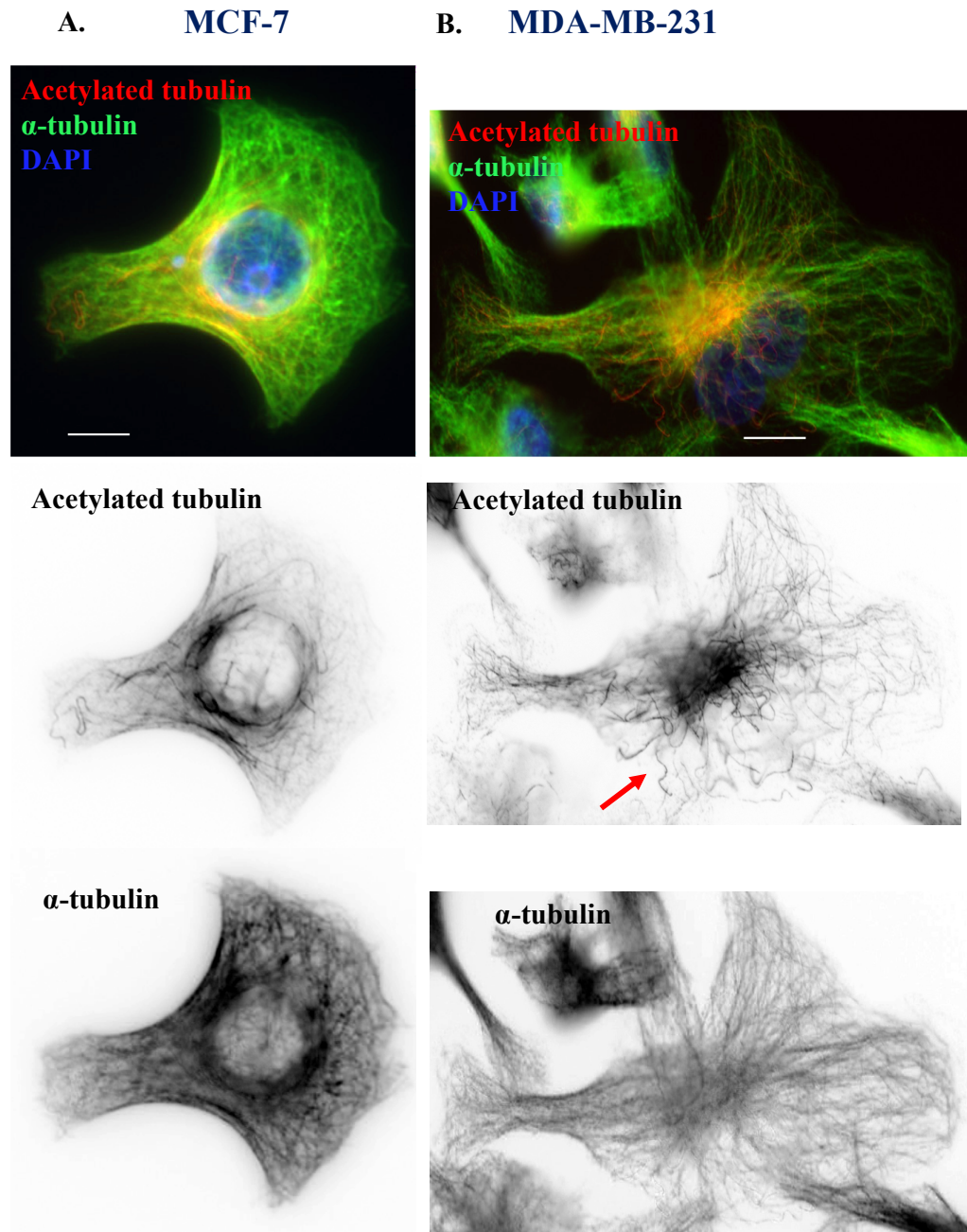


**Figure 3.17: MT acetylation in migrating MCF-7 and MDA-MB-231 cells.** Cells immunolabelled for acetylated tubulin (red, mAb) and  $\alpha$ -tubulin (green, pAb, ab15246). A) In a migrating MCF-7 cell, MTs appear disorganised with acetylated tubulin around the nucleus and some at the back. B) MDA-MB-231 cell exhibits a curly network of acetylated tubulin (red arrow) while there is a classic radial array of MTs. Scale bar = 10 $\mu$ m.

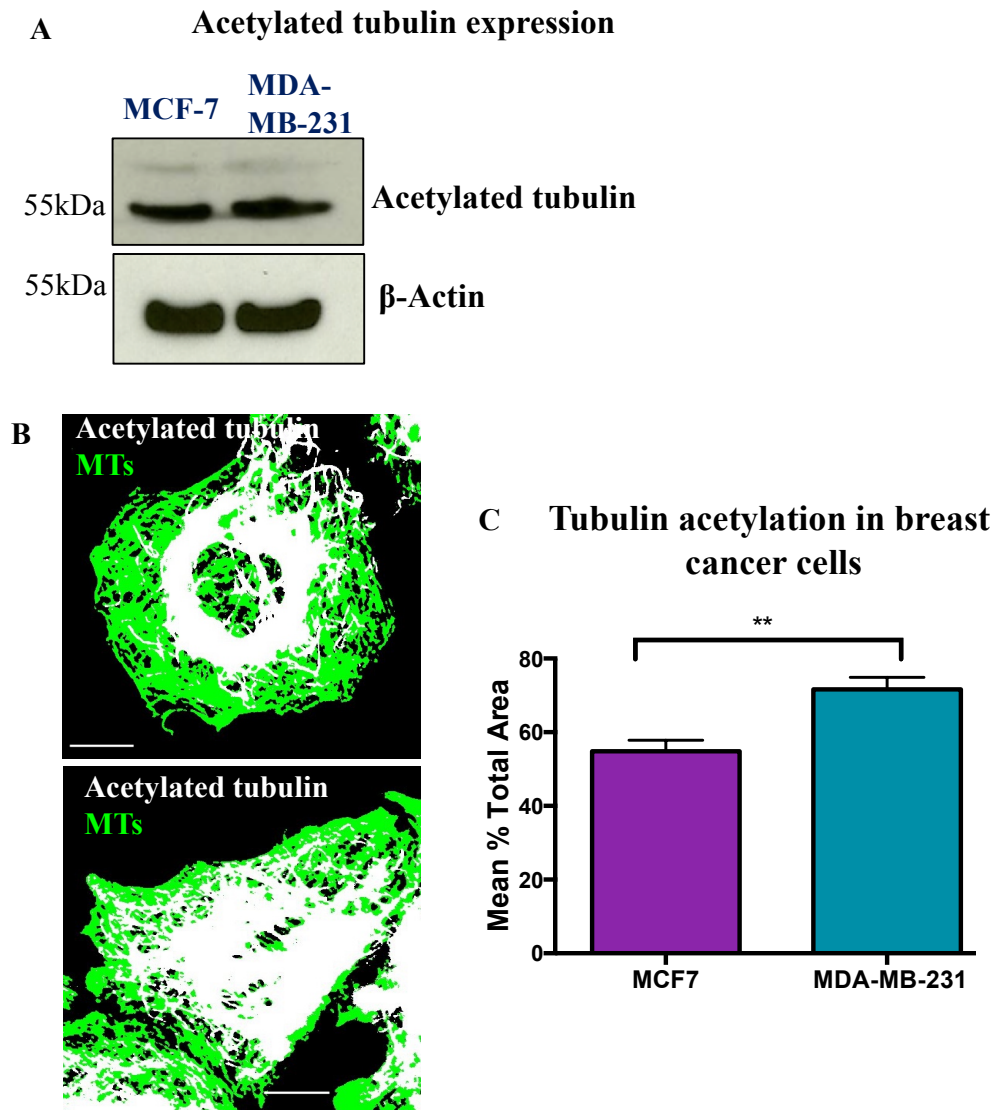


**Figure 3.18: Fluorescence intensity analysis suggest increased MT acetylation in highly metastatic breast cancer cells but no change seen in the expression levels.** A) Expression of acetylated tubulin suggests no difference in levels in MCF-7 compared to MDA-MB-231 cells. B) Overlay images show the proportional area acetylated tubulin occupied in relation to total tubulin. C) Fluorescence intensity analysis was used to estimate the proportion of acetylated tubulin compared to total  $\alpha$ -tubulin in the two cell lines using ImageJ. The same microscope settings were used for all images. Analysis by unpaired t-test showed a significant increase in acetylated area in MDA-MB-231 cells compared to MCF-7 cells. **\*\*** $p < 0.001$ . Error bars = SEM. No of cells measured = 10 per condition from one experiment.

Cold Treatment

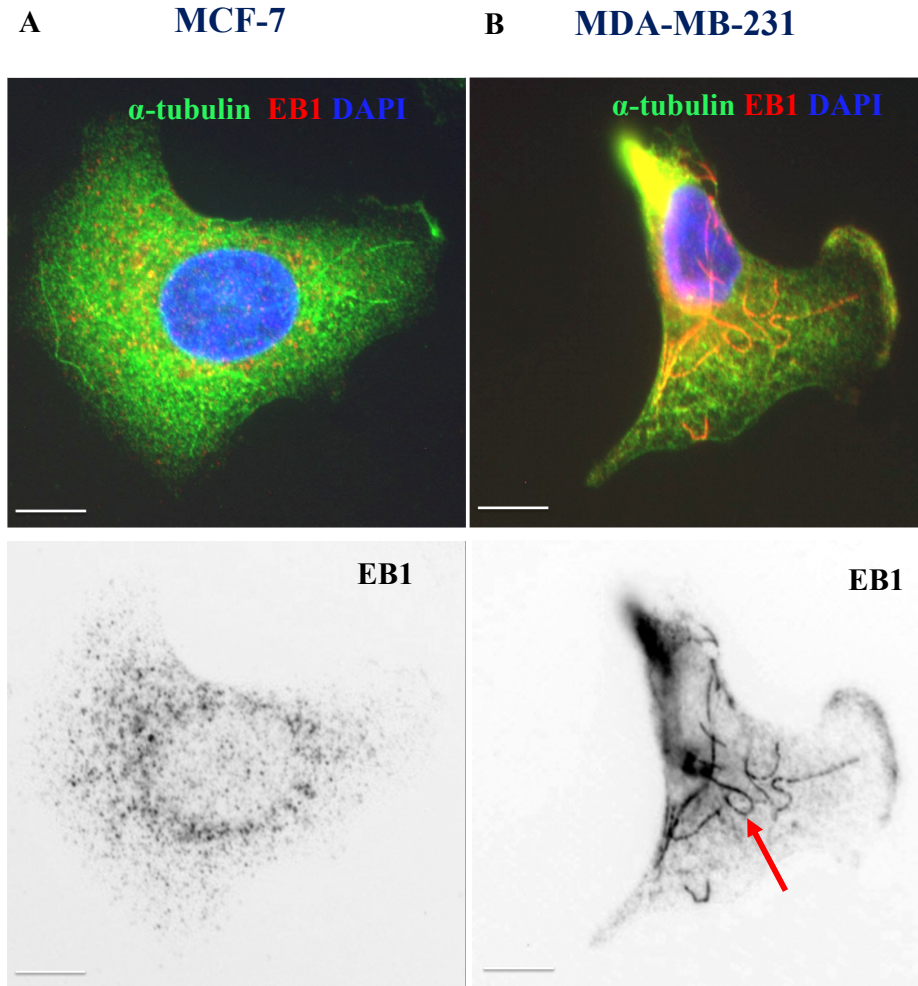


**Figure 3.19: Cold treatment resulted in total MT depolymerisation in most MCF-7 cells but revealed some stable MTs in MDA-MB-231 cells.**

Cells immunolabelled for EB1 (red, mAb, BD 610535) and  $\alpha$ -tubulin (green, pAb, ab15246). A) Cold treatment for 10 mins resulted in total MT depolymerisation in most MCF-7 cells. B) However, some stable MTs were observed in the MDA-MB-231 cells and these showed EB1 lattice association (red arrow). More stable MTs in the MDA-MB-231 cells suggest there is an increased balance between stable and dynamic MTs required for cell migration. This may explain the increased random cell migration in MDA-MB-231 cells. Scale bar = 10 $\mu$ m.

# **Chapter IV: Migration Studies in EB2 Overexpressing Cells**

## **4.1 Overview**

This chapter presents the effects of EB2-upregulation on cell migration in breast cancer cells and stably overexpressing EB2 epithelial cells. One of the questions we aimed to answer is whether high expression of EB2 influence random cell migration in terms of speed and distance travelled. The study also investigates if EB2-overexpression affects directional cell migration using wound healing assay and micro-patterned coverslips. If EB2 overexpression is shown to lead to increased migration and invasion, then EB2 protein could be used as a possible marker for invasive breast cancer. This is important because increased invasion and migration often leads to poor prognosis for patients.

## **4.2 Introduction**

Cell migration is important for normal physiological functions such as wound healing, embryonic development and immune responses. It also contributes to many pathological diseases such as multiple sclerosis and cancer including breast cancer. Breast cancer is a common cause of cancer death in the UK (Cancer Research UK, 2012), which is mainly from primary to secondary site migration. Thus, understanding the molecular mechanisms involved in cell migration is key to developing effective breast cancer treatments.

For migration to take place, all four processes of cell migration must be temporally and spatially coordinated. In migrating cells, the nucleus-centrosome axis is oriented in the same direction of migration whereby MTs accumulate at the front of the cell. Consequently, this leads to a polarised MT network important for transporting molecules to the leading edge of the cell (Etienne-Manneville, 2013). MT polarisation in migrating cells is further regulated by the Par complex. Cdc42 binds and recruits Par-6, then aPKC, which in turn leads to the phosphorylation and inhibition of GSK3 $\beta$  (Etienne-Manneville and Hall, 2003a, Etienne-Manneville and Hall, 2003b). Therefore, the Par complex acts by regulating GSK3 kinases before exerting its effect on many of its downstream substrates. For example, ACF7 an actin and MT crosslinker, is phosphorylated on its GSR domain by GSK3 $\beta$  to inhibit its binding to MTs. However, in skin stem cells, the inhibition of GSK3 $\beta$  creates a gradient at the leading edge,

allowing ACF7 to remain unphosphorylated and active, so that it can link actin and MTs for migration to occur (Wu et al., 2011).

The position of the centrosome, nucleus and Golgi complex contributes to the enhanced MT growth towards the leading edge (Efimov et al., 2007, Sütterlin and Colanzi, 2010). In migrating cells such as epithelial cells, the MTOC reorients towards the leading edge in a Cdc42 and dynein dependent manner (Palazzo et al., 2001b). Rho GTPases and integrins are vital for anchoring and stabilising MT plus-ends to the cortex (Gundersen et al., 2004, Watanabe et al., 2005). An example of this occurs in fibroblasts where focal adhesion kinase directs MT stabilisation and migration through RhoA, mDia, APC and EB1. EB1 enhances the interaction of MT plus ends with proteins that function to capture and stabilise MTs (Palazzo et al., 2001b, Wen et al., 2004). In addition to the formation of stabilised MTs, mDia induces the alignment of MTs parallel to actin bundles along the axes of cells (Wen et al., 2004). Interaction between MTs and focal adhesions are also needed to complete cell migration, which ACF-7 and actin cytoskeleton are thought to influence. Targeting MTs to focal adhesions create a feedback loop regulating Rho GTPases and then focal adhesion turnover (Watanabe et al., 2005, Stehbens and Wittmann, 2012a). EB proteins are important in regulating MT dynamics; EB2 downregulation has been observed in MT stability and bundle formation during differentiation in intestinal crypts (Goldspink et al., 2013). Therefore, it is possible that upregulation of EB2 in cancer cells could consequently stimulate migration of cancer cells. Interestingly, EB2 is upregulated in human pancreatic tissues and have been linked to perineural invasion (Abiatari et al., 2009).

Par-3 and dynein have been implicated in centrosome positioning during migration. It was discovered by co-immunoprecipitation in NIH 3T3 cell lysates that Par-3 associated strongly with dynein compared with other cell polarity or dynein-interacting proteins. This association occurred through the N-terminal dimerisation and PDZ1 domains of Par-3. Depletion of Par-3 or dynein inhibition disrupted centrosome positioning and decreased rate of migration compared to control cells. Increased MT pausing was also observed at the cell-cell contacts in wound healing fibroblasts as opposed to the leading edge where pausing is dependent on Par-3 and dynein light intermediate chain 2. Thus, Par-3 and dynein are believed to regulate correct

centrosome positioning and MT dynamics (Schmoranzer et al., 2009). The effect of Par-3 loss in human breast cancer is known to some degree. In human cells, Par-3 cooperated with ErbB2 (a epidermal growth factor receptor) to inhibit E-cadherin junction stability and to disrupt membrane and actin dynamics at cell-cell junctions. The Par complex have been directly connected in localising the force-generating interactions between MTs and the cortex that regulate the position and orientation of centrosomes. In cultured fibroblasts, Par-6/aPKC cooperate with dynein/dynactin to maintain the centrosome near the cell centroid, Cdc42 regulation drives actomyosin-based contraction and cortical flow to control the nucleus away from the leading edge, resulting in a reorientation of nucleus-MTOC axis towards the leading edge (Gomes et al., 2005).

Intercellular reorganisation is another important factor to be considered during EMT (Lamouille et al., 2014). A relatively new study showed that EMT is enabled by a reversal of cell polarity using MCF-10A culture as a model of mammary gland acini. This reversal results from centrosome repositioning. Specifically, centrosomes moved from their non-central, actin-rich position next to intercellular junctions to the cell centre and towards extracellular matrix adhesions on the opposite side of the nucleus. This movement is supported by controlled MT network disassembly whereby TGF- $\beta$  treatment caused a reduction in the total number of MTs via a decrease in MT nucleation and polymerisation; and the release of Par-3 from intercellular junctions resulting in disengagement promotion and mesenchymal cell scattering (Burute et al., 2017).

## 4.3 Results

### 4.3.1 Collagen-I provides a suitable ECM for cell migration in both MCF-7 and MDA-MB-231 cells

In order to determine which extracellular matrix (ECM) was most suitable for promoting migration in the two cell lines, cells were seeded on different matrices – fibronectin and collagen I, and also on tissue culture plastic. Cells seeded sparsely in 24-well plates, either on tissue culture plastic, fibronectin or collagen-I were left to adhere overnight before live time-lapse imaging. Images from live time-lapse recordings of sub-confluent MCF-7 and MDA-MB-231 cells showed different cellular morphologies. MDA-MB-231 cells showed elongated morphologies and a few slightly round cells were present when seeded on plastic (Fig 4.1A). Cells seeded on fibronectin also showed elongated morphologies but mainly with distinct lamellipodium (Fig 4.1B) while cells on collagen-I had marked longer protrusions (Fig 4.1C). MCF-7 cells on plastic showed mainly flat ‘fried-egg’ like structures (Fig 4.1D) while on fibronectin some cells still showed fried-like morphology with some having several small projections (Fig 4.1E). On collagen-I MCF-7 cells showing cells with longer protrusions (Fig 4.1F) compared to those on fibronectin.

The effect of ECM on random cell migration was analysed in MCF-7 and MDA-MB-231 cells when seeded on plastic, fibronectin or collagen-I both at 1mg/ml. Cells were seeded in a 24-well plate (four wells per condition) and time-lapse imaging was carried out for 16 h. Both fibronectin and collagen-1 were tested to determine the most suitable ECM component for these breast cancer cell lines. For analysis, eight separate positions were examined for each condition with five cells from each area therefore a total of 40 cells per condition were analysed. ImageJ was utilised to analyse cell movement by using the manual cell tracking plugin. To allow for the calculation of speed, the position of each analysed cell was recorded for each frame in the time course. If a cell that was being tracked entered mitosis, then only one of the daughter cells was followed for the rest of the time-lapse. The position results were used to calculate the average velocity for each of the tracked cells. Average velocities were plotted in a graph

to illustrate an overall average velocity for each condition. Statistical analysis was performed by using a one-way ANOVA with Tukey's multiple comparisons test.

Analysis of random migration revealed that the highly metastatic MDA-MB-231 cells had an average velocity of 0.464, 0.684 and 0.992  $\mu\text{m}/\text{min}$  when seeded on plastic, fibronectin and collagen-I respectively showing that the cells migrated faster on collagen-I (Fig 4.2A, Movie S3, S4 and S5). MCF-7 cells had an average velocity of 0.133, 0.171 and 0.456  $\mu\text{m}/\text{min}$  respectively (Fig 4.2B, Movie S6, S7 and S8) also revealing that MCF-7 had an increased velocity when seeded on collagen-I. Both MDA-MB-231 and MCF-7 cells migrated faster and further on collagen-I than on fibronectin or plastic. Collagen-I was therefore chosen as the most suitable ECM to support migration and was used for all subsequent migration studies unless stated otherwise.

### **4.3.2 MDA-MB-231 cells migrated faster and further than MCF-7 cells**

Using the results established in section 4.3.1, the experiment was repeated by seeding MCF-7 and MDA-MB-231 cells on collagen-I and analysed as previously described. The average velocity of MDA-MB-231 and MCF-7 cells were 1 and 0.4  $\mu\text{m}/\text{min}$  respectively. Forty cells per condition were analysed and statistical analysis by one-way ANOVA revealed that MDA-MB-231 cells had a significantly higher average speed of migration compared to MCF-7 cells (Fig 4.3, Movie S5 and S8). The graph shows one set of data from three independent experiments. The findings confirmed our hypothesis that MDA-MB-231 cells migrate significantly faster than MCF-7 cells. It is proposed that the increased migration of MDA-MB-231 compared to MCF-7 cells might be due to increased expression of EB2 in MDA-MB-231 cells and the highly specific localisation of EB2 at the leading edge (seen in Fig 3.10B). Chemotaxis and migration tool from Ibidi was used to show the distance travelled of individual cells during migration, and this is displayed in spider graphs. Spider graphs showed that MDA-MB-231 cells travelled an average distance of 229.28  $\mu\text{m}$  while that of MCF-7 cells were 92.60  $\mu\text{m}$ . This revealed that MDA-MB-231 cells travelled greater distances compared to MCF-7 cells, which mainly clustered in the centre (Fig 4.4).

### 4.3.3 Localisation of EB2 in MDCKII<sup>mChEmpty</sup> and MDCKII<sup>mChEB2Hi</sup> cells

A major difference between MCF-7 and MDA-MB-231 cells is that EB2 expression is higher in MDA-MB-231 than MCF-7 cells (described in 3.2.1.4). This raises the question whether high EB2 expression could contribute to the increased speed of migration observed in MDA-MB-231 cells. This was further investigated in non-cancerous MDCKII epithelial cells overexpressing EB2. The MDCKII<sup>mChEB2Hi</sup> cell clone stably express mCherry-EB2 and the control cell clone MDCKII<sup>mChEmpty</sup> were generated by Jonathan Gadsby (J Gadsby, Thesis).

Confirmation of mCherry-EB2 protein expression was carried out by Western blotting. Cell lysates were collected from untreated MDCKII and MDCKII cells stably transfected with mCherry-EB2 or mCherry-Empty construct before probing for RFP and the loading control  $\beta$ -actin. The bands corresponding to the tagged RFP construct was seen at around 65kDa in the RFP probed blot (Fig 4.5A) and  $\beta$ -actin below 55kDa marker. EB2 was also probed for, which can be seen in the MDCKII<sup>mChEB2Hi</sup> lane but not in untreated or MDCKII<sup>mChEmpty</sup> cells (Fig 4.5B). An explanation for this might be that all three sub-cell lines had low levels of endogenous EB2 expression, difficult to detect by the Odyssey machine, since the band in the MDCKII<sup>mChEB2Hi</sup> lane is above the usual 37kDa marker suggesting that the band detected is the one tagged to RFP. Therefore, it is difficult to draw conclusions and the experiment needs to be repeated.

Next, EB2 overexpression was verified in cells by immunolabelling. These new widefield fluorescent images of confluent MDCKII cells showed no differences in  $\alpha$ -tubulin localisation in MDCKII<sup>mChEB2Hi</sup> compared to MDCKII<sup>mChEmpty</sup> cells however EB2 expression is higher in MDCKII<sup>mChEB2Hi</sup> compared to MDCKII<sup>mChEmpty</sup> cells (Fig 4.6). Cells were then immunolabelled with an anti- $\alpha$ -tubulin antibody and anti-EB2 antibody. In a sub-confluent layer, EB2 was sparsely localised and dotted in MDCKII<sup>mChEmpty</sup> cells (Fig 4.7) as opposed to MDCKII<sup>mChEB2Hi</sup> cells where some EB2 is seen in the cytoplasm and not associating with MTs (Fig 4.8). More importantly, EB2

can be observed at the leading edge of cells and some accumulating along the MT lattice in MDCK<sup>mChEB2Hi</sup> cell (Fig 4.9).

### 4.3.4 Increased speed of random migration associated with EB2-overexpression in MDCKII cells

Stably expressing MDCKII<sup>mChEB2Hi</sup> cells were seeded in a 24-well plate (eight wells per condition) for time-lapse imaging. MDCKII<sup>mChEmpty</sup> cells had a ‘fried-egg’ like morphology (Fig 4.10A) with a few cells having protrusions. However, MDCKII<sup>mChEB2Hi</sup> cells had a more elongated morphology with more cells having protrusions (Fig 4.10B) compared to MDCKII<sup>mChEmpty</sup> cells. This is similar to the phenotypic changes seen in the more elongated MDA-MB-231 cells.

For analysis, eight separate positions were examined for each condition with ten cells from each area therefore a total of 80 cells per condition were analysed. ImageJ was utilised to analyse cell movement by using the manual cell tracking plugin as previously described. The average velocity result for each cell analysed was calculated and plotted in a graph to illustrate an overall average velocity for each condition. Statistical analysis was performed by using a one-way ANOVA with Tukey’s multiple comparisons test. Result shown is one out of two repeats. In MDCKII<sup>mChEB2Hi</sup> cells, the average velocity of random cell migration was 0.514  $\mu\text{m}/\text{min}$  compared with untreated and MDCKII<sup>mChEmpty</sup> cells of 0.324  $\mu\text{m}/\text{min}$  and 0.392  $\mu\text{m}/\text{min}$  respectively (Fig 4.11A, Movie S9, S10 and S11). The results show a statistical significance in MDCKII<sup>mChEB2Hi</sup> cells when compared with MDCKII<sup>mChEmpty</sup> cells. Analysis of the distance travelled by individual cells during migration was carried out. Spider graphs revealed that MDCKII<sup>mChEB2Hi</sup> cells travelled an average distance of 125.50  $\mu\text{m}$  while that of MDCKII<sup>mChEmpty</sup> cells were 105.68  $\mu\text{m}$  showing that MDCKII<sup>mChEB2Hi</sup> cells travelled greater distances when compared with MDCKII<sup>mChEmpty</sup> cells (Fig 4.11B).

### 4.3.5 Directional cell migration and centrosome positioning in MDCKII<sup>mChEB2Hi</sup> cells

Similar to random cell migration experiments, cells seeded to confluency for directional migration – scratch assays were analysed. MDCKII<sup>mChEmpty</sup> and MDCKII<sup>mChEB2Hi</sup> cells were seeded to confluency before using a p200 pipette tip to make a scratch in the cells then replacing the medium with 25 nM, 50 nM Taxol or 0.0005% DMSO. Cells were monitored over a 6 h time-period. Analysis by student's t-test revealed that at 6 h, the area closed in the DMSO-treated MDCKII<sup>mChEB2Hi</sup> cells ( $6.71 \times 10^5 \mu\text{m}^2$ ) was significantly greater compared to the DMSO-treated MDCKII<sup>mChEmpty</sup> cells ( $6.09 \times 10^5 \mu\text{m}^2$ ) (Fig 4.12 and 4.13). This is supported by results by a previous lab member (Jonathan Gadsby) where an increase in the rate of migration was found in untreated MDCKII<sup>mChEB2Hi</sup> cells compared to MDCKII<sup>mChEmpty</sup> cells (Data from Mogensen lab, 2014). Due to this result, it was thought to check whether Taxol could be used to try to rescue the effect of high level of EB2 on migration. Analysis by one-way ANOVA with Tukey's multiple comparisons test revealed a significant decrease in the area closed in MDCKII<sup>mChEB2Hi</sup> and MDCKII<sup>mChEmpty</sup> cells treated with Taxol (Fig 4.14A and B). Since the area closed in MDCKII<sup>mChEB2Hi</sup> cells decreased even more than the MDCKII<sup>mChEmpty</sup> cells, it is possible that the high expression of EB2 makes the cells more sensitive to Taxol. However, these are only preliminary findings so it was difficult to draw conclusions. The experiment would need to be repeated possibly with a lower concentration of Taxol.

To test the effect of EB2-overexpression in cells, on centrosome positioning experiments were carried out using micro-patterned coverslips (described in section 2.7.3). A cross-bow shaped micropattern was used to induce a migratory polarisation morphology in cells to determine if centrosome positioning was affected in EB2 overexpressing cells. Cells were seeded on collagen-I-coated CYTOO cross-bow micro-patterns for 8h before fixing and immunolabelling for  $\alpha$ -tubulin and  $\gamma$ -tubulin. Widefield fluorescent images taken showed that the centrosome position appears to in most cases to be in front of the nucleus in untreated and MDCKII<sup>mChEmpty</sup> cells compared to MDCKII<sup>mChEB2Hi</sup> cells where the centrosome appears to be behind the nucleus (Fig 4.15). Analysis of the centrosome position in respect to the centre of the

nucleus was carried out on 50 images per condition using ImageJ and Matlab (details in chapter 2). The analysis revealed that a significant number of cells had their centrosome at the back of the nucleus in MDCKII<sup>mChEB2Hi</sup> (26%) compared to MDCKII<sup>mChEmpty</sup> or untreated cells (16 and 10%) respectively (Fig 4.16). This finding suggests that the polarity was affected and it could potentially affect the directionality of cells.

## 4.4 Discussion

### 4.4.1 Collagen-I proved to be a suitable ECM for cell migration in both MCF-7 and MDA-MB-231 cells

Cells are provided with structural support through a network known as the ECM. Many cellular processes involve interactions between the ECM and the cell such as cellular migration where the ECM delivers environmental cues to cells. Insoluble fibronectin is a major component of the ECM. In this study, both MCF-7 and MDA-MB-231 cells migrated on fibronectin. Fibronectin is known to interact with integrins.  $\alpha 5\beta 1$ ,  $\alpha 8\beta 1$ ,  $\alpha \nu\beta 1$ ,  $\alpha \nu\beta 3$ ,  $\alpha \text{IIb}\beta 3$ ,  $\alpha \nu\beta 5$ ,  $\alpha \nu\beta 6$  and  $\alpha \nu\beta 8$  integrins recognise the Arg-Gly-Asp (RGD) motif found in many ECM components (Danen and Sonnenberg, 2003). Of these,  $\alpha 5\beta 1$  and  $\alpha \nu\beta 3$  are particularly efficient in mediating fibronectin matrix assembly (Wennerberg et al., 1996, Wu et al., 1996). The RGD motif is the site of cell attachment via  $\alpha 5\beta 1$  and  $\alpha \nu\beta 3$  integrins on the cell surface. Fibronectin has three types of modules – type I, II and III. Module III<sub>9</sub> acts together with the III<sub>10</sub> binding site to enhance integrin-mediated cell adhesion (Sechler et al., 1997).

Integrin  $\alpha 1\beta 1$  and  $\alpha 2\beta 1$  are expressed on epithelial cells and bind to collagen-I, but  $\alpha 2\beta 1$  integrin is the main collagen receptor. *In vitro* studies suggested that  $\alpha 1\beta 1$  prefers the monomeric form of collagen I to the fibrillar form that is present in mature connective tissues (Jokinen et al., 2004). Integrin and collagen-I interaction is promoted by magnesium and manganese (Tuckwell et al., 1996). In a relatively recent study, mice deficient in integrin  $\alpha 2$  was found to have an increased tumour cell intravasation, this suggests that the presence of  $\alpha 2$  serves as a metastasis suppressor (Ramirez et al., 2011).

This is further supported by microarray analysis on human breast cancer, which established that decreased expression of the gene encoding  $\alpha 2$  integrin, but not the  $\alpha 1$  or  $\beta 1$  integrin genes, was a predictor of metastatic dissemination and decreased survival (Ramirez et al., 2011).  $\beta 1$  expression was not reported to be significantly different between MCF-7 and MDA-MB-231 cells (Taherian et al., 2011), though no reports were found on  $\alpha 2$  expression in the two cell lines.

$\alpha 5$  and  $\alpha V\beta 3$  expression was found to be higher in invasive MDA-MB-231 cells compared to the non-invasive MCF-7 cells (Bauer et al., 2007, Mierke et al., 2011) and MDA-MB-231 was found to have little adhesive property compared to MCF-7 cells. Cell adhesion plays an essential role in cancer progression since integrin interaction with the ECM induces cell proliferation in some cancers while it prevents others from cell death. In metastatic cancers, cell adhesion undergoes rapid turnover that allow cells to disengage from the ECM and migrate. Therian and colleagues (2011) established that MCF-7 and MDA-MB-231 cells adhered better when plated on fibronectin compared to collagen while MCF-7 had a higher binding specificity to collagen in comparison with MDA-MB-231 cells (Taherian et al., 2011). Thus, an increased speed of migration when plated on collagen may be attributed to the increased rate of integrin turnover or reduced expression of  $\alpha 2\beta 1$  integrin in MDA-MB-231 compared to MCF-7 cells. This implies that collagen-I was the better ECM for studying migration in both cell lines compared to fibronectin where the cells had increased adhesive properties and were unable to turnover their interaction. Vargas et al (2012) established that during the transition of *in situ* ductal carcinoma (IDC) to breast cancer invasion, there was an increased expression of Col5 $\alpha 2$  and Col11 $\alpha 1$  in the IDC samples suggesting that these are ECM components used during breast cancer progression (Vargas et al., 2012).

#### **4.4.2 EB2 overexpression causes increased cell migration**

Increased EB2 expression has been linked with highly invasive cells and poor prognosis in pancreatic cancer (Abiatari et al., 2009). Evaluating the random cell migration in the breast cancer cells, there was a 60% increase in migrating MDA-MB-231 cells compared to the MCF-7 cells (Fig 4.3) and it was interesting to establish that the highly migratory MDA-MB-231 cells express elevated levels of EB2. Whether EB2

upregulation influence cell migration in these cells proved difficult to determine as attempts to deplete EB2 in MDA-MB-231 cells was not successful. A non-cancerous epithelial cell line generated to stably overexpress EB2 (MDCKII<sup>mChEB2Hi</sup>) was therefore used to investigate the effects of high EB2 expression on cell migration.

Wound healing and random cell migration experiments were performed on breast cancer cells and stably EB2-overexpressing MDCKII cells. Both types of migration are usually governed by different internal mechanisms that determine whether membrane protrusions form and are maintained at the front of the cell or a different location. This process is generally coordinated by Rho GTPase signalling (Petrie et al., 2009). Random migration assays of MDCKII<sup>mChEB2Hi</sup> cells showed that they moved more quickly than the MDCKII<sup>mChEmpty</sup> cells at an average velocity of 0.51  $\mu\text{m}/\text{min}$  and 0.39  $\mu\text{m}/\text{min}$  respectively resulting in a 31% increase overall (Fig 4.11). Therefore, in the random cell migration, EB2-overexpression was discovered to significantly increase the average speeds as well as the distance travelled. In the scratch assay, the increase in wound area closed in the DMSO-treated MDCKII<sup>mChEB2Hi</sup> cells closed on average 9.2% more than the MDCKII<sup>mChEmpty</sup> cells, which correlated to a significant increase in the degree to which the epithelial layer was able to migrate. A reduction was observed in the Taxol-treated MDCKII<sup>mChEB2Hi</sup> and MDCKII<sup>mChEmpty</sup> cells, and the data suggested that high expression of EB2 may make the cells more sensitive to Taxol. Further experiments including lower concentration of Taxol are required to verify this.

In migration, it is important for MTs protruding into the lamellipodium to be stable while the rest need to be dynamic so the regulation between the two parts need to be coordinated (Kaverina and Straube, 2011). EB2 contributes to focal adhesion turnover by directly associating with proteins, such as MAP4K4 and HAX1 (Yue et al., 2014a, Liu et al., 2015). These studies showed that depletion of EB2 or HAX1 resulted in focal adhesion stability and impaired epidermal cell migration. Therefore, in our studies, EB2-overexpression may contribute to increased cell migration by increasing focal adhesion turnover through HAX1 and MAP4K4. MT network polarisation during migration relies on centrosome repositioning to the front of the nucleus and on increased MT stability at the leading edge. Centrosomal position is regulated by different signalling pathways, and Par-3 and the MT motor dynein have been suggested

to play major roles. Depletion of Par-3 or dynein disrupted centrosome positioning at the cell centre and led to a decreased rate of migration compared to control cells (Schmoranzner et al., 2009). Centrosome mispositioning observed in MDCKII<sup>mChEB2Hi</sup> cells would be expected to cause a reduction in migration. It is possible that the effect of EB2 overexpression is a lot higher thereby overriding the effect caused by centrosome mispositioning explaining why an increased speed of migration was seen in these cells.

During cell migration, the Golgi is usually near the centrosome, which helps polarity and directionality. When this is lost, multiple lamellipodia form in cells making it difficult to follow the right cues hence, loss of directionality is observed. In wound healing, the centrosome is also located in front of the nucleus of directionally migrating cells (Etienne-Manneville and Hall, 2001, Manneville and Etienne-Manneville, 2006), and centrosome removal caused cells to lose their polarisation and directed migration (Wakida et al., 2010). Deregulated Rac1 activity has been implicated in several types of cancer and is known to drive cancer invasion and metastasis. These studies have demonstrated that Rac1 activation in cancer can be regulated by multiple mechanisms (Mack et al., 2011). Centrosome amplification leads to increased MT nucleation, which in turn triggered Rac1 activation and thus increased invasion (Godinho et al., 2014). Another possible explanation could be that EB2-overexpression prevents the plus-end capture of MTs at cortical Par-3/dynein sites thus maintenance of centrosome positioning at the front of the cell is lost. Involvement of Par-3/dynein at cortical sites for the maintenance of centrosome positioning have already been reported by (Schmoranzner et al., 2009).

## **4.5 Summary**

In summary, experiments carried out showed that collagen-I provide good ECM support for studying migration in both MCF-7 and MDA-MB-231 cells. The results also point towards EB2-overexpression causing an increase in cell migration and leading to an accumulation of EB2 at the leading edge. In addition, these preliminary data suggest that EB2-overexpression acts as a deregulator of centrosome positioning, therefore, there is scope for continuous investigations to expand on these exciting

results. For future experiments, investigations could be made on MDCKII<sup>mChEB2Hi</sup> and MDCKII<sup>mChEmpty</sup> cells using CYTOO micro-patterns to determine whether EB2 overexpression influences positioning of polarity proteins such as Par-3 and aPKC in centrosome positioning during migration (Schmoranzer et al., 2009). These micro-patterns are of great importance because they enable repeated samples of cells with the same architecture to be generated and this is beneficial for imaging and quantitative analyses. It is important to assess further whether there are any alterations in the expression of mesenchymal markers such as N-cadherin or vimentin, which are crucial following a switch to a mesenchymal phenotype.

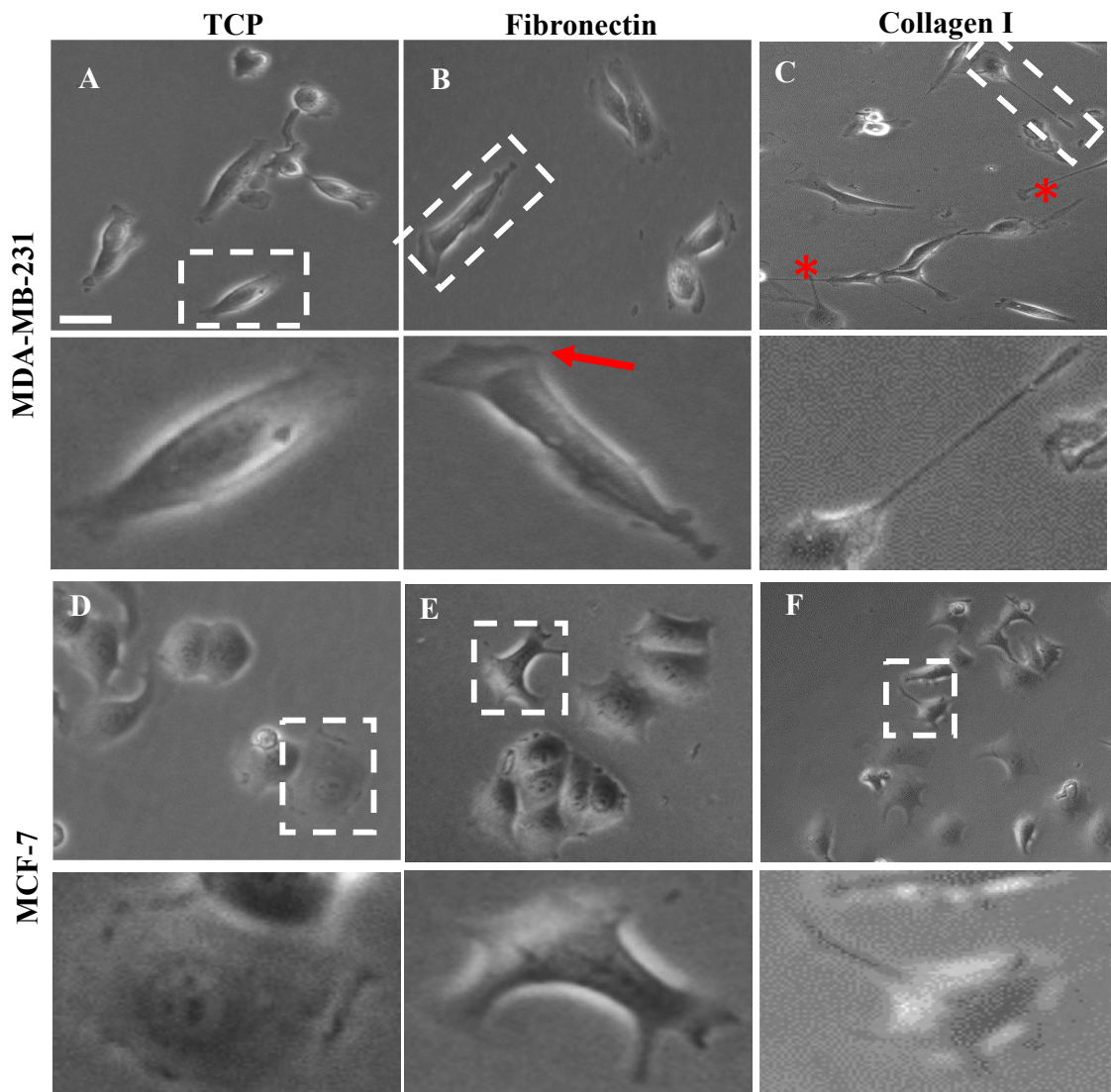


**Figure 4.1: Morphology of MDA-MB-231 and MCF-7 cells seeded on different ECM.**

Images from live time-lapse recordings (using X20 lens) of cells on tissue culture plastic (TCP), fibronectin (FN) and collagen-I (Col.I) A) MDA-MB-231 cells showing elongated morphologies (enlarged region) and a few slightly round cells are evident on plastic. B) MDA-MB-231 cells on fibronectin showing elongated shape with distinct lamellipodium (arrow in enlarged region) compared to those seeded on plastic. C) MDA-MB-231 cells on collagen-I with very distinct longer protrusions (asterisks & boxed region). D) MCF-7 cells on plastic show mainly flat ‘fried-egg’ like structure (enlarged region). E) MCF-7 cells on fibronectin showing fried-like morphology with some cells having several small projections (boxed and enlarged). F) MCF-7 cells on collagen-I showing cells mainly with short protrusions and some with ‘fried-egg’ like morphology (boxed region). Scale bar = 100  $\mu$ m.

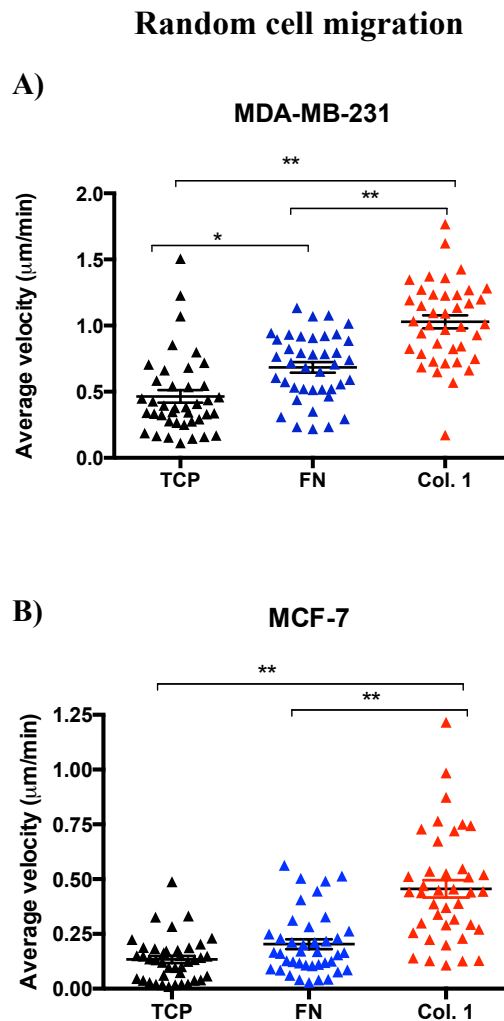


**Figure 4.2: Migration of MDA-MB-231 and MCF-7 cells when seeded on plastic, fibronectin and collagen I.** Live time-lapse imaging was used to take images every 10 min for 16 h. 40 cells per condition were analysed. The position of random cells were tracked in ImageJ and the average velocity of cells plotted. A) Average velocity of MDA-MB-231 cells on TCP, FN and Col.1 were 0.464, 0.68 and 0.992  $\mu\text{m}/\text{min}$  respectively. MDA-MB-231 cells had a higher velocity on collagen-1 compared to cells on TCP or FN. B) Average velocity of MCF-7 cells on TCP, FN and Col.1 were 0.133, 0.17 and 0.456  $\mu\text{m}/\text{min}$  respectively showing the cells migrated faster on collagen-1 compared to cells on TCP or FN. TCP = Tissue Culture Plastic, FN= Fibronectin and Col.1 = Collagen I. Statistical analysis using one-way ANOVA with Tukey's multiple comparisons test. Results shown is from one experiment. Mean  $\pm$  SEM.

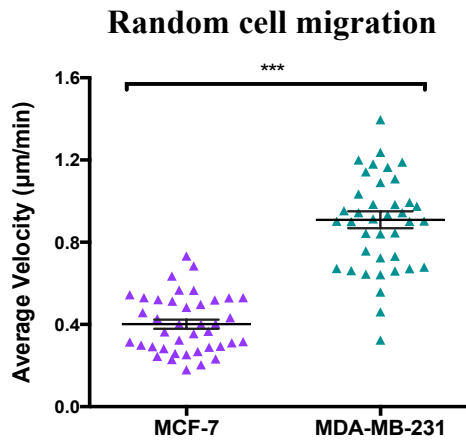


**Figure 4.3: MDA-MB-231 cells migrate with greater velocity than MCF-7 cells.**

Live time-lapse imaging of MDA-MB-231 and MCF7 cells seeded on collagen-I with images taken every 10 min for 16 h. Cells were tracked in ImageJ and their average velocity was plotted. MDA-MB-231 cells migrate at a higher average velocity of 1µm/min compared to 0.4 µm/min for MCF-7 cells. Number of cells per condition = 40. Graph shows one set of data from three independent experiments. Mean ± SEM.

### Spider graph

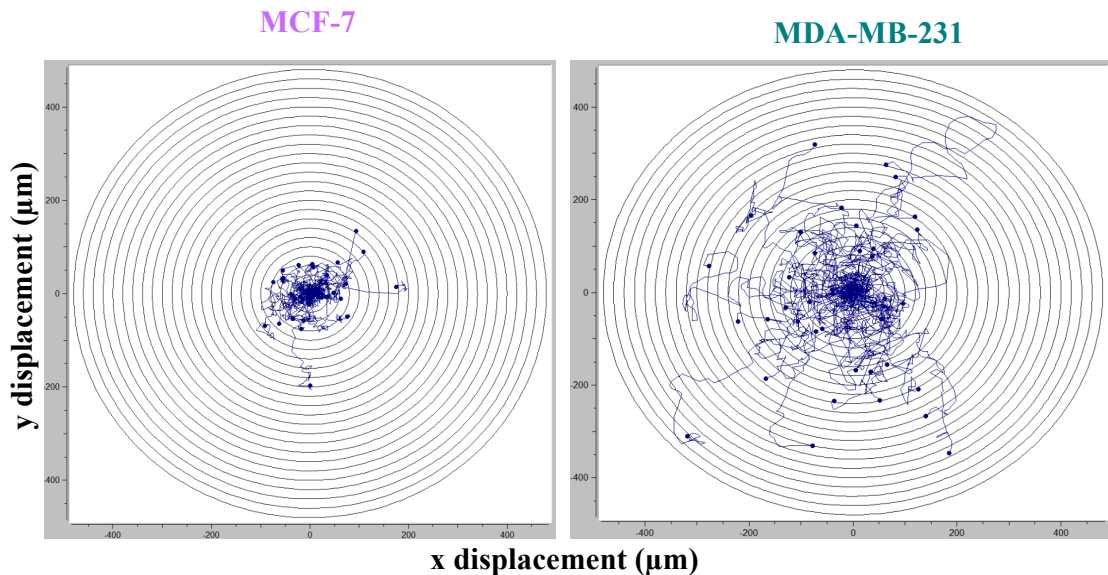


**Figure 4.4: MDA-MB-231 cells travel longer distances than MCF-7 cells.** Spider graphs show the distance of individual cells during a 16 hour migration period. MCF-7 cells travelled an average distance of 92.60 µm while that of MDA-MB-231 cells were 229.28 µm revealing an increase in spread in MDA-MB-231 compared to MCF-7 cells. No of cells analysed per condition = 40.

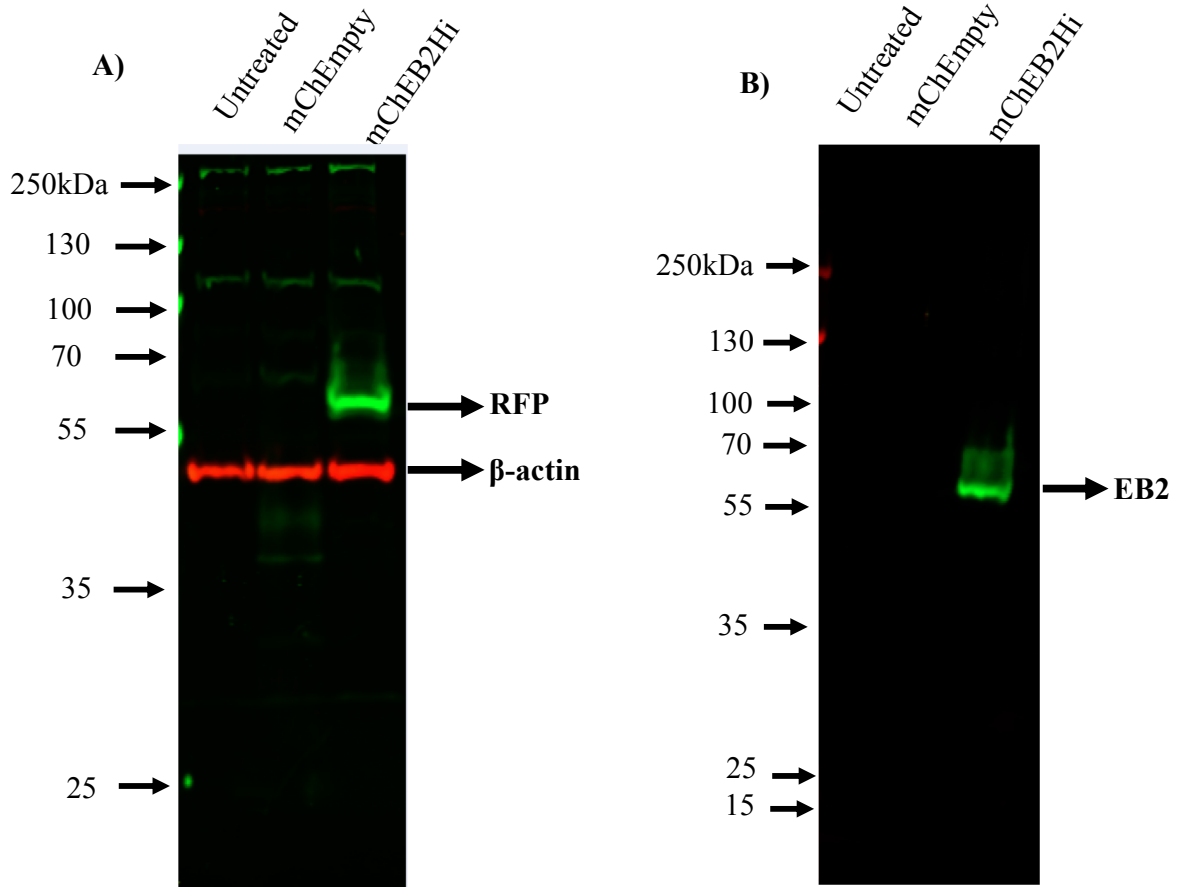


**Figure 4.5: Confirmation of mCherry-EB2 protein expression in MDCKII<sup>EB2Hi</sup> cells.** Cell extracts were obtained from untreated MDCKII<sup>WT</sup> and cells stably transfected with mCherry-EB2 or mCherry-Empty construct. Western blots of the cell lysates were probed for RFP and EB2 and  $\beta$ -actin for the loading control. A) The MDCKII<sup>mChEB2Hi</sup> lane show detection of mCherry-EB2 with the RFP antibody and  $\beta$ -actin below the 55kDa marker. mCherry is not detected with the RFP antibody in the MDCKII<sup>mChEmpty</sup> lane most likely due to the low molecular weight of mCherry (28.8kDa) and thus not being retained in the blot. B) EB2 expression is seen in the MDCKII<sup>mChEB2Hi</sup> lane but not in untreated MDCKII and MDCKII<sup>mChEmpty</sup> lanes possibly due to low levels of endogenous EB2 expression.

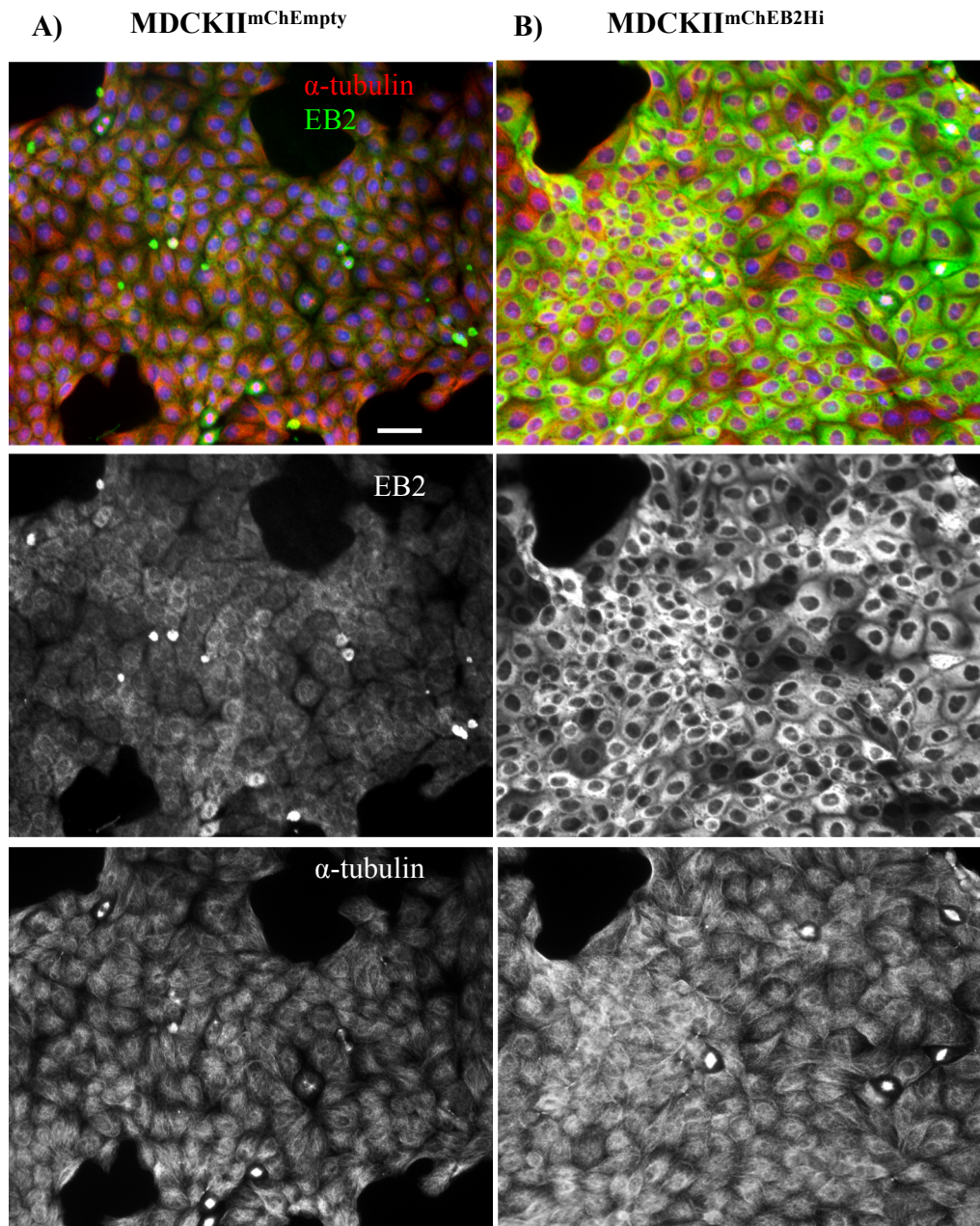


**Figure 4.6: EB2 expression in MDCKII<sup>mChEmpty</sup> and MDCKII<sup>mChEB2Hi</sup> cells.** Cells seeded on collagen I were immunolabelled with an anti- $\alpha$ -tubulin antibody (red, pAb, ab15246) and anti-EB2 antibody (green, mAb K52, ab45767). Widefield fluorescent images of confluent MDCKII<sup>mChEmpty</sup> and MDCKII<sup>mChEB2Hi</sup> cells reveal no apparent differences in  $\alpha$ -tubulin expression in MDCKII<sup>mChEB2Hi</sup> compared to MDCKII<sup>mChEmpty</sup> cells, however, EB2 expression is markedly higher in MDCKII<sup>mChEB2Hi</sup> (B) compared to MDCKII<sup>mChEmpty</sup> cells (A).

MDCKII<sup>mChEmpty</sup>

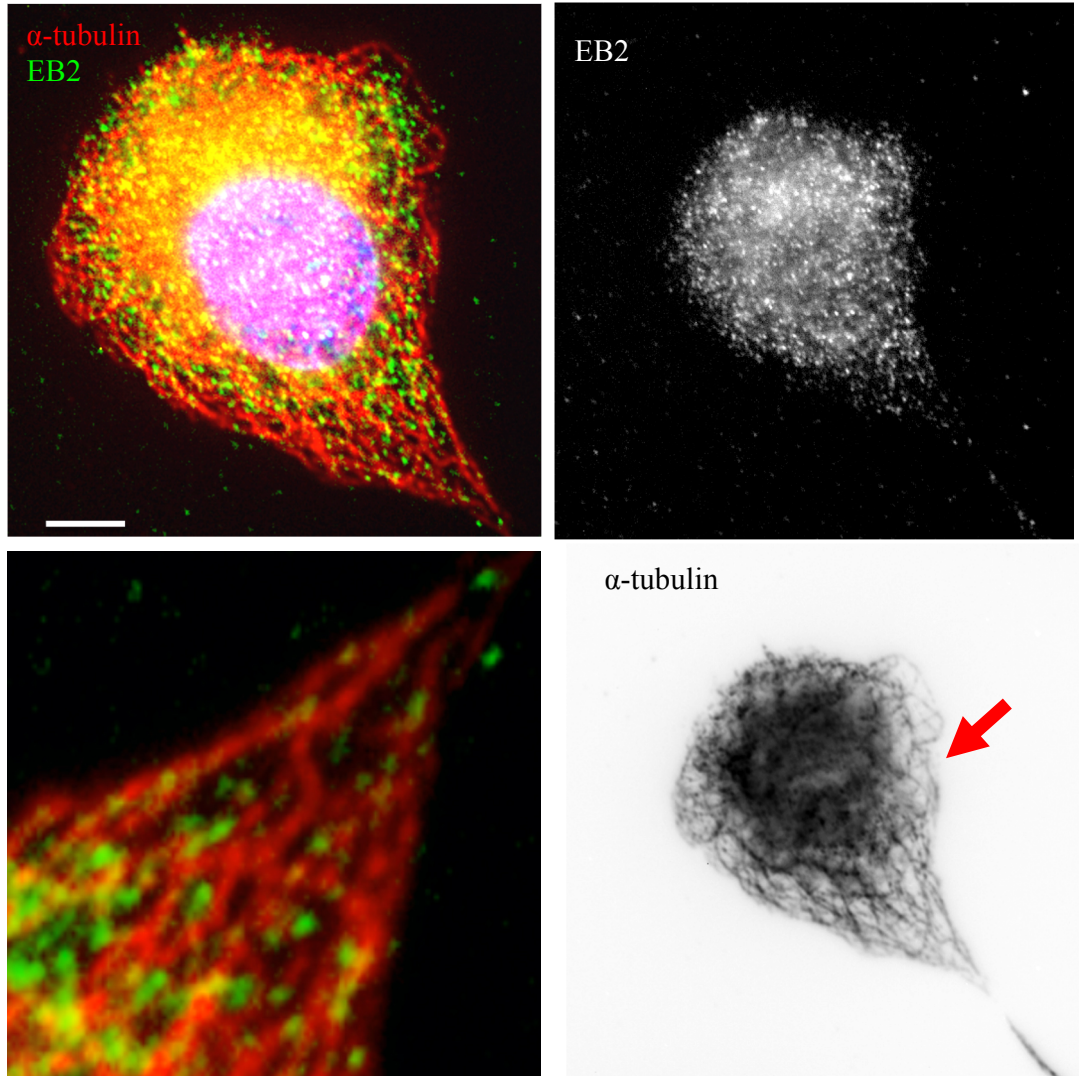


**Figure 4.7: EB2 localisation in MDCKII<sup>mChEmpty</sup> cell.**

Cell was immunolabelled with an anti- $\alpha$ -tubulin antibody (red, pAb, ab15246) and anti-EB2 K52 antibody (green, mAb, ab45767). Widefield fluorescent image of subconfluent MDCKII<sup>mChEmpty</sup> cell. Single channel image shows EB2 localisation is dotted and sparse around the cell while MTs appear curly and disorganised (red arrow inverted image). Some EB2 can be seen associating at MT ends. Scale bar = 10 $\mu$ m.

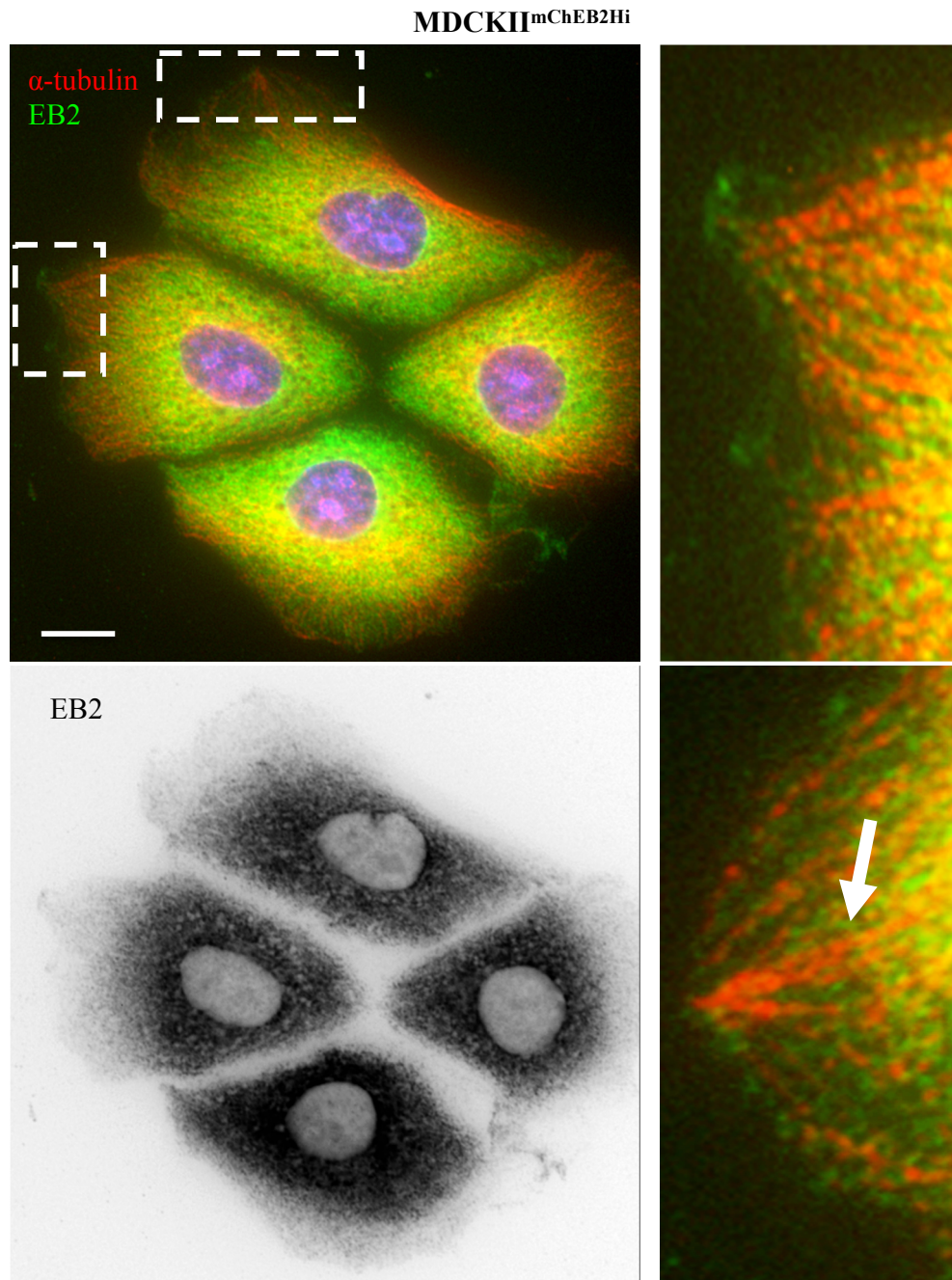


**Figure 4.8: EB2 localisation in MDCKII<sup>mChEB2Hi</sup> cells.**

Cells were immunolabelled with an anti- $\alpha$ -tubulin antibody (red, pAb, ab15246) and anti-EB2 K52 antibody (green, mAb, ab45767). Widefield fluorescent image of subconfluent MDCKII<sup>mChEB2Hi</sup> cells showing EB2 and  $\alpha$ -tubulin. Single channel image shows EB2 localises mainly in the cytoplasm with some EB2 seen concentrated at the periphery in MDCK<sup>mChEB2Hi</sup> cell (enlarged region). There is EB2 association with MTs (white arrow). EB2 localisation is higher in the centre of these cells compared to the MDCKII<sup>mChEmpty</sup> cell shown in the previous figure. Scale bar = 10 $\mu$ m.

MDCKII<sup>mChEB2Hi</sup>

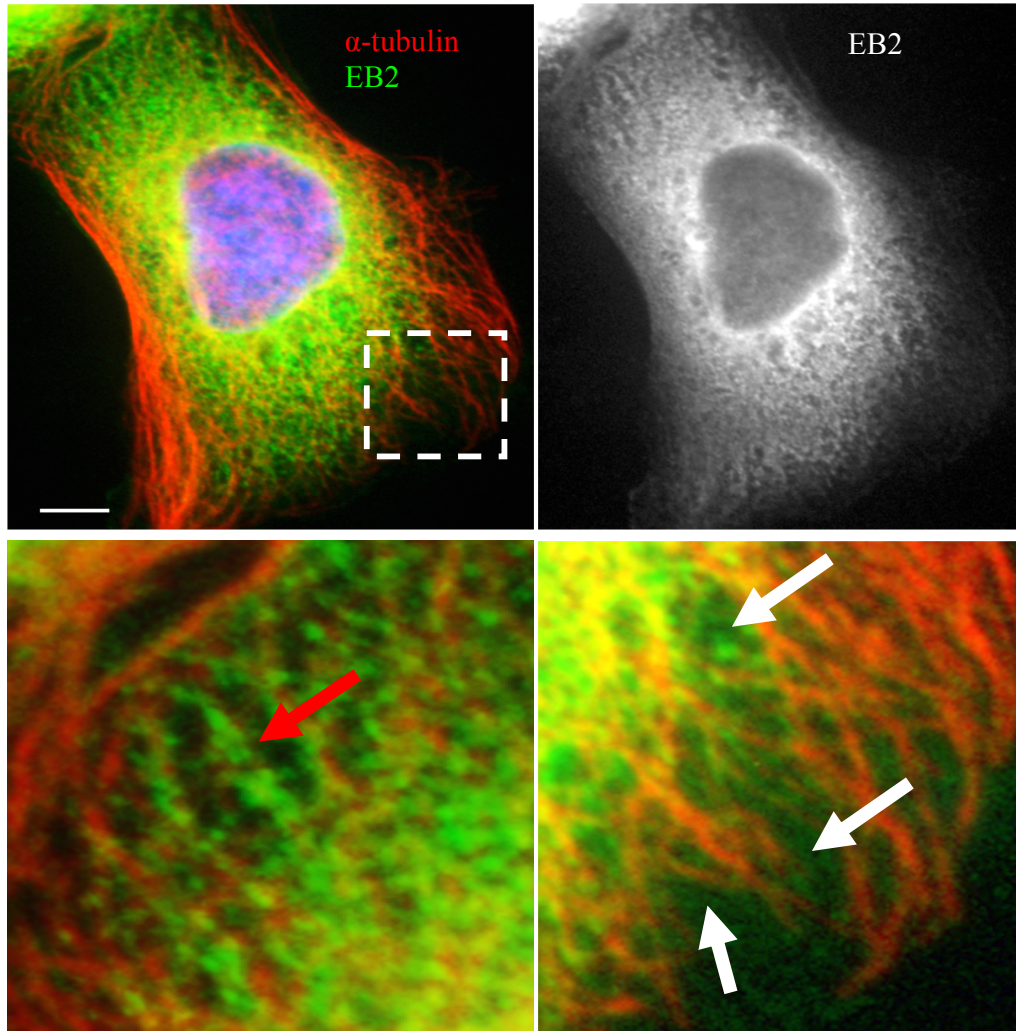


**Figure 4.9: EB2 localisation in MDCKII<sup>mChEB2Hi</sup> cells continued.**

Cells were immunolabelled with an anti- $\alpha$ -tubulin antibody (red, pAb ab15246) and anti-EB2 k52 antibody (green, mAb, ab45767). Widefield fluorescent images of subconfluent MDCK<sup>mChEB2Hi</sup> cell showing EB2 and  $\alpha$ -tubulin localisation. Single channel image shows the presence of EB2 but difficult to distinguish cytoplasmic EB2 or ones associating with MTs. Enlarged merged region shows EB2 accumulated along MT lattice (denoted by red arrow) in MDCK<sup>mChEB2Hi</sup> cell. White arrows indicate regions where EB2 appears in the cytoplasm and not associating with MTs. Scale bar = 10 $\mu$ m.

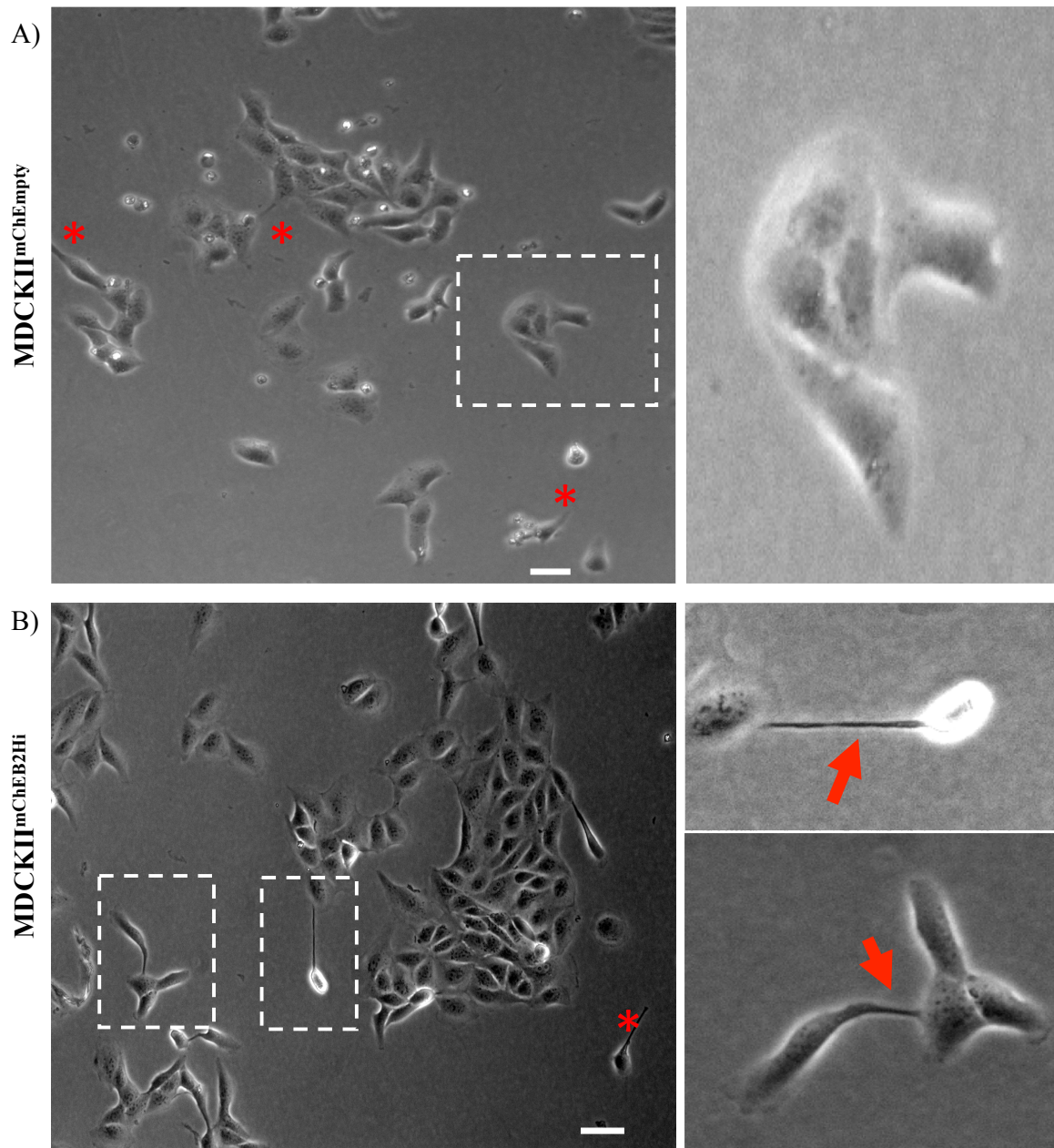


**Figure 4.10: Morphologies of MDCKII<sup>mChEmpty</sup> and MDCKII<sup>mChEB2Hi</sup> cells seeded on collagen-I.**

Frames from live time-lapse recording showing different cell morphologies. Images were taken every 10min for 16h. A) MDCKII<sup>mChEmpty</sup> cells had a flat, 'fried-egg' like morphology (denoted in the boxed region) with few cells having processes (asterisks). B) MDCKII<sup>mChEB2Hi</sup> cells had a more elongated morphology with more cells having protrusions (red arrow & asterisks) compared to MDCKII<sup>mChEmpty</sup> cells. Scale bar = 100  $\mu\text{m}$ .

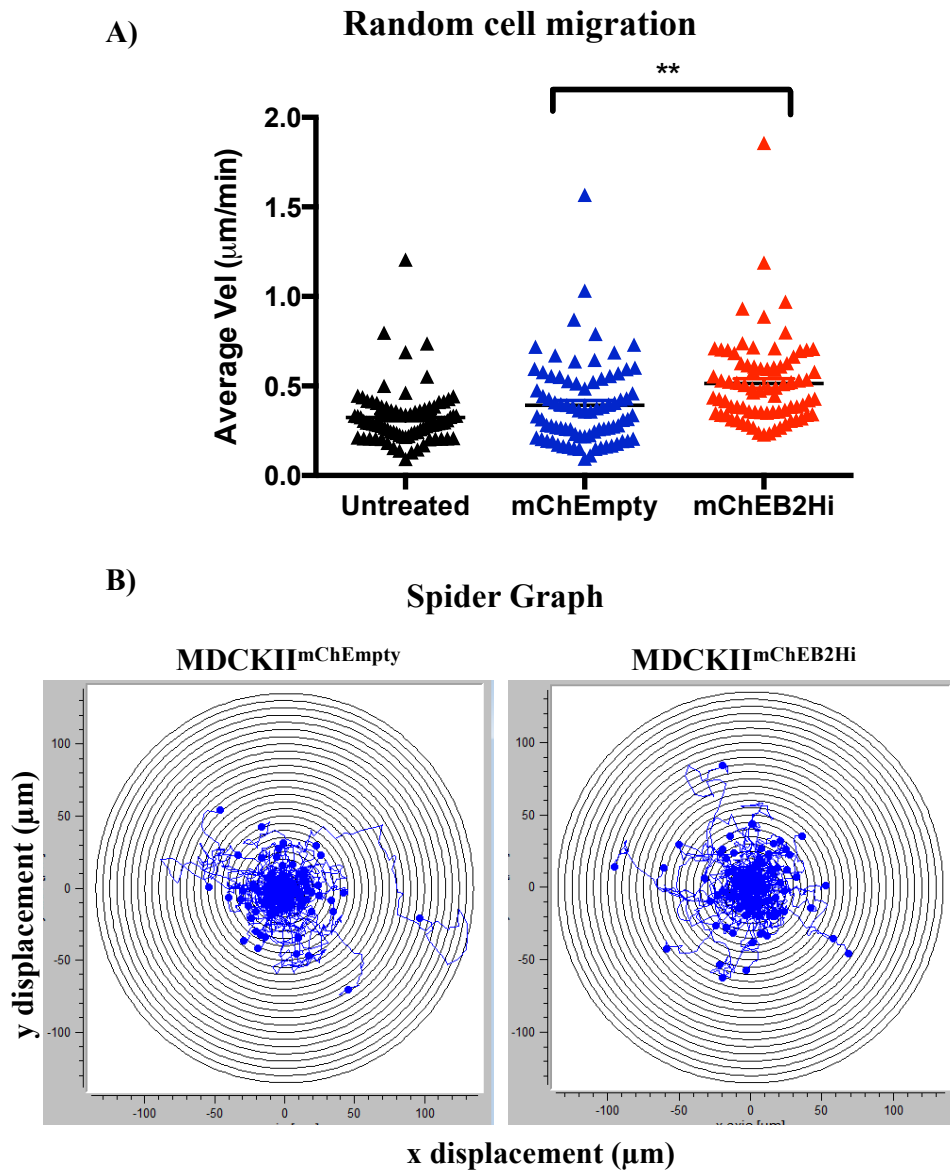


**Figure 4.11: EB2-overexpressing in MDCKII cells leads to increased migration.**

A) Live time-lapse imaging was used to take the images every 10 min for 16 h. Position of random cells were tracked in ImageJ and average velocity of cells plotted. Random migration of untreated, MDCKII<sup>mChEmpty</sup> and MDCKII<sup>mChEB2Hi</sup> cells when seeded on collagen-I had an average velocity of 0.362, 0.392 and 0.514  $\mu\text{m}/\text{min}$  respectively. Analysis revealed that MDCKII<sup>mChEB2Hi</sup> cells migrated faster when compared to MDCKII<sup>mChEmpty</sup> cells. Graph shows one set of data from two independent experiments. Statistical analysis using one-way ANOVA with Tukey's multiple comparisons test. Mean  $\pm$  SEM. B) Spider graph show further distances travelled in MDCKII<sup>mChEB2Hi</sup> cells (125.502 $\mu\text{m}$ ) compared to MDCKII<sup>mChEmpty</sup> cells (105.68 $\mu\text{m}$ ). No of cells analysed per condition = 80.

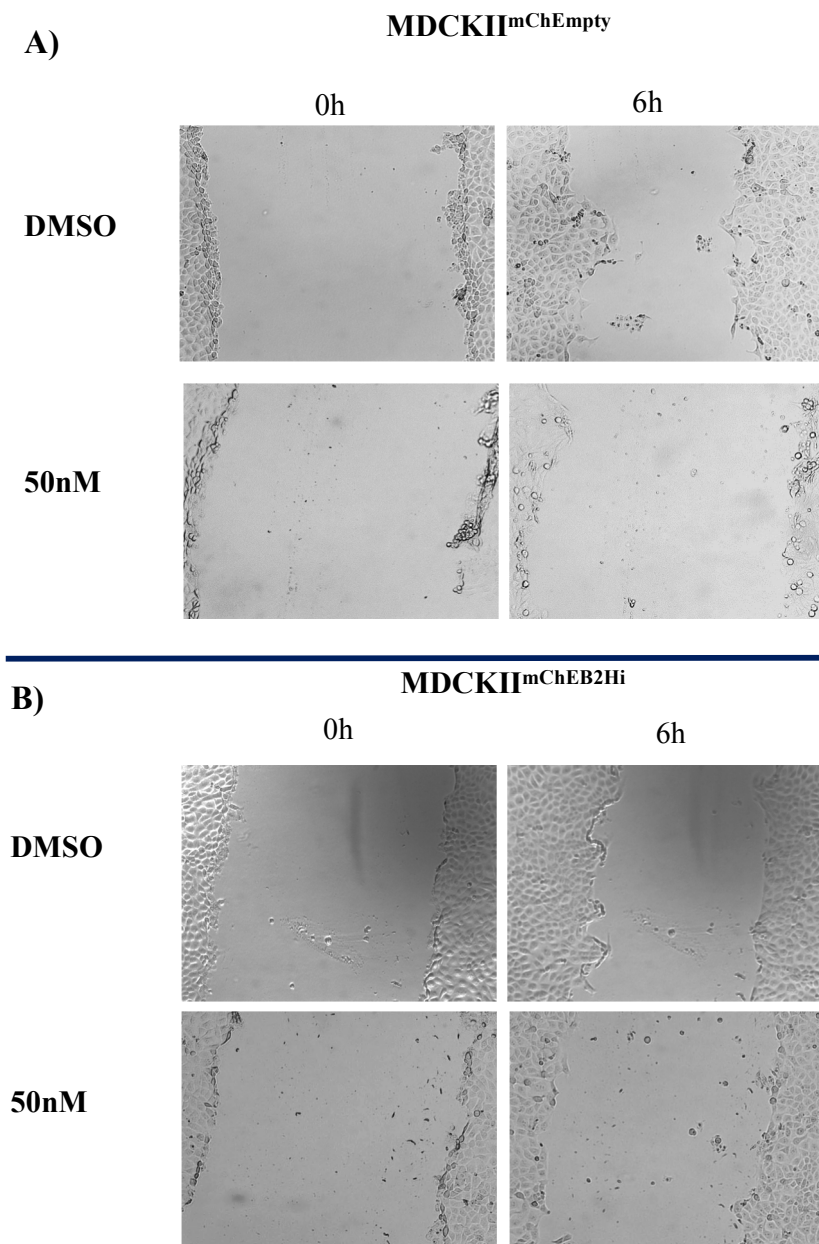


**Figure 4.12: Wound healing assay in MDCKII<sup>mChEmpty</sup> and MDCKII<sup>mChEB2Hi</sup> cells.** Cells were seeded for 24 h to adhere then a scratch was made using a P200 pipette tip before replacing the medium with one containing 50 nM Taxol or 0.0005% DMSO. A) The percentage area remaining in the MDCKII<sup>mChEmpty</sup> cells at 6h was reduced in the DMSO condition (64%) compared to area when the cells were treated with 50 nM of Taxol (95%). B) The percentage area remaining in the MDCKII<sup>mChEB2Hi</sup> cells at 6h was reduced in the DMSO condition (52%) compared to area when the cells were treated with 50 nM of Taxol (83%).

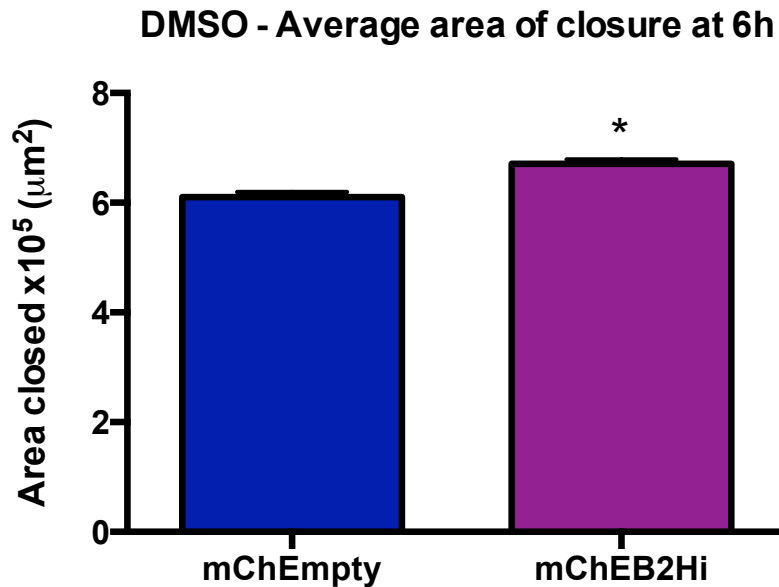


**Figure 4.13: Area of closure in scratch wound assays in MDCKII<sup>mChEmpty</sup> and MDCKII<sup>mChEB2Hi</sup> cells treated with DMSO.** MDCKII<sup>mChEmpty</sup> and MDCKII<sup>mChEB2Hi</sup> cells were seeded in a 24-well plate and allowed to grow to confluency. Cells were observed by time-lapse microscopy over a 6 h period. The area closed within the scratch was calculated for each condition by measuring the scratch area at t=6 h in ImageJ and a percentage calculated. Analysis by student's T-test revealed a significant increase in the area closed in DMSO-treated MDCKII<sup>mChEB2Hi</sup> compared to DMSO-treated MDCKII<sup>mChEmpty</sup> cells at 6h. Result is based on one experiment. Mean ± SEM.

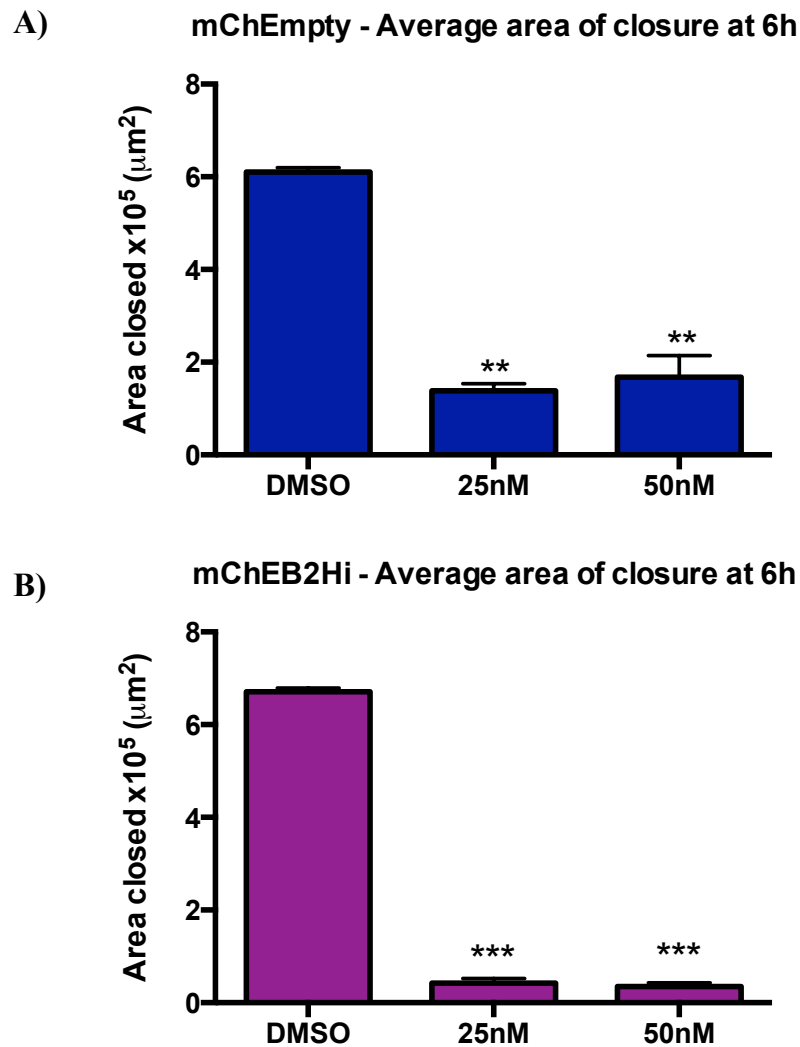


**Figure 4.14: Area of closure in scratch wound assays in MDCKII<sup>mChEmpty</sup> and MDCKII<sup>mChEB2Hi</sup> cells (Contd.).** MDCKII<sup>mChEmpty</sup> and MDCKII<sup>mChEB2Hi</sup> cells were seeded into 24-well plate and allowed to grow to confluency. Cells were observed by time-lapse widefield microscopy over a 6 h period. The area closed by the scratches for each condition were calculated by measuring the scratch area at t=0 h and at t=6 h in ImageJ. Scratches for each condition were analysed and plotted. A) Analysis by one way ANOVA with Tukey's multiple comparisons test revealed a significant decrease in the area closed in the Taxol-treated MDCKII<sup>mChEmpty</sup> cells compared to the DMSO. B) The average area closed in the Taxol-treated MDCKII<sup>mChEB2Hi</sup> cells were significantly reduced compared to DMSO-treated cells. The DMSO data here is the same as in Figure 4.13. Mean ± SEM.

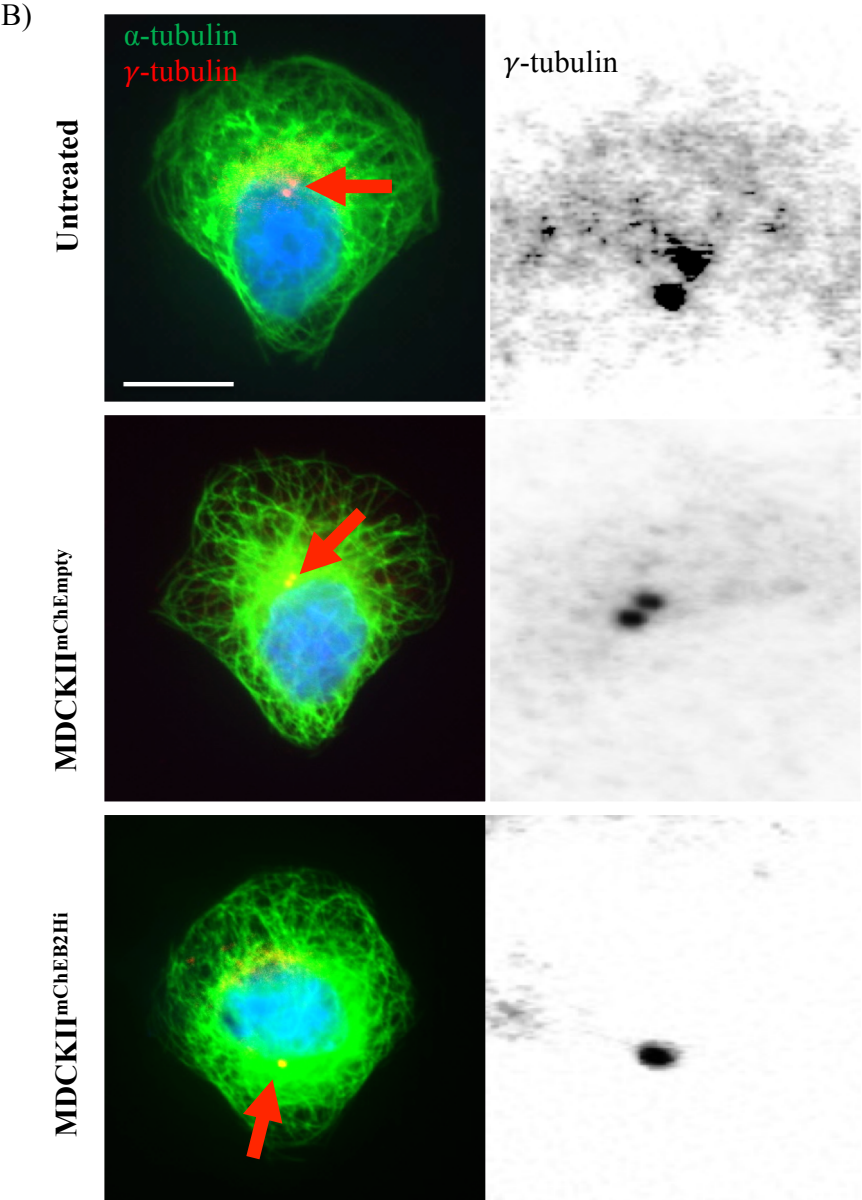
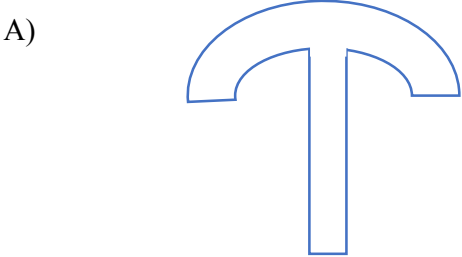


**Figure 4.15: Centrosome positioning in initiated directional migration of MDCKII cells.**

Cells were seeded on collagen-I-coated CYTOO micropatterns for 8h before fixing and immunolabelling with  $\alpha$ -tubulin (green, pAb, ab15246) and  $\gamma$ -tubulin (red, mAb, ab11316). Widefield fluorescent images were taken. A) A model showing the micropatterns used in the study. B) Centrosome position appears to be at the front of the nucleus towards the leading edge in untreated and MDCKII<sup>mChEmpty</sup> cells compared to MDCKII<sup>mChEB2Hi</sup> cells where the centrosome appears to be behind the nucleus. Inverted images show centrosome positioning in all three sub-cell lines. Scale bar = 10  $\mu$ m.

### Centrosome Position in directional migration

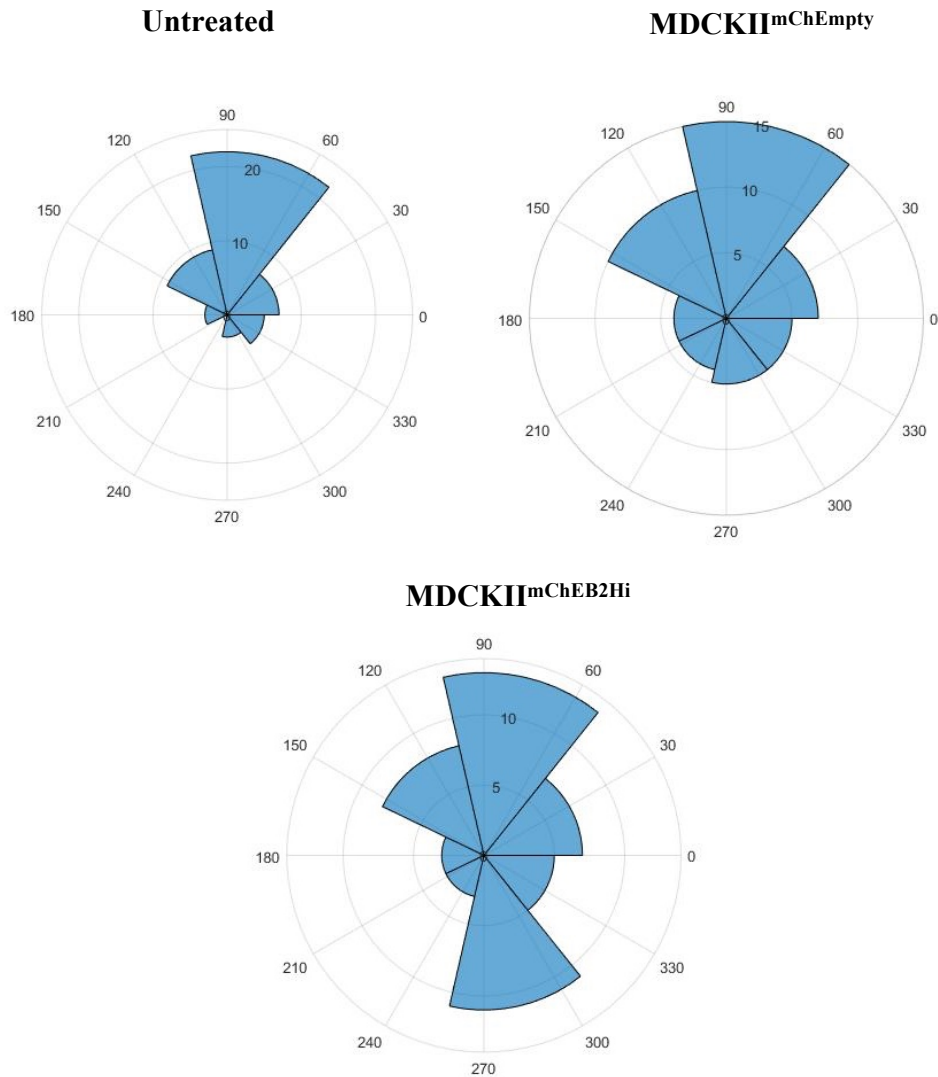


**Figure 4.16: EB2-overexpression appears to affect centrosome positioning.**

Analysis of the centrosome in respect to the centre of the nucleus. Fifty images were analysed per condition using ImageJ and Matlab. An increased percentage of cells had their centrosome at the back of the nucleus in MDCKII<sup>mChEB2Hi</sup> (26%) compared to MDCKII<sup>mChEmpty</sup> cells (16%) or untreated cells (10%).

# **Chapter V: Effects of Resveratrol on Cell Migration, MTs and End- binding Proteins in Breast Cancer Cells**

## 5.1 Overview

The purpose of this chapter is to investigate effects of resveratrol on breast cancer cell migration. The aims were to establish whether resveratrol affected the speed of migration and distance travelled in MCF-7 and MDA-MB-231 breast cancer cells and explore possible mechanisms involved. In particular, effects of resveratrol on MT dynamics and stability, focal adhesion turnover and on the organisation of end-binding proteins were investigated. Overall, the findings from this study will help to extend our knowledge on resveratrol and help determine whether it could be used as an adjuvant therapy for breast cancer patients.

## 5.2 Introduction

Breast cancer is a common cause of cancer death in the UK (Cancer Research UK, 2012) and strongly resistant to current cancer treatments (Osborne and Schiff, 2011, Hayes and Lewis-Wambi, 2015, Murphy and Dickler, 2016). Antimitotic drugs have been used for treating breast cancer though development of resistance over time due to loss of efficacy is a major drawback. Therefore, investigating new ways of treating the disease is of great importance.

MTs and actin filaments play crucial roles in cell motility by producing the force and tension required to initiate and maintain cell movement. Dynamic instability of MTs have been explored and used to engineer anticancer treatments that suppress instability (Azarenko et al., 2008, Nguyen et al., 2016, Yvon et al., 1999). For example, it has been reported that resveratrol suppresses MT polymerisation in human breast cancer cells (Hong et al., 2009) and other types of cancer such as pancreatic cancer, colon cancer, lung cancer and cervical cancer (Schneider et al., 2003, Thomas et al., 2016, Hong et al., 2009).

Resveratrol has been shown to have protective and therapeutic effects on different cancer types both *in vitro* and *in vivo*. Resveratrol has chemo-preventive and therapeutic potential mainly through suppressing MT polymerisation but has also been reported to inhibit cell proliferation, and initiate apoptosis in cancer cells (Thomas et

al., 2016, Traversi et al., 2017). Therefore, resveratrol has the capability of triggering apoptosis and inhibiting tumour progression and metastasis. The trimethoxy group (Fig 1.15A) of resveratrol is the most significant part because it integrates within the colchicine-binding hydrophobic pocket in tubulin thus blocking MT dynamics (Hong et al., 2009, Scherzberg et al., 2015, Schneider et al., 2003, Traversi et al., 2017).

EB proteins regulate MT dynamics by interacting with MT plus ends, which then have effects on processes such as cell division and migration (Vaughan, 2005, Lansbergen and Akhmanova, 2006). EB1 overexpression causes MT bundle formation and association along MT lattice, while EB2 overexpression does not induce bundles (Bu and Su, 2001, Goldspink et al., 2013). Depletion of EB2 leads to EB1 and ACF-7 localisation along MTs, and facilitates actin-MT co-alignment (Goldspink et al., 2013). In addition, reports have suggested that resveratrol decrease breast cancer cell migration by reducing Rac and Cdc42 signalling and lamellipodia formation. Furthermore, resveratrol has been shown to decrease the number of focal adhesions as well as FAK activity (Azios et al., 2007).

Cell invasion is associated with metastasis in solid tumours (Friedl and Gilmour, 2009). The ability of resveratrol to suppress cell invasion have been reported. For example, relatively high concentrations of resveratrol (100 and 200  $\mu\text{M}$ ) inhibit both the invasion and proliferation of hepatoma cells but only suppresses invasion and not proliferation at concentrations lower than 25  $\mu\text{M}$  suggesting that the anti-invasive activity of resveratrol is independent of the anti-proliferative activity (Kozuki et al., 2001). A very recent study also reported reduced invasion in colorectal cancer cells due to resveratrol inhibiting the phosphorylation of FAK, which led to a reduction in invasion, and an increase in apoptosis. The study also found that combined treatments of resveratrol with FAK-inhibitor or cytochalasin D (actin depolymerising agent) was more effective in reducing colorectal cancer cell invasion (Buhrmann et al., 2017). Extensive studies are required to further understand the effect of resveratrol, particularly its effect on MTs and EBs localisation, and whether such possible reorganisations influence cell migration, focal adhesion turnover and MT stability.

From the knowledge and understanding of resveratrol so far, the aim is to establish its effect on breast cancer cells by analysing how different concentrations

affects MT organisation and EB proteins localisation. These proteins are major regulators of MT dynamics therefore, the effect of resveratrol on EB proteins might have an impact on cellular migration and invasion.

## **5.3 Results**

### **5.3.1 Viability assessment of resveratrol in MCF-7 and MDA-MB-231 cells**

A MTT assay was used to evaluate the effect of resveratrol on cell viability. The assay is a colorimetric assay used for measuring cell's metabolic activity and reflects the presence of viable cells. The MTT assay is based on the reduction of the yellow dye MTT to purple formazan crystals. This occurs only in living cells, due to dehydrogenase activity in mitochondria. Viability was determined by using the MTT assay on MCF-7 and MDA-MB-231 cells treated with different concentrations of resveratrol for 24 h. Each cell line was seeded in a 96-well plate in triplicates, for each condition, and left to adhere overnight. Cells were either left untreated, treated with DMSO or different concentrations of resveratrol at 2.5, 5, 10, 20, 50 and 75  $\mu\text{M}$  and incubated for 24 h. Statistical analysis based on two experiments (each with three replicates) using one-way ANOVA with Tukey's showed that none of the concentrations used significantly affected the cell viability in either MCF-7 or MDA-MB-231 cells after a 24 h incubation (Fig 5.1). All concentrations were compared with the DMSO control. Resveratrol was dissolved in DMSO and therefore was used as the vehicle control. For the subsequent experiments the DMSO concentration was 0.038% (highest concentration used for the resveratrol solutions). These results indicate that resveratrol treatment up to 75  $\mu\text{M}$  had no significant effect on cell viability. Based on these findings, resveratrol concentrations from 10-75  $\mu\text{M}$  were used to investigate the effect on cell migration.

### **5.3.2 Resveratrol treatment causes morphological changes in both cell lines**

Breast cancer cells were seeded in a 24-well plate and incubated overnight for the cells to adhere. The following day, cells were treated with 10, 20, 50 and 75  $\mu\text{M}$  of resveratrol for 24 h and then used for live time-lapse imaging. DMSO-control cells adopted short protrusions (Fig 5.2A), similar to those seen in untreated MCF-7 cells (Fig 4.1F). Treatment with resveratrol at 10 and 20  $\mu\text{M}$  did not show marked morphological changes compared to the DMSO-treated cells (Fig 5.2B and C).

However, 50  $\mu\text{M}$  resveratrol-treatment showed MCF-7 cells adopting a ‘fried-egg’ like morphology with some membrane ruffling (Fig 5.2D).

In MDA-MB-231 cells, images of DMSO-treated cells revealed large protrusions at cell ends indicating migrating cells (Fig 5.3A), the morphologies were similar to those seen in untreated MDA-MB-231 cells (Fig 4.1C). The cells showed an elongated shape with membrane ruffling and short protrusions when treated with 20  $\mu\text{M}$  resveratrol (Fig 5.3B). Conversely, at 50  $\mu\text{M}$  and 75  $\mu\text{M}$  resveratrol, many cells revealed long elongated “tails” at one end (Fig 5.3C and D).

### **5.3.3 Resveratrol treatment causes a significant increase in cell size and decrease in cell proliferation in both cell lines**

Resveratrol has been reported to influence cell proliferation in various cancer types (Thomas et al., 2016, Traversi et al., 2017) It was therefore important to establish whether this was also the case for breast cancer cells. MCF-7 and MDA-MB-231 cells were seeded on collagen-I coated coverslips and treated with DMSO, 10, 20, 50 and 75  $\mu\text{M}$  resveratrol for 24 h. Cells were fixed in methanol at  $-20^{\circ}\text{C}$  for 5 min and immunolabelled. Images of resveratrol treated MCF-7 and MDA-MB-231 cells indicated a change in cell size. More specifically, resveratrol treated cells appeared larger in area compared to DMSO control cells (Fig 5.4A and B). ImageJ was used to analyse cell area by measuring the area of fixed cells to determined cell edge and measure the area. Statistical analysis was carried out using one-way analysis with Tukey’s multiple comparisons test. The weakness of this method is that the way of measuring cell area relies on the ability to accurately determine the cell edge.

The data revealed that in MCF-7 cells, DMSO cells displayed an average cell area of  $1458 \mu\text{m}^2$  compared to 1489, 1782 and  $2104 \mu\text{m}^2$  in 10, 20 and 50  $\mu\text{M}$  resveratrol respectively. An increase in the average cell area seems to be associated with resveratrol treatment compared to DMSO (Fig 5.5A). However, statistical analysis using one-way ANOVA with Tukey’s multiple comparisons, of thirty MCF7 cells per condition, revealed that only 50  $\mu\text{M}$  resveratrol showed a significant increase in cell

area compared to DMSO. However, in MDA-MB-231 cells, resveratrol treatment with 20, 50 and 75  $\mu\text{M}$  revealed significant increases in cell area with 2250  $\mu\text{m}^2$  for 20, 3052  $\mu\text{m}^2$  for 50, 3725  $\mu\text{m}^2$  for 75  $\mu\text{M}$  when compared to 1436  $\mu\text{m}^2$  in DMSO cells (Fig 5.5B). These changes in cell area following resveratrol treatment suggest that resveratrol influences cell proliferation and possibly adhesion, causing an increased cell area.

Cell proliferation was measured using ImageJ by counting the number of cells dividing per frame from time-lapse recordings. The average cell division observed in DMSO and resveratrol at 10, 20 and 50  $\mu\text{M}$  was 20, 19, 17 and 5 cells/frame respectively (Fig 5.6A). In MDA-MB-231 cells, the average cell division in DMSO and resveratrol at 20, 50 and 75  $\mu\text{M}$  was 24, 6, 2 and 1 cell/frame respectively (Fig 5.6B). Statistical analysis using One-way ANOVA with Tukey's multiple comparisons test (based on one experiment), showed that resveratrol caused a significant reduction in cell proliferation with 50  $\mu\text{M}$  in MCF7 cells but only 20  $\mu\text{M}$  was required in MDA-MB-231 cells.

### **5.3.4 Resveratrol treatment causes a reduction in speed and distance travelled during cell migration**

The effect of resveratrol on random cell migration was analysed in MCF-7 and MDA-MB-231 cells seeded on collagen-I at 1mg/ml. Cells were seeded in a 24-well plate (three wells per condition) for time-lapse imaging. For analysis, eight separate positions were examined for each condition with five cells from each area thus a total of 40 cells per condition were analysed. ImageJ was utilised to analyse cell movement by using the manual cell tracking plugin. To allow for the calculation of speed, the position of each analysed cell was recorded for each frame in the time course. If a cell that was being tracked underwent mitosis, only one of the daughter cells was followed for the rest of the time-lapse. The average velocity for each cell was calculated based on the positional information from the time-lapse. The average velocity result for each cell analysed was calculated and plotted in a graph to illustrate an overall average velocity for each condition. Statistical analysis was performed by using a one-way

ANOVA with Tukey's multiple comparisons test. The results are based on one experiment.

The average velocity of MCF-7 cells for each condition showed that DMSO treated cells moved at an average velocity of 0.382  $\mu\text{m}/\text{min}$  while the average velocities for 10, 20 and 50  $\mu\text{M}$  resveratrol treated cells were 0.252  $\mu\text{m}/\text{min}$ , 0.195  $\mu\text{m}/\text{min}$  and 0.160  $\mu\text{m}/\text{min}$  respectively (Fig 5.7A, Movie S12-S15). Resveratrol treatments at 10, 20 and 50  $\mu\text{M}$  had significant effects on the average velocity in MCF-7 cells compared to DMSO control cells. The average velocities of MDA-MB-231 cells for each condition showed that DMSO cells moved at an average velocity of 0.945  $\mu\text{m}/\text{min}$  while the average velocity for 20, 50 and 75  $\mu\text{M}$  resveratrol were 0.705  $\mu\text{m}/\text{min}$ , 0.492  $\mu\text{m}/\text{min}$  and 0.378  $\mu\text{m}/\text{min}$  respectively (Fig 5.8A, Movie S16-S19). A significant reduction in the average velocity was observed with resveratrol treatments of 20, 50 and 75  $\mu\text{M}$  in MDA-MB-231 cells compared to DMSO control cells.

The "chemotaxis and migration" tool (part of Ibidi software) was used to show the distance travelled by individual cells during migration. Spider graphs showed that DMSO, 10, 20 and 50  $\mu\text{M}$ -treated MCF-7 cells travelled average distances of 87.16, 62.24, 47.77 and 39.54  $\mu\text{m}$  respectively. This suggest that resveratrol causes a reduction in distance travelled during migration in MCF7 cells (Fig 5.7B). At 20 and 50  $\mu\text{M}$  most cells were concentrated in the centre, an indication of a reduction in distance travelled. The Spider graphs for MDA-MB-231 cells revealed that DMSO, 20, 50 and 75  $\mu\text{M}$ -resveratrol resulted in distances travelled of 233.26, 173.89, 121.54 and 93.28  $\mu\text{m}$  respectively, indication reductions in distances travelled with resveratrol treatment (Fig 5.8B). Resveratrol had a greater effect on MDA-MB-231 cells.

### **5.3.5 Resveratrol caused reduced invasion of MDA-MB-231 cells**

Invasion into neighbouring tissues is a step in cancer progression and a prerequisite to forming secondary tumours, called metastasis. Invasion and metastasis are causes of malignancy, which requires remodeling of the cytoskeleton. Metastasis is

responsible for poor prognosis and treatment failure. Therefore, understanding these events are crucial in developing new therapies.

The study here was done to test the ability of resveratrol to inhibit invasion in a 3D model (see Section 2.8) since it is closer to the *in vivo* environment. Both breast cancer cell lines were embedded in Matrigel with collagen I, fixed and immunolabelled for  $\alpha$ -tubulin. In MDA-MB-231 cells, a marked invasion was evident with mainly spindle shaped single cells and very few aggregates in the 3D matrix. Also, MDA-MB-231 cells had long protrusions with an extensive MT reorganisation observed at each end (Fig 5.9A). The invasive phenotype of MDA-MB-231 cells possibly confers its metastatic potential. Speculation could be made that the increased EB2 expression in these cells contributes to their increased invasion. In contrast, MCF-7 cells mainly formed aggregates with a few single migratory cells evident within the Matrigel and away from the aggregate (Fig 5.9B). Not all MCF-7 cells underwent MT reorganisation. Most of the cells were still rounded up further confirming their reduced invasive potential.

MCF-7 cells had been shown to be poorly invasive and not a good model for studying invasion (Valdivia-Silva et al., 2009, Franco-Barraza et al., 2010) only the MDA-MB-231 cells were used. MDA-MB-231 cells were seeded in a round-bottom 96-well plate for 48h to generate spheroids. The produced spheroids were collected and embedded in a Matrigel and Collagen I mixture for monitoring invasion with the medium supplemented with DMSO or resveratrol 20, 50 or 75 $\mu$ M. Phase-contrast images taken using a x2.5 objective lens revealed that the area of invasive cells was reduced in resveratrol concentrations of 20, 50 and 75  $\mu$ M compared to the DMSO control (Fig 5.10 and 5.11). The experiment was repeated once more to make a total of two. ImageJ was used to measure the area of the mass at 0 and 96h. Analysis by one way ANOVA with Tukey's multiple comparisons test revealed a significant reduction in the area of invasion in all resveratrol-treated cells compared to the invasive area of DMSO cells (Fig 5.12).

### **5.3.6 Resveratrol treatment leads to straighter MTs in MCF-7 and MDA-MB-231 cells but EB1 lattice association is observed in only MDA-MB-231 cells**

To investigate the effect of resveratrol on EB1 expression a Western blot was performed on lysates collected from resveratrol treated MCF-7 and MDA-MB-231 cells. The assay was used to analyse the level of EB1 expression in these cells with  $\beta$ -actin used as the loading control. In MCF-7 cells, there appears to be a slight decrease in EB1 expression with 50  $\mu$ M resveratrol compared to DMSO (Fig 5.13A). However, in MDA-MB-231 cells, there was no marked changes observed in EB1 expression following resveratrol treatment compared to DMSO (Fig 5.13B).

Next, the effect of resveratrol on MT organisation and EB1 localisation was determined. MCF-7 and MDA-MB-231 cells were seeded on collagen-I coated coverslips and treated with DMSO and various concentrations of resveratrol for 24 h. Cells were fixed in methanol at  $-20^{\circ}\text{C}$  for 5 min then immuno-labelled for  $\alpha$ -tubulin and EB1. Widefield fluorescent images of DMSO-treated MCF-7 cells showed disorganised MTs with a classic EB1 comet localisation at the plus ends (Fig 5.14A). At 10  $\mu$ M, there was no noticeable changes in MT organisation or EB1 localisation with EB1 still accumulated at the plus-ends of the MTs (Fig 5.14B). The 20 and 50  $\mu$ M resveratrol treated MCF-7 cells revealed that MTs were straighter with EB1 still localising at the plus ends though appearing more dotted compared with the DMSO control cells (Fig 5.15A and B). Analysis of EB1 comet shape revealed that EB1 circularity is significantly higher in 10, 20 and 50  $\mu$ M resveratrol treated MCF-7 cells at 0.592, 0.595 and 0.595 respectively compared to DMSO cells at 0.569 (Fig 5.16A). However, there was no significant difference in the feret's diameter when cells were treated with resveratrol (Fig 5.16B).

Images of DMSO-treated MDA-MB-231 cells showed most cells with highly disorganised MTs, forming interwoven networks at the front of the cell (Fig 5.17A). Comet lengths were longer in MDA-MB-231 compared to MCF-7 cells as seen in (Fig 5.14A) and previously in Chapter 3 (Fig 3.8). At 20  $\mu$ M resveratrol, there is no noticeable changes in organisation of MTs and in EB1 localisation compared to the

DMSO-treated cells (Fig 5.17B). However, the 50 and 75  $\mu\text{M}$  resveratrol treated MDA-MB-231 cells revealed alterations in MT organisation. These cells showed a radial array organisation of MTs. Furthermore, MTs appear considerably straighter compared with DMSO treated cells (Fig 5.18A and B). EB1 is also observed to associate along the MT lattice (Fig 5.18B). EB1 comet analysis in MDA-MB-231 cells showed a significant reduction in circularity in 20 and 50  $\mu\text{M}$  resveratrol treated MDA-MB-231 cells at 0.556 and 0.553 respectively compared to DMSO cells at 0.583 (Fig 5.19A). The comet Feret's diameters were significantly increased when cells were treated with 20 and 50  $\mu\text{M}$  resveratrol at 1.48 and 1.50  $\mu\text{m}$  respectively compared to DMSO cells at 1.38  $\mu\text{m}$  (Fig 5.19B). The 75  $\mu\text{M}$  resveratrol treated cells were not included in the comet analysis as EB1 localised along the lattice and not only as comets.

### **5.3.7 Resveratrol treatment leads to EB2 displacement from the leading edge and detachment from MTs in MDA-MB-231 cells**

Western Blot analyses indicated that resveratrol treatment did not affect the EB2 expression levels in MCF-7 cells (Fig 5.20A) but did appear to show a slight increase in the upper EB2 band in MDA-MB-231 cells treated with resveratrol compared to DMSO (Fig 5.20B).

In order to investigate the effect of resveratrol on EB2 localisation MCF-7 and MDA-MB-231 cells were seeded on collagen-I coated coverslips and treated with DMSO or resveratrol for 24 h. Cells were fixed in methanol at  $-20^{\circ}\text{C}$  for 5 min and immunolabelled for  $\alpha$ -tubulin and EB2. DMSO-treated MCF-7 cells show EB2 localises to MTs at the plus-ends (Fig 5.21A). The same results were also observed with 10  $\mu\text{M}$  treated cells (Fig 5.21B). In 20 and 50  $\mu\text{M}$  resveratrol treated cells, EB2 was observed associating along the MT lattice (Fig 5.22A and B). MDA-MB-231 DMSO and 20 $\mu\text{M}$  treated cells revealed some EB2 also associating along MT lattice and some concentrated at the edge of the cell (Fig 5.23A and B). However, 50  $\mu\text{M}$  and 75  $\mu\text{M}$  treated cells revealed reduced EB2 localisation at the leading edge of cells with more being dispersed in the cytoplasm (Fig 5.24A and B). In addition, there was a radial array

organisation of MTs, which appeared more straighter compared to DMSO cells (Fig 5.23A).

### **5.3.8 Resveratrol treatment causes actin depolymerisation**

To observe any changes in actin filaments relating to resveratrol treatment; subconfluent MCF-7 and MDA-MB-231 cells were fixed in methanol at -20°C for 5 min and then immunolabelled for  $\alpha$ -tubulin and phalloidin (actin). DMSO treated MCF-7 cells showed actin at the periphery with microspikes at the leading edge. Stress fibers were observed along the cell body with filopodia and microspikes at the leading edge (Fig 5.25). Images of 10, 20 and 50  $\mu$ M resveratrol treated MCF-7 cells indicated fewer actin filaments suggesting that resveratrol is causing actin depolymerisation. Similar results were also observed in resveratrol treated MDA-MB-231 cells. DMSO and 20  $\mu$ M treated cell shows actin localised at cell edges with some stress fibres noticed in the cell body. Transverse arcs were also noticeable at 20  $\mu$ M. Cells treated with 50 and 75  $\mu$ M resveratrol indicated fewer actin filaments at the leading edge (Fig 5.26) compared to the DMSO control. Analysis of actin fluorescent intensity was carried out on ten cells per condition using ImageJ. These preliminary data were based on one experiment. In MCF-7 cells, the average actin intensity of DMSO, 10, 20 and 50  $\mu$ M-treated cells were 5033, 4716, 3681 and 2800 respectively (Fig 5.27A) with a significant difference at 50  $\mu$ M. In MDA-MB-231 cells, the average actin intensity of DMSO, 20, 50 and 75  $\mu$ M-treated cells were 5037, 3265, 2350, 2187 respectively. A significant difference was seen at 20, 50 and 75  $\mu$ M-treated cells compared to the DMSO cells (Fig 5.27B).

### **5.3.9 Resveratrol treatment causes a decrease in size and number of focal adhesions**

Focal adhesions play an important role during cell migration. A dynamic MT network is vital to allow turnover, targeting and disassembly of focal adhesions (Kaverina et al., 2002). To establish whether resveratrol treatment affects focal adhesion turnover, MCF-7 and MDA-MB-231 cells were seeded on glass coverslips and incubated overnight. The cells were then treated with different concentrations of resveratrol and incubated for 24 h and then immunolabelled for FAK and  $\alpha$ -tubulin.

DMSO treated MCF-7 cells revealed focal adhesions at the cell edge, along with some focal adhesions in the cell body and this was also found for 10  $\mu\text{M}$  resveratrol (Fig 5.28). However, in 20  $\mu\text{M}$  and 50  $\mu\text{M}$  resveratrol treated cells, fewer focal adhesions were seen at the periphery or in the cell body (Fig 5.28). Similarly, in MDA-MB-231 cells, DMSO and 20  $\mu\text{M}$  resveratrol treated MDA-MB-231 cells showed focal adhesions at the cell periphery, along with some FAK staining that were diffused in the cytoplasm (Fig 5.29). However, the 50  $\mu\text{M}$  and 75  $\mu\text{M}$  resveratrol treated MDA-MB-231 cells revealed fewer focal adhesion in the cytoplasm and at the periphery. Images also suggested reduced focal adhesion size compared to the DMSO treated control cells (Fig 5.29).

The focal adhesions in 10 cells per condition were analysed using ImageJ software. The effects of resveratrol on focal adhesion number and size were assessed in 10 cells per treatment in both cell lines. The average number of focal adhesions in untreated, DMSO and 10, 20 and 50  $\mu\text{M}$  resveratrol treated MCF-7 cells were 1051, 983.6, 892.4, 741.9 and 653.4 respectively (Fig 5.30A). The average number of focal adhesions in untreated, DMSO and 20, 50 and 75  $\mu\text{M}$  resveratrol treated MDA-MB-231 cells were 1370, 1437, 1114, 691.4 and 577.9 respectively (Fig 5.30B). Using one-way ANOVA with Tukey's multiple comparisons test for analysis, a significant reduction in focal adhesions number was observed with 50  $\mu\text{M}$  in MCF-7 cells and in MDA-MB-231 cells, a significant reduction was seen with 50 and 75  $\mu\text{M}$  resveratrol. Additionally, the mean focal adhesion size was measured in both cell lines. In MCF-7 cells, the mean focal adhesion size in untreated, DMSO, 10, 20 and 50  $\mu\text{M}$  was 0.189, 0.199, 0.173, 0.161 and 0.169  $\mu\text{m}^2$  respectively (Fig 5.31A) and a significant reduction in focal adhesions size was observed at all resveratrol concentrations when compared to DMSO. However, in MDA-MB-231 cells, the mean focal adhesion size in untreated, DMSO and 20, 50 and 75  $\mu\text{M}$  resveratrol treated cells was 0.174, 0.180, 0.184, 0.150 and 0.142  $\mu\text{m}^2$  respectively, but a significant reduction was observed only with 50 and 75  $\mu\text{M}$  resveratrol (Fig 5.31B). Therefore, certain concentrations of resveratrol caused a significant reduction in focal adhesion number and size in both MCF-7 and MDA-MB-231 cells.

### **5.3.10 MT stability – tubulin acetylation**

Tubulin modifications affect MT dynamics as well as their organisation and interaction with other cellular components. Due to this, acetylated tubulin, which is thought to often associated with stable MTs and leads to reduced MT dynamics (Al-Bassam and Corbett, 2012, Howes et al., 2014) was analysed in both cell lines.

Resveratrol-treated MCF-7 and MDA-MB-231 cells were labelled for acetylated tubulin to determine the extent of this tubulin modification in the two cell lines. In DMSO, 10 and 20  $\mu\text{M}$  resveratrol treated MCF-7 cells, some acetylated tubulin was evident around the nucleus; sometimes adopting a curly nature. Cells treated with 50  $\mu\text{M}$  resveratrol revealed tubulin acetylation and disorganised acetylated MTs (Fig 5.32). In MDA-MB-231 cells, DMSO and 20  $\mu\text{M}$  resveratrol resulted in some acetylated tubulin mainly around the nucleus of each cell. However, in the 50 and 75  $\mu\text{M}$  resveratrol-treated cells, a broader area of acetylated tubulin spanning from the cell centre towards the periphery was observed rather than a cluster around the nucleus (Fig 5.33). The percentage of acetylated tubulin area in the cells were quantified using ImageJ. The acetylated tubulin area in one cell was divided by the total tubulin area of the same cell then shown as a percentage. The results illustrated that there was no significant difference in the area of acetylated tubulin in MCF-7 cells following resveratrol treatment (Fig 5.34A). Unlike the ImageJ analysis, the Western blot results indicated a decrease in acetylated tubulin expression following treatment with 50  $\mu\text{M}$  resveratrol (Fig 5.35A). However, in MDA-MB-231 cells, ImageJ analysis revealed a significant decrease in the area of acetylated tubulin with 75  $\mu\text{M}$  compared to DMSO control (Fig 5.34B) and Western blotting also showed a slight reduction in the level of acetylated tubulin expressed with 75  $\mu\text{M}$  resveratrol (Fig 5.35B). The Western blot quantification shows a reduction in acetylated tubulin in MCF-7 treated with 10, 20 and 50  $\mu\text{M}$  resveratrol while in MDA-MB-231 cells, a reduction is only seen at 75  $\mu\text{M}$  resveratrol (Fig 5.35C and D). Results are based on two experiments.

## 5.4 Discussion

### 5.4.1 Resveratrol caused an increase in cell area in both MCF-7 and MDA-MB-231 cells

Resveratrol-treated MCF-7 and MDA-MB-231 cells showed a significant increase in cell area. Widefield fluorescent images were used to analyse cell area and results showed a significant increase in cell area in 50 and 75  $\mu$ M resveratrol-treated MCF-7 and MDA-MB-231 cells. From our findings, resveratrol caused a decrease in cell proliferation only at 50  $\mu$ M in MCF-7 cells but at 20-75  $\mu$ M in MDA-MB-231 cells. These findings are consistent with other studies where resveratrol had higher anti-proliferative effect on MDA-MB-435 compared to MCF-7 cells (MDA-MB-435 cells have similar invasive properties to MDA-MB-231 cells) (Hsieh et al., 1999). Thus, a reduction in cell proliferation may have led to an increase in cell area.

Also, a resveratrol analogue, *cis*-3,4,5-trimethoxy-3'-hydroxystilbene was found to reduce cell proliferation in breast cancer cells by inhibiting MT polymerisation *in vitro* (Hong et al., 2009, Kim et al., 2004). These changes in cell area and proliferation following resveratrol treatment suggest that resveratrol may have an effect on cell adhesion which could be affecting cell migration. Cell migration requires dynamic MTs and focal adhesion (Ezratty et al., 2005) thus, any disruption in focal adhesions may lead to a reduction in cell migration. In addition, MTs contributes to the delivery of essential adhesion proteins such as MAP4K4 and HAX1 through EB2 (Yue et al., 2014b, Liu et al., 2015). Therefore, loss of EB2 association with MTs may affect focal adhesion turnover resulting in an increased cell area and cell migration reduction. A decrease in focal adhesions when cells are treated with resveratrol is supported by Azios and colleagues (2007) though an opposite effect was reported by Liu and co-workers (2015) when EB2 was depleted.

## **5.4.2 Resveratrol caused a dramatic decrease in cell migration in both MCF-7 and MDA-MB-231 cells**

Experiments were performed to establish the effect of resveratrol on random cell migration in MCF-7 and MDA-MB-231 cells. All resveratrol concentrations used (10-75  $\mu\text{M}$ ) revealed a significant reduction in the speed of migrating and distance travelled in MCF-7 and MDA-MB-231 cells. This is possibly due to the observed alteration of MTs – straighter MTs at higher concentrations of resveratrol, which might cause MT stability – and actin organisation and EB1 lattice association caused by resveratrol treatment (see section 5.3.3 and 5.3.7). Furthermore, the balance between dynamic and stable MTs could be the cause of reduced migration speed. This is related to changes in EB1 and EB2 plus tip localisation. EB1 was associated with the MT lattice, with more cytoplasmic EB2 in resveratrol treated MDA-MB-231 cells. However, there were no EB1 lattice association in resveratrol treated MCF-7 cells. This might be due to EB2 being highly expressed in MDA-MB-231 compared to MCF-7 cells (Fig 3.7B), which affects MT dynamics and possibly leading to increased migration speed. It has been reported that EB2 upregulation induces perineural invasion of pancreatic cancer cells (Abiatari et al., 2009). Furthermore, EB2 is evidently important for initial MT reorganisation during epithelial polarisation (Goldspink et al., 2013). Importantly, reduction in actin filaments were observed in resveratrol-treated cells. The inhibitory effect of resveratrol on random cell migration could be accounted for by its effect on the actin cytoskeleton and a reduction in filopodia extensions as previously reported (Azios and Dharmawardhane, 2005).

Using a three-dimensional model system to culture human breast cancer cells, we speculated that EB2-overexpression triggers cell invasion. Importantly, during invasion of MDA-MB-231 cells, the DMSO-treated cells showed invasive characteristics, as noted by the increased extension of cells around the mass into the Matrigel and collagen matrix. Reduction in MDA-MB-231 invasiveness following treatment with resveratrol is supported by (Buhrmann et al., 2017), which also revealed a reduction in colorectal cancer cell invasion by inhibiting FAK phosphorylation. Further studies could be carried out in these cells to establish the effect of resveratrol on focal adhesion kinases during invasion.

### **5.4.3 Resveratrol altered MT and actin organisation and resulted in EB1 associating along the MT lattice while EB2 became cytoplasmic in MDA-MB-231 cells**

In our study, comet analyses revealed increased EB1 circularity comets in resveratrol-treated MCF-7 cells while in MDA-MB-231 cells, comet circularity was reduced in resveratrol-treated cells and feret's diameter increased, which could suggest a reason for EB1 going along MT lattice. It is possible that the effect of resveratrol on these cells causes them to behave as if EB2 is depleted. As previously shown, EB2 depletion can inhibit microtubule dynamics and result in EB1 and ACF7 associating along the lattice, which leads to impaired migration (Goldspink et al., 2013). Resveratrol caused straighter MTs in both MCF-7 and MDA-MB-231 cells. Especially in the MDA-MB-231 cells where the cells adopted a radial array organisation of MTs at 50 and 75  $\mu$ M concentrations. It is possible that straighter MTs led to EB1 relocating from the plus ends and associating along the lattice in both treated cell lines. It is thought that EB1 lattice binding strengthens the lateral MT protofilaments and enhances MT stability (Zhang et al., 2009). This has been shown by the anticancer drug Taxol where this stabilisation of MTs enhanced EB1 lattice association (Jordan and Wilson, 2004, Goldspink et al., 2013, Shannon et al., 2005). Another explanation for EB1 binding along the lattice in addition to plus tips is due to their ability to recognise the GTP-tubulin state in MTs allowing straighter, stable MTs (Zhang et al., 2009, Maurer et al., 2012b). Therefore, because of straighter and possibly stable MTs, EB1 localisation was affected in resveratrol-treated cells.

In addition, EB2 localisation was affected in resveratrol-treated cells. DMSO-treated MCF-7 cells showed EB2 localisation at the plus-ends, as previously described (Komarova et al., 2009). EB2 localised at MT ends in MCF-7 resveratrol-treated cells. Usually, untreated or DMSO treated MDA-MB-231 cells had EB2 concentrated at the leading edge suggesting a higher ability for these cells to migrate, because EB2 is supposed to cause an increased MT dynamics required for cell migration however, in resveratrol-treated MDA-MB-231 cells, an increased amount of EB2 was diffused in the cytoplasm. In a recent publication, it was observed that phosphorylation of EB2

can lead to its disassociation from MTs and release into the cytoplasm (Iimori et al., 2016b). Also, a resveratrol analogue has been shown to increase the levels of Aurora B in MDA-MB-231 cells suggesting that the increased levels of Aurora B and CDK1 may be able to phosphorylate and dissociate EB2 from MTs (Hong et al., 2009). But while EB2 has dissociated from MTs in order for mitosis progression, resveratrol also binds to MTs inhibiting polymerisation, thereby, reducing cell proliferation and migration. This suggests that resveratrol may indirectly induce EB2 phosphorylation, which could be the second EB2 band noticed on the blot, an idea that needs to be investigated further. The results also suggest there was no change in the level of EB2 in both MCF-7 and MDA-MB-231 resveratrol treated cells. Additionally, resveratrol treatment altered actin filaments organisation. In both MCF-7 and MDA-MB-231 cells, resveratrol caused actin depolymerisation.

#### **5.4.4 Resveratrol caused a reduction in focal adhesions and altered MT acetylation in MDA-MB-231 cells**

In epithelial cells, migration is driven by cell polarisation, actin polymerisation, and generation of cross-linked actin filaments into leading edge lamellipodia that are stabilised by making focal adhesions with the ECM (Ridley et al., 2003). MTs are involved in two essential stages of cell migration, one being the reorientation of cellular organelles such as the Golgi complex towards the direction of movement and the other is the regulation of focal adhesion turnover (Ridley et al., 2003, Lauffenburger and Horwitz, 1996). Focal adhesion kinase (FAK) is one of the first signalling molecules recruited to nascent focal adhesions (Hu et al., 2014). Therefore, the observed reduced FAK number in response to resveratrol concentrations above 50  $\mu$ M may contribute to the inhibitory effect of resveratrol on cell migration. The effect on focal adhesion size occurred with resveratrol concentrations at 10  $\mu$ M and above. However, published data suggest that much higher concentration of 50 mM resveratrol is needed to cause reduction in focal adhesion size. Reduction in focal contacts is known to activate apoptosis (Schaller, 2001), thus, resveratrol-mediated decrease in focal adhesion number and size may represent another pathway by which resveratrol can induce apoptosis, an effect that needs to be fully examined in our study. Apoptosis could be shown by staining the cells with caspase-3 and then counting the number of cells that

took up the marker in the resveratrol-treated compared to the control cells. Buhrmann and co-workers (2017) established that a reduction in cancer cell invasion was mediated by resveratrol inhibiting FAK phosphorylation. Though how EB2 overexpression may affect this pathway in breast cancer cells need to be clarified.

MTs target focal adhesions, which correlates with focal adhesion disassembly. FAK (a protein that phosphorylates paxillin) and dynamin are needed for MT-induced focal adhesion disassembly. This occurs through FAK's interaction with dynamin during the early phases of focal adhesion disassembly. Localisation of dynamin around focal adhesions also occur through FAK (Ezratty et al., 2005). MT dynamics regulate focal adhesion turnover due to the delivery of important proteins (HAX1 and MAP4K4) to focal adhesion sites by MTs and EB2 (Yue et al., 2014b, Liu et al., 2015). More dynamic MTs can affect focal adhesion dynamics and turnover. As discovered, resveratrol-treated MDA-MB-231 but not MCF-7 cells showed a decrease in acetylated tubulin suggesting reduced MT stability, which may affect sites of focal adhesion. A decrease in acetylated MTs may therefore cause a reduction in the transportation of essential proteins needed to maintain their focal adhesion contact and sites. It has been suggested that EB2 contributes to focal adhesion turnover by associating with essential proteins, such as HAX1 and MAP4K4 (Liu et al., 2015). It is therefore possible to speculate that resveratrol has an influence on one of these proteins such as MAP4K4 whereby the effect caused is similar to the overexpression of MAP4K4 resulting in focal adhesion turnover.

Some MT-focused anticancer drugs have been reported to modify MT dynamics by binding to specific tubulin sites along MTs (Jordan and Wilson, 2004). For example, sulforaphane has been shown to modulate MTs dynamic instability by promoting acetylation of MTs in MCF-7-GFP- $\alpha$ -tubulin cells in a concentration-dependent manner (Azarenko et al., 2008). We demonstrate by fluorescence intensity analysis and Western blotting that resveratrol causes a reduction in MT acetylation, which has been connected with MT stability. In resveratrol-treated MCF-7 cells, even though the total area of tubulin acetylation was not significant, Western blot showed a reduction in the level of acetylated tubulin at 50  $\mu$ M. It has been demonstrated that Lys40 acetylation weakens lateral interactions between protofilaments, therefore, softening the MTs

(Portran et al., 2017). MT acetylation is also reported to reduce the frequency of nucleation and accelerate the rate of depolymerisation (Portran et al., 2017). As such those MTs are prone to depolymerisation, which might be the case in the 75  $\mu\text{M}$  resveratrol-treated MDA-MB-231 cells. Effects of resveratrol on MT stability might be brought on due to a conformational change of  $\alpha/\beta$ -tubulin dimer or by acting directly on resveratrol–tubulin complexes in MTs. It is already reported that resveratrol analogues can bind to colchicine-binding hydrophobic sites in tubulin, which dissociate very slowly once formed and stabilise the ends once they are incorporated (Hong et al., 2009, Scherzberg et al., 2015, Traversi et al., 2017). This seems to be the case as the MT localisation immunolabelling studies with resveratrol in MCF-7 and MDA-MB-231 cells revealed straighter MTs (section 5.3.3 and 5.3.4.). Further work into MT stability and dynamics need to be done. An example of this would be to carry out a pre-extraction study by cold-treatment, whereby free tubulin monomers in both treated cell lines are extracted in solution and then MT stability on the free tubulin monomers as well as the total polymerised tubulin are examined. Overall, the preliminary results suggest that the effects of resveratrol in MCF-7 and MDA-MB-231 cells are a result of its direct action on MTs and are not due to modification of the free tubulin levels as well as its effects on actin.

## **5.5 Summary**

In summary, resveratrol caused an increase in cell size in both breast cancer cell lines as well as a decrease in proliferation in MCF-7 cells with 50  $\mu\text{M}$  but in MDA-MB-231 cells above 20  $\mu\text{M}$ . Resveratrol seems to alter the organisation of MTs, in both cell lines, by making them straighter but only MDA-MB-231 cells showed EB1 lattice association. EB1 comets increased in circularity in MCF-7 cells and longer ‘tails’ were observed in only MDA-MB-231 cells with resveratrol treatment above 50  $\mu\text{M}$ . Usually, DMSO-treated MDA-MB-231 cells had EB2 concentrated at the leading edge suggesting a role in migration. However, in treated cells, an increased amount of EB2 diffused into the cytoplasm. In addition, 3D control invasive conditions resulted in long thin projections in MDA-MB-231 cells while most MCF-7 cells remained in aggregates. There was also a reduction in invasive cells following resveratrol treatment.

Resveratrol caused a decrease in cell migration speed and distances travelled. This implies that the decrease in migration was due to decreased actin polymerisation and also a decrease in focal adhesion size and number, which probably affected focal adhesion turnover. The intensity analysis of acetylated tubulin compared with total tubulin revealed no significant change while Western blotting suggested a reduction with 50  $\mu$ M in MCF-7 cells. In MDA-MB-231 cells, a reduction was observed with the intensity study as well as Western with 75  $\mu$ M resveratrol. It can be speculated that resveratrol causes its effects by increasing the levels of Aurora B (and possibly CDK1), which leads to the dissociation of EB2 from MTs. Loss of EB2 association with MTs then affects focal adhesion turnover resulting in an increased cell area and cell migration reduction. Resveratrol also directly inhibits MT polymerisation further preventing cell migration. However, the overall mechanism on how resveratrol causes these effects are not fully understood and further investigations are required.

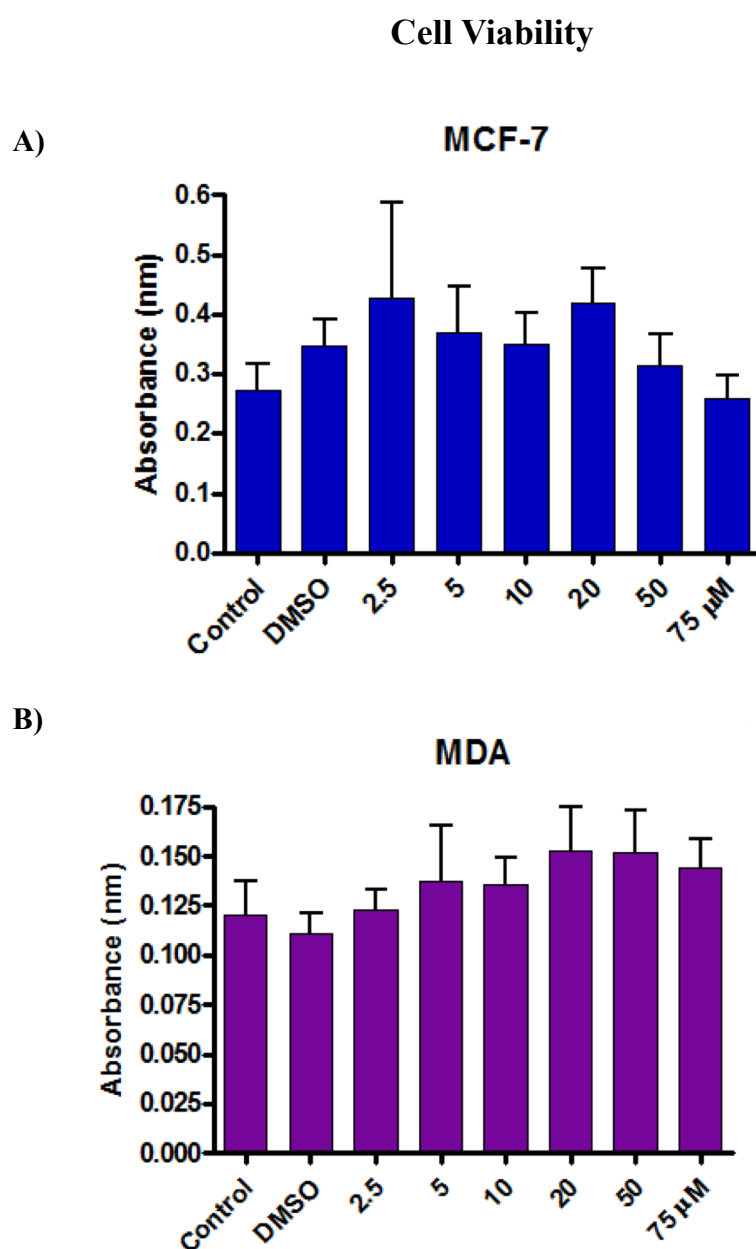


**Figure 5.1: Resveratrol cell viability assay in breast cancer cells.** Cells were treated with different concentrations of resveratrol then incubated for 24 h. Cell viability was examined with a MTT assay, which is based on the reduction of yellow tetrazole to purple formazan in living cells. A) and B) show that resveratrol concentrations up to 75  $\mu$ M did not cause significant changes in cell viability in MCF-7 and MDA-MB-231 cells using one-way ANOVA with Tukey's as statistical analysis. All concentrations were compared to the DMSO control. The results are based on two experiments.

**MCF-7**

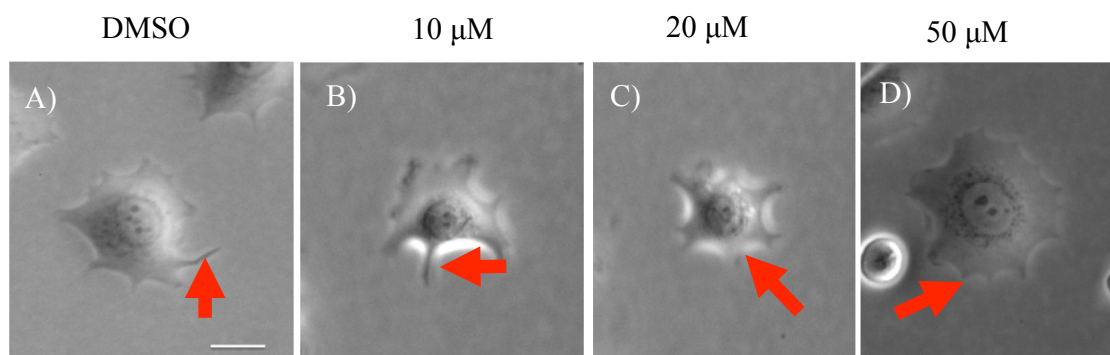


**Figure 5.2: Cell morphology of resveratrol-treated MCF-7 cells seeded on collagen I.** Representative images from live time-lapse recordings of subconfluent random migrating MCF-7 cells. A) DMSO treated cell showing a short protrusion (red arrow). B) Cell treated with 10  $\mu\text{M}$  resveratrol showing lamellipodium and tail projection (red arrow). C) Rounded cell showing several short projections and membrane ruffling (red arrow) following 20  $\mu\text{M}$  resveratrol treatment. D) A cell treated with 50  $\mu\text{M}$  resveratrol showing a 'fried-egg' like morphology with some membrane ruffling (red arrow). Scale bar = 100  $\mu\text{m}$ .

**MDA-MB-231**

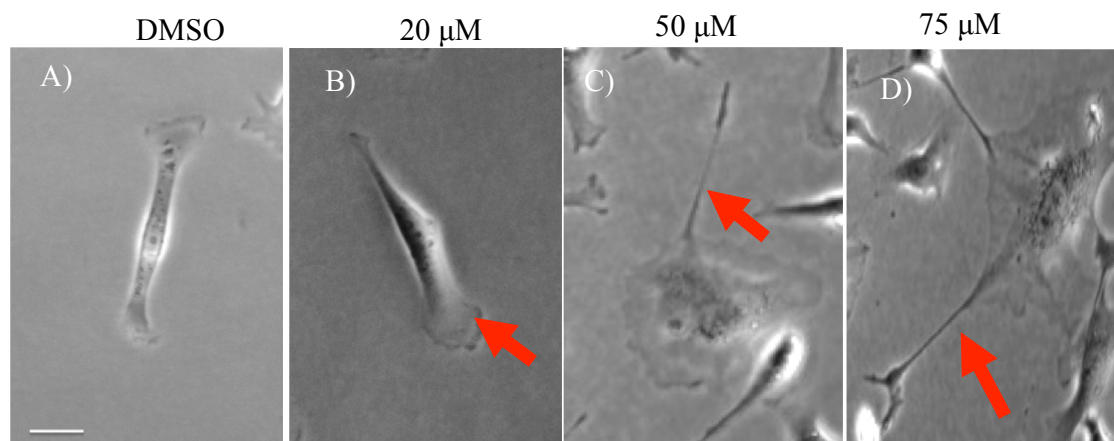


**Figure 5.3: Cell morphology of resveratrol-treated MDA-MB-231 cells seeded on collagen I.** Representative images from live time-lapse recordings of subconfluent random migrating MDA-MB-231 cells. A) DMSO treated cell showing an elongated morphology with large protrusions at both ends. B) Cell showing lamellipodium (red arrow) and elongated morphology following treatment with 20  $\mu\text{M}$  resveratrol. C) Cell showing cell body with lamellipodium and tail-like projection (red arrow) following treatment with 50  $\mu\text{M}$ . D) Treatment with 75  $\mu\text{M}$  resveratrol also led to formation of long tail-like projection. Scale bar = 100  $\mu\text{m}$ .

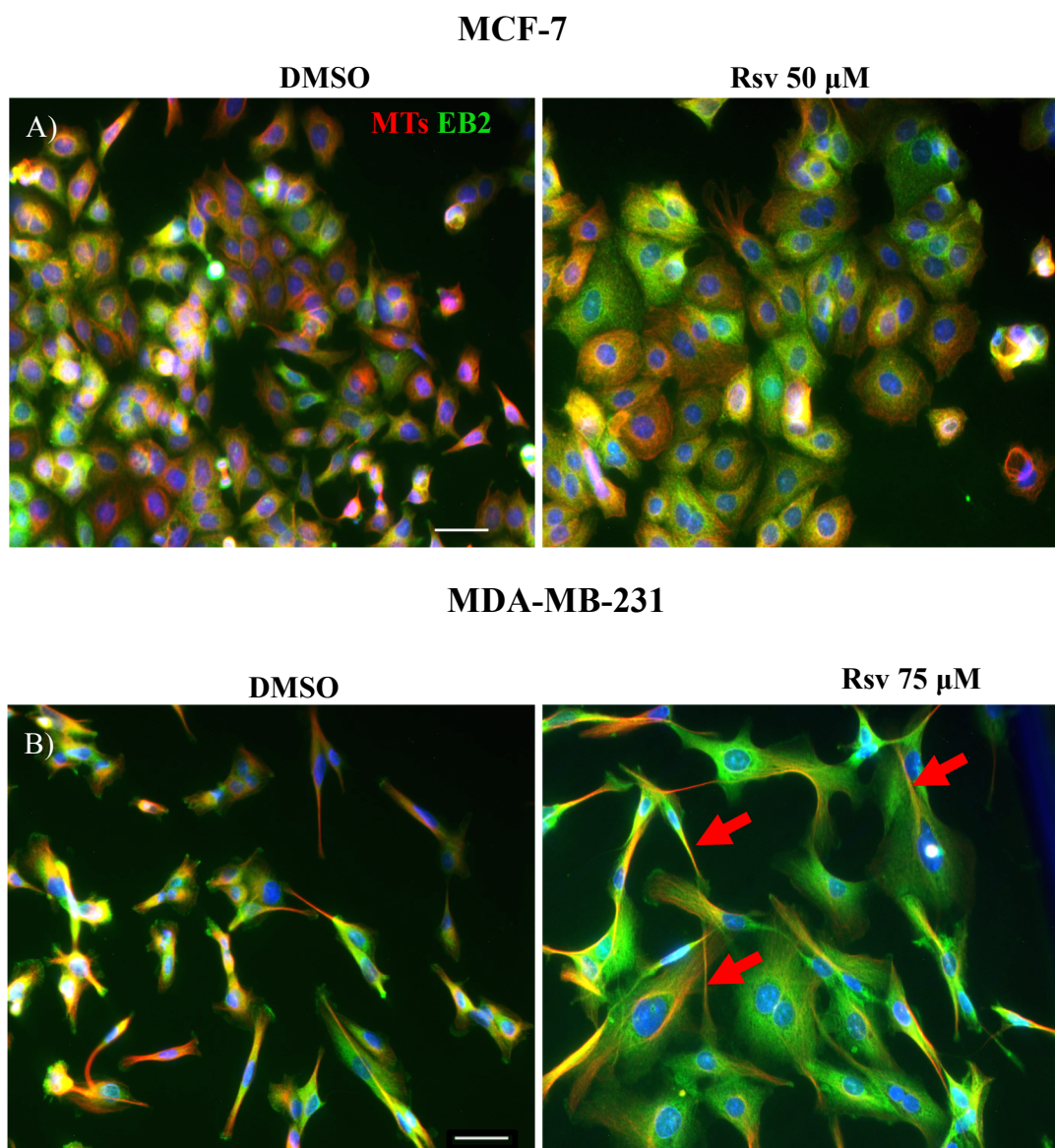


**Figure 5.4: Resveratrol affected the size of MCF-7 and MDA-MB-231 cells.** Cells seeded on collagen I were treated with different concentrations of resveratrol, incubated for 24 h. and then immunolabelled with an anti- $\alpha$ -tubulin antibody (red, pAb, ab15246) and anti-EB2 K52 antibody (green, ab45767). Widefield fluorescent images of MCF-7 and MDA-MB-231 cells obtained with a x20 objective lens. A) In MCF-7 cells 50  $\mu$ M resveratrol-treatment induced an increase in cell size compared to DMSO. B) In MDA-MB-231 cells 75  $\mu$ M resveratrol caused an increase in cell size and the appearance of long protrusions (red arrows) compared to the DMSO. Longer tails suggest that the cells are taking longer to move in its entirety. Images are to scale. Scale bars = 100  $\mu$ m.

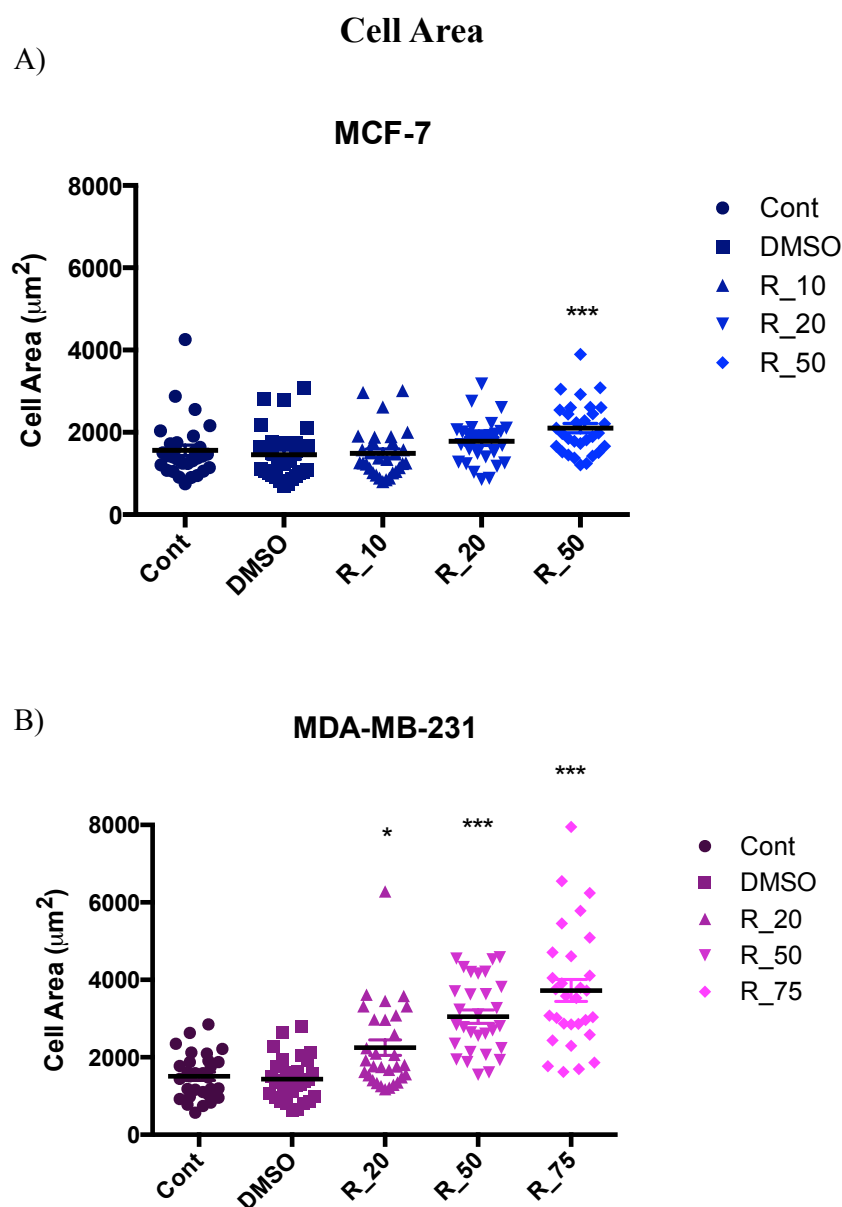


**Figure 5.5: Resveratrol caused an increase in the size of MCF-7 and MDA-MB-231 cells.** Cells seeded on collagen I were treated with different concentrations of resveratrol and incubated for 24 h. The cell area was measured using ImageJ. A and B) Analysis of both cell lines showed that 50  $\mu\text{M}$  resveratrol caused a significant increase in cell area compared to DMSO treated cells. Statistical analysis using one-way ANOVA with Tukey's multiple comparisons test. All concentrations were compared with DMSO control. Analysis is based on one experiment.

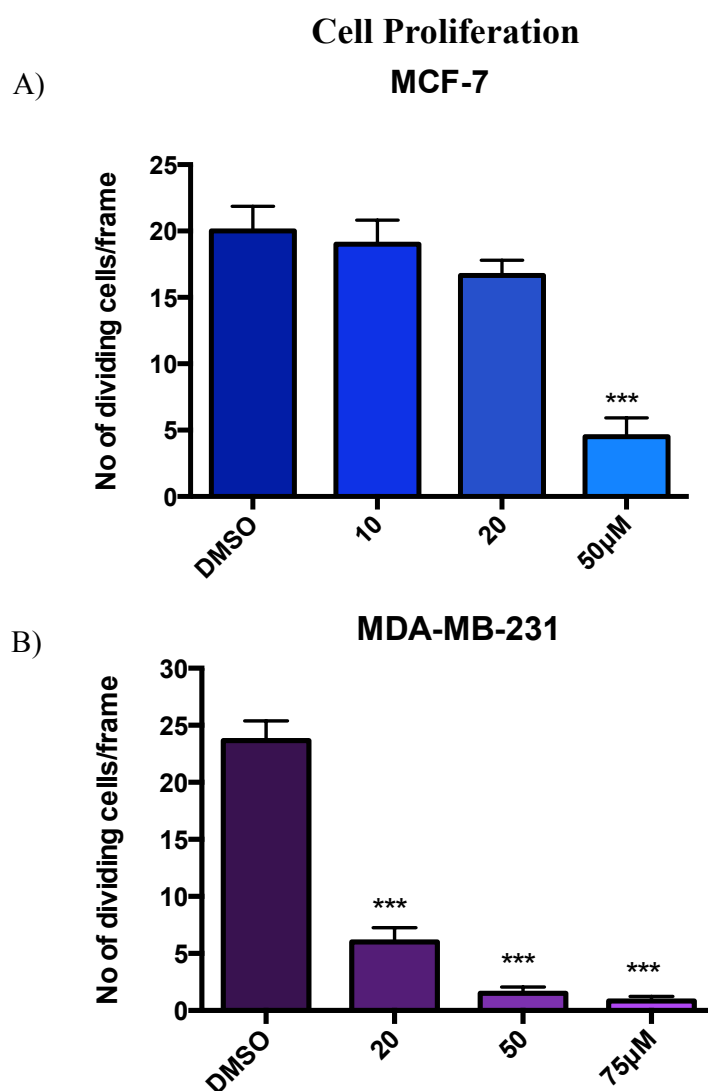


**Figure 5.6: Resveratrol caused a reduction in breast cancer cells proliferation.** Cells seeded on collagen-I were treated with different concentrations of resveratrol and incubated for 24 h. Cell proliferation was measured by counting the number of cells dividing per frame from time-lapse recordings. A) The average number of MCF7 cells dividing in DMSO and 10, 20 and 50  $\mu\text{M}$  resveratrol treated was 20, 19, 17 and 5 cells/frame respectively but only 50  $\mu\text{M}$  resveratrol resulted in a significant reduction in proliferation B) The average number of MDA-MB-231 cells dividing in DMSO treated and 20, 50 and 75  $\mu\text{M}$  resveratrol treated was 24, 6, 2 and 1 cell/frame respectively with all resveratrol treatments showing significant reductions in proliferation. Statistical analysis using One-way ANOVA with Tukey's multiple comparisons test. All concentrations were compared with DMSO control. Analysis is based on one experiment.

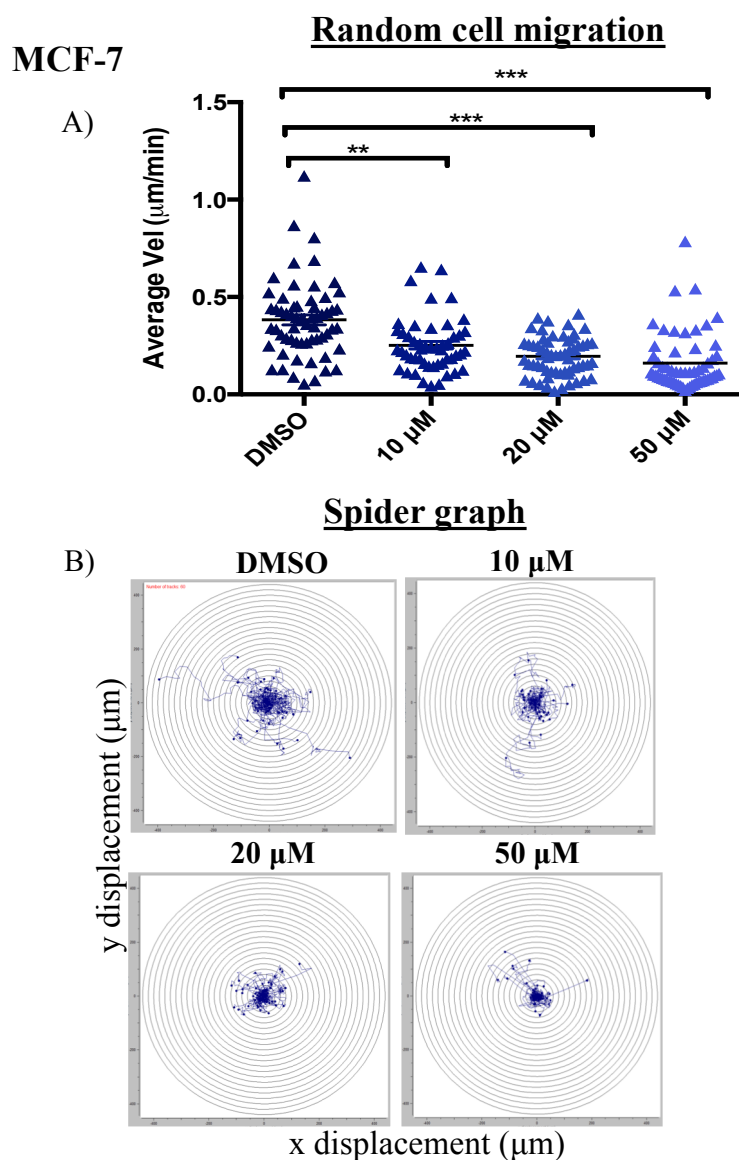


**Figure 5.7: Resveratrol caused a reduction in speed and distance travelled of randomly migrating MCF-7 cells.** Live time-lapse imaging was carried out with a frame taken every 10 min for 16 h. 40 cells per condition were analysed. A) Position of random cells were tracked in ImageJ and the average cell velocities were plotted. The average velocities of cells treated with DMSO and resveratrol of 10, 20 and 50  $\mu\text{M}$  were 0.382, 0.252, 0.195 and 0.160  $\mu\text{m}/\text{min}$  respectively, thus, a significant reduction in velocity when cells were treated with resveratrol compared with the DMSO. B) Spider graphs show the distance of individual cells during migration and revealed that DMSO, 10, 20 and 50  $\mu\text{M}$ -treated cells travelled a distance of 87.16, 62.24, 47.77 and 39.54  $\mu\text{m}$  respectively, thus resveratrol-treated cells travelled shorter distances compared to DMSO-treated cells. Mean  $\pm$  SEM. Analysis is based on one experiment.

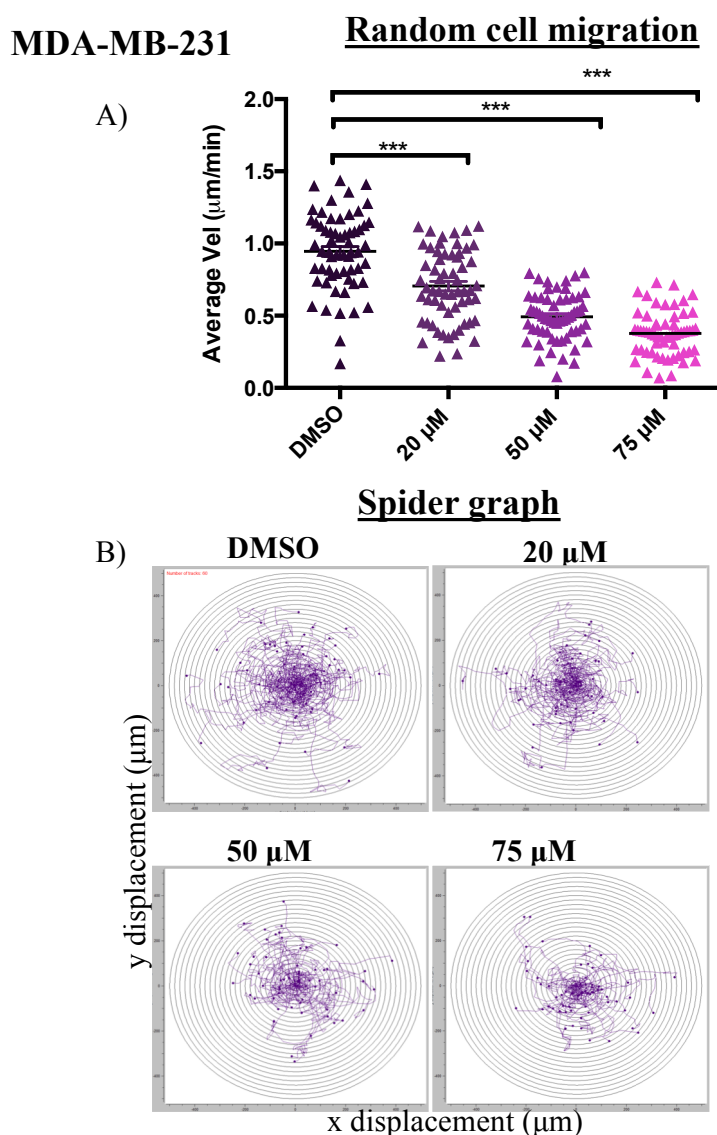


**Figure 5.8: Resveratrol caused a reduction in speed and distance travelled of random migrating MDA-MB-231 cells.** Live time-lapse recordings were used to take images every 10 min for 16 h. 40 cells per condition were analysed. The positions of random cells were tracked in ImageJ and average velocity of cells plotted. The average velocity of cells treated with DMSO and 20, 50 and 75  $\mu\text{M}$  resveratrol was 0.942, 0.675, 0.492 and 0.378  $\mu\text{m}/\text{min}$  respectively. A significant reduction in velocity was evident with all concentrations of resveratrol compared with the DMSO. B) Spider graphs showing the distance of individual cells during migration revealed that treatment with DMSO and 20, 50 and 75  $\mu\text{M}$  resveratrol resulted in travelled distances of 233.26, 173.89, 121.54 and 93.28  $\mu\text{m}$  respectively. Resveratrol-treated cells travelled shorter distances compared to DMSO-treated cells. Mean  $\pm$  SEM. Analysis is based on one experiment.

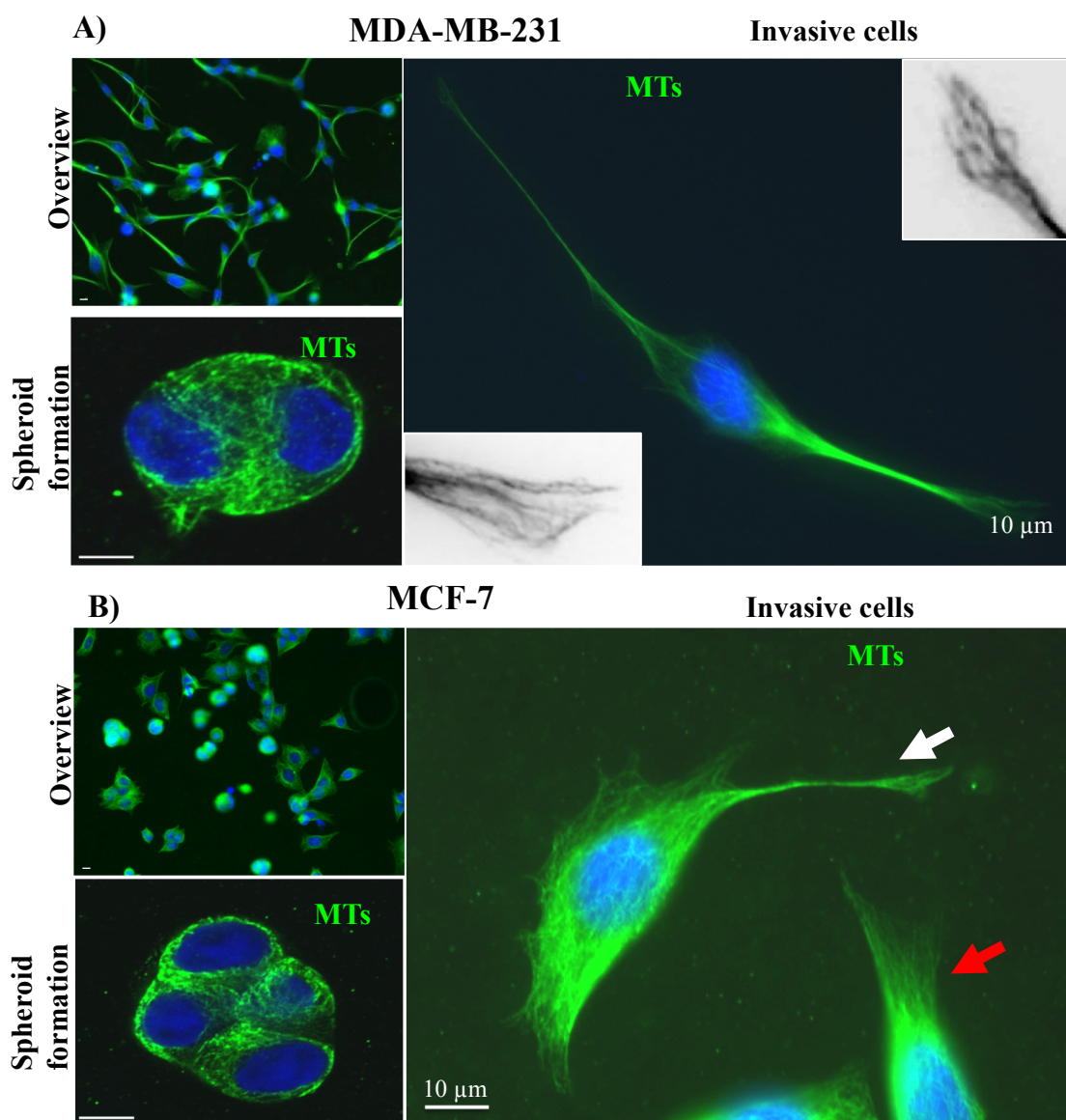


**Figure 5.9: Invasion of highly metastatic MDA-MB-231 cells.** Untreated MDA-MB-231 and MCF-7 cells were seeded in a round-bottom 96-well plate to generate spheroids. The spheroids were collected and embedded in a Matrigel with collagen (1mg/ml) and monitored for invasion. Cells were fixed in methanol and immunolabelled for  $\alpha$ -tubulin (green, pAb, ab15246). Widefield images were taken using a x2.5 obj lens, (not all the images some most have been with a higher lens). A) Mainly spindle shaped single cells and very few aggregates had formed in MDA-MB-231 cultures. Extensive MT reorganisation was seen at both ends of the cell (inverted image). B) MCF-7 cells mainly formed aggregates (overview image) and some single invasive cells with MT reorganisation (white arrow). An MCF-7 cell with no MT reorganisation (red arrow). Scale bar = 100  $\mu$ m for overview images.

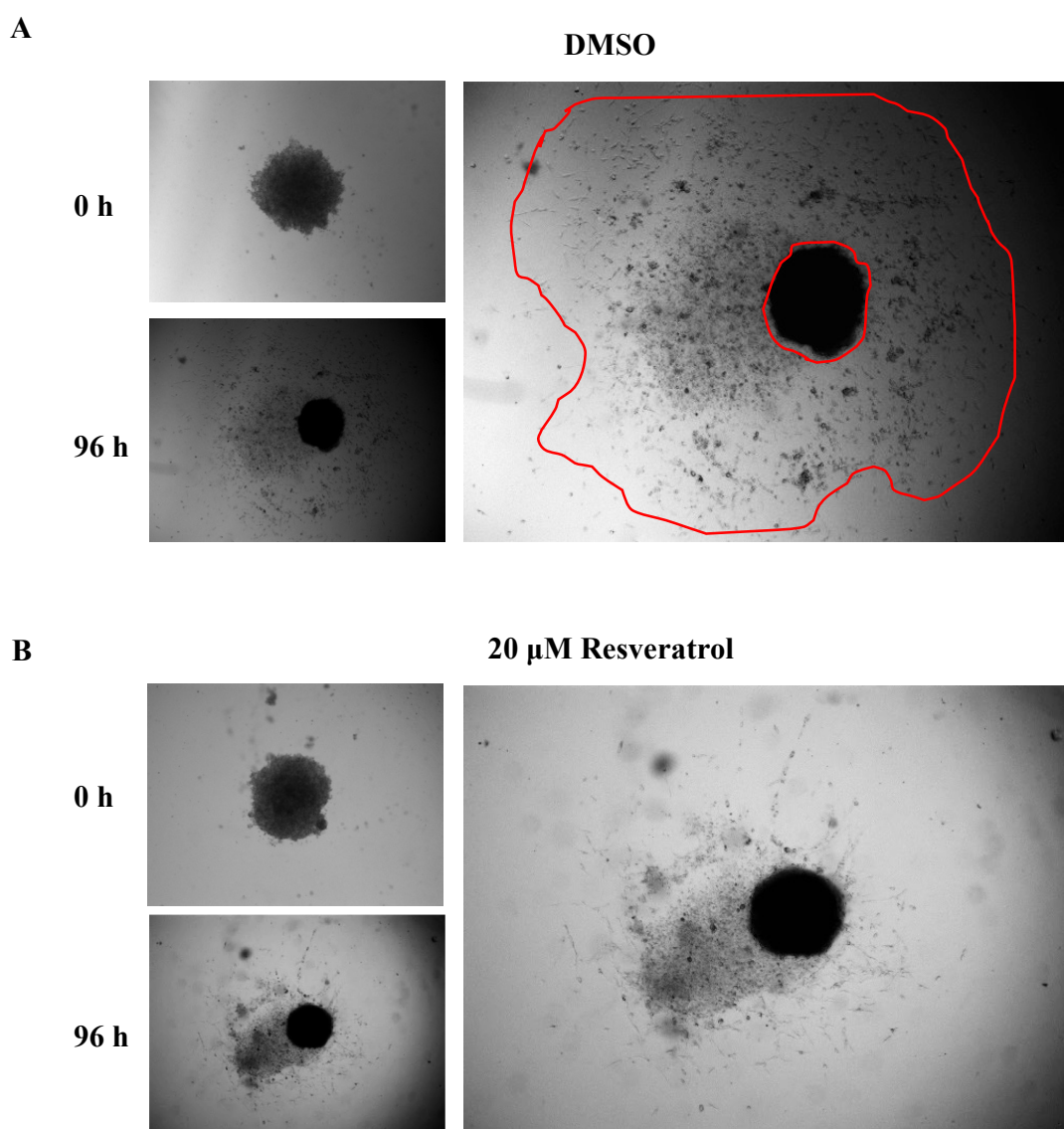


**Figure 5.10: Invasion of highly metastatic MDA-MB-231 cells.** MDA-MB-231 cells were seeded in a round-bottom 96-well plate for 48h to generate spheroids. The spheroids were then collected and embedded in a Matrigel with Collagen I (1mg/ml) and monitored for invasion. The medium was supplemented with DMSO or Resveratrol concentrations at 20, 50 or 75 $\mu$ M. Phase-contrast images were taken using a x2.5 obj lens. A) shows the area of invasion in MDA-MB-231 cells from the centre mass. B) A marked decrease in invasive area is apparent above with 20 $\mu$ M resveratrol.

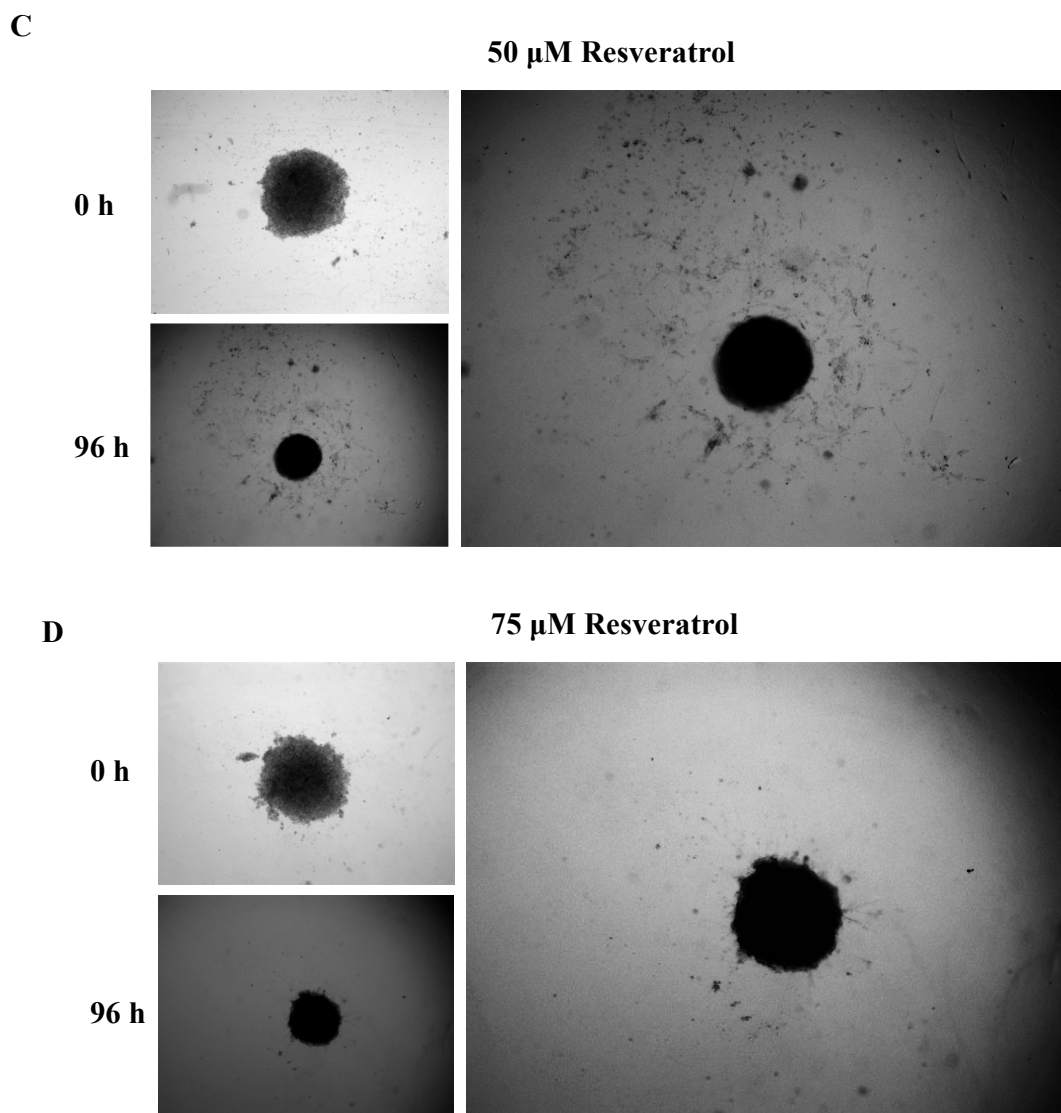


**Figure 5.11: Invasion of highly metastatic MDA-MB-231 cells continued:** The area of invasive cells was further reduced with 50  $\mu$ M (C) and 75 $\mu$ M (D) resveratrol compared to the DMSO control.

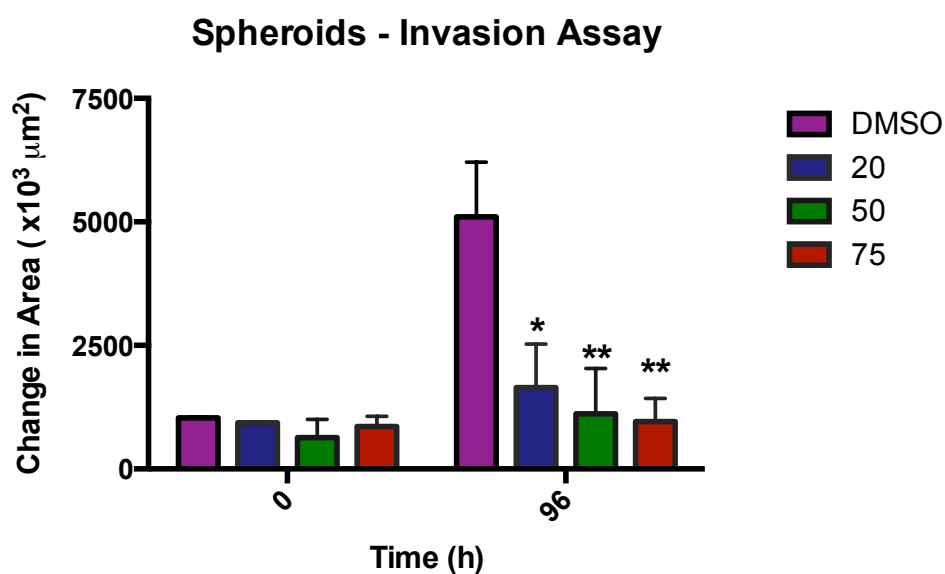


**Figure 5.12: Effect of resveratrol on MDA-MB-231 cell invasion.** ImageJ was used to measure the area of the cell mass at 0 and 96h. Analysis by one way ANOVA with Tukey's multiple comparisons test revealed a significant reduction in the invasive area in resveratrol-treated cells compared to DMSO after 96 h. Repeat of 2 experiments. Mean  $\pm$  SEM.

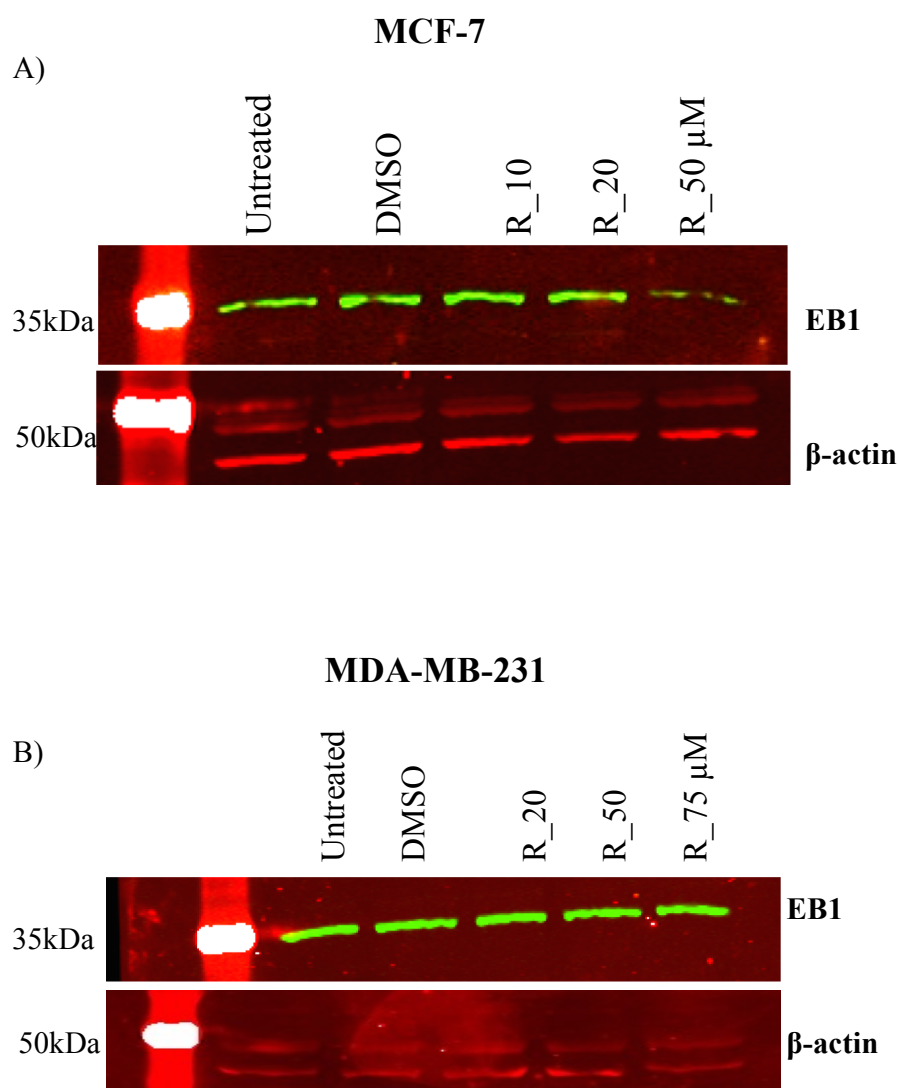


**Figure 5.13: EB1 expression in Resveratrol-treated MCF-7 and MDA-MB-231 cells.** Western blot showing the level of EB1 expression in untreated, DMSO and resveratrol-treated cells. A) In MCF-7 cells, there appears to be a slight decrease in EB1 expression with 50  $\mu$ M resveratrol compared to DMSO control cells. B) However, in MDA-MB-231 cells the Western blot suggests no change in the level of EB1 expression in resveratrol-treated cells compared to DMSO control cells.  $\beta$ -actin was used as the loading control. Result is based on one experiment.

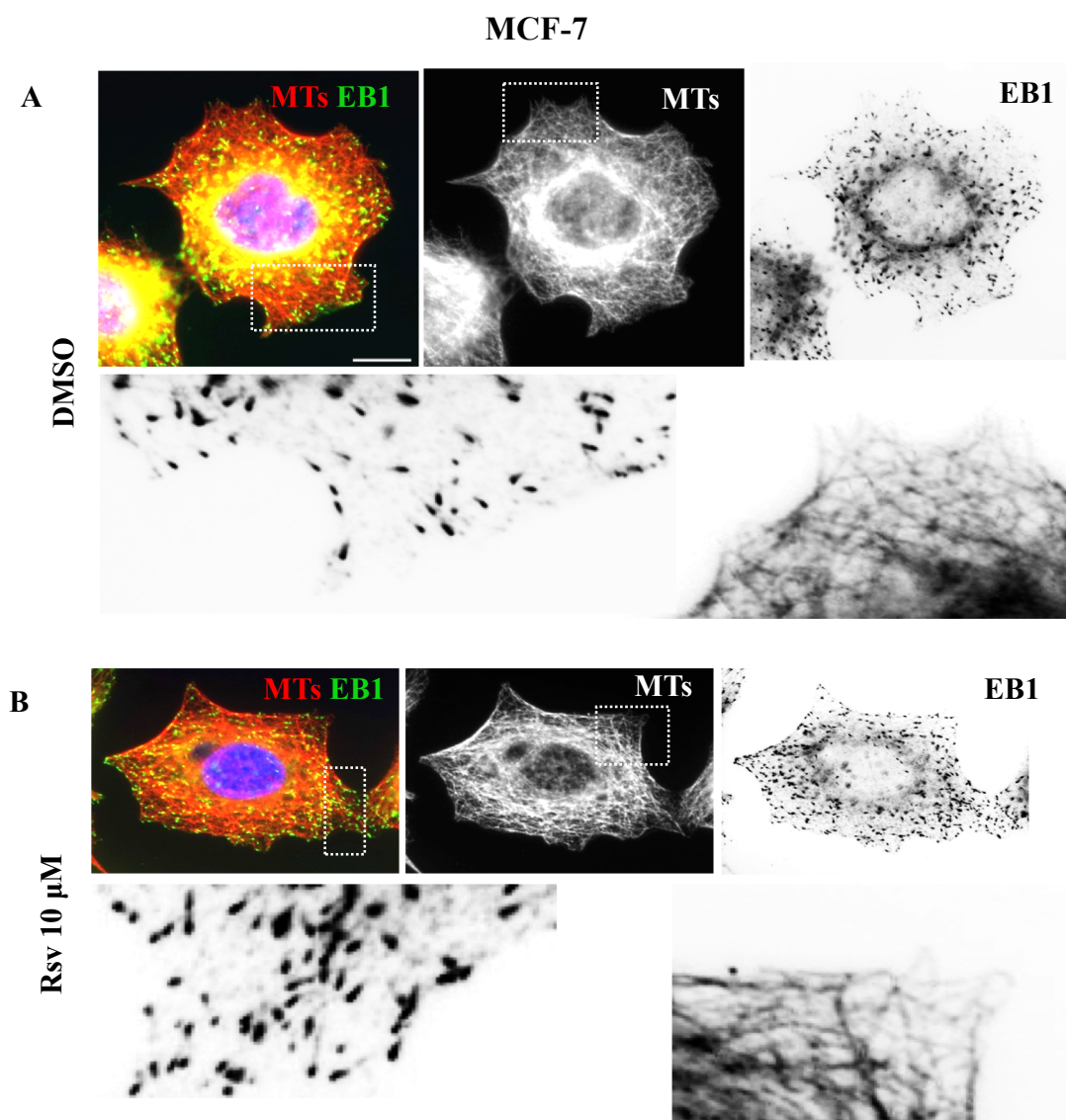


**Figure 5.14: EB1 localisation and MT organisation in Resveratrol-treated MCF-7 cells.** Cells were seeded on collagen I and treated with different concentrations of resveratrol, incubated for 24 h and immunolabelled with an anti- $\alpha$ -tubulin antibody (red, pAb, ab15246) and anti-EB1 antibody (green, mAb, 610535). Images were obtained with a widefield fluorescence microscope. A) Cell treated with DMSO showing MTs and EB1 in the merged image and single channel images of EB1 and MTs. EB1 localises as classic comets at MT ends (enlarged region) and the MTs are organised in curled bundles around the nucleus and as a disorganised network at the periphery. B) Cell treated with 10  $\mu$ M Resveratrol showing the merged image of MTs and EB1 and single channel images of EB1 and MTs show little changes in MT organisation or EB1 localisation compared with DMSO. Scale bar = 10  $\mu$ m.

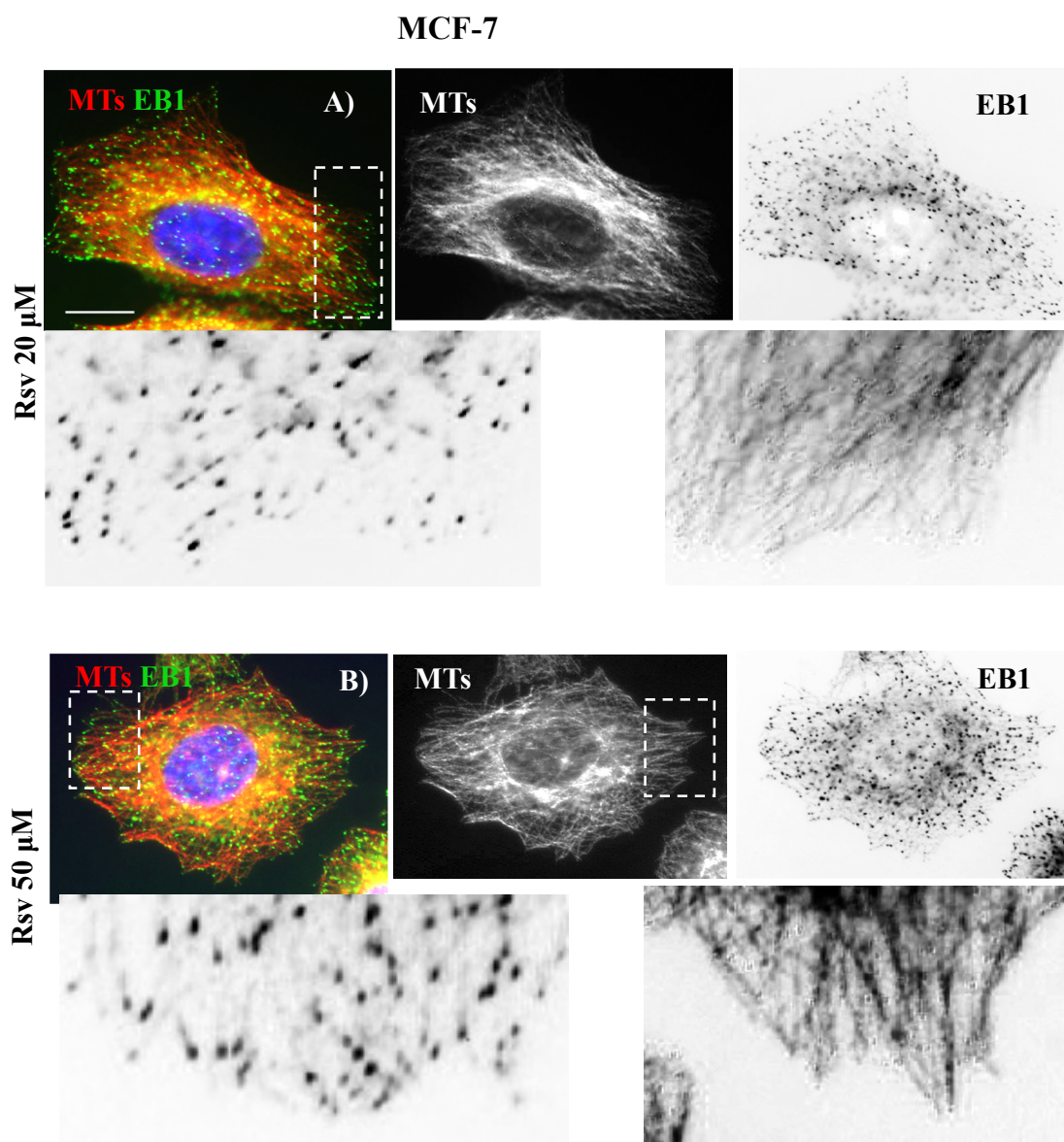


**Figure 5.15: EB1 localisation and MT organisation in Resveratrol-treated MCF-7 cells.** Cells seeded on collagen I were treated with different concentrations of resveratrol then incubated for 24 h. Cells were immunolabelled with an anti- $\alpha$ -tubulin antibody (red, pAb, ab15246) and anti-EB1 antibody (green, mAb, 610535) and widefield fluorescent images of MCF-7 cells were obtained. A) Cell treated with 20  $\mu$ M resveratrol reveal signs of straighter MTs (inverted enlarged image) and EB1 still localises at the plus ends though appears more dotted compared with the DMSO-control cell. B) The 50  $\mu$ M treated cell shows the appearance of straighter MTs (enlarged region). Single channel image shows dotted EB1 at MT ends (enlarged region). Scale bar = 10  $\mu$ m.

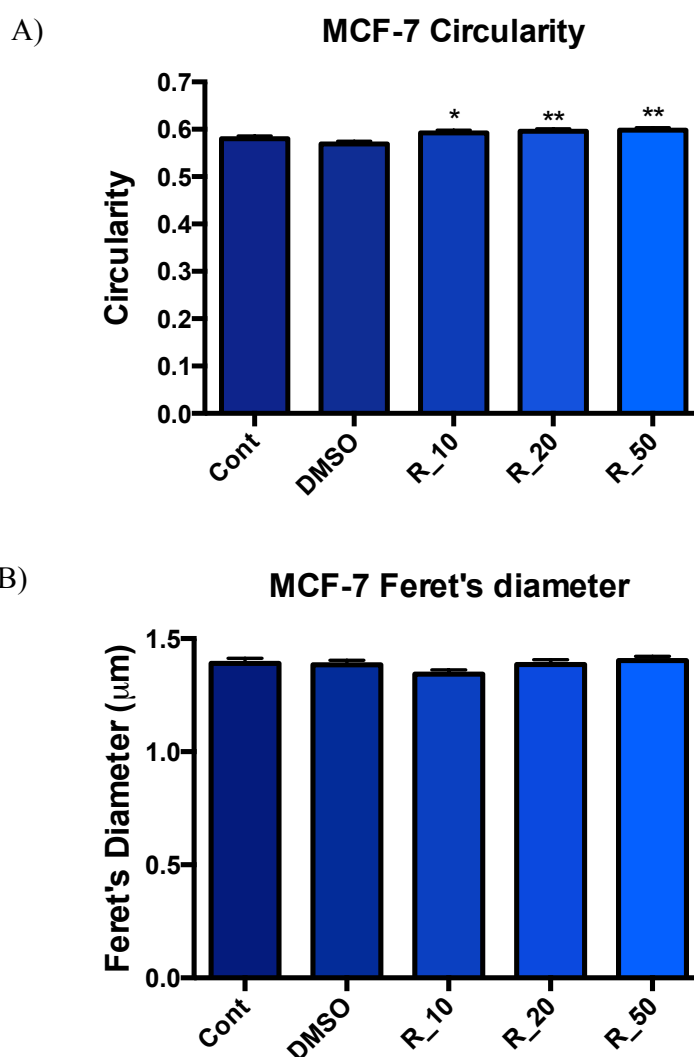


**Figure 5.16: EB1 comet analysis in Resveratrol-treated MCF-7 cells.**

ImageJ was used to analyse the circularity of comets and ferret's diameter. A) EB1 circularity is significantly higher in the 10, 20 and 50  $\mu\text{M}$  resveratrol-treated MCF-7 cells at 0.592, 0.595 and 0.595 respectively compared to DMSO cells at 0.569. B) Feret's diameter of comets were of no significant difference when cells were treated with resveratrol. Analysis was carried out by one-way ANOVA. Error bars = SEM. No of cells measured = 10. Based on one experiment.

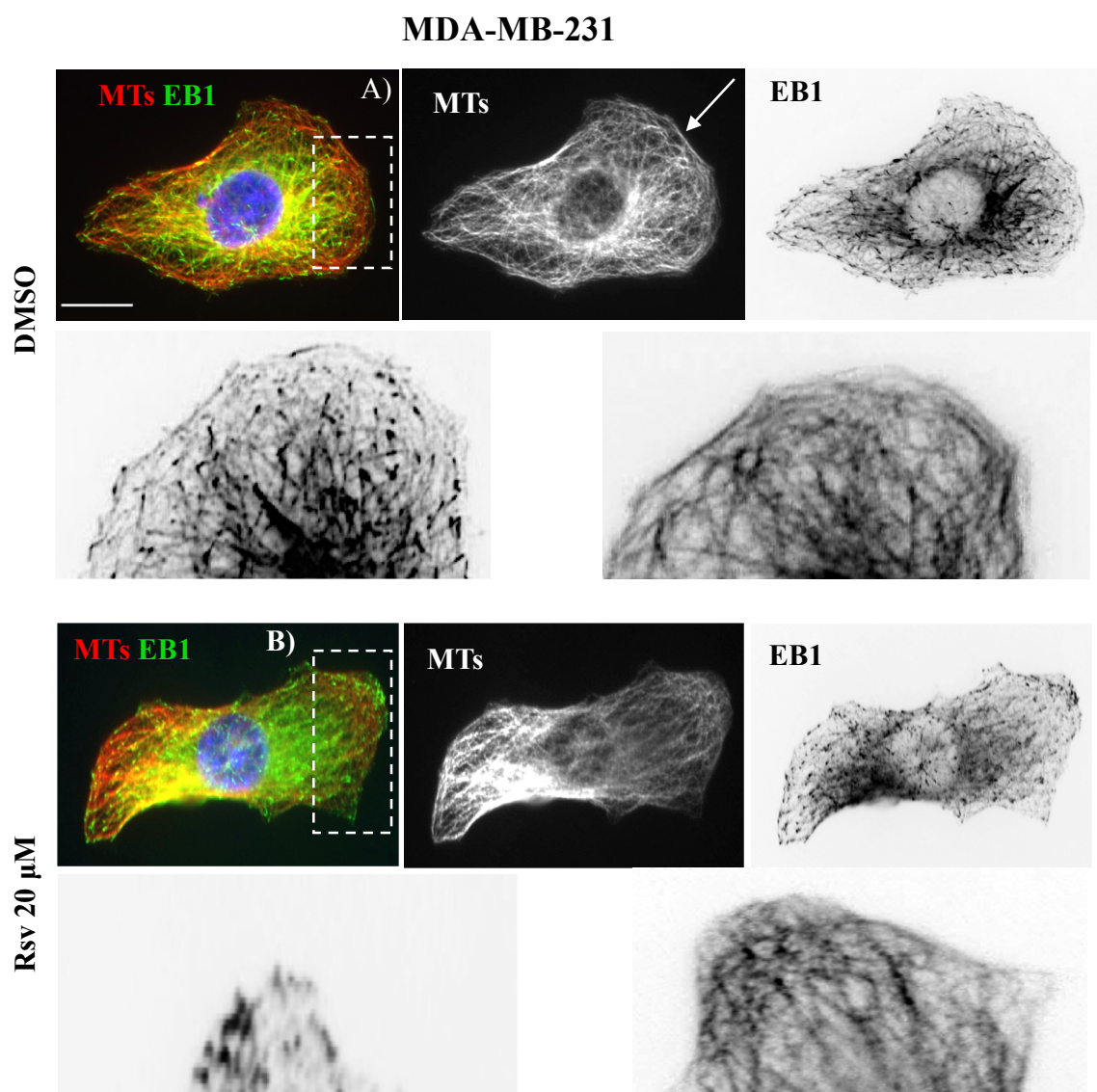


**Figure 5.17: EB1 localisation and MT organisation in Resveratrol-treated MDA-MB-231 cells.** Cells were seeded on collagen I and treated with different concentrations of resveratrol and incubated for 24 h. Cells were immunolabelled with an anti- $\alpha$ -tubulin antibody (red, pAb, ab15246) and anti-EB1 antibody (green, mAb, 610535) and widefield fluorescent images of MDA-MB-231 cells were obtained. A) DMSO-treated cell shows EB1 at the tip of MTs. Single channel image shows that the MTs are highly disorganised, forming interwoven networks at the front of the cell (white arrow and inverted enlarged region) while EB1 localises to the +TIP (enlarged region). Comets appear elongated in shape compared to the ones in MCF-7 cells. B) At 20  $\mu$ M resveratrol, the cell shows a disorganised organisation of MTs with EB1 at plus-ends (enlarged region). Scale bar = 10 $\mu$ m.

MDA-MB-231

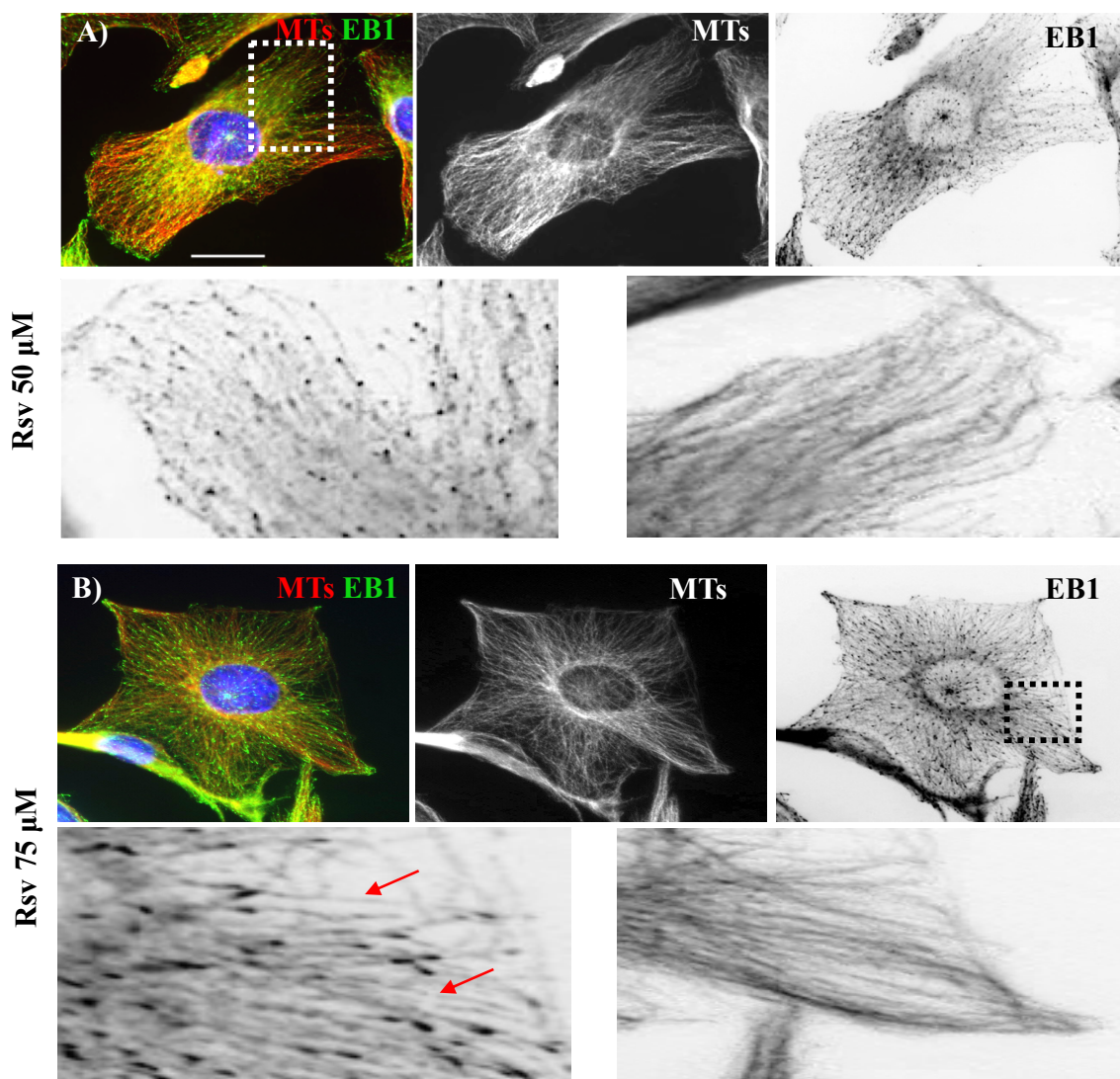


**Figure 5.18: EB1 localisation and MT organisation in Resveratrol-treated MDA-MB-231 cells.** Cells were seeded on collagen I and treated with different concentrations of resveratrol and incubated for 24 h. Cells were immunolabelled with an anti- $\alpha$ -tubulin antibody (red, pAb, ab15246) and anti-EB1 antibody (green, mAb, 610535) and widefield fluorescent images of MDA-MB-231 cells were obtained. A) Cell showing a radial array organisation of MTs (merged image) with MTs appearing straighter (inverted region) compared to DMSO. EB1 localises to the ends of the MTs. B) Cell showing a distinct radial array organisation of MTs (single channel image) and the appearance of straighter MTs (inverted enlarged region). Enlarged region shows association of EB1 along the MT lattice (red arrows enlarged region). Scale bar = 10  $\mu$ m.

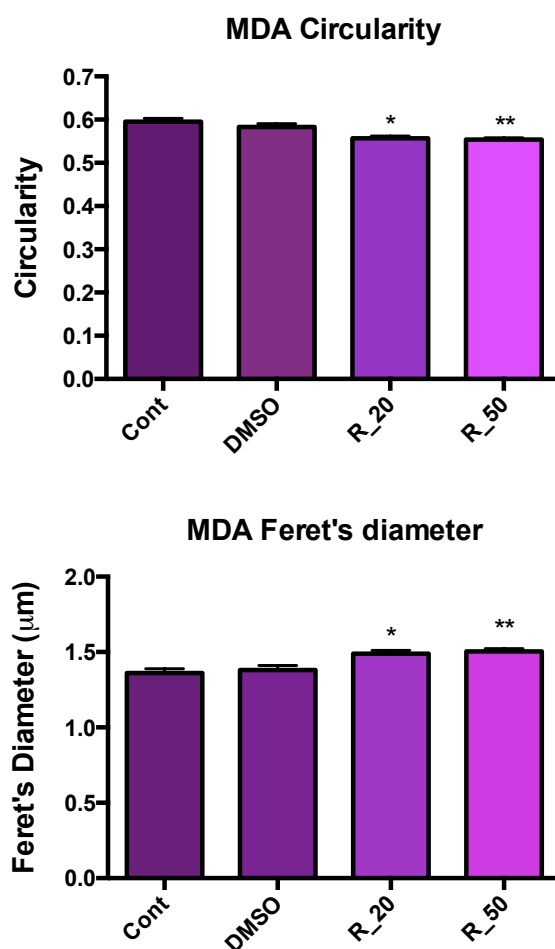


**Figure 5.19: EB1 comet analysis in Resveratrol-treated MDA-MB-231 cells.**

ImageJ was used to analyse the circularity of comets and ferret's diameter. A) EB1 circularity was reduced in 20 and 50 µM resveratrol treated MDA-MB-231 cells at 0.556 and 0.553 respectively compared to DMSO cells at 0.583. B) Feret's diameter of comets were significantly increased when cells were treated with 20 and 50 µM resveratrol at 1.48 and 1.50 µm respectively compared to DMSO cells at 1.38 µm. 75 µM resveratrol treated cells were not included in the analysis because EB1 localised along the lattice and not just as comets at MT ends). Analysis was carried out by one-way ANOVA. Error bars = SEM. No of cells measured = 10. Based on one experiment.

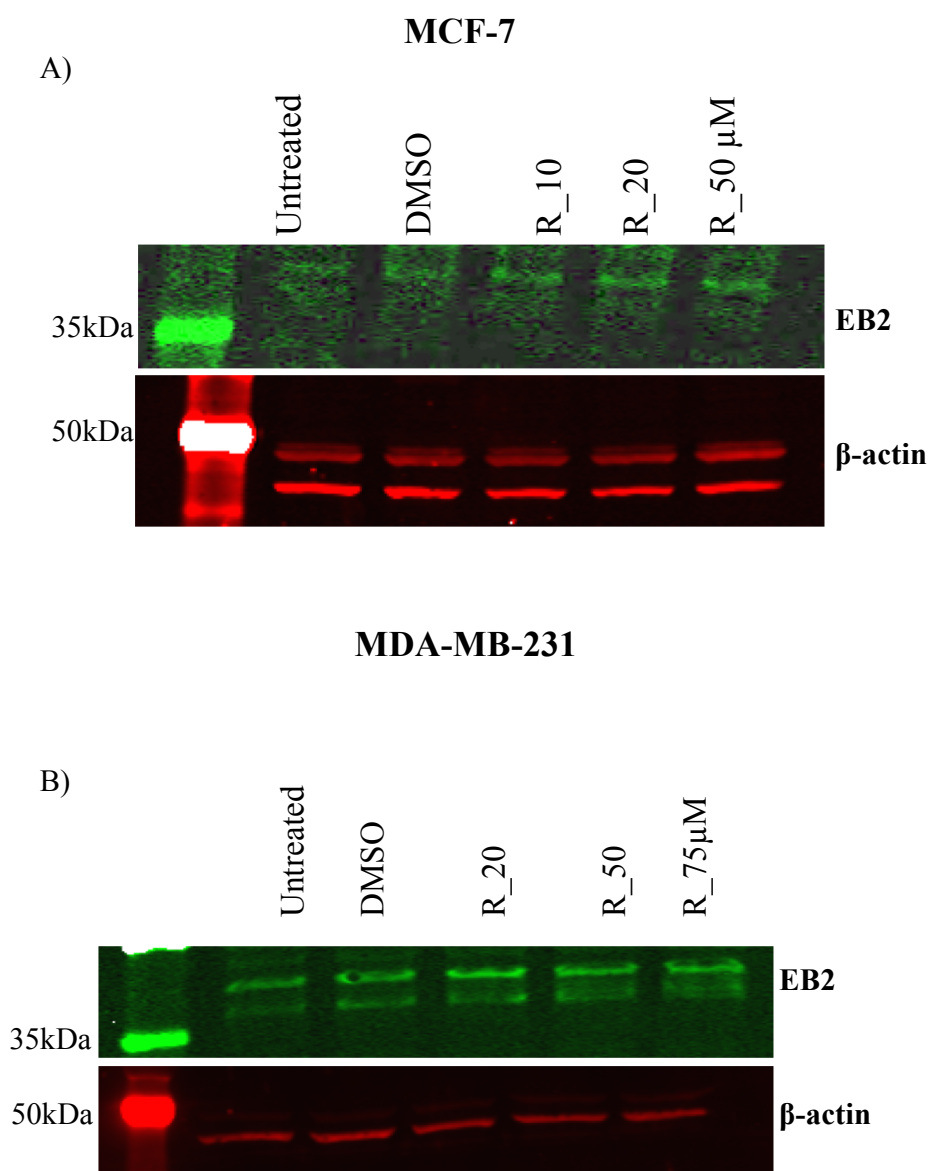


**Figure 5.20: EB2 expression in Resveratrol-treated MCF-7 and MDA-MB-231 cells.** A) A slight increase in EB2 expression is apparent in MCF-7 cells following resveratrol treatment. B) No increase in EB2 expression is evident in MDA-MB-231 cells following resveratrol treatment.  $\beta$ -actin was used as the loading control. Result is based on one experiment.

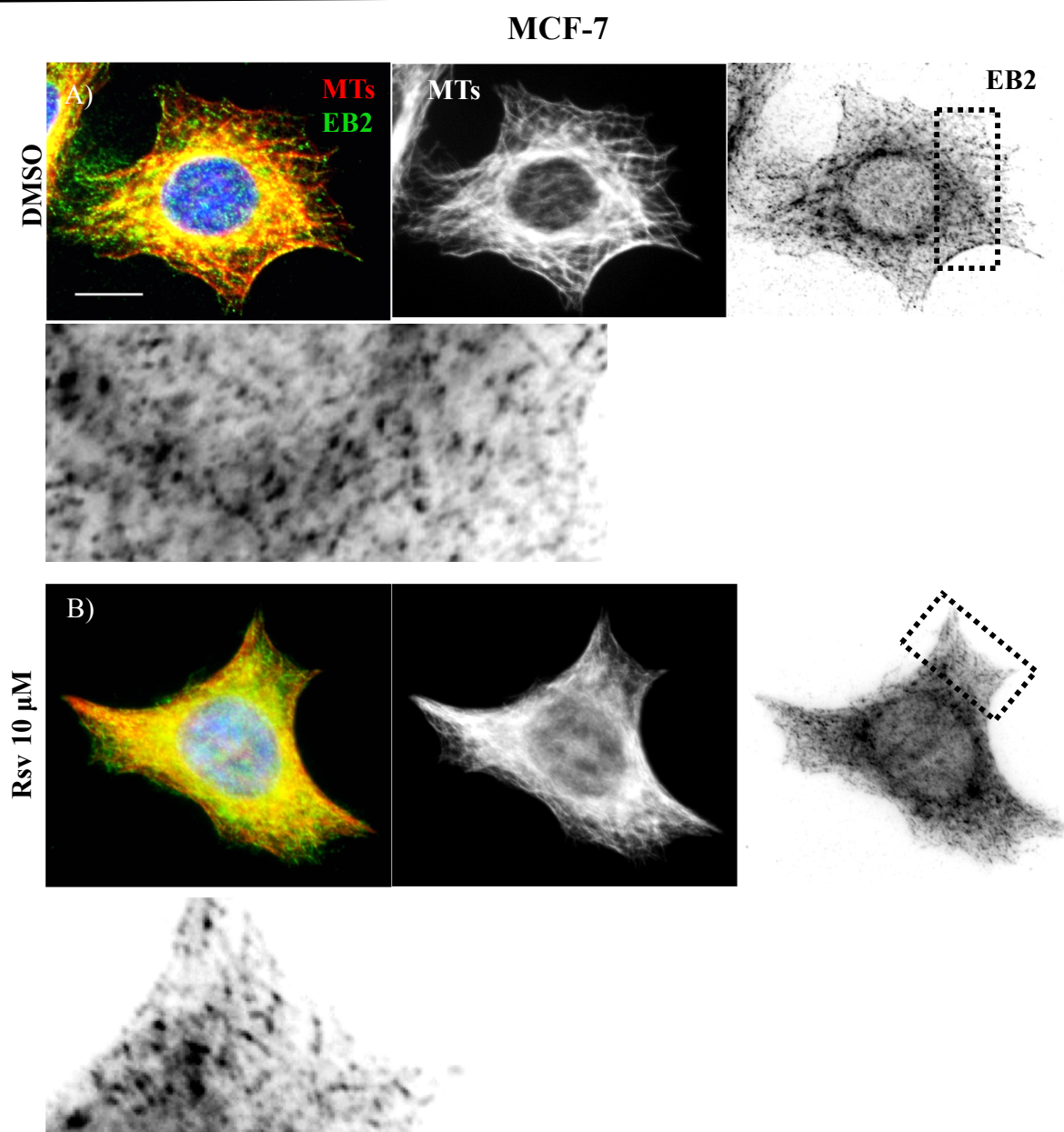


**Figure 5.21: EB2 localisation and MT organisation in resveratrol-treated MCF-7 cells.** Cells were seeded on collagen I and treated with different concentrations of resveratrol, incubated for 24 h. and immunolabelled with an anti- $\alpha$ -tubulin antibody (red, pAb, ab15246) and anti-EB2 K52 antibody (green, ab45767). Widefield fluorescent images of MCF-7 cells were obtained. A) DMSO treated cell showing EB2 localisation at MT ends (single channel image) with some at the plus-ends of MTs while others show lattice association. B) Treatment with 10  $\mu$ M resveratrol show EB2 association along the MT lattice (enlarged image). Scale bar = 10  $\mu$ m.

MCF-7

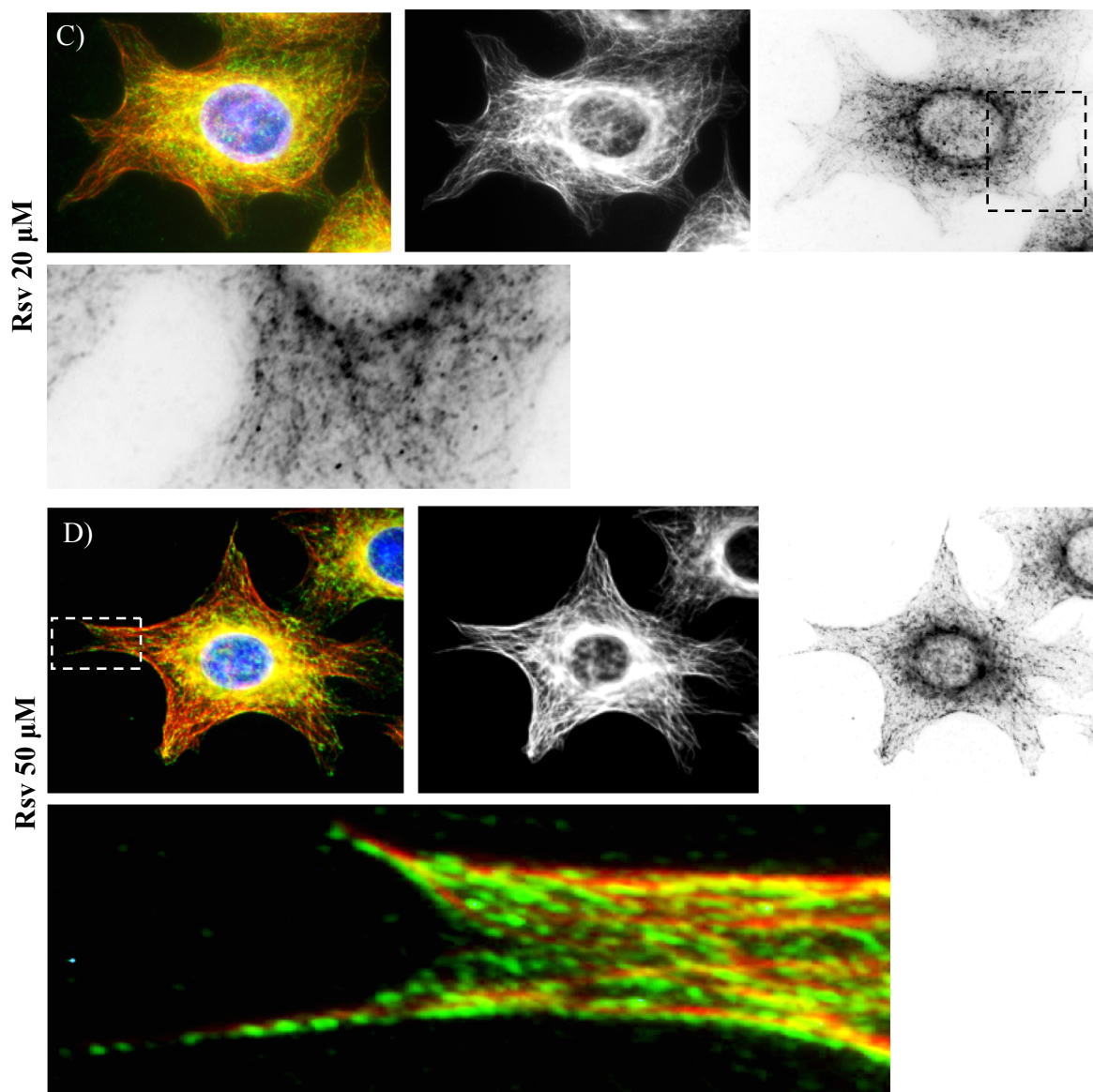


**Figure 5.22: EB2 localisation and MT organisation in Resveratrol-treated MCF-7 cells continued:** A) Treatment with 20  $\mu\text{M}$  resveratrol cell show EB2 associating with the MT lattice (enlarged image). B) 50  $\mu\text{M}$  resveratrol treated cell showing straighter and more radially organised MTs compared to the DMSO-control cell. EB2 show distinct association along the MT lattice (boxed and enlarged region). Scale bar = 10  $\mu\text{m}$ .

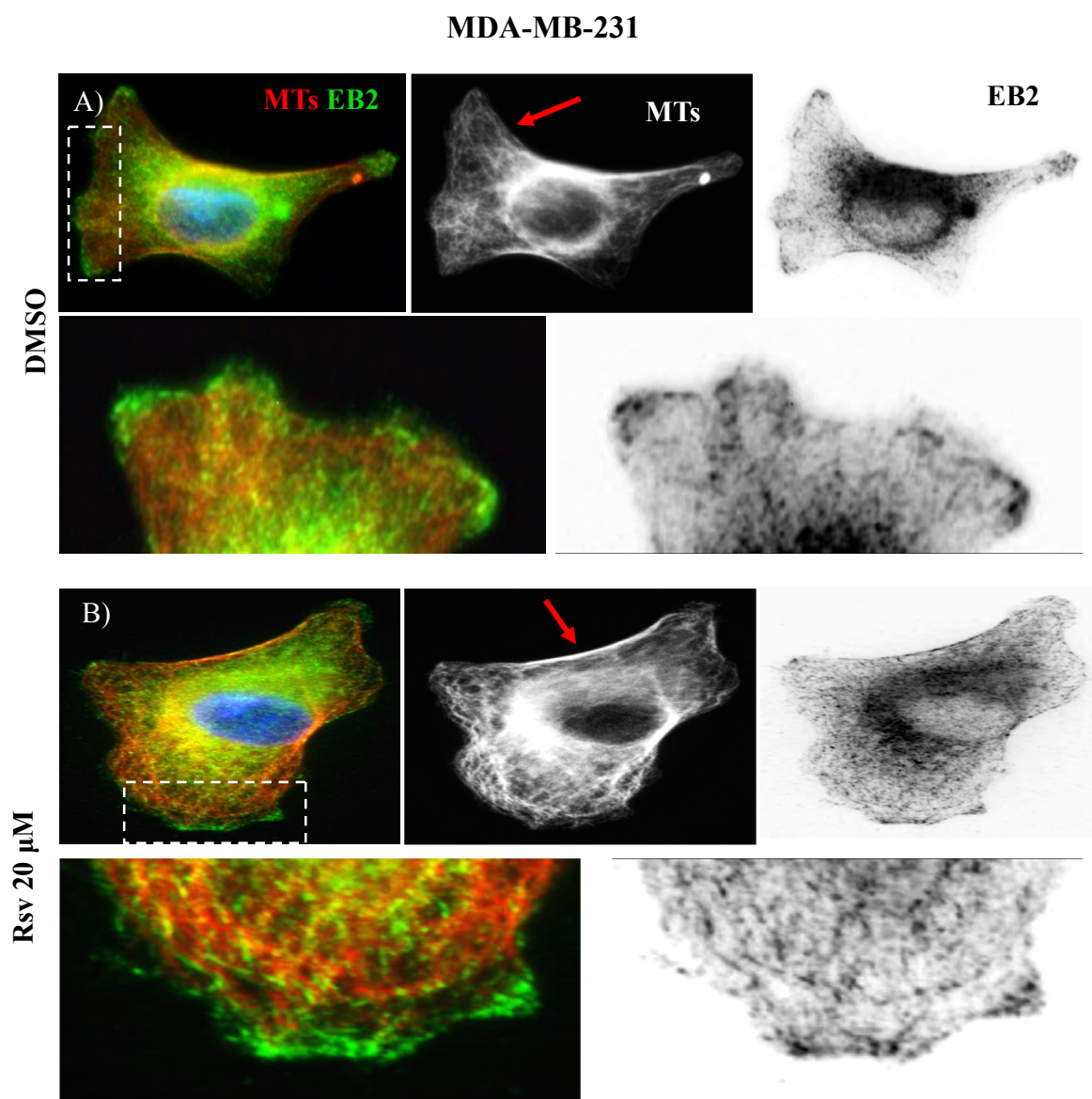


**Figure 5.23: EB2 localisation and MT organisation in resveratrol-treated MDA-MB-231 cells.** Cells were seeded on collagen I and treated with different concentrations of resveratrol, incubated for 24 h. and immunolabelled with an anti- $\alpha$ -tubulin antibody (red, pAb, ab15246) and anti-EB2 K52 antibody (green, ab45767). Widefield fluorescent images of MDA-MB-231 cells were obtained. A) DMSO-treated cell showing EB2 at the leading edge of the cell (boxed region). B) Cell treated with 20  $\mu$ M resveratrol showing some EB2 lattice association and some concentrated at the periphery (boxed region). Single channel image shows MT bundling at the side of the cell (red arrow). Scale bar = 10  $\mu$ m.

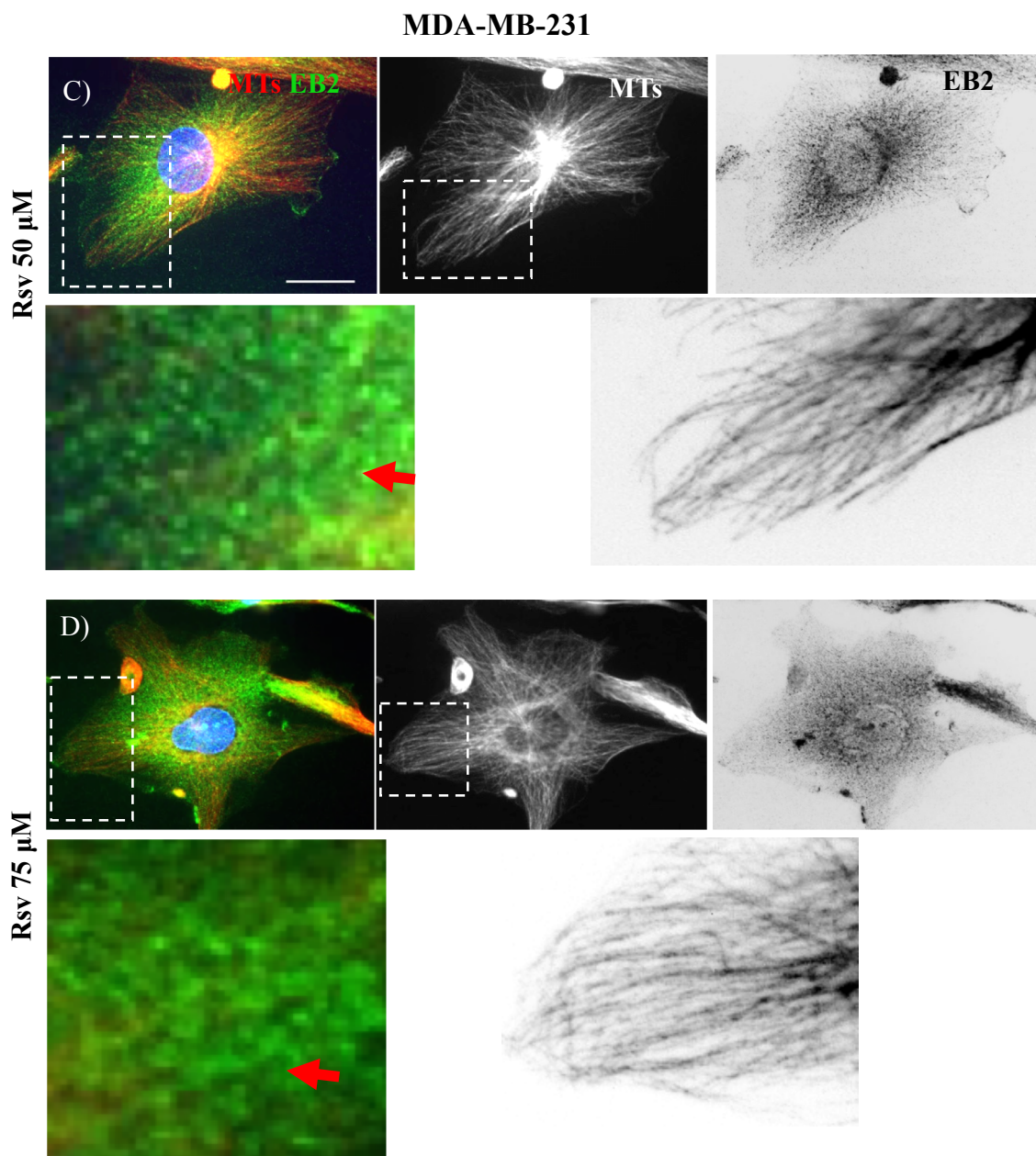


**Figure 5.24: EB2 localisation and MT organisation in Resveratrol-treated MDA-MB-231 cells continued]:** C) Treatment with 50  $\mu$ M resveratrol reveal EB2 association along the lattice but reduced EB2 at the leading edge. The MTs appear straighter with many making perpendicular cortical approaches and they are more radially organised than in DMSO treated cells. Evidence of EB2 free in the cytoplasmic is also apparent (arrow in enlarged merged regions). D). Treatment with 75  $\mu$ M resveratrol show similar results to 50  $\mu$ M. Scale bar = 10  $\mu$ m.

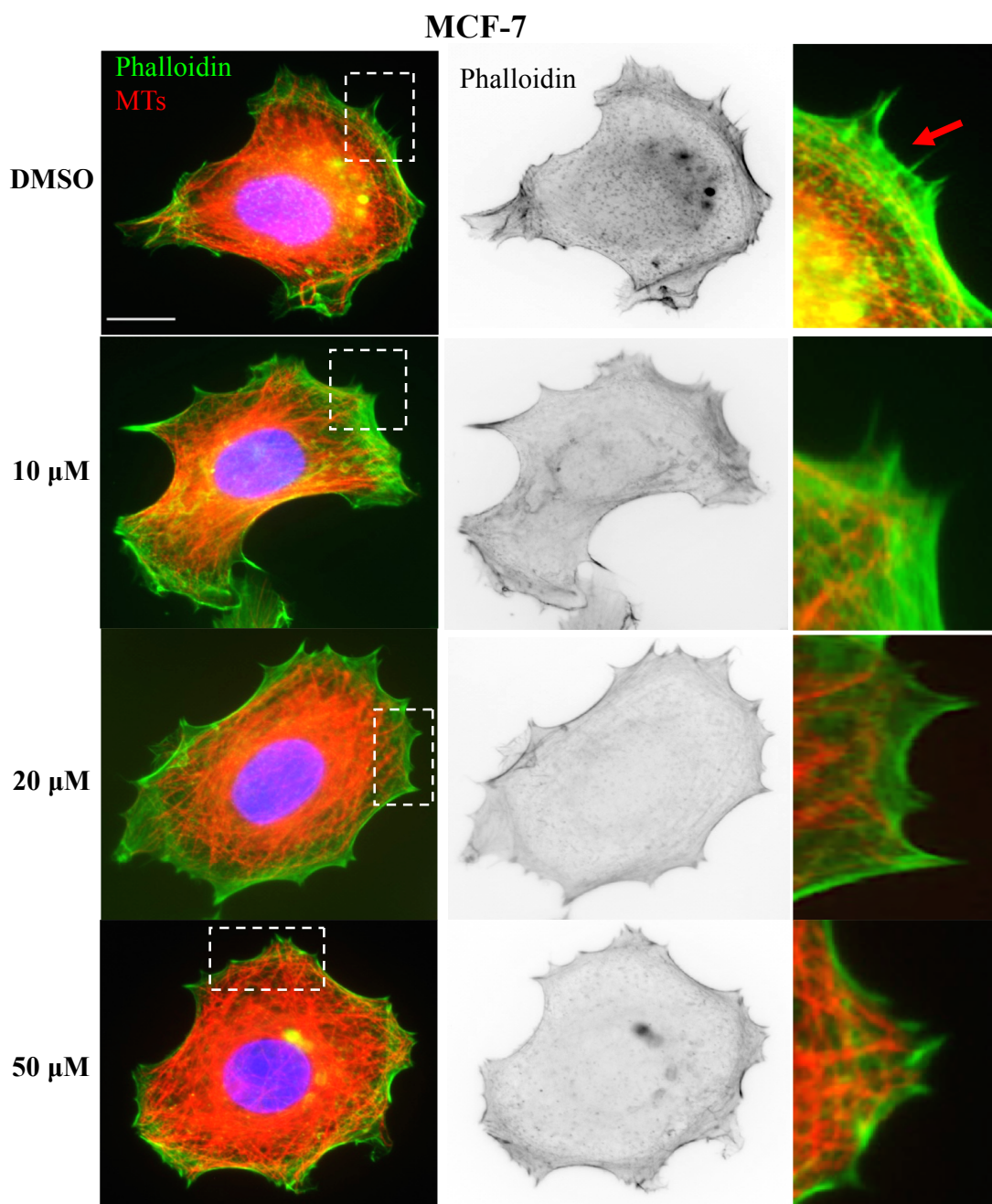


**Figure 5.25: Resveratrol leads to a reduction in actin filaments in MCF-7 cells.** Cells were seeded on collagen I and treated with different concentrations of resveratrol, incubated for 24 h. and immunolabelled with an anti- $\alpha$ -tubulin antibody (red, pAb, ab15246) and stained with phalloidin actin (green). Images were taken with the same settings on a Widefield fluorescence microscope. Merged images show actin mainly at the cell periphery. Single channel images show actin filaments localised at cell peripheries with a few more centrally located few stress fibres. However, treatment with 20 and 50  $\mu\text{M}$  resveratrol indicate a distinct reduction in actin filament especially within lamellipodia. This is highlighted in the enlarged regions. Scale bar = 10 $\mu\text{m}$ .

MDA-MB-231

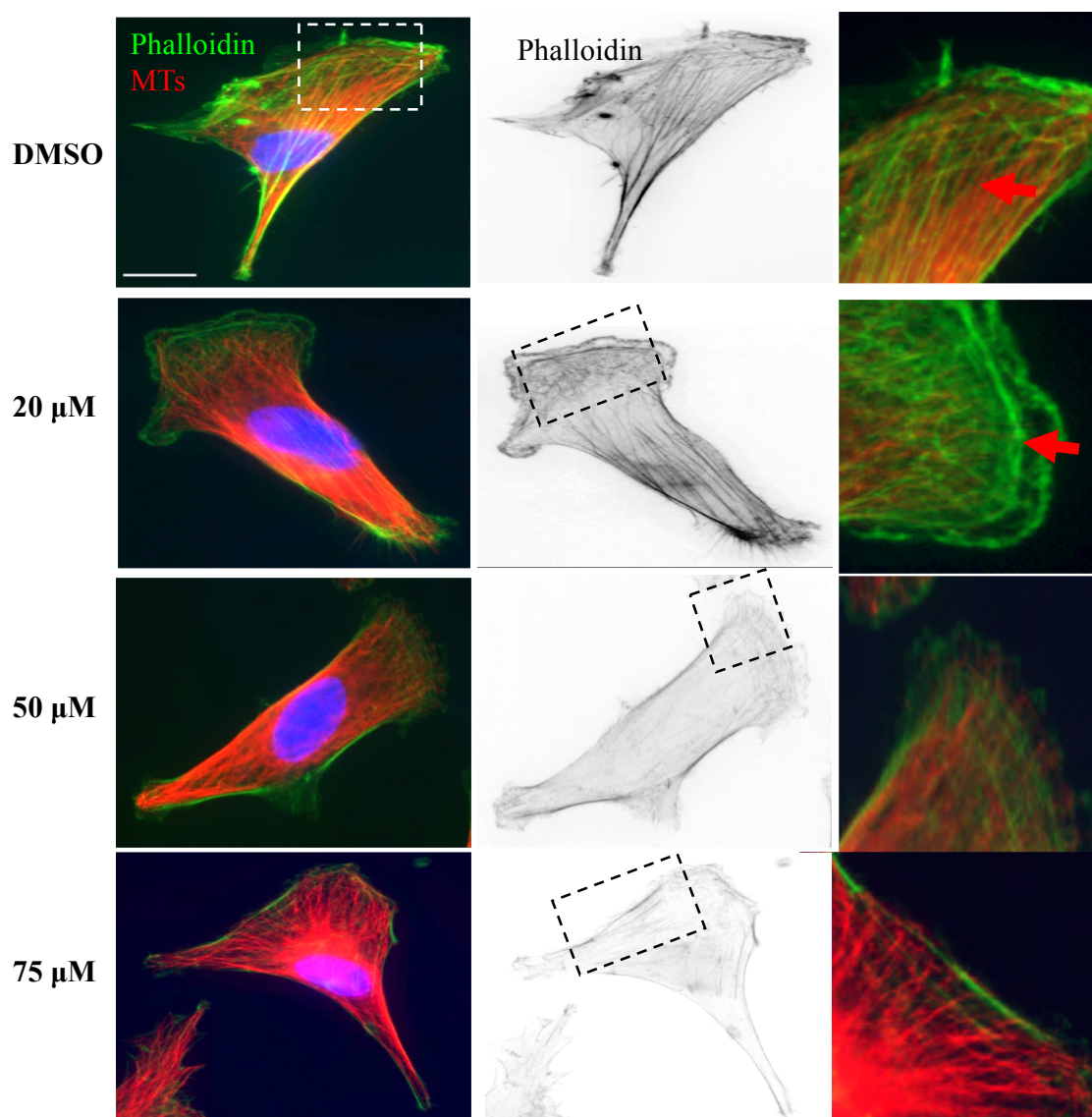


**Figure 5.26: Resveratrol caused actin filament depolymerisation in MDA-MB-231 cells.** Cells were seeded on collagen I and treated with different concentrations of resveratrol, incubated for 24 h. and immunolabelled with an anti- $\alpha$ -tubulin antibody (red, pAb, ab15246) and stained with phalloidin actin (green). Images were taken with the same settings on a Widefield fluorescence microscope. Cells treated with DMSO and 20  $\mu$ M resveratrol show actin localised to the cell periphery with some stress fibres noticed in the cell body (red arrow). Transverse arcs were also noticeable at 20  $\mu$ M (arrow in enlarged region). Cells treated with 50 and 75  $\mu$ M resveratrol have fewer actin filaments at the leading edge (enlarged regions) compared to the DMSO control. Scale bar = 10 $\mu$ m.

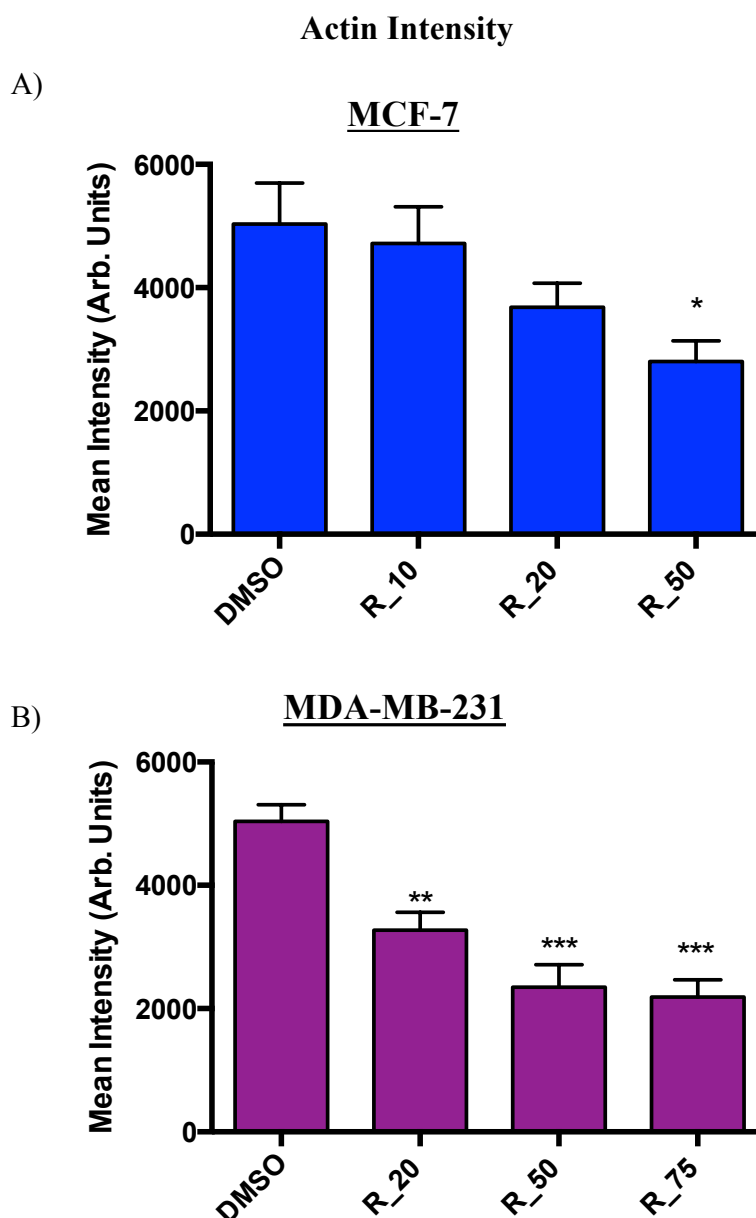


**Figure 5.27: Analysis of the actin fluorescence intensity.** Whole cell actin analysis was carried out using ImageJ. A) In MCF-7 cells, the average actin intensities in DMSO and 10, 20 and 50  $\mu$ M resveratrol treated cells were 5033, 4716, 3681 and 2800 respectively with a significant difference observed at 50 $\mu$ M. B) In MDA-MB-231 cells, the average actin intensities in DMSO and 20, 50 and 75  $\mu$ M resveratrol treated cells were 5037, 3265, 2350, 2187 respectively. A significant reduction was seen in 20, 50 and 75  $\mu$ M resveratrol treated cells. Statistical analysis was done using Tukey's one-way ANOVA. No of cells measured for each condition = 10. Error bars = SEM.

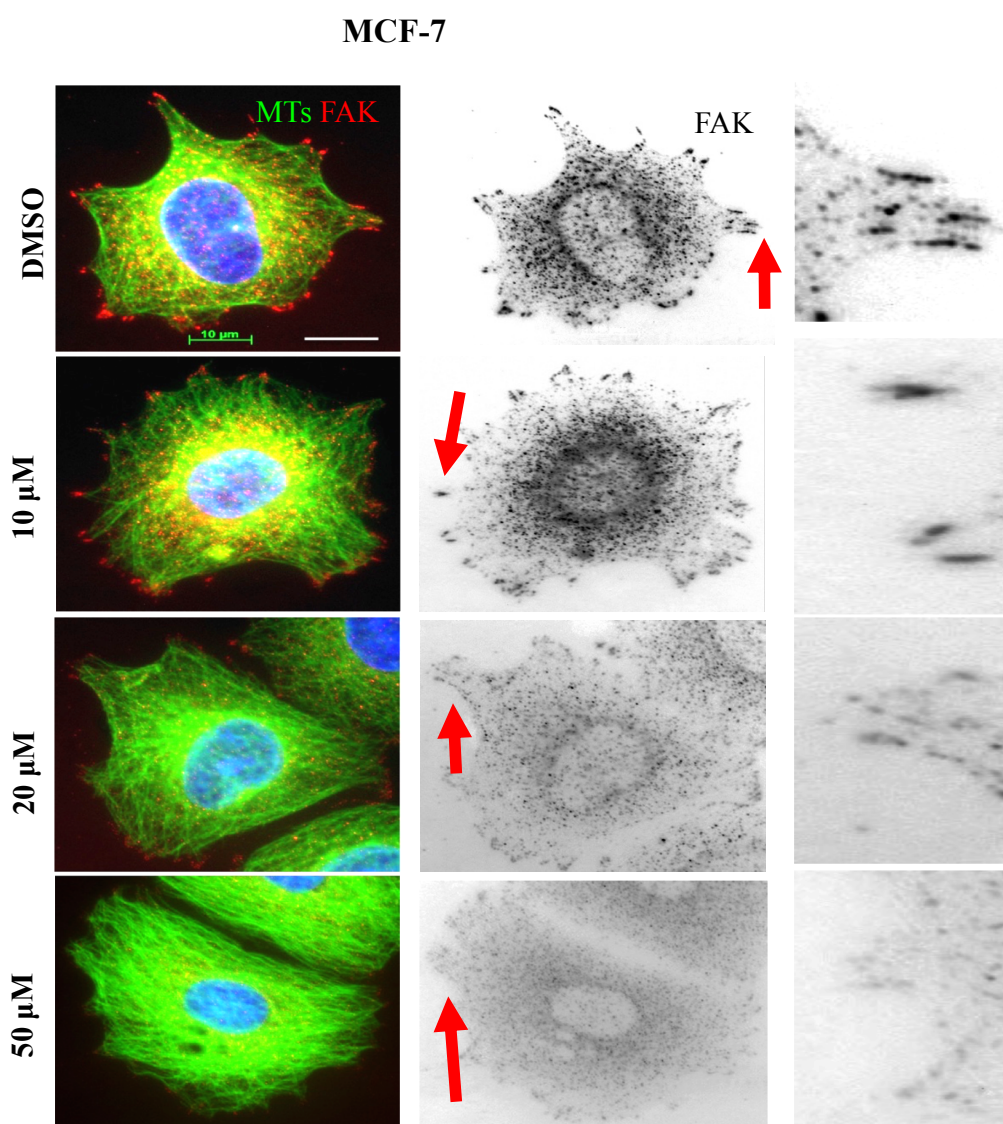


**Figure 5.28: Resveratrol cause a decrease in focal adhesions in MCF-7 cells.** Cells were seeded on collagen I, treated with different concentrations of resveratrol, incubated for 24 h and immunolabelled with an anti- $\alpha$ -tubulin antibody (green, mAb YL1/2, ab6160) and FAK (red, pAb). Images were taken on a widefield fluorescence microscope. DMSO and 10  $\mu$ M resveratrol treated cells reveal focal adhesions mainly at the cell periphery (enlarged regions) and some in the centre of the cell (inverted images). However, fewer focal adhesions are evident in cells treated with 20  $\mu$ M and 50  $\mu$ M resveratrol (inverted images and enlarged regions). Scale bar = 10 $\mu$ m.

MDA-MB-231

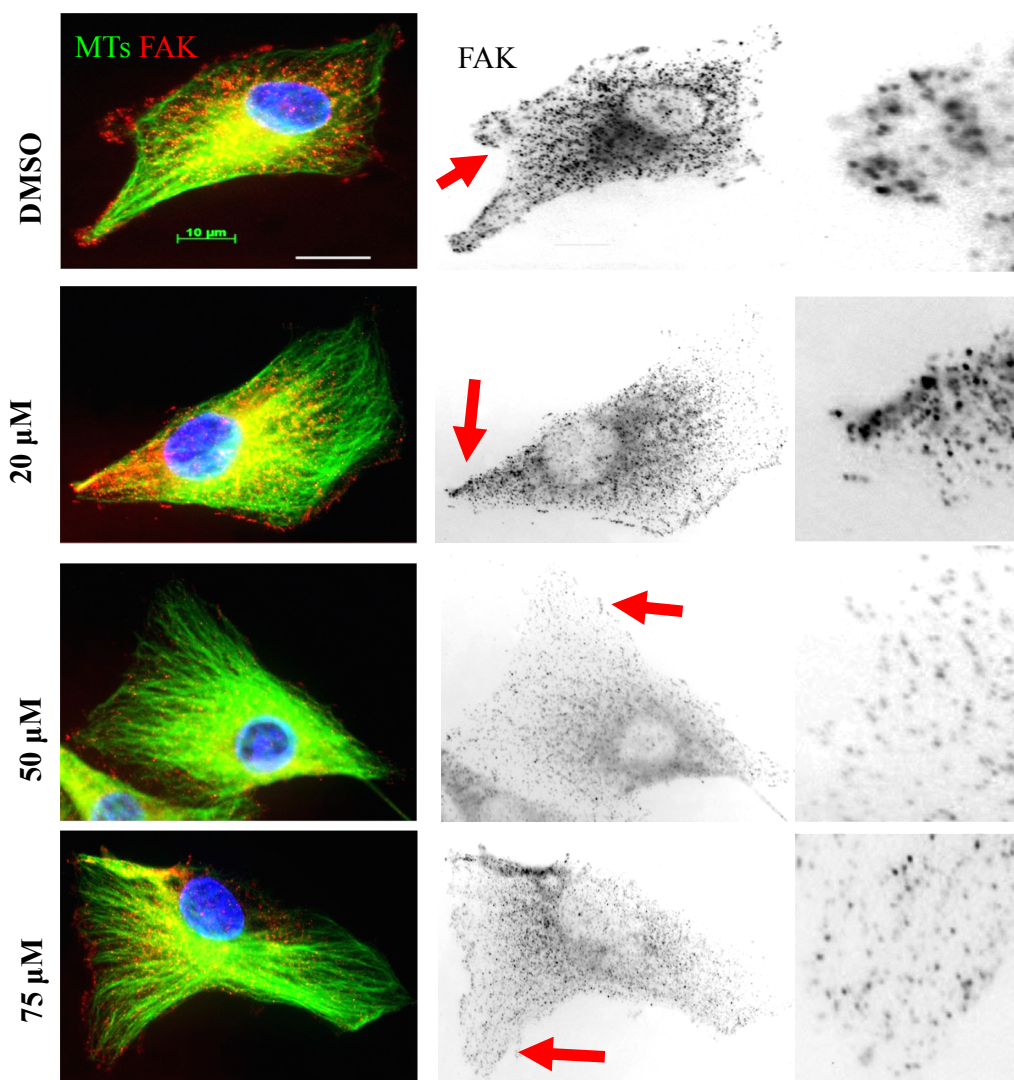


**Figure 5.29: Resveratrol cause a decrease in focal adhesions in MCF-7 cells.** Cells were seeded on collagen I, treated with different concentrations of resveratrol, incubated for 24 h and immunolabelled with an anti- $\alpha$ -tubulin antibody (green, mAb YL1/2, ab6160) and FAK (red, pAb). Images were taken on a widefield fluorescence microscope. Treatment with DMSO and 20  $\mu$ M resveratrol show cells with focal adhesions in the centre and the periphery (inverted image). However, treatment with 50  $\mu$ M and 75  $\mu$ M resveratrol result in fewer focal adhesions at the periphery and in the cell body (enlarged regions). In addition, the focal adhesions appear smaller in size compared to the DMSO control cell (enlarged regions). Scale bar = 10 $\mu$ m.

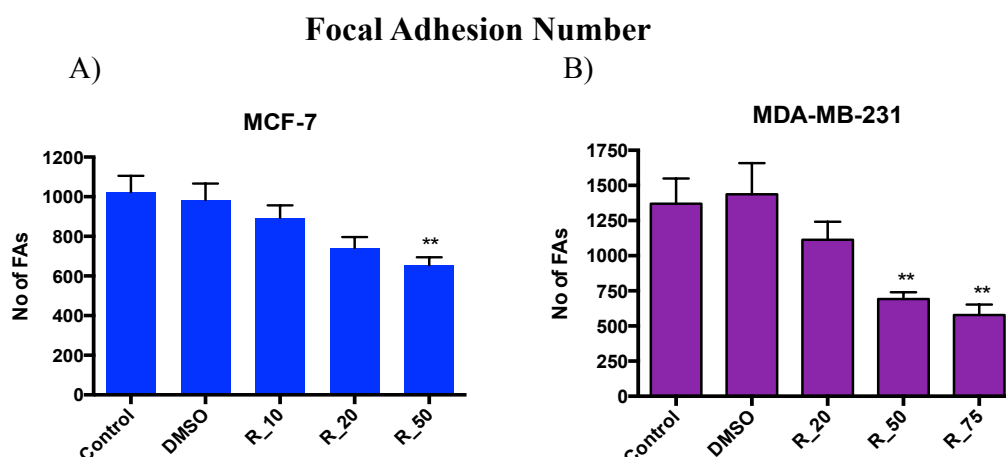


**Figure 5.30: Resveratrol led to a reduction in the number of focal adhesions breast cancer cells.** ImageJ was used for analysis. A) The average number of focal adhesions in control, DMSO and 10, 20 and 50  $\mu\text{M}$  resveratrol treated cells were 1051, 983.6, 892.4, 741.9 and 653.4 respectively. A significant reduction in focal adhesions number was observed at 50  $\mu\text{M}$  in MCF-7 cells. B) In MDA-MB-231 cells the average number of focal adhesions in control and DMSO, 20, 50 and 75  $\mu\text{M}$  resveratrol treated cells were 1370, 1437, 1114, 691.4 and 577.9 respectively. A significant reduction was seen with 50 and 75  $\mu\text{M}$  resveratrol. Statistical analysis using One-way ANOVA with Tukey's multiple comparisons test. No of cells measured = 10. Error bars = SEM. Analysis is based on one experiment.

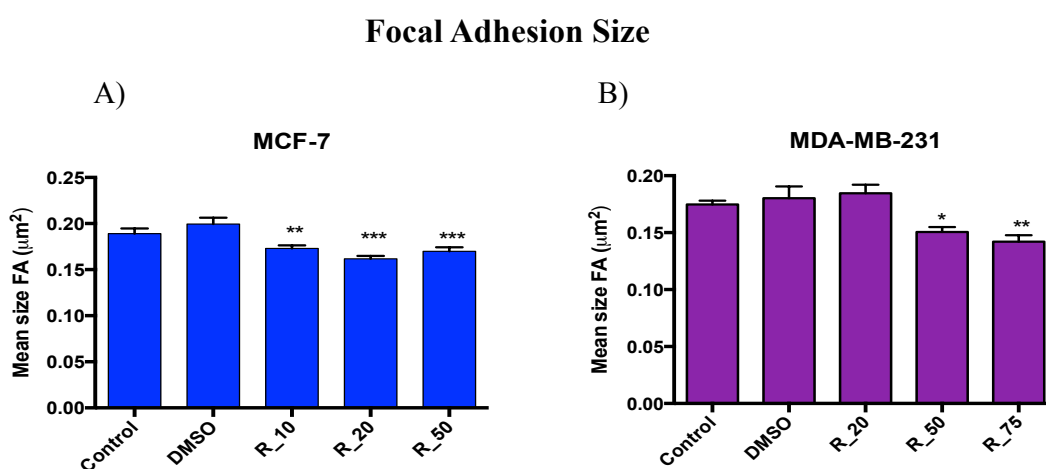


**Figure 5.31: Resveratrol led to a reduction in the size of focal adhesions breast cancer cells.** ImageJ was used for analysis. A) The mean focal adhesion size in control, DMSO and 10, 20 and 50  $\mu\text{M}$  resveratrol treated MCF7 cells were 0.189, 0.199, 0.173, 0.161 and 0.169  $\mu\text{m}^2$  respectively. A significant reduction in focal adhesions size was observed with all resveratrol concentrations compared to DMSO control. B) In MDA-MB-231 cells, the mean focal adhesion size in control, DMSO and 20, 50 and 75  $\mu\text{M}$  resveratrol treated cells were 0.174, 0.180, 0.184, 0.150 and 0.142  $\mu\text{m}^2$  respectively. A significant reduction was observed only with 50 and 75  $\mu\text{M}$  resveratrol. Statistical analysis using One-way ANOVA with Tukey's multiple comparisons test. No of cells measured = 10. Error bars = SEM. Analysis is based on one experiment.

MCF-7

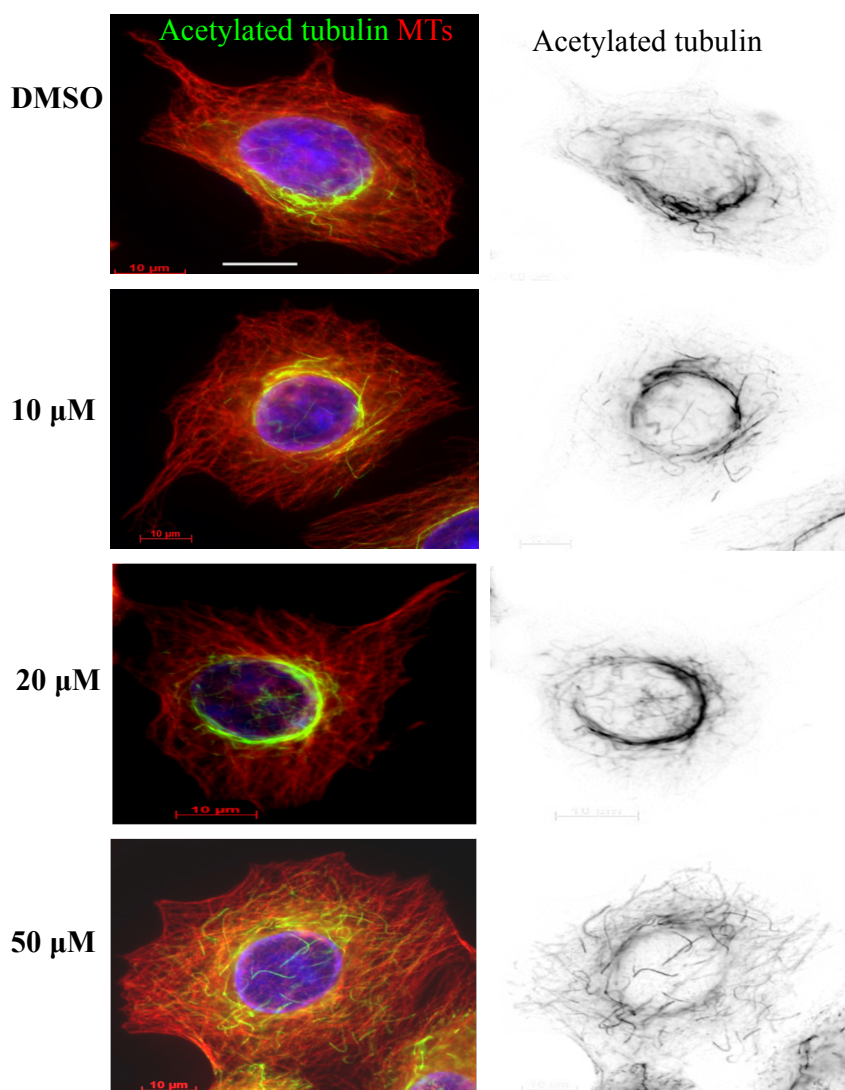


**Figure 5.32: MT acetylation in Resveratrol-treated MCF-7 cells.** Cells seeded on collagen I were treated with different concentrations of resveratrol, incubated for 24 h. and immunolabelled with an anti- $\alpha$ -tubulin antibody (red, pAb, ab15246) and anti-acetylated tubulin (green, mAb). Widefield fluorescent images were obtained of MCF-7 cells. Cells treated with DMSO or 10 and 20  $\mu\text{M}$  resveratrol show some acetylated tubulin mainly around the nucleus of the cell whereas cells treated with 50  $\mu\text{M}$  resveratrol reveal broad MT acetylation. Scale bars =10 $\mu\text{m}$ .

**MDA-MB-231**

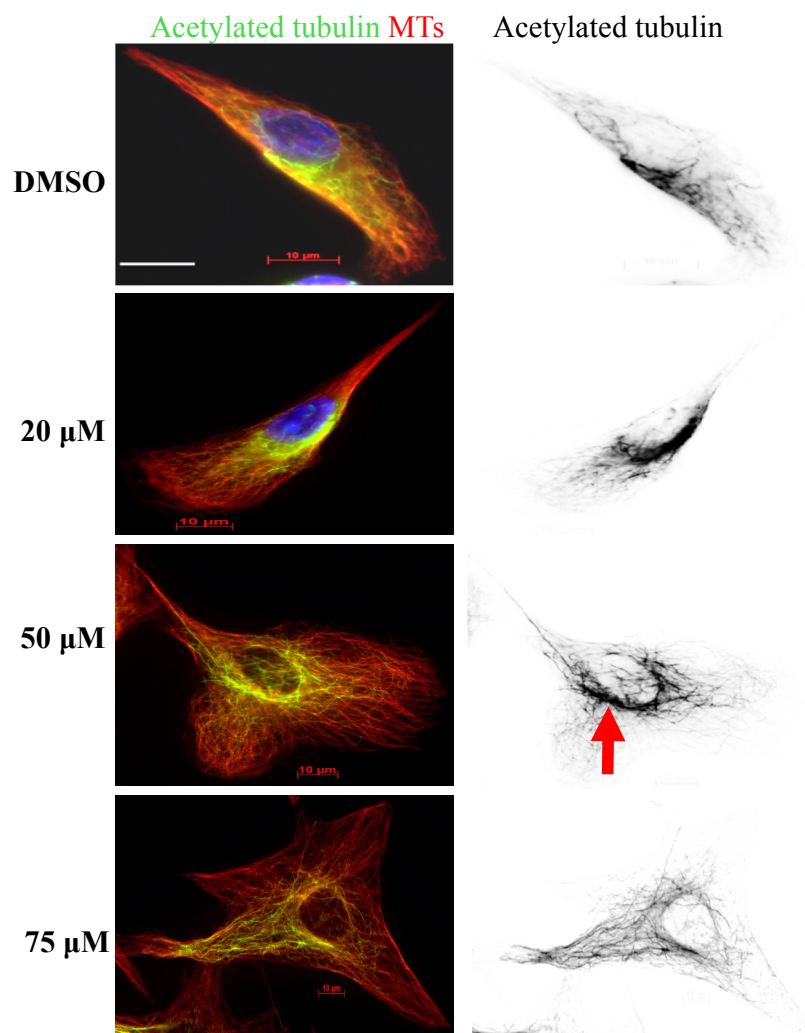


**Figure 5.33: MT acetylation in Resveratrol-treated MDA-MB-231 cells.** Cells seeded on collagen I were treated with different concentrations of resveratrol, incubated for 24 h. and immunolabelled with an anti- $\alpha$ -tubulin antibody (red, pAb, ab15246) and anti-acetylated tubulin (green, mAb). Widefield fluorescent images were obtained of MDA-MB-231 cells. Cells treated with DMSO or 20  $\mu\text{M}$  resveratrol show some acetylated tubulin mainly around the nucleus whereas cells treated with 50  $\mu\text{M}$  resveratrol reveal a broad area of acetylated tubulin that extends from the cell centre towards the periphery as well as bundles around the nucleus (red arrow). Scale bars =10 $\mu\text{m}$ .

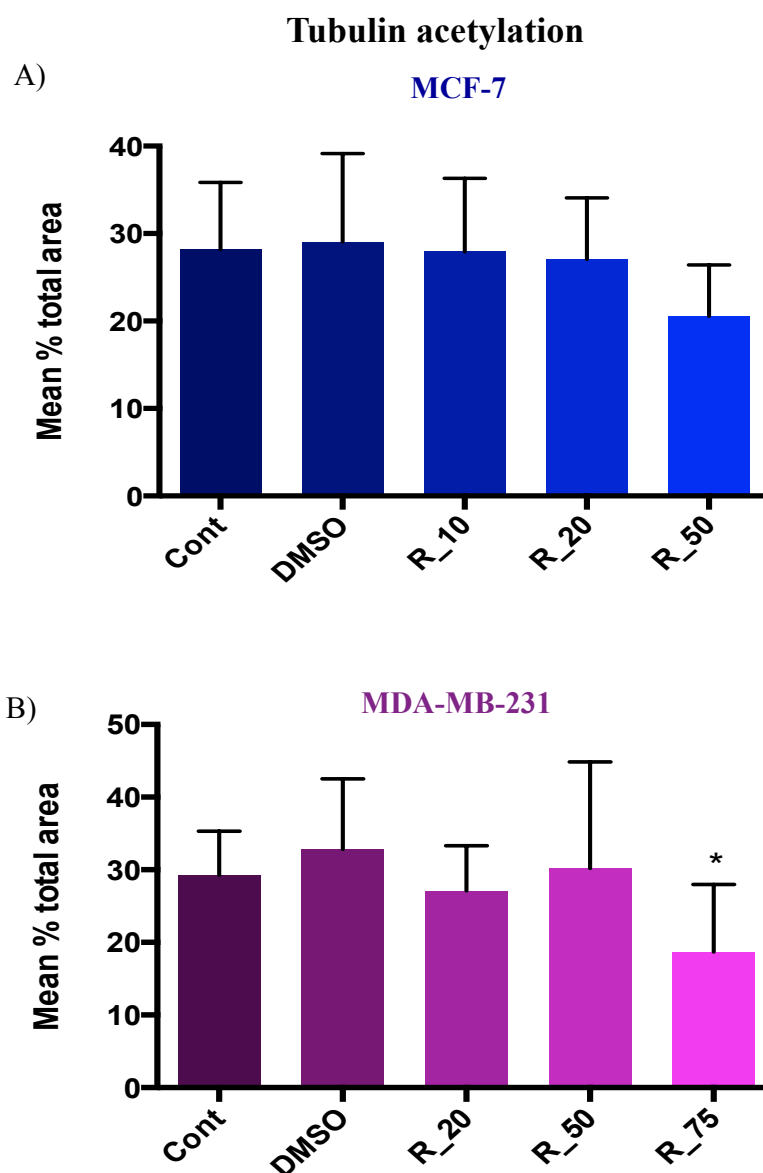


**Figure 5.34: Resveratrol decreases MT acetylation in MDA-MB-231 cells.** ImageJ was used to analyse the areas of acetylated tubulin compared to total tubulin area. A) In MCF-7 cells, there was no significant difference in the area of acetylated tubulin. B) In MDA-MB-231 cells, there was a significant decrease in area of acetylated tubulin with 75  $\mu$ M resveratrol compared to DMSO control. Statistical analysis using One-way ANOVA with Tukey's multiple comparisons test. No of cells measured = 10. Error bars = SEM. Analysis is based on one experiment.

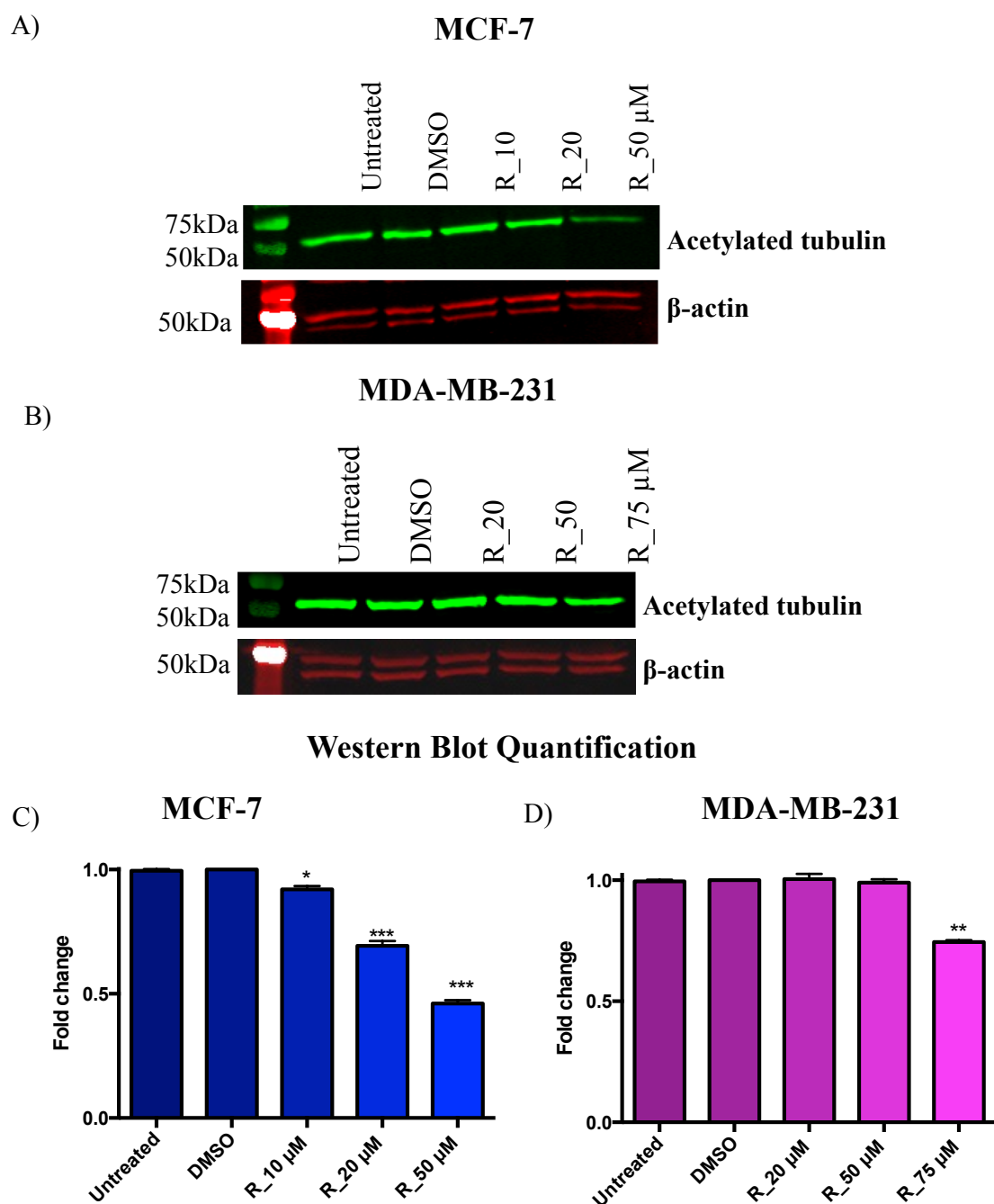


**Figure 5.35: Acetylated tubulin expression measured by Western Blotting.** A) In MCF-7 cells, the amount of acetylated tubulin expressed decreased at 50  $\mu\text{M}$  as shown by the Western blot. B) In MDA-MB-231 cells, a slight reduction in the level of acetylated tubulin is evident with 75  $\mu\text{M}$  resveratrol. C) Western blot quantification (based on two experiments) shows a significant reduction in acetylated tubulin at 10, 20 and 50  $\mu\text{M}$  resveratrol in MCF-7 cells. D) Western blot quantification shows a significant reduction in acetylated tubulin at 75  $\mu\text{M}$  resveratrol in MDA-MB-231 cells.

# **Chapter VI: Effects of EB2 Overexpression on Epithelial Lumen Formation**

## **6.1 Overview**

The objective of this chapter is to investigate effects of EB2 overexpression on epithelial lumen formation and the mechanism involved. The overall aim was to investigate the effect of EB2 overexpression in epithelial remodelling in order to enhance our knowledge on the processes leading to loss of normal tissue architecture and ultimately an invasive breast cancer state. Breast biopsies usually contain cells with abnormal architecture; some of these are benign but others may represent cancer precursors. Strategies that aim to identify precursors and early stages of cancer in breast biopsies are urgently needed. Thus, it is important to find out if EB2 is associated with cell and tissue changes commonly noticed in breast biopsies.

## **6.2 Introduction**

Epithelial cells organise into groups so that their apical surface faces a central lumen whilst the basolateral surface contacts the extracellular matrix or adjacent cells (Bryant and Mostov, 2008, Nelson, 2003). The two domains are usually separated by adherens and tight junctions. Lumen formation is a complex process that involves dynamic restructuring of the cytoskeleton, endocytic membrane transport, and the localisation of specialised polarity proteins. Although progress has been made, several questions remain unanswered. For example, how do these proteins interact to establish a single lumen site? How is the single lumen maintained and what role do associated MT proteins have? Correct lumen formation is important for maintaining the positioning of cells within a tissue and thus controlling the overall tissue architecture.

Cord hollowing lumen formation process takes advantage of one cell undergoing coordinated cell division. Here the formation of the midbody during the first cell division is the key event that initiates polarisation of two daughter cells. In the two-cell stage, polarisation begins whereby E-cadherin, occludin, and the multimeric exocyst tethering subunit, Sec10, are found along the zone for cell–cell adhesion, while Par-3 and Sec8 are enriched in the periphery. Polarity is established by forming an apical membrane domain at the interface of the two cells. The apical lumen forms between two cells and is dependent on the trafficking of cargo proteins to the apical membrane initiation site (AMIS). Fundamental to AMIS formation is a progression of

trafficking occasions that incorporate transportation of apical proteins, for example, gp135 and the Crb complex to Rab11a-positive recycling endosomes and lastly their exocytosis. Polarity proteins are involved in lumen formation. The apical Par complex consists of the proteins Par-3, Par-6 and aPKC (Goldstein and Macara, 2007). The Par complex localises to tight junctions and are therefore important in regulating apical and lateral domains (Schluter and Margolis, 2012). Par-3 restricts aPKC at the apical membrane, resulting in the binding and phosphorylation of Par-3 by aPKC. Loss of Par-3 triggers both the mislocalisation and activation of aPKC, which then triggers JAK-dependent activation of Stat3. However, activated Stat3 is known to promote breast cancer metastasis (Barbieri et al., 2010). Though, the work was carried out in mice, it certainly suggests that Par-3 may play a significant role in human breast cancer progression. The effect of Par-3 loss in human breast cancer is now known to some degree, though the mechanism discovered was different from the aPKC-JAK/Stat pathway found in mice. One of the many consequences of unregulated Par-3 protein is tumourigenesis as shown by (McCaffrey et al., 2012). Cells from murine mammary glands lacking Par-3 had a significant increase in the levels of active Tiam-1 Rac-1 under no ErbB2 induction suggesting that the phenotype observed was in fact due to the loss of Par-3 and not an effect of ErbB2. While the loss of Par-3 seems to be responsible in breast tumourigenesis, in ovarian cancer it was high Par-3 expression that proved problematic, which was associated with peritoneal metastases (Xue et al., 2013).

As the lumen matures, tight junctions form separating the apical domain from the basolateral domain (see Figure 1.8). They do this by forming a tight seal between neighbouring cells hence regulating paracellular permeability. U5 is required for targeting ZO-1 to tight junctions while the U6 motif inhibits the binding of occludin to the SH3-GUK motif in ZO-1. In 3D MDCK cysts, downregulation of ZO-1 generated cysts of normal size but with no clear lumen or organised structures (Sourisseau et al., 2006). Further work was done to understand the role of ZO-1 in lumen formation. Epithelial cells lacking ZO-1 had defects in the early stages of polarisation and consequently formed cysts with multiple lumens. The U5 domain of ZO-1 is critical due to its ability to organise cortical actin (Fanning et al., 2012). Once lumens are formed they must expand to their mature, functional size. Turgor is generated by hydrostatic pressure. Hydrostatic pressure and the activation of pumps and ion channels

is thought to account for part of luminal expansion in most tissues (Bagnat et al., 2007). Once this is established, the lumen is matured and stabilised.

Mitotic spindle orientation determines the division plane, fate and positioning of cells within a tissue and thus control the overall tissue architecture (Di Pietro et al 2016). Loss of epithelial organisation and incorrect spindle orientation are hallmarks of many types of cancers. Apico-basal polarised epithelial cells, such as those lining the acini in breast tissues orient their mitotic spindles parallel to the apical surface and thus divide in the plane of the epithelial layer. Defects in spindle positioning may lead to hyperplasia though the mechanisms responsible are not fully understood (Overeem et al 2015). MTs that anchor the spindle poles to the cell membrane during mitosis are referred to as astral MTs and these interact with several cortical proteins at the membrane, including NuMA, LGN, Gai, and dynein. The N-terminus of NuMA is used for binding to dynein while the C-terminus binds both LGN and MTs, with each of these interactions being a requirement for correct spindle orientation (Seldin et al., 2016, Kotak et al., 2012). In addition, the LGN- and MT-binding domains of NuMA overlap and stimulate mutually exclusive interactions. Regulation of NuMA occurs through phosphorylation on a serine residue by Aurora A. This promotes the release of phosphorylated NuMA from the poles and thereby allow its association with LGN (Gallini et al., 2016).

In addition to polarity markers, tight junctions and spindle orientation, cell confinement is also necessary for correct lumen formation. Cell confinement limits peripheral actin contractility by controlling cell spreading. This promotes centrosome positioning and lumen initiation after the first cell division. The study by (Rodriguez-Fraticelli et al., 2012) suggested that peripheral actin contractility, directed by myosin II activity, is increased in cells in low confinement conditions, which led to delays in early apicobasal cell polarisation and lumen initiation after the first cell division. In animal cells, the centrosome is a key organelle for cell polarity (Bornens, 2012). In division, the centrosomes organise the mitotic spindle, which should be properly oriented for normal lumen formation. It is also well established that cortical actomyosin contractility controls the position of the centrosome in different animal species during both interphase and cell division (Thery et al., 2005, Paluch et al., 2006, Fink et al., 2011). The use of blebbistatin to inhibit myosin II suppressed actin contractility. Indeed,

blebbistatin-treated cells showed a significant reduction in peripheral actin fibers, indicating that these structures are myosin II dependent.

Furthermore, blebbistatin led to a rectified centrosome orientation toward the cell junctions in low confinement conditions. Proper centrosome positioning is vital for the vesicular trafficking machinery required for normal lumen formation. Further work revealed that positioning of the centrosome at the cell junctions depends on aPKC activity independent of actin contractility. Therefore, cell confinement through myosin II and aPKC activity controls nuclear-centrosomal orientation and lumen initiation during 3D lumenogenesis (Rodriguez-Fraticelli et al., 2012). IQGAP1 is a protein not involved in centrosome positioning (Inmaculada et al., 2014). Ezrin, an actin regulator, has been implicated in centrosome positioning. After the 1<sup>st</sup> cell division in Caco2 epithelial cells, the interphase centrosome localises below the Ezrin-positive apical surface, however, the spindle rotates 90° to affect symmetric division. This rotation may involve transient Ezrin inactivation at the apical pole and the force-generating activity of lateral adherens junctions. In the absence of Merlin, Ezrin is not restricted to the apical surface, and interphase centrosomes localise near ectopic cortical Ezrin leading to spindle misorientation and the formation of multiple lumens, emphasising the dual function of Ezrin in positioning the centrosome and maintaining an apical domain during epithelial morphogenesis. Hence, Merlin functions to control the cortical distribution of Ezrin, which in turn positions the centrosome in epithelial lumen formation (Hebert et al., 2012).

The centrosome is linked with the establishment of cell polarity. A recent study discovered that the essential mother centriole distal appendage protein CEP164 was not involved in the formation of cell polarity but the subdistal appendages were vital (Hung et al., 2016). In interphase, cenexin a subdistal appendage protein, attaches ninein and centriolin to subdistal appendages (Gromley et al., 2003). Cenexin depletion did not alter the localisation of the distal appendage protein CEP164 and vice versa however, subdistal appendage proteins were disrupted. Therefore, it can be concluded that cenexin specifically targeted subdistal appendages. Depletion of cenexin did not modify the localisation of proteins needed for polarity generation for example Par-3 and E-cadherin. Although it did lead to the formation of cysts with multiple lumens suggesting a role of cenexin in centrosome positioning and spindle orientation (Hung

et al., 2016).

The overall aim was to investigate the effect of EB2 overexpression in epithelial remodelling in order to enhance our knowledge on the processes leading to loss of normal tissue architecture and ultimately an invasive breast cancer state. To investigate the potential effects of EB2 overexpression on key aspects of epithelial lumen formation, MDCKII cells were used as a cell model because they readily form cysts and are non-cancerous epithelial cells. A stable MDCKII<sup>mCherry-EB2</sup> overexpressing epithelial cell line and the control MDCKII<sup>mCherryEmpty-vector</sup> were created by Jonathan Gadsby (a former PhD student in the lab as described in Chapter II) and used to examine cell polarity and MT organisation. Polarity was assessed by embedding these cells in 3D Matrigel matrix to form cysts. Next, the localisation of key polarity and junctional proteins were monitored, especially at the early stages, in both EB2-overexpressing and control cells. Elucidating the mechanisms responsible for lumen formation and how EB2 overexpression played a role were aims of this chapter.

## **6.3 Results**

### **6.3.1 EB2 overexpression causes the formation of 3D cysts with multiple lumens**

It was important first to establish whether EB2 overexpression influence cell polarity and tissue architecture. MDCKII cells stably overexpressing EB2 (hereafter referred to as MDCKII<sup>mChEB2Hi</sup>) or empty-vector (MDCKII<sup>mChEmpty</sup>) were therefore seeded in Matrigel and cultured for 5 days before fixing in Formaldehyde/Methanol at -20°C for 30 min. Cysts were immunolabelled for  $\alpha$ -tubulin and the tight junction marker ZO-1 and optical sections taken on the confocal microscope. The findings revealed that both MDCKII<sup>mChEB2Hi</sup> and MDCKII<sup>mChEmpty</sup> cysts had maintained their apico-basal MT arrays (Fig. 6.1). At day 5, both MDCKII<sup>mChEB2Hi</sup> and MDCKII<sup>mChEmpty</sup> cysts had ZO-1 localised to the apical junctions most likely tight junctions as seen in the enlarged regions of Fig 6.2, and revealed MTs in apico-basal arrays. There appears to be no difference in the localisation pattern of ZO-1 in the MDCKII<sup>mChEB2Hi</sup> and MDCKII<sup>mChEmpty</sup> cell lines. MDCKII<sup>mChEmpty</sup> and MDCKII<sup>mChEB2Hi</sup> cells formed cysts with single lumens (Fig 6.3), however, multiple lumens were prominent in MDCKII<sup>mChEB2Hi</sup> cells as seen in Fig 6.2. Localisation of the adherens junction protein  $\beta$ -catenin in both sub-cell lines also suggested no difference (Fig 6.3). Analysis revealed that 45% of MDCKII<sup>mChEB2Hi</sup> cells formed multiple lumens compared with 20% of control cysts (Fig 6.4). Statistical analysis by two-way ANOVA showed that the number of cysts with multiple lumens observed in MDCKII<sup>mChEB2Hi</sup> were significant greater than control (MDCKII<sup>mChEmpty</sup>) cysts while the number of cysts with no lumens was not significant. Results were based on 75 cysts per condition from three independent experiments.

### **6.3.2 Localisation of polarity markers during 3D cyst formation**

EB2 overexpression clearly influence cyst formation leading to an increase in cysts with multiple lumens. Could this be due to mis-localisation of polarity proteins? This was investigated next. MDCKII cells stably expressing EB2, empty-vector or

untreated cells were seeded in Matrigel and cultured for 1-6 days before fixing in Formaldehyde/Methanol at -20°C for 30 min. Cysts were immunolabelled for  $\alpha$ -tubulin and Par-3. Par-3 is a well-known polarity marker. By day 5, as the cysts mature, Par-3 is excluded from the basal surface and is observed to localise to junctional sites that is around the apical periphery while MTs become apico-basally oriented (Fig 6.5). Par-3 continues to localise at the junctional sites by day 6 as illustrated by images in Fig 6.6. In the MDCKII<sup>mChEmpty</sup> cysts, a dividing cell depicts almost a planar spindle orientation making sure that the division plane maintains the single cell layer and normal tissue architecture. The localisation of Par-3 in the MDCKII<sup>mChEB2Hi</sup> cyst was similar to those observed in the MDCKII<sup>mChEmpty</sup> cyst (Fig 6.6). Finally, EB2 overexpression does not prevent the formation of apico-basal MTs (seen in Fig 6.2, 6.3, 6.5 & 6.6).

Immunofluorescent staining for the tight junction marker ZO-1 at day 1 revealed localisation to the centre at the two-cell stage (Fig 6.7). By day 2, cells have gone through another round of division and the localisation of ZO-1 becomes stronger in the centre, known as the 'pre-apical patch' (Fig 6.8). Day 3 cysts revealed that the lumen is starting to take shape, which is supported by the ring appearance of ZO-1 suggesting localisation at apical junctions (Fig 6.9). By day 4, slightly oblique optical section images in both MDCKII<sup>mChEB2Hi</sup> and MDCKII<sup>mChEmpty</sup> cysts show an intense ZO-1 staining at the junctional periphery (Fig 6.10). By day 5 and 6, ZO-1 is continually observed to localise to the junctions of the lumen with exclusion from the basal region. Some MDCKII<sup>mChEB2Hi</sup> cells formed cysts with four lumens. More ZO-1 localisation was revealed in the basal region of MDCKII<sup>mChEB2Hi</sup> cyst when compared with the MDCKII<sup>mChEmpty</sup> cyst, which is based on 10 cysts (Fig 6.12). Though, the MT array in MDCKII<sup>mChEB2Hi</sup> cysts is like that of the control (Fig 6.11 and 6.12).

### **6.3.3 EB2 overexpression impairs centrosome positioning in MDCKII<sup>mChEB2Hi</sup> cells**

Centrosome positioning to specific sites near the plasma membrane is regarded as fundamental for protein trafficking systems, for example, the delivery of secretory granules for axon arrangement during the progression of neuronal polarity (Stinchcombe et al., 2006); and is important for repositioning the vesicular trafficking

machinery toward the cell junctions during normal lumen formation (Rodriguez-Fraticelli et al., 2012). MDCKII<sup>mChEmpty</sup> and MDCKII<sup>mChEB2Hi</sup> cells were seeded in Matrigel for 20 h before fixing and immunolabelling with  $\gamma$ -tubulin and Par-3 and analysing cells at the two-cell stage for centrosome positioning. Images were then taken on the confocal microscope. In MDCKII<sup>mChEmpty</sup> cells, the centrosome was typically positioned towards the cell-cell junction at the AMIS and where the future lumen will form (Fig 6.13A). However, in MDCKII<sup>mChEB2Hi</sup> cells, centrosomes on one side is further away from the midbody compared to centrosomes on the other side of the midbody (Fig 6.13A). For centrosome positioning, we analysed the distance between the two centrosomes and the apical surface (AMIS) (Par-3 staining) to determine the position of the centrosome. Fifteen cells from each sub-clone of one experiment were analysed using ImageJ by measuring the centre of the two cells, marking the two centrosomes before measuring the distance between the centrosome and the AMIS. The results for this section are only preliminary so further experiments will be needed to confirm this. Analysis using unpaired t-test revealed a significant difference in the distance between the two centrosomes and the AMIS in the MDCKII<sup>mChEB2Hi</sup> when compared with MDCKII<sup>mChEmpty</sup> cells (Fig 6.13B). As aforementioned, proper centrosome positioning is vital for the vesicular trafficking machinery required for normal lumen formation. Work by Rodriguez-Fraticelli (2012) has shown that positioning of the centrosome at the cell junctions depends on aPKC activity, which is independent of actin contractility. Therefore, centrosome mispositioning possibly affects the transport of proteins required for the subsequent stages of lumen formation.

### **6.3.4 EB2 overexpression alters spindle orientation in MDCKII cells**

Spindle orientation is a key process during epithelial lumen formation and misorientation has been linked to cancer (Noatynska et al., 2012, Hung et al., 2016). So, to measure the effect EB2-overexpression had on spindle orientation, it was necessary to have an increased mitotic number per experiment. Therefore, thymidine, was chosen for synchronisation so that more cells will be in mitosis and the same phase after the drug is washed out. Thymidine arrests cells at the G1/S border preventing progression beyond S phase. To increase synchronisation, cells were blocked twice.

This contained an initial block of 17 h, followed by a wash out and a 9 h passage through the cell cycle then a second 17 h treatment followed by a final release.

To assess the optimal time point for fixation and spindle analysis after the second release, monolayer cells were fixed at several time points after the second release and then immunolabelled for  $\alpha$ -tubulin (black and white). Widefield fluorescence microscopy images revealed a few cells undergoing mitosis at 0, 1 and 3 h post treatment wash out in untreated and thymidine-treated cells (Fig 6.14). From the next set of time points, 6 & 9 h, a proportional increase in the number of cells in mitosis were observed in the thymidine-treated cells when compared to the untreated (Fig 6.15A). ImageJ was utilised to quantify any changes seen in the images by counting all the cells per frame and deducing the number of mitotic cells then taking a percentage of those for all the time points. Following this, a graph was produced which showed that there was a proportional increase in mitotic cells as the timepoint increased when cells were treated with thymidine as opposed to the untreated control cells (Fig 6.15B). Thus, 9 h was chosen as the optimal time point for fixation.

MDCKII cells were seeded on a thin layer of Matrigel and allowed to adhere for 24 h prior to double-blocking with thymidine and then immunolabelling for  $\alpha$ -tubulin and  $\gamma$ -tubulin. Matrigel was used to generate partially polarised cells. Confocal microscopy optical sections through the entire spindle were taken at 0.2  $\mu\text{m}$  intervals. Optical sections were obtained of bipolar spindles with astral MTs radiating out from the spindle pole towards the cell cortex in untreated, MDCKII<sup>mChEmpty</sup> and MDCKII<sup>mChEB2Hi</sup> cells (Fig 6.16B-D, Movie S20-S22). The orthogonal views (generated in ImageJ) are also illustrated, which show the difference in height and angle between the two spindle poles in MDCKII<sup>mChEmpty</sup> and MDCKII<sup>mChEB2Hi</sup> cells. An increased number of multiple spindles were observed in MDCKII<sup>mChEB2Hi</sup> cells but these are described in chapter 7. Spindle orientation angle in respect to the substratum in these cells were calculated by measuring the distance (D) between the centre of each spindle pole and the angle (A) of the division plane (Fig 6.16E). Volocity software was used for obtaining those values. Result illustrates a significant increase in the height of the spindle poles of MDCKII<sup>mChEB2Hi</sup> compared to MDCKII<sup>mChEmpty</sup> cells (Fig 6.17A). Bipolar spindle orientation analysis revealed a significant increase in the spindle angle in MDCKII<sup>mChEB2Hi</sup> cells (5°) compared to MDCKII<sup>mChEmpty</sup> cells (2.5°) (Fig 6.17B).

Further analysis illustrated a significant decrease in the percentage of cells with spindle angles  $<5^\circ$  in EB2 overexpressing compared to control (MDCKII<sup>mChEmpty</sup>) cells while there was a significant increase in MDCKII<sup>mChEB2Hi</sup> cells with spindle angles  $>5^\circ$  (Fig 6.17C). Forty cells were analysed per condition and statistical significance was assessed by one-way ANOVA with Tukey's multiple comparison test based on one experiment.

### **6.3.5 EB2-overexpressing cells exhibit defects in astral MT cortical contact**

Spindle orientation is controlled by astral MTs emanating from the spindle poles and captured by cortical complexes (Wittmann et al., 2001). Mechanisms that regulate astral MT nucleation, anchoring, dynamics and interactions with the cortex thus control spindle orientation and the plane of division (Di Pietro et al 2016; Seldin and Macara 2017). Our data suggest that EB2 overexpression perturbs the normal spindle angle and this could be due to defects in the astral MTs. The number of astral MTs and their contact with the cortex was therefore investigated.

To assess whether EB2 overexpression influenced astral MTs, cells were seeded on a thin-layer of Matrigel (for partial polarisation) and allowed to adhere for 24 h. Thymidine was used in cell synchronisation prior to immunolabelling with  $\alpha$ -tubulin and staining for actin with phalloidin to mark the cell cortex. Confocal optical sections were taken at 0.2  $\mu\text{m}$  intervals. Z-stacks taken show a normal bipolar spindle formation in the untreated and MDCKII<sup>mChEmpty</sup> with astral MTs radiating out from the spindle pole towards the cell cortex (Fig 6.18A, Movie S23 and S24). While some MDCKII<sup>mChEB2Hi</sup> cells also showed bipolar spindle formation with the rest exhibiting multipolar spindles (described in Chapter 7). Analysis revealed that there were fewer astral MTs making contact with the cortex in the MDCKII<sup>mChEB2Hi</sup> cells compared to MDCKII<sup>mChEmpty</sup> control cells (Movie S25). However, actin localisation seems unaffected. ImageJ was used to analyse astral MT length based on twenty cells per condition from one experiment. A significant decrease in the length of astral MTs emanating from the spindle pole was evident in EB2 overexpressing cells. The average astral MT length in MDCKII<sup>mChEB2Hi</sup> cells was 4  $\mu\text{m}$  compared to 8  $\mu\text{m}$  for control thus a 50% reduction (Fig 6.18B), a significant decrease in the number of cells with more

than 5 astral MTs reaching the cortex was observed in MDCKII<sup>mChEB2Hi</sup> cells compared to the MDCKII<sup>mChEmpty</sup> cells (Fig 6.18C).

These defects in astral MTs, may suggest that proteins responsible for the capture of astral MTs at the cortex are functionally impaired. Localisation of the key cortical protein NuMA was therefore studied. NuMA is known to interact with MTs and play a role in the formation and organisation of the mitotic spindle during mitosis. Cells immunolabelled for NuMA and  $\alpha$ -tubulin were taken on the widefield microscope using the same exposure time to allow comparison. Cells were analysed and the cortical fluorescence intensity of NuMA was assessed. The images revealed that NuMA localised to the cortex in both MDCKII<sup>mChEB2Hi</sup> and MDCKII<sup>mChEmpty</sup> cells (Fig 6.19A). ImageJ was used to analyse the cortical fluorescence intensity of NuMA by using two boxes of sizes 25  $\mu$ m by 25  $\mu$ m. After image processing by subtracting the background and adjusting the brightness, each 25  $\mu$ m box was placed at the cell cortex directly opposite the spindle pole and then intensity measured (Fig 6.19B). Twenty cells per condition were analysed. The graph obtained showed no significant difference in the cortical intensity in both MDCKII<sup>mChEB2Hi</sup> and MDCKII<sup>mChEmpty</sup> cells (Fig 6.19C).

### **6.3.6 EB2 overexpression leads to increased GFP-CLIP-170 comet speed**

Taxol stabilises MTs and addition of taxol to MDCKII<sup>mChEB2Hi</sup> cells seemed to rescue the spindle angle restoring it to that of the control cells. This suggests that EB2 overexpression may make MTs less stable and more dynamic and this was therefore pursued next.

To evaluate whether EB2-overexpression influenced microtubule dynamics, GFP-CLIP-170 comet dynamics were analysed in MDCKII<sup>mChEB2Hi</sup> and MDCKII<sup>mChEmpty</sup> cells. Both cell lines were grown as a monolayer in 3 cm glass-bottomed dishes at 75,000 cells per dish and left to adhere overnight. Cells were then transfected with 2  $\mu$ g GFP-CLIP-170 construct for 6 h before replacing the medium

with the normal medium. Cells expressing GFP-CLIP-170 were imaged using live time-lapse fluorescence microscopy for three minutes, with frame acquisition every three seconds. GFP-CLIP-170 comets were acquired using the U-Track automated tracking software, formerly packaged as plusTipTracker (Applegate et al., 2011). Post-tracking analyses were conducted on ten cells from one experiment using the MATLAB software. It is worth mentioning that shrinking or stable MTs cannot be classified using this method.

U-Track analysis of GFP-CLIP-170 comets were carried out in MDCKII<sup>mChEmpty</sup> and MDCKII<sup>mChEB2Hi</sup> cells over a three-minute period (Movie S26 and S27). GFP-CLIP-170 tracking suggested that EB2 overexpression may affect MT dynamics. Analysis of GFP-CLIP-170 comets in MDCKII<sup>mChEB2Hi</sup> cells revealed a significant increase in the mean comet's growth speed compared to MDCKII<sup>mChEmpty</sup> cells. The increase in growing speed in MDCKII<sup>mChEB2Hi</sup> cells might suggest an increased ability for the MTs in these cells to grow and possibly have an effect on pausing and shrinkage. This needs to be done as a further study in order to fully establish that EB2 overexpression increases MT dynamics. The MDCKII<sup>mChEmpty</sup> cells had an average CLIP-170 comet speed of 7.5  $\mu\text{m min}^{-1}$  while MDCKII<sup>mChEB2Hi</sup> cells revealed a speed of 8.5  $\mu\text{m min}^{-1}$  (Fig 6.20A). However, analysis of the growth lifetime of MTs was not statistically significant in the MDCKII<sup>mChEB2Hi</sup> cells when compared to the MDCKII<sup>mChEmpty</sup> cells (Fig 6.20B). Similarly, MDCKII<sup>mChEB2Hi</sup> cells showed no significant difference in mean growth length and the overall percentage MTs spent in the growth phase compared to MDCKII<sup>mChEmpty</sup> cells (Fig 6.21A & B).

Western blots were carried out to establish the level of MT stability in all three sub-cell lines by checking the levels of acetylated and detyrosinated tubulin. This was to support the results from the MT dynamics experiments. Western blot analysis (from two independent experiments) suggested an increase in the level of acetylated and detyrosinated tubulin expression in the MDCKII<sup>mChEB2Hi</sup> cells compared with the MDCKII<sup>mChEmpty</sup> cells (Figure 6.22A). This marked increase in acetylated and detyrosinated tubulin suggests an increase in MT stability. This theory was tested in both cell lines using cold treatment. Incubation of cells on ice causes MT depolymerisation with MTs remaining polymerised being resistant to cold and therefore stable. The incubation of MDCKII<sup>mChEmpty</sup> cells on ice for 10 min revealed that all but

very few MTs had depolymerised. Similarly, MDCKII<sup>mChEB2Hi</sup> cells also revealed a marked reduction in MTs (Figure 6.22B). These preliminary cold treatment experiments suggest that the MTs in EB2 overexpressing cells are not more stable than those of the control cells.

### **6.3.7 Spindle misorientation in MDCKII<sup>mChEB2Hi</sup> cells could be rescued by Taxol**

Following on from the results in section 6.3.5 and 6.3.6 that showed a decrease in MT length and the number of MTs making cortical contact and an increased GFP CLIP-170 speed in MDCKII<sup>mChEB2Hi</sup> cells respectively; it was speculated that maybe the MTs in the MDCKII<sup>mChEB2Hi</sup> cells were not stable enough to maintain cortical contact therefore, we decided to treat these cells with a MT-stabilising drug, Taxol, and monitor the effects on spindle orientation.

Taxol, a taxane, is well-known anti-cancer chemotherapy drug. It works by stabilising the MT lattice and stimulating polymerisation. This prevents the rapid MT dynamics required for rearrangement into mitotic spindles thus inhibiting cell division and promoting cell death. Bearing in mind that MT bundling was induced in ARPE-19 cells at 2  $\mu$ M Taxol (Goldspink et al., 2013), we needed to induce enough MT dynamics if it was to correct astral MT defects in MDCKII<sup>mChEB2Hi</sup> cells without causing bundle formation. Therefore, a lower concentration than the one known to cause MT bundle formation was chosen (50 and 100 nM). To evaluate whether Taxol corrected defects observed in astral MTs in MDCKII<sup>mChEB2Hi</sup> cells, cells were seeded on a thin-layer of Matrigel then double-blocked with thymidine. Thymidine, was chosen for synchronisation so that all the cells in mitosis will be in the same phase after the drug is washed out. Thymidine arrest cells at the G1/S border preventing progression beyond the S phase. To increase synchronisation, cells were blocked twice. This contained an initial block of 17 h, followed by a wash out and a 9 h passage through the cell cycle then a second 17 h treatment followed by a final release. However, as the second treatment is washed out, Taxol, at 50 and 100 nM were added to the cells and allowed to go through the cell cycle for 9 h before fixing and immunolabelling. Volocity software was utilised for analysing the spindle angle. Angle in thirty cells per condition

from one repeated experiment were calculated. Analysis showed no significant difference when MDCKII<sup>mChEB2Hi</sup> cells were treated with 50 nM Taxol in comparison to the DMSO-control cells. However, a 0.3x fold decrease in angle was observed, although not significant. In contrast, at 100 nM, a significant decrease was noticed with a 0.58x fold difference when compared to the DMSO-control cells (Fig 6.23).

## **6.4 Discussion**

### **6.4.1 EB2-overexpression leads to an increase in multiple lumen formation**

EB2 is a crucial factor for initial MT reorganisation during apico-basal differentiation while its downregulation enhances bundle formation (Goldspink et al., 2013). In this present study, culturing of the stable MDCKII-EB2-overexpressing cell line in Matrigel showed that EB2 overexpression does affect single lumen cyst formation. However, there was a significant reduction in the number of cysts with single lumens and an increase in the number of multiple lumens when EB2 was overexpressed. On further assessment, it was discovered that EB2-overexpression did not affect the localisation of apical polarity markers or junctional proteins as the overexpressing cells were able to effectively localise Par-3 and ZO-1 proteins. This implies that EB2-overexpression does not affect polarity establishment. Also, it means that the generation of multiple lumens in these cells was not caused by limitations to the polarity or junctional proteins and likely to be due to other mechanisms. Par-3 was studied as it is already implicated as one of the first polarity markers observed during epithelial lumen formation (Schluter and Margolis, 2009) so it was necessary to check whether the process at which multiple lumens are formed in MDCKII<sup>mChEB2Hi</sup> cells goes awry during AMIS formation.

MDCKII<sup>mChEB2Hi</sup> and MDCKII<sup>mChEmpty</sup> cysts were stained at various days to monitor differences in MTs. Unfortunately, it was difficult to say from immunofluorescent images whether there were any apparent differences in MT arrays between the MDCKII<sup>mChEB2Hi</sup> and MDCKII<sup>mChEmpty</sup> cells. Further investigations of MT

organisation in overexpressing and control cells would be needed in order to determine whether subtle differences are apparent using super-resolution microscopy techniques. From the images, it could be said that lumens are formed in MDCKII cells by hollowing rather than cavitation where the cells in the centre die by apoptosis due to deprived cell-ECM contact. There was little evidence of apoptosis in the cells as lumens formed (Fig 6.5 & 6.6) possibly due to the presence of laminin – a major component of Matrigel. A study by (Martin-Belmonte et al., 2008) showed that when laminin is present there was a reduced need for lumen formation by apoptosis. Cells cultured in Matrigel had a rapid polarisation and caspase-3 was not present while those cells cultured in collagen-I polarised slowly with caspase-3 being present. Not only is laminin required but also Cdc42 because when it was depleted, it forced cells to undergo cavitation and delayed lumen formation. Apoptosis is only required when the acquisition of polarity is perturbed thus, acting as a control mechanism. This supports our findings as there were no defects in the localisation of polarity markers. The study by Odenwald and colleagues (2017) found that epithelial cells lacking ZO-1 or occludin had defects in the early stages of polarisation and consequently formed cysts with multiple lumens where ZO-1 functions through its U5 domain by organising cortical actin (Fanning et al., 2012). Therefore, both proteins are able to regulate the orientation of cell division during single lumen formation (Odenwald et al., 2017). Furthermore, Hao et al., (2012) discovered that Par-3 inhibition caused spindle misorientation in MDCKII cells. In our study there was no indication that Par-3 or ZO-1 were the cause of multiple lumen formation in MDCKII<sup>mChEB2Hi</sup> cells, thus other processes required for lumen formation are likely to be involved.

Centrosome positioning is known to be vital for vesicular transport during cell division (Rodriguez-Fraticelli et al., 2012). During lumen formation, as the cells differentiate the centrosome is reoriented towards the apical pole, this leads to the components of the vesicular trafficking pathway to be repositioned together with the centrosome (Datta et al., 2011). Our preliminary data indicate that EB2-overexpression may impair centrosomal positioning and possibly lumen initiation in MDCKII<sup>mChEB2Hi</sup> cells during the two-cell stage. Furthermore, we showed that centrosome positioning was altered during directional migration in MDCKII<sup>mChEB2Hi</sup> cells (Figs 4.15 and 4.16). The location of the centrosome during the two-cell stage is critical during lumen formation because both centrosomes need to be in synergy with tight junctions and

apical proteins in order to form the PAP. In MDCKII cysts, Par-3 and aPKC kinase activity are required for apical trafficking to the AMIS to expand to a PAP (Bryant et al., 2010). Therefore, further studies will need to be conducted to establish whether aPKC affects centrosome positioning and consequently lumen formation.

### **6.4.2 EB2-overexpression leads to spindle misorientation**

Spindle orientation and positioning are key processes during epithelial lumen formation and misorientation has been linked with cancer (Noatynska et al., 2012). Spindle orientation play important roles in cell fate determination and tissue morphogenesis. Spindle pole proteins are involved in nucleating and anchoring MTs. EB2-overexpression caused an increase in the height difference in spindle poles consequently increasing the angle of spindle pole orientation leading to multiple lumen formation (Fig 6.17A-C). This is consistent with findings that spindle orientation is important for lumen formation in MDCKII cells, whereby depletion of cenexin did not modify the localisation of polarity proteins such as E-cadherin and Par-3 but did lead to the formation of multiple lumens through its inability to organise and stabilise MTs consequently leading to spindle misorientation. Cenexin usually modulates dynamic astral MTs and cortical NuMA localisation thus proper spindle orientation (Hung et al., 2016). Spindle angles established in our study when EB2 is overexpressed was around 5°, which is also supported by (Hung et al., 2016) where cenexin-depleted MDCK cells also achieved an average of 5°.

The fact that EB2-overexpression affects the length of astral MTs and the number reaching the cell cortex suggested that either MT dynamics or proteins required for capturing the astral MTs are affected so both possibilities were pursued. Polarity proteins at the lateral cell cortex such as NuMA, LGN and Gai are examples of proteins responsible for capturing the astral MT at the cortex. MT nucleation and anchorage proteins are critical for maintaining MT organisation (Mogensen et al., 2000). Ninein is a protein responsible for MT anchorage at the centrosome and might be important for regulating astral MT dynamics at spindle poles (Moss et al., 2007, Goldspink et al., 2017a). Therefore, loss of spindle pole integrity proteins affect astral MT dynamics (Chen et al., 2014). The study found a spindle pole-anchored complex where pericentrin

recruits Cep215, which, in turn recruits centriolin and ninein. This centrosome-based complex was required for controlling spindle orientation and hence, the division plane. In the absence of pericentrin, centriolin, Cep215 and ninein are lost from spindle poles, inhibiting astral MT assembly and proper spindle orientation (Chen et al., 2014). Phosphorylation of EB1 by ASK1 helps to stabilise astral MTs (Luo et al., 2016), however, in MDCKII<sup>mChEB2Hi</sup> cells, EB2 goes along the MT lattice (Fig 4.9) and thus, may be able to remove EB1 from the plus ends causing weaker astral MTs therefore spindle misorientation. ASK1 might be controlling astral MTs in these cells indirectly. Furthermore, it is also possible that the level of EB2 in MDCKII<sup>mChEB2Hi</sup> cells is a lot higher than the levels of Aurora B and CDK1, therefore not all EB2 is phosphorylated, which means the non-phosphorylated EB2 are still able to bind MTs resulting in weaker MTs in mitotic cells and spindle misorientation. EB2 overexpression could inhibit the activities of Aurora B and CDK1 in a negative feedback loop in such a way that even less EB2 is phosphorylated enhancing the possibility of spindle misorientation. This could be a mechanism cancer cells have created to increase epithelial remodelling.

Results from MT dynamics established that EB2-overexpression caused an increase in comet speed. An increased comet speed could also highlight one of the reasons astral MTs are not captured at the cortex resulting in relatively weak, unstable astral MTs. It is possible that these MTs touch the cortex of the cell and then retract thus, causing shrinkage. This is more likely as there were no significant differences in the intensity of NuMA at the cortex in the overexpressing and control cells. This implies that astral MTs are not necessary for the delivery of NuMA to the cortex, which contradicts the findings by (Hung et al., 2016) where astral MTs were found to be important; and instead other cortical proteins may be more relevant in sequestering the plus ends of astral MTs to the cortex in MDCKII<sup>mChEB2Hi</sup> cells although our findings are still preliminary. This is a possibility since (Kotak et al., 2014) have established that NuMA can directly associate with phosphoinositides such as phosphatidylinositol 4,5-bisphosphate for cortical delivery during mitosis. To fully validate this, the activity and effect of other cortical proteins need to be explored. It is worth mentioning that the amount of NuMA delivered to the cortex is not exclusively dependent on the number of astral MTs but also on the activity of motor proteins, which may explain the localisation of NuMA at the cortex. Rapid growth of spindle MTs by EB2 results in an incomplete attachment of MTs to chromosomes at their kinetochores, incomplete

formation of metaphase spindles and a possible reduction in spindle tension, all of which are required for progression into anaphase and satisfaction of the spindle assembly checkpoint.

Since EB2-overexpression seemed to increase the speed of MT growth, there was a rescue attempt by stabilising MTs with Taxol. Taxol treatment reversed the spindle angle effects caused by EB2-overexpression suggesting that more stable MTs are desired for correct spindle orientation. The fact that Taxol is able to significantly reduce the angle of spindle poles towards the angle of control cells suggests that Taxol may be able to reduce the number of multiple lumens generated by the overexpression of EB2 however, more work is needed to confirm this. The findings that EB2-overexpression in MDCKII cells affect MT stability was further supported by cold treatment experiment where there was a marked reduction in stable MTs. However, Western blot results revealed an increase in acetylated and detyrosinated tubulin expression levels (markers for stable MTs), which was surprising. An explanation for this might be that expression pattern experiments consider both interphase and mitotic cells where there is a mixture in the level of stable and dynamic MTs. Our findings suggest that EB2 overexpression affects lumen formation through spindle misorientation.

## **6.5 Summary**

In summary, experiments involving overexpression of EB2 have produced particularly interesting results connecting overexpression of EB2 in a previously unknown role in multiple lumen formation. The results showed that EB2-overexpression caused no localisation changes in polarity and junctional proteins during epithelial lumen formation but led to the formation of multiple lumens. Defects observed in spindle orientation and astral MTs length in MDCKII<sup>mChEB2Hi</sup> cells were possible reasons for multiple lumens. In the future, further experiments need to be carried out to establish the role of other cortical proteins involved in astral MT stabilisation and whether EB2 is phosphorylated; since EB2 phosphorylation leads to dispersal in the cytoplasm reducing its affinity for binding along the MT lattice, which is necessary for mitosis (Iimori et al., 2016a). Also, work needs to be done to evaluate if EB1 is still functional in MDCKII<sup>mChEB2Hi</sup> cells. It might be worthwhile to repeat

these experiments in a normal mammary epithelial cell line such as the MCF-10A overexpressing EB2 to confirm results seen using MDCKII cells.

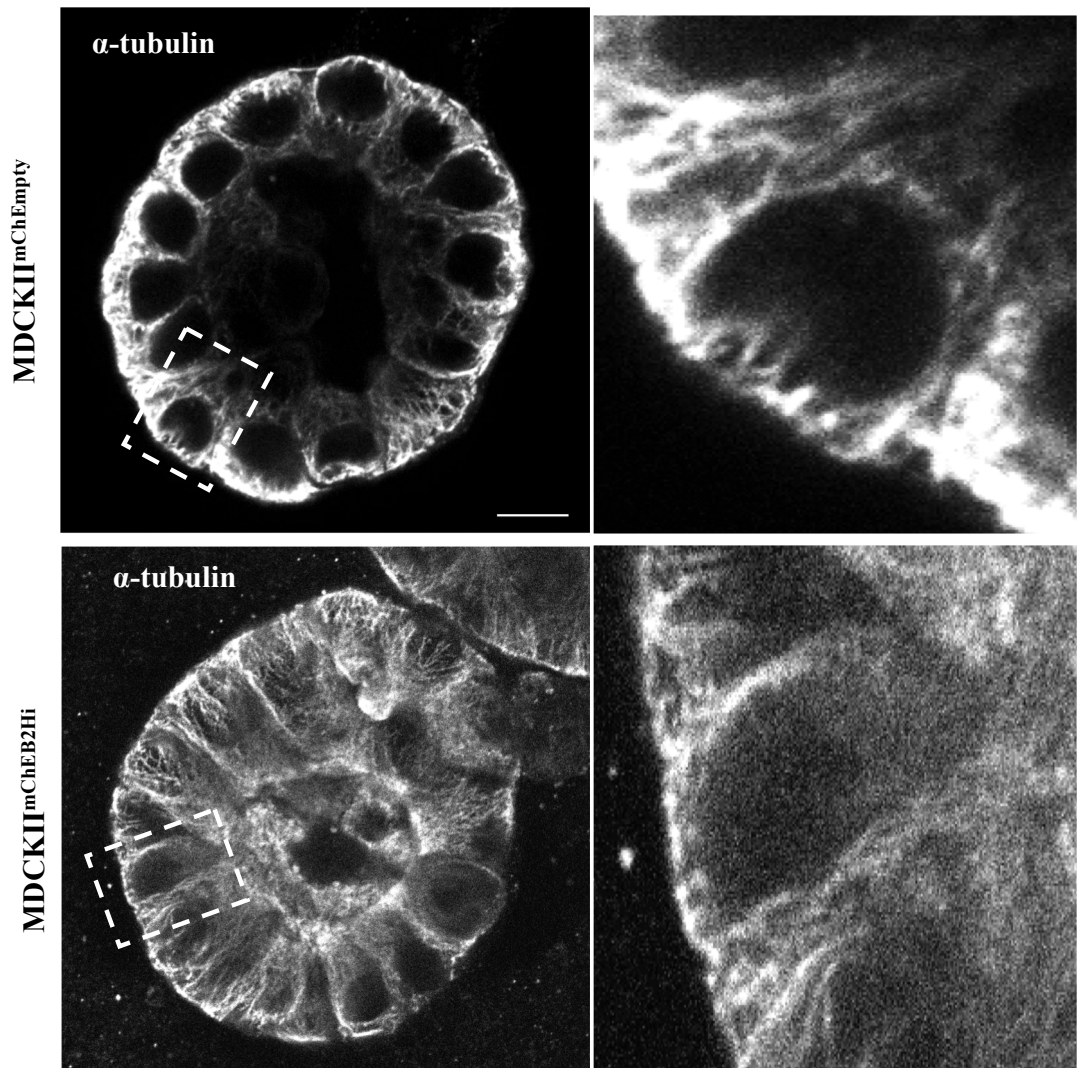


**Figure 6.1: MT organisation in MDCKII<sup>mChEmpty</sup> and MDCKII<sup>mChEB2Hi</sup> cells.**

Cells cultured in Matrigel then fixed in Methanol/Formaldehyde and stained on day 5 for MTs (pAb, green). Single optical sections showing MDCKII<sup>mChEmpty</sup> and MDCKII<sup>mChEB2Hi</sup> epithelial cells produced cysts with single lumens surrounded by a layer of polarised cells. Images highlight apico-basal array organisation of MTs in polarised cells (see also boxed regions enlarged). Scale bar = 10 $\mu$ m.

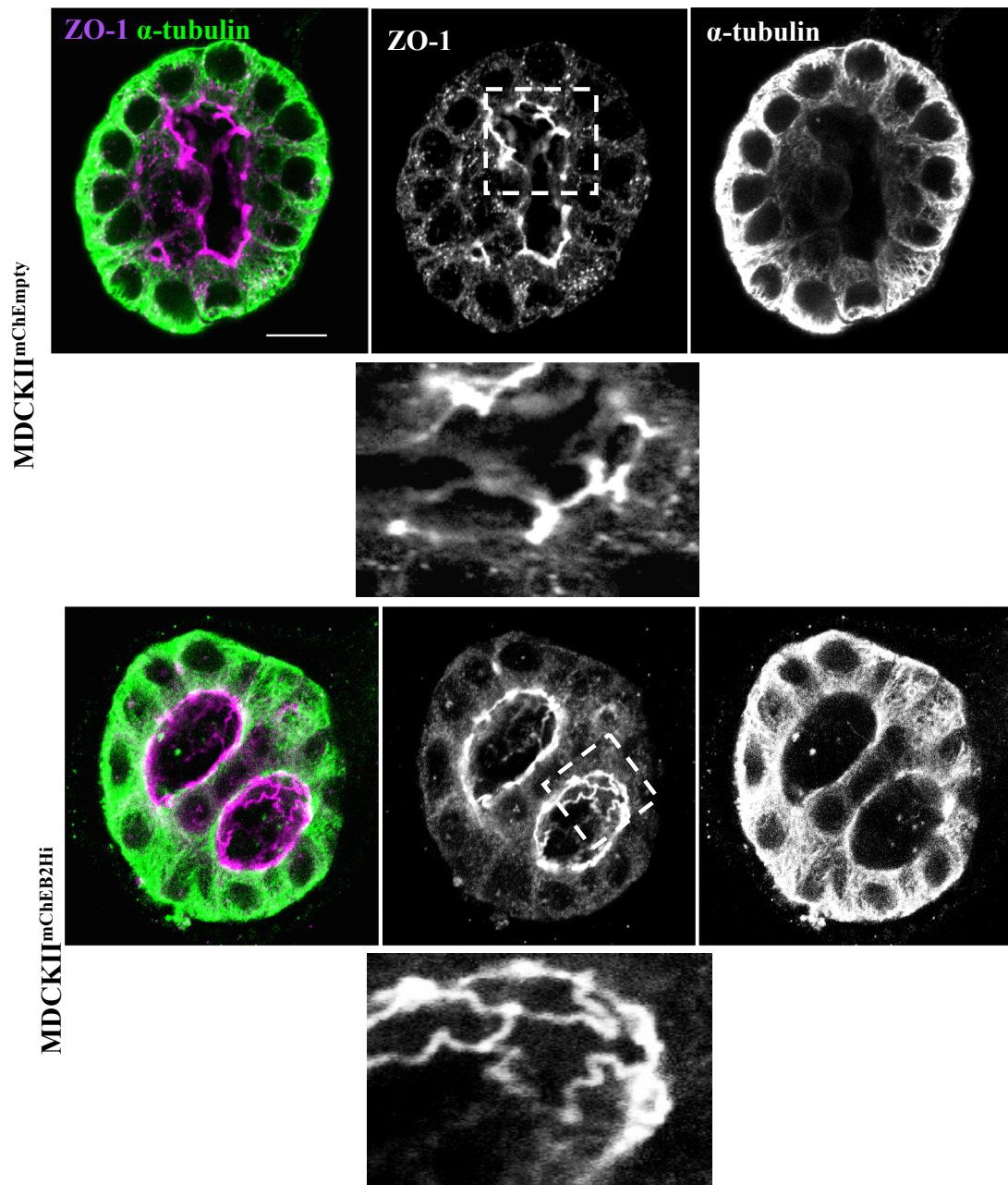


**Figure 6.2: Localisation of the tight junction marker ZO-1 in MDCKII<sup>mChEmpty</sup> and MDCKII<sup>mChEB2Hi</sup> cells reveal multiple lumens in EB2 overexpressing cells.**

Cells were cultured in Matrigel then fixed in Methanol/Formaldehyde and stained on day 5, ZO-1 (pAb, purple) and MT (mAb YL1/2, green). Images show single optical sections taken using a confocal microscope. The mCherry Empty-vector MDCKII epithelial cyst reveal a single lumen surrounded by a layer of polarised cells with apico-basal MTs. The EB2-overexpressing cyst shows two distinctive lumens with the polarised cells still indicate apico-basal MT organisation. The enlarged region shows junctional localisation of ZO-1. Scale bar = 10µm.

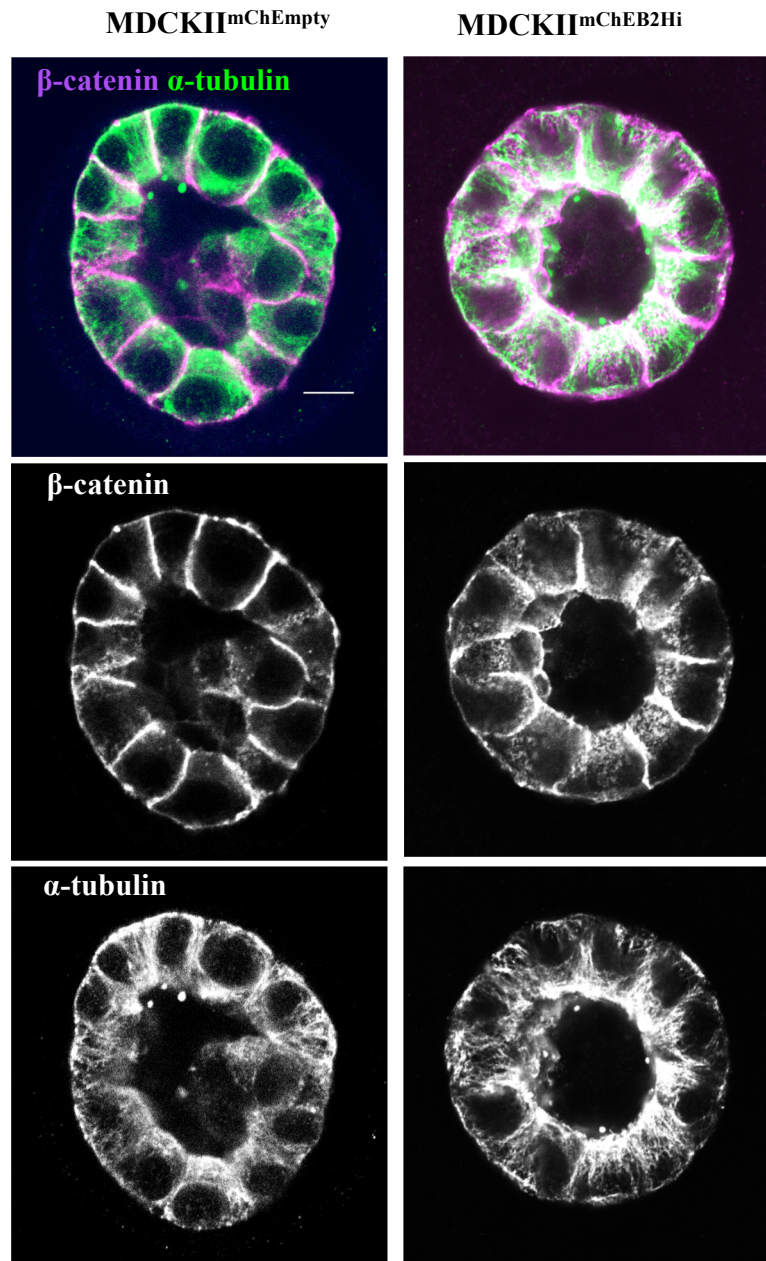


**Figure 6.3:  $\beta$ -catenin localises to adherens junctions in EB2 overexpressing cells.**

Cells were cultured in Matrigel then fixed in Methanol/Formaldehyde and stained on day 5 for  $\beta$ -catenin (mAb, purple) and MTs (pAb, green). Images were taken using a confocal microscope. Single optical sections showing  $\beta$ -catenin localisation observed in MDCKII<sup>mChEB2Hi</sup> cells were not different when compared with MDCKII<sup>mChEmpty</sup> cells. Apico-basal MT organisation evident in both control and EB2 overexpressing cysts. Scale bar = 10 $\mu$ m.

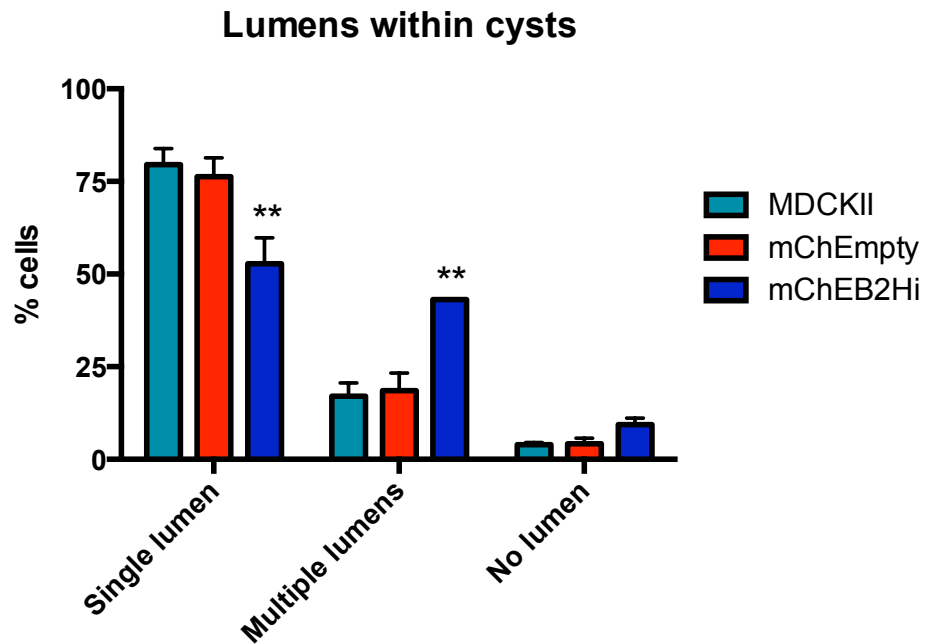


**Figure 6.4: EB2-overexpressing MDCKII cysts revealed an increased number of cysts with multiple lumens.**

Significantly more MDCKII<sup>mChEB2Hi</sup> cysts contained multiple lumens and fewer a single lumen than MDCKII<sup>mChEmpty</sup> and untreated MDCKII cysts. The number of cysts with no lumens were not significant. Statistical significance was assessed by two-way ANOVA, n=75. Graph shows combined data from three independent experiments. Mean ± SEM

Day 5

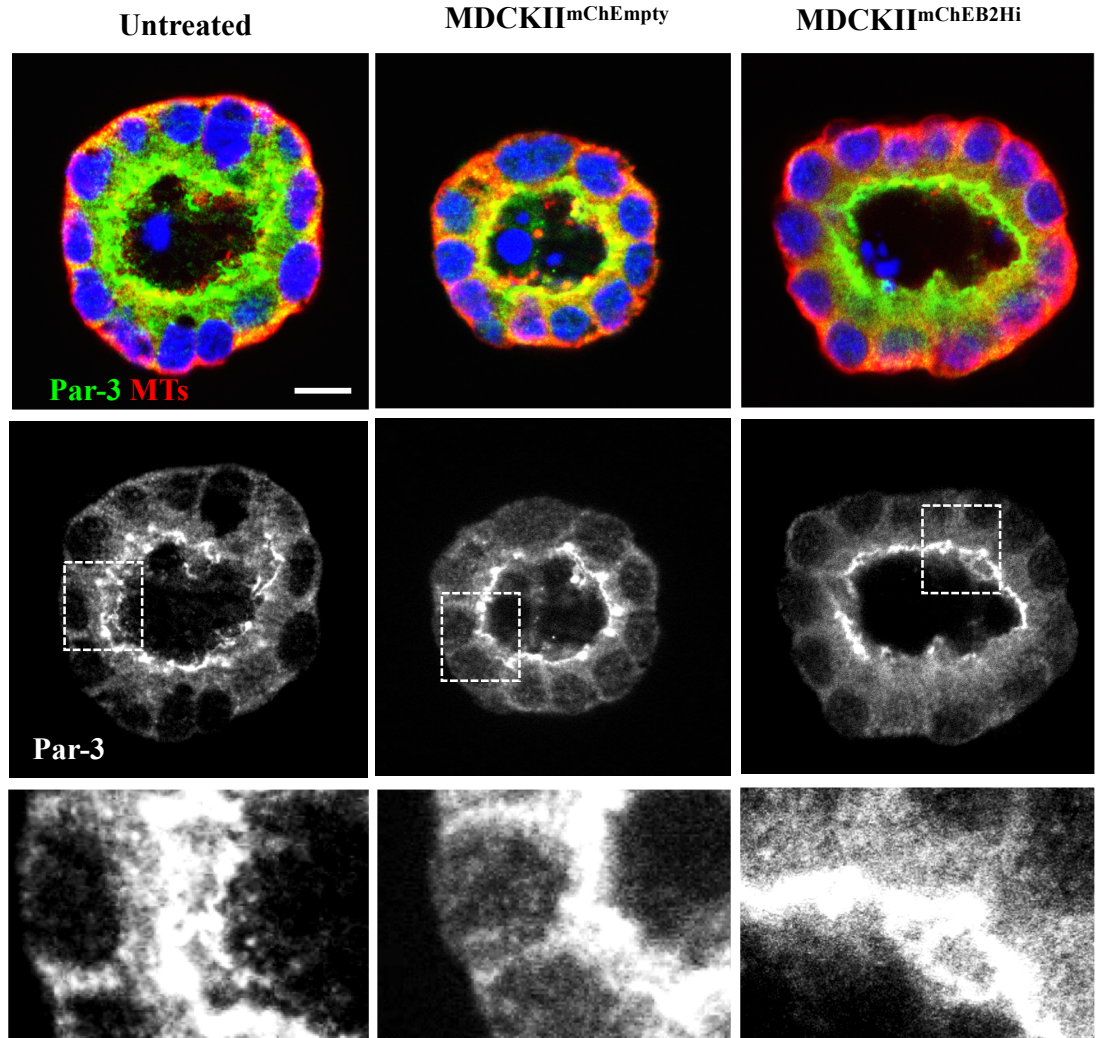


**Figure 6.5: EB2 overexpression in 5 day MDCKII cysts does not affect localisation of the polarity marker Par-3 to apical junctions.**

Cells were cultured in Matrigel for 5 days before fixing in Methanol/Formaldehyde and immunolabelling for Par-3 (green; pAb), MTs (red; mAb YL1/2) and DAPI. Images highlight apico-basal organisation of MTs in polarised cells similar in all three sub-cell lines. Par-3 is observed to localise to the junctional region of the lumen. There were no significant changes in the localisation of Par-3 in the MDCKII<sup>mChEB2Hi</sup> cysts when compared with the MDCKII<sup>mChEmpty</sup> cysts as seen by the enlarged regions. Scale bars=10µm.

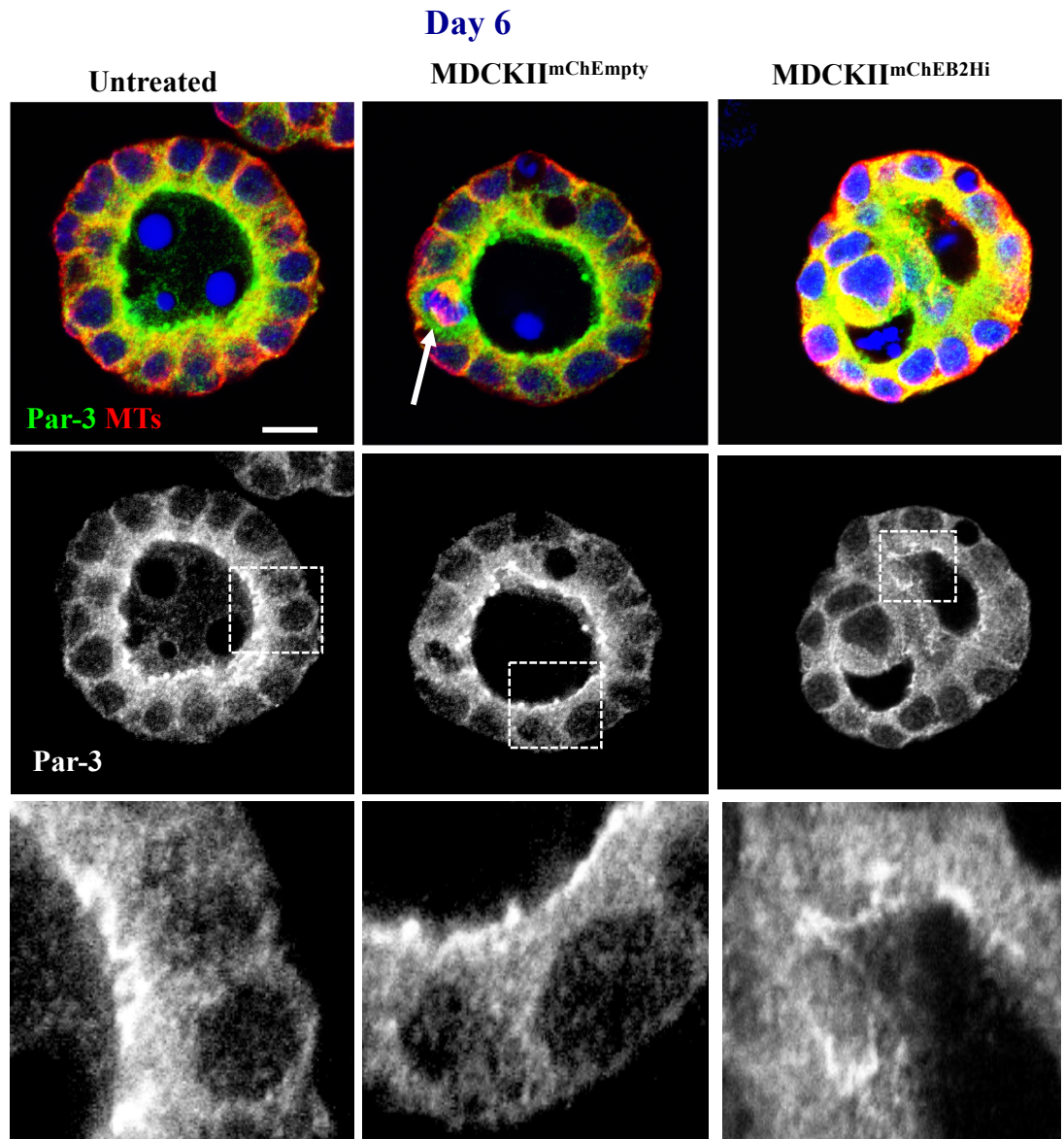


**Figure 6.6: EB2 overexpression in 6 day MDCKII cysts revealed maintenance of the polarity marker Par-3 localisation to apical junctions.**

Cells were cultured in Matrigel for 6 days before fixing in Methanol/Formaldehyde and immunolabelling for Par-3 (green; pAb), MTs (red; mAb YL1/2) and DAPI. Images highlight apico-basal organisation of MTs in polarised cells similar in all three cell lines. Par-3 is observed to localise to the junctional region of the lumen. In the empty-vector MDCK cysts, a dividing cell (white arrow) depicts a planar spindle orientation making sure that the division plane maintains the single cell layer and normal tissue architecture. The localisation of Par-3 in the MDCKII<sup>mChEB2Hi</sup> cyst to the apical junctions similar to the MDCKII<sup>mChEmpty</sup> cyst. Scale bars =10µm.

Day 1

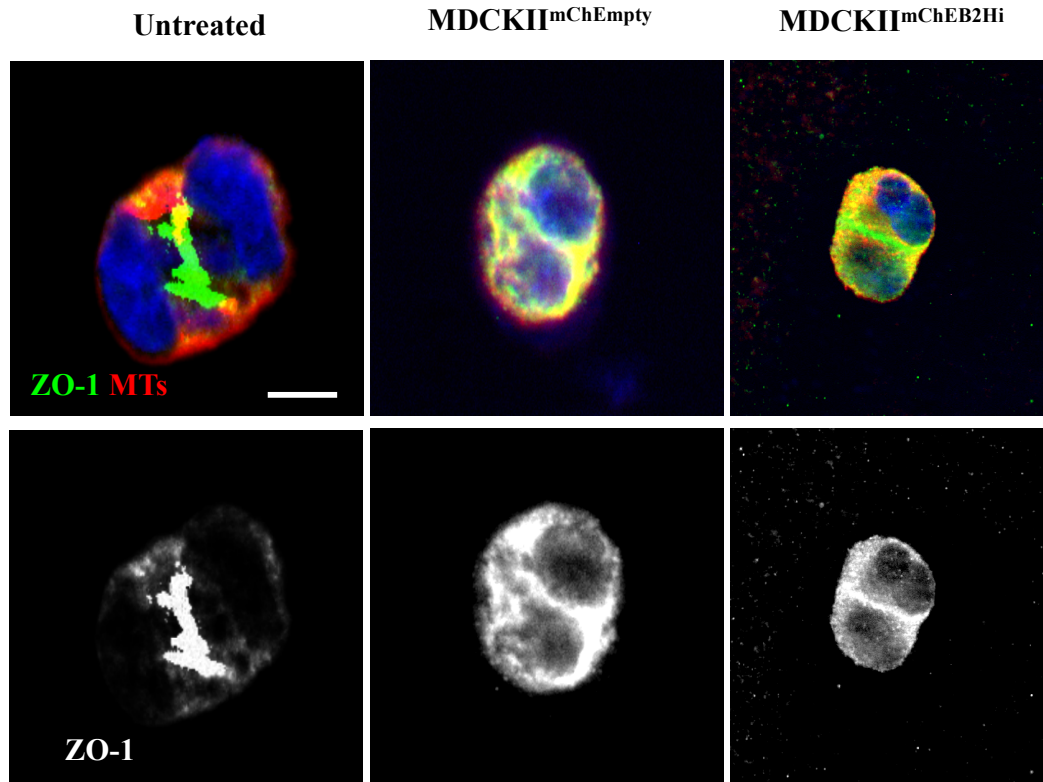


**Figure 6.7: EB2 overexpression in MDCKII cells does not affect localisation of the tight junction marker ZO-1 to the apical membrane at the two cell stage.**

Cells were cultured in Matrigel for 24 h before fixing in Methanol/Formaldehyde and immunolabelling for ZO-1 (pAb, green), MT (mAb YL1/2, red) and DAPI. ZO-1 is observed to localise to the centre between the two divided cells. There were no significant changes in the localisation of ZO-1 in the MDCKII<sup>mChEB2Hi</sup> cells when compared with the MDCKII<sup>mChEmpty</sup> cells at the two-cell stage. Scale bars=10µm.

Day 2

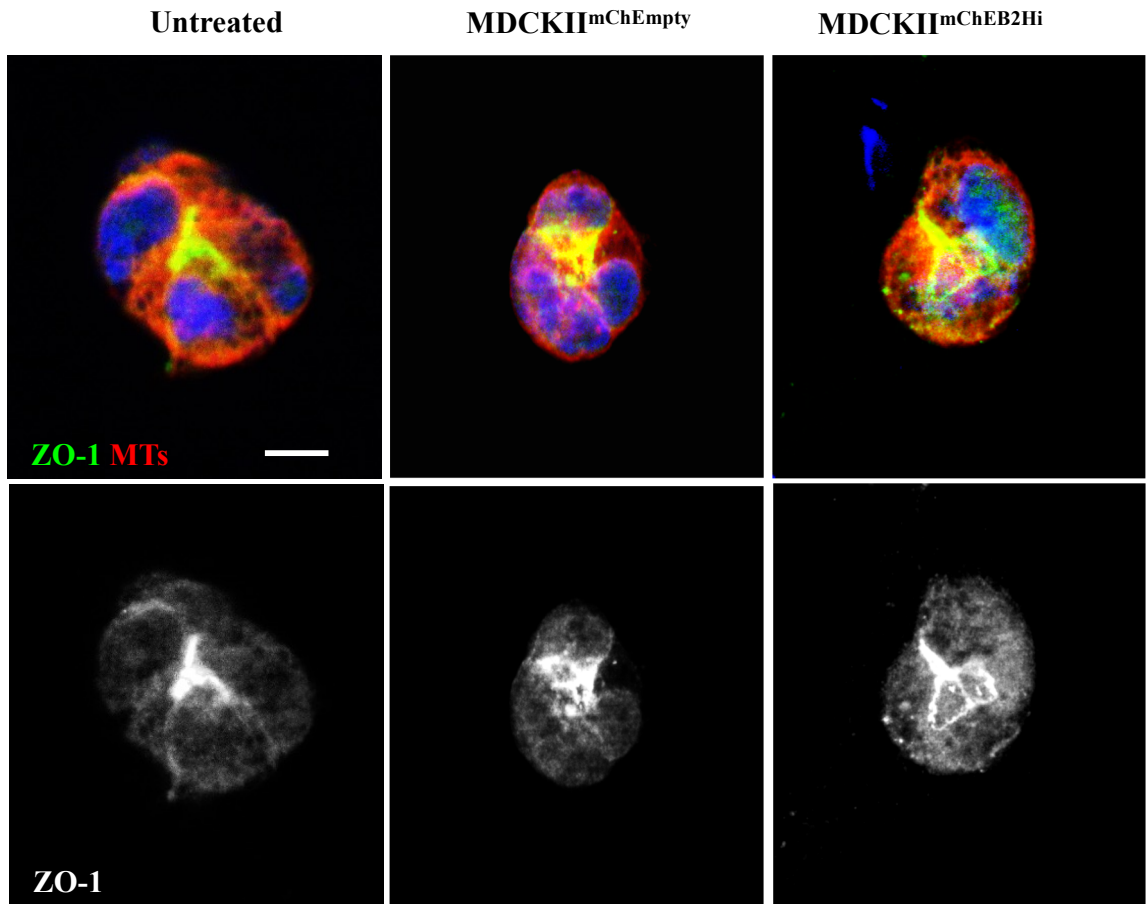


**Figure 6.8: EB2 overexpression in MDCKII cells does not affect the localisation of tight junctional marker ZO-1 to the apical membrane at the four-cell stage.**

Cells were cultured in Matrigel for 2 days before fixing in Methanol/Formaldehyde and immunolabelling for ZO-1 (pAb, green), MT (mAb YL1/2, red) and DAPI. ZO-1 is observed to localise to the pre-apical patch of the cells. There were no significant changes in the localisation of ZO-1 in the MDCKII<sup>mChEB2Hi</sup> cysts when compared with the MDCKII<sup>mChEmpty</sup> cysts. Scale bars=10 $\mu$ m.

Day 3

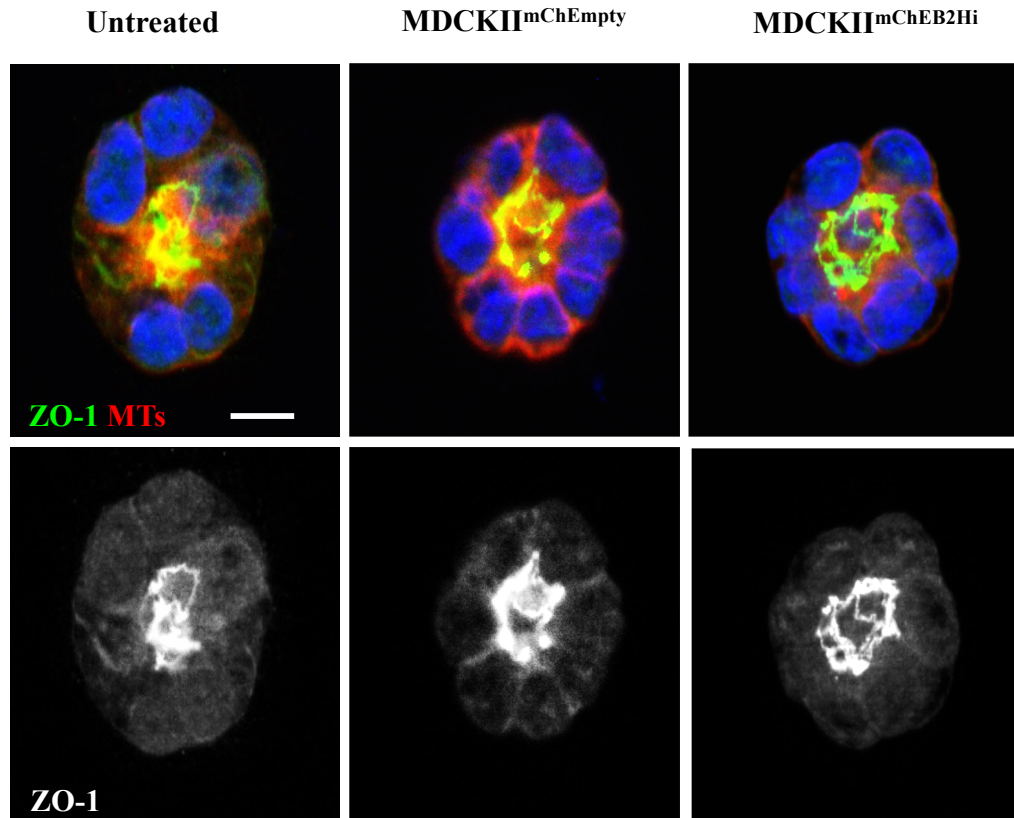


**Figure 6.9: EB2 overexpression in 3 day MDCKII cysts does not affect localisation of the tight junction protein ZO-1 to the apical membrane.**

Cells were cultured in Matrigel for 3 days before fixing in Methanol/Formaldehyde and immunolabelling for ZO-1 (pAb, green), MT (mAb YL1/2, red) and DAPI. The lumen is starting to take shape, which is supported by the ring appearance of ZO-1. There were no significant changes in the localisation of ZO-1 in the MDCKII<sup>mChEB2Hi</sup> cysts when compared with the MDCKII<sup>mChEmpty</sup> cysts. Scale bars=10µm.

Day 4

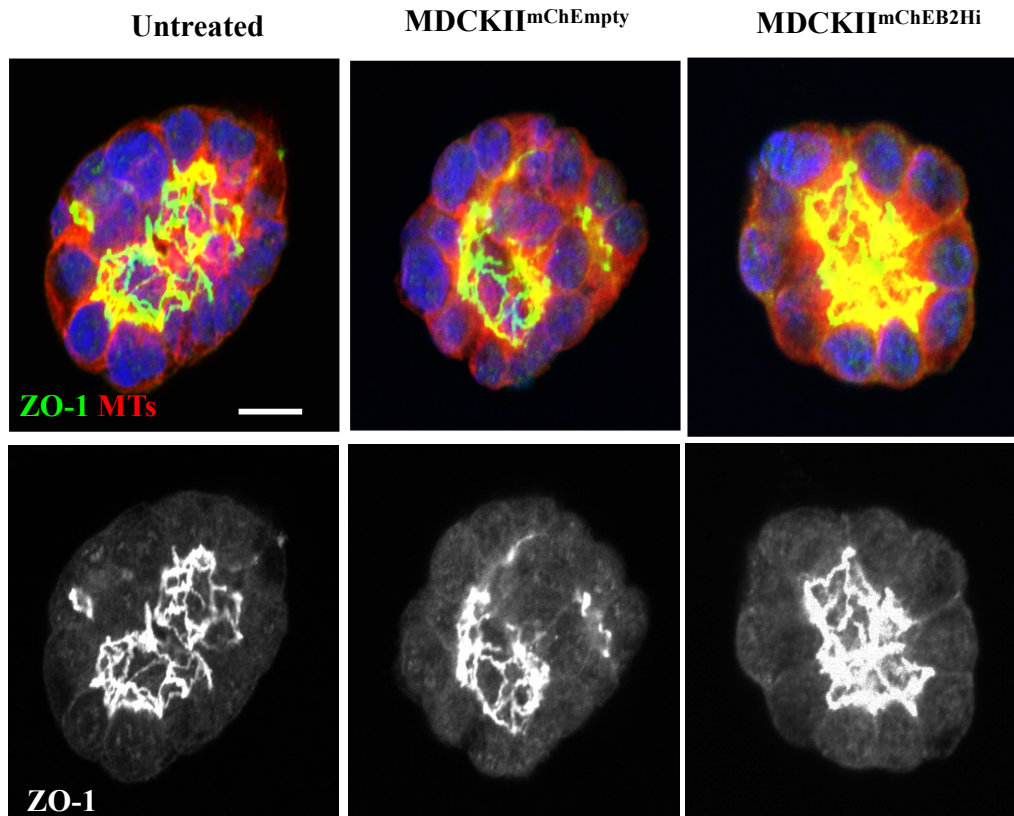


**Figure 6.10: EB2 overexpression in 4 day MDCKII cysts does not affect localisation of the tight junction protein ZO-1 to apical junctions.**

Cells were cultured in Matrigel for 4 days before fixing in Methanol/Formaldehyde and immunolabelling for ZO-1 (pAb, green), MT (mAb YL1/2, red) and DAPI. ZO-1 is observed to localise to the apical surface of the cells. There were no significant changes in the localisation of ZO-1 in the MDCKII<sup>mChEB2Hi</sup> cysts when compared with the MDCKII<sup>mChEmpty</sup> cysts. Scale bars=10 $\mu$ m.

Day 5

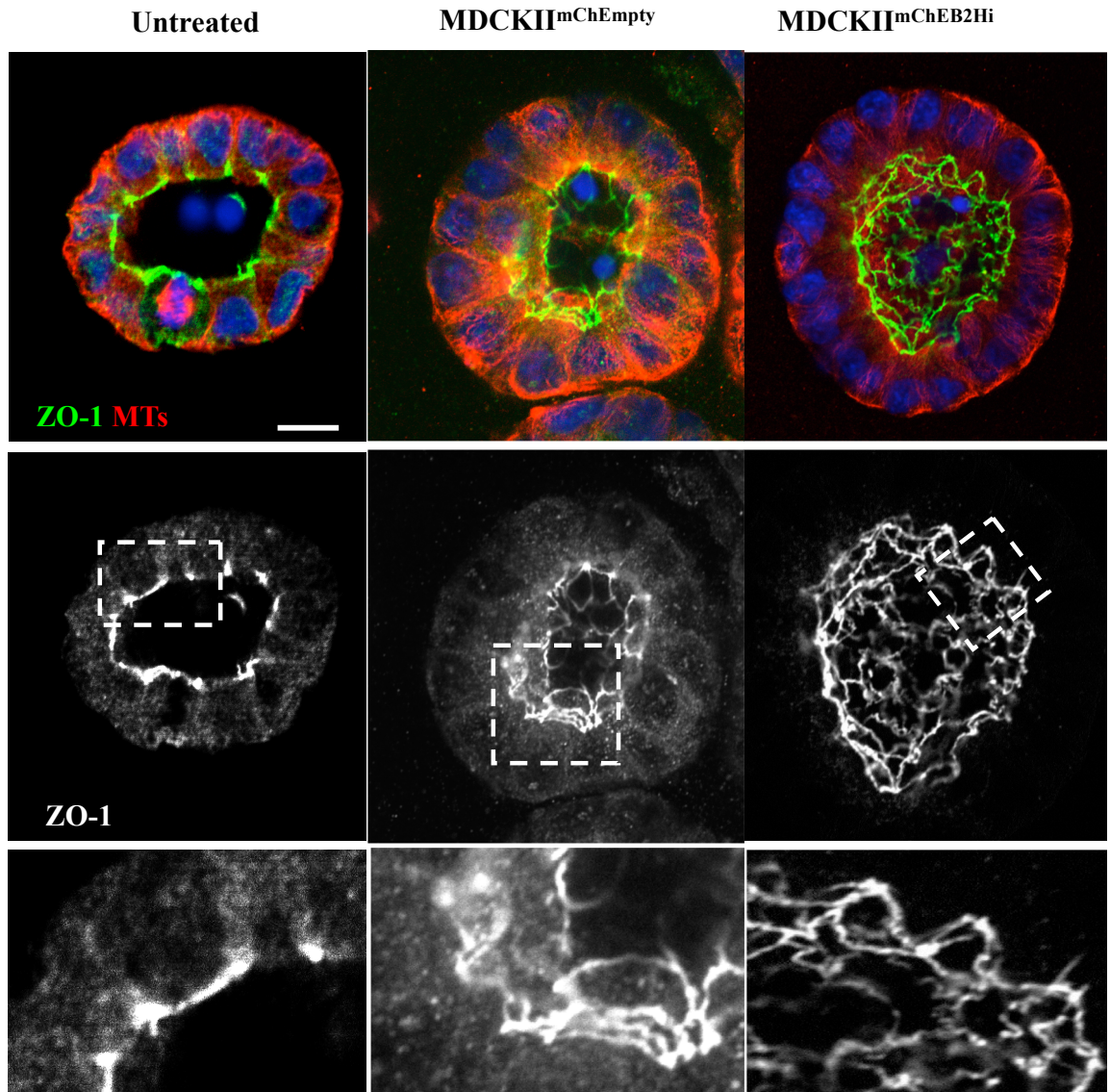


**Figure 6.11: EB2 overexpression in 5 day MDCKII cysts does not affect localisation of the tight junction protein ZO-1 to apical junctions.**

Cells were cultured in Matrigel for 5 days before fixing in Methanol/Formaldehyde and immunolabelling for ZO-1 (pAb, green), MT (mAb YL1/2, red) and DAPI. Images highlight apico-basal organisation of MTs in polarised cells similar in all three cell lines. ZO-1 is observed to localise to the apical surface of the lumen with exclusion from the basal region. There were no significant changes in the localisation of ZO-1 in the MDCKII<sup>mChEB2Hi</sup> cysts when compared with the MDCKII<sup>mChEmpty</sup> cysts. Scale bars =10µm.

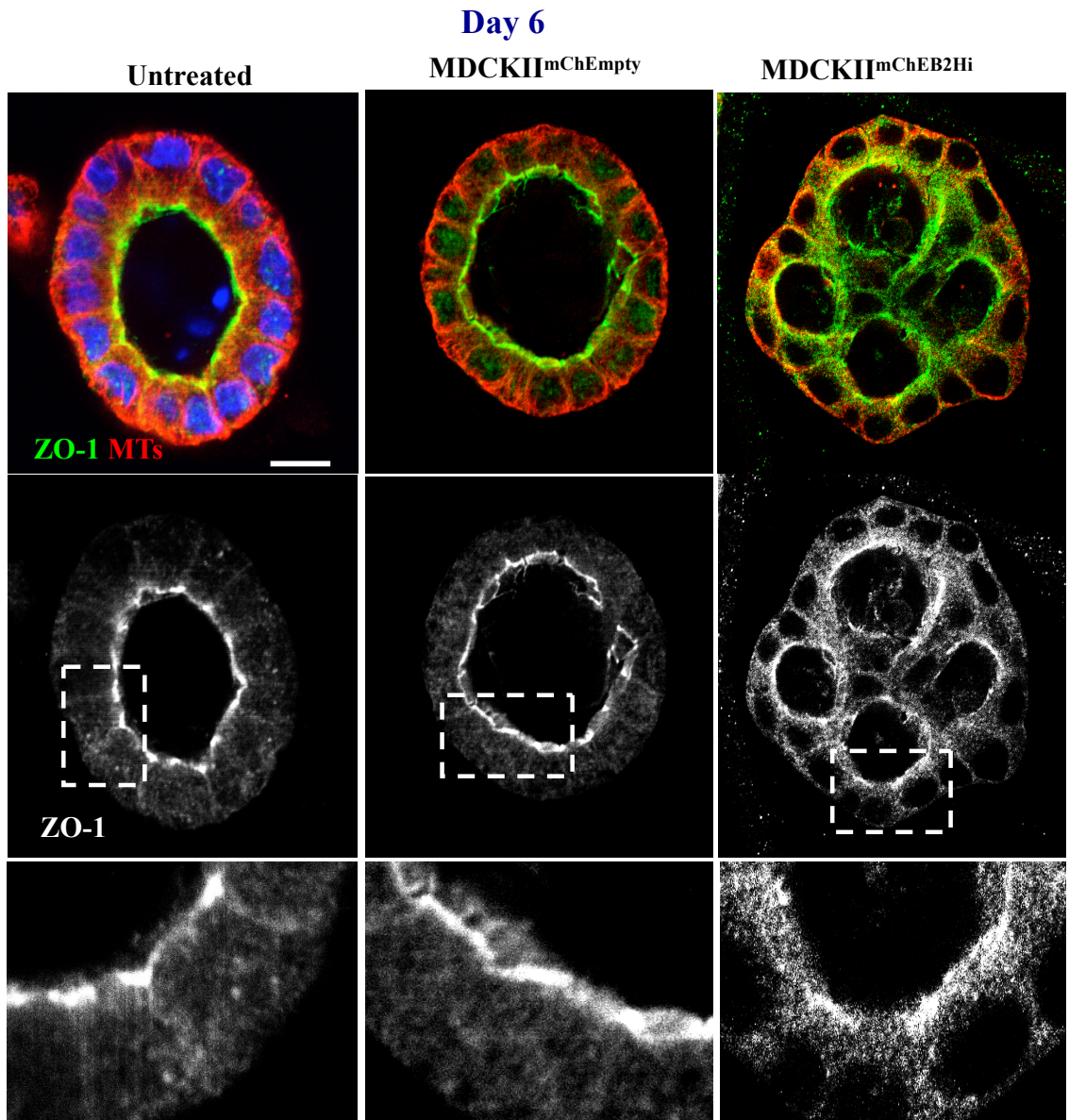


**Figure 6.12: EB2 overexpression in 6 day MDCKII cysts does not affect localisation of the tight junction protein ZO-1 to apical junctions**

Cells were cultured in Matrigel for 6 days before fixing in Methanol/Formaldehyde and immunolabelling for ZO-1 (pAb, green), MT (mAb YL1/2, red) and DAPI. Images highlight apico-basal organisation of MTs in polarised cells similar in all three cell lines. ZO-1 is observed to localise to the apical surface of the lumen with exclusion from the basal region. There were no significant changes in the localisation of ZO-1 in the MDCKII<sup>mChEB2Hi</sup> cysts when compared with the MDCKII<sup>mChEmpty</sup> cysts. The MDCKII<sup>mChEB2Hi</sup> cells formed cysts with four lumens in this case. The localisation of ZO-1 in the MDCKII<sup>mChEB2Hi</sup> cyst revealed a lower degree in the basal region of the cyst. Scale bars =10 $\mu$ m.

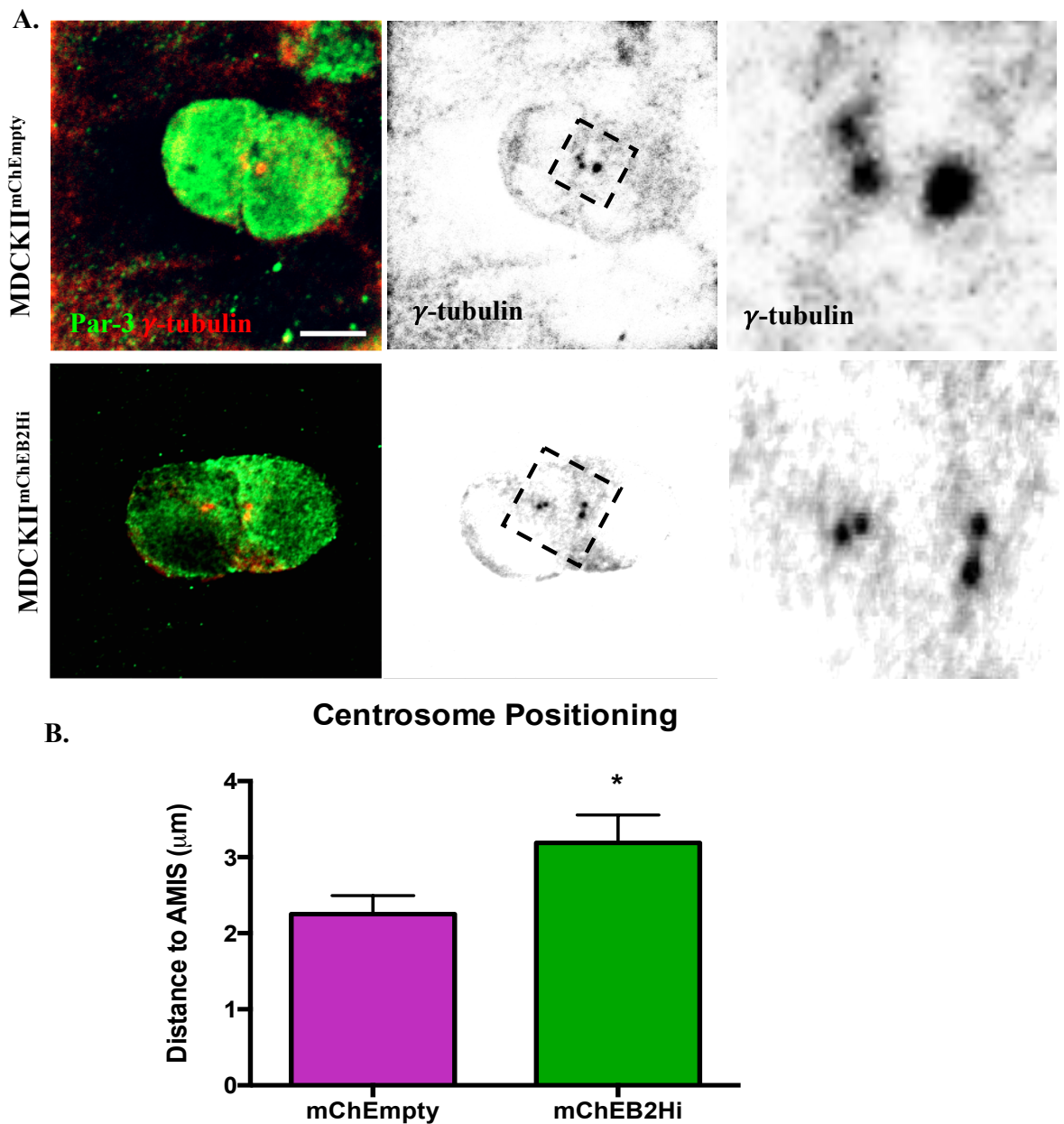


**Figure 6.13: EB2 overexpression in MDCKII cells affects centrosome positioning at the two-cell stage.**

A) Cells were cultured in Matrigel for 20 h before fixing and immunolabelling for Par-3 (green, pAb) and  $\gamma$ -tubulin (red, mAb). Images were taken on the confocal microscope. In MDCKII<sup>mChEmpty</sup> cells, Par-3 is observed in the centre of the two cells referred to as the midpoint while the MTOC labelled with  $\gamma$ -tubulin is seen to be in close proximity with the midpoint. In the MDCKII<sup>mChEB2Hi</sup> cells, Par-3 is also observed at the midpoint, however, the centrosomes on the left side is further away from the midpoint compared to centrosomes on the right side of the midpoint. B) Quantification of centrosome positioning using ImageJ. The graph shows a significant difference in centrosome positioning from the midpoint in MDCKII<sup>mChEB2Hi</sup> cells compared with the MDCKII<sup>mChEmpty</sup> cells. No of cells analysed = 15 per condition. Mean  $\pm$  SEM.

MDCKII Cells

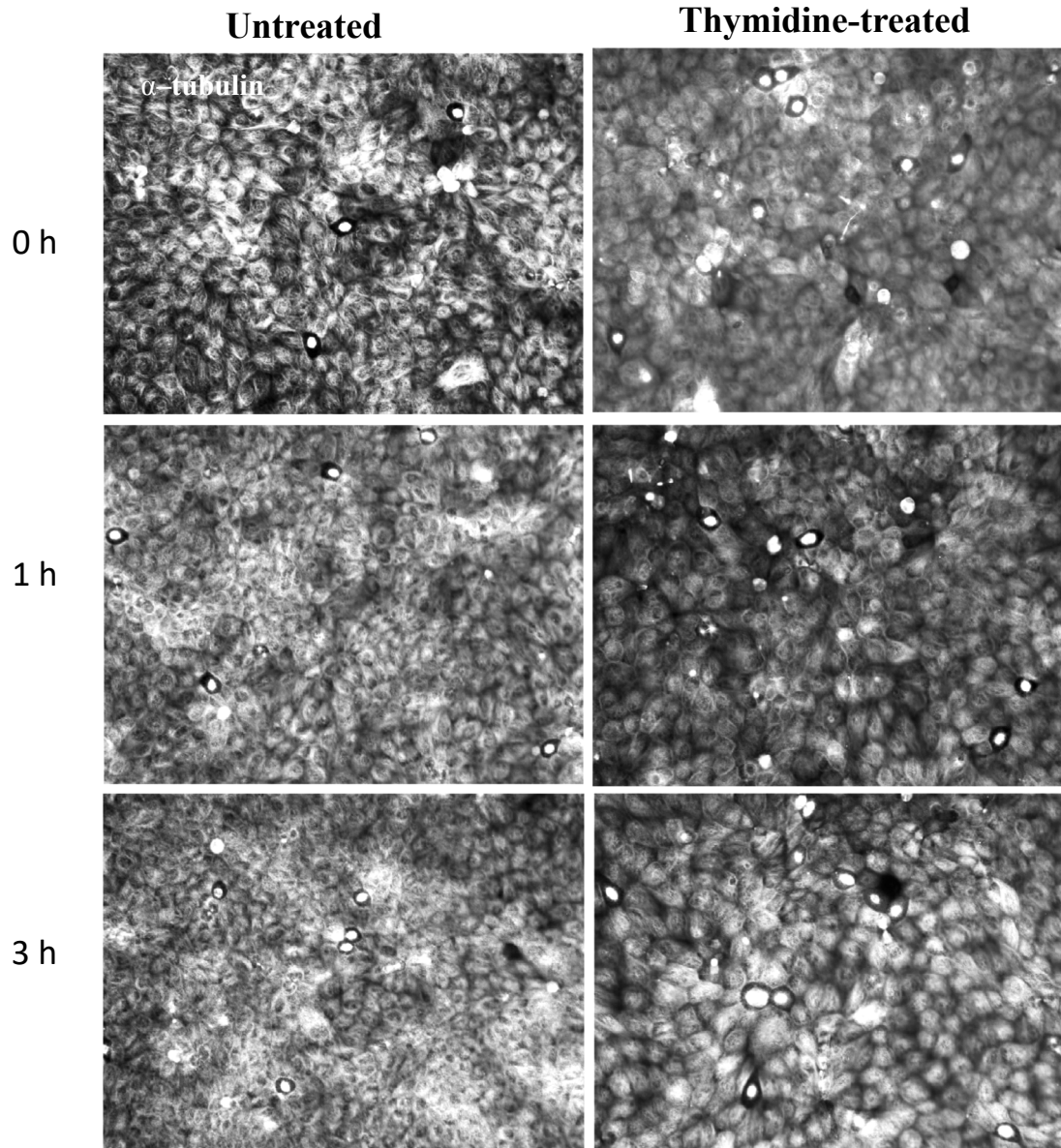


**Figure 6.14: Cell synchronisation using Thymidine treatment in MDCKII cells.**

MDCKII cells were treated with a double-block of thymidine for 17 h then washed out before fixing and immunolabelling at different time points (0, 1, 3, 6 and 9 h).  $\alpha$ -tubulin (B&W). The number of cells in mitosis were similar in the untreated and thymidine-treated cells at 0, 1 and 3 h post thymidine treatment.

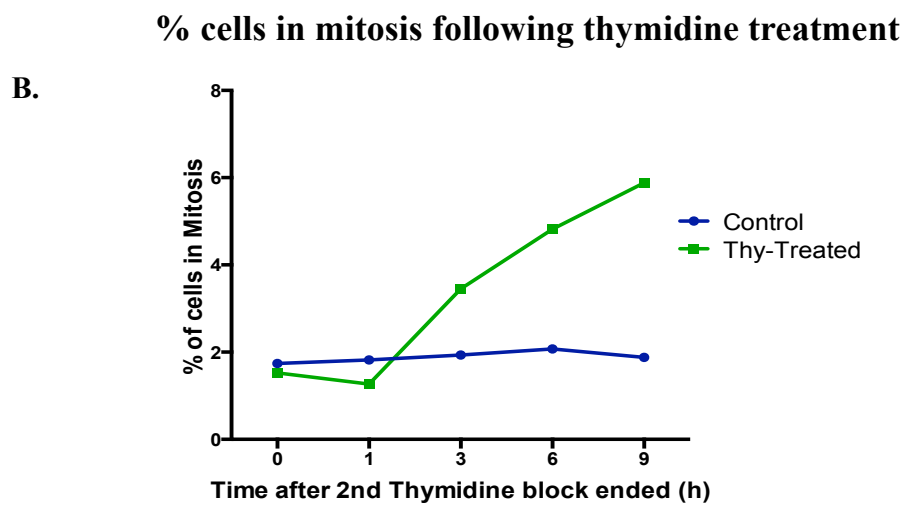
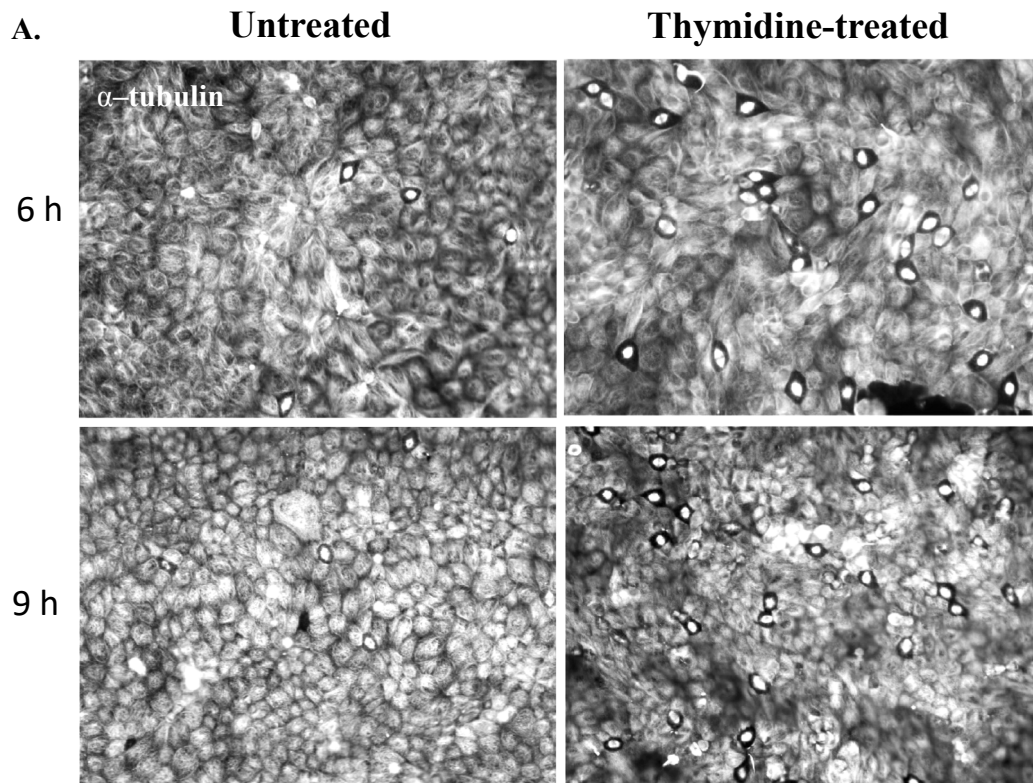


**Figure 6.15: Cell synchronisation using Thymidine treatment in MDCKII cells.**

A) MDCKII cells were treated with a double-block of thymidine for 17 h then washed before fixing and immunolabelling at different time points (0, 1, 3, 6 and 9 h). There were more cells in mitosis in the thymidine-treated cells at 6 and 9 h post thymidine treatment compared to the untreated cells. B) The graph shows a proportional increase in mitotic cells compared to the time after the second thymidine treatment ended.

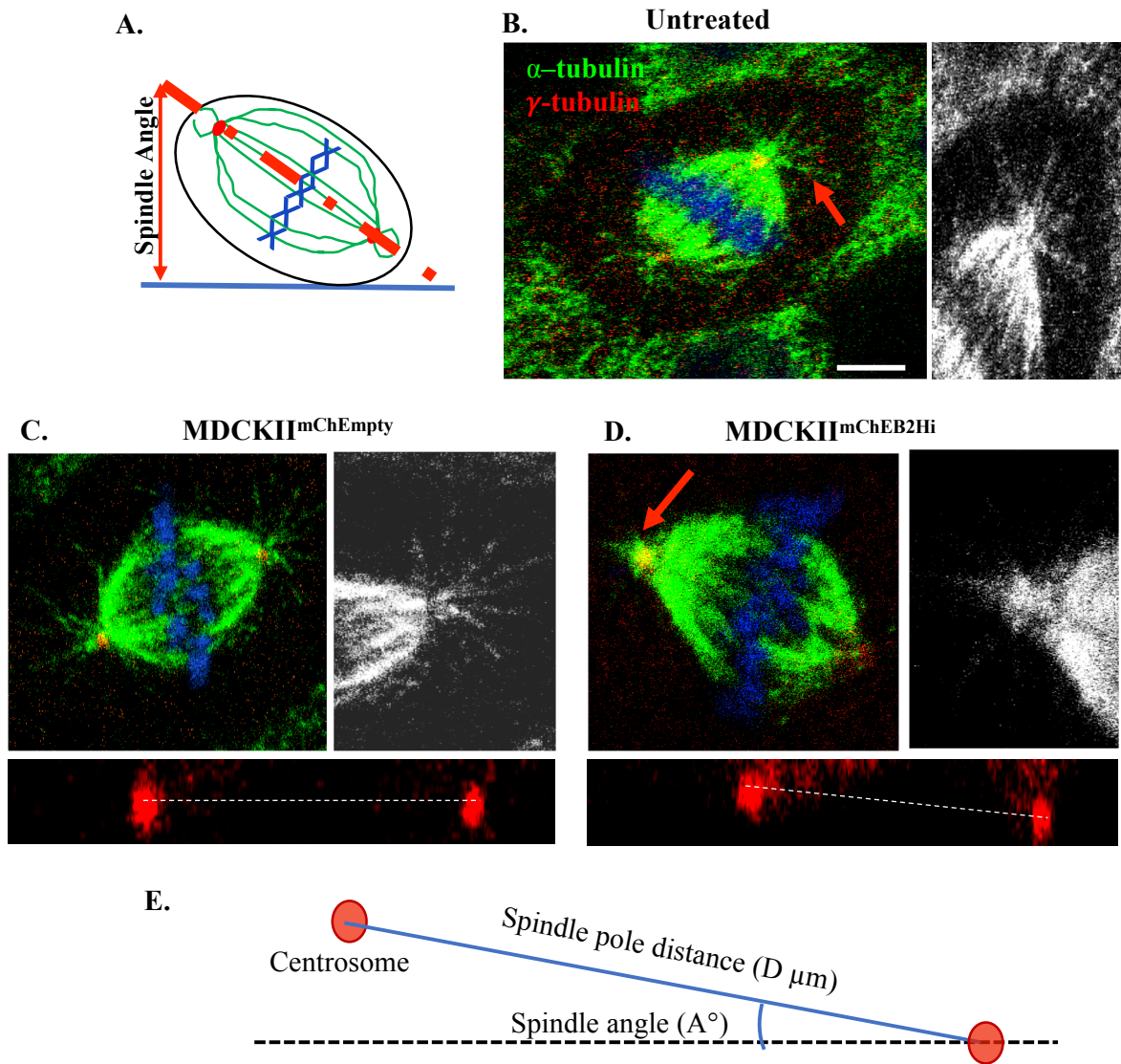


**Figure 6.16: EB2 overexpression in MDCKII cells affects the bipolar spindle angle.**

A) A model depicting the angle of the bipolar spindle of a cell undergoing mitosis. B-D) Cells were double-blocked with thymidine, allowed to go through mitosis for 9 h and then fixed and immunolabelled for MTs (green, mAb YL1/2),  $\gamma$ -tubulin (red, pAb) and DAPI. Z-stacks were taken on the confocal microscope at intervals of 0.2  $\mu$ m. Optical sections taken from the Z-stacks show a normal bipolar spindle untreated MDCKII, MDCKII<sup>mChEmpty</sup> and MDCKII<sup>mChEB2Hi</sup> cells with astral MTs radiating out from the spindle pole towards the cell cortex (black and white images). The orthogonal views show the difference in height between the two centrosomes in the MDCKII<sup>mChEmpty</sup> and MDCKII<sup>mChEB2Hi</sup> cells. E) Schematic showing the spindle angle in relation to the spindle poles. The spindle pole distance ( $D$ ) measures the difference between both centrosomes; the difference in height measures the distance between the height of both centrosomes; Spindle angle ( $A$ ) is calculated from the difference in height with respect to the substratum. Scale bar = 10  $\mu$ m.

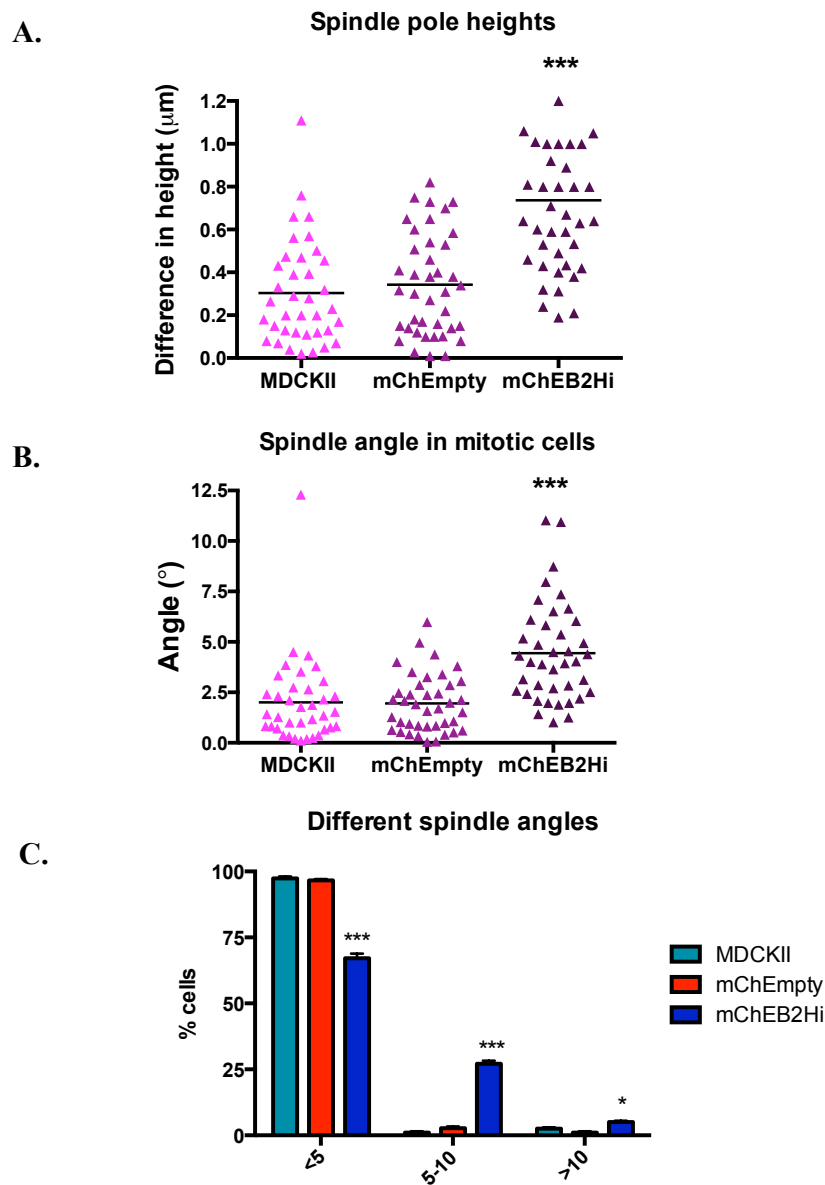


**Figure 6.17: EB2 overexpression affects the angle and height of bipolar spindles in MDCKII cells.** A) Analysis illustrates a significant increase in the height of the spindle poles of MDCKII<sup>mChEB2Hi</sup> compared to MDCKII<sup>mChEmpty</sup> cells. B) Bipolar spindle orientation analysis shows a significant increase in spindle angle MDCKII<sup>mChEB2Hi</sup> compared to MDCKII<sup>mChEmpty</sup> cells. Volocity software was used for analysing the spindle angles. C) Analysis revealed a significant decrease in cells with spindle angles <5° in MDCKII<sup>mChEB2Hi</sup> cells compared to MDCKII<sup>mChEmpty</sup> cells while a significant increase in cells with spindle angles >5°. Statistical significance was assessed by two-way ANOVA. Statistical significance was assessed by one-way ANOVA with Tukey's multiple comparison test. Graphs B and C were derived from the same data. No of cells per condition = 40 based on one experiment. Mean ± SEM

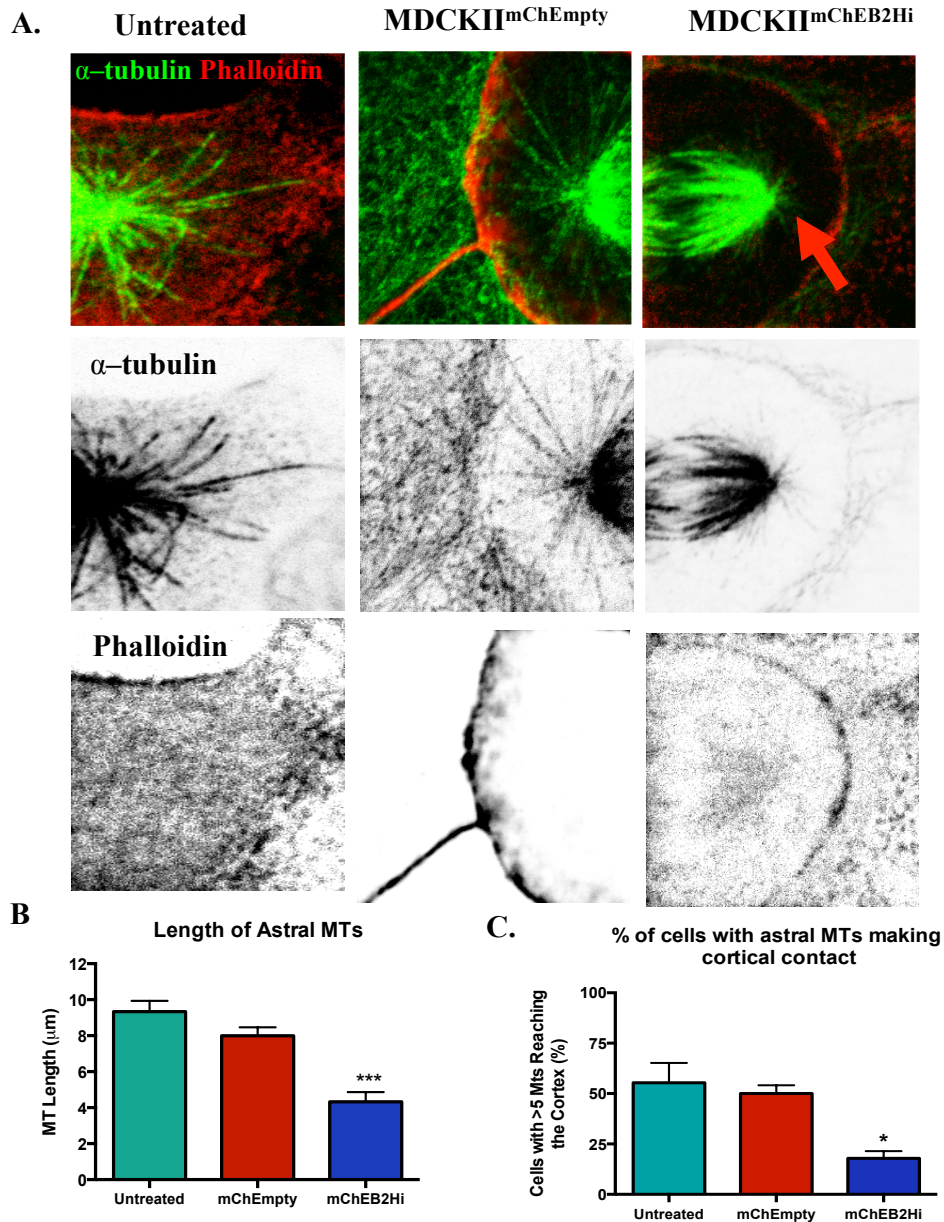


**Figure 6.18: EB2-overexpressing MDCKII cells exhibited defects in astral MTs making contact with the periphery.**

Synchronised cells were fixed in PHEMO and immunolabelled with an anti- $\alpha$ -tubulin antibody (green, pAb) and stained for actin (red) with phalloidin to outline the periphery. A) Images taken on the confocal microscope shows astral MTs radiating out from the spindle poles towards the cell cortex. The images indicate that fewer astral MTs make contact with the cortex in MDCKII<sup>mChEB2Hi</sup> compared to MDCKII<sup>mChEmpty</sup> cells. B) ImageJ was used to analyse the MT length. The graph shows a significant decrease in the length of astral MTs emanating from the spindle pole in MDCKII<sup>mChEB2Hi</sup> cells. C) ImageJ was used to analyse the number of MTs reaching the cortex. The graph shows a significant decrease in the number of cells with more than 5 astral MTs reaching the cortex in MDCKII<sup>mChEB2Hi</sup> cells. Statistical significance was assessed by one-way ANOVA with Tukey's multiple comparisons test based on 20 cells per condition from one experiment. Mean  $\pm$  SEM.

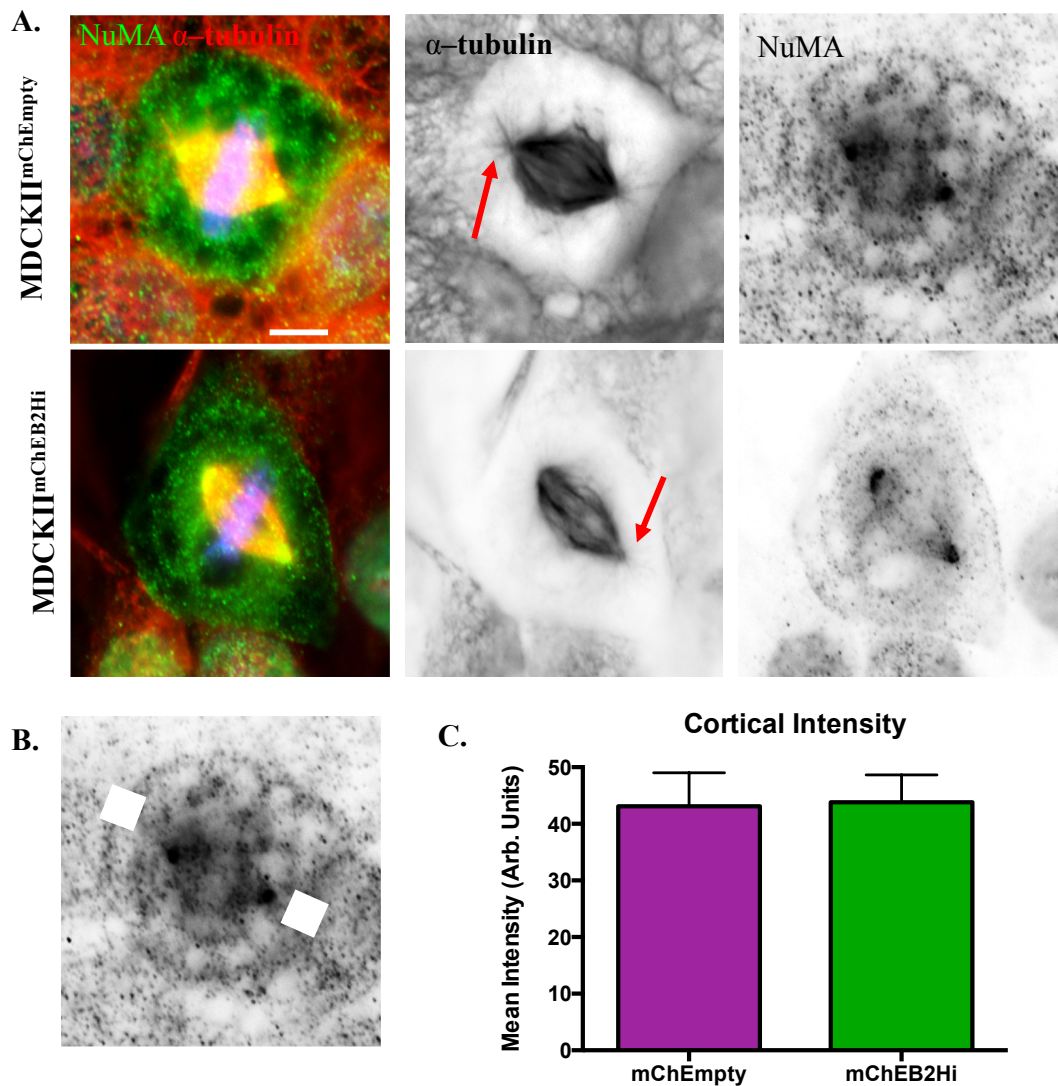


**Figure 6.19: EB2-overexpressing cells exhibited no significant change in cortical NuMA intensity.** Synchronised cells were fixed in methanol and immunolabelled for  $\alpha$ -tubulin (red, mAb YL1/2) and NuMA (green, pAb) to analyse NuMA accumulation at the cortex A) Images taken on the widefield fluorescent microscope shows MTs radiating out from the spindle poles towards the cell cortex (red arrows). Images suggest no changes in NuMA at the cortex in MDCKII<sup>mChEB2Hi</sup> cells compared to MDCKII<sup>mChEmpty</sup> cells. B) Illustrates analysis of each cell. A box of 25  $\mu$ m by 25  $\mu$ m is placed at the cell cortex directly opposite the spindle poles and then fluorescence intensity measured. C) ImageJ was used to analyse NuMA fluorescence intensity at the cortex. The graph shows no significant change in the intensity of cortical NuMA in MDCKII<sup>mChEB2Hi</sup> compared to MDCKII<sup>mChEmpty</sup> cells. Statistical significance was assessed by unpaired t-test. Results based on 20 cells from one experiment. Mean  $\pm$  SEM. Scale bar = 10  $\mu$ m.

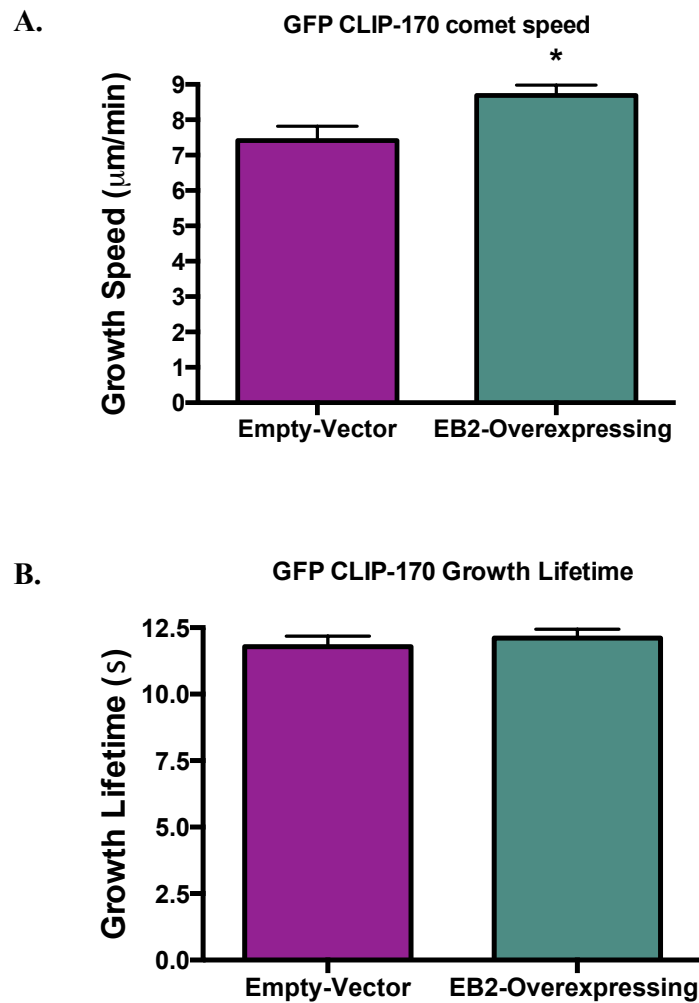


**Figure 6.20: EB2-overexpression leads to increased CLIP-170 comet speed but not growth lifetime events.**

GFP-CLIP-170 comet in MDCKII<sup>mChEmpty</sup> and MDCKII<sup>mChEB2Hi</sup> cells were analysed to assess MT dynamics. A) MDCKII<sup>mChEB2Hi</sup> cells reveal a significant increase in the mean of comets speed compared to MDCKII<sup>mChEmpty</sup> cells. B) The growth lifetime of MTs is not statistically significant in the MDCKII<sup>mChEB2Hi</sup> cells when compared to the MDCKII<sup>mChEmpty</sup> cells. Statistical significance was assessed by unpaired t-test.

[\*P<0.05] Ten cells analysed based on one experiment. Mean  $\pm$  SEM

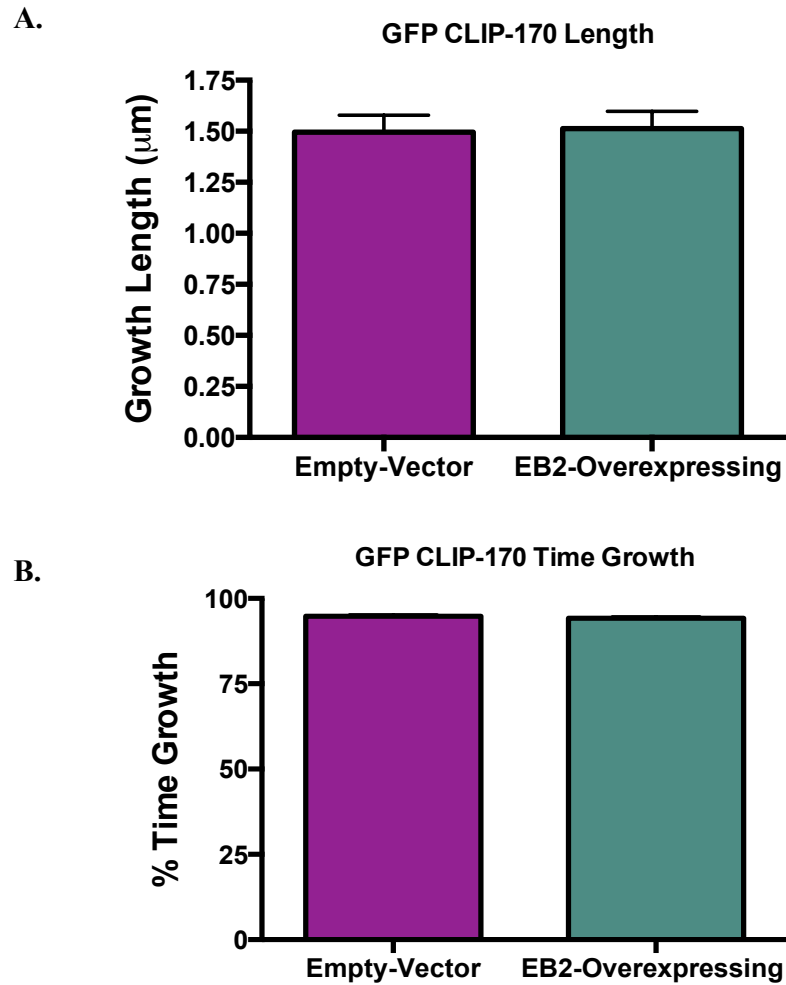


**Figure 6.21: EB2-overexpression does not alter the MT growth length and overall % time growth.** GFP-CLIP-170 comet in MDCKII<sup>mChEmpty</sup> and MDCKII<sup>mChEB2Hi</sup> cells were analysed to assess MT dynamics. A) MDCKII<sup>mChEB2Hi</sup> cells show no significant difference in the mean of growth length compared to MDCKII<sup>mChEmpty</sup> cells. B) The overall percentage MTs spent in the growth phase is not statistically significant in the MDCKII<sup>mChEB2Hi</sup> cells when compared to the MDCKII<sup>mChEmpty</sup> cells. Statistical significance was assessed by unpaired t-test. Ten cells analysed based on one experiment. Mean  $\pm$  SEM

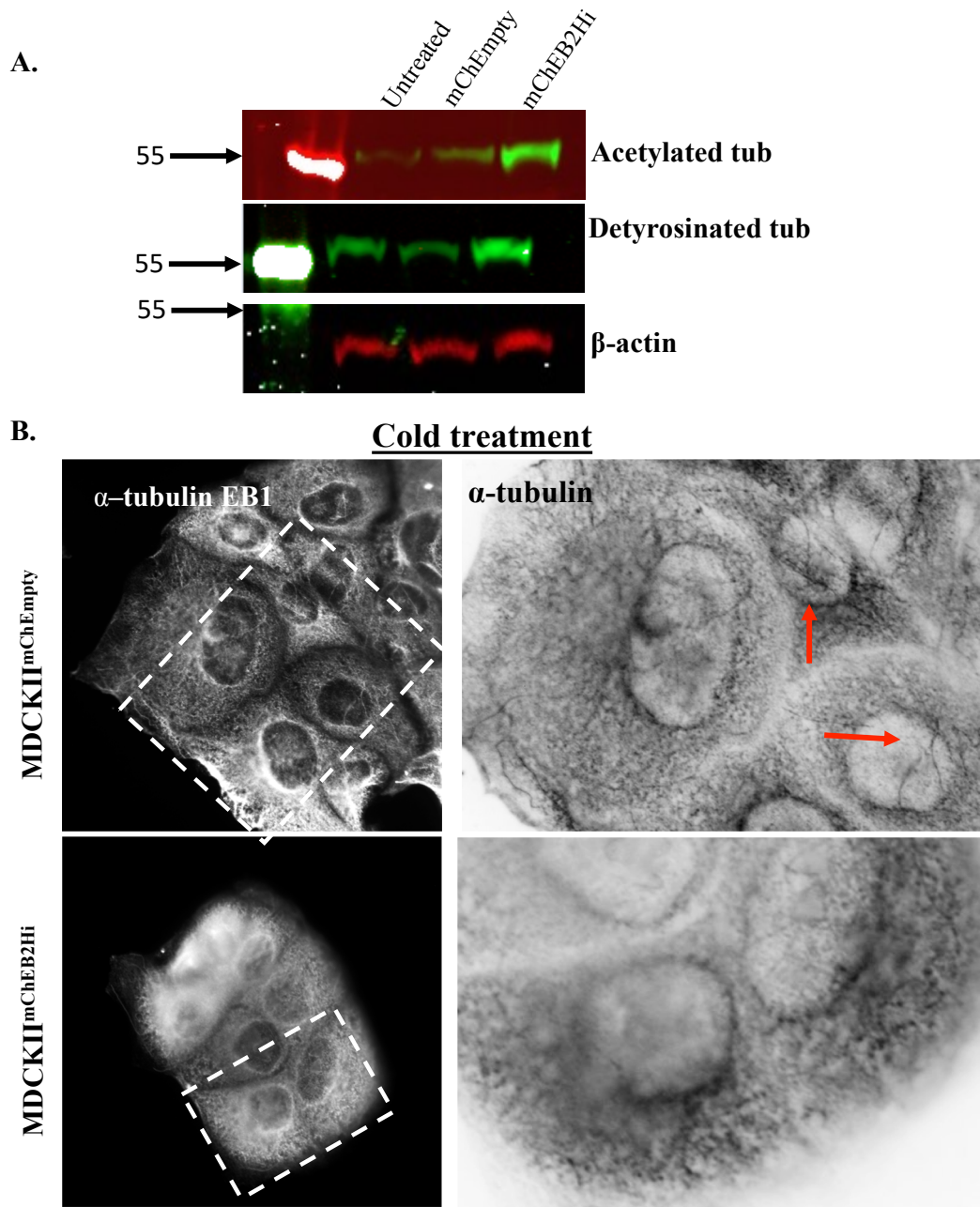


**Figure 6.22: EB2-overexpression led to increased acetylated and detyrosinated tubulin but reduced stability of MTs when 2D MDCKII cells are cold treated.** A) Western blot suggests there is a slight increase in acetylated tubulin and detyrosinated tubulin expression levels in MDCKII<sup>mChEB2Hi</sup> cells compared to the MDCKII<sup>mChEmpty</sup> cells. Molecular weight of both acetylated and detyrosinated tubulin = 50kDa.  $\beta$ -actin was used as loading control, molecular weight = 42kDa. B) The incubation of MDCKII<sup>mChEmpty</sup> cells on ice for 10 min revealed that all but a few MTs had depolymerised (arrows in enlarged region). Similarly, MDCKII<sup>mChEB2Hi</sup> cells also revealed a marked reduction in stable MTs (enlarged single channel). Scale bar =10 $\mu$ m.

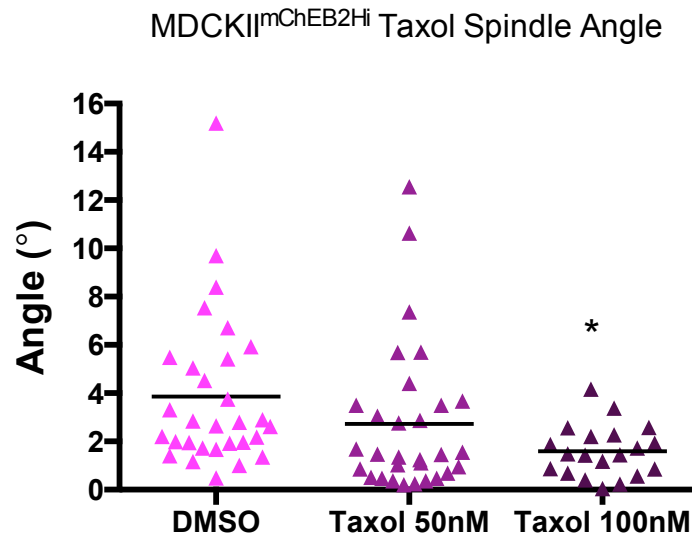


**Figure 6.23: Taxol Treatment rescued spindle orientation defects in MDCKII<sup>mChEB2Hi</sup> cells.** Thymidine-treated MDCKII<sup>mChEB2Hi</sup> cells were treated with DMSO or Taxol for 9 h before fixing in PHEMO and immunolabelling. Volocity software was used for analysing the spindle poles. The graph shows no significant difference in spindle angle when cells were treated with 50 nM Taxol compared to DMSO-control cells. A significant decrease in spindle angle was evident in cells treated with 100 nM taxol resulting in a 0.58x fold change. Statistical significance was assessed by one-way ANOVA with Tukey's multiple comparison test. No of cells per condition = 30. Results derived from one experiment. Mean  $\pm$  SEM.

# **Chapter VII: EB2 Overexpression and Multispindle Formation**

## **7.1 Overview**

The objective of this chapter is to investigate how EB2 overexpression plays a role in multipolar spindle formation. Multipolar spindles are associated with supernumerary centrosomes and chromosome instability that may arise from the activation or deactivation of oncogenes or tumour suppressor genes, which may contribute to cancer progression. The process is well-studied in contexts such as in Plk4 overexpression. However, since multipolar spindles were mainly observed in the MDCKII<sup>mChEB2<sup>Hi</sup></sup> cells, it was important to understand the molecular role of EB2 overexpression that leads to supernumerary centrosomes, cytokinesis failure and/or loss of spindle pole integrity.

## **7.2 Introduction**

Centrosome amplification is a hallmark of cancer. Monopolar spindles arise when centrosome separation fails during mitosis while multipolar spindle formation is caused by the presence of extra centrosomes. Plk4 is a major protein that regulates centriole duplication. Levels of Plk4 are regulated by SCF/Slimb ubiquitin ligase proteolysis, which is controlled by its autophosphorylation (Cunha-Ferreira et al., 2009). Plk4 overexpression leads to the generation of extra centrioles and thus also centrosomes as shown in a non-transformed mammary cell line (Godinho et al., 2014). When centrosomes are amplified through Plk4 overexpression, the consequences are chromosome missegregation and aneuploidy, and these extra centrosomes can direct spontaneous intestinal tumour development (Levine et al., 2017). Plk4 overexpression in connection with a truncated APC was utilised to study the impact on centrosome number. Tumour numbers but not size was altogether increased in intestines of mice bearing the truncated APC allele and Plk4 overexpression. This was because of the inactivation of the p53 pathway resulting in p53 not being able completely block the advancement of tumourigenesis (Levine et al., 2017). Centrin is also required for centriole duplication, which moves distally as the procentriole elongates. Depletion of centrin-2 led to centriole duplication defects in HeLa cells (Salisbury et al., 2002). Also, it is a good marker for studying centriole overduplication.

Centrosome amplification or cytokinesis failure are ways supernumerary centrosomes and chromosome instability arise that often lead to multiple spindles observed in certain cancers (Lingle et al., 1998, Chan, 2011). One way to suppress multipolar cell division is by clustering supernumerary centrosomes into two groups for mitosis thus forming pseudo-bipolar spindles (Brinkley, 2001, Quintyne et al., 2005). Multipolar spindles are often observed in cancer cell lines as evidenced in cultured vertebrate cells whereby extra centrosomes failed to cluster (Ganem et al., 2009, Quintyne et al., 2005). The presence of p53 in mouse embryonic fibroblasts prevents the formation of multipolar spindles while the knock-out of p53 or mutation led to impaired centrosome clustering by suppressing RhoA/ROCK signalling pathway (Yi et al., 2011). Chromosome instability is generated in cells with centrosomes amplification when majority of the spindles are bipolar. This was due to the establishment of merotelic attachments, in which a single kinetochore is attached to both spindle poles (Ganem et al., 2009, Holland and Cleveland, 2009, Silkworth et al., 2009). These types of attachments are not always corrected at the spindle assembly checkpoint because there are MT attachments, even though they are incorrect thus, allowing mitosis progression. Uncorrected merotelic attachments generates an increased frequency of lagging chromosomes during anaphase.

A recent study in glioblastoma (SGB4) cells reported that in a significant number of cells, bipolar mitoses with failed cytokinesis occurred prior to multipolar mitoses (Telentschak et al., 2015). Failed cytokinesis is expected to cause an increase in chromosome and centrosome numbers. The study also found that multipolar mitoses in SGB4 cells produced viable daughter cells and were able to undergo subsequent mitoses, which is in contrast to the study by Ganem and co-workers (2009). There are times when multipolar spindles are not caused by centrosome amplification but rather through centriole disengagement or PCM fragmentation (Maiato and Logarinho, 2014), which was considered in this study. Centriole disengagement precedes centriole duplication initiation during the centrosome duplication cycle and occurs when there are defects in centriole cohesion that drives centriole partition before the end of chromatid segregation causing multipolar spindle formation (Stevens et al., 2011).

Cep215 (also known as CDK5RAP2) and Cep68 are proteins required for maintaining centrosome cohesion. Graser and colleagues (2007) found that Cep215

remained at the centrosome throughout mitosis but not particularly at a certain phase therefore, was probably not directly involved in regulating the linker structure. However, they proposed an indirect mechanism by which Cep215 would be involved in regulating centrosome cohesion. This would be through Cep215 interacting with centrosome-MTs possibly affecting the transport of structural proteins required for centrosome cohesion. (Graser et al., 2007). It has been reported that Cep215 has a MT plus-end tracking motif, SXIP motif, that allows it to bind to MTs via EB1 and regulate its dynamics (Fong et al., 2009). In addition to the SXIP motif, Cep215 also interacts with EB1 via its dimerisation domain. It is thought that Cep215 has a regulatory role when associated with EB1 for MT tracking because the MT plus-end tracking of EB1 is increased and its exchange reduced due to the di-/multimerisation of the bound SXIP sequence thus, Cep215 plays an active role on EB1 rather than passively hitchhiking (Fong et al., 2017). A proteomics analysis of SXIP domain interaction found Cep215 as a possible binding partner of EB2 (Jiang et al., 2012) and the aim is to confirm this with co-IP in future experiments.

Apart from centriole disengagement, loss of spindle pole integrity may be due to PCM fragmentation. PCM fragmentation is caused by loss of centrosome integrity, which generates acentriolar fragments that can nucleate spindle MTs that associate with chromosomes. Several centrosomal proteins such as ninein, centrin-2 and PCM-1 are known to accumulate at pericentriolar satellites and are transported along MTs by dynein. Ninein, chTOG or Aurora A depletion caused PCM fragmentation and led to the formation of multipolar spindles irrespective of p53 present or not (Dammermann and Merdes, 2002, Kimura et al., 2013, De Luca et al., 2008). Therefore, these proteins are required to maintain spindle pole integrity.

## 7.3 Results

### 7.3.1 EB2-overexpression leads to a significant increase in cells with multipolar spindles

MDCKII cells were seeded on a thin layer of Matrigel and allowed to adhere for 24 h prior to double-blocking with thymidine and then immunolabelling for  $\alpha$ -tubulin and  $\gamma$ -tubulin. Matrigel was used to generate partially polarised cells. Confocal microscopy optical sections through the entire spindle were taken at 0.2  $\mu\text{m}$  intervals. Unexpectedly, some MDCKII<sup>mChEB2Hi</sup> cells exhibited multipolar spindles (Fig 7.1 and 7.2, Movie S28). Forty cells per condition, from randomly acquired images, were analysed from one experiment by counting the numbers of cells with bipolar and multiple spindles. The results showed that about 40% of MDCKII<sup>mChEB2Hi</sup> cells had multipolar spindles compared to MDCKII<sup>mChEmpty</sup> cells, while the rest formed bipolar spindles. Statistical assessment by two-way ANOVA revealed a significant increase in the number of multiple spindles in MDCKII<sup>mChEB2Hi</sup> cells compared to MDCKII<sup>mChEmpty</sup> cells (Fig 7.3).

### 7.3.2 Supernumerary Centrioles

Centrin is a protein required for centriole duplication (Salisbury et al., 2002). It is concentrated within the central lumen of the centrioles and is therefore well suited as a centriole marker and for studying centriole overduplication. Cells were fixed in methanol and immunolabelled for centrin,  $\gamma$ -tubulin and DAPI. Widefield fluorescent images of mitotic cells revealed bipolar spindle formation in MDCKII<sup>mChEmpty</sup> cells and in some MDCKII<sup>mChEB2Hi</sup> cells (Fig 7.4A and B). However, some MDCKII<sup>mChEB2Hi</sup> cells showed multipolar formation with centrioles at each spindle pole (Fig 7.4C). Supernumerary centrioles caused by PCM fragmentation was ruled out because centrioles were present at each spindle pole in MDCKII<sup>mChEB2Hi</sup> cells. In interphase, MDCKII<sup>mChEmpty</sup> cells had mainly two centrioles (Fig 7.5A) as was also the case for some of the MDCKII<sup>mChEB2Hi</sup> cells while other cells revealed multiple centrioles (Fig 7.5B). Analysis established that there was a significant increase in the number of MDCKII<sup>mChEB2Hi</sup> cells with more than 4 centrioles compared to MDCKII<sup>mChEmpty</sup> cells

(Fig 7.6). This preliminary analysis was based on one experiment of 20 cells per condition and the statistical significance was assessed by two-way ANOVA.

### **7.3.3 PLK4 is not overexpressed in EB2-overexpressing MDCKII cells**

These preliminary findings suggested that EB2 overexpression is associated with centriole amplification and not PCM fragmentation. Plk4 is the master regulator of centriole duplication (Habedanck et al., 2005, Godinho et al., 2014). The expression of Plk4 was therefore investigated in MDCKII<sup>mChEmpty</sup> and MDCKII<sup>mChEB2Hi</sup> cells (Godinho et al., 2014). Synchronised cells were fixed in PHEMO and immunolabelled for Plk4,  $\gamma$ -tubulin and stained for DAPI. Widefield fluorescent images showed Plk4 co-localising with  $\gamma$ -tubulin at the spindle poles (centrosomes) within bipolar spindles in MDCKII, MDCKII<sup>mChEmpty</sup> and MDCKII<sup>mChEB2Hi</sup> cells (Fig 7.7A and B). MDCKII<sup>mChEB2Hi</sup> cells with, for example, tripolar spindle formation showed Plk4 and  $\gamma$ -tubulin at all three spindle poles (Fig 7.7C).

Simultaneously, all three sub-cell lines were cultured to confluency and lysates collected for Western blotting. In all three cell lysates. A double band at 109kDa for Plk4 was evident. The second band might be due to post-translational modification but needs to be verified. The western did not suggest that Plk4 is overexpressed in MDCKII<sup>mChEB2Hi</sup> cells compared to MDCKII<sup>mChEmpty</sup> or MDCKII cell lysates (Fig 7.8).  $\beta$ -actin was used as a loading control. The Western Blot shown is one of two independent experiments.

### **7.3.4 EB2 overexpression in MDCKII cells may induce cytokinesis failure while centriole engagement seems unaffected.**

As mentioned in the introduction above, cytokinesis failure is a mechanism through which centrosomes could increase in number and cause multipolar spindles. This was therefore important to establish whether this was the case for MDCKII<sup>mChEB2Hi</sup>

cells. Cells were seeded to confluency, fixed in methanol and immunolabelled for E-cadheren and stained for DAPI. E-cadheren was used to mark the cell periphery in all three sub-cell lines. Widefield fluorescent images show E-cadheren localisation to the periphery of cells. MDCKII and MDCKII<sup>mChEmpty</sup> cells revealed a single nucleus per cell while some MDCKII<sup>mChEB2Hi</sup> cells had more than one nucleus (Fig 7.9A-C). Subsequently, randomly acquired image frames were analysed for cells with more than one nucleus. Analysis of the number of nuclei per cell showed no significant difference in the number of cells with more than one nucleus in MDCKII, MDCKII<sup>mChEmpty</sup> and MDCKII<sup>mChEB2Hi</sup> (Fig 7.10A). However, cytokinesis failure could also be manifested by an increase in nuclear size as a consequence of nuclear fusion. Nuclear diameter was assessed, and ImageJ was used to mark the circumference of each nucleus. The data presented is from one experiment and based on twenty cells per condition and shows a significant increase in the diameter of MDCKII<sup>mChEB2Hi</sup> compared with MDCKII<sup>mChEmpty</sup> cells suggesting that cytokinesis failure could be a reason for the supernumerary centrosomes. However, further analysis would be needed to verify this (Fig 7.10B).

Apart from centrosome amplification, there are times when multipolar spindles are caused through centriole disengagement (Maiato and Logarinho, 2014), so this was also tested using Cep215 as a marker. EB2 may interact with Cep215 as indicated in a proteomics analysis, but this remains to be verified by Co-IP (Jiang et al., 2012). However, it was hypothesised that overexpression of EB2 leads to the sequestering of Cep215 from the centrosome thus causing centriole disengagement. Cells were fixed in methanol and immunolabelled for Cep215,  $\gamma$ -tubulin and stained for DAPI. Images were taken using the same exposure time for all in order for intensity analysis to be completed. Widefield fluorescent images showed mitotic MDCKII<sup>mChEmpty</sup> and MDCKII<sup>mChEB2Hi</sup> cells with Cep215 localisation at each pole (Fig 7.11A and B). ImageJ was used to analyse the fluorescence intensity of Cep215. Very preliminary data show no significant differences in Cep215 fluorescent intensity in MDCKII<sup>mChEB2Hi</sup> cells compared to MDCKII<sup>mChEmpty</sup> cells based on twenty cells per condition from one experiment suggesting no centriole sequestering by EB2 in MDCKII<sup>mChEB2Hi</sup> cells (Fig 7.11C).

## 7.4 Discussion

### 7.4.1 EB2-overexpression leads to the formation of multipolar spindles but not through Plk4 overexpression

The results acquired in this chapter were unexpected and occurred towards the end of this PhD project, therefore, limited number of experiments could be carried out and the findings are very preliminary.

The present study identified an unexpected, possible role of EB2-overexpression in multispindle formation. MDCKII<sup>mChEB2Hi</sup> cells had an increased proportion of cells with multiple spindles (approx. 40%), an observation that was not seen in MDCKII<sup>mChEmpty</sup> cells. In a normal cell during mitosis, centrioles duplicate once per cell cycle and only one daughter centriole is formed per mother centriole. Some studies have mentioned that multispindles are due to centrosome amplification (Lingle et al., 1998, Pihan et al., 1998, Chan, 2011). Though our findings suggest centriole overduplication in MDCKII<sup>mChEB2Hi</sup> cells was not due to Plk4 overexpression as previously reported (Godinho et al., 2009, Habedanck et al., 2005, Rosario et al., 2010). However, it is possible that the amount of active Plk4 is higher in EB2 overexpressing cells and this needs to be investigated further. Western blot images in Fig 7.8 show double bands for Plk4 expression suggesting some form of post-translational modification, maybe phosphorylation. A next step would be to use a phosphorylated-specific Plk4 antibody to probe the cell lines to confirm whether Plk4 is phosphorylated or not.

Maiato and Logarinho (2014) reported that centrosome amplification may sometimes be due to cytokinesis failure, centriole disengagement or PCM fragmentation. So, steps were taken to check if there was disruption during cytokinesis (i.e. cytokinesis failure), centriole disengagement or PCM fragmentation. The preliminary data indicated no change in Cep215 at the spindle poles in MDCKII<sup>mChEB2Hi</sup> compared to MDCKII<sup>mChEmpty</sup> and MDCKII<sup>WT</sup> thus suggesting that EB2 does not sequester Cep215 from the centrosomes. However, preliminary findings suggest MDCKII<sup>mChEB2Hi</sup> cells may possess more than one nucleus. Cytokinesis failure may not

only cause supernumerary centrosomes but also a particularly dangerous event, whereby cells emerging from disrupted divisions will possess both multiple centrosomes and duplicated genomes. In essence, cytokinesis failure leads to both centrosome amplification and polyploidy (Nigg, 2006). Duplicated genome and polyploidy in the MDCKII<sup>mChEB2Hi</sup> and MDCKII<sup>mChEmpty</sup> could be established by using FACS analysis to determine if the set of chromosomes are diploid or tetraploid in the MDCKII<sup>mChEmpty</sup> and MDCKII<sup>mChEB2Hi</sup> cells.

There are three members of the Aurora kinase family – Aurora A, B and C. All three kinases share similar structures, with their catalytic domains flanked by very short C-terminal tails and N-terminal domains of variable lengths but differ in their expression patterns, subcellular localisation and timing of activity (Adams et al., 2001). Aurora A localises to both spindle poles and spindle MTs during early mitosis whereas Aurora B first associates with kinetochores then relocates to the midzone of the central spindle, and at the midbody between dividing cells (Adams et al., 2001). Aurora A is frequently overexpressed in human cancers including breast, bladder, ovarian and pancreatic cancer, and has been used to provide evidence for cytokinesis failure causing centrosome amplification (Meraldi et al., 2002, Meraldi et al., 2004). Though, very recently, Aurora B was found to phosphorylate EB2 during mitosis (Iimori et al., 2016b). Aurora B and EB1 colocalise on the central spindle during anaphase and in the midbody during cytokinesis. Overexpression of EB1 augments Aurora B activity by inhibiting its dephosphorylation by protein phosphatase 2A (Sun et al., 2008). The opposite may be true when EB2 is overexpressed that is the activity of Aurora B is reduced or non-functional, which prevents the detachment of EB2 from MTs. The reduction of aurora B activity might then prevent the recruitment of one of its substrates TACC1 to the midbody as reported by (Delaval et al., 2004). Thereby the lack of TACC1 recruitment prevents correct cytokinesis and eventually leads to the formation of multipolar spindles.

Furthermore, it is possible that the proportion of cells having multipolar spindles would have been higher but due to the centrosome clustering mechanism (though this was not particularly observed in my fixed staining experiments), some cells with extra centrosomes can still undergo a bipolar spindle assembly thus, producing two daughter cells. The remaining cells, which are unable to cluster their centrosomes are the ones

with multipolar spindles. It is not clear what happens to the chromosomes once the cells have gone through division. A way this could be verified is by fluorescent tagging the MTs and chromosomes, then follow some cells from the beginning of the cell division to the end, using live-imaging microscopy. This approach should help establish the subsequent fate of chromosomes from multipolar spindles. Since there was no observation of Plk4 overexpression in MDCKII<sup>mChEB2Hi</sup> cells, we could speculate that the supernumerary centrioles seen in MDCKII<sup>mChEB2Hi</sup> cells are caused after the centriole duplication phase of the centrosome duplication cycle; because Plk4 has a major role in the centriole duplication phase but no alterations were observed.

## **7.5 Summary**

In summary, experiments involving overexpression of EB2 have produced extremely promising results connecting EB2 to previously unknown role in multiple spindle formation. MDCKII<sup>mChEB2Hi</sup> cells were found to have a significant number of multispindles compared to the MDCKII<sup>mChEmpty</sup> cells. The mechanism appears to be through cytokinesis failure with MDCKII<sup>mChEB2Hi</sup> cells showing a significant increase in nucleus size. The study also discovered through Western blots and immunolabelling experiments that Plk4 was not overexpressed in MDCKII<sup>mChEB2Hi</sup> cells therefore, may not be the cause of multispindles formation although it is still possible that more active Plk4 is associated with MDCKII<sup>mChEB2Hi</sup> compared to MDCKII<sup>mChEmpty</sup> cells. Further investigations need to be done to fully understand the mechanism governing EB2 overexpression and multispindle formation.

**Fig 7.1: Multipolar spindle formation in MDCKII<sup>mChEB2Hi</sup> cells.** Synchronised cells were fixed in PHEMO and immunolabelled for  $\alpha$ -tubulin (green, pAb, ab15246) and  $\gamma$ -tubulin (red, mAb, ab11316) and stained with DAPI. Confocal optical section show one cell with four spindle poles denoted by red arrows in the single channel. Note that spindle MTs originate from the four poles appear to make contact with chromosomes and the chromosomes can be seen to be organised in several planes. Scale bar = 10 $\mu$ m.

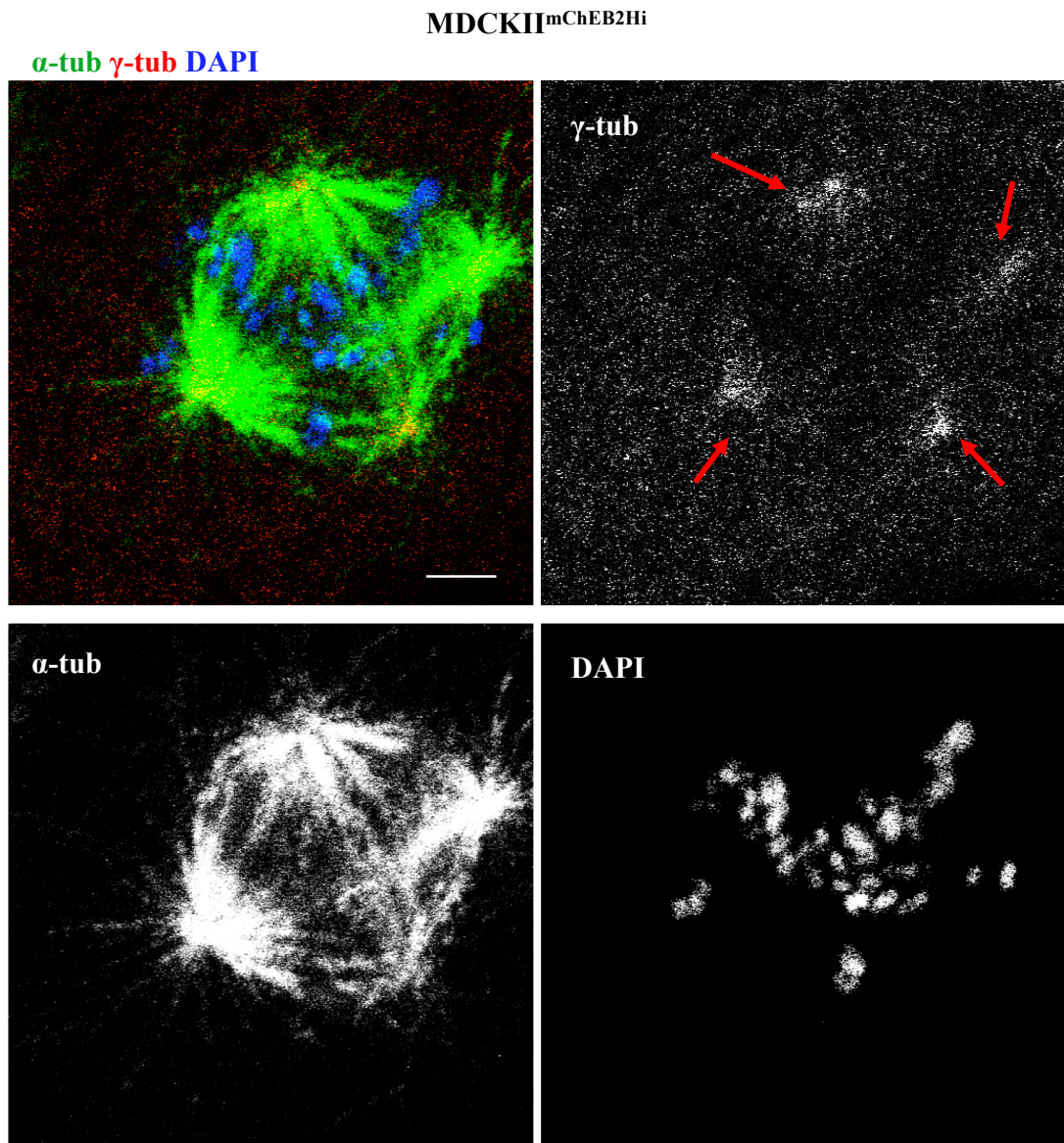


**Figure 7.1: Multipolar spindle formation in MDCKII<sup>mChEB2Hi</sup> cells.** Synchronised cells were fixed in PHEMO and immunolabelled for  $\alpha$ -tubulin (green, pAb, ab15246) and  $\gamma$ -tubulin (red, mAb, ab11316) and stained with DAPI. Confocal optical section show one cell with four spindle poles denoted by red arrows in the single channel. Note that spindle MTs originate from the four poles appear to make contact with chromosomes and the chromosomes can be seen to be organised in several planes. Scale bar = 10 $\mu$ m.

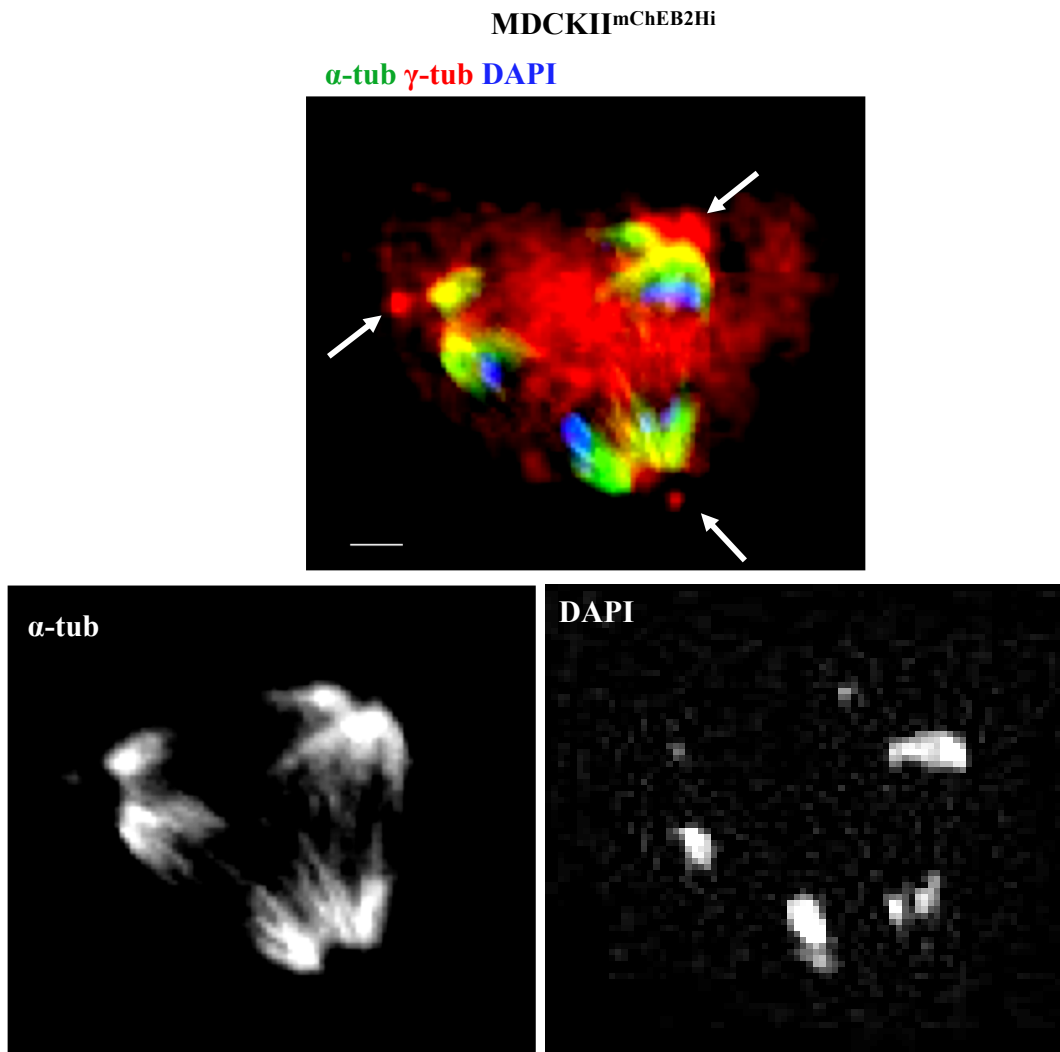


**Figure 7.2: Multipolar spindle formation in MDCKII<sup>mChEB2Hi</sup> cells.** Synchronised cells were fixed in PHEMO and immunolabelled for  $\alpha$ -tubulin (green, pAb, ab15246) and  $\gamma$ -tubulin (red, mAb, ab11316) and stained with DAPI. Widefield image using a x20 objective lens reveals one cell with three spindle poles denoted by white arrows. Parts of the chromosomes appear pulled towards each of the three poles. Scale bar = 10 $\mu$ m.

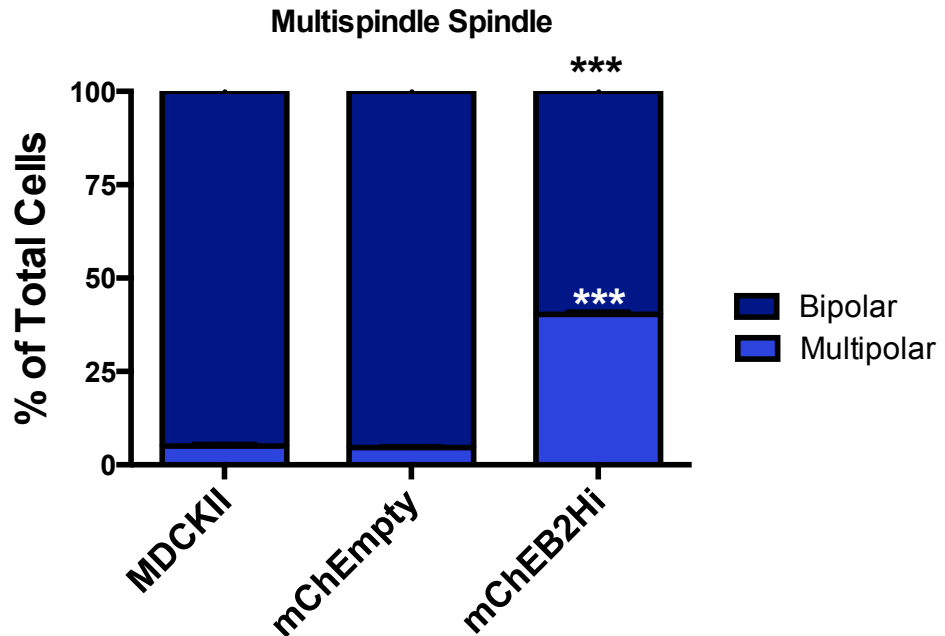


**Figure 7.3: Multipolar spindle formation in MDCKII<sup>mChEB2Hi</sup> cells.** Graph illustrates that formation of multipolar spindles is significantly increased in MDCKII<sup>mChEB2Hi</sup> cells compared to MDCKII<sup>mChEmpty</sup> and MDCKII cells. In MDCKII cells, 95% of cells still formed bipolar spindles, similarly 95.4% of MDCKII<sup>mChEmpty</sup> cells formed bipolar spindles whilst in MDCKII<sup>mChEB2Hi</sup> cells, it was 59.6%. Statistical significance was assessed by two-way ANOVA, N=40 per condition. Graph shows data from one experiment. Mean  $\pm$  SEM.

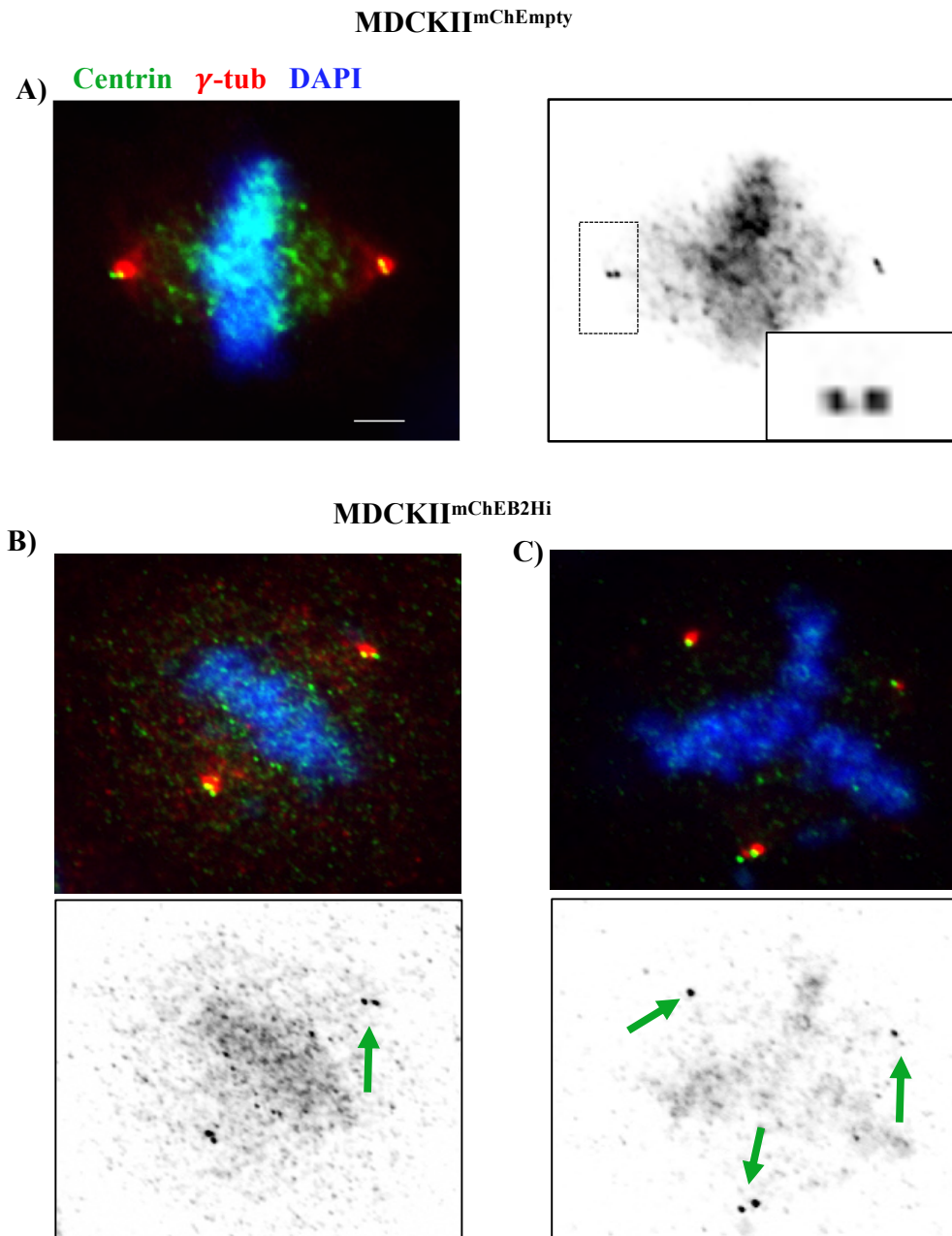


**Figure 7.4: Supernumerary centrioles in MDCKII cells.** Synchronised cells were fixed in methanol and immunolabelled for centrin (green, mAb),  $\gamma$ -tubulin (red, pAb, ab16504) and stained with DAPI. A) Widefield fluorescent image showing bipolar spindle in MDCKII<sup>mChEmpty</sup> cell with two centrioles visible at each pole (inverted image). B) Image shows MDCKII<sup>mChEB2Hi</sup> cell with two centrioles at each pole (denoted by green arrows). C) Image shows a MDCKII<sup>mChEB2Hi</sup> cell with a tripolar spindle. Centrioles can be seen at each pole (green arrows). Scale bar = 10 $\mu$ m.

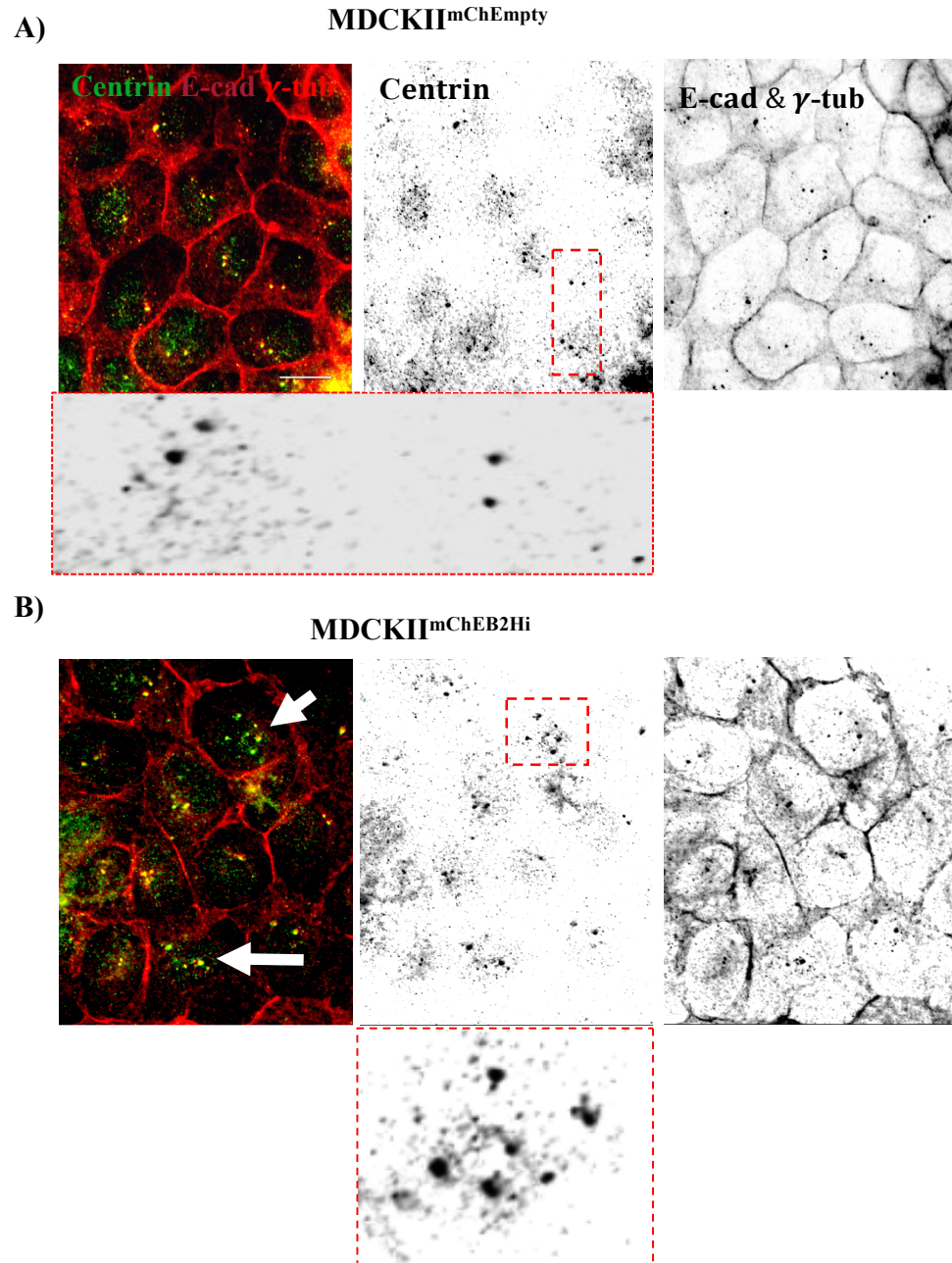


**Figure 7.5: Supernumerary centrioles in MDCKII cells.** Interphase cells were fixed in methanol and immunolabelled for centrin (green, mAb),  $\gamma$ -tubulin (red, pAb, ab16504) and E-cadheren (red, mAb, BD610181). E-cadheren was used to denote the periphery of each cell. A) Widefield fluorescent image showing MDCKII<sup>mChEmpty</sup> cells with mainly two centrioles visible in each cell (inverted enlarged region). B) Image showing some MDCKII<sup>mChEB2Hi</sup> cells with two centrioles as well as some with more than two centrioles (denoted by white arrows and enlarged region). Scale bar = 10 $\mu$ m.

### Centriole Overduplication

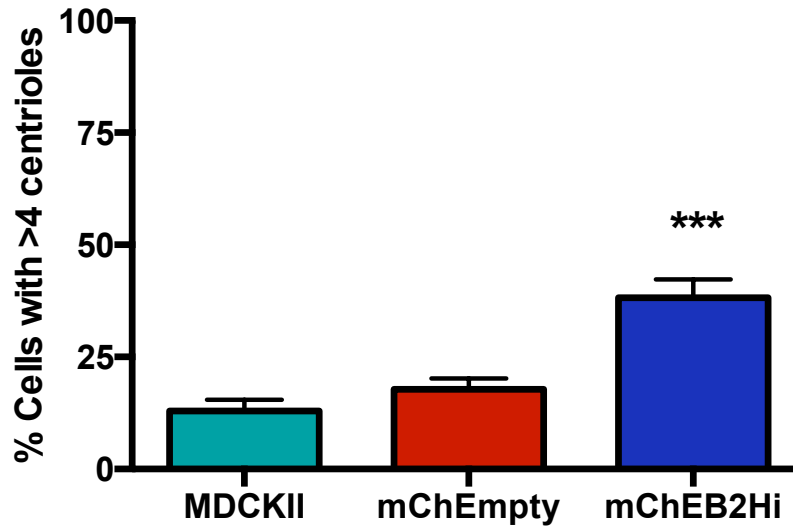


**Figure 7.6: Supernumerary centrioles in MDCKII<sup>mChEB2Hi</sup> cells.**

Graph shows a significant increase in the number of MDCKII<sup>mChEB2Hi</sup> cells with more than 4 centrioles compared to MDCKII<sup>mChEmpty</sup> cells. Results based on 20 cells per condition from one experiment. Statistical significance was assessed by two-way ANOVA. Mean  $\pm$  SEM.

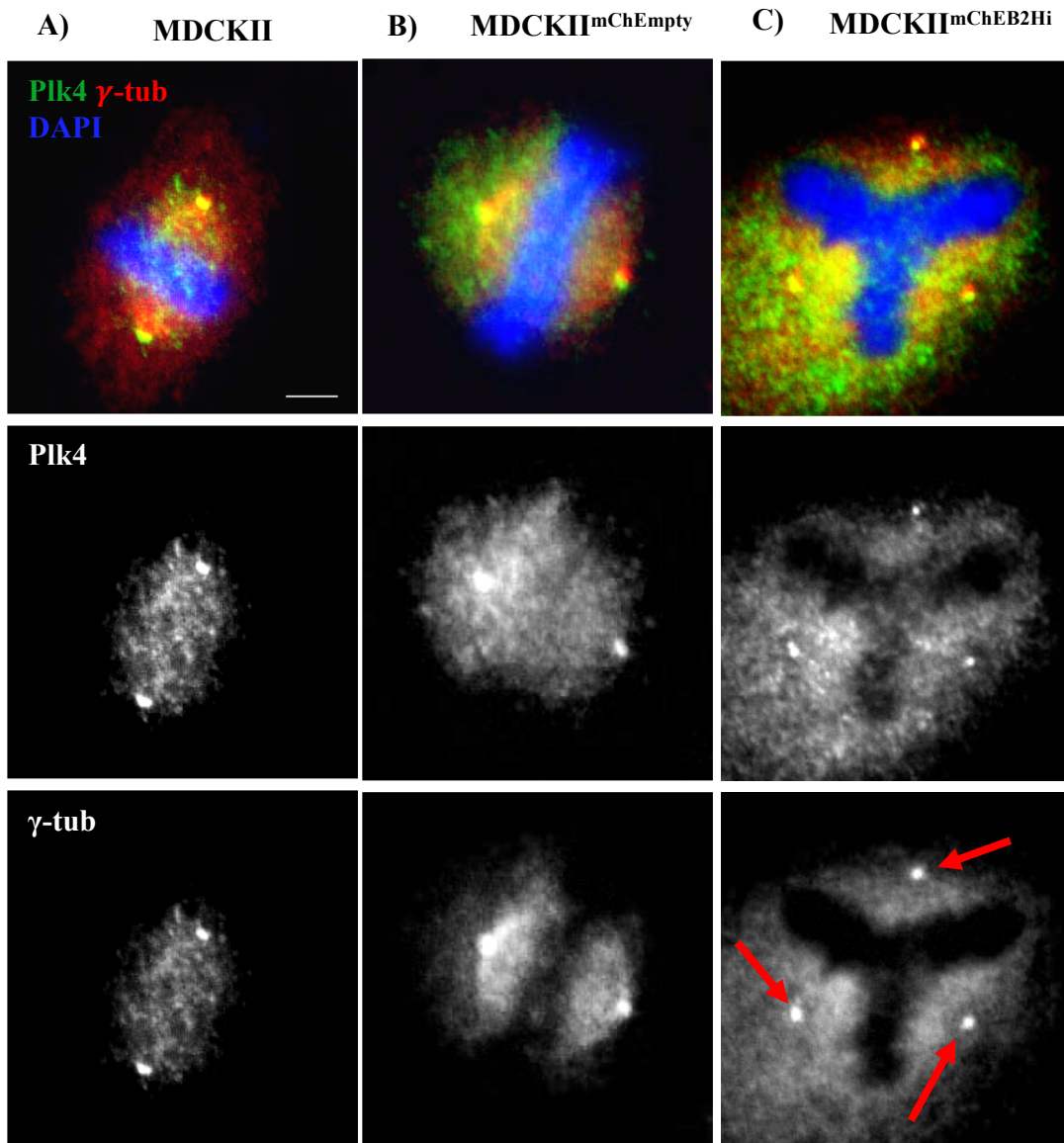


**Figure 7.7: Plk4 localisation in MDCKII, MDCKII<sup>mChEmpty</sup> and MDCKII<sup>mChEB2Hi</sup> cells.** Synchronised cells were fixed in PHEMO and immunolabelled for Plk4 (green, pAb),  $\gamma$ -tubulin (red, mAb, ab11316) and stained with DAPI. A) Widefield fluorescent image shows bipolar spindle formation in MDCKII cell with Plk4 co-localising with  $\gamma$ -tubulin at the spindle poles (centrosomes). B) Image shows MDCKII<sup>mChEmpty</sup> cell with with Plk4 co-localizing with  $\gamma$ -tubulin at the spindle poles (centrosomes).. C) Image shows MDCKII<sup>mChEB2Hi</sup> cell with tripolar spindle formation and Plk4 co-localising with  $\gamma$ -tubulin at each of the three spindle poles (centrosomes, red arrows). Scale bar = 10 $\mu$ m.

### Plk4 Expression

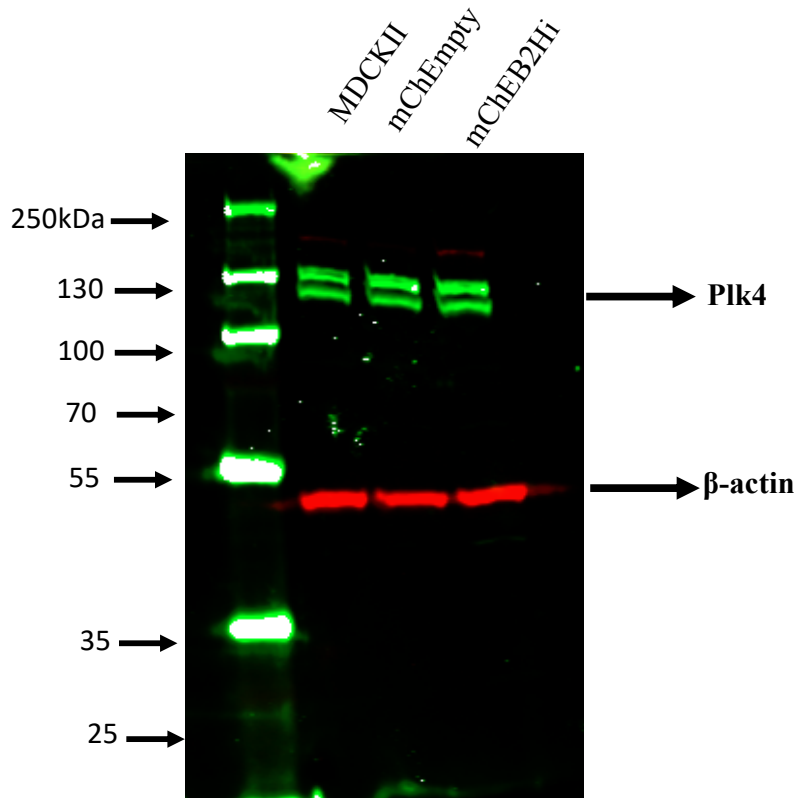


**Figure 7.8: PLK4 is not overexpressed in MDCKII cells.**

Western blot showing similar levels of expression of Plk4 in MDCKII<sup>mChEB2Hi</sup> as for MDCKII<sup>mChEmpty</sup> and MDCKII. PLK4 shows double bands at 109kDa in all of the cell lines. The second band might be due to post-translational modification but this needs to be verified. β-actin was used as a loading control. Blot shown is one of two independent experiments.

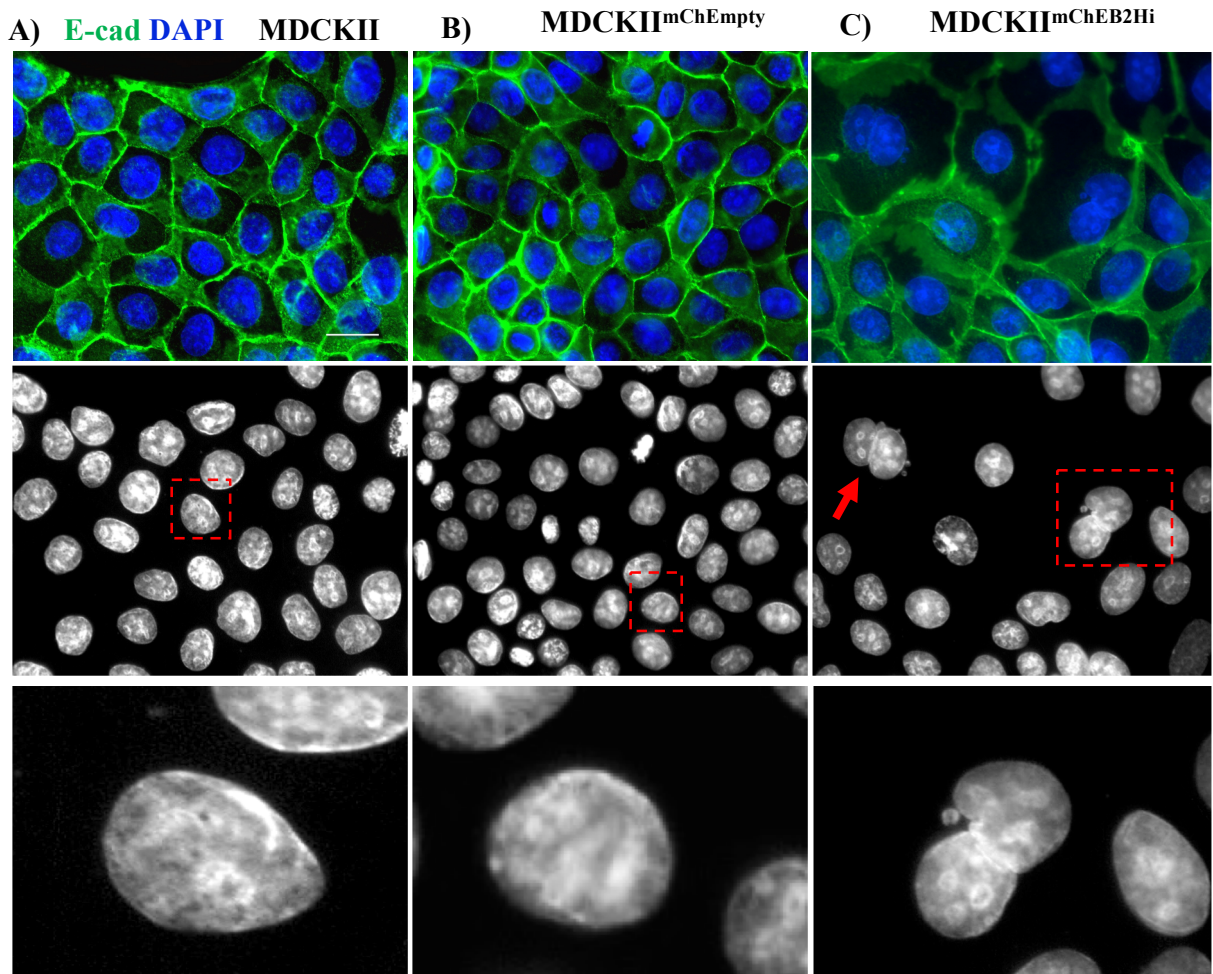


**Figure 7.9: EB2 overexpressing MDCKII cells may possess more than one nucleus.** Interphase cells were fixed in methanol and immunolabelled for E-cadherin (green, mAb, BD610181) and stained with DAPI. Widefield fluorescent images showing E-cadherin localisation at cell junctions in all three sub-cell lines. A and B) MDCKII and MDCKII<sup>mChEmpty</sup> cells showing one nucleus per cell. Single channel images show the nuclei. C) Some MDCKII<sup>mChEB2Hi</sup> cells showing more than one nucleus (red arrows and enlarged region). Scale bar = 10  $\mu$ m.

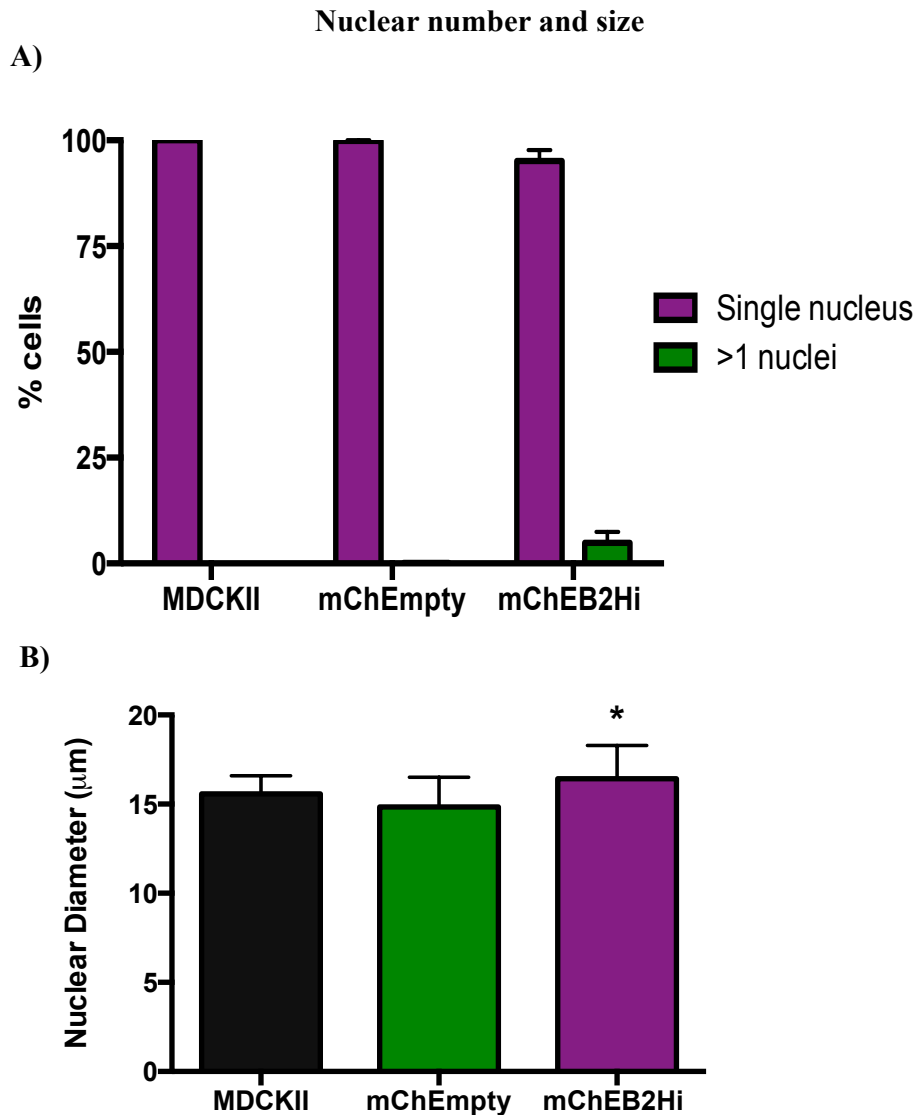


**Figure 7.10: EB2 overexpressing MDCKII cells may possess an increase in nucleus diameter.**

A) Images were used to analyse for numbers of nuclei per cells and the number of cells with more than one nucleus is presented as a percentage. Graph shows no significant difference in the number of cells with more than one nucleus. B) ImageJ was used to mark the circumference of each nucleus in order to determine the diameter. The graph shows a significant increase in the diameter of MDCKII<sup>mChEB2Hi</sup> cells compared with MDCKII<sup>mChEmpty</sup> cells. Results are based on one experiment. No of cells analysed per condition = 20. Scale bar = 10 µm.

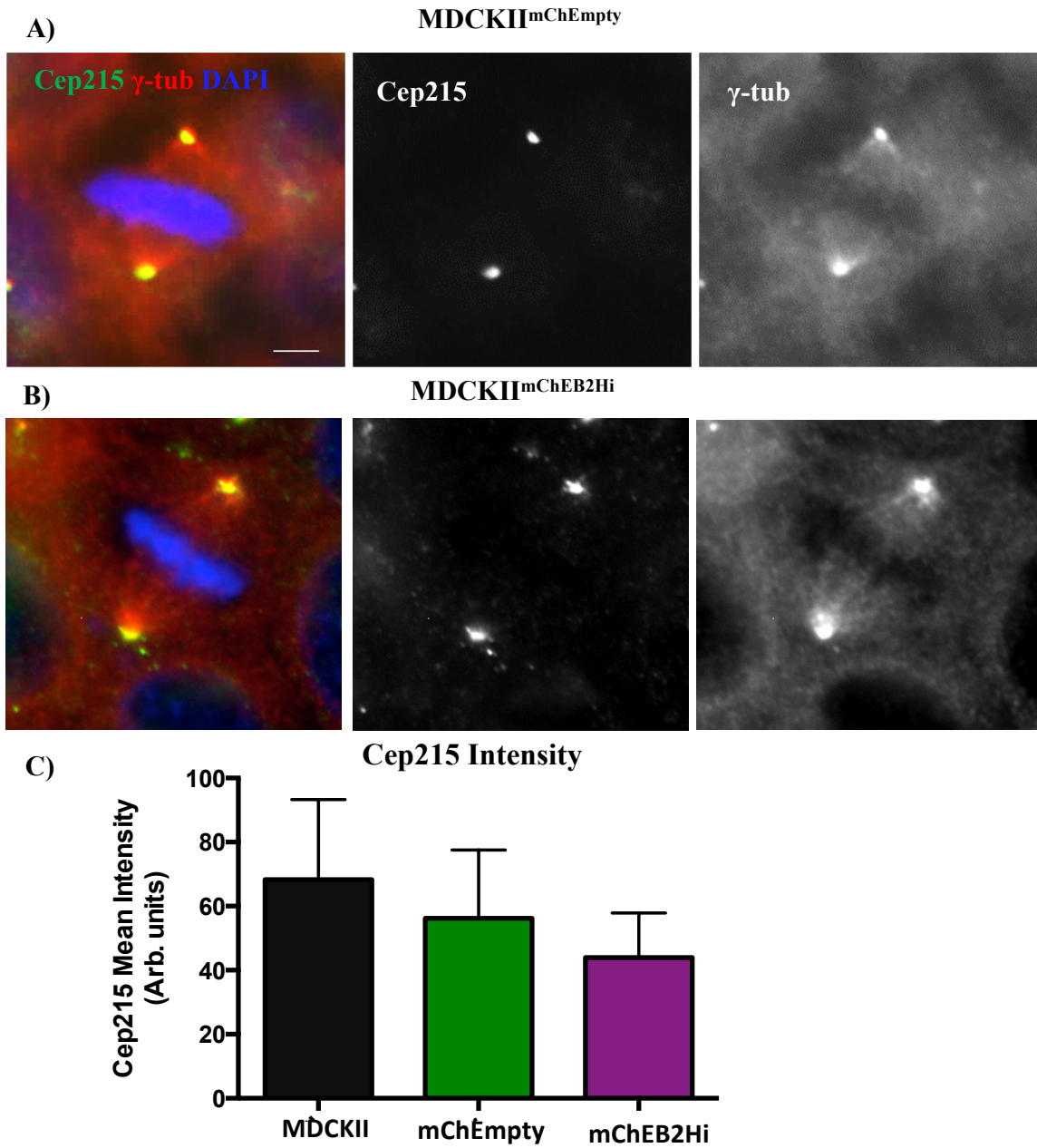


**Figure 7.11: Cep215 polar localisation suggests that EB2 does not sequester Cep215 from the poles in MDCKII<sup>mChEB2Hi</sup> cells.** Cells were fixed in methanol and immunolabelled for Cep215 (green, pAb),  $\gamma$ -tubulin (red, mAb, ab11316) and stained with DAPI. Images were acquired using the same exposure time. A) Widefield fluorescent image showing MDCKII<sup>mChEmpty</sup> cell with Cep215 localisation at each pole. B) Image showing a MDCKII<sup>mChEB2Hi</sup> cell with a bipolar spindle formation and Cep215 localisation at each pole. C) The graph shows no significant difference in Cep215 intensity in MDCKII<sup>mChEB2Hi</sup> cells compared to MDCKII<sup>mChEmpty</sup> cells. Data acquired from one experiment. No of cells analysed per condition = 20. Scale bar = 10  $\mu$ m.

# **Chapter VIII: General Discussion**

## 8.1 Introduction

Breast cancer is one of the most common type of cancer in the UK with poor prognosis hence, a major health issue. Therefore, understanding the mechanisms involved in this disease and identifying new targets that can act as diagnostic biomarkers or drugs for treatment are of great importance. Breast cancer starts in the inner lining of milk ducts or the lobules that supply them with milk. From there, if the cells acquire mutations and lose their polarised epithelial characteristics, they could metastasise to other parts of the body.

The MT cytoskeleton is important for several processes such as cell differentiation, cell division, protein trafficking, polarity establishment and migration. Due to these, MTs have been a major target for research in cancer treatment. In many cell types, the centrosome and Golgi apparatus relocate to the front of the nucleus facing the leading edge, which is important for directed migration. Here stable MTs extend to the leading edge while dynamic MTs are found at the rear (Ridley et al., 2003, Etienne-Manneville, 2013).

A better understanding of the roles of MTs in breast cancer cell migration and invasion, and in epithelial remodelling are required. A critical property of MTs is their inherent dynamics that allows them to undergo rearrangements. This property is tightly regulated by a group of proteins known as MT associating proteins, which +TIPs are a category of. Therefore, the aims of this project were to determine whether upregulation of proteins that regulate MT dynamics influence epithelial architecture, remodelling and migration and thereby contribute to transition to a more invasive phenotype? EB2 is a member of the EB family, which associate with MT ends and regulate growth (Komarova et al., 2009). EB2 has also been reported to be a key regulator of MT reorganisation during apico-basal epithelial differentiation (Goldspink et al., 2013). Implications of EB2 upregulation in migration and invasion is extremely limited however, it is known that EB2 does not have the same potency abilities for MT ends like other EB family members (Komarova et al., 2009). Overall, the objective of the project was to establish the effect of EB2 overexpression on breast cancer cells and MDCKII cells stably expressing mCherry-EB2 in terms of promoting migration and invasion. In addition, the aim was to investigate the role of EB2 overexpression on epithelial cyst formation, polarity and MT dynamics. Another area that was examined

was the effect of resveratrol on breast cancer cell models, specifically on the cytoskeleton, EB2, speed of migration and focal adhesions.

## 8.2 Increased EB2 expression promotes cell migration

EB2 expression plays a role in MT reorganisation during apico-basal epithelial differentiation (Goldspink et al., 2013). Previous studies have shown that the gene (MAPRE2) encoding for EB2 expression was found to be upregulated in pancreatic cancer cells (Abiatari et al., 2009) whereas EB2 depletion reduced the rate of cell migration and induced the formation of bundled and less dynamic MTs (Goldspink et al., 2013). Thereby these reports suggested a role of EB2 in cell migration and invasion, which needed to be further explored.

Migration and metastasis are reasons for poor prognosis in patients (Hanahan and Weinberg, 2011) and as such important therapeutic treatments need to be targeted towards these processes. Of major concern is understanding the mechanism governing MT regulators and how they contribute to cancer cell migration. During migration, plus tip proteins are known to regulate the MT network. For example, EB1 and APC bind to mDia, which function to capture and stabilise MTs thereby promoting cell migration (Wen et al., 2004). Also, in 3D migration, EB1 and dynein regulate migration by modulating cell protrusions through the activity of RhoA (Jayatilaka et al., 2017). It is important for stable MTs to be present at the front of the cell and dynamic ones at the rear for effective delivery, turnover and recycling, and interaction with other proteins during migration (Etienne-Manneville, 2013).

This project reports, for the first time, that EB2 expression is higher in the highly invasive MDA-MB-231 cells compared to MCF-7 cells. This EB2 upregulation may contribute to an increased velocity of random cancer cell migration. EB2 overexpression was therefore investigated in a non-cancerous cell line. Increased cell migration was also observed in MDCKII<sup>mChEB2Hi</sup> compared to MDCKII<sup>mChEmpty</sup> cells. These results may well be due to changes in MT organisation, changes in expression

and localisation of EB proteins as well as focal adhesions where these may affect MT dynamics. Evidence of EB2 overexpression also leading to an increased area of invasion in MDA-MB-231 cells was shown suggesting a possible role in metastasis (Chapter V). Depleting EB2 in MDA-MB-231 cells is one way to establish whether the invasiveness of MDA-MB-231 cells was specifically due to elevated levels of EB2. Initial experiments, using siRNA transfection, were carried out but proved unsuccessful. An alternative method would be to use CRISP/Cas9 to knockout the gene.

How EB2 is regulated, and particularly which signalling pathways are involved in the promotion of cell migration remains to be determined. Rho GTPases are known regulators of cell migration and could be interactors of EB2. Their levels are altered depending on the migratory structures required and location in the cell. Disrupted level of Rho GTPases are linked to cancer progression (Reymond et al., 2012, Ridley, 2013). Specifically, Rac1 has been found overexpressed in certain types of cancers including breast and gastric cancer (Ji et al., 2015, Ma et al., 2013). Downstream effectors of Rho GTPases, formins, are also implicated in migration (Vega et al., 2011). It is now known that formin inhibition in EB2 depleted ARPE-19 cells led to MTs that were less organised and lacked co-alignment with actin filaments (Goldspink et al., 2013). Further studies will help identify if any of the Rho GTPases are directly involved in EB2 regulation.

Our findings using cross-bow micropatterns which simulate a migratory morphology showed altered centrosome positioning in MDCKII<sup>mChEB2Hi</sup> compared to MDCKII<sup>mChEmpty</sup> cells. The centrosome and nucleated MTs are important for defining and maintaining cell directionality and polarity. The implications of Par-3 and dynein have been reported in centrosome positioning during migration in fibroblasts (Schmoranzer et al., 2009). Disruption of aPKC, Rac1 and Par-3 also affect centrosome positioning and cell migration (Rodriguez-Fraticelli et al., 2012, Godinho et al., 2014, Burute et al., 2017) therefore, the consequences of EB2 overexpression on these proteins should be checked in further studies. Centrosome amplification leads to increased MT nucleation and elongation, which in turn triggered Rac1 activation and thus increased invasion (Godinho et al., 2014). One could speculate that EB2-overexpression prevents the plus-end capture of MTs at cortical Par-3/dynein sites thus maintenance of centrosome positioning at the front of the cell is lost. According to

Schmoranzner et al., (2009) MT contact with Par-3/dynein complexes at lateral sides of the leading edge is needed to maintain centrosome positioning at the front of the nucleus.

### **8.3 Resveratrol alters MT organisation and reduces migration and invasion in breast cancer cells**

Migration and metastases of breast cancer cells to secondary sites are one of the reasons the disease is difficult to treat therefore, new treatments are necessary. Resveratrol has been shown to have protective and therapeutic effects on different cancer types both *in vitro* and *in vivo* (Schneider et al., 2003, Hong et al., 2009, Thomas et al., 2016, Traversi et al., 2017). Therefore, it was used to help determine whether it could be used as an adjuvant therapy for breast cancer patients. MCF-7 and MDA-MB-231 breast cancer cells were treated with resveratrol and then the effects were monitored. Resveratrol concentrations, from 10-75  $\mu\text{M}$ , were found to significantly inhibit cell migration in both cell lines (Chapter V). This effect seemed to be due to changes in MT and EB proteins localisation, which may affect MT dynamics. EB1 was observed to associate with the MT lattice in MDA-MB-231 cells but not in MCF-7 cells. Following high resveratrol treatment in MDA-MB-231 cells, EB2 became highly dispersed in the cytoplasm. A recent report presented data on EB2 phosphorylation by Aurora B and CDK1, which ensures EB2 is released from MTs (Iimori et al., 2016b). There is also evidence for the effects of resveratrol on Aurora B kinase activity. Hong and co-workers (2009) showed that a resveratrol analogue increased the levels of cell cycle checkpoint proteins, Aurora B and cyclin B, in breast cancer cells. After EB2 has been phosphorylated and dissociated, the main effect of the analogue comes from inhibiting MT polymerisation *in vitro*. This suggests that resveratrol may indirectly cause the phosphorylation of EB2 in breast cancer cells, however, further studies are required to investigate this.

Additionally, resveratrol led to an increase in cell area in both cell lines while the number and size of focal adhesions reduced. Cell migration requires dynamic MTs and focal adhesion (Ezratty et al., 2005) thus, any disruption in focal adhesions may

lead to a reduction in cell migration. Moreover, it has been indicated that EB2 associates with MAP4K4 or HAX1 and they play a vital role in focal adhesion turnover and cell migration, where knockdown EB2 resulted in focal adhesion stability and impaired cell migration (Yue et al., 2014a, Liu et al., 2015). Besides, MTs contribute to the delivery of essential adhesion proteins such as MAP4K4 and HAX1 through EB2. Therefore, loss of EB2 association with MTs, which may be induced by resveratrol, may affect focal adhesion turnover therefore causing a reduction in cell migration.

Our results revealed 3D control invasive conditions resulted in long thin projections in MDA-MB-231 cells while most MCF-7 cells remained in aggregates. MCF-7 cells had been shown to be poorly invasive and not a good model for studying invasion (Valdivia-Silva et al., 2009, Franco-Barraza et al., 2010) thus, only the MDA-MB-231 cells were used, which revealed a reduction in 3D spheroid invasion following resveratrol treatment suggesting a possible role of resveratrol in breast cancer treatment.

## **8.4 EB2 overexpression induces formation of multiple lumens and multipolar spindle formation in MDCKII<sup>mChEB2Hi</sup> cells**

EB2 expression is required during the early phase of differentiation to maintain a dynamic population of MTs while its downregulation is important for the formation of stabilised MT arrays in epithelial cells enabling EB1 lattice association (Goldspink et al., 2013). It was interesting therefore to focus on what would happen when EB2 is overexpressed using a 3D model that closely mimics the *in vivo* environment. Would the dysregulation of EB2 i.e. overexpression in cancer cells, compromise epithelial polarity and architecture. MDCKII kidney cells were used because they readily formed 3D cysts and were already generated to stably express EB2. Results from this would give an idea on the role of EB2 in promoting an invasive phenotype in breast cancer cells.

Our results revealed that cells with EB2 overexpression had an increased number of cysts with multiple lumens compared to the empty-vector counterpart

suggesting that EB2 overexpression was the reason behind this finding (Chapter VI). The mechanism for this could be speculated to be through defects in centrosome integrity, positioning and/or spindle orientation. Centrosome positioning is essential during cell migration, cell division and vesicular transport of proteins (Rodriguez-Fraticelli et al., 2012). Preliminary data indicate that mispositioning of centrosomes observed in MDCKII<sup>mChEB2Hi</sup> cells occurred at the two-cell stage. In MDCKII cysts, Par-3 and aPKC kinase activity are required for apical trafficking to the AMIS to expand to a PAP (Bryant et al., 2010). Therefore, further studies will be needed to establish whether aPKC affects centrosome positioning and consequently lumen formation.

Correct spindle orientation is critical for the correct maintenance of an epithelial sheet as it determines the division plane and the overall tissue architecture (Hung et al., 2016, di Pietro et al., 2016). Incorrect spindle orientation may lead to a multi-layered epithelium and loss of the overall tissue architecture (Hung et al., 2016). Results established in this project suggest that EB2 overexpression perturbs the normal spindle angle leading to the formation of multiple lumens (also seen in the study by Hung and co-workers (2016)), and upon further investigation it is likely due to defects in astral MTs. Regulation of astral MTs are important as they are believed to interact with proteins such as ninein or NuMA to ensure spindle poles are in the right position (Goldspink et al., 2017a, Hung et al., 2016). Preliminary findings suggest that EB2 overexpression caused a shortening and reduction in the number of astral MTs reaching the cortex in MDCKII<sup>mChEB2Hi</sup> cells. Further experiments need to be carried out to establish the role of other cortical proteins involved in astral MT stabilisation since NuMA did not appear to affect astral MTs.

Protein kinases are important during cell division (Nigg, 2001) and have been linked with astral MTs (Luo et al., 2016). In MDCKII<sup>mChEB2Hi</sup> cells, EB2 is seen along the lattice (Chapter IV), so it is possible that EB1, which is phosphorylated by ASK1 to aid astral MT stabilisation (Luo et al., 2016), is competitively removed from the plus ends by EB2 resulting in relatively weaker astral MTs thus, spindle misorientation. Another point to note is that since EB2 is overexpressed in these MDCKII cells, its effect could be linked to a feedback loop mechanism. Aurora B and CDK1 are known to phosphorylate EB2 (Iimori et al., 2016b). The level of EB2 overexpressed might be

a lot higher than the levels of Aurora B and CDK1 thereby not phosphorylating all EB2, which means the non-phosphorylated EB2 are still able to bind MTs resulting in weaker MTs in mitotic cells, spindle misorientation and eventually formation of multiple lumens. The type of protein kinase directly or indirectly interacting with EB2 in MDCKII cells need to confirmed.

Experiments involving EB2 overexpression also showed interesting results linking EB2 in multispindle formation (Chapter VII). MDCKII<sup>mChEB2Hi</sup> cells were found to have a significant number of multispindles compared to MDCKII<sup>mChEmpty</sup> cells. Of the areas investigated, cytokinesis failure in MDCKII<sup>mChEB2Hi</sup> cells appears to be the mechanism through which the cells possess more than one nucleus and thus centrosome amplification. In addition, Plk4 was found not to be overexpressed in MDCKII<sup>mChEB2Hi</sup> cells so, may not be the cause of multispindles formation. Further investigations need to be done to verify these data and to fully understand the mechanism governing EB2 overexpression and multispindle formation.

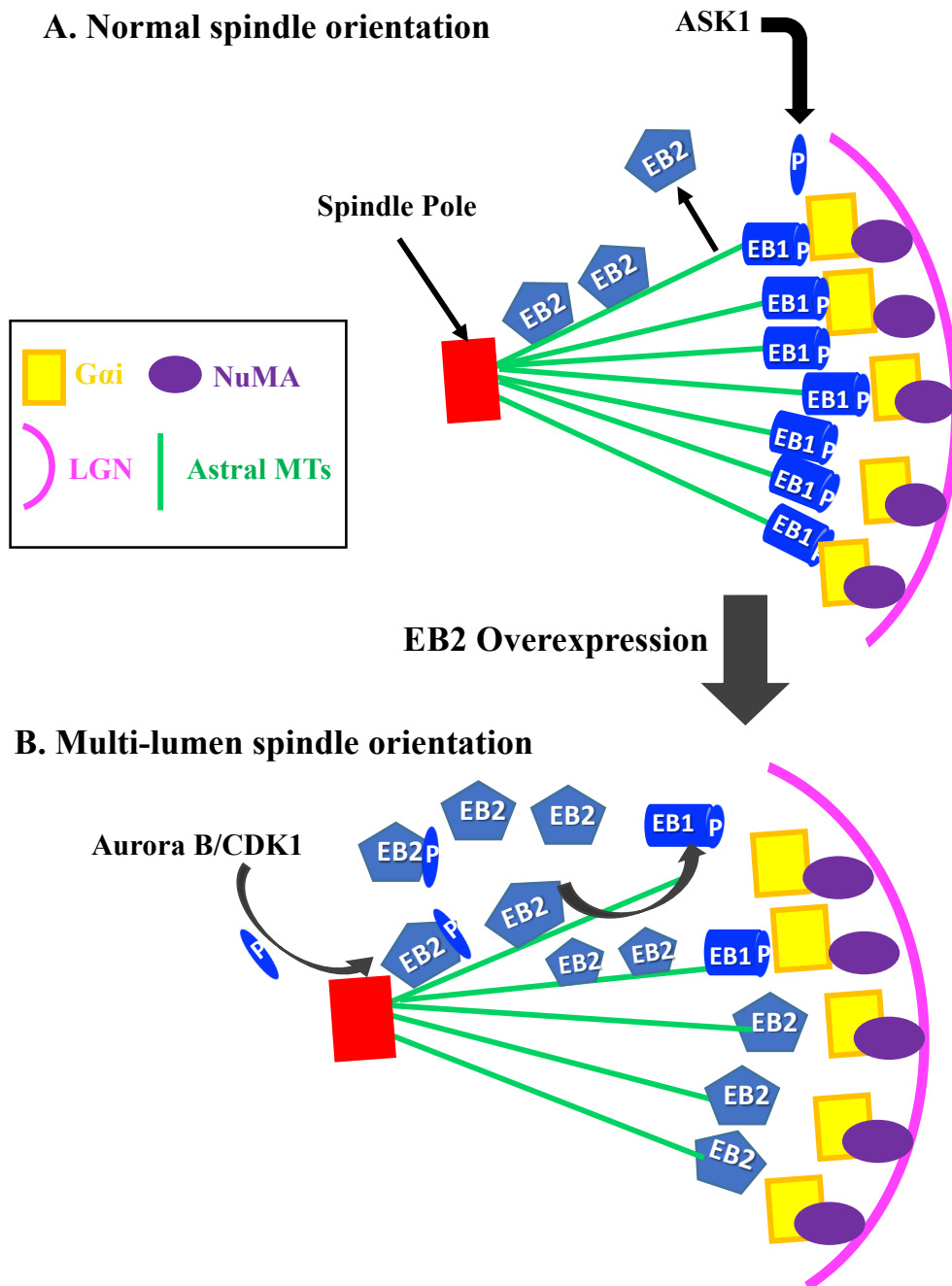
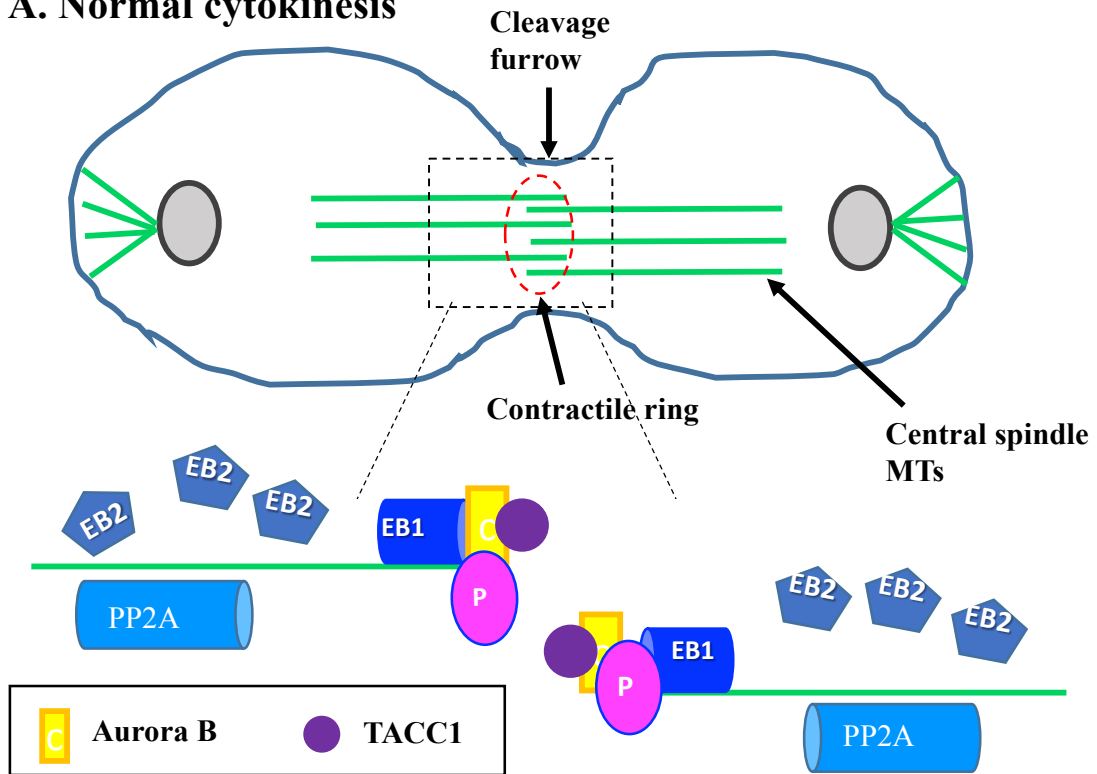


**Figure 8.1: Model for a possible mechanism by which astral MTs defects may lead to multiple lumen formation.** A) ASK1 phosphorylates EB1, which associates with the plus-ends of MTs aiding astral MT stabilisation and correct spindle orientation. Aurora B/CDK1 phosphorylates EB2 detaching it from MTs. B) When EB2 is overexpressed, there is insufficient Aurora B/CDK1 to phosphorylate EB2 and remove it from MTs, therefore, it is able to competitively remove EB1 from the MT plus-ends resulting in a shortening and reduction in the number of astral MTs reaching the cortex consequently causing multiple lumen formation. Also EB2 at plus-end may not enable MT capture at cortex.

### A. Normal cytokinesis



### B. Cytokinesis failure – EB2 Overexpression

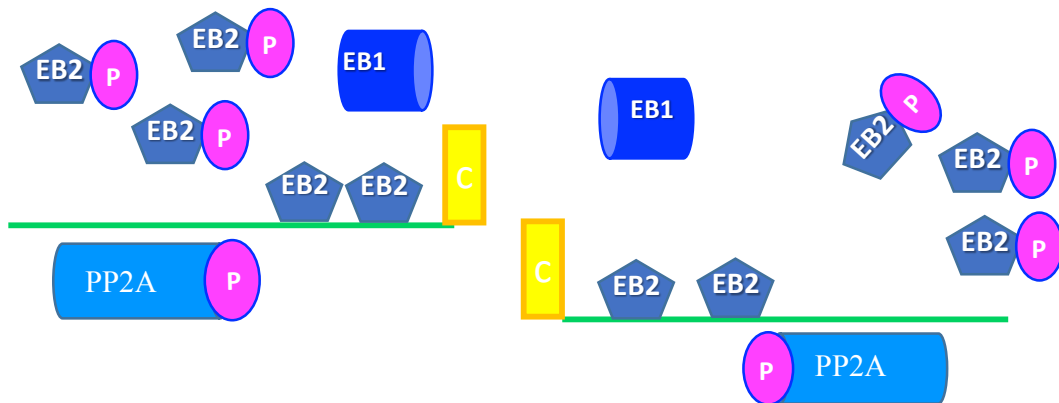


**Figure 8.2: Model for a possible mechanism by which cytokinesis failure may lead to supernumerary centrosomes and multiple spindle formation.** A) During cytokinesis, EB1 associates with the MT plus-ends as well as phosphorylated Aurora B. Due to the presence of EB1, PP2A is unable to dephosphorylate Aurora B allowing the recruitment of TACC1, which leads to correct cytokinesis. B) However, when EB2 is overexpressed, not all EB2 gets phosphorylated by Aurora B so some are still bound to MTs removing EB1. PP2A dephosphorylates Aurora B thereby preventing the recruitment of TACC1 leading to cytokinesis failure, supernumerary centrosomes and multispindle formation.

## 8.5 Summary

Key findings of this project includes:

1. MDA-MB-231 cells and MDCKII<sup>mChEB2Hi</sup> cells, both with an increased EB2 expression, had an increased average cell velocity compared to MCF-7 and MDCKII<sup>mChEmpty</sup> cells respectively. In the MDCKII<sup>mChEB2Hi</sup> cells, centrosome positioning appears to be behind the nucleus compared to the MDCKII<sup>mChEmpty</sup> cells where the centrosome appears to be at the front of the nucleus (Chapter IV).
2. Resveratrol alters MT organisation and EB2 appears to detach from MTs; and dramatically reduces cell velocity in breast cancer cells. Resveratrol also appeared to reduce invasiveness in MDA-MB-231 spheroid assays (Chapter V).
3. EB2 overexpression led to formation of cysts with multiple lumens. Mitotic spindle orientation was affected and this seems to be due to reduced cortical astral MTs interactions (Chapter VI). EB2 overexpression also caused multipolar spindles with supernumerary centrioles in MDCKII<sup>mChEB2Hi</sup> cells (Chapter VII).

## 8.6 Future work

The interesting data suggesting the role of EB2 overexpression on migration suggests an immediate requirement for further investigation. Initially, it would be exciting to find out if EB2-overexpression contributes to increased cell migration by increasing focal adhesion turnover through HAX1 and MAP4K4, since an interaction between EB2 and these proteins have been reported (Liu et al., 2015, Yue et al., 2014a). Next, positioning of centrosomes are regulated by signalling pathways including Par-3 (Schmoranzer et al., 2009) thus, whether EB2 overexpression interferes with the interaction of MTs with Par-3/dynein at the cortex leading to centrosome mispositioning needs to be studied. Also, in terms of invasion, it would be interesting

to find out the how EB2 plays a role through MT reorganisation either directly or indirectly.

Some effects of resveratrol on breast cancer cells have been established, for example, EB2 becomes more cytoplasmic in resveratrol-treated breast cancer cells, which suggest EB2 coming off MTs. This implies more stable MTs due to EB1 going along the MT lattice. To fully verify if EB2 becomes cytoplasmic, it would be necessary to check if EB2 is phosphorylated by resveratrol as a recent report suggested that EB2 phosphorylation leads to dissociation from MTs (Iimori et al., 2016b).

Another area where knowledge is limiting is the mechanism governing the role of EB2 overexpression in multiple lumens and multiple spindle formation. It would be interesting to examine the point where multi spindles form by labelling cells with a MT marker then live-tracking the cells during cell division. This model could also be used to monitor astral MT dynamics. There seems to be promising results in terms of Taxol rescuing spindle orientation in MDCKII<sup>mChEB2Hi</sup> cells however, an increased concentration needs to be used to probably get similar angles to the ones in MDCKII<sup>mChEmpty</sup> cells, without causing MT bundling. A stably EB2 overexpressing cell line will be generated in a non-tumourigenic, mammary epithelial cell line (MCF-10A) thus, allowing for some of the experiments carried out using the MDCKII model to be repeated. Further investigations of MT organisation and regulation in epithelial cancers are therefore essential, and could provide interesting therapeutic targets. To conclude, these studies will hopefully further enhance knowledge on the role of EB2 overexpression on processes leading to the loss of normal tissue architecture to an invasive breast cancer state.

# Appendix A: Reagents and Solutions

## Western Blotting Solutions

### Protein Lysis Buffer

In ddH<sub>2</sub>O:

50 mM	HEPES	pH 7.5
50 mM	NaCl	
1%	Triton X-100	
1 mM	EDTA	
10%	Glycerol	

### Sample Buffer

In ddH<sub>2</sub>O:

125 mM	Tris-HCl at	pH 6.8
2%	SDS (Sodium dodecyl sulphate)	
0.02%	Bromophenol Blue	
20%	Glycerol	

### Lower Gel Buffer (6%)

In final volume 250 ml ddH<sub>2</sub>O:

45.375 g	Tris (1.5M)	pH 6.8
1 g	SDS (0.4% w/v)	

### Upper Gel Buffer

In final volume of 250 ml ddH<sub>2</sub>O:

15.125 g	Tris (500Mm)	pH 6.8
1 g	SDS (0.4% w/v)	

### 6% Lower Resolving Gel

Per gel (12 ml total volume):

1.8 ml 40%	Acrylamide (Sigma, Poole, Dorset)
3 ml	Lower Gel Buffer

7.2 ml ddH<sub>2</sub>O  
72 µl 10% Ammonium persulphate (Sigma, Poole, Dorset)  
14 µl TEMED (N,N,N',N'-tetramethylethylenediamine) (Sigma, Poole, Dorset)

### **8% Lower Resolving Gel**

Per gel (12ml total volume):

2.4ml 40% Acrylamide  
3ml Lower Gel Buffer  
6.6ml ddH<sub>2</sub>O  
72µl 10% Ammonium persulphate  
14µl TEMED

### **5% Upper Stacking Gel**

Per gel (8ml total volume):

1ml 40% Acrylamide  
2ml Upper Gel Buffer  
5ml ddH<sub>2</sub>O  
72µl 10% Ammonium persulphate  
14µl TEMED

### **10x SDS Running Buffer**

In a final volume of 5L ddH<sub>2</sub>O:

151g Tris (250 mM)  
720g Glycine (1.9M)  
50g SDS (1% w/v)

### **Transfer Buffer**

In a final volume of 1L:

800ml ddH<sub>2</sub>O  
2.9g Glycine (39mM)  
5.8g Tris (48mM) adjusted to pH 8.3  
0.375g SDS (0.0375% w/v)

200ml          Methanol (20% v/v)

### **PBS-T**

In a final volume of 200ml PBS:

100µl          Tween-20

### **Tris-HCl**

In ddH<sub>2</sub>O:

100mM          Tris                  adjusted to pH 8.5 with HCl

### **ECL Solution A**

In 10ml Tris-HCl, pH 8.5:

45µl                  Coumaric acid (91 mM stock solution: 0.15g in 10ml DMSO)  
(Sigma, Poole, Dorset)

100µl                  Luminol (250 mM stock solution: 0.44g in 10ml DMSO)  
(Sigma, Poole, Dorset)

### **ECL Solution B**

In 10ml Tris-HCl, pH 8.5:

6µl 30%          Hydrogen peroxide solution

## Appendix B: Supplementary Data

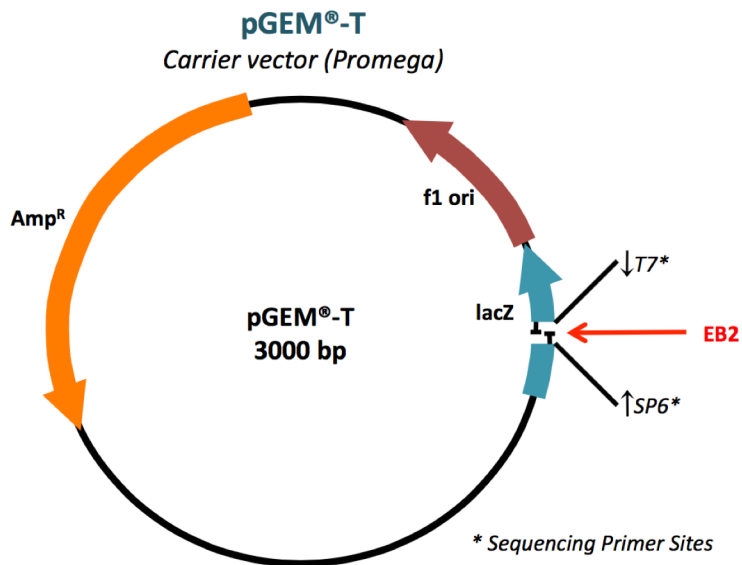
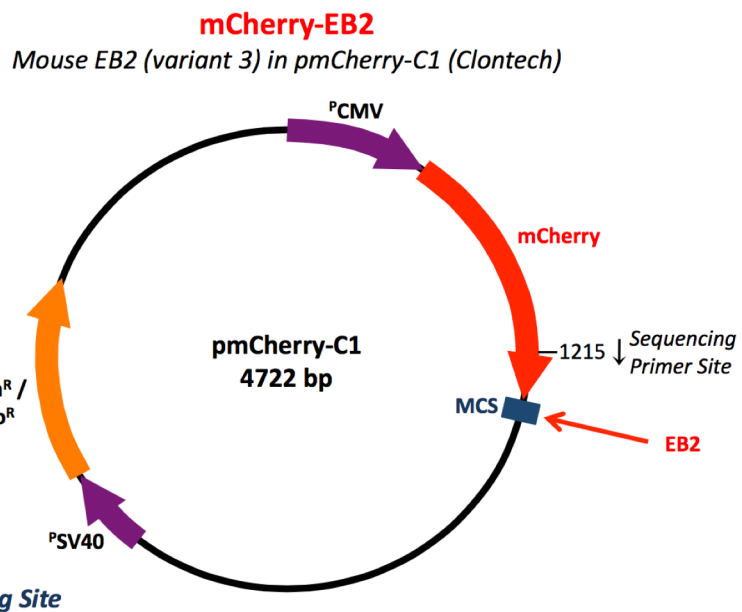


Figure S1A: A construct map of pGEM<sup>®</sup>-T, kindly gifted by P. Powell, University of East Anglia, and used as a carrier vector in the cloning of mouse EB2 (variant 3).



### Multiple Cloning Site

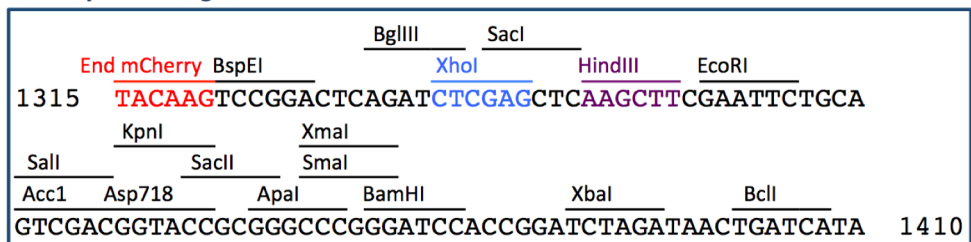
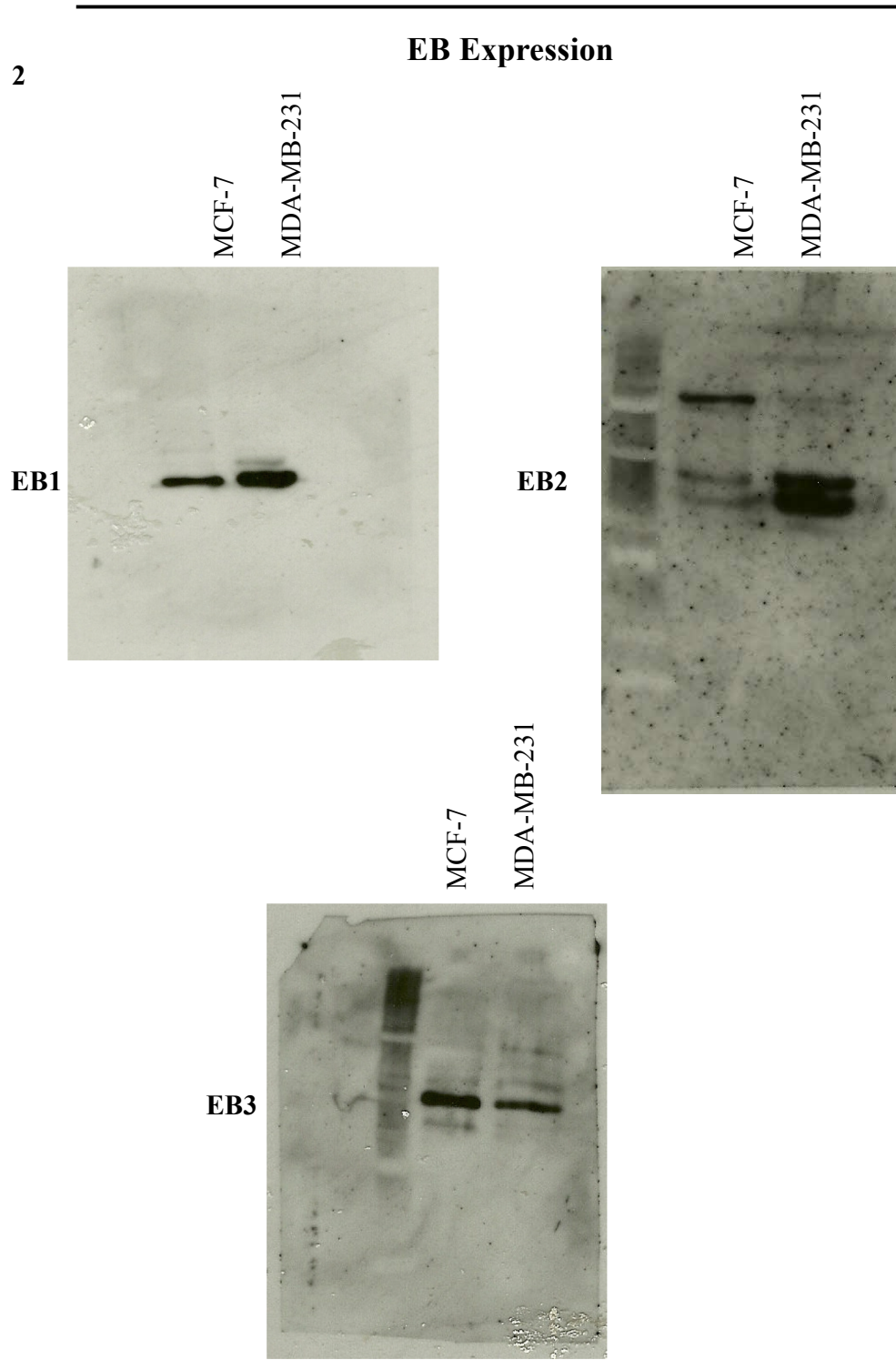
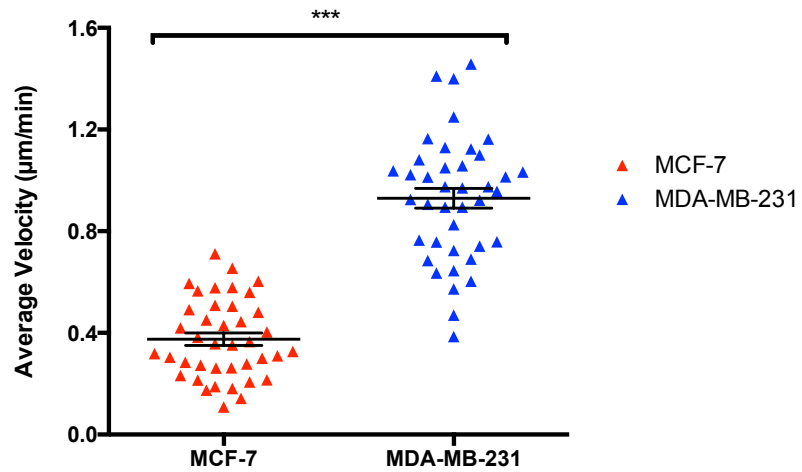


Figure S1B: A construct map of pmCherry-C1, kindly gifted by P. Powell, University of East Anglia, and used to directionally clone mouse EB2 (variant 3) into the MCS via the XhoI and HindIII restriction sites.



**Figure S2: Full blots of EB expression in MCF-7 and MDA-MB-231 cells.**

**Random cell migration: Experiment 2**

**Figure S3: Speed of random migration in MCF-7 and MDA-MB-231 cells.**

Live time-lapse imaging of MDA-MB-231 and MCF7 cells seeded on collagen-I with images taken every 10 min for 16 h. Cells were tracked in ImageJ and their average velocity was plotted. MDA-MB-231 cells migrate at a higher average velocity of 1µm/min compared to 0.4 µm/min for MCF-7 cells. Number of cells per condition = 40. Graph shows data from the 2nd experiment. Mean  $\pm$  SEM.

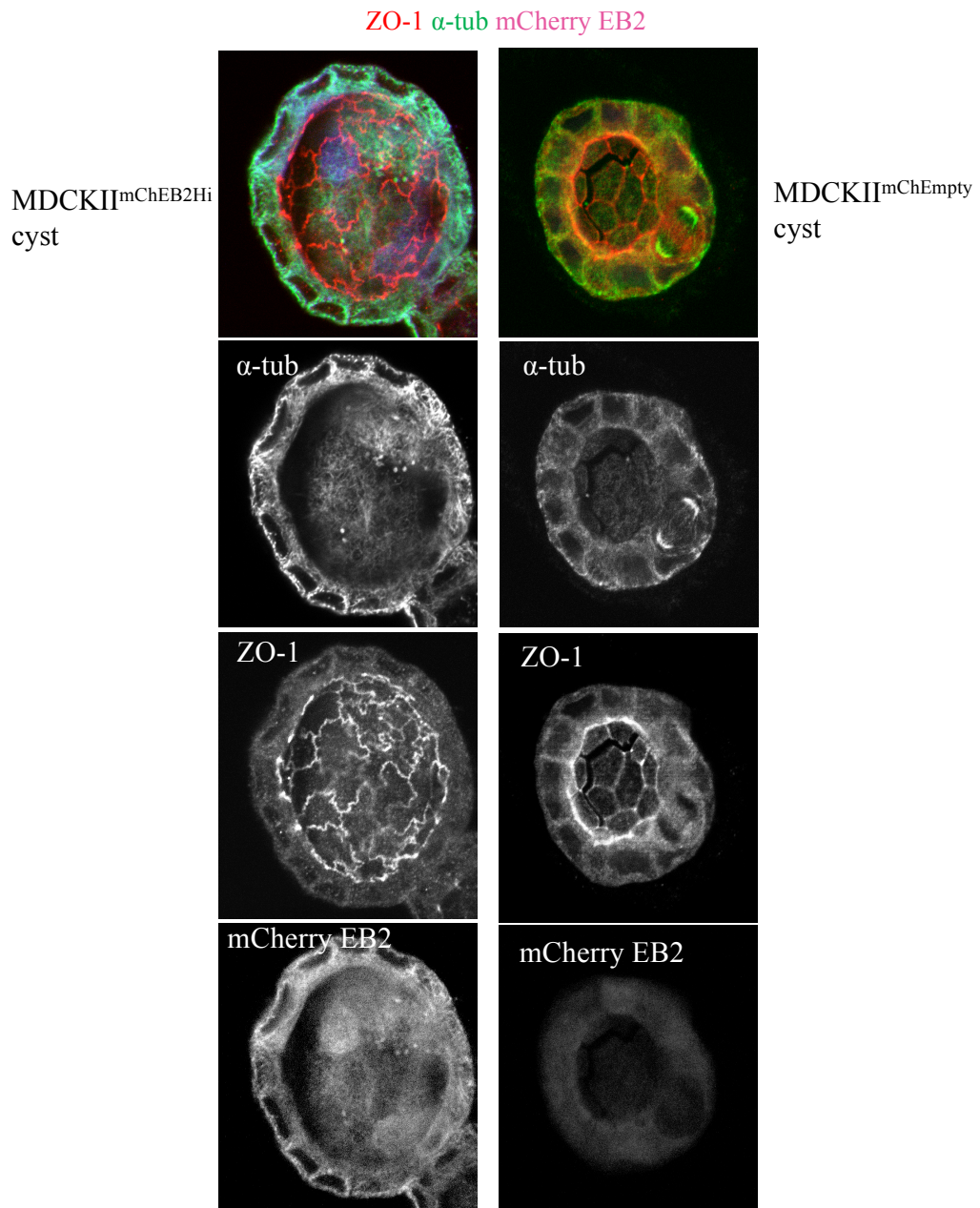


**Figure S4: mCherry-EB2 expression in MDCKII<sup>mChEmpty</sup> and MDCKII<sup>mChEB2Hi</sup> cysts.**

## **Movies**

### **Chapter III**

#### **Movie S1: Time-lapse of MCF-7 cell transiently expressing GFP-CLIP-170.**

Images were taken every three-seconds over three-minute period and replayed at 5 frames per second. The movie shows U-Track analysis of GFP-CLIP-170 comets over the acquisition period.

#### **Movie S2: Time-lapse of MDA-MB-231 cell transiently expressing GFP-CLIP-170.**

Images were taken every three-seconds over three-minute period and replayed at 5 frames per second. The movie shows U-Track analysis of GFP-CLIP-170 comets over the acquisition period.

### **Chapter IV**

#### **Movie S3: Cell tracking in sub-confluent MDA-MB-231 cells seeded on tissue culture plastic.**

Time-lapse movie of MDA-MB-231 cells, where 10 cells were randomly selected and tracked. For each cell, the position was tracked for each frame over a 16-hour time-lapse experiment with images taken every 10-minutes using a x10 objective, and movies replayed at 5 frames per second.

#### **Movie S4: Cell tracking in sub-confluent MDA-MB-231 cells seeded on fibronectin.**

Time-lapse movie of MDA-MB-231 cells, where 10 cells were randomly selected and tracked. For each cell, the position was tracked for each frame over a 16-hour time-lapse experiment with images taken every 10-minutes using a x10 objective, and movies replayed at 5 frames per second.

#### **Movie S5: Cell tracking in sub-confluent MDA-MB-231 cells seeded on Collagen-I.**

Time-lapse movie of MDA-MB-231 cells, where 10 cells were randomly selected and tracked. For each cell, the position was tracked for each frame over a 16-hour time-lapse experiment with images taken every 10-minutes using a x10 objective, and movies replayed at 5 frames per second.

**Movie S6: Cell tracking in sub-confluent MCF-7 cells seeded on tissue culture plastic.** Time-lapse movie of MCF-7 cells, where 10 cells were randomly selected and tracked. For each cell, the position was tracked for each frame over a 16-hour time-lapse experiment with images taken every 10-minutes using a x10 objective, and movies replayed at 5 frames per second.

**Movie S7: Cell tracking in sub-confluent MCF-7 cells seeded on fibronectin.** Time-lapse movie of MCF-7 cells, where 10 cells were randomly selected and tracked. For each cell, the position was tracked for each frame over a 16-hour time-lapse experiment with images taken every 10-minutes using a x10 objective, and movies replayed at 5 frames per second.

**Movie S8: Cell tracking in sub-confluent MCF-7 cells seeded on Collagen-I.** Time-lapse movie of MCF-7 cells, where 10 cells were randomly selected and tracked. For each cell, the position was tracked for each frame over a 16-hour time-lapse experiment with images taken every 10-minutes using a x10 objective, and movies replayed at 5 frames per second.

**Movie S9: Cell tracking in sub-confluent MDCKII cells seeded on Collagen-I.** Time-lapse movie of MDCKII cells, where 10 cells were randomly selected and tracked. For each cell, the position was tracked for each frame over a 16-hour time-lapse experiment with images taken every 10-minutes using a x10 objective, and movies replayed at 5 frames per second.

**Movie S10: Cell tracking in sub-confluent MDCKII<sup>mChEmpty</sup> cells seeded on Collagen-I.** Time-lapse movie of MDCKII<sup>mChEmpty</sup> cells, where 10 cells were randomly selected and tracked. For each cell, the position was tracked for each frame over a 16-hour time-lapse experiment with images taken every 10-minutes using a x10 objective, and movies replayed at 5 frames per second.

**Movie S11: Cell tracking in sub-confluent MDCKII<sup>mChEB2Hi</sup> cells seeded on Collagen-I.** Time-lapse movie of MDCKII<sup>mChEB2Hi</sup> cells, where 10 cells were randomly selected and tracked. For each cell, the position was tracked for each frame over a 16-

hour time-lapse experiment with images taken every 10-minutes using a x10 objective, and movies replayed at 5 frames per second.

## **Chapter V**

**Movie S12: Cell tracking in sub-confluent DMSO treated MCF-7 cells.** Time-lapse movie of DMSO treated cells, where 10 cells were randomly selected and tracked. For each cell, the position was tracked for each frame over a 16-hour time-lapse experiment with images taken every 10-minutes using a x10 objective, and movies replayed at 5 frames per second.

**Movie S13: Cell tracking in sub-confluent 10  $\mu$ M resveratrol-treated MCF-7 cells.** Time-lapse movie of 10  $\mu$ M treated cells, where 10 cells were randomly selected and tracked. For each cell, the position was tracked for each frame over a 16-hour time-lapse experiment with images taken every 10-minutes using a x10 objective, and movies replayed at 5 frames per second. Cells moved similarly to those in untreated cells. Movie showed a marked reduction in the speed of 10  $\mu$ M resveratrol cells compared to DMSO cells.

**Movie S14: Cell tracking in sub-confluent 20  $\mu$ M resveratrol-treated MCF-7 cells.** Time-lapse movie of 20  $\mu$ M treated cells, where 10 cells were randomly selected and tracked. For each cell, the position was tracked for each frame over a 16-hour time-lapse experiment with images taken every 10-minutes using a x10 objective, and movies replayed at 5 frames per second. Cells moved similarly to those in untreated cells. Movie showed a marked reduction in the speed of 20  $\mu$ M resveratrol cells compared to DMSO cells.

**Movie S15: Cell tracking in sub-confluent 50  $\mu$ M resveratrol-treated MCF-7 cells.** Time-lapse movie of 50  $\mu$ M treated cells, where 10 cells were randomly selected and tracked. For each cell, the position was tracked for each frame over a 16-hour time-lapse experiment with images taken every 10-minutes using a x10 objective, and movies replayed at 5 frames per second. Cells moved similarly to those in untreated cells. Movie showed a marked reduction in the speed of 50  $\mu$ M resveratrol cells compared to DMSO cells.

**Movie S16: Cell tracking in sub-confluent DMSO treated MDA-MB-231 cells.**

Time-lapse movie of DMSO treated cells, where 10 cells were randomly selected and tracked. For each cell, the position was tracked for each frame over a 16-hour time-lapse experiment with images taken every 10-minutes using a x10 objective, and movies replayed at 5 frames per second.

**Movie S17: Cell tracking in sub-confluent 20  $\mu\text{M}$  resveratrol-treated MDA-MB-231 cells.** Time-lapse movie of 20  $\mu\text{M}$  treated cells, where 10 cells were randomly selected and tracked. For each cell, the position was tracked for each frame over a 16-hour time-lapse experiment with images taken every 10-minutes using a x10 objective, and movies replayed at 5 frames per second. Cells moved similarly to those in untreated cells. Movie showed a marked reduction in the speed of 20  $\mu\text{M}$  resveratrol cells compared to DMSO cells.

**Movie S18: Cell tracking in sub-confluent 50  $\mu\text{M}$  resveratrol-treated MDA-MB-231 cells.** Time-lapse movie of 50  $\mu\text{M}$  treated cells, where 10 cells were randomly selected and tracked. For each cell, the position was tracked for each frame over a 16-hour time-lapse experiment with images taken every 10-minutes using a x10 objective, and movies replayed at 5 frames per second. Cells moved similarly to those in untreated cells. Movie showed a marked reduction in the speed of 50  $\mu\text{M}$  resveratrol cells compared to DMSO cells.

**Movie S19: Cell tracking in sub-confluent 75  $\mu\text{M}$  resveratrol-treated MDA-MB-231 cells.** Time-lapse movie of 75  $\mu\text{M}$  treated cells, where 10 cells were randomly selected and tracked. For each cell, the position was tracked for each frame over a 16-hour time-lapse experiment with images taken every 10-minutes using a x10 objective, and movies replayed at 5 frames per second. Cells moved similarly to those in untreated cells. Movie showed a marked reduction in the speed of 75  $\mu\text{M}$  resveratrol cells compared to DMSO cells.

## **Chapter VI**

**Movie S20: MDCKII cell bipolar spindle orientation**

Z-stack images of MDCKII cell treated with thymidine, washed out then immunolabelled with  $\alpha$ -tubulin and  $\gamma$ -tubulin. Images of mitotic cells at metaphase were taken at 0.2  $\mu\text{m}$  intervals.

**Movie S21: MDCKII<sup>mChEmpty</sup> cell bipolar spindle orientation**

Z-stack images of MDCKII<sup>mChEmpty</sup> cell treated with thymidine, washed out then immunolabelled with  $\alpha$ -tubulin and  $\gamma$ -tubulin. Images of mitotic cells at metaphase were taken at 0.2  $\mu\text{m}$  intervals.

**Movie S22: MDCKII<sup>mChEB2Hi</sup> cell bipolar spindle orientation**

Z-stack images of MDCKII<sup>mChEB2Hi</sup> cell treated with thymidine, washed out then immunolabelled with  $\alpha$ -tubulin and  $\gamma$ -tubulin. Images of mitotic cells at metaphase were taken at 0.2  $\mu\text{m}$  intervals.

**Movie S23: MDCKII cell astral MT dynamics**

Z-stack images of MDCKII cell treated with thymidine, washed out then immunolabelled with  $\alpha$ -tubulin and phalloidin (actin). Images of mitotic cells at metaphase were taken at 0.2  $\mu\text{m}$  intervals.

**Movie S24: MDCKII<sup>mChEmpty</sup> cell astral MT dynamics**

Z-stack images of MDCKII<sup>mChEmpty</sup> cell treated with thymidine, washed out then immunolabelled with  $\alpha$ -tubulin and phalloidin (actin). Images of mitotic cells at metaphase were taken at 0.2  $\mu\text{m}$  intervals.

**Movie S25: MDCKII<sup>mChEB2Hi</sup> cell astral MT dynamics**

Z-stack images of MDCKII<sup>mChEB2Hi</sup> cell treated with thymidine, washed out then immunolabelled with  $\alpha$ -tubulin and phalloidin (actin). Images of mitotic cells at metaphase were taken at 0.2  $\mu\text{m}$  intervals.

**Movie S26: MDCKII<sup>mChEmpty</sup> cell GFP-CLIP-170 dynamics**

Time-lapse of MDCKII<sup>mChEmpty</sup> cell transiently expressing GFP-CLIP-170. Images were taken every three-seconds over three-minute period and replayed at 5 frames per

second. The movie shows U-Track analysis of GFP-CLIP-170 comets over the acquisition period.

**Movie S27: MDCKII<sup>mChEB2Hi</sup> cell GFP-CLIP-170 dynamics**

Time-lapse of MDCKII<sup>mChEB2Hi</sup> cell transiently expressing GFP-CLIP-170. Images were taken every three-seconds over three-minute period and replayed at 5 frames per second. The movie shows U-Track analysis of GFP-CLIP-170 comets over the acquisition period.

**Chapter VII**

**Movie S28: MDCKII<sup>mChEB2Hi</sup> cell multipolar spindle formation**

Z-stack images of MDCKII<sup>mChEB2Hi</sup> cell treated with thymidine, washed out then immunolabelled with  $\alpha$ -tubulin and  $\gamma$ -tubulin. Images of multipolar cells were taken at 0.2  $\mu\text{m}$  intervals.

# References

- ABE, Y., OHSUGI, M., HARAGUCHI, K., FUJIMOTO, J. & YAMAMOTO, T. 2006. LATS2-Ajuba complex regulates gamma-tubulin recruitment to centrosomes and spindle organization during mitosis. *FEBS Lett*, 580, 782-8.
- ABIATARI, I., GILLEN, S., DEOLIVEIRA, T., KLOSE, T., BO, K., GIESE, N. A., FRIESS, H. & KLEEFF, J. 2009. The microtubule-associated protein MAPRE2 is involved in perineural invasion of pancreatic cancer cells. *Int J Oncol*, 35, 1111-6.
- ADAMS, R. R., CARMENA, M. & EARNSHAW, W. C. 2001. Chromosomal passengers and the (aurora) ABCs of mitosis. *Trends Cell Biol*, 11, 49-54.
- AGUIRRE-GHISO, J. A. 2007. Models, mechanisms and clinical evidence for cancer dormancy. *Nature Reviews Cancer*, 7, 834-846.
- AKHMANOVA, A. & HOOGENRAAD, C. C. 2005. Microtubule plus-end-tracking proteins: mechanisms and functions. *Current opinion in cell biology*, 17, 47-54.
- AKHMANOVA, A. & MAIATO, H. 2017. Closing the tubulin detyrosination cycle. *Science*, 358, 1381-1382.
- AKHMANOVA, A., MAUSSET-BONNEFONT, A. L., VAN CAPPELLEN, W., KEIJZER, N., HOOGENRAAD, C. C., STEPANOVA, T., DRABEK, K., VAN DER WEES, J., MOMMAAS, M., ONDERWATER, J., VAN DER MEULEN, H., TANENBAUM, M. E., MEDEMA, R. H., HOOGERBRUGGE, J., VREEBURG, J., URINGA, E. J., GROOTEGOED, J. A., GROSVELD, F. & GALJART, N. 2005. The microtubule plus-end-tracking protein CLIP-170 associates with the spermatid manchette and is essential for spermatogenesis. *Genes Dev*, 19, 2501-15.
- AKHMANOVA, A. & STEINMETZ, M. O. 2008. Tracking the ends: a dynamic protein network controls the fate of microtubule tips. *Nat Rev Mol Cell Biol*, 9, 309-22.
- AKHMANOVA, A. & STEINMETZ, M. O. 2010. Microtubule +TIPs at a glance. *J Cell Sci*, 123, 3415-9.
- AKHMANOVA, A. & STEINMETZ, M. O. 2015. Control of microtubule organization and dynamics: two ends in the limelight. *Nat Rev Mol Cell Biol*, 16, 711-26.
- AKHTAR, N. & STREULI, C. H. 2013. An integrin-ILK-microtubule network orients cell polarity and lumen formation in glandular epithelium. *Nat Cell Biol*, 15, 17-27.
- AL-BASSAM, J. & CHANG, F. 2011. Regulation of microtubule dynamics by TOG-domain proteins XMAP215/Dis1 and CLASP. *Trends in cell biology*, 21, 604-614.
- AL-BASSAM, J. & CORBETT, K. D. 2012.  $\alpha$ -Tubulin acetylation from the inside out. *Proc Natl Acad Sci U S A*, 109, 19515-6.
- APODACA, G., GALLO, L. I. & BRYANT, D. M. 2012. Role of membrane traffic in the generation of epithelial cell asymmetry. *Nat Cell Biol*, 14, 1235-43.
- APPLEGATE, K. T., BESSON, S., MATOV, A., BAGONIS, M. H., JAQAMAN, K. & DANUSER, G. 2011. plusTipTracker: quantitative image analysis software for the measurement of microtubule dynamics. *Journal of structural biology*, 176, 168-184.
- ARPIN, M., CHIRIVINO, D., NABA, A. & ZWAENEPOEL, I. 2011. Emerging role for ERM proteins in cell adhesion and migration. *Cell Adh Migr*, 5, 199-206.
- AU, F. K., JIA, Y., JIANG, K., GRIGORIEV, I., HAU, B. K., SHEN, Y., DU, S., AKHMANOVA, A. & QI, R. Z. 2017. GAS2L1 Is a Centriole-Associated Protein Required for Centrosome Dynamics and Disjunction. *Dev Cell*, 40, 81-94.
- AZARENKO, O., OKOUNEVA, T., SINGLETARY, K. W., JORDAN, M. A. & WILSON, L. 2008. Suppression of microtubule dynamic instability and turnover in MCF7 breast cancer cells by sulforaphane. *Carcinogenesis*, 29, 2360-8.

- AZIMZADEH, J. & MARSHALL, W. F. 2010. Building the centriole. *Curr Biol*, 20, R816-25.
- AZIOS, N. G. & DHARMAWARDHANE, S. F. 2005. Resveratrol and estradiol exert disparate effects on cell migration, cell surface actin structures, and focal adhesion assembly in MDA-MB-231 human breast cancer cells. *Neoplasia*, 7, 128-40.
- AZIOS, N. G., KRISHNAMOORTHY, L., HARRIS, M., CUBANO, L. A., CAMMER, M. & DHARMAWARDHANE, S. F. 2007. Estrogen and resveratrol regulate Rac and Cdc42 signaling to the actin cytoskeleton of metastatic breast cancer cells. *Neoplasia*, 9, 147-58.
- BAGNAT, M., CHEUNG, I. D., MOSTOV, K. E. & STAINIER, D. Y. 2007. Genetic control of single lumen formation in the zebrafish gut. *Nat Cell Biol*, 9, 954-60.
- BAGNAT, M., NAVIS, A., HERBSTREITH, S., BRAND-ARZAMENDI, K., CURADO, S., GABRIEL, S., MOSTOV, K., HUISKEN, J. & STAINIER, D. Y. 2010. Cse1l is a negative regulator of CFTR-dependent fluid secretion. *Curr Biol*, 20, 1840-5.
- BAILEY, M. J. & PREHODA, K. E. 2015. Establishment of Par-Polarized Cortical Domains via Phosphoregulated Membrane Motifs. *Dev Cell*, 35, 199-210.
- BARBIERI, I., PENSA, S., PANNELLINI, T., QUAGLINO, E., MARITANO, D., DEMARIA, M., VOSTER, A., TURKSON, J., CAVALLO, F., WATSON, C. J., PROVERO, P., MUSIANI, P. & POLI, V. 2010. Constitutively active Stat3 enhances neu-mediated migration and metastasis in mammary tumors via upregulation of Cten. *Cancer Res*, 70, 2558-67.
- BARRETTA, M. L., SPANO, D., D'AMBROSIO, C., CERVIGNI, R. I., SCALONI, A., CORDA, D. & COLANZI, A. 2016. Aurora-A recruitment and centrosomal maturation are regulated by a Golgi-activated pool of Src during G2. *Nat Commun*, 7, 11727.
- BASTO, R., BRUNK, K., VINADOGROVA, T., PEEL, N., FRANZ, A., KHODJAKOV, A. & RAFF, J. W. 2008. Centrosome amplification can initiate tumorigenesis in flies. *Cell*, 133, 1032-42.
- BAUER, K., MIERKE, C. & BEHRENS, J. 2007. Expression profiling reveals genes associated with transendothelial migration of tumor cells: a functional role for alphavbeta3 integrin. *Int J Cancer*, 121, 1910-8.
- BELLETT, G., CARTER, J. M., KEYNTON, J., GOLDSPIK, D., JAMES, C., MOSS, D. K. & MOGENSEN, M. M. 2009. Microtubule plus - end and minus - end capture at adherens junctions is involved in the assembly of apico - basal arrays in polarised epithelial cells. *Cell motility and the cytoskeleton*, 66, 893-908.
- BENTON, R. & ST JOHNSTON, D. 2003. Drosophila PAR-1 and 14-3-3 inhibit Bazooka/PAR-3 to establish complementary cortical domains in polarized cells. *Cell*, 115, 691-704.
- BERTRAN, M. T., SDELICI, S., REGUE, L., AVRUCH, J., CAELLES, C. & ROIG, J. 2011. Nek9 is a Plk1-activated kinase that controls early centrosome separation through Nek6/7 and Eg5. *EMBO J*, 30, 2634-47.
- BETSCHINGER, J., MECHTLER, K. & KNOBLICH, J. A. 2003. The Par complex directs asymmetric cell division by phosphorylating the cytoskeletal protein Lgl. *Nature*, 422, 326-30.
- BIELING, P., KANDELS-LEWIS, S., TELLEY, I. A., VAN DIJK, J., JANKE, C. & SURREY, T. 2008. CLIP-170 tracks growing microtubule ends by dynamically recognizing composite EB1/tubulin-binding sites. *J Cell Biol*, 183, 1223-33.
- BLASKY, A. J., MANGAN, A. & PREKERIS, R. 2015. Polarized protein transport and lumen formation during epithelial tissue morphogenesis. *Annu Rev Cell Dev Biol*, 31, 575-91.
- BOBINNEC, Y., MOUDJOU, M., FOUQUET, J. P., DESBRUYERES, E., EDDE, B. & BORNENS, M. 1998. Glutamylation of centriole and cytoplasmic tubulin in proliferating non-neuronal cells. *Cell Motil Cytoskeleton*, 39, 223-32.
- BOMPARD, G., RABEHARIVELO, G., CAU, J., ABRIEU, A., DELSERT, C. & MORIN, N. 2013. P21-activated kinase 4 (PAK4) is required for metaphase spindle positioning and anchoring. *Oncogene*, 32, 910-9.

- BRANDT, D. T. & GROSSE, R. 2007. Get to grips: steering local actin dynamics with IQGAPs. *EMBO Rep*, 8, 1019-23.
- BRE, M. H., REDEKER, V., QUIBELL, M., DARMANADEN-DELORME, J., BRESSAC, C., COSSON, J., HUITOREL, P., SCHMITTER, J. M., ROSSLER, J., JOHNSON, T., ADOUTTE, A. & LEVILLIERS, N. 1996. Axonemal tubulin polyglycylation probed with two monoclonal antibodies: widespread evolutionary distribution, appearance during spermatozoan maturation and possible function in motility. *J Cell Sci*, 109 ( Pt 4), 727-38.
- BREITSPRECHER, D. & GOODE, B. L. 2013. Formins at a glance. *J Cell Sci*, 126, 1-7.
- BRINKLEY, B. R. 2001. Managing the centrosome numbers game: from chaos to stability in cancer cell division. *Trends Cell Biol*, 11, 18-21.
- BRITTLE, A. L. & OHKURA, H. 2005. Centrosome maturation: Aurora lights the way to the poles. *Curr Biol*, 15, R880-2.
- BROUHARD, G. J., STEAR, J. H., NOETZEL, T. L., AL-BASSAM, J., KINOSHITA, K., HARRISON, S. C., HOWARD, J. & HYMAN, A. A. 2008. XMAP215 is a processive microtubule polymerase. *Cell*, 132, 79-88.
- BRYANT, D. M., DATTA, A., RODRIGUEZ-FRATICELLI, A. E., PERANEN, J., MARTIN-BELMONTE, F. & MOSTOV, K. E. 2010. A molecular network for de novo generation of the apical surface and lumen. *Nat Cell Biol*, 12, 1035-45.
- BRYANT, D. M. & MOSTOV, K. E. 2008. From cells to organs: building polarized tissue. *Nat Rev Mol Cell Biol*, 9, 887-901.
- BU, W. & SU, L.-K. 2001. Regulation of microtubule assembly by human EB1 family proteins. *Oncogene*, 20.
- BU, W. & SU, L.-K. 2003. Characterization of Functional Domains of Human EB1 Family Proteins. *Journal of Biological Chemistry*, 278, 49721-49731.
- BUHRMANN, C., SHAYAN, P., GOEL, A. & SHAKIBAEI, M. 2017. Resveratrol Regulates Colorectal Cancer Cell Invasion by Modulation of Focal Adhesion Molecules. *Nutrients*, 9.
- BURRIDGE, K. & WENNERBERG, K. 2004. Rho and Rac take center stage. *Cell*, 116, 167-79.
- BURUTE, M., PRIOUX, M., BLIN, G., TRUCHET, S., LETORT, G., TSENG, Q., BESSY, T., LOWELL, S., YOUNG, J., FILHOL, O. & THERY, M. 2017. Polarity Reversal by Centrosome Repositioning Primes Cell Scattering during Epithelial-to-Mesenchymal Transition. *Dev Cell*, 40, 168-184.
- BUZDAR, A. U. 2007. Preoperative chemotherapy treatment of breast cancer--a review. *Cancer*, 110, 2394-407.
- CANCER RESEARCH UK. 2012. Available: <http://www.cancerresearchuk.org/cancer-info/cancerstats/mortality/cancerdeaths/#Twenty> [Accessed 8th December 2014].
- CANCER RESEARCH UK. 2013a. Cancer Research UK. Available: <http://www.cancerresearchuk.org/cancer-info/cancerstats/incidence/> [Accessed 8th December 2014].
- CANCER RESEARCH UK. 2013b. Available: <http://www.cancerresearchuk.org/cancer-info/cancerstats/mortality/uk-cancer-mortality-statistics> [Accessed 8th December 2014].
- CANCER RESEARCH UK. 2013c. Available: <http://www.cancerresearchuk.org/about-cancer/what-is-cancer> [Accessed 8th December 2014].
- CANCER RESEARCH UK. 2014a. Available: <http://www.cancerresearchuk.org/cancer-info/cancerstats/types/breast/mortality/uk-breast-cancer-mortality-statistics> [Accessed 8th December 2014].
- CANCER RESEARCH UK. 2014b. Available: <http://www.cancerresearchuk.org/about-cancer/type/breast-cancer/treatment/tnm-breast-cancer-staging> [Accessed 26th April 2015].

- CARMINATI, M., GALLINI, S., PIROVANO, L., ALFIERI, A., BISI, S. & MAPELLI, M. 2016. Concomitant binding of Afadin to LGN and F-actin directs planar spindle orientation. *Nat Struct Mol Biol*, 23, 155-63.
- CASSIMERIS, L. 2009. Microtubule assembly: lattice GTP to the rescue. *Current Biology*, 19, R174-R176.
- CAUSSINUS, E. & GONZALEZ, C. 2005. Induction of tumor growth by altered stem-cell asymmetric division in *Drosophila melanogaster*. *Nat Genet*, 37, 1125-9.
- CERAMI, E., GAO, J., DOGRUSOZ, U., GROSS, B. E., SUMER, S. O., AKSOY, B. A., JACOBSEN, A., BYRNE, C. J., HEUER, M. L., LARSSON, E., ANTIPIN, Y., REVA, B., GOLDBERG, A. P., SANDER, C. & SCHULTZ, N. 2012. The cBio cancer genomics portal: an open platform for exploring multidimensional cancer genomics data. *Cancer Discov*, 2, 401-4.
- CHANEAU, M., IOANNOU, M. S. & MCPHERSON, P. S. 2013. Rab35: GEFs, GAPs and effectors. *Traffic*, 14, 1109-17.
- CHAKRABORTY, S., LEVENSON, A. S. & BISWAS, P. K. 2013. Structural insights into Resveratrol's antagonist and partial agonist actions on estrogen receptor alpha. *BMC Struct Biol*, 13, 27.
- CHAN, J. Y. 2011. A clinical overview of centrosome amplification in human cancers. *Int J Biol Sci*, 7, 1122-44.
- CHAVEZ, K. J., GARIMELLA, S. V. & LIPKOWITZ, S. 2010. Triple negative breast cancer cell lines: one tool in the search for better treatment of triple negative breast cancer. *Breast Dis*, 32, 35-48.
- CHEN, C. T., HEHNLY, H., YU, Q., FARKAS, D., ZHENG, G., REDICK, S. D., HUNG, H. F., SAMTANI, R., JURCZYK, A., AKBARIAN, S., WISE, C., JACKSON, A., BOBER, M., GUO, Y., LO, C. & DOXSEY, S. 2014. A unique set of centrosome proteins requires pericentrin for spindle-pole localization and spindle orientation. *Curr Biol*, 24, 2327-2334.
- CHOI, S. Y., CHACON-HESZELE, M. F., HUANG, L., MCKENNA, S., WILSON, F. P., ZUO, X. & LIPSCHUTZ, J. H. 2013. Cdc42 deficiency causes ciliary abnormalities and cystic kidneys. *J Am Soc Nephrol*, 24, 1435-50.
- CLUCAS, J. & VALDERRAMA, F. 2014. ERM proteins in cancer progression. *J Cell Sci*, 127, 267-75.
- COLE, N. B. & LIPPINCOTT-SCHWARTZ, J. 1995a. Organization of organelles and membrane traffic by microtubules. *Current opinion in cell biology*, 7, 55-64.
- COLE, N. B. & LIPPINCOTT-SCHWARTZ, J. 1995b. Organization of organelles and membrane traffic by microtubules. *Curr Opin Cell Biol*, 7, 55-64.
- CONDUIT, P. T., FENG, Z., RICHENS, J. H., BAUMBACH, J., WAINMAN, A., BAKSHI, S. D., DOBBELAERE, J., JOHNSON, S., LEA, S. M. & RAFF, J. W. 2014. The centrosome-specific phosphorylation of Cnn by Polo/Plk1 drives Cnn scaffold assembly and centrosome maturation. *Dev Cell*, 28, 659-69.
- COOK, T. A., NAGASAKI, T. & GUNDERSEN, G. G. 1998. Rho guanosine triphosphatase mediates the selective stabilization of microtubules induced by lysophosphatidic acid. *The Journal of cell biology*, 141, 175-185.
- COOMBES, C., YAMAMOTO, A., MCCLELLAN, M., REID, T. A., PLOOSTER, M., LUXTON, G. W., ALPER, J., HOWARD, J. & GARDNER, M. K. 2016. Mechanism of microtubule lumen entry for the  $\alpha$ -tubulin acetyltransferase enzyme  $\alpha$ TAT1. *Proc Natl Acad Sci U S A*, 113, E7176-E7184.
- COTA, R. R., TEIXIDÓ-TRAVESA, N., EZQUERRA, A., EIBES, S., LACASA, C., ROIG, J. & LÜDERS, J. 2017. MZT1 regulates microtubule nucleation by linking  $\gamma$ TuRC assembly to adapter-mediated targeting and activation. *J Cell Sci*, 130, 406-419.
- CROWELL, J. A., KORYTKO, P. J., MORRISSEY, R. L., BOOTH, T. D. & LEVINE, B. S. 2004. Resveratrol-associated renal toxicity. *Toxicol Sci*, 82, 614-9.

- CUNHA-FERREIRA, I., RODRIGUES-MARTINS, A., BENTO, I., RIPARBELLI, M., ZHANG, W., LAUE, E., CALLAINI, G., GLOVER, D. M. & BETTENCOURT-DIAS, M. 2009. The SCF/Slimb ubiquitin ligase limits centrosome amplification through degradation of SAK/PLK4. *Curr Biol*, 19, 43-9.
- DAMMERMANN, A. & MERDES, A. 2002. Assembly of centrosomal proteins and microtubule organization depends on PCM-1. *J Cell Biol*, 159, 255-66.
- DANEN, E. H. & SONNENBERG, A. 2003. Integrins in regulation of tissue development and function. *J Pathol*, 201, 632-41.
- DATTA, A., BRYANT, D. M. & MOSTOV, K. E. 2011. Molecular regulation of lumen morphogenesis. *Curr Biol*, 21, R126-36.
- DE CRAENE, B. & BERX, G. 2013. Regulatory networks defining EMT during cancer initiation and progression. *Nature Reviews Cancer*, 13, 97-110.
- DE FORGES, H., PILON, A., CANTALOUBE, I., PALLANDRE, A., HAGHIRI-GOSNET, A. M., PEREZ, F. & POÛS, C. 2016. Localized Mechanical Stress Promotes Microtubule Rescue. *Curr Biol*, 26, 3399-3406.
- DE GROOT, C. O., JELESAROV, L., DAMBERGER, F. F., BJELIĆ, S., SCHÄRER, M. A., BHAVESH, N. S., GRIGORIEV, L., BUEY, R. M., WÜTHRICH, K., CAPITANI, G., AKHMANOVA, A. & STEINMETZ, M. O. 2010. Molecular insights into mammalian end-binding protein heterodimerization. *J. Biol. Chem.*, 285, 5802-5814.
- DE LUCA, M., BRUNETTO, L., ASTERITI, I. A., GIUBETTINI, M., LAVIA, P. & GUARGUAGLINI, G. 2008. Aurora-A and ch-TOG act in a common pathway in control of spindle pole integrity. *Oncogene*, 27, 6539-49.
- DEBNATH, J., MUTHUSWAMY, S. K. & BRUGGE, J. S. 2003. Morphogenesis and oncogenesis of MCF-10A mammary epithelial acini grown in three-dimensional basement membrane cultures. *Methods*, 30, 256-68.
- DELAVAL, B., FERRAND, A., CONTE, N., LARROQUE, C., HERNANDEZ-VERDUN, D., PRIGENT, C. & BIRNBAUM, D. 2004. Aurora B -TACC1 protein complex in cytokinesis. *Oncogene*, 23, 4516-22.
- DESAI, A. & MITCHISON, T. J. 1997. Microtubule polymerization dynamics. *Annual review of cell and developmental biology*, 13, 83-117.
- DETAMPEL, P., BECK, M., KRAHENBUHL, S. & HUWYLER, J. 2012. Drug interaction potential of resveratrol. *Drug Metab Rev*, 44, 253-65.
- DEWEY, E. B., SANCHEZ, D. & JOHNSTON, C. A. 2015. Warts phosphorylates mud to promote pins-mediated mitotic spindle orientation in *Drosophila*, independent of Yorkie. *Curr Biol*, 25, 2751-2762.
- DI PIETRO, F., ECHARD, A. & MORIN, X. 2016. Regulation of mitotic spindle orientation: an integrated view. *EMBO Rep*, 17, 1106-30.
- DIMITROV, A., QUESNOIT, M., MOUTEL, S., CANTALOUBE, I., POÛS, C. & PEREZ, F. 2008. Detection of GTP-tubulin conformation in vivo reveals a role for GTP remnants in microtubule rescues. *Science*, 322, 1353-6.
- DOMINGUEZ, R. & HOLMES, K. C. 2011. Actin structure and function. *Annu Rev Biophys*, 40, 169-86.
- DOMPIERRE, J. P., GODIN, J. D., CHARRIN, B. C., CORDELIÈRES, F. P., KING, S. J., HUMBERT, S. & SAUDOU, F. 2007. Histone deacetylase 6 inhibition compensates for the transport deficit in Huntington's disease by increasing tubulin acetylation. *The Journal of neuroscience*, 27, 3571-3583.
- DONG, X., LIU, F., SUN, L., LIU, M., LI, D., SU, D., ZHU, Z., DONG, J. T., FU, L. & ZHOU, J. 2010. Oncogenic function of microtubule end - binding protein 1 in breast cancer. *The Journal of pathology*, 220, 361-369.
- DU, Q. & MACARA, I. G. 2004. Mammalian Pins is a conformational switch that links NuMA to heterotrimeric G proteins. *Cell*, 119, 503-16.

- DU, Y., ENGLISH, C. A. & OHI, R. 2010. The kinesin-8 Kif18A dampens microtubule plus-end dynamics. *Curr Biol*, 20, 374-80.
- DURGAN, J., KAJI, N., JIN, D. & HALL, A. 2011. Par6B and atypical PKC regulate mitotic spindle orientation during epithelial morphogenesis. *J Biol Chem*, 286, 12461-74.
- DUTERTRE, S., CAZALES, M., QUARANTA, M., FROMENT, C., TRABUT, V., DOZIER, C., MIREY, G., BOUCHE, J. P., THEIS-FEBVRE, N., SCHMITT, E., MONSARRAT, B., PRIGENT, C. & DUCOMMUN, B. 2004. Phosphorylation of CDC25B by Aurora-A at the centrosome contributes to the G2-M transition. *J Cell Sci*, 117, 2523-31.
- DZHINDZHEV, N. S., ROGERS, S. L., VALE, R. D. & OHKURA, H. 2005. Distinct mechanisms govern the localisation of Drosophila CLIP-190 to unattached kinetochores and microtubule plus-ends. *J Cell Sci*, 118, 3781-90.
- EFIMOV, A., KHARITONOV, A., EFIMOVA, N., LONCAREK, J., MILLER, P. M., ANDREYEVA, N., GLEESON, P., GALJART, N., MAIA, A. R., MCLEOD, I. X., YATES, J. R., MAIATO, H., KHODJAKOV, A., AKHMANOVA, A. & KAVERINA, I. 2007. Asymmetric CLASP-dependent nucleation of noncentrosomal microtubules at the trans-Golgi network. *Dev Cell*, 12, 917-30.
- ELIAS, B. C., DAS, A., PAREKH, D. V., MERNAUGH, G., ADAMS, R., YANG, Z., BRAKEBUSCH, C., POZZI, A., MARCIANO, D. K., CARROLL, T. J. & ZENT, R. 2015. Cdc42 regulates epithelial cell polarity and cytoskeletal function during kidney tubule development. *J Cell Sci*, 128, 4293-305.
- ERIKSSON, J. E., DECHAT, T., GRIN, B., HELFAND, B., MENDEZ, M., PALLARI, H. M. & GOLDMAN, R. D. 2009. Introducing intermediate filaments: from discovery to disease. *J Clin Invest*, 119, 1763-71.
- ERSFELD, K., WEHLAND, J., PLESSMANN, U., DODEMONT, H., GERKE, V. & WEBER, K. 1993. Characterization of the tubulin-tyrosine ligase. *J Cell Biol*, 120, 725-32.
- ESPIRITU, E. B., KRUEGER, L. E., YE, A. & ROSE, L. S. 2012. CLASPs function redundantly to regulate astral microtubules in the C. elegans embryo. *Dev Biol*, 368, 242-54.
- ETIENNE-MANNEVILLE, S. 2013. Microtubules in cell migration. *Annu Rev Cell Dev Biol*, 29, 471-99.
- ETIENNE-MANNEVILLE, S. & HALL, A. 2001. Integrin-mediated activation of Cdc42 controls cell polarity in migrating astrocytes through PKCzeta. *Cell*, 106, 489-98.
- ETIENNE-MANNEVILLE, S. & HALL, A. 2002. Rho GTPases in cell biology. *Nature*, 420, 629-635.
- ETIENNE-MANNEVILLE, S. & HALL, A. 2003a. Cdc42 regulates GSK-3beta and adenomatous polyposis coli to control cell polarity. *Nature*, 421, 753-6.
- ETIENNE-MANNEVILLE, S. & HALL, A. 2003b. Cell polarity: Par6, aPKC and cytoskeletal crosstalk. *Curr Opin Cell Biol*, 15, 67-72.
- EZRATTY, E. J., PARTRIDGE, M. A. & GUNDERSEN, G. G. 2005. Microtubule-induced focal adhesion disassembly is mediated by dynamin and focal adhesion kinase. *Nat Cell Biol*, 7, 581-90.
- FANNING, A. S., VAN ITALLIE, C. M. & ANDERSON, J. M. 2012. Zonula occludens-1 and -2 regulate apical cell structure and the zonula adherens cytoskeleton in polarized epithelia. *Mol Biol Cell*, 23, 577-90.
- FEHON, R. G., MCCLATCHEY, A. I. & BRETSCHER, A. 2010. Organizing the cell cortex: the role of ERM proteins. *Nat Rev Mol Cell Biol*, 11, 276-87.
- FERRARI, A., VELIGODSKIY, A., BERGE, U., LUCAS, M. S. & KROSCHEWSKI, R. 2008. ROCK-mediated contractility, tight junctions and channels contribute to the conversion of a preapical patch into apical surface during isochoric lumen initiation. *J Cell Sci*, 121, 3649-63.

- FIELDING, A. B., DOBREVA, I., MCDONALD, P. C., FOSTER, L. J. & DEDHAR, S. 2008. Integrin-linked kinase localizes to the centrosome and regulates mitotic spindle organization. *J Cell Biol*, 180, 681-9.
- FIFE, C. M., MCCARROLL, J. A. & KAVALLARIS, M. 2014. Movers and shakers: cell cytoskeleton in cancer metastasis. *Br J Pharmacol*, 171, 5507-23.
- FINK, J., CARPI, N., BETZ, T., BETARD, A., CHEBAH, M., AZIOUNE, A., BORNENS, M., SYKES, C., FETLER, L., CUVELIER, D. & PIEL, M. 2011. External forces control mitotic spindle positioning. *Nat Cell Biol*, 13, 771-8.
- FIRAT-KARALAR, E. N. & STEARNS, T. 2014. The centriole duplication cycle. *Philos Trans R Soc Lond B Biol Sci*, 369.
- FONG, K. W., AU, F. K. C., JIA, Y., YANG, S., ZHOU, L. & QI, R. Z. 2017. Microtubule plus-end tracking of end-binding protein 1 (EB1) is regulated by CDK5 regulatory subunit-associated protein 2. *J Biol Chem*, 292, 7675-7687.
- FONG, K. W., HAU, S. Y., KHO, Y. S., JIA, Y., HE, L. & QI, R. Z. 2009. Interaction of CDK5RAP2 with EB1 to track growing microtubule tips and to regulate microtubule dynamics. *Mol Biol Cell*, 20, 3660-70.
- FRANCO-BARRAZA, J., VALDIVIA-SILVA, J. E., ZAMUDIO-MEZA, H., CASTILLO, A., GARCÍA-ZEPEDA, E. A., BENÍTEZ-BRIBIESCA, L. & MEZA, I. 2010. Actin cytoskeleton participation in the onset of IL-1beta induction of an invasive mesenchymal-like phenotype in epithelial MCF-7 cells. *Arch Med Res*, 41, 170-81.
- FRIEDL, P. & GILMOUR, D. 2009. Collective cell migration in morphogenesis, regeneration and cancer. *Nat Rev Mol Cell Biol*, 10, 445-57.
- FRY, A. M. 2015. Solving the centriole disengagement puzzle. *Nat Cell Biol*, 17, 3-5.
- FUCHS, E. & WEBER, K. 1994. Intermediate filaments: structure, dynamics, function, and disease. *Annu Rev Biochem*, 63, 345-82.
- FUJII, K., KONDO, T., YOKOO, H., YAMADA, T., IWATSUKI, K. & HIROHASHI, S. 2005. Proteomic study of human hepatocellular carcinoma using two - dimensional difference gel electrophoresis with saturation cysteine dye. *Proteomics*, 5, 1411-1422.
- FUKASAWA, K. 2005. Centrosome amplification, chromosome instability and cancer development. *Cancer Lett*, 230, 6-19.
- GALJART, N. 2010. Plus-end-tracking proteins and their interactions at microtubule ends. *Curr Biol*, 20, R528-37.
- GALLINI, S., CARMINATI, M., DE MATTIA, F., PIROVANO, L., MARTINI, E., OLDANI, A., ASTERITI, I. A., GUARGUAGLINI, G. & MAPELLI, M. 2016. NuMA Phosphorylation by Aurora-A Orchestrates Spindle Orientation. *Curr Biol*, 26, 458-69.
- GALVEZ-SANTISTEBAN, M., RODRIGUEZ-FRATICELLI, A. E., BRYANT, D. M., VERGARAJAUREGUI, S., YASUDA, T., BANON-RODRIGUEZ, I., BERNASCONE, I., DATTA, A., SPIVAK, N., YOUNG, K., SLIM, C. L., BRAKEMAN, P. R., FUKUDA, M., MOSTOV, K. E. & MARTIN-BELMONTE, F. 2012. Synaptotagmin-like proteins control the formation of a single apical membrane domain in epithelial cells. *Nat Cell Biol*, 14, 838-49.
- GANEM, N. J., GODINHO, S. A. & PELLMAN, D. 2009. A mechanism linking extra centrosomes to chromosomal instability. *Nature*, 460, 278-82.
- GARD, D. L. & KIRSCHNER, M. W. 1987. A microtubule-associated protein from *Xenopus* eggs that specifically promotes assembly at the plus-end. *J Cell Biol*, 105, 2203-15.
- GARDNER, M. K., ZANIC, M., GELL, C., BORMUTH, V. & HOWARD, J. 2011. Depolymerizing kinesins Kip3 and MCAK shape cellular microtubule architecture by differential control of catastrophe. *Cell*, 147, 1092-103.
- GARNHAM, C. P. & ROLL - MECAK, A. 2012. The chemical complexity of cellular microtubules: tubulin post - translational modification enzymes and their roles in tuning microtubule functions. *Cytoskeleton*, 69, 442-463.

- GEHM, B. D., MCANDREWS, J. M., CHIEN, P. Y. & JAMESON, J. L. 1997. Resveratrol, a polyphenolic compound found in grapes and wine, is an agonist for the estrogen receptor. *Proc Natl Acad Sci U S A*, 94, 14138-43.
- GIERKE, S. & WITTMANN, T. 2012. EB1-recruited microtubule +TIP complexes coordinate protrusion dynamics during 3D epithelial remodeling. *Curr Biol*, 22, 753-62.
- GLOERICH, M., BIANCHINI, J. M., SIEMERS, K. A., COHEN, D. J. & NELSON, W. J. 2017. Cell division orientation is coupled to cell-cell adhesion by the E-cadherin/LGN complex. *Nat Commun*, 8, 13996.
- GODINHO, S. A., KWON, M. & PELLMAN, D. 2009. Centrosomes and cancer: how cancer cells divide with too many centrosomes. *Cancer Metastasis Rev*, 28, 85-98.
- GODINHO, S. A., PICONE, R., BURUTE, M., DAGHER, R., SU, Y., LEUNG, C. T., POLYAK, K., BRUGGE, J. S., THERY, M. & PELLMAN, D. 2014. Oncogene-like induction of cellular invasion from centrosome amplification. *Nature*, 510, 167-71.
- GOLDSPINK, D. A., GADSBY, J. R., BELLETT, G., KEYNTON, J., TYRRELL, B. J., LUND, E. K., POWELL, P. P., THOMAS, P. & MOGENSEN, M. M. 2013. The microtubule end-binding protein EB2 is a central regulator of microtubule reorganisation in apico-basal epithelial differentiation. *Journal of cell science*, 126, 4000-4014.
- GOLDSPINK, D. A., ROOKYARD, C., TYRRELL, B. J., GADSBY, J., PERKINS, J., LUND, E. K., GALJART, N., THOMAS, P., WILEMAN, T. & MOGENSEN, M. M. 2017a. Ninein is essential for apico-basal microtubule formation and CLIP-170 facilitates its redeployment to non-centrosomal microtubule organizing centres. *Open Biology*, 7, 160274.
- GOLDSTEIN, B. & MACARA, I. G. 2007. The PAR proteins: fundamental players in animal cell polarization. *Dev Cell*, 13, 609-22.
- GOMES, E. R., JANI, S. & GUNDERSEN, G. G. 2005. Nuclear movement regulated by Cdc42, MRCK, myosin, and actin flow establishes MTOC polarization in migrating cells. *Cell*, 121, 451-63.
- GONZALO, S. 2010. Epigenetic alterations in aging. *J Appl Physiol (1985)*, 109, 586-97.
- GOS, M., MIŁOSZEWSKA, J. & PRZYBYSZEWSKA, M. 2008. [Epithelial-mesenchymal transition in cancer progression]. *Postepy biochemii*, 55, 121-128.
- GOTO, H., KOSAKO, H., TANABE, K., YANAGIDA, M., SAKURAI, M., AMANO, M., KAIBUCHI, K. & INAGAKI, M. 1998. Phosphorylation of vimentin by Rho-associated kinase at a unique amino-terminal site that is specifically phosphorylated during cytokinesis. *J Biol Chem*, 273, 11728-36.
- GRASER, S., STIERHOF, Y. D. & NIGG, E. A. 2007. Cep68 and Cep215 (Cdk5rap2) are required for centrosome cohesion. *J Cell Sci*, 120, 4321-31.
- GREEN, R. A., WOLLMAN, R. & KAPLAN, K. B. 2005. APC and EB1 function together in mitosis to regulate spindle dynamics and chromosome alignment. *Mol Biol Cell*, 16, 4609-22.
- GRIMALDI, A. D., MAKI, T., FITTON, B. P., ROTH, D., YAMPOLSKY, D., DAVIDSON, M. W., SVITKINA, T., STRAUBE, A., HAYASHI, I. & KAVERINA, I. 2014. CLASPs are required for proper microtubule localization of end-binding proteins. *Dev Cell*, 30, 343-52.
- GROMLEY, A., JURCZYK, A., SILLIBOURNE, J., HALILOVIC, E., MOGENSEN, M., GROISMAN, I., BLOMBERG, M. & DOXSEY, S. 2003. A novel human protein of the maternal centriole is required for the final stages of cytokinesis and entry into S phase. *J Cell Biol*, 161, 535-45.
- GRUBER, J., HARBORTH, J., SCHNABEL, J., WEBER, K. & HATZFELD, M. 2002. The mitotic-spindle-associated protein astrin is essential for progression through mitosis. *J Cell Sci*, 115, 4053-9.
- GUICHARD, P., DESFOSES, A., MAHESHWARI, A., HACHET, V., DIETRICH, C., BRUNE, A., ISHIKAWA, T., SACHSE, C. & GONCZY, P. 2012. Cartwheel architecture of *Trichonympha* basal body. *Science*, 337, 553.

- GUNDERSEN, G. G., GOMES, E. R. & WEN, Y. 2004. Cortical control of microtubule stability and polarization. *Curr Opin Cell Biol*, 16, 106-12.
- GUNDERSEN, G. G., KALNOSKI, M. H. & BULINSKI, J. C. 1984. Distinct populations of microtubules: tyrosinated and nontyrosinated alpha tubulin are distributed differently in vivo. *Cell*, 38, 779-89.
- GUTZMAN, J. H. & SIVE, H. 2010. Epithelial relaxation mediated by the myosin phosphatase regulator Mypt1 is required for brain ventricle lumen expansion and hindbrain morphogenesis. *Development*, 137, 795-804.
- HABEDANCK, R., STIERHOF, Y. D., WILKINSON, C. J. & NIGG, E. A. 2005. The Polo kinase Plk4 functions in centriole duplication. *Nat Cell Biol*, 7, 1140-6.
- HALLAK, M. E., RODRIGUEZ, J. A., BARRA, H. S. & CAPUTTO, R. 1977. Release of tyrosine from tyrosinated tubulin. Some common factors that affect this process and the assembly of tubulin. *FEBS Lett*, 73, 147-50.
- HALLOWS, K. R., KOBINGER, G. P., WILSON, J. M., WITTERS, L. A. & FOSKETT, J. K. 2003. Physiological modulation of CFTR activity by AMP-activated protein kinase in polarized T84 cells. *Am J Physiol Cell Physiol*, 284, C1297-308.
- HAMMOND, J. W., CAI, D. & VERHEY, K. J. 2008. Tubulin modifications and their cellular functions. *Curr Opin Cell Biol*, 20, 71-6.
- HANAHAN, D. & WEINBERG, R. A. 2011. Hallmarks of cancer: the next generation. *Cell*, 144, 646-74.
- HANNAK, E., KIRKHAM, M., HYMAN, A. A. & OEGEMA, K. 2001. Aurora-A kinase is required for centrosome maturation in *Caenorhabditis elegans*. *J Cell Biol*, 155, 1109-16.
- HAO, Y., DU, Q., CHEN, X., ZHENG, Z., BALSBAUGH, J. L., MAITRA, S., SHABANOWITZ, J., HUNT, D. F. & MACARA, I. G. 2010. Par3 controls epithelial spindle orientation by aPKC-mediated phosphorylation of apical Pins. *Curr Biol*, 20, 1809-18.
- HATCH, E. M., KULUKIAN, A., HOLLAND, A. J., CLEVELAND, D. W. & STEARNS, T. 2010. Cep152 interacts with Plk4 and is required for centriole duplication. *J Cell Biol*, 191, 721-9.
- HAWKINS, T., MIRIGIAN, M., SELCUK YASAR, M. & ROSS, J. L. 2010. Mechanics of microtubules. *J Biomech*, 43, 23-30.
- HAYES, E. L. & LEWIS-WAMBI, J. S. 2015. Mechanisms of endocrine resistance in breast cancer: an overview of the proposed roles of noncoding RNA. *Breast Cancer Res*, 17, 40.
- HEBERT, A. M., DUBOFF, B., CASALETTO, J. B., GLADDEN, A. B. & MCCLATCHEY, A. I. 2012. Merlin/ERM proteins establish cortical asymmetry and centrosome position. *Genes Dev*, 26, 2709-23.
- HESSE, M., MAGIN, T. M. & WEBER, K. 2001. Genes for intermediate filament proteins and the draft sequence of the human genome: novel keratin genes and a surprisingly high number of pseudogenes related to keratin genes 8 and 18. *J Cell Sci*, 114, 2569-75.
- HOLLAND, A. J. & CLEVELAND, D. W. 2009. Boveri revisited: chromosomal instability, aneuploidy and tumorigenesis. *Nat Rev Mol Cell Biol*, 10, 478-87.
- HOLLAND, A. J., FACHINETTI, D., ZHU, Q., BAUER, M., VERMA, I. M., NIGG, E. A. & CLEVELAND, D. W. 2012. The autoregulated instability of Polo-like kinase 4 limits centrosome duplication to once per cell cycle. *Genes Dev*, 26, 2684-9.
- HOLLIDAY, D. L. & SPEIRS, V. 2011. Choosing the right cell line for breast cancer research. *Breast Cancer Res*, 13, 215.
- HONG, Y. B., KANG, H. J., KIM, H. J., ROSEN, E. M., DAKSHANAMURTHY, S., RONDANIN, R., BARUCHELLO, R., GRISOLIA, G., DANIELE, S. & BAE, I. 2009. Inhibition of cell proliferation by a resveratrol analog in human pancreatic and breast cancer cells. *Exp Mol Med*, 41, 151-60.

- HONNAPPA, S., GOUVEIA, S. M., WEISBRICH, A., DAMBERGER, F. F., BHAVESH, N. S., JAWHARI, H., GRIGORIEV, I., VAN RIJSSEL, F. J., BUEY, R. M., LAWERA, A., JELESAROV, I., WINKLER, F. K., WUTHRICH, K., AKHMANOVA, A. & STEINMETZ, M. O. 2009. An EB1-binding motif acts as a microtubule tip localization signal. *Cell*, 138, 366-76.
- HONNAPPA, S., OKHRIMENKO, O., JAUSSE, R., JAWHARI, H., JELESAROV, I., WINKLER, F. K. & STEINMETZ, M. O. 2006. Key interaction modes of dynamic +TIP networks. *Mol Cell*, 23, 663-71.
- HORWITZ, K. B., COSTLOW, M. E. & MCGUIRE, W. L. 1975. MCF-7; a human breast cancer cell line with estrogen, androgen, progesterone, and glucocorticoid receptors. *Steroids*, 26, 785-95.
- HOTULAINEN, P. & LAPPALAINEN, P. 2006. Stress fibers are generated by two distinct actin assembly mechanisms in motile cells. *J Cell Biol*, 173, 383-94.
- HOWARD, J. & HYMAN, A. A. 2007. Microtubule polymerases and depolymerases. *Curr Opin Cell Biol*, 19, 31-5.
- HOWES, S. C., ALUSHIN, G. M., SHIDA, T., NACHURY, M. V. & NOGALES, E. 2014. Effects of tubulin acetylation and tubulin acetyltransferase binding on microtubule structure. *Mol Biol Cell*, 25, 257-66.
- HSIEH, T. C., BURFEIND, P., LAUD, K., BACKER, J. M., TRAGANOS, F., DARZYNKIEWICZ, Z. & WU, J. M. 1999. Cell cycle effects and control of gene expression by resveratrol in human breast carcinoma cell lines with different metastatic potentials. *Int J Oncol*, 15, 245-52.
- HU, Y. L., LU, S., SZETO, K. W., SUN, J., WANG, Y., LASHERAS, J. C. & CHIEN, S. 2014. FAK and paxillin dynamics at focal adhesions in the protrusions of migrating cells. *Sci Rep*, 4, 6024.
- HUBBERT, C., GUARDIOLA, A., SHAO, R., KAWAGUCHI, Y., ITO, A., NIXON, A., YOSHIDA, M., WANG, X. F. & YAO, T. P. 2002. HDAC6 is a microtubule-associated deacetylase. *Nature*, 417, 455-8.
- HUNG, H. F., HEHNLY, H. & DOXSEY, S. 2016. The Mother Centriole Appendage Protein Cenexin Modulates Lumen Formation through Spindle Orientation. *Curr Biol*, 26, 793-801.
- HURD, D. D. & KEMPHUES, K. J. 2003. PAR-1 is required for morphogenesis of the *Caenorhabditis elegans* vulva. *Dev Biol*, 253, 54-65.
- IIMORI, M., WATANABE, S., KIYONARI, S., MATSUOKA, K., SAKASAI, R., SAEKI, H., OKI, E., KITAO, H. & MAEHARA, Y. 2016a. Phosphorylation of EB2 by Aurora B and CDK1 ensures mitotic progression and genome stability. *Nat Commun*, 7, 11117.
- IIMORI, M., WATANABE, S., KIYONARI, S., MATSUOKA, K., SAKASAI, R., SAEKI, H., OKI, E., KITAO, H. & MAEHARA, Y. 2016b. Phosphorylation of EB2 by Aurora B and CDK1 ensures mitotic progression and genome stability. *Nature communications*, 7.
- IOANNOU, M. S. & MCPHERSON, P. S. 2016. Rab-mediated membrane trafficking and the control of epithelial cell polarity. *J Cell Biol*, 213, 301-3.
- IWAO, Y., MURAKAWA, T., YAMAGUCHI, J. & YAMASHITA, M. 2002. Localization of gamma-tubulin and cyclin B during early cleavage in physiologically polyspermic newt eggs. *Dev Growth Differ*, 44, 489-99.
- JACQUEMET, G., HAMIDI, H. & IVASKA, J. 2015. Filopodia in cell adhesion, 3D migration and cancer cell invasion. *Curr Opin Cell Biol*, 36, 23-31.
- JAFFE, A. B., KAJI, N., DURGAN, J. & HALL, A. 2008. Cdc42 controls spindle orientation to position the apical surface during epithelial morphogenesis. *J Cell Biol*, 183, 625-33.
- JANKE, C. & MONTAGNAC, G. 2017. Causes and Consequences of Microtubule Acetylation. *Curr Biol*, 27, R1287-R1292.
- JANKE, C., ROGOWSKI, K., WLOGA, D., REGNARD, C., KAJAVA, A. V., STRUB, J. M., TEMURAK, N., VAN DIJK, J., BOUCHER, D., VAN DORSSELAER, A., SURYAVANSHI, S., GAERTIG, J.

- & EDDE, B. 2005. Tubulin polyglutamylase enzymes are members of the TTL domain protein family. *Science*, 308, 1758-62.
- JANSEN, S., COLLINS, A., YANG, C., REBOWSKI, G., SVITKINA, T. & DOMINGUEZ, R. 2011. Mechanism of actin filament bundling by fascin. *J Biol Chem*, 286, 30087-96.
- JAULIN, F. & KREITZER, G. 2010. KIF17 stabilizes microtubules and contributes to epithelial morphogenesis by acting at MT plus ends with EB1 and APC. *J Cell Biol*, 190, 443-60.
- JAYATILAKA, H., GIRI, A., KARL, M., AIFUWA, I., TRENTON, N. J., PHILLIP, J. M., KHATAU, S. & WIRTZ, D. 2017. EB1 and cytoplasmic dynein mediate protrusion dynamics for efficient 3-dimensional cell migration. *FASEB J*.
- JI, J., FENG, X., SHI, M., CAI, Q., YU, Y., ZHU, Z. & ZHANG, J. 2015. Rac1 is correlated with aggressiveness and a potential therapeutic target for gastric cancer. *Int J Oncol*, 46, 1343-53.
- JIANG, K., HUA, S., MOHAN, R., GRIGORIEV, I., YAU, K. W., LIU, Q., KATRUKHA, E. A., ALTELAAR, A. F., HECK, A. J., HOOGENRAAD, C. C. & AKHMANOVA, A. 2014. Microtubule minus-end stabilization by polymerization-driven CAMSAP deposition. *Dev Cell*, 28, 295-309.
- JIANG, K., TOEDT, G., MONTENEGRO GOUVEIA, S., DAVEY, N. E., HUA, S., VAN DER VAART, B., GRIGORIEV, I., LARSEN, J., PEDERSEN, L. B., BEZSTAROSTI, K., LINCE-FARIA, M., DEMMERS, J., STEINMETZ, M. O., GIBSON, T. J. & AKHMANOVA, A. 2012. A Proteome-wide screen for mammalian SxIP motif-containing microtubule plus-end tracking proteins. *Curr Biol*, 22, 1800-7.
- JOKINEN, J., DADU, E., NYKVIST, P., KÄPYLÄ, J., WHITE, D. J., IVASKA, J., VEHVILÄINEN, P., REUNANEN, H., LARJAVA, H., HÄKKINEN, L. & HEINO, J. 2004. Integrin-mediated cell adhesion to type I collagen fibrils. *J Biol Chem*, 279, 31956-63.
- JORDAN, M. A. & WILSON, L. 2004. Microtubules as a target for anticancer drugs. *Nat Rev Cancer*, 4, 253-65.
- KALININA, E., BISWAS, R., BEREZNIUK, I., HERMOSO, A., AVILES, F. X. & FRICKER, L. D. 2007. A novel subfamily of mouse cytosolic carboxypeptidases. *FASEB J*, 21, 836-50.
- KANDASWAMI, C., PERKINS, E., SOLONIUK, D. S., DRZEWIECKI, G. & MIDDLETON, E. 1991. Antiproliferative effects of citrus flavonoids on a human squamous cell carcinoma in vitro. *Cancer Lett*, 56, 147-52.
- KAPUR, J. N. 1985. A New Method for Gray-Level Picture Thresholding Using the Entropy of the Histogram. **29** 273-285.
- KAVERINA, I., KRYLYSHKINA, O. & SMALL, J. V. 2002. Regulation of substrate adhesion dynamics during cell motility. *The international journal of biochemistry & cell biology*, 34, 746-761.
- KAVERINA, I., ROTTNER, K. & SMALL, J. V. 1998. Targeting, capture, and stabilization of microtubules at early focal adhesions. *The Journal of cell biology*, 142, 181-190.
- KAVERINA, I. & STRAUBE, A. 2011. Regulation of cell migration by dynamic microtubules. *Semin Cell Dev Biol*, 22, 968-74.
- KERN, D. M., NICHOLLS, P. K., PAGE, D. C. & CHEESEMAN, I. M. 2016. A mitotic SKAP isoform regulates spindle positioning at astral microtubule plus ends. *J Cell Biol*, 213, 315-28.
- KESSENBROCK, K., PLAKS, V. & WERB, Z. 2010. Matrix metalloproteinases: regulators of the tumor microenvironment. *Cell*, 141, 52-67.
- KHODJAKOV, A., COLE, R. W., OAKLEY, B. R. & RIEDER, C. L. 2000. Centrosome-independent mitotic spindle formation in vertebrates. *Curr Biol*, 10, 59-67.
- KIM, S. & COULOMBE, P. A. 2007. Intermediate filament scaffolds fulfill mechanical, organizational, and signaling functions in the cytoplasm. *Genes Dev*, 21, 1581-97.
- KIM, Y. A., CHOI, B. T., LEE, Y. T., PARK, D. I., RHEE, S. H., PARK, K. Y. & CHOI, Y. H. 2004. Resveratrol inhibits cell proliferation and induces apoptosis of human breast carcinoma MCF-7 cells. *Oncol Rep*, 11, 441-6.

- KIMURA, M., YOSHIOKA, T., SAIO, M., BANNO, Y., NAGAOKA, H. & OKANO, Y. 2013. Mitotic catastrophe and cell death induced by depletion of centrosomal proteins. *Cell Death Dis*, 4, e603.
- KINOSHITA, K., NOETZEL, T. L., PELLETIER, L., MECHTLER, K., DRECHSEL, D. N., SCHWAGER, A., LEE, M., RAFF, J. W. & HYMAN, A. A. 2005. Aurora A phosphorylation of TACC3/maskin is required for centrosome-dependent microtubule assembly in mitosis. *J Cell Biol*, 170, 1047-55.
- KIRSCHNER, M. W. 1980. Implications of treadmilling for the stability and polarity of actin and tubulin polymers in vivo. *J Cell Biol*, 86, 330-4.
- KITAGAWA, D., VAKONAKIS, I., OLIERIC, N., HILBERT, M., KELLER, D., OLIERIC, V., BORTFELD, M., ERAT, M. C., FLUCKIGER, I., GONCZY, P. & STEINMETZ, M. O. 2011. Structural basis of the 9-fold symmetry of centrioles. *Cell*, 144, 364-75.
- KIYOMITSU, T. & CHEESEMAN, I. M. 2012. Chromosome- and spindle-pole-derived signals generate an intrinsic code for spindle position and orientation. *Nat Cell Biol*, 14, 311-7.
- KLINKERT, K., ROCANCOURT, M., HOUDUSSE, A. & ECHARD, A. 2016. Rab35 GTPase couples cell division with initiation of epithelial apico-basal polarity and lumen opening. *Nat Commun*, 7, 11166.
- KNOBLICH, J. A. 2010. Asymmetric cell division: recent developments and their implications for tumour biology. *Nat Rev Mol Cell Biol*, 11, 849-60.
- KOLLMAN, J. M., MERDES, A., MOUREY, L. & AGARD, D. A. 2011. Microtubule nucleation by gamma-tubulin complexes. *Nat Rev Mol Cell Biol*, 12, 709-21.
- KOMAROVA, Y., DE GROOT, C. O., GRIGORIEV, I., GOUVEIA, S. M., MUNTEANU, E. L., SCHOBER, J. M., HONNAPPA, S., BUEY, R. M., HOOGENRAAD, C. C. & DOGTEROM, M. 2009. Mammalian end binding proteins control persistent microtubule growth. *The Journal of cell biology*, 184, 691-706.
- KOMAROVA, Y., LANSBERGEN, G., GALJART, N., GROSVELD, F., BORISY, G. G. & AKHMANOVA, A. 2005. EB1 and EB3 control CLIP dissociation from the ends of growing microtubules. *Mol Biol Cell*, 16, 5334-45.
- KOMAROVA, Y. A., AKHMANOVA, A. S., KOJIMA, S., GALJART, N. & BORISY, G. G. 2002. Cytoplasmic linker proteins promote microtubule rescue in vivo. *J Cell Biol*, 159, 589-99.
- KOTAK, S., BUSSO, C. & GONCZY, P. 2012. Cortical dynein is critical for proper spindle positioning in human cells. *J Cell Biol*, 199, 97-110.
- KOTAK, S., BUSSO, C. & GONCZY, P. 2014. NuMA interacts with phosphoinositides and links the mitotic spindle with the plasma membrane. *EMBO J*, 33, 1815-30.
- KOTAK, S. & GONCZY, P. 2013. Mechanisms of spindle positioning: cortical force generators in the limelight. *Curr Opin Cell Biol*, 25, 741-8.
- KOZUKI, Y., MIURA, Y. & YAGASAKI, K. 2001. Resveratrol suppresses hepatoma cell invasion independently of its anti-proliferative action. *Cancer Lett*, 167, 151-6.
- KRATZ, A. S., BARENZ, F., RICHTER, K. T. & HOFFMANN, I. 2015. Plk4-dependent phosphorylation of STIL is required for centriole duplication. *Biol Open*, 4, 370-7.
- KREPLAK, L. & FUDGE, D. 2007. Biomechanical properties of intermediate filaments: from tissues to single filaments and back. *Bioessays*, 29, 26-35.
- KUMAR, M., MEHRA, S., THAKAR, A., SHUKLA, N. K., ROYCHOUDHARY, A., SHARMA, M. C., RALHAN, R. & CHAUHAN, S. S. 2016. End Binding 1 (EB1) overexpression in oral lesions and cancer: A biomarker of tumor progression and poor prognosis. *Clin Chim Acta*, 459, 45-52.
- KUMAR, P. & WITTMANN, T. 2012. +TIPs: SxIPping along microtubule ends. *Trends Cell Biol*, 22, 418-28.

- KWON, M., GODINHO, S. A., CHANDHOK, N. S., GANEM, N. J., AZIOUNE, A., THERY, M. & PELLMAN, D. 2008. Mechanisms to suppress multipolar divisions in cancer cells with extra centrosomes. *Genes Dev*, 22, 2189-203.
- LAMOUILLE, S., XU, J. & DERYNCK, R. 2014. Molecular mechanisms of epithelial-mesenchymal transition. *Nat Rev Mol Cell Biol*, 15, 178-96.
- LANSBERGEN, G. & AKHMANOVA, A. 2006. Microtubule plus end: a hub of cellular activities. *Traffic*, 7, 499-507.
- LAUFFENBURGER, D. A. & HORWITZ, A. F. 1996. Cell migration: a physically integrated molecular process. *Cell*, 84, 359-69.
- LE CORRE, L., CHALABI, N., DELORT, L., BIGNON, Y. J. & BERNARD-GALLON, D. J. 2005. Resveratrol and breast cancer chemoprevention: molecular mechanisms. *Mol Nutr Food Res*, 49, 462-71.
- LECHTRECK, K. F., TELTENKÖTTER, A. & GRUNOW, A. 1999. A 210 kDa protein is located in a membrane-microtubule linker at the distal end of mature and nascent basal bodies. *J Cell Sci*, 112 ( Pt 11), 1633-44.
- LEE, K. & RHEE, K. 2012. Separase-dependent cleavage of pericentrin B is necessary and sufficient for centriole disengagement during mitosis. *Cell Cycle*, 11, 2476-85.
- LENARD, A., ELLERTSDOTTIR, E., HERWIG, L., KRUDEWIG, A., SAUTEUR, L., BELTING, H. G. & AFFOLTER, M. 2013. In vivo analysis reveals a highly stereotypic morphogenetic pathway of vascular anastomosis. *Dev Cell*, 25, 492-506.
- LEVENSON, A. S. & JORDAN, V. C. 1997. MCF-7: the first hormone-responsive breast cancer cell line. *Cancer Res*, 57, 3071-8.
- LEVENSON, A. S. & JORDAN, V. C. 1999. Selective oestrogen receptor modulation: molecular pharmacology for the millennium. *Eur J Cancer*, 35, 1628-39.
- LEVENSON, A. S., KLIAKHANDLER, I. L., SVOBODA, K. M., PEASE, K. M., KAISER, S. A., WARD, J. E., 3RD & JORDAN, V. C. 2002. Molecular classification of selective oestrogen receptor modulators on the basis of gene expression profiles of breast cancer cells expressing oestrogen receptor alpha. *Br J Cancer*, 87, 449-56.
- LEVINE, M. S., BAKKER, B., BOECKX, B., MOYETT, J., LU, J., VITRE, B., SPIERINGS, D. C., LANSDORP, P. M., CLEVELAND, D. W., LAMBRECHTS, D., FOIJER, F. & HOLLAND, A. J. 2017. Centrosome Amplification Is Sufficient to Promote Spontaneous Tumorigenesis in Mammals. *Dev Cell*, 40, 313-322 e5.
- LI, B., ZHAO, W. D., TAN, Z. M., FANG, W. G., ZHU, L. & CHEN, Y. H. 2006. Involvement of Rho/ROCK signalling in small cell lung cancer migration through human brain microvascular endothelial cells. *FEBS Lett*, 580, 4252-60.
- LI, B. X., SATOH, A. K. & READY, D. F. 2007. Myosin V, Rab11, and dRip11 direct apical secretion and cellular morphogenesis in developing *Drosophila* photoreceptors. *J Cell Biol*, 177, 659-69.
- LI, D., KUEHN, E. W. & PREKERIS, R. 2014a. Kinesin-2 mediates apical endosome transport during epithelial lumen formation. *Cell Logist*, 4, e28928.
- LI, D., MANGAN, A., CICCHINI, L., MARGOLIS, B. & PREKERIS, R. 2014b. FIP5 phosphorylation during mitosis regulates apical trafficking and lumenogenesis. *EMBO Rep*, 15, 428-37.
- LINGLE, W. L., LUTZ, W. H., INGLE, J. N., MAIHLE, N. J. & SALISBURY, J. L. 1998. Centrosome hypertrophy in human breast tumors: implications for genomic stability and cell polarity. *Proc Natl Acad Sci U S A*, 95, 2950-5.
- LIPPMAN, M., BOLAN, G. & HUFF, K. 1976. The effects of estrogens and antiestrogens on hormone-responsive human breast cancer in long-term tissue culture. *Cancer Res*, 36, 4595-601.

- LIU, H., YUE, J., HUANG, H., GOU, X., CHEN, S.-Y., ZHAO, Y. & WU, X. 2015. Regulation of Focal Adhesion Dynamics and Cell Motility by the EB2 and Hax1 Protein Complex. *Journal of Biological Chemistry*, 290, 30771-30782.
- LOWERY, J., KUCZMARSKI, E. R., HERRMANN, H. & GOLDMAN, R. D. 2015. Intermediate Filaments Play a Pivotal Role in Regulating Cell Architecture and Function. *J Biol Chem*, 290, 17145-53.
- LU, X., ERRINGTON, J., CURTIN, N. J., LUNEC, J. & NEWELL, D. R. 2001. The impact of p53 status on cellular sensitivity to antifolate drugs. *Clin Cancer Res*, 7, 2114-23.
- LUDERS, J., PATEL, U. K. & STEARNS, T. 2006. GCP-WD is a gamma-tubulin targeting factor required for centrosomal and chromatin-mediated microtubule nucleation. *Nat Cell Biol*, 8, 137-47.
- LUO, Y., LI, D., RAN, J., YAN, B., CHEN, J., DONG, X., LIU, Z., LIU, R., ZHOU, J. & LIU, M. 2014. End-binding protein 1 stimulates paclitaxel sensitivity in breast cancer by promoting its actions toward microtubule assembly and stability. *Protein & cell*, 5, 469-479.
- LUO, Y., RAN, J., XIE, S., YANG, Y., CHEN, J., LI, S., SHUI, W., LI, D., LIU, M. & ZHOU, J. 2016. ASK1 controls spindle orientation and positioning by phosphorylating EB1 and stabilizing astral microtubules. *Cell Discov*, 2, 16033.
- LY, N., ELKHATIB, N., BRESTEAU, E., PIÉTREMENT, O., KHALED, M., MAGIERA, M. M., JANKE, C., LE CAM, E., RUTENBERG, A. D. & MONTAGNAC, G. 2016.  $\alpha$ TAT1 controls longitudinal spreading of acetylation marks from open microtubules extremities. *Sci Rep*, 6, 35624.
- LÓPEZ, M. P., HUBER, F., GRIGORIEV, I., STEINMETZ, M. O., AKHMANOVA, A., KOENDERINK, G. H. & DOGTEROM, M. 2014. Actin–microtubule coordination at growing microtubule ends. *Nature communications*, 5.
- MA, J., XUE, Y., LIU, W., YUE, C., BI, F., XU, J., ZHANG, J., LI, Y., ZHONG, C. & CHEN, Y. 2013. Role of activated Rac1/Cdc42 in mediating endothelial cell proliferation and tumor angiogenesis in breast cancer. *PLoS One*, 8, e66275.
- MACK, N. A., WHALLEY, H. J., CASTILLO-LLUVA, S. & MALLIRI, A. 2011. The diverse roles of Rac signaling in tumorigenesis. *Cell Cycle*, 10, 1571-81.
- MADRID, R., ARANDA, J. F., RODRIGUEZ-FRATICELLI, A. E., VENTIMIGLIA, L., ANDRES-DELGADO, L., SHEHATA, M., FANAYAN, S., SHAHHEYDARI, H., GOMEZ, S., JIMENEZ, A., MARTIN-BELMONTE, F., BYRNE, J. A. & ALONSO, M. A. 2010. The formin INF2 regulates basolateral-to-apical transcytosis and lumen formation in association with Cdc42 and MAL2. *Dev Cell*, 18, 814-27.
- MAIATO, H. & LOGARINHO, E. 2014. Mitotic spindle multipolarity without centrosome amplification. *Nat Cell Biol*, 16, 386-94.
- MAN, X., MEGRAW, T. L. & LIM, Y. P. 2015. Cep68 can be regulated by Nek2 and SCF complex. *Eur J Cell Biol*, 94, 162-72.
- MANGAN, A. J., SIETSEMA, D. V., LI, D., MOORE, J. K., CITI, S. & PREKERIS, R. 2016. Cingulin and actin mediate midbody-dependent apical lumen formation during polarization of epithelial cells. *Nat Commun*, 7, 12426.
- MANNA, T., HONNAPPA, S., STEINMETZ, M. O. & WILSON, L. 2008. Suppression of microtubule dynamic instability by the +TIP protein EB1 and its modulation by the CAP-Gly domain of p150glued. *Biochemistry*, 47, 779-86.
- MANNEVILLE, J. B. & ETIENNE-MANNEVILLE, S. 2006. Positioning centrosomes and spindle poles: looking at the periphery to find the centre. *Biol Cell*, 98, 557-65.
- MARCIANO, D. K. 2017. A holey pursuit: lumen formation in the developing kidney. *Pediatr Nephrol*, 32, 7-20.
- MARDIN, B. R. & SCHIEBEL, E. 2012. Breaking the ties that bind: new advances in centrosome biology. *J Cell Biol*, 197, 11-8.

- MARTHIENS, V., RUJANO, M. A., PENNETIER, C., TESSIER, S., PAUL-GILLOTEAUX, P. & BASTO, R. 2013. Centrosome amplification causes microcephaly. *Nat Cell Biol*, 15, 731-40.
- MARTIN-BELMONTE, F., YU, W., RODRIGUEZ-FRATICELLI, A. E., EWALD, A. J., WERB, Z., ALONSO, M. A. & MOSTOV, K. 2008. Cell-polarity dynamics controls the mechanism of lumen formation in epithelial morphogenesis. *Curr Biol*, 18, 507-13.
- MATTSON, M. P., SON, T. G. & CAMANDOLA, S. 2007. Viewpoint: mechanisms of action and therapeutic potential of neurohormetic phytochemicals. *Dose Response*, 5, 174-86.
- MAURER, S. P., BIELING, P., COPE, J., HOENGER, A. & SURREY, T. 2011. GTPγS microtubules mimic the growing microtubule end structure recognized by end-binding proteins (EBs). *Proceedings of the National Academy of Sciences*, 108, 3988-3993.
- MAURER, S. P., FOURNIOL, F. J., BOHNER, G., MOORES, C. A. & SURREY, T. 2012a. EBs recognize a nucleotide-dependent structural cap at growing microtubule ends. *Cell*, 149, 371-82.
- MAURER, S. P., FOURNIOL, F. J., BOHNER, G., MOORES, C. A. & SURREY, T. 2012b. EBs recognize a nucleotide-dependent structural cap at growing microtubule ends. *Cell*, 149, 371-382.
- MCCAFFREY, L. M., MONTALBANO, J., MIHAI, C. & MACARA, I. G. 2012. Loss of the Par3 polarity protein promotes breast tumorigenesis and metastasis. *Cancer Cell*, 22, 601-14.
- MCNULTY, D. E., LI, Z., WHITE, C. D., SACKS, D. B. & ANNAN, R. S. 2011. MAPK scaffold IQGAP1 binds the EGF receptor and modulates its activation. *J Biol Chem*, 286, 15010-21.
- MEDER, D., SHEVCHENKO, A., SIMONS, K. & FÜLLEKRUG, J. 2005. Gp135/podocalyxin and NHERF-2 participate in the formation of a preapical domain during polarization of MDCK cells. *J Cell Biol*, 168, 303-13.
- MENG, X., MALIAKAL, P., LU, H., LEE, M. J. & YANG, C. S. 2004. Urinary and plasma levels of resveratrol and quercetin in humans, mice, and rats after ingestion of pure compounds and grape juice. *J Agric Food Chem*, 52, 935-42.
- MERALDI, P., HONDA, R. & NIGG, E. A. 2002. Aurora-A overexpression reveals tetraploidization as a major route to centrosome amplification in p53<sup>-/-</sup> cells. *EMBO J*, 21, 483-92.
- MERALDI, P., HONDA, R. & NIGG, E. A. 2004. Aurora kinases link chromosome segregation and cell division to cancer susceptibility. *Curr Opin Genet Dev*, 14, 29-36.
- MIALHE, A., LAFANECHERE, L., TREILLEUX, I., PELOUX, N., DUMONTET, C., BREMOND, A., PANH, M. H., PAYAN, R., WEHLAND, J., MARGOLIS, R. L. & JOB, D. 2001. Tubulin detyrosination is a frequent occurrence in breast cancers of poor prognosis. *Cancer Res*, 61, 5024-7.
- MIERKE, C. T., FREY, B., FELLNER, M., HERRMANN, M. & FABRY, B. 2011. Integrin α5β1 facilitates cancer cell invasion through enhanced contractile forces. *J Cell Sci*, 124, 369-83.
- MIKSTACKA, R., STEFANSKI, T. & ROZANSKI, J. 2013. Tubulin-interactive stilbene derivatives as anticancer agents. *Cell Mol Biol Lett*, 18, 368-97.
- MILLER, P. M., FOLKMANN, A. W., MAIA, A. R., EFIMOVA, N., EFIMOV, A. & KAVERINA, I. 2009. Golgi-derived CLASP-dependent microtubules control Golgi organization and polarized trafficking in motile cells. *Nat Cell Biol*, 11, 1069-80.
- MITCHISON, T. & KIRSCHNER, M. 1984. Dynamic instability of microtubule growth. *Nature*, 312, 237-242.
- MOGENSEN, M. M. 2004. Microtubule organizing centers in polarized epithelial cells. *Centrosomes in Development and Disease*, 299-319.
- MOGENSEN, M. M., MACKIE, J. B., DOXSEY, S. J., STEARNS, T. & TUCKER, J. B. 1997. Centrosomal deployment of gamma-tubulin and pericentrin: evidence for a

- microtubule-nucleating domain and a minus-end docking domain in certain mouse epithelial cells. *Cell Motil Cytoskeleton*, 36, 276-90.
- MOGENSEN, M. M., MALIK, A., PIEL, M., BOUCKSON-CASTAING, V. & BORNENS, M. 2000. Microtubule minus-end anchorage at centrosomal and non-centrosomal sites: the role of ninein. *J Cell Sci*, 113 ( Pt 17), 3013-23.
- MOHAN, R., KATRUKHA, E. A., DOODHI, H., SMAL, I., MEIJERING, E., KAPITEIN, L. C., STEINMETZ, M. O. & AKHMANOVA, A. 2013. End-binding proteins sensitize microtubules to the action of microtubule-targeting agents. *Proc Natl Acad Sci U S A*, 110, 8900-5.
- MONTESANO, R., SCHALLER, G. & ORCI, L. 1991. Induction of epithelial tubular morphogenesis in vitro by fibroblast-derived soluble factors. *Cell*, 66, 697-711.
- MOON, R. C. & MEHTA, R. G. 1990. Chemoprevention of mammary cancer by retinoids. *Basic Life Sci*, 52, 213-24.
- MORIN, X., JAOUEN, F. & DURBEC, P. 2007. Control of planar divisions by the G-protein regulator LGN maintains progenitors in the chick neuroepithelium. *Nat Neurosci*, 10, 1440-8.
- MOSS, D. K., BELLETT, G., CARTER, J. M., LIOVIC, M., KEYNTON, J., PRESCOTT, A. R., LANE, E. B. & MOGENSEN, M. M. 2007. Ninein is released from the centrosome and moves bidirectionally along microtubules. *J Cell Sci*, 120, 3064-74.
- MOUSTAKAS, A. & HELDIN, C. H. 2007. Signaling networks guiding epithelial–mesenchymal transitions during embryogenesis and cancer progression. *Cancer science*, 98, 1512-1520.
- MULLER, P. A., TRINIDAD, A. G., TIMPSON, P., MORTON, J. P., ZANIVAN, S., VAN DEN BERGHE, P. V., NIXON, C., KARIM, S. A., CASWELL, P. T., NOLL, J. E., COFFILL, C. R., LANE, D. P., SANSOM, O. J., NEILSEN, P. M., NORMAN, J. C. & VOUSDEN, K. H. 2013. Mutant p53 enhances MET trafficking and signalling to drive cell scattering and invasion. *Oncogene*, 32, 1252-65.
- MULLER, P. A. & VOUSDEN, K. H. 2014. Mutant p53 in cancer: new functions and therapeutic opportunities. *Cancer Cell*, 25, 304-17.
- MURPHY, C. G. & DICKLER, M. N. 2016. Endocrine resistance in hormone-responsive breast cancer: mechanisms and therapeutic strategies. *Endocr Relat Cancer*, 23, R337-52.
- NAGAI-TAMAI, Y., MIZUNO, K., HIROSE, T., SUZUKI, A. & OHNO, S. 2002. Regulated protein-protein interaction between aPKC and PAR-3 plays an essential role in the polarization of epithelial cells. *Genes Cells*, 7, 1161-71.
- NELSON, K. S., FURUSE, M. & BEITEL, G. J. 2010. The Drosophila Claudin Kune-kune is required for septate junction organization and tracheal tube size control. *Genetics*, 185, 831-9.
- NELSON, W. J. 2003. Adaptation of core mechanisms to generate cell polarity. *Nature*, 422, 766-74.
- NGUYEN, C. B., KOTTURI, H., WARIS, G., MOHAMMED, A., CHANDRAKESAN, P., MAY, R., SUREBAN, S., WEYGANT, N., QU, D., RAO, C. V., DHANASEKARAN, D. N., BRONZE, M. S., HOUCHE, C. W. & ALI, N. 2016. (Z)-3,5,4'-Trimethoxystilbene Limits Hepatitis C and Cancer Pathophysiology by Blocking Microtubule Dynamics and Cell-Cycle Progression. *Cancer Res*, 76, 4887-96.
- NIESSEN, C. M. & GOTTARDI, C. J. 2008. Molecular components of the adherens junction. *Biochim Biophys Acta*, 1778, 562-71.
- NIGG, E. A. 2001. Mitotic kinases as regulators of cell division and its checkpoints. *Nat Rev Mol Cell Biol*, 2, 21-32.
- NIGG, E. A. 2002. Centrosome aberrations: cause or consequence of cancer progression? *Nat Rev Cancer*, 2, 815-25.

- NIGG, E. A. 2006. Origins and consequences of centrosome aberrations in human cancers. *Int J Cancer*, 119, 2717-23.
- NIGG, E. A. & STEARNS, T. 2011. The centrosome cycle: Centriole biogenesis, duplication and inherent asymmetries. *Nat Cell Biol*, 13, 1154-60.
- NISHIGAKI, R., OSAKI, M., HIRATSUKA, M., TODA, T., MURAKAMI, K., JEANG, K. T., ITO, H., INOUE, T. & OSHIMURA, M. 2005. Proteomic identification of differentially expressed genes in human gastric carcinomas. *Proteomics*, 5, 3205-3213.
- NOATYNSKA, A., GOTTA, M. & MERALDI, P. 2012. Mitotic spindle (DIS)orientation and DISease: cause or consequence? *J Cell Biol*, 199, 1025-35.
- NORITAKE, J., WATANABE, T., SATO, K., WANG, S. & KAIBUCHI, K. 2005. IQGAP1: a key regulator of adhesion and migration. *J Cell Sci*, 118, 2085-92.
- NORTH, B. J., MARSHALL, B. L., BORRA, M. T., DENU, J. M. & VERDIN, E. 2003. The human Sir2 ortholog, SIRT2, is an NAD<sup>+</sup>-dependent tubulin deacetylase. *Mol Cell*, 11, 437-44.
- O'BRIEN, L. E., JOU, T. S., POLLACK, A. L., ZHANG, Q., HANSEN, S. H., YURCHENCO, P. & MOSTOV, K. E. 2001. Rac1 orientates epithelial apical polarity through effects on basolateral laminin assembly. *Nat Cell Biol*, 3, 831-8.
- OAKLEY, B. R., PAOLILLO, V. & ZHENG, Y. 2015.  $\gamma$ -Tubulin complexes in microtubule nucleation and beyond. *Mol Biol Cell*, 26, 2957-62.
- OAKLEY, C. E. & OAKLEY, B. R. 1989. Identification of gamma-tubulin, a new member of the tubulin superfamily encoded by mipA gene of *Aspergillus nidulans*. *Nature*, 338, 662-4.
- ODENWALD, M. A., CHOI, W., BUCKLEY, A., SHASHIKANTH, N., JOSEPH, N. E., WANG, Y., WARREN, M. H., BUSCHMANN, M. M., PAVLYUK, R., HILDEBRAND, J., MARGOLIS, B., FANNING, A. S. & TURNER, J. R. 2017. ZO-1 interactions with F-actin and occludin direct epithelial polarization and single lumen specification in 3D culture. *J Cell Sci*, 130, 243-259.
- OHTA, K., SHIINA, N., OKUMURA, E., HISANAGA, S., KISHIMOTO, T., ENDO, S., GOTOH, Y., NISHIDA, E. & SAKAI, H. 1993. Microtubule nucleating activity of centrosomes in cell-free extracts from *Xenopus* eggs: involvement of phosphorylation and accumulation of pericentriolar material. *J Cell Sci*, 104 ( Pt 1), 125-37.
- OKADA, K., BARTOLINI, F., DEACONESCU, A. M., MOSELEY, J. B., DOGIC, Z., GRIGORIEFF, N., GUNDERSEN, G. G. & GOODE, B. L. 2010. Adenomatous polyposis coli protein nucleates actin assembly and synergizes with the formin mDia1. *J Cell Biol*, 189, 1087-96.
- OLIVEIRA, R. A. & NASMYTH, K. 2013. Cohesin cleavage is insufficient for centriole disengagement in *Drosophila*. *Curr Biol*, 23, R601-3.
- OLIVIER, M., EELES, R., HOLLSTEIN, M., KHAN, M. A., HARRIS, C. C. & HAINAUT, P. 2002. The IARC TP53 database: new online mutation analysis and recommendations to users. *Hum Mutat*, 19, 607-14.
- OSBORNE, C. K. & SCHIFF, R. 2011. Mechanisms of endocrine resistance in breast cancer. *Annu Rev Med*, 62, 233-47.
- OVEREEM, A. W., BRYANT, D. M. & VAN, I. S. C. 2015. Mechanisms of apical-basal axis orientation and epithelial lumen positioning. *Trends Cell Biol*, 25, 476-85.
- PALAZZO, A., ACKERMAN, B. & GUNDERSEN, G. G. 2003. Cell biology: Tubulin acetylation and cell motility. *Nature*, 421, 230.
- PALAZZO, A. F., COOK, T. A., ALBERTS, A. S. & GUNDERSEN, G. G. 2001a. mDia mediates Rho-regulated formation and orientation of stable microtubules. *Nat Cell Biol*, 3, 723-9.
- PALAZZO, A. F., JOSEPH, H. L., CHEN, Y. J., DUJARDIN, D. L., ALBERTS, A. S., PFISTER, K. K., VALLEE, R. B. & GUNDERSEN, G. G. 2001b. Cdc42, dynein, and dynactin regulate

- MTOC reorientation independent of Rho-regulated microtubule stabilization. *Curr Biol*, 11, 1536-41.
- PALAZZO, R. E., VOGEL, J. M., SCHNACKENBERG, B. J., HULL, D. R. & WU, X. 2000. Centrosome maturation. *Curr Top Dev Biol*, 49, 449-70.
- PALUCH, E., VAN DER GUCHT, J. & SYKES, C. 2006. Cracking up: symmetry breaking in cellular systems. *J Cell Biol*, 175, 687-92.
- PARSONS, J. T., HORWITZ, A. R. & SCHWARTZ, M. A. 2010. Cell adhesion: integrating cytoskeletal dynamics and cellular tension. *Nat Rev Mol Cell Biol*, 11, 633-43.
- PASDAR, M. & NELSON, W. J. 1988. Kinetics of desmosome assembly in Madin-Darby canine kidney epithelial cells: temporal and spatial regulation of desmoplakin organization and stabilization upon cell-cell contact. I. Biochemical analysis. *J Cell Biol*, 106, 677-85.
- PELLEGRIN, S. & MELLOR, H. 2007. Actin stress fibres. *J Cell Sci*, 120, 3491-9.
- PEREZ, F., DIAMANTOPOULOS, G. S., STALDER, R. & KREIS, T. E. 1999. CLIP-170 highlights growing microtubule ends in vivo. *Cell*, 96, 517-27.
- PETRIE, R. J., DOYLE, A. D. & YAMADA, K. M. 2009. Random versus directionally persistent cell migration. *Nat Rev Mol Cell Biol*, 10, 538-49.
- PEYRE, E., JAOUEN, F., SAADAOU, M., HAREN, L., MERDES, A., DURBEC, P. & MORIN, X. 2011. A lateral belt of cortical LGN and NuMA guides mitotic spindle movements and planar division in neuroepithelial cells. *J Cell Biol*, 193, 141-54.
- PIHAN, G. A., PUROHIT, A., WALLACE, J., KNECHT, H., WODA, B., QUESENBERRY, P. & DOXSEY, S. J. 1998. Centrosome defects and genetic instability in malignant tumors. *Cancer Res*, 58, 3974-85.
- POLLARD, T. D. & BORISY, G. G. 2003. Cellular motility driven by assembly and disassembly of actin filaments. *Cell*, 112, 453-65.
- POLLARD, T. D. & COOPER, J. A. 2009. Actin, a central player in cell shape and movement. *Science*, 326, 1208-12.
- PORTRAN, D., SCHAEDEL, L., XU, Z., THÉRY, M. & NACHURY, M. V. 2017. Tubulin acetylation protects long-lived microtubules against mechanical ageing. *Nat Cell Biol*, 19, 391-398.
- PROVENZANO, P. P. & KEELY, P. J. 2011. Mechanical signaling through the cytoskeleton regulates cell proliferation by coordinated focal adhesion and Rho GTPase signaling. *Journal of cell science*, 124, 1195-1205.
- QUINTYNE, N. J., REING, J. E., HOFFELDER, D. R., GOLLIN, S. M. & SAUNDERS, W. S. 2005. Spindle multipolarity is prevented by centrosomal clustering. *Science*, 307, 127-9.
- RAMIREZ, N. E., ZHANG, Z., MADAMANCHI, A., BOYD, K. L., O'REAR, L. D., NASHABI, A., LI, Z., DUPONT, W. D., ZIJLSTRA, A. & ZUTTER, M. M. 2011. The  $\alpha_2\beta_1$  integrin is a metastasis suppressor in mouse models and human cancer. *J Clin Invest*, 121, 226-37.
- RASBAND, W. 1997-2016. *ImageJ* [Online]. U. S. National Institutes of Health, Bethesda, Maryland, USA,. Available: <https://imagej.nih.gov/ij/> [Accessed].
- REGINATO, M. J. & MUTHUSWAMY, S. K. 2006. Illuminating the center: mechanisms regulating lumen formation and maintenance in mammary morphogenesis. *J Mammary Gland Biol Neoplasia*, 11, 205-11.
- REYMOND, N., RIOU, P. & RIDLEY, A. J. 2012. Rho GTPases and cancer cell transendothelial migration. *Methods Mol Biol*, 827, 123-42.
- RIDLEY, A. J. 2001. Rho GTPases and cell migration. *Journal of Cell Science*, 114, 2713-2722.
- RIDLEY, A. J. 2006. Rho GTPases and actin dynamics in membrane protrusions and vesicle trafficking. *Trends Cell Biol*, 16, 522-9.
- RIDLEY, A. J. 2013. RhoA, RhoB and RhoC have different roles in cancer cell migration. *J Microsc*, 251, 242-9.

- RIDLEY, A. J., SCHWARTZ, M. A., BURRIDGE, K., FIRTEL, R. A., GINSBERG, M. H., BORISY, G., PARSONS, J. T. & HORWITZ, A. R. 2003. Cell migration: integrating signals from front to back. *Science*, 302, 1704-1709.
- RODRIGUEZ, O. C., SCHAEFER, A. W., MANDATO, C. A., FORSCHER, P., BEMENT, W. M. & WATERMAN-STORER, C. M. 2003a. Conserved microtubule-actin interactions in cell movement and morphogenesis. *Nat Cell Biol*, 5, 599-609.
- RODRIGUEZ, O. C., SCHAEFER, A. W., MANDATO, C. A., FORSCHER, P., BEMENT, W. M. & WATERMAN-STORER, C. M. 2003b. Conserved microtubule-actin interactions in cell movement and morphogenesis. *Nature cell biology*, 5, 599-609.
- RODRIGUEZ-FRATICELLI, A. E., AUZAN, M., ALONSO, M. A., BORNENS, M. & MARTIN-BELMONTE, F. 2012. Cell confinement controls centrosome positioning and lumen initiation during epithelial morphogenesis. *J Cell Biol*, 198, 1011-23.
- RODRIGUEZ-FRATICELLI, A. E., VERGARAJAUREGUI, S., EASTBURN, D. J., DATTA, A., ALONSO, M. A., MOSTOV, K. & MARTIN-BELMONTE, F. 2010. The Cdc42 GEF Intersectin 2 controls mitotic spindle orientation to form the lumen during epithelial morphogenesis. *J Cell Biol*, 189, 725-38.
- RONGHE, A., CHATTERJEE, A., SINGH, B., DANDAWATE, P., ABDALLA, F., BHAT, N. K., PADHYE, S. & BHAT, H. K. 2016. 4-(E)-{(p-tolylimino)-methylbenzene-1,2-diol}, 1 a novel resveratrol analog, differentially regulates estrogen receptors alpha and beta in breast cancer cells. *Toxicol Appl Pharmacol*, 301, 1-13.
- ROONEY, C., WHITE, G., NAZGIEWICZ, A., WOODCOCK, S. A., ANDERSON, K. I., BALLESTREM, C. & MALLIRI, A. 2010. The Rac activator STEF (Tiam2) regulates cell migration by microtubule-mediated focal adhesion disassembly. *EMBO Rep*, 11, 292-8.
- ROSARIO, C. O., KO, M. A., HAFFANI, Y. Z., GLADDY, R. A., PADEROVA, J., POLLETT, A., SQUIRE, J. A., DENNIS, J. W. & SWALLOW, C. J. 2010. Plk4 is required for cytokinesis and maintenance of chromosomal stability. *Proc Natl Acad Sci U S A*, 107, 6888-93.
- ROSS, J. L., ALI, M. Y. & WARSHAW, D. M. 2008. Cargo transport: molecular motors navigate a complex cytoskeleton. *Curr Opin Cell Biol*, 20, 41-7.
- SALISBURY, J. L., SUINO, K. M., BUSBY, R. & SPRINGETT, M. 2002. Centrin-2 is required for centriole duplication in mammalian cells. *Curr Biol*, 12, 1287-92.
- SALMON, W. C., ADAMS, M. C. & WATERMAN-STORER, C. M. 2002. Dual-wavelength fluorescent speckle microscopy reveals coupling of microtubule and actin movements in migrating cells. *J Cell Biol*, 158, 31-7.
- SARRIÓ, D., RODRIGUEZ-PINILLA, S. M., HARDISSON, D., CANO, A., MORENO-BUENO, G. & PALACIOS, J. 2008. Epithelial-mesenchymal transition in breast cancer relates to the basal-like phenotype. *Cancer research*, 68, 989-997.
- SCHAEDEL, L., JOHN, K., GAILLARD, J., NACHURY, M. V., BLANCHOIN, L. & THÉRY, M. 2015. Microtubules self-repair in response to mechanical stress. *Nat Mater*, 14, 1156-63.
- SCHALLER, M. D. 2001. Biochemical signals and biological responses elicited by the focal adhesion kinase. *Biochim Biophys Acta*, 1540, 1-21.
- SCHERZBERG, M. C., KIEHL, A., ZIVKOVIC, A., STARK, H., STEIN, J., FÜRST, R., STEINHILBER, D. & ULRICH-RÜCKERT, S. 2015. Structural modification of resveratrol leads to increased anti-tumor activity, but causes profound changes in the mode of action. *Toxicol Appl Pharmacol*, 287, 67-76.
- SCHLUTER, M. A. & MARGOLIS, B. 2009. Apical lumen formation in renal epithelia. *J Am Soc Nephrol*, 20, 1444-52.
- SCHLUTER, M. A. & MARGOLIS, B. 2012. Apicobasal polarity in the kidney. *Exp Cell Res*, 318, 1033-9.
- SCHMIDT, T. I., KLEYLEIN-SOHN, J., WESTENDORF, J., LE CLECH, M., LAVOIE, S. B., STIERHOF, Y. D. & NIGG, E. A. 2009. Control of centriole length by CPAP and CP110. *Curr Biol*, 19, 1005-11.

- SCHMORANZER, J., FAWCETT, J. P., SEGURA, M., TAN, S., VALLEE, R. B., PAWSON, T. & GUNDERSEN, G. G. 2009. Par3 and dynein associate to regulate local microtubule dynamics and centrosome orientation during migration. *Curr Biol*, 19, 1065-74.
- SCHNEIDER, Y., CHABERT, P., STUTZMANN, J., COELHO, D., FOUGEROUSSE, A., GOSSÉ, F., LAUNAY, J. F., BROUILLARD, R. & RAUL, F. 2003. Resveratrol analog (Z)-3,5,4'-trimethoxystilbene is a potent anti-mitotic drug inhibiting tubulin polymerization. *Int J Cancer*, 107, 189-96.
- SECHLER, J. L., CORBETT, S. A. & SCHWARZBAUER, J. E. 1997. Modulatory roles for integrin activation and the synergy site of fibronectin during matrix assembly. *Mol Biol Cell*, 8, 2563-73.
- SEETAPUN, D., CASTLE, B. T., MCINTYRE, A. J., TRAN, P. T. & ODDE, D. J. 2012. Estimating the microtubule GTP cap size in vivo. *Curr Biol*, 22, 1681-7.
- SELDIN, L., MUROYAMA, A. & LECHLER, T. 2016. NuMA-microtubule interactions are critical for spindle orientation and the morphogenesis of diverse epidermal structures. *Elife*, 5.
- SEN, I., VEPRINTSEV, D., AKHMANOVA, A. & STEINMETZ, M. O. 2013. End binding proteins are obligatory dimers. *PLoS One*, 8, e74448.
- SERCIN, O., LARSIMONT, J. C., KARAMBELAS, A. E., MARTHIENS, V., MOERS, V., BOECKX, B., LE MERCIER, M., LAMBRECHTS, D., BASTO, R. & BLANPAIN, C. 2016. Transient PLK4 overexpression accelerates tumorigenesis in p53-deficient epidermis. *Nat Cell Biol*, 18, 100-10.
- SHAMON, L. A., CHEN, C., MEHTA, R. G., STEELE, V., MOON, R. C. & PEZZUTO, J. M. 1994. A correlative approach for the identification of antimutagens that demonstrate chemopreventive activity. *Anticancer Res*, 14, 1775-8.
- SHANNON, K. B., CANMAN, J. C., BEN MOREE, C., TIRNAUER, J. S. & SALMON, E. D. 2005. Taxol-stabilized microtubules can position the cytokinetic furrow in mammalian cells. *Mol Biol Cell*, 16, 4423-36.
- SHARMA, S., STUTZMAN, J. D., KELLOFF, G. J. & STEELE, V. E. 1994. Screening of potential chemopreventive agents using biochemical markers of carcinogenesis. *Cancer Res*, 54, 5848-55.
- SHIN, K., FOGG, V. C. & MARGOLIS, B. 2006. Tight junctions and cell polarity. *Annu Rev Cell Dev Biol*, 22, 207-35.
- SIDDIQUI, A., DANDAWATE, P., RUB, R., PADHYE, S., APHALE, S., MOGHE, A., JAGYASI, A., VENKATESWARA SWAMY, K., SINGH, B., CHATTERJEE, A., RONGHE, A. & BHAT, H. K. 2013. Novel Aza-resveratrol analogs: synthesis, characterization and anticancer activity against breast cancer cell lines. *Bioorg Med Chem Lett*, 23, 635-40.
- SIGURBJORNSDOTTIR, S., MATHEW, R. & LEPTIN, M. 2014. Molecular mechanisms of de novo lumen formation. *Nat Rev Mol Cell Biol*, 15, 665-76.
- SILKWORTH, W. T., NARDI, I. K., SCHOLL, L. M. & CIMINI, D. 2009. Multipolar spindle pole coalescence is a major source of kinetochore mis-attachment and chromosome mis-segregation in cancer cells. *PLoS One*, 4, e6564.
- SKAU, C. T. & WATERMAN, C. M. 2015. Specification of Architecture and Function of Actin Structures by Actin Nucleation Factors. *Annu Rev Biophys*, 44, 285-310.
- SLEP, K. C. & VALE, R. D. 2007. Structural basis of microtubule plus end tracking by XMAP215, CLIP-170, and EB1. *Mol Cell*, 27, 976-91.
- SMALL, J. V., ROTTNER, K., KAVERINA, I. & ANDERSON, K. I. 1998. Assembling an actin cytoskeleton for cell attachment and movement. *Biochim Biophys Acta*, 1404, 271-81.
- SNIDER, N. T. & OMARY, M. B. 2014. Post-translational modifications of intermediate filament proteins: mechanisms and functions. *Nat Rev Mol Cell Biol*, 15, 163-77.

- SOBIN, L. H. & FLEMING, I. D. 1997. TNM Classification of Malignant Tumors, fifth edition (1997). Union Internationale Contre le Cancer and the American Joint Committee on Cancer. *Cancer*, 80, 1803-4.
- SONNEN, K. F., GABRYJONCZYK, A. M., ANSELM, E., STIERHOF, Y. D. & NIGG, E. A. 2013. Human Cep192 and Cep152 cooperate in Plk4 recruitment and centriole duplication. *J Cell Sci*, 126, 3223-33.
- SOURISSEAU, T., GEORGIADIS, A., TSAPARA, A., ALI, R. R., PESTELL, R., MATTER, K. & BALDA, M. S. 2006. Regulation of PCNA and cyclin D1 expression and epithelial morphogenesis by the ZO-1-regulated transcription factor ZONAB/DbpA. *Mol Cell Biol*, 26, 2387-98.
- SPERKA, T., GEISLER, K. J., MERKEL, U., SCHOLL, I., RUBIO, I., HERRLICH, P. & MORRISON, H. L. 2011. Activation of Ras requires the ERM-dependent link of actin to the plasma membrane. *PLoS One*, 6, e27511.
- STEBBENS, S. & WITTMANN, T. 2012a. Targeting and transport: how microtubules control focal adhesion dynamics. *J Cell Biol*, 198, 481-9.
- STEBBENS, S. & WITTMANN, T. 2012b. Targeting and transport: How microtubules control focal adhesion dynamics. *The Journal of cell biology*, 198, 481-489.
- STEVENS, D., GASSMANN, R., OEGEMA, K. & DESAI, A. 2011. Uncoordinated loss of chromatid cohesion is a common outcome of extended metaphase arrest. *PLoS One*, 6, e22969.
- STINCHCOMBE, J. C., MAJOROVITS, E., BOSSI, G., FULLER, S. & GRIFFITHS, G. M. 2006. Centrosome polarization delivers secretory granules to the immunological synapse. *Nature*, 443, 462-5.
- STOOPS, E. H., HULL, M., OLESEN, C., MISTRY, K., HARDER, J. L., RIVERA-MOLINA, F., TOOMRE, D. & CAPLAN, M. J. 2015. The periciliary ring in polarized epithelial cells is a hot spot for delivery of the apical protein gp135. *J Cell Biol*, 211, 287-94.
- STRAUB, F. 1943. Actin. 3, 23-37
- STRILIC, B., EGLINGER, J., KRIEG, M., ZEEB, M., AXNICK, J., BABAL, P., MULLER, D. J. & LAMMERT, E. 2010. Electrostatic cell-surface repulsion initiates lumen formation in developing blood vessels. *Curr Biol*, 20, 2003-9.
- STRILIC, B., KUCERA, T., EGLINGER, J., HUGHES, M. R., MCNAGNY, K. M., TSUKITA, S., DEJANA, E., FERRARA, N. & LAMMERT, E. 2009. The molecular basis of vascular lumen formation in the developing mouse aorta. *Dev Cell*, 17, 505-15.
- STROUD, M. J., KAMMERER, R. A. & BALLESTREM, C. 2011. Characterization of G2L3 (GAS2-like 3), a new microtubule- and actin-binding protein related to spectraplakins. *J Biol Chem*, 286, 24987-95.
- SU, L.-K., BURRELL, M., HILL, D. E., GYURIS, J., BRENT, R., WILTSHIRE, R., TRENT, J., VOGELSTEIN, B. & KINZLER, K. W. 1995. APC binds to the novel protein EB1. *Cancer research*, 55, 2972-2977.
- SU, L.-K. & QI, Y. 2001. Characterization of Human MAPRE Genes and Their Proteins. *Genomics*, 71, 142-149.
- SUN, L., GAO, J., DONG, X., LIU, M., LI, D., SHI, X., DONG, J. T., LU, X., LIU, C. & ZHOU, J. 2008. EB1 promotes Aurora-B kinase activity through blocking its inactivation by protein phosphatase 2A. *Proc Natl Acad Sci U S A*, 105, 7153-8.
- SUN, X., LI, D., YANG, Y., REN, Y., LI, J., WANG, Z., DONG, B., LIU, M. & ZHOU, J. 2012. Microtubule-binding protein CLIP-170 is a mediator of paclitaxel sensitivity. *J Pathol*, 226, 666-73.
- SUN, X., LI, F., DONG, B., SUO, S., LIU, M., LI, D. & ZHOU, J. 2013. Regulation of tumor angiogenesis by the microtubule-binding protein CLIP-170. *Protein & cell*, 4, 266-276.
- SZENT-GYÖRGYI, A. G. 1953. Meromyosins, the subunits of

- myosin. *Archives of biochemistry and biophysics*, 42, 305-320.
- SÜTTERLIN, C. & COLANZI, A. 2010. The Golgi and the centrosome: building a functional partnership. *J Cell Biol*, 188, 621-8.
- TAHERIAN, A., LI, X., LIU, Y. & HAAS, T. A. 2011. Differences in integrin expression and signaling within human breast cancer cells. *BMC Cancer*, 11, 293.
- TAMURA, N. & DRAVIAM, V. M. 2012. Microtubule plus-ends within a mitotic cell are 'moving platforms' with anchoring, signalling and force-coupling roles. *Open Biol*, 2, 120132.
- TELENTSCHAK, S., SOLIWODA, M., NOHROUDI, K., ADDICKS, K. & KLINZ, F. J. 2015. Cytokinesis failure and successful multipolar mitoses drive aneuploidy in glioblastoma cells. *Oncol Rep*, 33, 2001-8.
- TEPASS, U. 2012. The apical polarity protein network in Drosophila epithelial cells: regulation of polarity, junctions, morphogenesis, cell growth, and survival. *Annu Rev Cell Dev Biol*, 28, 655-85.
- THERY, M., RACINE, V., PEPIN, A., PIEL, M., CHEN, Y., SIBARITA, J. B. & BORNENS, M. 2005. The extracellular matrix guides the orientation of the cell division axis. *Nat Cell Biol*, 7, 947-53.
- THOMAS, E., GOPALAKRISHNAN, V., HEGDE, M., KUMAR, S., KARKI, S. S., RAGHAVAN, S. C. & CHOUDHARY, B. 2016. A Novel Resveratrol Based Tubulin Inhibitor Induces Mitotic Arrest and Activates Apoptosis in Cancer Cells. *Sci Rep*, 6, 34653.
- THOMAS, G. E., SREEJA, J. S., GIREESH, K. K., GUPTA, H. & MANNA, T. K. 2015. +TIP EB1 downregulates paclitaxel-induced proliferation inhibition and apoptosis in breast cancer cells through inhibition of paclitaxel binding on microtubules. *Int J Oncol*, 46, 133-46.
- TOJKANDER, S., GATEVA, G. & LAPPALAINEN, P. 2012. Actin stress fibers--assembly, dynamics and biological roles. *J Cell Sci*, 125, 1855-64.
- TOJKANDER, S., GATEVA, G., SCHEVZOV, G., HOTULAINEN, P., NAUMANEN, P., MARTIN, C., GUNNING, P. W. & LAPPALAINEN, P. 2011. A molecular pathway for myosin II recruitment to stress fibers. *Curr Biol*, 21, 539-50.
- TRAVERSI, G., FIORE, M., PERCARIO, Z., DEGRASSI, F. & COZZI, R. 2017. The resveratrol analogue trimethoxystilbene inhibits cancer cell growth by inducing multipolar cell mitosis. *Mol Carcinog*, 56, 1117-1126.
- TSOU, M. F., WANG, W. J., GEORGE, K. A., URYU, K., STEARNS, T. & JALLEPALLI, P. V. 2009. Polo kinase and separase regulate the mitotic licensing of centriole duplication in human cells. *Dev Cell*, 17, 344-54.
- TUCKWELL, D. S., REID, K. B., BARNES, M. J. & HUMPHRIES, M. J. 1996. The A-domain of integrin alpha 2 binds specifically to a range of collagens but is not a general receptor for the collagenous motif. *Eur J Biochem*, 241, 732-9.
- UZBEKOV, R., KIREYEV, I. & PRIGENT, C. 2002. Centrosome separation: respective role of microtubules and actin filaments. *Biol Cell*, 94, 275-88.
- VALDIVIA-SILVA, J. E., FRANCO-BARRAZA, J., SILVA, A. L., PONT, G. D., SOLDEVILA, G., MEZA, I. & GARCÍA-ZEPEDA, E. A. 2009. Effect of pro-inflammatory cytokine stimulation on human breast cancer: implications of chemokine receptor expression in cancer metastasis. *Cancer Lett*, 283, 176-85.
- VAN BREUGEL, M., HIRONO, M., ANDREEVA, A., YANAGISAWA, H. A., YAMAGUCHI, S., NAKAZAWA, Y., MORGNER, N., PETROVICH, M., EBONG, I. O., ROBINSON, C. V., JOHNSON, C. M., VEPRINTSEV, D. & ZUBER, B. 2011. Structures of SAS-6 suggest its organization in centrioles. *Science*, 331, 1196-9.
- VAN DER VAART, B., AKHMANOVA, A. & STRAUBE, A. 2009. Regulation of microtubule dynamic instability. *Biochem Soc Trans*, 37, 1007-13.

- VARGAS, A. C., MCCART REED, A. E., WADDELL, N., LANE, A., REID, L. E., SMART, C. E., COCCIARDI, S., DA SILVA, L., SONG, S., CHENEVIX-TRENCH, G., SIMPSON, P. T. & LAKHANI, S. R. 2012. Gene expression profiling of tumour epithelial and stromal compartments during breast cancer progression. *Breast Cancer Res Treat*, 135, 153-65.
- VAUGHAN, K. T. 2005. TIP maker and TIP marker; EB1 as a master controller of microtubule plus ends. *J Cell Biol*, 171, 197-200.
- VEGA, F. M., FRUHWIRTH, G., NG, T. & RIDLEY, A. J. 2011. RhoA and RhoC have distinct roles in migration and invasion by acting through different targets. *J Cell Biol*, 193, 655-65.
- VEGA, F. M. & RIDLEY, A. J. 2008. Rho GTPases in cancer cell biology. *FEBS Lett*, 582, 2093-101.
- VERHEY, K. J. & GAERTIG, J. 2007. The tubulin code. *Cell cycle*, 6, 2152-2160.
- VINZENZ, M., NEMETHOVA, M., SCHUR, F., MUELLER, J., NARITA, A., URBAN, E., WINKLER, C., SCHMEISER, C., KOESTLER, S. A. & ROTTNER, K. 2012. Actin branching in the initiation and maintenance of lamellipodia. *J Cell Sci*, 125, 2775-2785.
- VITRE, B., COQUELLE, F. M., HEICHETTE, C., GARNIER, C., CHRÉTIEN, D. & ARNAL, I. 2008. EB1 regulates microtubule dynamics and tubulin sheet closure in vitro. *Nat Cell Biol*, 10, 415-21.
- WAKIDA, N. M., BOTVINICK, E. L., LIN, J. & BERNS, M. W. 2010. An intact centrosome is required for the maintenance of polarization during directional cell migration. *PLoS One*, 5, e15462.
- WALTHER, R. F. & PICHAUD, F. 2010. Crumbs/DaPKC-dependent apical exclusion of Bazooka promotes photoreceptor polarity remodeling. *Curr Biol*, 20, 1065-74.
- WANG, C., CHANG, K. C., SOMERS, G., VIRSHUP, D., ANG, B. T., TANG, C., YU, F. & WANG, H. 2009. Protein phosphatase 2A regulates self-renewal of Drosophila neural stem cells. *Development*, 136, 2287-96.
- WANG, Q. & MARGOLIS, B. 2007. Apical junctional complexes and cell polarity. *Kidney Int*, 72, 1448-58.
- WANG, T., YANGER, K., STANGER, B. Z., CASSIO, D. & BI, E. 2014. Cytokinesis defines a spatial landmark for hepatocyte polarization and apical lumen formation. *J Cell Sci*, 127, 2483-92.
- WANG, X., YANG, Y., DUAN, Q., JIANG, N., HUANG, Y., DARZYNKIEWICZ, Z. & DAI, W. 2008. sSgo1, a major splice variant of Sgo1, functions in centriole cohesion where it is regulated by Plk1. *Dev Cell*, 14, 331-41.
- WANG, Y., ZHOU, X., ZHU, H., LIU, S., ZHOU, C., ZHANG, G., XUE, L., LU, N., QUAN, L. & BAI, J. 2005. Overexpression of EB1 in human esophageal squamous cell carcinoma (ESCC) may promote cellular growth by activating  $\beta$ -catenin/TCF pathway. *Oncogene*, 24, 6637-6645.
- WATANABE, T., NORITAKE, J. & KAIBUCHI, K. 2005. Regulation of microtubules in cell migration. *Trends Cell Biol*, 15, 76-83.
- WATERMAN-STORER, C., DUEY, D. Y., WEBER, K. L., KEECH, J., CHENEY, R. E., SALMON, E. D. & BEMENT, W. M. 2000. Microtubules remodel actomyosin networks in Xenopus egg extracts via two mechanisms of F-actin transport. *J Cell Biol*, 150, 361-76.
- WATERMAN-STORER, C. M. & SALMON, E. 1997. Actomyosin-based retrograde flow of microtubules in the lamella of migrating epithelial cells influences microtubule dynamic instability and turnover and is associated with microtubule breakage and treadmilling. *The Journal of cell biology*, 139, 417-434.
- WATERMAN-STORER, C. M. & SALMON, E. 1999. Positive feedback interactions between microtubule and actin dynamics during cell motility. *Curr Opin Cell Biol*, 11, 61-7.

- WATERS, J. C., CHEN, R. H., MURRAY, A. W. & SALMON, E. D. 1998. Localization of Mad2 to kinetochores depends on microtubule attachment, not tension. *J Cell Biol*, 141, 1181-91.
- WATSON, D. L. 1980. Immunological functions of the mammary gland and its secretion-- comparative review. *Aust J Biol Sci*, 33, 403-22.
- WEE, B., JOHNSTON, C. A., PREHODA, K. E. & DOE, C. Q. 2011. Canoe binds RanGTP to promote Pins(TPR)/Mud-mediated spindle orientation. *J Cell Biol*, 195, 369-76.
- WEGNER, A. 1976. Head to tail polymerization of actin. *J Mol Biol*, 108, 139-50.
- WEIDNER, K. M., ARAKAKI, N., HARTMANN, G., VANDEKERCKHOVE, J., WEINGART, S., RIEDER, H., FONATSCH, C., TSUBOUCHI, H., HISHIDA, T. & DAIKUCHARA, Y. 1991. Evidence for the identity of human scatter factor and human hepatocyte growth factor. *Proc Natl Acad Sci U S A*, 88, 7001-5.
- WEISENBERG, R. C. 1972. Microtubule formation in vitro in solutions containing low calcium concentrations. *Science*, 177, 1104-1105.
- WEN, Y., ENG, C. H., SCHMORANZER, J., CABRERA-POCH, N., MORRIS, E. J., CHEN, M., WALLAR, B. J., ALBERTS, A. S. & GUNDERSEN, G. G. 2004. EB1 and APC bind to mDia to stabilize microtubules downstream of Rho and promote cell migration. *Nat Cell Biol*, 6, 820-30.
- WENNERBERG, K., LOHIKANGAS, L., GULLBERG, D., PFAFF, M., JOHANSSON, S. & FÄSSLER, R. 1996. Beta 1 integrin-dependent and -independent polymerization of fibronectin. *J Cell Biol*, 132, 227-38.
- WESTERMANN, S. & WEBER, K. 2003. Post-translational modifications regulate microtubule function. *Nature Reviews Molecular Cell Biology*, 4, 938-948.
- WESTLAKE, C. J., BAYE, L. M., NACHURY, M. V., WRIGHT, K. J., ERVIN, K. E., PHU, L., CHALOUNI, C., BECK, J. S., KIRKPATRICK, D. S., SLUSARSKI, D. C., SHEFFIELD, V. C., SCHELLER, R. H. & JACKSON, P. K. 2011. Primary cilia membrane assembly is initiated by Rab11 and transport protein particle II (TRAPP II) complex-dependent trafficking of Rabin8 to the centrosome. *Proc Natl Acad Sci U S A*, 108, 2759-64.
- WHITSETT, T., CARPENTER, M. & LAMARTINIERE, C. A. 2006. Resveratrol, but not EGCG, in the diet suppresses DMBA-induced mammary cancer in rats. *J Carcinog*, 5, 15.
- WICKSTROM, S. A., LANGE, A., HESS, M. W., POLLEUX, J., SPATZ, J. P., KRUGER, M., PFALLER, K., LAMBACHER, A., BLOCH, W., MANN, M., HUBER, L. A. & FASSLER, R. 2010. Integrin-linked kinase controls microtubule dynamics required for plasma membrane targeting of caveolae. *Dev Cell*, 19, 574-88.
- WILLENBORG, C., JING, J., WU, C., MATERN, H., SCHAACK, J., BURDEN, J. & PREKERIS, R. 2011. Interaction between FIP5 and SNX18 regulates epithelial lumen formation. *J Cell Biol*, 195, 71-86.
- WITTMANN, T., HYMAN, A. & DESAI, A. 2001. The spindle: a dynamic assembly of microtubules and motors. *Nat Cell Biol*, 3, E28-34.
- WITTMANN, T. & WATERMAN-STORER, C. M. 2005. Spatial regulation of CLASP affinity for microtubules by Rac1 and GSK3beta in migrating epithelial cells. *J Cell Biol*, 169, 929-39.
- WLOGA, D. & GAERTIG, J. 2010. Post-translational modifications of microtubules. *Journal of cell science*, 123, 3447-3455.
- WOJNACKI, J., QUASSOLLO, G., MARZOLO, M.-P. & CÁCERES, A. 2014. Rho GTPases at the crossroad of signaling networks in mammals: impact of Rho-GTPases on microtubule organization and dynamics. *Small GTPases*, 5, e28430.
- WORDEMAN, L. 2005. Microtubule-depolymerizing kinesins. *Curr Opin Cell Biol*, 17, 82-8.
- WOZNIAK, M. A., MODZELEWSKA, K., KWONG, L. & KEELY, P. J. 2004. Focal adhesion regulation of cell behavior. *Biochim Biophys Acta*, 1692, 103-19.
- WU, B. & GUO, W. 2015. The Exocyst at a Glance. *J Cell Sci*, 128, 2957-64.

- WU, C., HUGHES, P. E., GINSBERG, M. H. & MCDONALD, J. A. 1996. Identification of a new biological function for the integrin alpha v beta 3: initiation of fibronectin matrix assembly. *Cell Adhes Commun*, 4, 149-58.
- WU, J. & AKHMANOVA, A. 2017. Microtubule-Organizing Centers. *Annu Rev Cell Dev Biol*, 33, 51-75.
- WU, X., SHEN, Q. T., ORISTIAN, D. S., LU, C. P., ZHENG, Q., WANG, H. W. & FUCHS, E. 2011. Skin stem cells orchestrate directional migration by regulating microtubule-ACF7 connections through GSK3 $\beta$ . *Cell*, 144, 341-52.
- XUE, B., KRISHNAMURTHY, K., ALLRED, D. C. & MUTHUSWAMY, S. K. 2013. Loss of Par3 promotes breast cancer metastasis by compromising cell-cell cohesion. *Nat Cell Biol*, 15, 189-200.
- YAMAGUCHI, H. & CONDEELIS, J. 2007. Regulation of the actin cytoskeleton in cancer cell migration and invasion. *Biochim Biophys Acta*, 1773, 642-52.
- YANG, B., SONAWANE, N. D., ZHAO, D., SOMLO, S. & VERKMAN, A. S. 2008. Small-molecule CFTR inhibitors slow cyst growth in polycystic kidney disease. *J Am Soc Nephrol*, 19, 1300-10.
- YI, Q., ZHAO, X., HUANG, Y., MA, T., ZHANG, Y., HOU, H., COOKE, H. J., YANG, D. Q., WU, M. & SHI, Q. 2011. p53 dependent centrosome clustering prevents multipolar mitosis in tetraploid cells. *PLoS One*, 6, e27304.
- YOON, M., MOIR, R. D., PRAHLAD, V. & GOLDMAN, R. D. 1998. Motile properties of vimentin intermediate filament networks in living cells. *J Cell Biol*, 143, 147-57.
- YU, I., GARNHAM, C. P. & ROLL-MECAK, A. 2015. Writing and reading the tubulin code. *Journal of Biological Chemistry*, 290, 17163-17172.
- YU, W., DATTA, A., LEROY, P., O'BRIEN, L. E., MAK, G., JOU, T. S., MATLIN, K. S., MOSTOV, K. E. & ZEGERS, M. M. 2005. Beta1-integrin orients epithelial polarity via Rac1 and laminin. *Mol Biol Cell*, 16, 433-45.
- YU, W., SHEWAN, A. M., BRAKEMAN, P., EASTBURN, D. J., DATTA, A., BRYANT, D. M., FAN, Q. W., WEISS, W. A., ZEGERS, M. M. & MOSTOV, K. E. 2008. Involvement of RhoA, ROCK I and myosin II in inverted orientation of epithelial polarity. *EMBO Rep*, 9, 923-9.
- YUE, J., XIE, M., GOU, X., LEE, P., SCHNEIDER, M. D. & WU, X. 2014a. Microtubules regulate focal adhesion dynamics through MAP4K4. *Developmental cell*, 31, 572-585.
- YUE, J., XIE, M., GOU, X., LEE, P., SCHNEIDER, M. D. & WU, X. 2014b. Microtubules regulate focal adhesion dynamics through MAP4K4. *Dev Cell*, 31, 572-85.
- YVON, A. M., WADSWORTH, P. & JORDAN, M. A. 1999. Taxol suppresses dynamics of individual microtubules in living human tumor cells. *Mol Biol Cell*, 10, 947-59.
- ZACK, G. W., ROGERS, W. E. & LATT, S. A. 1977. Automatic measurement of sister chromatid exchange frequency. *J Histochem Cytochem*, 25, 741-53.
- ZANIC, M., STEAR, J. H., HYMAN, A. A. & HOWARD, J. 2009. EB1 recognizes the nucleotide state of tubulin in the microtubule lattice. *PLoS One*, 4, e7585.
- ZEGERS, M. M., O'BRIEN, L. E., YU, W., DATTA, A. & MOSTOV, K. E. 2003. Epithelial polarity and tubulogenesis in vitro. *Trends Cell Biol*, 13, 169-76.
- ZHANG, J., PIONTEK, J., WOLBURG, H., PIEHL, C., LISS, M., OTTEN, C., CHRIST, A., WILLNOW, T. E., BLASIG, I. E. & ABDELILAH-SEYFRIED, S. 2010. Establishment of a neuroepithelial barrier by Claudin5a is essential for zebrafish brain ventricular lumen expansion. *Proc Natl Acad Sci U S A*, 107, 1425-30.
- ZHANG, T., ZAAL, K. J., SHERIDAN, J., MEHTA, A., GUNDERSEN, G. G. & RALSTON, E. 2009. Microtubule plus-end binding protein EB1 is necessary for muscle cell differentiation, elongation and fusion. *J Cell Sci*, 122, 1401-1409.
- ZHENG, J., FURNESS, D., DUAN, C., MILLER, K. K., EDGE, R. M., CHEN, J., HOMMA, K., HACKNEY, C. M., DALLOS, P. & CHEATHAM, M. A. 2013. Marshalin, a microtubule

minus-end binding protein, regulates cytoskeletal structure in the organ of Corti.  
*Biology open*, 2, 1192-1202.

ZHU, W., QIN, W., ZHANG, K., ROTTINGHAUS, G. E., CHEN, Y. C., KLIETHERMES, B. & SAUTER, E. R. 2012. Trans-resveratrol alters mammary promoter hypermethylation in women at increased risk for breast cancer. *Nutr Cancer*, 64, 393-400.

ZYSS, D. & GERGELY, F. 2009. Centrosome function in cancer: guilty or innocent? *Trends Cell Biol*, 19, 334-46.